

– An international journal for New Concepts in Global Tectonics –

NCGT JOURNAL

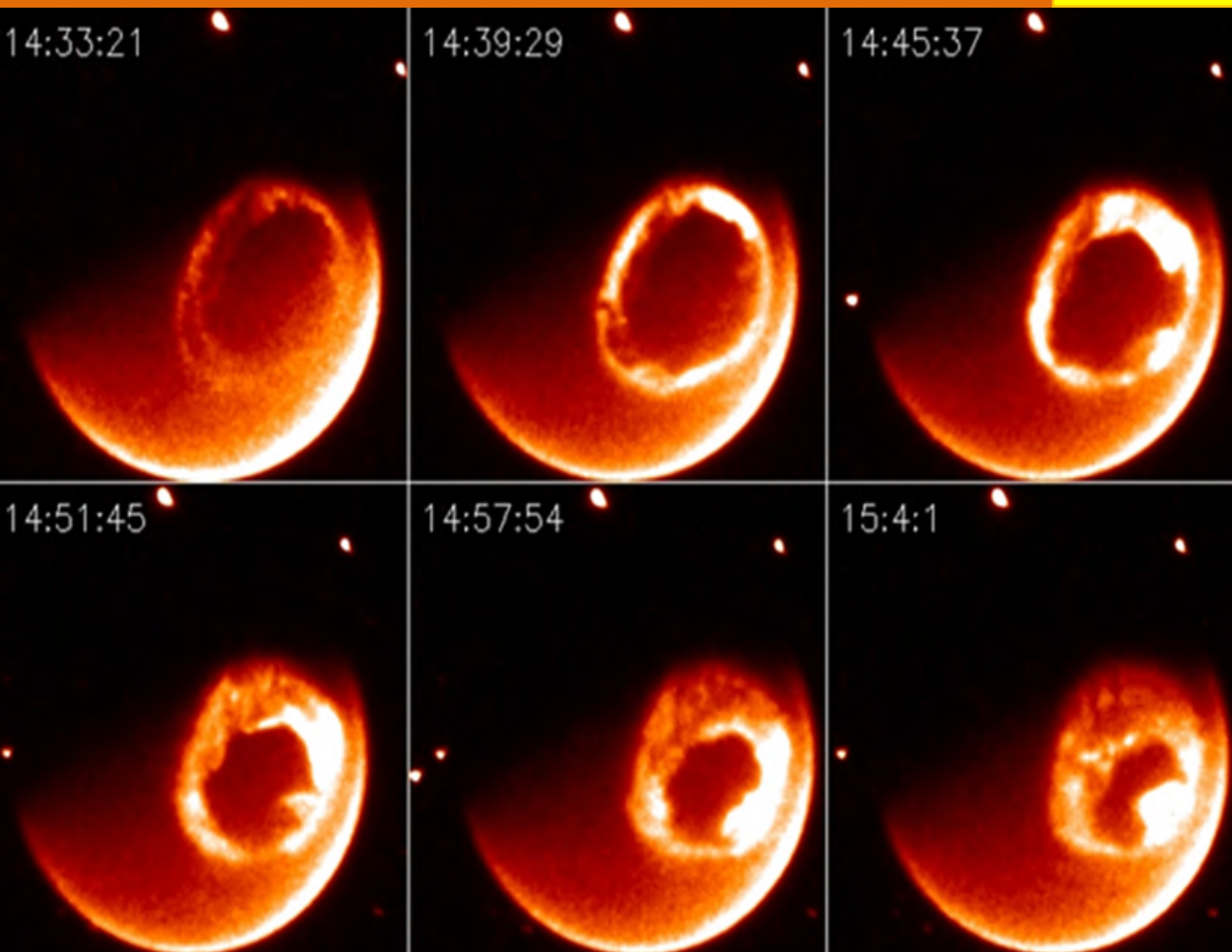
Editor-in-Chief: Bruce LEYBOURNE (leybourneb@iascc.org)

Volume 13, Number 4
June 2025



ISSN 2202-0039

WWW.ncgtjournal.com



Auroral substorm observed by the FUV (Far Ultraviolet) photometers on IMAGE (Imager for Magnetopause-to-Aurora Global Exploration). After <http://sprg.ssl.berkeley.edu/image/>. Credit: NASA. NASA copyright free policy.

Auroral Substorms

2nd Quarterly Issue

– An international journal for New Concepts in Global Tectonics –

NCGT  **JOURNAL**

Volume 13, Number 4, June 2025. ISSN 2202-0039.

EDITORIAL BOARD

Editor-in-Chief: Bruce LEYBOURNE, USA (leybourneb@iascc.org)
Co-Editor-in-Chief: Masahiro SHIBA, Japan (shiba@dino.or.jp)
Giovanni P. GREGORI, Italy (giovannipgregori38@gmail.com)
Louis HISSINK Australia (louis.hissink@outlook.com)
Per MICHAELSEN, Mongolia (perm@must.edu.mn)
Biju LONGHINOS, India (biju.longhinos@gmail.com)
Vladimir ANOKHIN, Russia (vladanokhin@yandex.ru)

CONTENTS

EDITOR'S CORNER - Comments by Editor in Chief - Bruce Leybourne.....475
Announcements on Upcoming Conferences - "CALL FOR PAPERS".....475

Articles

Energy and physical mechanisms in the magnetosphere: Giovanni P. Gregori, Bruce A. Leybourne, Giorgio Maria Gregori.....476

Solar and Earth's Geomagnetic Activity Related to the M6.2 Earthquake Recorded in Chile on November 8, 2024: Valentino Straser, Gabriele Cataldi, Daniele Cataldi.....546

Solar and Earth's Geomagnetic Activity Related to the M6+ Earthquake Recorded Between 12 and 18 November 2024: Valentino Straser, Gabriele Cataldi, Daniele Cataldi.....556

Plate Tectonic Issues, The Influence Of Electricity In Rock Forming Processes And A Coherent Connection Between Science, Mythology And History Of Finland Part III: Stefan Ahmala.....564

Interpretation of the Data on the Kursk Magnetic Anomaly Based on Recordings by Artificial Earth Satellites: Vadim V. Gordienko and Victor N. Tarasov.....598

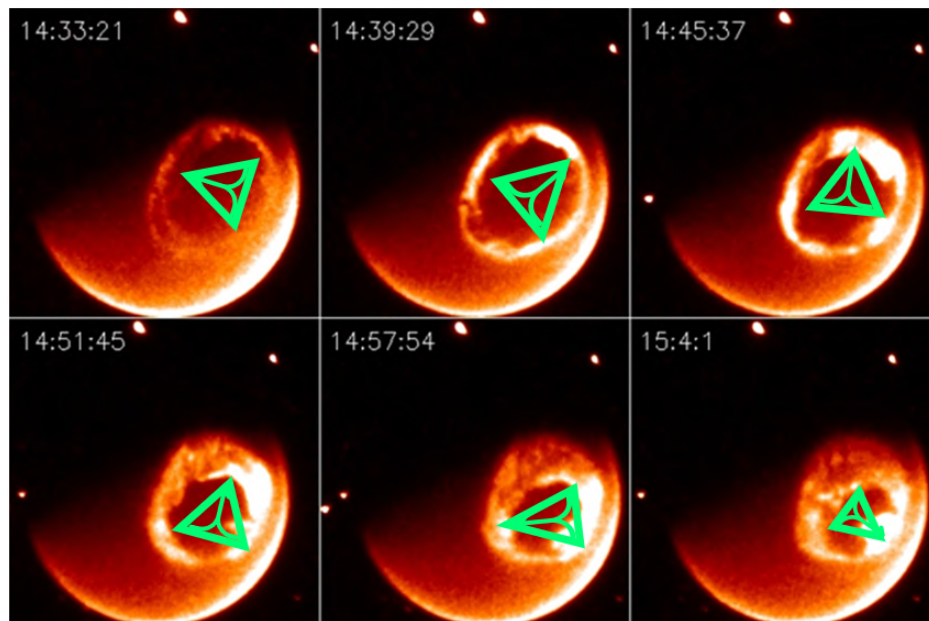
Comets like probes of the solar wind Magnetospheres and Cometospheres: Giovanni P. Gregori, Bruce A. Leybourne.....605

About the NCGT Journal676

For donations, please feel free to contact the Research Director of the Geoplasma Research Institute, Mr. Bruce Leybourne, at leybourneb@iascc.org. For contact, correspondence, or inclusion of material in the NCGT Journal please use the following methods: *NEW CONCEPTS IN GLOBAL TECTONICS*. 1. E-mail: leybourneb@iascc.org (files in MS Word or ODT format, and figures in gif, bmp or tif format) as separate files; 3. Telephone, +61 402 509 420. *DISCLAIMER:* The opinions, observations and ideas published in this journal are the responsibility of the contributors and do not necessarily reflect those of the Editor and the Editorial Board. *NCGT Journal* is a refereed quarterly international online journal and appears in March, June, September and December. ISSN number; ISSN 2202-0039.

EDITOR'S CORNER - Comments by Editor in Chief - Bruce Leybourne

Our regular quarterly issue this month includes an interesting cover image from NASA on an **Auroral substorm observed by the FUV (Far Ultraviolet) photometers**. The tetrahedron added inside the ring current that was rarefied during the auroral substorm is inserted to indicate the possibility of a rotating Delta-Wye circuit embedded at the polar-space interface indicating the presence of an electric current traversing through the Earth. The upper middle image portrays three bright segments highlighting the suspected effect, although this is only somewhat portrayed in the other images. These currents are speculatively suspected to exist in dark mode and interconnect with the Sun and other planets near the heliopause within a rotating Birkeland current associated with the spiraling arm of our galaxy likely related to the ~26,000 year rotation of the precession cycle. These circuits are mapped out with John Quinn's deep seated satellite magnetic modeling data delineating Giovanni Gregori's sea urchin spikes in an Electric Universe (2016) presentation by me. See: <https://www.youtube.com/watch?v=Q355Haapq-0>



See: **Comets like probes of the solar wind Magnetospheres and Cometospheres** : Giovanni P. Gregori, Bruce A. Leybourne in this issue - Fig. 13. Auroral substorm observed by the FUV (Far Ultraviolet) photometers on IMAGE (Imager for Magnetopause -to- Aurora Global Exploration). After <http://sprg.ssl.berkeley.edu/image/>. Credit: NASA. NASA copyright free policy.

Announcements on Upcoming Conferences - “CALL FOR PAPERS”

We have initiated planning committees for 2 upcoming conferences:

January/February 2026 – NCGT in Trivandrum, India is being organized by Biju Longhinos (biju.longhinos@gmail.com), where we are planning about 6 - half day sessions over 4 days with a post conference field trip. Details to be announced with a “CALL FOR PAPERS”. Please contact Biju, if you wish to become involved in any aspect of the conference. We are looking for Session Topics, Abstracts, Papers, Session Chairs, Organizers, Workers, Financial Contributions etc. Let me and Biju know how you'd like to be involved, and we may accommodate.

September 2026 – NCGT in Italy is being organized by Valentino Straser (valentino.straser@gmail.com) where we are planning a similar event with details to be determined. Please contact Valentino if you wish to become involved in any aspect of the conference. Again, we are looking for Session Topics, Abstracts, Papers, Session Chairs, Organizers, Workers, Financial Contributions etc. Let me and Valentino know how you'd like to be involved, and we may accommodate.

Energy and physical mechanisms in the magnetosphere

Giovanni Pietro Gregori¹, Bruce Allen Leybourne², Giorgio Maria Gregori³

¹ IDASC-Istituto di Acustica e Sensoristica O. M. Corbino (CNR), Roma, now merged into IMM-Istituto per la Microelettronica e Microsistemi (CNR); and ISSO-International Seismic Safety Organization, Italy

²GeoPlasma Research Institute-(GeoPlasmaResearchInstitute.org), Aurora, CO 80014, USA

³Master of Science in Physics of Biosystems at University La Sapienza in Rome

Corresponding Author: G. P. Gregori, IDASC-Istituto di Acustica e Sensoristica O. M. Corbino (CNR), Roma, now merged into IMM-Istituto per la Microelettronica e Microsistemi (CNR);
Email: giovannipgregori38@gmail.com

Abstract: The magnetosphere is a dynamic structure, which represents the response of the time-varying flow of solar wind, following the expansion of the solar corona. Hence, at every time instant, the magnetosphere represents a different physical system, and the magnetosphere is not a closed domain of space. The physical mechanisms that determine the structure of the magnetosphere imply a time varying exchange of energy content between different components parts. This is the focus of the present paper. The problem can be tackled from a “top-down” approach - i.e., starting from the laws of physics and deriving the expected observations. An alternative approach is “bottom-up”, i.e., one relies on available observations and, in some way, one constructs an empirical model interpolating over observations. The present paper deals with the “top-down” approach. One can tackle the problem according to two viewpoints, either in terms of loops of electric currents (or \mathbf{j} -loops), or in terms of *MHD* algorithms. Both viewpoints are here discussed and the result compared each other. The problem is quite intricate, and this implied that this topic is somewhat unfashionable, enjoying some interest only in the 1960s and 1970s. In any case, real quantitative applications should require observational information that, in general, are at present unavailable. However, by clarifying the entire conceptual procedure, we attain a better understanding of the real physical mechanisms that govern the magnetosphere. All these items are here discussed in detail, including the comparison with a few “bottom-up” investigations.

Keywords: neutral sheet – plasmashet - magnetospheric substorms and geomagnetic storms - plasma mantle - current loop formulation - phase space approach - steady state - time varying conditions – variational principles - minimum potential energy - energy contents, stresses and torques - electromagnetic drag of the Earth

Table of content

1 - Introduction	5.2.5 - The work spent by the electric field (the energy equation)
2 - The Earth’s magnetosphere. A model in terms of \mathbf{j} -loops	5.2.6 - Summary
3 - The Earth’s magnetosphere. Magnetospheric substorms and geomagnetic storms	6 - The energy of the magnetosphere - Time varying conditions
4 - The Earth’s magnetosphere. Forelocks and plasma mantle	7 - The minimum potential energy of the magnetosphere.
5 - Energy in the magnetosphere	8 - Energy contents, stresses and torques in magnetospheric subvolumes
5.1 - Steady state - The current loop formulation	8.1 - The geomagnetic field in absence of solar wind
5.1.1 - Screened Earth’s core	8.2 - $U_j(\mathbf{B}_M, \mathbf{b})$ and its time derivative
5.1.2 - Unscreened Earth’s core	8.3 - The Earth’s core
5.2 - Steady state - The phase space approach	8.4 - $U_s(\mathbf{b})$ and the total magnetic energy of the magnetosphere
5.2.1 - The virial equation	8.5 - Other self- and joint energies and their respective currents and geometrical factors. Partial <i>DPS</i> ratios and their time derivatives
5.2.2 - The Dessler-Parker-Sckopke (<i>DPS</i>) ratio	8.6 - The electromagnetic drag of the Earth
5.2.3 – Forces	8.7 – Conclusion
5.2.4 – Torques	

9 - Energy computations. Case histories reported in the literature

Appendix

- A.1. *In terms of c-loops and of m-loops*
- A.2. *c-loops linking m-loops.*
- A.3. *m-loops linking c-loops*
- A.4. Computation of the magnetic self-energies for specific models
- A.5. Loops
- A.6. Two rigid loops
- A.7. Spherical shell
- A.8. 2D current distribution of arbitrary shape (general shell)

Introduction

The present study is based on notes by the senior author, written in the late 1960s and early 1970s, when – while seeking a physical explanation of the Earth’s magnetosphere - he actively investigated the energy content and relations between different components of the magnetosphere.¹ Differently stated, while searching for a physical explanation of the formation of the magnetosphere - including the neutral sheet and all observational details that were collected in those hectic years - an obvious concern was about how to compute the energy content (and its variation) inside different parts of the magnetosphere.

Indeed, this entire item resulted quite intricate. It has been quite a job. Nevertheless, it can be shown how it is possible to exploit this analysis, up to some extent, depending - however - on available observations. The present paper reports this intricate analysis. Owing to the intrinsic formal complication, this topic has always been somewhat unfashionable, and always implied a considerable amount of hard thinking. The reader should forgive for some eventually apparently complicated formalism, and consider, rather, the underlying physical content.

The magnetosphere is not a closed domain of space. Rather, it is a dynamic structure, which represents the response of the time-varying flow of solar wind, following the expansion of the solar corona. Hence, every time instant deals with a different physical system. The expanding solar corona is represented by a sphere of surface $4\pi R_{ecl}^2$ where $R_{ecl} = 1 AU$ is the mean radius of the Earth’s orbit around the Sun. If the magnetosphere has a cross-section with a surface, say, $\pi (10 R_E)^2$ where R_E is the Earth’s radius, the Earth’ magnetosphere interacts with a fraction $\sim 0.45 \times 10^{-9}$ of the expanding solar corona. Therefore, we must expect that the magnetosphere feels the large scatter of the solar wind

flow.

The previous literature addressed the entire magnetosphere. The present analysis focuses, rather, on the energy content inside subvolumes of the instant structure of the magnetosphere. It is reasonable to expect that, in general, the available instant observational monitoring is not sufficiently detailed for computing distinct energy contents. However, the discussion, which is here carried out, permits to understand the way energy migrates between different component parts of the magnetosphere.

In general, two kinds of approach can be distinguished: a *top-down* and a *bottom-up* approach. The *top-down* approach begins by the laws of electromagnetism (e.m.), and attempts to implement a formal exhaustive theory of the energy content and relations, focusing on the different components of the magnetosphere. Conversely, the *bottom-up* approach is semi-empirical, as it begins by a set of experimental records and it attempts to implement some energy balance that fits with observations.

The present study focuses the *top-down* approach - while a comparatively limited number of papers, mostly in the comparably more recent literature, focus on the *bottom-up* approach, by means of some records collected by satellite and space probes. These *bottom-up* papers are here only briefly mentioned for completeness sake, with no devoted discussion.

We must, however, face some drawback, as the present generally reported model of the magnetosphere relies on a semi-empirical approach, combining laws of physics altogether with experimental observations. For instance, let us mention the most amazing example, as nobody seems to give a physical explanation for the formation of the neutral sheet. Therefore, as a first step for the exploitation of our *top-down* approach, we must begin and explain a few key physical features of the magnetosphere by avoiding every semi-empirical model. For brevity purpose, only a few essential items are here mentioned, while a somewhat more extended - although concise - description is given in Gregori and Leybourne (2025m). However, we must begin and mention a few basic warning.

A theorem hold, which is universal and applies everywhere - on every scale from the micro-world of a tiny water droplet through the huge galactic superclusters. This theorem was proven in Gregori (2002), even though the author formerly did not realize its key relevance. The theorem deals with the rigorous proof of the *generalized Cowling theorem*. In fact, Larmor² (1919a, 1920) gave the first explanation of the magnetic field **B** that had been observed on the solar

¹ This was his first target and achievement, after having entered, in the mid-1960s, into the study of solar-terrestrial relations.

² Sir Joseph Larmor (1857–1942), Irish mathematician and physicist.

photosphere. The violent endogenous processes of the solar interior originate violent motions of the ionized environment, thus supplying what is called a “stellar dynamo”. This explanation is still generally accepted, and the object of extensive modeling. However, in the 1930s, Cowling³ showed a famous theorem (Gregori et al., 2025d), which was soon considered a classical result. Cowling showed that, in the case of an ideal cylindrical symmetry, no stellar dynamo can originate a **B**. Thus, the theorem soon became a nightmare for all solar and stellar physicists. Several proofs were later given, everyone based on different reasonable assumptions, but every proof led to the same conclusion.

Gregori (2002) unexpectedly found a rigorous proof of the *generalized Cowling theorem*⁴ that can be briefly synthesized as follows.

Under very general conditions, every system of charged particles with an internal dynamics - such as, e.g., a convection cell - is an effective dynamo that can display only either one of the two patterns shown in Figure 1. Figure 1a has poloidal **B** and toroidal **E**, while Figure 1b has poloidal **E** and toroidal **B**. The theorem states that the case of Figure 1a is *unstable*, hence never observed, while the case of Figure 1b is *stable*. In addition, the argument shows that, in the case of ideal cylindrical symmetry, the stable case of Figure 1b has *null* energy – being thus in close agreement with the old-fashioned classical Cowling theorem.

Hence, it is concluded that every closed loop of the motion of some ionized medium – such as a convective cell of any size – operates like a true dynamo, which can be named “*Cowling dynamo*”.

The next key item claims that every stellar dynamo must soon stop due to “*Biermann blocking*”. In fact, Biermann⁵ (1941) showed that inside sunspots electrons cannot cool, due to the violent **B**. In fact, it can be shown (Gregori, 2002) that every stellar dynamo attempts to lock the entire star inside a huge toroidal **B**. That is, we should not even observe the star. Conversely, the enormous endogenous energy causes a continuous disruption of the blocking. That is, a star is the balance between thermonuclear energy and e.m. blocking. This blocking is therefore named Biermann blocking.

The subsequent step deals with the *electrostatics of a star*. Indeed, a star is composed of electrons and protons, ions, etc. The great difference of mass between different particles implies a difference of the respective gyration radii. Hence, the evaporation process is expected to be much more effective on protons and ions than on electrons, because they have much larger gyration radii, and are therefore less firmly locked by the stellar **B**.

Thus, the star progressively acquires a negative total electric charge, while the expanding stellar corona transports a mainly positive charge. Therefore, when the negative charge of the star overwhelms some given threshold, enormous van de Graaff accelerators launch violent electron jets that break through the photosphere of the star. This is the explanation of sunspots (Gregori and Leybourne, 2025g).

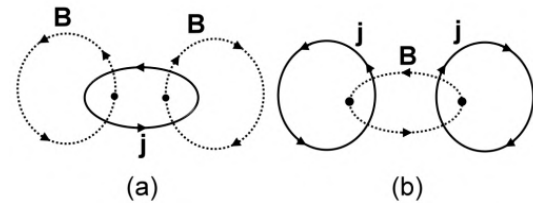


Figure 1. Idealized scheme of every most general dynamo composed of charge matter with some internal dynamics. Only two configurations are possible. The generalized Cowling theorem proves that case (a) is unstable while case (b) is stable. In either case, the system attains the maximum possible dynamo performance, even though in the case of the perfect cylindrical symmetric configuration, the total energy of the stable dynamo of case (b) is *null*. In contrast, with no cylindrical symmetry the energy for case (b) is not null. After Gregori (2002), also in Gregori et al. (2025d), with kind permission of the late Wilfried Schröder.

This explains the observed mainly positive charge of the “regular” *solar wind*, which is eventually crossed by sporadic huge clouds of electrons that originate spectacular polar auroras and very large e.m. perturbations.

A key feature is related to the internal micro-thermal inhomogeneity that originates micro-convective cells, hence Cowling micro-dynamos. The consequent result is an observed, and otherwise unexplained, self-focusing of the solar wind that displays *collimation effects* into filaments.

In this respect, note that - in the case of infinite conductivity σ of the solar wind - the classical “*frozen-in*” concept of Alfvén⁶ applies, as the solar wind particles have a null gyration radius. This implies, however, the paradox that, when $\sigma \rightarrow \infty$, the solar wind is a perfect ideal mirror. Hence, we could not even see any kind of radiation coming from the Sun, at any frequency. This paradox, however, is solved upon considering the “*illusion of continuity*”.

In fact, it is customary to treat the solar wind by means of *MHD*. That is, the solar wind is considered a continuous fluid. However, at very low particle concentration, an ideal continuity must imply to smear

³ Thomas George Cowling, FRS (1906–1990), English astronomer.

⁴ An extensive account is given in Gregori et al. (2025d).

⁵ Ludwig Biermann (1907-1986), German astronomer.

⁶ Hannes Olof Gösta Alfvén (1908-1995), Swedish physicist.

every single electron or proton into smaller charged particles. Conversely, behind a given limit, we must refer to discrete particle collision. That is, the assumption $\sigma \rightarrow \infty$ no more applies. Thus, the solar wind is not a perfect mirror, and we can in fact observe the solar radiation within some given frequency band.

For future reference, let us remind about a classical and well known argument. Inside the solar wind the *kinetic energy density* overwhelms the *magnetic energy density*, hence \mathbf{B} is “frozen-in” the solar wind, and is transported by the kinetic field of particles. This originates the well-known spiral pattern of the interplanetary magnetic field \mathbf{B}_{int} , often called *IMF*. In contrast, close to the Earth the magnetic energy density overwhelms the kinetic energy density of particles, which are therefore trapped and form the radiation belts (see below).

Another key - and often considered - concept is the so-called “*reconnection*” of \mathbf{B} field lines (Figure 2). Suppose that some discontinuity occurs, e.g., in the solar wind. Hence, a gap of particles cannot supply the needed “regular” continuous flow of the solar wind. It is claimed that a “*plasma cavity*” occurs inside the solar wind. In reality, in this way the composition of the system changes.

Conversely, it has become customary to consider, intuitively, the Earth’s magnetosphere like a model aircraft inside a wind tunnel, where air molecules regularly enter into - and exit from - the tunnel. On the other hand, the solar wind flow is other than this simple model. When the physical system changes composition due to missing particles in the solar wind, the general topology changes of the e.m. field embedded in the solar wind. In any case, if one wants to save the *MHD* formalisms that presumes a “continuous” flow of plasma, one must admit that a breaking occurred of \mathbf{B} field lines, with subsequent “*reconnection*” with a different pattern. This is obviously in contrast with the Maxwell⁷ law requirement $div \mathbf{B} = 0$.

Given any two most general distributions (in 2D or 3D) of electric current C_1 and C_2 ,

I) – when Joule heat can be neglected, either it is

$$\delta U_{s1} \equiv \delta U_{s2} \equiv -\delta U_j \equiv -\delta W \quad (1)$$

or either one of the following conditions hold

$$\text{Max } U_j \quad \text{min } U_{s1} \quad \text{min } U_{js2} \quad (2)$$

being

$$\delta U_{s1} + \delta U_{s2} + \delta U_j + \delta W = \delta E \quad (3)$$

where U_{sk} is the self energy of C_k ($k = 1,2$), U_j is the joint magnetic energy of C_1 and C_2 , W is kinetic energy, and E includes all other forms of energy that are eventually either supplied to the system (when positive) or released by it (when negative).

An additional warning deals with the origin of the \mathbf{B} of a celestial object. In addition to the obvious case of an iron meteorite - which is a remnant of a disruption of a larger magnetized object - four mechanisms can be envisaged.

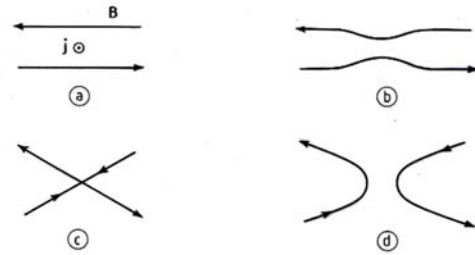


Figure 2. “*Reconnection*”. A lack of supply of the current j [figure (a)], associated, e.g., with a “*plasma cavity*” in the solar wind, compels the system to change its geometry [figure (b)], because $curl \mathbf{B}$ can no more be sustained by j . On the occasion of some extreme case history, the topology of the \mathbf{B} field-lines can even be drastically changed [figure (c)], eventually evolving into some new pattern [figure (d)]. This process is mathematically described by stating that the former \mathbf{B} field-lines were “cut” and “reconnected”. However, this is a mathematical fiction, because it violates the Maxwell relation $div \mathbf{B} = 0$. After Gregori (1991, 2000, 2001), and Gregori and Leybourne (2025m). With kind permission of *SIF*.

The aforementioned Larmor dynamo applies to stars - equivalently one can consider the generation of toroidal \mathbf{B} by Cowling dynamo.

In addition, the orbital motion, or spin, of objects with a non-null electric charge is a source of \mathbf{B} . In fact, if the solar wind has a non-null total electric charge (see above), all objects in the Solar System experience a varying total electric charge. This is nicely shown, e.g., by the four mini-satellites of the Pluto-Charon binary system (Gregori, 2016a).

However, a tide-driven (*TD*) dynamo is a most important and frequent mechanism for the origin of the \mathbf{B} of a celestial object. This mechanism applies to large objects, which are significantly smaller than stars, and that are composed of unbound components that can move relative to one another due to tidal pull. This is the focus of Gregori (2002). See additional comments in Gregori and Leybourne (2025m).

In the following, we need the “*principle of magnetic energy variation*” (see Gregori et al., 2025e for a general account). The proof relies on college physics (see brief mentions in section A.6), and the related theorem is as follows.

II) – Whenever Joule heat cannot be neglected,

⁷ James Clerk Maxwell, FRS FRSE (1831–1879), Scottish physicist and mathematician.

U_{s1} , and U_{s2} progressively damp off, while U_j , is transferred step-by-step into either U_{s1} , or U_{s2} , where it later decays by Joule heat.

We can now focus on some crucial - and generally reported as unexplained - features of the Earth's magnetosphere.

Two viewpoints apply. One viewpoint considers the Earth's magnetosphere as an ensemble of current loops, or j -loops. The other viewpoint applies the phase space approach. We discuss separately the two approaches.

The mathematical formalism is sometimes intricate. We refer to the standard symbols that, at present, are widely applied in the geomagnetic literature. In this respect, we warn the reader about the impossibility to report here the detailed definition of every symbol, as this can be made only on a devoted textbook. We report formulas that can give a feeling of the general approach to this intricate problem, while we suppose that the reader is acquainted to deal with the geomagnetic literature. A few formulas are given in the Appendix, being however, only a part of the needed formulas.

We add that the two viewpoints can be approached almost independent each other. The reader who is not acquainted with the reference to phase-space methods can, in any case, read and understand the paper concerning to computations in terms of j -loops.

2 - The Earth's magnetosphere. A model in terms of j -loops

The present generally accepted model of the magnetosphere is largely empirical, and relies on observational evidence independent of physical interpretation. This model is often reported to have been first proposed by Heikkila⁸ (1972), who synthesized the most current beliefs of that time. As already mentioned, recall the well-known energy balance argument. Inside the solar wind, the kinetic energy density overwhelms the magnetic energy density, hence \mathbf{B} is "frozen-in" the solar wind. In contrast, close to the Earth the magnetic energy density overwhelms the kinetic energy density of particles, which are therefore trapped and form the radiation belts. The region where the two kinds of energy density approximately balance each other is called "magnetopause". This is emblematically represented by a closed surface - and this is the rationale for defining the "drop-model" magnetosphere (Figure 3, left panel). The drop-model magnetosphere was the generally agreed concept before the discovery in the 1960s of the neutral sheet, and - in some way - this model favored the erroneous intuitive concept of magnetosphere conceived like a given closed domain in space.

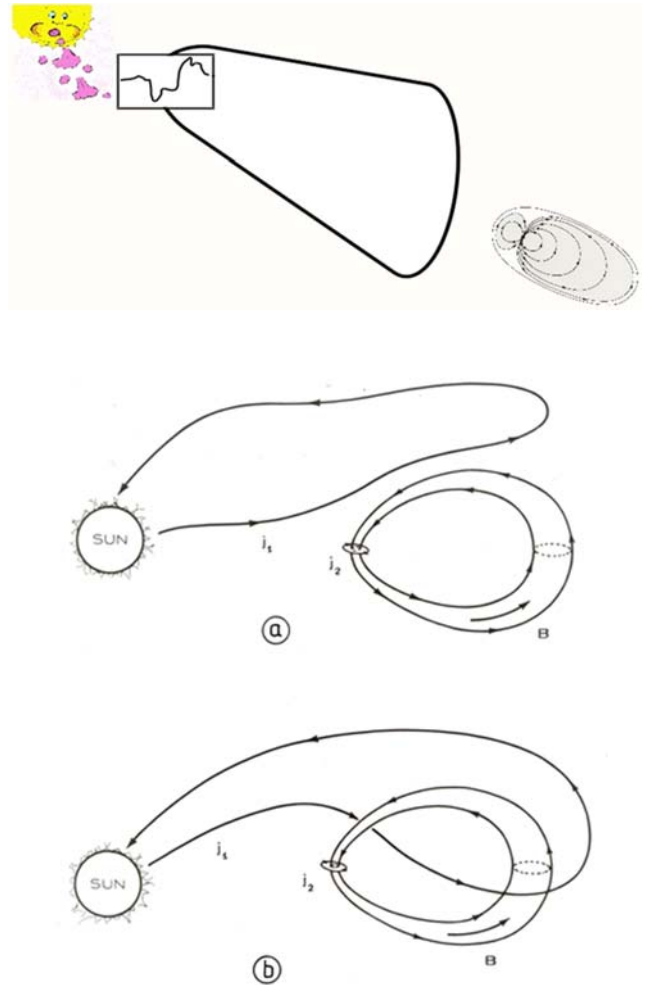


Figure 3. (top) A j -loop of the solar wind approaches the j -loop that symbolizes the j currents that originate the \mathbf{B} of the Earth. The solar wind j -loop contains a j -generator, i.e., a generator of electric current - not of voltage. The j -generator is indicated by the top-left rectangle. Historically, only the gravitational interaction was first considered, and only later also the thermodynamic and e.m. implications were addressed. After Gregori (2002). With kind permission of the late Wilfried Schröder. (bottom) The solar wind is here symbolized (with no loss of generality) only by one loop of electric current j_1 and the source of the Earth \mathbf{B} is here symbolized only by one loop j_2 . Within a "drop-model" magnetosphere [Figure (a)] j_1 flows all outside the magnetopause and it links no flux Φ_2 of the magnetic field \mathbf{B}_2 generated by j_2 . However, whenever some physical cause is such that j_1 links as much Φ_2 as possible, such as it occurs in Figure (b), the Hamilton's principle states that - by this and only by this - stable equilibrium can be attained. Thus, (a) and (b) can be considered as physically possible and meaningful states of equilibrium, although (a) is unstable, while (b) is stable. After Gregori (1989, 1998, 1999a), also in Gregori and Leybourne (2025m), and after Figure 1 of Gregori et al. (2025e). With kind permission of SIF.

⁸ Walter John Heikkila, a nice gentleman, Professor Emeritus at the University of Texas at Dallas, TX.

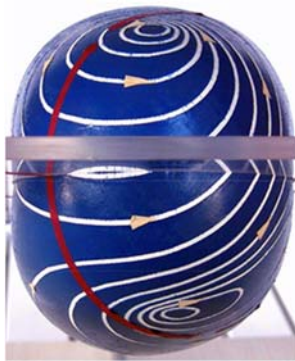
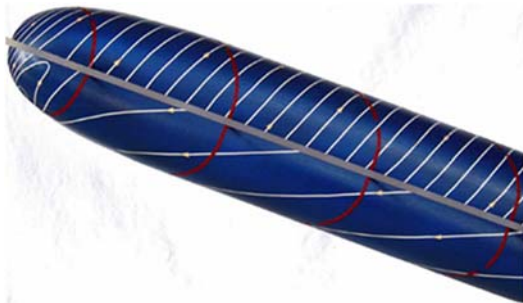


Figure 4. 3D model of the magnetosphere (not to scale), to investigate the topology of \mathbf{j} currents, in the case of an “away” sector of \mathbf{B}_{int} . The \mathbf{B}_{int} field lines are shown by red arrows, tracked on a transparent slab that represents the ecliptic plane. Note the great asymmetry between the Northern and Southern lobes. Other images are in Gregori and Leybourne (2025m). The top figure shows the senior author. See text. Unpublished figure.

Within a “drop-model” magnetosphere [Figure 3a] \mathbf{j}_1 flows all outside the magnetopause and it links no flux Φ_2 of the magnetic field \mathbf{B}_2 generated by \mathbf{j}_2 . However, occasionally some micro-plasma cavity in the solar wind permits that \mathbf{j}_1 currents link as much Φ_2 as possible, such as it occurs in Figure 3b. Thus, owing to the Hamilton's principle, a stable equilibrium is attained - by this and only by this. See additional details below and also in Gregori (1999) and in Gregori et al. (2025e). That is, Figure 3a and Figure 3b can be considered as physically possible and meaningful states of equilibrium, although Figure 3a is unstable, while Figure 3b is stable. To our understanding, this is *the unique ever proposed* physical explanation for the formation of the neutral sheet, relying on the well known Hamilton's variation principle (see Gregori et al., 2025e).

We stress that the concept of magnetopause does not imply that the magnetosphere is a closed domain in space, where the magnetopause separates the domain of interplanetary environment. Conversely, several phenomena cross through the magnetopause, due the corpuscular nature of the solar wind, which implies micro-plasma cavities. These several phenomena are well known and are named in different ways - and observed by space probes by means of different sensors (see some account *passim* here below).

The 1960s were hectic years, and space probes discovered the “neutral sheet”. At present, the literature refers to the aforementioned Heikkila's model of the magnetosphere, relying – however - on an interpolation of available observations. In contrast, as already stressed, no physical explanation is given for the formation of the neutral sheet, which is, rather, here explained in terms of a variational principle. Indeed, a key concept deals with the Maxwell law $\text{div } \mathbf{j} = 0$, by which all currents \mathbf{j} can be expressively imagined, e.g., as a flow of water inside a water-pipe of varying cross-section. A comparably more intense \mathbf{j} is thus associated to a smaller cross-section of the pipe, etc. That is, the role of particle gaps (or “plasma cavities”) in the solar wind is intuitively considered a secondary effect, which causes a perturbation of the main pattern – reminding, e.g., about an air bubble that flows within the “water-pipe”.

Upon a close and detailed analysis, it is found that the whole \mathbf{j} -system is surprisingly composed of three loops (Figure 5). One \mathbf{j} -loop is denoted by J_1 and by a green arrow in the left panel of Figure 5. It flows away from the Sun, and – when seen from the Sun – it confines the Northern lobe of the magnetosphere by a clockwise current. In normal conditions the solar wind has mainly positive charges. Hence, this loop is composed of protons and *He* ions.

A similar \mathbf{j} -loop, denoted by J_2 , shown by a blue

arrow in the top panel of Figure 5, must envelop the Southern lobe by a clockwise current – when observed from the Sun – although the current must flow towards the Sun.

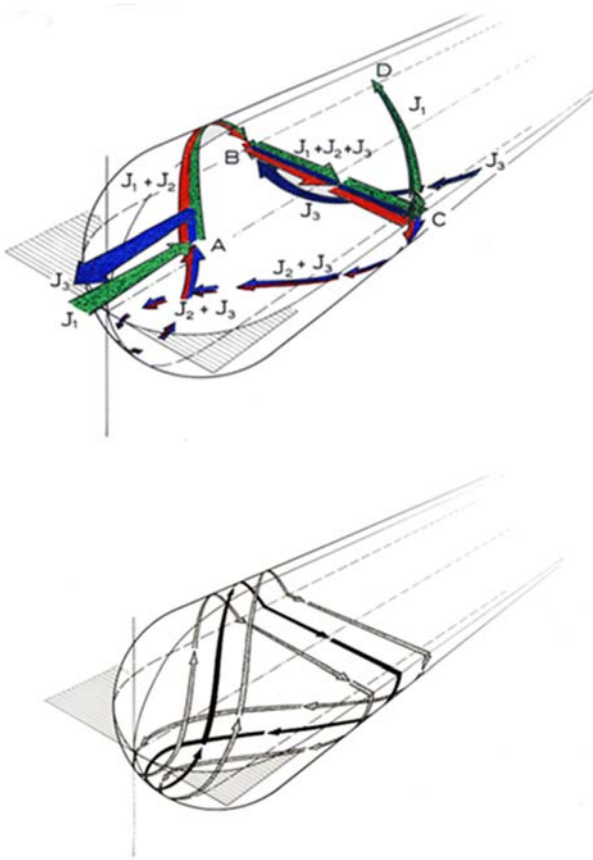


Figure 5. The \mathbf{j} -system of Figure 4 is composed of three loops. One \mathbf{j} -loop, denoted by J_1 , is shown in the left panel by a green arrow. It flows away from the Sun, and – when observed from the Sun – it confines the Northern lobe of the magnetosphere by a clockwise current. Another \mathbf{j} -loop, denoted by J_2 , shown in the left panel by a blue arrow, confines the Southern lobe of the magnetosphere by a clockwise current – when observed from the Sun – although the current flows towards the Sun. A third \mathbf{j} -loop is partially shown in the left panel by a red arrow. It has a curious and unexpected character of “trapped” radiation, and is shown in detail by the right panel, where it must be stressed that only two, not three, \mathbf{j} -loops are shown. Just one \mathbf{j} -loop, denoted by a black circuit, has a unique winding around both lobes of the magnetosphere. The other \mathbf{j} -loop, shown by grey arrows, winds up twice each lobe of the magnetosphere, and crosses twice through the neutral sheet, once earthward and once tailward with respect to the crossing of the black \mathbf{j} -loop. Only one unique loop like the black circuit exists, and an infinite number of loops similar to the grey arrows circuit. See text. Figure after Gregori and Leybourne (2025m).

This loop is the leading current when intense clouds of electrons are ejected from the Sun. Therefore, this

loop is typically much intensified during magnetospheric substorms and geomagnetic storms (see section 3).

A third \mathbf{j} -loop has a curious and unexpected character of “trapped” radiation, and is partially shown in the left panel of Figure 5 by a red arrow. The full \mathbf{j} -loop is shown by the right panel of Figure 5. Note that only two, *not* three, \mathbf{j} -loops are shown in the right panel of Figure 5. One \mathbf{j} -loop (the black circuit) has a unique winding around both lobes of the magnetosphere. The second \mathbf{j} -loop (the grey arrow) winds up twice each lobe of the magnetosphere, and it crosses through the neutral sheet once earthward and once tailward with respect to the crossing of the black \mathbf{j} -loop. That is, these third \mathbf{j} -loops look like curious trapping orbits for electrons, protons and ions.

Note that the anti-sunward flow of \mathbf{j} -currents determines the formation of the *neutral sheet* and *plasmashet*, according to the energy rationale expressed by Figure 3 (right panel), according to section 3.

Consider what happens when the Earth’s magnetosphere crosses through the so-called heliospheric neutral sheet (*HNS*). In fact, the \mathbf{B}_{int} spiral structure is bent, (at 1 *AU*) approximately by $\sim 45^\circ$ with respect to the sunward direction. Owing to $\text{curl } \mathbf{H} = (4\pi/\gamma_0)\mathbf{j}$ the separation of “toward” and “away” sectors of the \mathbf{B}_{int} spiral structure must contain a sheet of electric currents, which are the *HNS*. Since \mathbf{B}_{int} is always recorded to lie almost perfectly in the ecliptic plane, the *HNS* is almost perpendicular to the ecliptic plane. The tail of the magnetosphere is directed in the radial direction away from the Sun. When the Earth’s magnetosphere crosses through the *HNS*, the *HNS* looks almost like a “blade” of \mathbf{j} -currents that impinge on the Earth’s magnetosphere. The spiral pattern of \mathbf{B}_{int} rotates with a period of the order of ~ 27 days, while the Earth moves comparably slower, along its orbit around the Sun. Hence, the *HNS* \mathbf{j} -currents merge with the magnetospheric J_1 and J_2 loops, and progressively – although “quietly” and regularly – reverse the asymmetry between the \mathbf{j} -loops that twist around the two lobes of the magnetosphere.

3 - The Earth’s magnetosphere. Magnetospheric substorms and geomagnetic storms

When some small or large plasma cavity occurs in the solar wind, the magnetospheric J_1 and J_2 loops of Figure 5 abruptly experience an either small or large perturbation. The relation $\text{curl } \mathbf{H} = (4\pi/\gamma_0)\mathbf{j}$ requests a change of topology due to a lack of \mathbf{j} supply. That is, imagine that an “air-bubble” propagates along the water-pipes that represent the J_1 and J_2 \mathbf{j} -loops.

The physical system is substantially changed, and “reconnection” must occur wherever the “air-bubble” (or

plasma cavity) is located. Owing to a variational principle (see section 2, or Gregori et al., 2025e, and references therein), the system must attempt to obviate to the missing particle supply by the solar wind. Hence, the system uses all available particles from other sources. Therefore, all particles that are available downstream are accelerated both earthward and downstream in the neutral sheet. The result is the observed *plasmashet*, - which is well known to be a layer a few R_E (Earth's radii) thick, with earthward flowing particles, observed - like an almost permanent feature - to flow around the neutral sheet.

How far particles in the plasmashet can penetrate earthward? Apply a balance between the kinetic energy density of the particles in the plasmashet, and the B energy density close to the Earth. The argument is identical to the aforementioned definition of the *drop-model* magnetopause (Figure 3, left panel), although the pressure balance is now applied, rather than in 3D, in 2D in the approximate plane of the plasmashet.

Indeed, the kinetic energy density of the particle flow in the plasmashet is intensified during magnetospheric substorms and geomagnetic storm (see below). Hence, two types of patterns must be expected, qualitatively shown in the cartoon of Figure 6. When the plasma cavity is more intense, the aforementioned "reconnection" process along the tail occurs for a longer time, hence the earthward flow of particles in the plasmashet is more intense.

Note that a huge flow of particles occurs in the plasmashet, both earthward and downward, even though - on the Earth - we detect the effect of the earthward flow. Thus, concerning observations at Earth's surface, polar auroras display the typical morphology that Syun-Ichi Akasofu⁹ (1964) named "*auroral substorm*" - and he later interpreted the phenomenon (Akasofu, 1968, 1977) like a facet of a more general *magnetospheric substorm*.

A check of this explanation is as follows. The typical observed duration of an auroral substorm is $\sim 2 - 3$ hours. The plasma cavity in the solar wind (and of the "air bubble" in the water pipe) propagates downstream at the mean speed of the solar wind ($\sim 400 \text{ km sec}^{-1}$). The tail of the magnetosphere is reported having been observed with a typical length of the order of $\sim 1,000 R_E$. Hence, the earthward flow in the plasmashet should last $\sim 1,000 R_E / 400 \text{ km sec}^{-1} \cong 4.4 \text{ hours}$. That is, the order of magnitude is certainly correct.

⁹ Syun-Ichi Akasofu (1930-), was the founding Director of the *International Arctic Research Center* of the *University of Alaska Fairbanks (UAF)*, and served in that position from the *Center's* establishment in 1998 until January 2007. From 1986 he had been the previous Director of the *University's Geophysical Institute*. He discovered auroral substorms by exploiting a most impressive visual and empirical analysis of

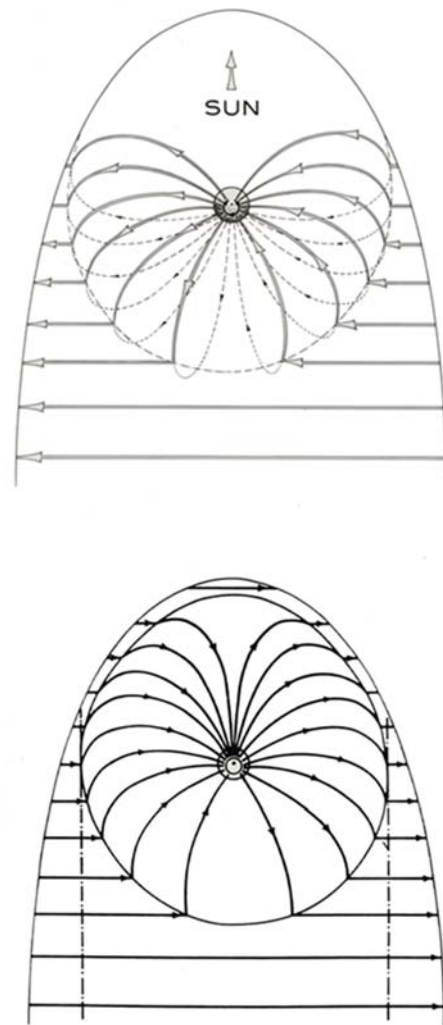


Figure 6. Earthward termination of the earthward flow of particles in the plasmashet. The left figure (out of scale) shows the typical standard case history observed in the case of the Earth. In contrast, when the pressure by the particle flux in the plasmashet is more intense, the earthward termination of the plasmashet affords to surround the Earth, i.e., even on the noon side. This typical pattern is observed in the case of the Jupiter magnetosphere, and is called "*magnetodisk*". See text. After Gregori and Leybourne (2025m).

Note that, before the onset of the substorm, the B energy density along the tail is responsible for the balance between internal and external pressure across the

the whole set of all-sky camera pictures collected during the *International Geophysical Year* (1957-1959). This impressive achievement reminds about the old-fashioned investigations carried out with no computer aids. Professor Syun-Ichi Akasofu will be remembered in the history of Earth sciences for this almost unbelievable achievement.

magnetopause. However, owing to the plasma cavity, j -currents and the B energy density fade off (as per Figure 5, left panel). Thus, the magnetosphere squeezes the tail, almost reminding about a toothpaste tube. In fact, the system attempts to use all available particles in the plasmashet, as it must recover from the missing internal magnetic pressure.

Hence, an observer located on the Earth monitors a magnetospheric substorm exhausting when the plasma cavity (or the “air-bubble” in the water-pipe) gets out of the last fringes of the tail. That is, the particle supply must exhaust, which is originated by the earthward flow of particles in the plasmashet.

Conversely, consider that - as a standard - a large plasma cavity endures in the solar wind much longer than a few hours. Hence, as long as the plasma cavity does not fade off, a sequence of substorm starts, as, indeed, we observe. Thus, we observe substorms triggered in sequence, while a new substorm eventually begins when the previous substorm is not over. In summary, the phenomenon altogether is the well-known classical “geomagnetic storm”, which is observed having a typical duration of a few days.

To our knowledge, this is the *unique available physical* explanation for the occurrence of substorms and of geomagnetic storms. In fact, as expected, the recorded horizontal component H of the geomagnetic field displays the typical classical morphology of the reversed shape of a lognormal distribution (Campbell, 1996). This is consistent with statistics (i.e., with the Kapteyn¹⁰ class distributions), which implies that the occurrence of an event is proportional to the number of already occurring similar events (this is the same logic of rush hours; Arley and Buch, 1950, or Paparo and Gregori, 2003). That is, the probability of the trigger of a new substorm during a “geomagnetic storm” is proportional to the number of substorms that are already in progress.

4 - The Earth’s magnetosphere. Forelocks and plasma mantle

Plasma cavities affect “reconnection”, hence they affect all phenomena that occur across the magnetopause, and that control the flow of particles inside the two lobes of the magnetosphere - other than what happens inside the neutral sheet. Figure 7 shows a single case history.

In fact, some kind of secondary neutral sheet is developed on the pole, because “reconnection” implies particles that propagate downstream, much like in the neutral sheet. However, owing to the internal micro-Cowling dynamos (see section 1), particles twist, and

experience collimation, of the flow downstream, always at the mean speed of the solar wind. That is, a phenomenon occurs that can be considered like a “forelock”¹¹ of B flux tube.

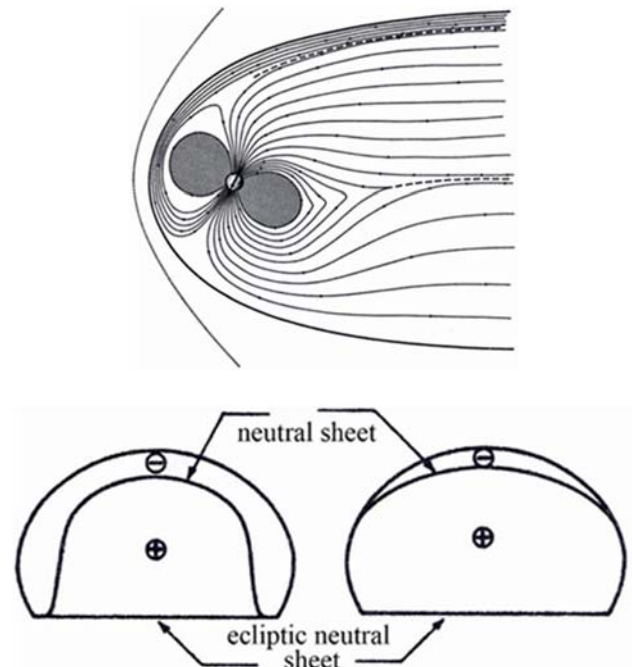


Figure 7. Noon-midnight meridional cross-section [left panel] and tail cross-section [right panel] (out of scale) that show the formation of “forelocks” of B flux tubes caused by missing particles (plasma cavities) in the solar wind flow. Every “forelock” is collimated by a twisting B due to the toroidal B generated by micro-Cowling dynamos. See text. This forerunning sketch is loaned after Gregori (1968) with permission by *Annales de Géophysique*, licensed under “Open Access” CC BY 4.0.

In summary, we must expect that *filamentary patterns are observed* inside the magnetopause, and this phenomenon occurs above both polar caps. In the case of the Earth, the result was named “*plasma mantle*”¹² as shown in the cartoon of Figure 8.

For the sake of completeness, let us remind about so-called *polar wind* - which is a steady leakage of a tiny fraction of the Earth’s atmosphere over both polar caps. This topic is classical, and observations are now available, including sunspot cycle dependence, but no details are here needed.

Another closely related – and generally not well acknowledged – phenomenon is concerned with the palæovariations of the total mass of the atmosphere, which imply variations of the *palæodensity of the atmosphere*. There is no need to discuss this item in the

¹⁰ Jacobus Cornelius Kapteyn (1851–1922), Dutch astronomer.

¹¹ The term “forelock” is not found in the literature.

¹² See, e.g., Paschmann et al. (1976), Philipp and Morfill (1976), Scoppe and Paschmann (1978), Schwenn (1981), etc.

framework of the present paper. Refer to Gregori and Leybourne (2025m) and references therein.

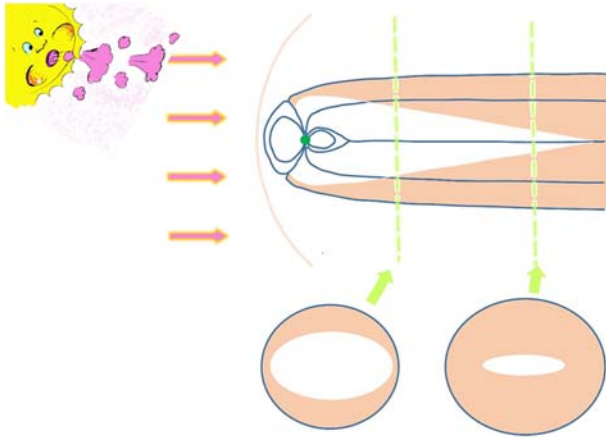


Figure 8. Rough hand-made sketch showing what is called “plasma mantle”. The pink region shows where some diffuse flux of particles is observed by space probes, originated by the penetration of particles across the magnetopause. According to the interpretation here given, these particles represent temporary “forelocks” of B flux tubes. The lower sketch shows a transversal cross-section along the tail. See text. The sketch is based on an idea after Schulz (1991, p. 157, Figure 26). Figure after Gregori and Leybourne (2025m).

Instead, let us consider the effect of the “reconnection” process that involves some temporary, varying, and more or less extended, area around both “singular points” over both polar caps - characterized by closed j -loops encircling them – as shown in the lower photographs of Figure 4.

These “singular points” are a mathematical fiction, because, in reality, “reconnection” always occurs due to the always present micro-cavity in the solar wind. Thus, direct precipitation of solar wind particles occurs directly over the high polar atmosphere. The literature reports this phenomenon as a “cleft” that penetrates over both polar regions, directly from the front side of the magnetosphere. In this respect, for the sake of completeness, we remind about the PCA (polar cap absorption events)¹³ observed as an abrupt fading off of the radio-signals impinging from a celestial source. The phenomenon is due to the abrupt enhancement of ionization in the upper atmosphere. Thus, the radio-signal is reflected outward by the ionosphere and disappears from the observations at Earth’s surface.

In addition, a possible phenomenon related to “cleft” precipitation deals with noon-side auroræ. “Auroral oval” denotes the instant location of polar auroræ. In

contrast, “auroral zone” is named the statistical, time integrated, distribution of the auroral oval. The auroral zone shows a maximum in the midnight sector, and a secondary maximum in the noon sector. In contrast, auroræ are less frequent in the sunrise and sunset sectors. The noon maximum of the auroral zone could be associated, maybe, to the “cleft”. However, another realistic possibility is that the earthward penetration of the plasmashet continues on the flanks of the magnetosphere (see Figure 6, right panel). In this way, the plasmashet forms a temporary “magnetodisk” around the Earth - which, in fact, is observed as a regularly feature of the Jupiter’s magnetosphere. These features, and others, are briefly mentioned in Gregori and Leybourne (2025m), but are not of direct concern for the present discussion.

Before entering into the discussion of the energy content in the magnetosphere, we must warn the reader about some fashionable and frequently mentioned features, which cannot fit into our general physical interpretation of the Earth’s magnetosphere, even though they are reported as “generally agreed” facts.

One feature deals with the direction of B_{int} that, in fact, is always observed to lie approximately in the ecliptic plane, apart at most a scatter of very few degrees. In contrast, it is now customary to plot B_{int} perpendicular to the ecliptic plane. This belief derives from the so called “open model” of the magnetosphere, dating back to the late Dungey¹⁴ (1961, 1963). This assumption unfortunately bias a large fraction of the literature, as follows:

- The belief that the inversion of the tiny “vertical” (North/South) component of B_{int} is crucial for Earth phenomena
- The formation of a unique “neutral line” crossing the night side of the Earth magnetosphere inside the neutral sheet, which, in fact, was never observed, even though several researchers intensively searched for it.
- The assumption of “convection” inside the magnetosphere - i.e., the magnetosphere in conceived like a closed system, with anti-sunward flow of particles along the lobes of the magnetosphere, and earthward flow inside the plasmashet.

Our criticism relies on physical arguments that are concisely outlined here above. Unfortunately, these items are now considered “classical”. However, e.g., the often claimed correlation of phenomena, with a tiny “vertical” component of the observed B_{int} , generally displays a very low correlation coefficient, thus raising a

¹³ This topic seems somewhat unfashionable. Some old reviews are, e.g., Reid (1963), Lassen (1967, 1969), Hultqvist (1969a).

¹⁴ James Wynne Dungey (1923-2015), British space scientist, at the Imperial College in London, who in 1961 pioneered “reconnection” in the Sun–Earth system.

serious doubt about the significance of any such a correlation. A more extensive critical discussion can, however, be pertinent only in a devoted monograph on the Earth's magnetosphere, and is outside the perspective of the present study.

In addition, as already stressed, *no physical reason* requests that the magnetosphere is a closed system. The particle flow inside the magnetopause is part of the solar wind flow. The particles, which are detected inside the magnetopause, are associated to the aforementioned "forelocks" - and share the same fate of other particles of the expanding solar corona. *No return flow of particles* occurs inside the magnetosphere, and no "convection" can occur inside the Earth's magnetosphere, which is an open system. The earthward flow of particles in the plasmashet must be explained in a different way. In addition, as mentioned in section 3, this concept is explained in a straightforward way when dealing with the *j*-loops in the magnetosphere. A better detail of these processes is explained in section 7.

5 - Energy in the magnetosphere

The investigation of the energy relations in the magnetosphere is a way to show how a magnetosphere must be considered as a lesser constituent of the whole solar wind system, and it cannot be singled out as an independent closed entity. At present, owing also to its difficulty, this topic seems to be only seldom considered in the literature, and - except a few exceptions (see section 9) - in general it is only a marginal concern. The reader ought to be warned that no systematic search was carried out for papers that can be either directly or indirectly related to the treatment here given. However, during several decades, no mention was found in the whole literature on the magnetosphere, which the senior author (GPG) had the chance to scan for other purposes. In any case, we must stress that the approach, which is here considered, is "top-down" (like some older literature), unlike the more recent references that are "bottom-up" - and that, therefore, cannot be pertinent for the present discussion.

Compared to the previous "top-down" papers, the formal general theory relies on a distinction between suitable subvolumes of the Earth's "magnetosphere". Hence, we deal with a largely original derivation, even though - unfortunately - a direct application to observational data cannot be straightforward, as it requires devoted collections of records by space probes that - to our knowledge - are not yet available. In fact, every application ought to rely on formal integration of observed physical quantities over suitable geometrically defined surfaces. These observations, on the other hand, can often be available only by devoted *in situ* monitoring by space probes. Hence, no direct application can be here carried out by means of standard available observations. Rather, the present discussion is an extensive discussion of the needed

tools for investigating the energy relations between different component parts of the Earth's magnetosphere.

In any case, as shown in detail in section 7, it is possible to understand on a quantitative ground the specific energy flux and exchange between different parts of the magnetosphere. That is, the quantitative energy balance is awkward - if feasible at all - while the qualitative processes can be understood in detail, concerning all phenomena that occur at every instant inside the magnetosphere. This is certainly an achievement in understanding the energy flux between different components of the magnetosphere.

Our starting point are a few simple formulations that can be found in the literature, and that are here extensively generalized. The formalism relies on classical electromagnetism, and some needed details are eventually better specified in other papers or in a devoted appendix. These algorithms are classical, although sometimes not common. Hence, a standard reader can sometimes find some difficulty to follow the arguments. We confirm that the whole formulation has been carefully checked in detail, and that it is certain that every reader can quickly get rid of difficulties and he can follow the entire mathematical development.

A crucial issue is that the energy balance of the system can be equivalently formulated by means of either one of two approaches, i.e., either in terms of *j*-loops, or in terms of *MHD*, i.e., of particle electrodynamics and plasma physics.

We consider first the steady state of the magnetosphere. The treatment in terms of *j*-currents is the object of section 5.1, while the treatment in terms of *MHD* is the focus of section 5.2. Time varying conditions are discussed in section 6, and this completes the mathematically more intricate discussion of the present study. The minimum potential energy of the magnetosphere is investigated in section 7, while the focus of section 8 is on the energy contents, on the stresses and on the torques in magnetospheric subvolumes. Some computations dealing with specific case histories that are reported in the literature are mentioned in section 9. These case histories are, however, only marginal applications of the more general theoretical formulation that is here briefly illustrated.

5.1 - Steady state - The current loop formulation

Let us assume that the solar wind is cold, collisionless, and infinitely conducting ($\sigma \rightarrow \infty$). This implies that the solar wind is everywhere in perfect equilibrium. Hence, we can safely use the picture of closed *j*-loops (as in the Appendix). This is the same as the "frozen-in" assumption by Alfvén (see section 1). The energy of the system can be described as the integral over all space of the magnetic energy density. In fact, the electric energy density is negligible. This can be shown

by referring to the Poynting theorem,¹⁵ in the case of a stationary state (with $\sigma \rightarrow \infty$).

Hence, we can consider the model with perfectly flexible wires. It can be shown that the ratio of the electric energy to the magnetic energy density is¹⁶

$$\frac{[1/(8\pi)] \mathbf{E} \times \mathbf{D}}{[1/(8\pi)] \mathbf{H} \times \mathbf{B}} = \gamma_0^2 \epsilon_r \mu_r \left(\frac{v_{\perp}}{c}\right)^2 \quad (4)$$

where ϵ_r is the relative permittivity. This is a dimensionless number, which results $\ll 1$ when considering all unit systems for which $\gamma_0 = 1$. As far as the $(cgs)_{sym}$ or $(cgs)_{Gauss}$ units are concerned, it is $\gamma_0 = c$. However, the ratio is a dimensionless number and is always the same, and the \mathbf{E} , \mathbf{D} , \mathbf{H} , and \mathbf{B} units must therefore to be defined in such a way as to justify such a very dimensionless ratio. Therefore, in a stationary state the total e.m. energy of the system is only magnetic. This energy equals the work spent by the e.m.f. to generate the currents \mathbf{j} that flow within all \mathbf{j} -loops.

As far as the internal origin \mathbf{B} is concerned, i.e., the tide-driven (TD) dynamo (see section 1), consider that the present section refers to a perfectly steady state. Hence, the system is supposed to be at equilibrium, and the \mathbf{j} -loops of the TD dynamo are supposed stationary and supplied by their respective TD driver.

In general, Joule heat is neglected. However, up to some extent it can be eventually included, although in this case one must envisage an energy input aimed to refill the system in order to agree with the steady-state assumption.

The energy of a steady state magnetosphere was investigated – according to a “top-down” approach - in a series of papers (Chapman,¹⁷ 1964; Carovillano¹⁸ and Maguire, 1966 and 1968; Maguire and Carovillano, 1966; Carovillano and Siscoe,¹⁹ 1973; Siscoe, 1974), where a few theorems are shown under the following hypotheses:

- the magnetosphere is strictly closed, i.e., no “reconnection” should occur across the magnetopause;
- the magnetosphere is piecewise continuous;
- the magnetosphere is simply connected, i.e., the neutral sheet does not exist;
- the magnetosphere is void of particles, i.e., no radiation belt, no ionosphere, but the telluric currents are taken into account;
- the interplanetary field is null, i.e.

$$\mathbf{B}_{int} = 0 \quad (5)$$

Call \mathbf{B}_M the unperturbed purely internal origin field

(but, there is no need to suppose that it is necessarily dipolar). Call \mathbf{B} the real observed field, and \mathbf{b} the “perturbation” field

$$\mathbf{B} = \mathbf{B}_M + \mathbf{b} \quad (6)$$

Owing to (5), the magnetic energy of the system is

$$\int_{V_{sc}} \frac{\mathbf{B}^2}{8\pi K_0 \mu_r} d\tau = \int_{V_{\infty}} \frac{\mathbf{B}_M^2}{8\pi K_0 \mu_r} d\tau + \int_{V_{\infty}} \frac{\mathbf{B} \times \mathbf{b}}{8\pi K_0 \mu_r} d\tau + \int_{V_{\infty}} \frac{\mathbf{b}^2}{8\pi K_0 \mu_r} d\tau \quad (7)$$

where V_{sc} is the volume of the closed magnetosphere (“sc” is the acronym for “surface currents”, i.e., currents flowing on an ideal surface identified with the magnetopause), $d\tau$ is the volume differential, and V_{∞} is all space; (7) can also be written by means of the symbols U_s and U_j , respectively, of the self- and joint magnetic energy of different current systems

$$U_s(\mathbf{B}) = U_s(\mathbf{B}_M) + U_j(\mathbf{B}_M, \mathbf{b}) + U_s(\mathbf{b}) \quad (8)$$

The aforementioned theorems reported in the literature deal with two general cases.

5.1.1 - Screened Earth’s core

The perturbation field \mathbf{b} is supposed to be screened (by lithosphere and mantle) from any interaction with the internal origin currents \mathbf{j} . That is, it is assumed that a volume V_{tc} exists, enclosed by a surface S_{tc} , which includes all sources of the internal origin field. The acronym “tc” is for “telluric currents”, which flow in the lithosphere and mantle and represent a supposed ideal Faraday screen between the space inside and outside S_{tc} . Hence, by this it is supposed that inside S_{tc} it is $\mathbf{b} = 0$.

The following theorems have been proven (respectively by Chapman, 1964, and by Carovillano and Maguire, 1966 and 1968):

$$U_j(\mathbf{B}_M, \mathbf{b}) = 0 \quad (9)$$

$$U_s(\mathbf{b}) = -\frac{1}{2} \mathbf{M} \times \mathbf{b}_{sc}(0) \geq 0 \quad (10)$$

where \mathbf{M} is the dipole moment of the Earth, and its field is here assumed purely dipolar (the generalization to non-dipolar field was given by Maguire and Carovillano, 1966; see below); $\mathbf{b}_{sc}(0)$ is the \mathbf{b} contribution at the origin where \mathbf{M} is located, a contribution that is originated by the “surface currents” on the magnetopause.

Analogously to the aforementioned S_{tc} and V_{tc} , let

mentioned in a previous footnote, this concern is quite intricate and is discussed in detail by Gregori et al. (2025o).

¹⁷ Sydney Chapman FRS (1888-1970).

¹⁸ Robert L. Carovillano (1932-2015).

¹⁹ George L. Siscoe (1937-).

¹⁵ The concept is classical in college electromagnetism.

¹⁶ The symbol \times denotes scalar product, the symbol \wedge denotes vector product, and μ_r is the relative magnetic permeability. The constant K_0 is defined depending on the unit system used. Owing to the use of historical models of the geomagnetic field - which are based on different unit systems - it is essential to use formulas that can refer to every unit system. As already

us also define in the following S_{sc} and V_{sc} that are associated with the ideal surface identified with the magnetopause, which is assumed to be a perfect Faraday screen.

5.1.2 - Unscreened Earth's core

This is a more realistic condition. Since equilibrium conditions are considered, it is supposed that \mathbf{b} is constant vs. time. The following theorems were proven (Maguire and Carovillano, 1966; Carovillano and Maguire, 1968)

$$U_j(\mathbf{B}_M, \mathbf{b}) = \mathbf{M} \times \mathbf{b}(0) \leq 0 \quad (11)$$

where $\mathbf{b}(0)$ is the \mathbf{b} field at the origin, and

$$U_s(\mathbf{b}) = -\frac{1}{2} \mathbf{M} \times \mathbf{b}(0) \geq 0 \quad (12)$$

Theorems (9), (10), (11), and (12) have been shown in two different ways: (i) by direct computation, with the additional assumption of simple geometry (Chapman, 1964; Carovillano and Maguire, 1966; Maguire and Carovillano, 1966), and (ii) by another method (that is here generalized), applied by Carovillano and Maguire (1968), and also by Carovillano and Siscoe (1973). A third proof of theorem (12) is given by Siscoe (1970) under the assumption of vanishing \mathbf{B}_{int} . In another paper, Maguire and Carovillano (1968) gave a generalization and avoided the assumption (5). They used the same conceptual approach as Carovillano and Maguire (1968), although at a more limited extent – when compared to the treatment outlined here below.

In contrast, a more realistic magnetosphere is here considered. We are not concerned about whether the magnetosphere is “open” or “closed”. Therefore, any amount of “reconnection” can occur across the magnetopause. In addition, a neutral sheet can be considered, and also the ionospheric currents and the telluric currents. We stress, however, that some less realistic assumptions are here implied when some other currents are assumed null, i.e., air-earth currents,²⁰ and the currents between the telluric current system and the geodynamo \mathbf{j} -system.

On the other hand, every “simple” model must rely on some abstraction, suited to simplify the substantial and intrinsic great complication of natural reality. Every choice of a simplifying assumption ought therefore to be suited to focus on some leading and hopefully essential “first-order” approximation of the driving mechanisms, while eventual suitable subsequent improvements can provide some better insight in the details of some

“second-order” effect.

For the sake of simplicity, for the time being we neglect also collision and dissipative phenomena. Hence, we neglect Joule heat and we assume $\sigma \rightarrow \infty$. We neglect also electric and magnetic polarizations. These assumptions, however, can be easily dropped, only at the expense of some formal complication, by generalizing the formulas here given. The approach outlined here below is identical to the procedure used by Carovillano and Maguire (1968).

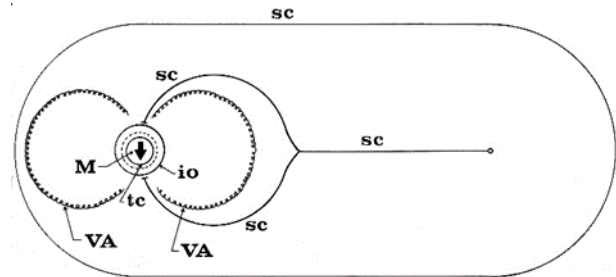


Figure 9. Schematic model used to compute the energy content in the magnetosphere. Subscripts mean: *sc* surface currents (including also solar wind currents) that flow over the magnetopause and in the neutral sheet, and are eventually connected with the solar wind (see Figure 5); other *sc* \mathbf{j} -loops do not flow on the magnetopause or in the neutral sheet, but are only part of the solar wind; *VA* means Van Allen belts; *io* ionospheric currents; it is supposed that the *sc* pattern flows in the ionosphere only through currents aligned along \mathbf{B} filed lines (Birkeland²¹-Alfvén currents); *tc* means telluric currents; \mathbf{M} stands for Earth's dipole/multipole, even though it is intended as a suitable \mathbf{j} -loop in the core, responsible for the whole internal origin \mathbf{B} (dipolar and non-dipolar field). We assume that the magnetosphere closes somewhere downstream, and that the neutral sheet stops somewhere, but this restriction is not essential for the present approximate model. A major drawback of this whole model is due to neglecting air-earth currents, because in the 1960s-1970s air-earth currents were considered to play a negligible role, when averaged over to planetary scale. Unpublished figure.

Consider the aforementioned Poynting theorem, and refer to the simplified scheme outlined by the sketch of figure 9, which is self-explanatory, where the acronyms *VA* and *io* denote, respectively, Van Allen belts and ionosphere.

In general, owing to the very large (practically infinite) σ , the electric field \mathbf{E} spends no work over \mathbf{j} , while $\mathbf{j} \wedge \mathbf{B} \neq 0$, because the \mathbf{j} -loops - which represent either one of the *VA*, or *io*, or *tc*, or \mathbf{M} system - cannot be

scheme of Figure 565. We can only guess that a computation of the energy content in the magnetosphere - when air-earth currents are neglected - can be compared in some way with actual observations, in order to assess how much air-earth currents affect the overall energy processes in the magnetosphere.

²¹ Kristian Birkeland (1886-1917), Norwegian physicist.

²⁰ This is the most severe physical constraint of our treatment, as stressed *passim*. When the notes for the present study were written in the early 1970s, the general feeling was that air-earth currents contribute a mean effect that - on the planetary scale - can be neglected. Now, several evidences show that this Gauss' reasonable working hypothesis is untenable. On the other hand, the observational knowledge of the real air-earth currents is still insufficient, for adding any “correction” to the

depicted like flexible \mathbf{j} -loops. They are, rather, concerned with well defined geometrical constraints. One must therefore consider that the currents \mathbf{j} can flow only over these pre-defined geometrical surfaces - or, differently stated, if one refers to a model in terms of point particles, every particle is said to be subject to "holonomic" constraints. Hence, the relation holds $\mathbf{v} \times \mathbf{j} \wedge \mathbf{B} = \mathbf{0}$, where \mathbf{v} is the bulk velocity of charged particles. That is, the model here considered relies on a few implicit assumptions, although - as a first order approximation - they can be considered to be reasonably satisfactory.

Call \mathbf{A} the vector potential of \mathbf{B} , and according to Carovillano and Maguire (1968) consider the identity (the present procedure is identical to the treatment explained in sections A.1 and A.3)

$$\mathbf{B}^2 = \text{div } \mathbf{A} \wedge \mathbf{B} + \frac{4\pi K_0 \mu_r}{\gamma_0} \mathbf{j} \times \mathbf{A} \quad (13)$$

hence, the self-energy of \mathbf{B} is (the symbols are self-explanatory and $\hat{\mathbf{n}}$ is the unit vector perpendicular to S_∞ and pointing outward)

$$\mathbf{B}_1 \times \mathbf{B}_2 = \text{div } (\mathbf{A}_1 \wedge \mathbf{B}_2) + \frac{4\pi K_0 \mu_r}{\gamma_0} \mathbf{j}_2 \times \mathbf{A}_1 = \text{div } (\mathbf{A}_1 \wedge \mathbf{B}_2) + \frac{4\pi K_0 \mu_r}{\gamma_0} \mathbf{j}_1 \times \mathbf{A}_2 \quad (16)$$

where each field \mathbf{B}_k is generated by a current \mathbf{j}_k and it is

$$U_j(\mathbf{B}_1, \mathbf{B}_2) = \int_{V_\infty} \frac{\mathbf{B}_1 \times \mathbf{B}_2}{8\pi K_0 \mu_r} d\tau = \frac{1}{\gamma_0} \int_{V_\infty} \mathbf{j}_1 \times \mathbf{A}_2 d\tau = \frac{1}{\gamma_0} \int_{V_\infty} \mathbf{j}_2 \times \mathbf{A}_1 d\tau \quad (17)$$

It is now possible to express the energy of the whole system in terms of c -loops linking m -loops (see details in section A.2) or in terms of m -loops linking c -loops (see details in section A.3), and by this it is possible to distinguish:

- (i) the selfenergies, by means of the linking of c - and m -loops generated by one and the same subsystem of figure 9, and
- (ii) the joint-energies, by means of the linking of c and m -loops generated by two different subsystems of figure 9.

Note that, as already mentioned, every term can always be equivalently interpreted in a twofold way, either in terms of c -loops linking m -loops or in terms of m -loops linking c -loops. Thus, it is possible to apply the energy variational principles, and specifically the "principle of magnetic energy variation" (see 1).

The relation with theorems (9), (10), (11) and (12) ought sometimes to rely on formulas expressed in terms of the magnetostatic limit, e.g., when reference is made to the geomagnetic dipole \mathbf{M} . This is, however, of no direct concern for the present discussion.

For the sake of completeness, let us recall that

$$U_s(\mathbf{B}) = \int_{V_\infty} \frac{\mathbf{B}^2}{8\pi K_0 \mu_r} d\tau \quad (14)$$

$$= \frac{1}{8\pi K_0 \mu_r} \oint_{S_\infty} \hat{\mathbf{n}} \times \mathbf{A} \wedge \mathbf{B} d\sigma$$

$$+ \frac{1}{2\gamma_0} \int_{V_\infty} \mathbf{j} \times \mathbf{A} d\tau$$

The surface integral in (14) vanishes when (as it is here assumed) no singular point exists at any finite distance from the origin. That is, the presence is neglected of dipoles, multipoles or magnetic layers. If they exist one should exclude these singularities by enveloping them by additional closed surfaces, etc. Hence, if the surface integral vanishes, (14) becomes

$$U_s(\mathbf{B}) = \int_{V_\infty} \frac{\mathbf{B}^2}{8\pi K_0 \mu_r} d\tau \quad (15)$$

$$= \frac{1}{2\gamma_0} \int_{V_\infty} \mathbf{j} \times \mathbf{A} d\tau$$

that is a well-known result (e.g., Stratton, 1941) and it coincides with (263).

Concerning the joint energy of two fields \mathbf{B}_1 and \mathbf{B}_2 (one field is \mathbf{B} and the other \mathbf{b}) the corresponding formulas are

associated with a vector potential \mathbf{A}_k

Maguire and Carovillano (1968) (see also Carovillano and Siscoe, 1973) neglect the presence of the neutral sheet, although they take into account the contribution by a non-vanishing \mathbf{B}_{int} . However, compared to the present treatment, they use a different algorithm. They introduce one additional coil of currents that envelop the magnetosphere. They also distinguish the case in which \mathbf{B}_{int} does not penetrate into the magnetopause (no-merging case), and the case in which \mathbf{B}_{int} completely enters into it (complete merging). In the case of complete merging an additional shell of currents must be introduced in order to forbid \mathbf{B}_{int} to penetrate inside the Earth. The formal treatment is identical to the aforementioned derivation. They try to consider also the case of an intermediate amount of merging. They carry out a linear combination of the two extreme cases of null or of complete merging. These items, however, are of no concern for the present discussion.

It is now a simple matter of a formal algebra to reconsider theorems (9), (10), (11), and (12), and to assess how they can be generalized to the more realistic model that is here considered. The general starting

formula, which is the analytical expression of the abstraction and approximations represented by figure 9, is

$$2 U_s(\mathbf{B}) = [I_M \Phi_M(I_M)] + [I_M \Phi_M(I_{tc} + I_{io} + I_{VA} + I_{sc}) + I_{tc} \Phi_{tc}(I_M) + I_{io} \Phi_{io}(I_M) + I_{VA} \Phi_{VA}(I_M) + I_{sc} \Phi_{sc}(I_M)] + [I_{tc} \Phi_{tc}(I_{tc} + I_{io} + I_{VA} + I_{sc}) + I_{io} \Phi_{io}(I_{tc} + I_{io} + I_{VA} + I_{sc}) + I_{VA} \Phi_{VA}(I_{tc} + I_{io} + I_{VA} + I_{sc}) + I_{sc} \Phi_{sc}(I_{tc} + I_{io} + I_{VA} + I_{sc})] \quad (18)$$

where the expressions in square brackets represent, respectively, $U_s(\mathbf{B}_M)$, $U_j(\mathbf{B}_M, \mathbf{b})$, and $U_s(\mathbf{b})$.

In the case of *screened Earth's core*, we have that inside V_{tc} it is $\mathbf{b} = 0$. This case history can therefore be applied also to perturbed conditions, which can even change very slowly - although such a physical occurrence should require a different and more correct treatment as discussed in sections 6 and 8.

No details about the formal derivation is here given, as it is only a simple matter of algebra. It can thus be shown that theorem (9) holds

$$U_j(\mathbf{B}, \mathbf{b}) = 0 \quad (19)$$

while theorem (10) is generalized into (where "magnp" is the acronym for magnetopause)

$$U_s(\mathbf{b}) = \frac{1}{2} [I_{ns} \Phi_{ns}(\mathbf{B}) + I_{magnp} \Phi_{magnp}(\mathbf{B}) + I_{io} \Phi_{io}(\mathbf{B}) + I_{VA} \Phi_{VA}(\mathbf{B}) - \frac{1}{2} \mathbf{M} \times [\mathbf{b}_{io}(0) + \mathbf{b}_{VA}(0) + \mathbf{b}_{sc}(0)]] \quad (20)$$

or, upon considering that inside S_{tc} it is assumed that

$$\mathbf{b} = \mathbf{b}_{tc} + \mathbf{b}_{io} + \mathbf{b}_{VA} + \mathbf{b}_{sc} \equiv 0 \quad (21)$$

$$U_s(\mathbf{b}) = \frac{1}{2} [I_{ns} \Phi_{ns}(\mathbf{B}) + I_{magnp} \Phi_{magnp}(\mathbf{B}) + I_{io} \Phi_{io}(\mathbf{B}) + I_{VA} \Phi_{VA}(\mathbf{B}) + \frac{1}{2} \mathbf{M} \times \mathbf{b}_{tc}(0)] \quad (22)$$

Let us refer to the case of unscreened Earth's core. Theorem (11) is

$$U_j(\mathbf{B}_M, \mathbf{b}) = I_M \Phi_M(\mathbf{b}) = \mathbf{M} \times \mathbf{b}(0) \quad (23)$$

that, when $\mathbf{b}(0) = 0$, becomes (19). Theorem (12) is generalized into

$$U_s(\mathbf{b}) = Q - \frac{1}{2} \mathbf{M} \times \mathbf{b}(0) = Q - \frac{1}{2} U_j(\mathbf{B}_M, \mathbf{b}) \quad (24)$$

$$Q = \frac{1}{2} [I_{ns} \Phi_{ns}(\mathbf{B}) + I_{magnp} \Phi_{magnp}(\mathbf{B}) + I_{VA} \Phi_{VA}(\mathbf{B}) + I_{io} \Phi_{io}(\mathbf{B}) + I_{tc} \Phi_{tc}(\mathbf{B})] \quad (25)$$

that, when $\mathbf{b}(0) = 0$, becomes (20).

Hence, the final expression for the total energy of the magnetosphere is

$$U_s(\mathbf{b}) = \frac{1}{2} I_M \Phi_M(I_M) + Q + \frac{1}{2} \mathbf{M} \times \mathbf{b}(0) \quad (26)$$

and by (23) and (24)

$$U_j(\mathbf{B}_M, \mathbf{b}) = 2Q - 2 U_s(\mathbf{b}) \quad (27)$$

5.2. Steady state - The phase space approach

5.2.1 - The virial equation

The energy content in the magnetosphere can be treated by making reference to charged particle motions and plasma physics. The starting items are some moments of the collisionless Boltzmann²² equation (momentum, angular momentum conservation, energy, and virial equations). Previous treatments were reviewed by Siscoe (1970). The energy content in different subvolumes of the magnetosphere can be computed and separated according to their different forms (kinetic plus thermal, power spent by electric field, magnetic energy). The total forces and moments exchanged between different subvolumes can also be evaluated. In the present treatment the collision terms and the relativistic effects are systematically neglected.

The conceptual basis for this approach can be found on several standard books on plasma physics or, e.g., in a concise presentation given by Rossi²³ and Olbert²⁴ (1970, Ch. 9 and 10). Owing to brevity purpose, no extensive review can be here made of this theoretical formulation and of its algorithms. The reader who is not familiar with these items can, however, take for granted only a few starting formulas. Then, he can follow the entire physical discussion. In any case, *the content of the present section 5.2 is not strictly required for the remaining discussion, and it is here inserted only for the sake of completeness*, in order to show how it agrees with the results outlined in the previous section, which were derived by means of different algorithms and approximations.

The previous literature about this approach began with Dessler²⁵ and Parker²⁶ (1959), with subsequent developments by Parker (1962, 1966a), Scokopke (1966), Baker and Hurley (1967), Olbert et al. (1968), Carovillano and Maguire (1968) and Siscoe (1970). In addition, see also the reviews by Carovillano and Siscoe (1973) and by Siscoe (1974). The starting point was the

²² Ludwig Eduard Boltzmann (1844-1906), Austrian theoretical physicist and philosopher.

²³ Bruno Benedetto Rossi (1905-1993) Italian-American physicist.

²⁴ Stanislaw "Stan" Olbert (1923-1994), Polish-American physicist.

²⁵ Alexander J. Dessler (1928-2023) American physicist.

²⁶ Eugene Newman Parker (1927- 2022) American physicist.

evaluation of the so-called Dessler-Parker-Sckopke (*DPS*) ratio, which is the ratio between $b_z(0)$, i.e., the z -component of the geomagnetic perturbation field extrapolated to Earth's center, and the intensity B_0 of the unperturbed geomagnetic field at the equator at Earth's surface. The \hat{z} -axis is along (and opposite to) the Earth's dipole moment \mathbf{M} . The term "*DPS* ratio" was proposed by Olbert et al. (1968), but see also Akasofu and Chapman (1972).

Siscoe (1970) gave some substantial, new and more general, expressions for the *DPS* ratio, and he used a more systematic approach by means of the virial theorem applied to plasmas. He used some drastic assumptions ($\mathbf{B}_{int} = 0$, no neutral sheet, no reconnection, no ionosphere, no telluric currents). His innovative mathematical methods, however, can be used for the problem here of concern, and are here generalized.

Sckopke (1972) is an example of the way this kind of energetic relationship in the magnetosphere can be used to infer self-consistent models of specific subsets of currents \mathbf{j} that partake to the physical system of the magnetosphere. In general, the same geophysical assumptions are used, which were already defined in section 5.1. Since $\sigma \rightarrow \infty$, the \mathbf{E} contribution can be neglected, altogether with the dissipative phenomena such as Joule heat.

The solar wind is assumed perfectly continuous and steady, while there is no concern about "merging" or "reconnection" across the magnetopause or across the neutral sheet. The solar wind must be assumed to be infinitely extended, because - if it is finite - we should assume that the currents \mathbf{j} of the *sc* system must expand in space, i.e., this would be just the expansion of the solar corona. However, this would contradict the assumption of equilibrium conditions. On the other hand, the assumption of infinite extension of the solar wind introduces divergent terms that, however, can be easily handled and subtracted.

Let us deal with the problem by means of the phase space of the charged particles that compose the solar wind. Specifically, refer to the virial equation. Reference is made, e.g., to Brandstatter (1963), Longmire (1963), Olbert et al. (1968), Rossi and Olbert (1970), Siscoe (1970), and references therein. In addition, Baker and Hurley (1967) and Carovillano and Maguire (1968), and references therein, use essentially the same argument, although at a more limited extent. Their arguments are here generalized, including the arguments by Siscoe (1970).

Let us consider microscopically every \mathbf{j} -loop, i.e., in terms of its particles in their phase space (see, e.g., Rossi and Olbert, 1970, Ch. 9 and 10). Call \mathbf{b}_1 the field produced by the particles that are assumed to move in an

externally applied field \mathbf{B}_1 (originated by all other \mathbf{j} -loops). It is

$$\mathbf{B} = \mathbf{B}_1 + \mathbf{b}_1 \quad (28)$$

Let us suppose that also the total current density \mathbf{J} that produces \mathbf{B} is separated into two parts (note a slight change of symbols, as the former \mathbf{j} is now called \mathbf{J})

$$\mathbf{J} = \mathbf{J}_1 + \mathbf{j}_1 \quad (29)$$

where \mathbf{J} , \mathbf{J}_1 and \mathbf{j}_1 are responsible for \mathbf{B} , \mathbf{B}_1 and \mathbf{b}_1 , respectively. Let us consider a strictly stationary state. Thus, the momentum balance equation is as follows, when $\mathbf{j}_1 \wedge \mathbf{B}_1$ is considered as an external force and the effect of \mathbf{b}_1 is taken into account through its magnetic stress tensor $t_{ij}(1)$ (the convention is here used to raise in parentheses any subscript like 1 in \mathbf{b}_1 whenever there is need to specify vector or tensor indexes)

$$\frac{\partial}{\partial x^j} [p^{ij}(1) - t^{ij}(1) - \gamma^{ij}(1)] \quad (30)$$

$$= (\mathbf{J}_1 \wedge \mathbf{B}_1)^i + \sum \mathbf{f}^i$$

where $p^{ij}(1)$ is the particle momentum flow tensor and $\gamma^{ij}(1)$ is the gravity tensor. It is [see e.g. Rossi and Olbert, 1970, p. 298 (10.167)]

$$t^{ij}(1) = -\frac{1}{8\pi K_0 \mu_r} [\mathbf{b}(1)^2 \delta^{ij} - 2 b^i(1) b^j(1)] \quad (31)$$

where δ^{ij} is the Kronecker²⁷ δ -symbol. In addition, the contribution of the electric field \mathbf{E} is neglected, because it was already neglected in section 5.1, and it might be very easily inserted in the present formulation by means only of some unessential complication. Moreover, it is

$$p^{ij}(1) = \mathbf{p}^{ij}(1) + \rho(1) v^i(1) v^j(1) \quad (32)$$

where, in the non-relativistic approximation, $\mathbf{p}(1)$ is the pressure tensor, $\rho(1)$ is the mass density, and $\mathbf{v}(1)$ is the bulk velocity, i.e., the velocity of the proper frame of the plasma (i.e., of the frame where the total momentum density vanishes). Moreover, following Siscoe (1970), let us introduce the pressures \tilde{p}_{\parallel} parallel to \mathbf{B} and \tilde{p}_{\perp} perpendicular to \mathbf{B} (note that they are defined with respect to \mathbf{B} , not with respect to \mathbf{b}_1). Thus, it is

$$p^{ij}(1) = \tilde{p}_{\perp}(1) \delta^{ij} + [\tilde{p}_{\parallel}(1) \frac{B^i B^j}{B^2} - \tilde{p}_{\perp}(1)] \quad (33)$$

Finally [see, e.g., Rossi and Olbert, 1970, p. 299 (10.173)]

$$\gamma^{ij}(1) = -\frac{1}{4\pi \kappa} \left[g^i(1) g^j(1) - \frac{1}{2} g^2(1) \delta^{ij} \right] \quad (34)$$

where κ and \mathbf{g} are the gravitational constant and field, respectively.

All previous symbols refer to \mathbf{b}_1 , which is supposed to be generated by particles in their phase space. In what follows, whenever reference has to be made to \mathbf{B} or \mathbf{B}_1 that are produced by other sets of particles in their respective phase space, the self-explanatory symbols are

²⁷Leopold Kronecker (1823-1891), German mathematician.

used that are defined in Table 16.

Table 16. Symbols for the computation of the energy contents in the magnetosphere in terms of particle phase space (1)

for									
\mathbf{b}_1	$t^{ij}(1)$	$p^{ij}(1)$	$\mathbf{p}^{ij}(1)$	$\varrho(1)$	$\mathbf{v}(1)$	$\tilde{\mathbf{p}}_{\perp}(1)$	$\tilde{\mathbf{p}}_{\parallel}(1)$	$\mathbf{g}(1)$	$\gamma^{ij}(1)$
\mathbf{B}_1	$T^{ij}(1)$	$P^{ij}(1)$	$\mathfrak{P}^{ij}(1)$	$\varrho(1)$	$\mathbf{V}(1)$	$\tilde{\mathfrak{P}}_{\perp}(1)$	$\tilde{\mathfrak{P}}_{\parallel}(1)$	$\mathbf{G}(1)$	$\Gamma^{ij}(1)$
\mathbf{B}	T^{ij}	P^{ij}	\mathfrak{P}^{ij}	ϱ	\mathbf{V}	$\tilde{\mathfrak{P}}_{\perp}$	$\tilde{\mathfrak{P}}_{\parallel}$	\mathbf{G}	Γ^{ij}

The addendum $\sum \mathbf{f}^i$ in (30) is defined as

$$\sum \mathbf{f}^i = \mathbf{f}_M + \mathbf{f}_{tc} + \mathbf{f}_{io} \quad (35)$$

which includes the forces exerted by the holonomic constraints, which operate respectively on the \mathbf{M} , tc , and io \mathbf{j} -systems as a consequence of their fixed geometry. For the sake of simplicity, let us hereafter assume that \mathbf{f}_M acts over \mathbf{M} as a 2D force perpendicular to the circular \mathbf{j} -loop, which generates \mathbf{M} and that is called L_M . Conversely, \mathbf{f}_{tc} and \mathbf{f}_{io} are simple 1D radial components, perpendicular to their respective spherical shells (ss) over which the tc and io currents \mathbf{j} flow. These two ss are called here below S_{tc} and S_{io} , respectively.

These holonomic terms must be inserted in (30) only

$$\int_V x_i \frac{\partial}{\partial x^j} [p^{ij}(1) - t^{ij}(1) - \gamma^{ij}(1)] d\tau = \int_V \mathbf{r} \times \mathbf{j}_1 \wedge \mathbf{B}_1 d\tau + \int_V \sum \mathbf{r} \times \mathbf{f} d\tau \quad (36)$$

The last integral is, when V includes L_M , S_{tc} and S_{io}

$$\int_V \sum \mathbf{r} \times \mathbf{f} d\tau = \oint_{L_M} |\mathbf{f}_M| r_M d\lambda + \oint_{S_{tc}} f_{tc} r_{tc} d\sigma + \oint_{S_{io}} f_{io} r_{io} d\sigma \quad (37)$$

where $d\lambda$ is a length differential, and r_M is the radius of L_M , and r_{tc} and r_{io} are the radii of S_{tc} and S_{io} , respectively. It is also

$$\int_V \sum \mathbf{r} \times \mathbf{f} d\tau = r_M |\mathbf{F}_M| + r_{tc} |\mathbf{F}_{tc}| + r_{io} |\mathbf{F}_{io}| \quad (38)$$

where \mathbf{F}_M , \mathbf{F}_{tc} , and \mathbf{F}_{io} are the resultant total forces of the holonomic constraints over L_M , r_{tc} and r_{io} , respectively. Note that the resultant force

$$\mathbf{F} = \mathbf{F}_M + \mathbf{F}_{tc} + \mathbf{F}_{io} \quad (39)$$

plays the role of an electrodynamic perturbation on the orbital motion of the Earth, originated by the solar wind. This item is discussed in sections 6 and 8.

Let us define the following symbols, where it is supposed that V contains either the whole L_M or the whole S_{tc} or the whole S_{io} , and the corresponding holonomic terms must be included

$$\mathfrak{D} = \int_V \sum \mathbf{r} \times \mathbf{f} d\tau = \mathfrak{D}_M + \mathfrak{D}_{tc} + \mathfrak{D}_{io}$$

$$\mathfrak{D}_M = r_M |\mathbf{F}_M| \quad \mathfrak{D}_{tc} = r_{tc} |\mathbf{F}_{tc}|$$

$$\mathfrak{D}_{io} = r_{io} |\mathbf{F}_{io}| \quad (40)$$

The left hand side of (36) can be transformed by commuting x_i and $\partial/\partial x^j$ and by applying the Gauss' theorem

when \mathbf{b}_1 includes either one (or a few) of the \mathbf{j} -systems that are responsible for \mathbf{M} and/or tc and/or io . When \mathbf{b}_1 does not comprise either one of them, the corresponding addendum in (35) must be deleted, because (30) is not concerned with the constraints applied for the generation of \mathbf{B}_1 , rather it deals with constraints on the charged particles that originate \mathbf{b}_1 .

The corresponding energy relationship can be obtained by computing the scalar product of both sides of (30) with the radial vector $\mathbf{r} \equiv (x_1, x_2, x_3)$ and by integrating over a given volume V of space that is enclosed by a surface S

$$\oint_S \hat{\mathbf{n}}_j x_i [p^{ij}(1) - t^{ij}(1) - \gamma^{ij}(1)] d\sigma - \int_V Tr [p^{ij}(1) - t^{ij}(1) - \gamma^{ij}(1)] d\tau \quad (41)$$

where Tr denotes the trace of a tensor and $\hat{\mathbf{n}}$ is the outward unit vector perpendicular to S . The trace of $p^{ij}(1)$ is $2\tilde{\kappa}(1)$, where $\tilde{\kappa}(1)$ is the total kinetic energy density of the plasma particles that originate \mathbf{b}_1 . In addition, let us call $k_1 = \int_{V_{\infty}} \tilde{\kappa}(1) d\tau$ their total kinetic energy. The trace of $t^{ij}(1)$ is minus the magnetic energy density of \mathbf{b}_1 , hence its integral over V_{∞} is $-U_s(\mathbf{b}_1)$. The trace of $\gamma^{ij}(1)$ is minus the gravitational energy density, and its integral over V_{∞} is $-U_g(\mathbf{b}_1)$ being

$$U_g(\mathbf{b}_1) = - \int_{V_{\infty}} \frac{g^2(1)}{8\pi \kappa} d\tau < 0 \quad (42)$$

that, in the case of a finite density distribution, is not singular.

The corresponding different symbols for \mathbf{B}_1 and \mathbf{B} are defined according to the scheme of Table 17, while the symbols for the gravitational constant κ , the coordinates x^i , the unit vector $\hat{\mathbf{n}}$ perpendicular to S , and the \mathbf{f} and \mathbf{F} vectors, are unchanged.

Table 17. Symbols for the computation of the energy

contents in the magnetosphere in terms of particle phase space (II)

for \mathbf{b}_1	$\tilde{\kappa}(1)$	k_1	$U_g(\mathbf{b}_1)$
for \mathbf{B}_1	$\tilde{K}(1)$	K_1	$U_g(\mathbf{B}_1)$
for \mathbf{B}	\tilde{K}	K	$U_g(\mathbf{B})$

Therefore (36) can be rewritten as

$$\oint_S \hat{n}_j x_i [p^{ij}(1) - t^{ij}(1) - \gamma^{ij}(1)] d\sigma - \int_V Tr [p^{ij}(1) - t^{ij}(1) - \gamma^{ij}(1)] d\tau = \int_V \mathbf{r} \times \mathbf{j}_1 \wedge \mathbf{B}_1 d\tau + \mathfrak{D} \quad (43)$$

Let us first suppose $V \equiv V_\infty$, $S \equiv S_\infty$, and thus generalize the arguments that can be found in Baker and Hurley (1967), Carovillano and Maguire (1968) and Olbert et al. (1968). The volume integral on the left hand

which is derived as follows

$$\begin{aligned} \int_{V_\infty} (\mathbf{r} \times \mathbf{j}_1 \wedge \mathbf{b}_2 + \mathbf{r} \times \mathbf{j}_2 \wedge \mathbf{b}_1) d\tau &= \frac{\gamma_0}{4\pi} \int_{V_\infty} \mathbf{r} \times (\text{curl } \mathbf{b}_1 \wedge \mathbf{b}_2 + \mathbf{r} \times \text{curl } \mathbf{b}_2 \wedge \mathbf{b}_1) d\tau \\ &= \frac{\gamma_0}{4\pi} \int_{V_\infty} x^m [\varepsilon^{ijk} b_{k/j}(1) b^h(2) \varepsilon_{ihm} + \varepsilon^{ijk} b_{k/j}(2) b^h(1) \varepsilon_{ihm}] d\tau \\ &= \frac{\gamma_0}{4\pi} \int_{V_\infty} x^m (\delta_h^j \delta_m^k - \delta_m^j \delta_h^k) [b_{k/j}(1) b^h(2) + b_{k/j}(2) b^h(1)] d\tau \\ &= \frac{\gamma_0}{4\pi} \int_{V_\infty} [(x^m b_m(1) b^h(2))_{/h} + (x^m b_m(2) b^h(1))_{/h} - (x^m b_h(1) b^h(2))_{/m} \\ &\quad - x^m_{/h} (b_m(1) b^h(2) + b_m(2) b^h(1)) + x^m_{/m} b_h(1) b^h(2)] d\tau \\ &= \frac{\gamma_0}{4\pi} \int_{S_\infty} [\hat{n}_h x^m b_m(1) b^h(2) + \hat{n}_h x^m b_m(2) b^h(1) - \hat{n}_m x^m b_h(1) b^h(2)] d\sigma \\ &\quad + \frac{\gamma_0}{4\pi} \int_{V_\infty} \{-\delta_h^m [b_m(1) b^h(2) + b_m(2) b^h(1)] + 3 b_h(1) b^h(2)\} d\tau \end{aligned} \quad (46)$$

where, as already stated, the subscripts 1 and 2 are put in parentheses in order to avoid confusion with tensor indices. Moreover, we use the Gauss' theorem, and ε^{ijk} is the elementary anti-symmetric tensor (Ricci's tensor; see Gregori et al., 2025o).

When $\mathbf{b}_1 = \mathbf{b}_2 = \mathbf{b}$ and $\mathbf{j}_1 = \mathbf{j}_2 = \mathbf{j}$, (45) becomes

$$\int_{V_\infty} \mathbf{r} \times \mathbf{j} \wedge \mathbf{b} d\tau = U_s(\mathbf{b}) + \frac{\gamma_0}{4\pi} \oint_{S_\infty} \left[(\hat{\mathbf{n}} \times \mathbf{b})(\mathbf{r} \times \mathbf{b}) - \frac{1}{2} (\hat{\mathbf{n}} \times \mathbf{r}) b^2 \right] d\sigma \quad (47)$$

Note that (45) and (47) hold also for a finite volume V enclosed by a surface S (but, U_j refers only to a volume $V \subset V_\infty$). The relation (47) is used by Sckopke

side becomes

$$\int_V Tr [p^{ij}(1) - t^{ij}(1) - \gamma^{ij}(1)] d\tau = 2 k_1 + U_s(\mathbf{b}_1) + U_g(\mathbf{b}_1) \quad (44)$$

In contrast, the computation of the first integral on the right hand side of (43) is normally much more involved, due to its dependence on the geometry of the current distribution. Two useful relations can be shown.

Let us call \mathbf{b}_1 and \mathbf{b}_2 the fields produced by any two current distributions \mathbf{j}_1 and \mathbf{j}_2 [and unlike in (28) we do not request $\mathbf{b}_1 + \mathbf{b}_2 = \mathbf{B}$]. It can be shown that

$$\begin{aligned} \int_{V_\infty} \mathbf{r} \times \mathbf{j}_1 \wedge \mathbf{b}_2 + \mathbf{r} \times \mathbf{j}_2 \wedge \mathbf{b}_1 d\tau &= U_j(\mathbf{b}_1, \mathbf{b}_2) \\ &\quad + \frac{\gamma_0}{4\pi} \oint_{S_\infty} [(\hat{\mathbf{n}} \times \mathbf{b}_1)(\mathbf{r} \times \mathbf{b}_2) \\ &\quad + (\hat{\mathbf{n}} \times \mathbf{b}_2)(\mathbf{r} \times \mathbf{b}_1) - (\hat{\mathbf{n}} \times \mathbf{r})(\mathbf{b}_1 \times \mathbf{b}_2)] d\sigma \end{aligned} \quad (45)$$

(1972).

The second relation is shown by Baker and Hurley (1967) in the following way. A purely dipolar \mathbf{b}_2 is considered, let us call it \mathbf{b}_D , and it is

$$\int_{V_\infty} \mathbf{r} \times \mathbf{j}_1 \wedge \mathbf{b}_D d\tau = -U_j(\mathbf{j}_1, \mathbf{b}_D) \quad (48)$$

This can be shown by representing \mathbf{b}_D by the expression

$$\mathbf{b}_D = -3M \frac{\cos \vartheta}{r^3} \hat{\mathbf{r}} + \frac{M}{r^3} \hat{\mathbf{z}} \quad (49)$$

where $\hat{\mathbf{z}}$ and $\hat{\mathbf{r}}$ are unit vectors, being $\mathbf{M} = -M \hat{\mathbf{z}}$ the dipole moment vector, and ϑ the colatitude reckoned from $-\mathbf{M}$. Thus, it is

$$\int_{V_\infty} \mathbf{r} \times \mathbf{j}_1 \wedge \mathbf{b}_D \, d\tau = -M \hat{\mathbf{z}} \times \int_{V_\infty} \frac{\mathbf{r} \wedge \mathbf{j}_1}{r^3} \, d\tau \quad (50)$$

$$= -\mathbf{M} \times \mathbf{b}_1(0)$$

where $\mathbf{b}_1(0)$ is expressed by means of the Laplace's law,

$$\int_{V_\infty} \mathbf{r} \times \mathbf{j}_D \wedge \mathbf{b}_1 \, d\tau = \frac{\gamma_0}{4\pi} \int_{V_\infty} \mathbf{r} \times \text{curl } \mathbf{b}_D \wedge \mathbf{b}_1 \, d\tau$$

$$= 2 U_j(\mathbf{j}_D, \mathbf{b}_1) + \frac{\gamma_0}{4\pi} \oint_{S_\infty} [(\hat{\mathbf{n}} \times \mathbf{b}_D)(\mathbf{r} \times \mathbf{b}_1) + (\hat{\mathbf{n}} \times \mathbf{b}_1)(\mathbf{r} \times \mathbf{b}_D) - (\hat{\mathbf{n}} \times \mathbf{r})(\mathbf{b}_1 \times \mathbf{b}_D)] \, d\sigma$$

that shows that the two addenda on the left hand side of (45) give, in general, quite different contributions. Note also that the argument relying on the Laplace' law in (50) can be applied only considering the l/r^3 dependence in (49), i.e., higher multipolar terms give more complicated expressions for (50). Finally, note that (50) and (51) also hold for a finite volume V , the only condition being that V must contain the entire \mathbf{b}_1 system.

In summary, the previous results become, when $V = V_\infty$ (43),

$$\mathfrak{S}(\mathbf{b}_1) - 2 k_1 - U_s(\mathbf{b}_1) - U_g(\mathbf{b}_1) \quad (52)$$

$$= \int_{V_\infty} \mathbf{r} \times \mathbf{j}_1 \wedge \mathbf{B}_1 \, d\tau + \mathfrak{D}$$

where \mathfrak{D} is defined by (40) and

$$\mathfrak{S}(\mathbf{b}_1) = \oint_{S_\infty} \hat{n}_j x_i [p^{ij} - t^{ij} - \gamma^{ij}] \, d\sigma \quad (53)$$

where \mathbf{b}_1 is explicitly indicated as an argument of \mathfrak{S} to mean that \mathfrak{S} depends on the choice made while separating \mathbf{B} and \mathbf{J} according to (28) and (29).

A comment has to be made dealing with the argument \mathbf{b}_1 that is specified for U_g . In order to keep a perfect analogy between the gravitational and magnetic fields (see Rossi and Olbert, 1970) we should suppose that the gravitational tensor (34) should refer only to the gravitational field originated by particles that compose the current systems that produce \mathbf{b}_1 . In this case, the gravitational field - which is due to all neutral matter in the Earth and its environment - should be considered an external field that enters as a fourth addendum in \mathfrak{D} , i.e., in (40). In this case, it is correct to specify \mathbf{b}_1 as an argument of U_g .

An alternative way is to consider γ^{ij} in (34) as referring to the total actual gravitational field that is experienced by particles, i.e., including also contribution by neutral matter. In this case, U_g is independent of the choice of \mathbf{b}_1 . It is a volume integral over V_∞ and its value is practically unaffected by the current systems.

As a conclusion,

- (i) either we specify the \mathbf{b}_1 argument for U_g in (52) - and we suppose that in (40) a fourth addendum must be included in \mathfrak{D} , which is the space integral over V_∞ of the gravitational field energy density originated by all existing matter (minus the matter that is part of the current systems that

and $\mathbf{b}_1(0)$ is the \mathbf{b}_1 field at the origin where \mathbf{M} is located. Finally, one gets (48) by (23) (even when $\mathbf{b}_1 + \mathbf{b}_D \neq \mathbf{B}$). From (45) and (48) one gets also (recall that according to the present assumption it is $\text{curl } \mathbf{b}_D \neq 0$)

$$(51)$$

cause \mathbf{b}_1); but in this case $U_g(\mathbf{b}_1)$ is negligible compared to the aforementioned fourth addendum; or

- (ii) we do not specify the \mathbf{b}_1 argument for U_g and we add a constant to \mathfrak{D} . This second choice is formally much simpler.

A third point of view is to avoid the use of γ^{ij} , and to describe \mathbf{g} as a purely external force that acts on \mathbf{j}_1 . According to such a viewpoint, we have to add to \mathfrak{D} a term

$$\mathfrak{S}(V) = \int_V \varrho(1) \mathbf{r} \times \mathbf{g} \, d\tau \quad (54)$$

Note that, if we assume a spherically symmetric or slightly ellipsoidal distribution, it is $\mathbf{r} \times \mathbf{g} \cong -r \mathbf{g}$ and $\mathfrak{S} < 0$. [When $V = V_\infty$ let us call $\mathfrak{S}(V_\infty) = \mathfrak{S}$.] This is different compared to $U_g(V)$ [where the V argument means that in (42) the integration volume is $V \subset V_\infty$] because the surface integral in (41) does not vanish when V is finite. In the following, such a third viewpoint is adopted, and the surface integral of (41) is thus avoided.

In this same respect, the \mathfrak{D} constraints are simply determined by the electrical conductivity σ of the medium where the respective currents flow. The \mathbf{M} currents flow in the Earth's core, and fade off as soon as σ decreases. Owing to the Hamilton's principle (see section 2 and Gregori et al., 2025e), these currents \mathbf{j} tend to expand as much as possible, and are thus confined inside a finite volume defined by the drop of σ . The same argument applies also for the tc currents (indeed, they flow as much as possible on the outermost crustal layer, unless σ requests a deeper flow). As far as the io \mathbf{j} -system is concerned, the currents flows inside a thick layer, which is the result both of the local ionization and of the interaction of the ionosphere with the \mathbf{B} that is embedded in a rotating and dynamic atmosphere. The induced currents \mathbf{j} are only a part of a much more complicated phenomenon, but - strictly speaking - they must be comparatively more intense in the outermost ionosphere.

Consider (52) and suppose that all \mathbf{j} -systems, with the only exception of sc , can be enclosed inside a finite volume. Their contribution to p^{ij} , whenever they enter in the definition of \mathbf{b}_1 , is identically zero at infinity (because the particle density-function in phase space,

which enters into the p^{ij} definition, vanishes at infinity). Moreover, t^{ij} tends to infinity like $1/r^6$ (i.e., like the dipolar component of \mathbf{b}_1 , while the higher order terms decrease more rapidly). Thus, in any case (when \mathbf{j}_1 does not include sc)

$$\mathfrak{S}(\mathbf{b}_1) = 0 \quad (55)$$

Let us put $\mathbf{B}_1 = \mathbf{J}_1 = 0$ in (28) and (29) (i.e., all \mathbf{j} -systems contribute to define \mathbf{b}_1). Thus, (52) becomes

$$\mathfrak{S}(\mathbf{b}_1) = 2\mathfrak{K} + U_s(\mathbf{B}) + \mathfrak{D} + \mathfrak{S} \quad (56)$$

where \mathfrak{K} is the total kinetic and thermal energy of all particles that generate all \mathbf{j} -systems.

First, let us neglect $\mathfrak{D} + \mathfrak{S}$ and conclude that, in this case, $\mathfrak{S}(\mathbf{B})$ must be positive and cannot vanish. This is the well-known argument by which it is shown that a plasma cannot be self-contained, but it must in any case expand (see section 6 and, e.g., Brandstatter, 1963, or Rossi and Olbert, 1970). This is also known as *Chandrasekhar-Fermi theorem* (Chandrasekhar and Fermi, 1953). In order to investigate the role of \mathfrak{D} and \mathfrak{S} in (56), let us suppose that also the sc system is in equilibrium, and that it is entirely contained inside a finite volume. Thus, also \mathfrak{S} vanishes and (56) gives

$$\mathfrak{D} + \mathfrak{S} = -2\mathfrak{K} - U_s(\mathbf{B}) < 0 \quad (57)$$

that is, $\mathfrak{D} + \mathfrak{S}$ should reflect forces directed towards the center of the Earth, or - which is the same, as already mentioned - that the L_M , S_{tc} and S_{io} are stretched outside either by self-induction or by the interaction with the solar wind.

Now, let us consider a box of solar wind so huge that, at its surface, the effects of all \mathbf{j} -systems other than sc can be neglected. In order to keep equilibrium, the wider is the huge box of solar wind, the larger should be \mathfrak{D} [because, if one neglects the gravitational field of the solar wind particles, \mathfrak{S} decreases as l/r^4 , and when one considers also the gravitational field of the solar wind particles, the increase in \mathfrak{S} is much slower than that the increase either of \mathfrak{K} or of $U_s(\mathbf{B})$]. This is very unlikely, because \mathfrak{D} has to be supposed in any case to be finite. By this, it is concluded that in (56) $\mathfrak{S}(\mathbf{B})$ cannot vanish, or we have to consider an infinitely extended solar wind, which is the same thing (otherwise, we should account for its actual expansion and we could not consider a steady equilibrium situation). This statement implies that in (56) $\mathfrak{S}(\mathbf{B})$, \mathfrak{K} , $U_s(\mathbf{B})$, and \mathfrak{S} tend to infinity when the box of solar wind tends to V_∞ . However, the quantity

$$\begin{aligned} \mathfrak{S}(\mathbf{B}) - 2\mathfrak{K} - U_s(\mathbf{b}) - \mathfrak{S} \\ = U_s(\mathbf{B}_M) + U_j(\mathbf{B}_M, \mathbf{b}) \\ + \mathfrak{D} \end{aligned} \quad (58)$$

tends, in any case, to a finite limit. An alternate expression for $U_j(\mathbf{B}_M, \mathbf{b})$ is

$$U_j(\mathbf{B}_M, \mathbf{b}) = [\mathfrak{S}(\mathbf{B}) - 2\mathfrak{K} - U_s(\mathbf{b}) - \mathfrak{S}] - U_s(\mathbf{B}_M) - \mathfrak{D} \quad (59)$$

Moreover, owing to (55) it is

$$\mathfrak{S}(\mathbf{B}) \equiv \mathfrak{S}(\mathbf{b}_{sc}) \quad (60)$$

where \mathbf{b}_{sc} means \mathbf{b} contribution originated only by sc .

Indeed, only a finite portion of the infinitely extended solar wind interacts with the geomagnetic field (which, physically, must have a finite energy). In section 8 it is shown how to compute $U_s(\mathbf{b})$ on an experimental basis, but we are unable to give a practical criterion by which we can select a finite volume, inside the solar wind, which contains the magnetosphere and the fraction of solar wind that actually interacts with it. We can only show that its $U_s(\mathbf{b})$ is finite and it is also possible to evaluate its value experimentally.

Let us apply (52) and state that \mathbf{b}_1 is the field of any set of \mathbf{j} -systems, and \mathbf{B}_1 the field of the set of all other \mathbf{j} -systems that are not considered in the definition of \mathbf{b}_1 [they must include all other \mathbf{j} -systems as otherwise the momentum balance (30) cannot be satisfied]. Therefore, we can exchange the role of the two sets of currents and write anew (52). Add the two virial equations that are thus found, apply (45) and find anew (56).

Let us choose $\mathbf{b}_1 = \mathbf{B}_M$ and obtain from (52), (55) and (51) (upon assuming that \mathbf{B}_M is dipolar)

$$\begin{aligned} -2k_M - U_s(\mathbf{B}_M) - \mathfrak{S} \\ = 2 U_j(\mathbf{B}_M, \mathbf{b}) \\ + \frac{\gamma_0}{4\pi} \oint [(\hat{\mathbf{n}} \times \mathbf{B}_M) (\mathbf{r} \times \mathbf{b}) \\ + (\hat{\mathbf{n}} \times \mathbf{b}) (\mathbf{r} \times \mathbf{B}_M) - (\hat{\mathbf{n}} \\ \times \mathbf{r}) (\mathbf{b} \times \mathbf{B}_M)] d\sigma + \sigma_M \end{aligned} \quad (61)$$

where k_M is the total kinetic and thermal energy of the particles that partake to the M system. Similarly, by taking $\mathbf{b}_1 = \mathbf{b}$ one gets from (52), (48) and (40) (still assuming that \mathbf{B}_M is dipolar)

$$\begin{aligned} \mathfrak{S}(\mathbf{B}_{sc}) - 2(\mathfrak{K} - k_M) - U_s(\mathbf{b}) - \mathfrak{S} \\ = -U_j(\mathbf{B}_M, \mathbf{b}) + \sigma_{tc} + \sigma_{io} \end{aligned} \quad (62)$$

It can be shown that, if we assume that, asymptotically, $\mathbf{b} \rightarrow \mathbf{b}_{sc} = const$, the surface integral in (61) vanishes. This can be shown by assuming that S_∞ is a very large sphere. Then, $B_M \rightarrow l/r^3$ and $r d\sigma \rightarrow r^3$. But, owing to the symmetry of the dipole field \mathbf{B}_M , it can be concluded that the integral vanishes. Thus, by (61) one finds

$$U_j(\mathbf{B}_M, \mathbf{b}) = -\frac{1}{2} [2k_M + U_s(\mathbf{B}_M) + \sigma_M + \mathfrak{S}] \quad (63)$$

Finally, skip in (62) the terms with infinite limits [by means of (58) and (60)] and find anew (63). Hereafter call

$$\mathcal{T}_M = 2k_M + U_s(\mathbf{B}_M) + \sigma_M + \mathfrak{S} \quad (64)$$

Let us consider (43) and suppose that V is a finite region of space. The surface integral in (43) can be expressed [by means of (31), (32), and (33)] in the following way

$$\begin{aligned} \mathfrak{S}(b_1, S) = \int_S \hat{n}_j x_i \left\{ \left[\hat{p}_\perp \delta^{ij} \right. \right. & (65) \\ & + (\hat{p}_\parallel(1) - \hat{p}_\perp) \frac{B^i B^j}{B^2} \\ & + \varrho(1) v^i(1) v^j(1) \left. \right] \\ & + \frac{1}{8\pi K_0 \mu_r} [b^2(1) \delta^{ij} \\ & - 2 b^i(1) b^j(1)] \left. \right\} d\sigma \end{aligned}$$

[note that $\mathfrak{S}(b_1) = \mathfrak{S}(b_1, \mathfrak{S}_\infty)$]. Let us divide V into sub-domains of integration and let us define them, e.g., by means of flux tubes of \mathbf{B} cut by surfaces perpendicular to \mathbf{B} (figure 10). Change the frame of reference in such a way that \mathbf{B} has only its third component different from zero. Thus, it is

$$\begin{aligned} p^{11}(1) &= \hat{p}_\perp(1) & p^{22}(1) &= \hat{p}_\perp(1) & p^{33}(1) &= \hat{p}_\parallel(1) & (66) \\ p^{ij}(1) &= 0 & & & & & (i \neq j) \end{aligned}$$

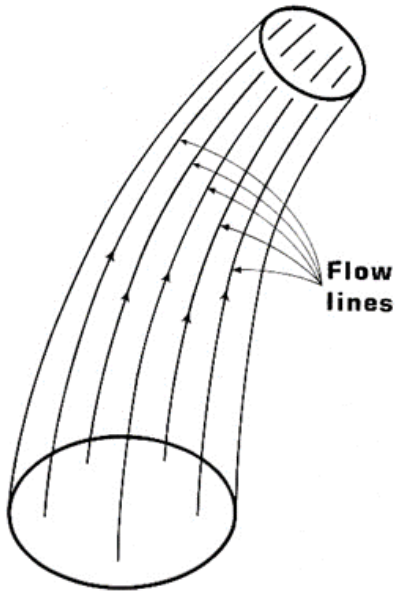


Figure 10. Sub-domain of integration defined as a flow tube of a given vector field, cut by surfaces perpendicular to the vector field itself. Unpublished figure.

Over any piece of S parallel to \mathbf{B} , (since $\hat{n}_3 = 0$) we can pose

$$\hat{n}_j x_i p^{ij}(1) = (\hat{\mathbf{n}} \times \mathbf{r}) \hat{p}_\perp(1) \quad (67)$$

Over any piece of S perpendicular to \mathbf{B} (since $\hat{n}_1 = \hat{n}_2 = 0$) we can pose

$$\hat{n}_j x_i p^{ij}(1) = (\hat{\mathbf{n}} \times \mathbf{r}) \hat{p}_\parallel(1) \quad (68)$$

Note that (67) and (68) are independent of the reference frame.

Concerning the t^{ij} contribution, consider sub-domains of integration that are flux tubes of \mathbf{b}_1 (figure 10). When $\mathbf{b}_1 = \mathbf{B}$ and $\mathbf{B}_1 = 0$, they coincide with the previous sub-domains. Let us change frame of reference.

The new reference frame is defined in such a way that only the third component of \mathbf{b}_1 is not zero. It is

$$\begin{aligned} t^{11} &= -\frac{1}{8\pi K_0 \mu_r} b_1^2 & t^{22} &= -\frac{1}{8\pi K_0 \mu_r} b_1^2 \\ t^{33} &= -\frac{1}{8\pi K_0 \mu_r} b_1^2 & t^{ij} &= 0 \quad (i \neq j) \end{aligned} \quad (69)$$

Over any piece of S parallel to \mathbf{b}_1 , it is (being $\hat{n}_3 = 0$)

$$\hat{n}_j x_i t^{ij}(1) = -(\hat{\mathbf{n}} \times \mathbf{r}) \frac{b_1^2}{8\pi K_0 \mu_r} \quad (70)$$

and over any piece of S perpendicular to \mathbf{b}_1 , it is (being $\hat{n}_1 = \hat{n}_2 = 0$)

$$\hat{n}_j x_i t^{ij}(1) = (\hat{\mathbf{n}} \times \mathbf{r}) \frac{b_1^2}{8\pi K_0 \mu_r} \quad (71)$$

According to usual definitions (refer, e.g., to Rossi and Olbert, 1970), (66) is called “pressure tensor”, (69) “e.m. pressure tensor”, and $\varrho(1) v^i(1) v^j(1)$ the “dynamic pressure tensor”. As far as the dynamic pressure tensor is concerned, let us consider sub-domains of integration defined by flux tubes of $\mathbf{v}(1)$ that are cut by surfaces perpendicular to $\mathbf{v}(1)$ (figure 10). According to arguments similar to the previous ones, it is shown (see, e.g., Rossi and Olbert, 1970) that over any piece of S parallel to $\mathbf{v}(1)$ it is

$$\hat{n}_j x_i \varrho(1) v^i(1) v^j(1) = 0 \quad (72)$$

and over any piece of S perpendicular to $\mathbf{v}(1)$ it is

$$\hat{n}_j x_i \varrho(1) v^i(1) v^j(1) = \varrho(1) v^2(1) \frac{\mathbf{v}(1) \times \mathbf{r}}{|\mathbf{v}(1)|} \quad (73)$$

We can thus summarize (72) and (73) and state that

$$\begin{aligned} \hat{n}_j x_i \varrho(1) v^i(1) v^j(1) &= \varrho(1) (\mathbf{v}(1) \times \hat{\mathbf{n}}) (\mathbf{v}(1) \\ &\times \mathbf{r}) \end{aligned} \quad (74)$$

Equations (67), (68), (70), (71) and (74) are well-known and give relations among partial magnetospheric energies. The scheme of figure 11 can be proposed, where the magnetosphere is divided by means of a few spherical surfaces and of \mathbf{B} flux tubes, cut by surfaces perpendicular to \mathbf{B} . In addition, we assume that in (28) it is $\mathbf{b}_1 = \mathbf{B}$ and $\mathbf{B}_1 = 0$. The argument of the surface integral in (43) is:

- for a piece of S parallel to \mathbf{B}

$$\begin{aligned} \hat{n}_j x_i (P^{ij} - T^{ij}) &= \hat{n}_j x_i \mathfrak{P}^{ij} + \hat{n}_j x_i \varrho V^i V^j \\ &- \hat{n}_j x_i T^{ij} \\ &= (\hat{\mathbf{n}} \\ &\times \mathbf{r}) \left(\mathfrak{P}_\perp + \frac{B^2}{8\pi K_0 \mu_r} \right) \\ &+ \hat{n}_j x_i \varrho V^i V^j \end{aligned} \quad (75)$$

- and for a piece of S perpendicular to \mathbf{B}

$$\begin{aligned} \hat{n}_j x_i (P^{ij} - T^{ij}) &= (\hat{\mathbf{n}} \times \mathbf{r}) \left(\mathfrak{P}_\parallel - \frac{B^2}{8\pi K_0 \mu_r} \right) \\ &+ \hat{n}_j x_i \varrho V^i V^j \end{aligned} \quad (76)$$

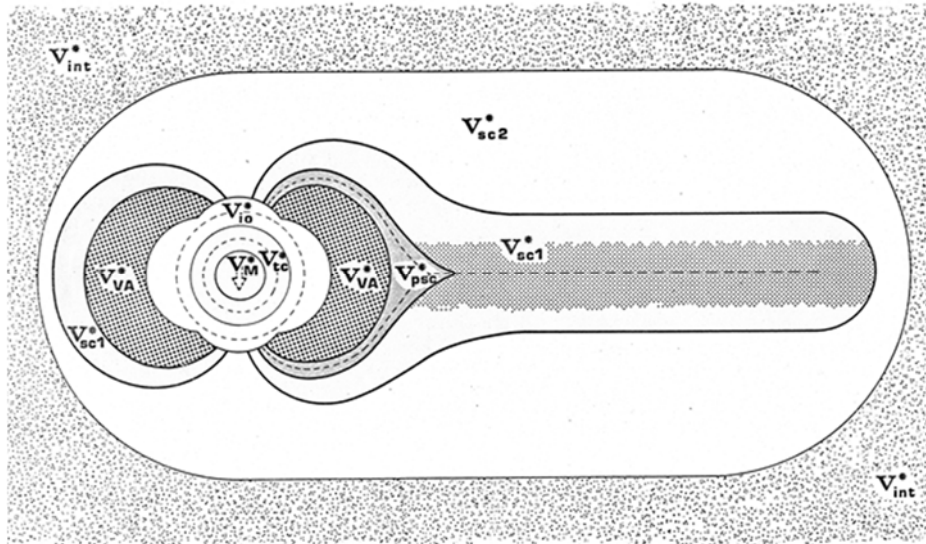


Figure 11. Definition of sub-domains of integration in the magnetosphere. Dotted lines or shaded areas denote \mathbf{j} -systems. The surfaces that confine the sub-domains are indicated according to the following convention: S_a^* confines the sub-domain V_a^* ; S_a^* can be composed of a part comparatively closer to the Earth, which is called “internal” and denoted by S_{ai}^* , and of an “external” part S_{ae}^* ; in addition, a surface S^* can be either parallel to \mathbf{B} or perpendicular to it, being denoted by S_{\parallel}^* and S_{\perp}^* , respectively. Conventionally, every unit vector perpendicular to any S^* is always directed outward with respect to the Earth. Note that V_{tc}^* is comprised between S_M^* and S_{tc}^* , i.e., sub-domains never overlap one another. V_{va}^* is approximately toroidal, and it encloses, longitudinally, the Earth. V_{psc}^* (psc = plasmasheet cusp) has a similar shape, but it is not closed longitudinally. V_{sc1}^* comprises only field-lines that are “reconnected” across the neutral sheet. V_{sc2}^* comprises only fieldlines that are “reconnected” across the magnetopause (see figure 8). Concerning the specific properties of every S^* , no assumption is made dealing with the roughly spherical S_M^* and S_{io}^* . In contrast, $S_{VA\perp}^*$, $S_{psc\perp}^*$, $S_{sc1\perp}^*$, and $S_{sc2\perp}^*$ are perpendicular to \mathbf{B} , while $S_{VA\parallel}^*$, $S_{psc\parallel}^*$, $S_{sc1\parallel}^*$, and $S_{sc2\parallel}^*$ are parallel to \mathbf{B} . S_{sc}^* is a surface immediately outside the magnetopause. The space outside the magnetopause is called V_{int}^* . See text. Unpublished figure.

These expressions can be further simplified whenever the \mathbf{B} energy density is much larger than the kinetic energy density (e.g., as it occurs close to the Earth). In this case, particles move along \mathbf{B} field-lines with orbits of the kind of the trapped (or quasi-trapped, or ionospheric precipitating “Birkeland currents”) particles. That is, the velocity of their proper frame is just \mathbf{V}_{\parallel} , which is their velocity component along the \mathbf{B} field-line. Therefore, S is composed of surfaces either parallel or perpendicular to both \mathbf{B} and \mathbf{V}_{\parallel} and by (74) it is found, from (75) and (76),

$$\hat{n}_j x_i (P^{ij} - T^{ij}) = (\hat{n} \times \mathbf{r}) \left(\mathfrak{P}_{\perp} + \frac{\mathbf{B}^2}{8\pi K_0 \mu_r} \right) \quad (77)$$

and

$$\hat{n}_j x_i (P^{ij} - T^{ij}) = (\hat{n} \times \mathbf{r}) \left(\mathfrak{P}_{\parallel} - \frac{\mathbf{B}^2}{8\pi K_0 \mu_r} \right) + \varrho V_{\parallel} (\mathbf{V} \times \mathbf{r}) \quad (78)$$

In figure 11, according to a simplifying abstraction, it is arbitrarily assumed that the \mathbf{M} and tc currents are not connected to each other, and that also the tc and io currents are not connected. In natural reality the system is much more intricate, as mentioned *passim*. However, an extensive discussion of air-earth currents is premature, and should request a much larger room, and cannot be exploited in the present paper.

Let us write the energy balance (43) for every volume defined in figure 11. The surface integrals that enter into these relations are composed by addenda of the kind (67), (68), (70), (71) and (74), all of which, in principle, can be measured experimentally (e.g., on the basis of measured particle fluxes and energies, or on the basis of some mathematical model for \mathbf{B}). By this, one can infer – in principle for every given volume V - an experimental relationship among the total magnetic energy, the total thermal plus kinetic energy of particles, their gravitational energy and eventually the total constraint effects (caused by the intrinsic properties of the conducting medium). In addition, in section 8 it is shown how to evaluate experimentally several partial self- and joint-energies, thus improving the general picture of the energetic interactions inside the magnetosphere. These relations are (where volumes and surfaces are defined in figure 11, and the integration volume is indicated before every respective equation)

$$\begin{aligned} [V_M^*] & - \oint_{S_M^*} \psi_1 d\sigma = \mathcal{J}_M^* \\ [V_{tc}^*] & - \oint_{S_{tc}^* - S_M^*} \psi_1 d\sigma = \mathcal{J}_{tc}^* \end{aligned} \quad (79)$$

$$\begin{aligned}
 [V_{io}^*] & - \oint_{-S_{tc}^*} \psi_1 d\sigma + \oint_{S_{VA\parallel i}^*} \psi_2 d\sigma \\
 & + \oint_{S_{VA\perp}^* + S_{psc1}^* + S_{sc1\perp}^* + S_{sc2\perp}^*} \psi_3 d\sigma = \mathcal{T}_{io}^* \\
 [V_{VA}^*] & \oint_{-S_{VA\parallel i}^* + S_{VA\parallel e}^*} \psi_2 d\sigma + \oint_{-S_{VA\perp}^*} \psi_3 d\sigma = \mathcal{T}_{VA}^* \\
 [V_{psc}^*] & \oint_{-S_{VA\parallel e}^* + S_{sc1\parallel i}^*} \psi_2 d\sigma + \oint_{S_{sc1\parallel i}^*} \psi_4 d\sigma \\
 & + \oint_{-S_{psc\parallel}^*} \psi_3 d\sigma = \mathcal{T}_{psc}^* \\
 [V_{sc1}^*] & \oint_{-S_{sc1\parallel i}^* + S_{sc1\parallel e}^*} \psi_2 d\sigma + \oint_{-S_{sc1\parallel i}^* + S_{sc1\parallel e}^*} \psi_4 d\sigma \\
 & + \oint_{-S_{sc1\perp}^*} \psi_3 d\sigma = \mathcal{T}_{sc1}^* \\
 [V_{sc2}^*] & \oint_{-S_{sc1\parallel e}^*} \psi_2 d\sigma + \oint_{-S_{sc1\parallel e}^*} \psi_4 d\sigma + \oint_{S_{sc}^*} \psi_5 d\sigma \\
 & + \oint_{-S_{sc2\perp}^*} \psi_3 d\sigma = \mathcal{T}_{sc2}^* \\
 [V_{int}^*] & \mathfrak{E}(\mathbf{B}) + \oint_{-S_{sc}^*} \psi_5 d\sigma \\
 & = 2k_{sw} + U_s(\mathbf{B}, V_{int}^*) \\
 & + \mathfrak{E}(V_{int}^*)
 \end{aligned}$$

where

$$\psi_1 = \hat{n}_j x_i T^{ij} \quad (80)$$

$$\psi_2 = (\hat{\mathbf{n}} \times \mathbf{r}) \left(\mathfrak{P}_{\perp} + \frac{\mathbf{B}^2}{8\pi K_0 \mu_r} \right) \quad (81)$$

$$\psi_3 = (\hat{\mathbf{n}} \times \mathbf{r}) \left(\mathfrak{P}_{\parallel} - \frac{\mathbf{B}^2}{8\pi K_0 \mu_r} \right) + \varrho \mathbf{V}_{\parallel}(\mathbf{V}_{\parallel} \times \mathbf{r}) \quad (82)$$

$$\psi_4 = \hat{n}_j x_i \varrho V^i V^j \quad (83)$$

$$\psi_5 = \hat{n}_j x_i (P^{ij} - T^{ij}) \quad (84)$$

$$\begin{aligned}
 \mathcal{T}_a^* & = 2k_a + U_s(\mathbf{B}, V_a^*) + \mathfrak{E}(V_a^*) + \sigma_a \\
 & = \mathcal{T}_a - U_s(\mathbf{B}, V_{\infty} - V_a^*) \\
 & - \mathfrak{E}(V_{\infty} - V_a^*)
 \end{aligned} \quad (85)$$

where a is any index that denotes a \mathbf{j} -system or sub-domain of integration, and it is assumed $\sigma_a \equiv 0$ when $a \neq \mathbf{M}, tc, io$. The relation is also shown between \mathcal{T}_M^* and \mathcal{T}_M defined by (64).

A reminder is also deserved about the following additional properties.

- (I) - It is $\oint_{-S} f d\sigma = - \oint_S f d\sigma$ (f and S arbitrary).
- (II) - The sum of all (79) gives just (56).
- (III) - The shape of the external surface of V_{io}^* is of the kind sketched in figure 12. Define it by neglecting the \mathbf{B} generated by particles that cross it. Then, describe \mathbf{B} by

a potential and take two portions (AB and CD) of equipotential surface. The external toroidal surface (AD and BC) is defined by \mathbf{B} field-lines.

- (IV) - This same figure can be introduced also for S_M^* and S_{tc}^* , depending on the distance between \mathbf{M} and tc , and between tc and io . The corresponding surface integrals in (79)a and b should be modified by means of (70) and (71).

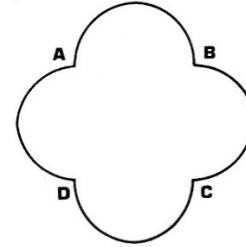


Figure 12. Example of configuration of S_{io}^* (and, possibly, also of S_M^* or of S_{tc}^*). AB and CD are equipotential surfaces, BC and AD are meridional intersections of an approximately cylindrical surface defined by a portion (BC or AD) of field-line longitudinally shifted through 360° . Unpublished figure.

- (V) - If one neglects the leakage of trapped particles in the atmosphere, the ϱV_{\parallel}^2 term across $S_{VA\perp}^*$ should be neglected in (79)c and d.
- (VI) - The simplification that from (75) and (76) leads to (77) and (78) cannot be applied in only three cases:
 - ✓ first, across the magnetopause, i.e., the surface integral across S_{sc}^* in (79)f and (79)g;
 - ✓ second, across $S_{sc1\parallel e}^*$ corresponding to the connection of the magnetopause currents with the neutral sheet and plasmasheet currents (in this respect, note that it is assumed that V_{sc2}^* completely surrounds V_{sc1}^* even on the flanks); and
 - ✓ third, across $S_{sc1\parallel i}^*$ in the region where the plasmasheet particles are injected from V_{sc1}^* into V_{psc}^* [after which they start to spiral towards the atmosphere, and (77) and (78) hold again].
- (VII) - The total (thermal plus kinetic) energies of the \mathbf{M} , tc , io and VA \mathbf{j} -systems are called k_M , k_{tc} , k_{io} , and k_{VA} , respectively. The corresponding energy of the plasmasheet particles that precipitate along the boundaries of the (night) cusp is called k_{psc} ($psc =$ plasmasheet cusp). The corresponding energy of all particles that wander through V_{sc1}^* is called k_{sc1} , and contain mainly plasmasheet particles. In this respect, let us assume that the plasmasheet particles - which are observed to flow earthward, e.g., during a substorm post-breakup condition - have been accelerated by “reconnection” of \mathbf{B} field-lines in the neutral sheet (i.e., by a mechanism similar to the auroral particle acceleration, see, e.g., Hasegawa,²⁸ 1971). Hence, the thickness of V_{sc1}^* should be identified, roughly, with

²⁸ Akira Hasegawa (1934-) Japanese theoretical physicist and engineer.

the thickness of the plasmashet, and no more than that. Concerning k_{sc2} , it deals with particles that move inside V_{sc2}^* , such as the polar wind and, possibly, also the day-cusp particles (see figure 8).

(VIII) - The surface integral over S_{sc}^* can be explicitly expressed in a more direct and intuitive form, depending on the kind of experimental information, which is supposed to be available dealing with “reconnection” and particle flux across the magnetopause.

(IX) - The surface integrals over $S_{sc1||e}^*$ of $\hat{n}_j x_i \varrho V^i V^j$ in (79)f and (79)g are relative to the neutral sheet and plasmashet particle exchange between V_{sc1}^* and V_{sc2}^* .

(X) - Particle and current exchanges are neglected across S_M^* , S_{tc}^* , $S_{VA||i}^*$ and $S_{VA||e}^*$.

(XI) - Concerning the last expression (79)h, one can use (56) in order to get rid of divergent terms. The total thermal plus kinetic energy of the solar wind inside V_{int}^* is called k_{sw} . Let us call k_{magnp} the total thermal plus kinetic energy of particles that flow on the magnetopause. It is

$$\mathcal{K} = k_{sw} + k_{sc}^* \quad (86)$$

$$k_{sc}^* = k_{magnp} + k_{sc2} + k_{sc1} + k_{psc} + k_{VA} \quad (87)$$

$$+ k_{io} + k_{tc} + k_M \quad (88)$$

$$V_{\infty} = V_{int}^* + V_{sc}^* \quad (88)$$

Hence, from (79)h it follows,

$$\oint_{S_{sc}^*} \hat{n}_j x_i (P^{ij} - T^{ij}) d\sigma \quad (89)$$

$$= 2 k_{sc}^* + U_s(\mathbf{B}, V_{sc}^*) + \mathcal{D} + \mathcal{G}(V_{sc}^*)$$

that could be inserted in (79)g and that immediately results also by applying (43) to V_{sc}^* .

Concerning the possibility of applying experimentally (79), a few comments are needed.

- (i) - In general the gravitational terms can be neglected.
- (ii) - Magnetic self-energies can be supposed to be computed, either experimentally as per section 8, or by means of some mathematical \mathbf{B} model.
- (iii) - All surface integrals (with the only exception of the integral over S_{sc}^*) can be supposed to be deduced on the basis of averaged experimental data (some difficulty can arise for $S_{sc1||e}^*$).

(iv) - Some quantities can hardly be estimated experimentally. They include all thermal plus kinetic energies k (7 unknowns) plus the three holonomic constraint terms σ_M , σ_{tc} and σ_{io} . If (89) is used to compute the surface integral over S_{sc}^* , the other 7 equations permit, in principle, to compute $2k_M + \sigma_M$, $2k_{tc} + \sigma_{tc}$, $2k_{io} + \sigma_{io}$, k_{VA} , k_{psc} , k_{sc1} and k_{sc2} , respectively.

Consider (89) and, upon recalling (7), decompose

$$U_s(\mathbf{B}, V_{sc}^*) = U_s(\mathbf{B}_M) + U_j(\mathbf{B}_M, \mathbf{b}) \quad (90)$$

$$+ U_s(\mathbf{b}) - U_s(\mathbf{B}, V_{int}^*)$$

thus, obtain

$$U_s(\mathbf{B}, V_{sc}^*) = \oint_{S_{sc}^*} \hat{n}_j x_i (P^{ij} - T^{ij}) d\sigma \quad (91)$$

$$+ U_s(\mathbf{B}, V_{sc}^*) - 2 k_{sc}^* - U_s(\mathbf{B}_M) - U_s(\mathbf{b}) - \mathcal{D} - \mathcal{G}(V_{sc}^*)$$

Note the similarity of this relation with (59), while (91) can be obtained from (59) by skipping the divergent contribution from the square bracket in (59).

Relations (27), (63) and (91) link the quantities $U_s(\mathbf{b})$, $U_j(\mathbf{B}_M, \mathbf{b})$, \mathcal{Q} , \mathcal{T}_M , $\left[\oint_{S_{sc}^*} \hat{n}_j x_i (P^{ij} - T^{ij}) d\sigma \right]$, $k_{sc}^* - k_M$, $\sigma_{tc} + \sigma_{io}$, and $\mathcal{G}(V_{sc}^* - V_M^*)$. For instance, we can either solve them with respect to $U_j(\mathbf{B}_M, \mathbf{b})$, $U_s(\mathbf{b})$ and to the surface integral, or we can eliminate \mathcal{T}_M in (91) by means of (63) and thus get

$$U_j(\mathbf{B}_M, \mathbf{b}) = 2(k_{sc}^* - k_M) + U_s(\mathbf{b}) + \sigma_{tc} \quad (92)$$

$$+ \sigma_{io} + \mathcal{G}(V_{sc}^* - V_M^*) - \oint_{S_{sc}^*} \hat{n}_j x_i (P^{ij} - T^{ij}) d\sigma - U_s(\mathbf{B}_M, V_{sc}^*)$$

Compare this relation with formula (41) in Carovillano and Siscoe (1973). This relation, when the \mathcal{D} and \mathcal{G} terms and the last addendum are neglected, is used by Siscoe (1970) in order to compute the *DPS* ratio (see below). In reality, he considers what is here called $M+tc$ as the source of the internal origin \mathbf{B} , and he treats it as a dipolar field. Thus, σ_{tc} should be skipped from (92), and the gravitational term $\mathcal{G}(V_{sc}^* - V_M^* - V_{tc}^*)$ should be used. Moreover, a perfect similarity between (92) and the Siscoe’s result can be obtained by defining S_{sc}^* as a surface immediately inside the magnetopause, so that k_{magnp} should be skipped from (87). This is only a matter of convention. It is here preferred to define S_{sc}^* as containing also the magnetopause currents, because - in the opposite case - we should account for the penetration of magnetopause currents \mathbf{j} into the neutral sheet, thus introducing a formal and useless complication.

Another relation obtained by (27), (63) and (91) is

$$\oint_{S_{sc}^*} \hat{n}_j x_i (P^{ij} - T^{ij}) d\sigma \quad (93)$$

$$= 3 U_s(\mathbf{b}) - 2\mathcal{Q} + 2(k_{sc}^* - k_M^*) + \sigma_{tc} + \sigma_{io} + \mathcal{G}(V_{sc}^* - V_M^*) - U_s(\mathbf{B}, V_{int}^*)$$

which is the generalization of another result by Siscoe (1970) [his formula (31)+1], who however neglects all addenda on the right hand side of (93), except the first one. Compare (93) also with formula (43) of Carovillano and Siscoe (1973). Several other similar relations can be obtained by means of (27), (63) and (91).

A more direct comparison with previous treatments can be inferred upon introducing the nonphysical assumption of no “reconnection” and no particle flow across the magnetopause. In such a case, V_{sc2}^* collapses to zero and let us call $S_{sc1||e}^*$ the internal surface of the magnetopause. The relations that are thus obtained are the generalization

of the Siscoe's (1970) treatment. Moreover, let us call S_{sc}^* the surface immediately outside the magnetopause, and let us consider the volume V_{magnp}^* defined by the thin layer

$$\oint_{S_{sc1||e}^*} (\hat{n} \times \mathbf{r}) \frac{B^2}{8\pi K_0 \mu_r} d\sigma + \oint_{S_{sc}^*} \left[(\hat{n} \times \mathbf{r}) \left(\mathfrak{P}_\perp + \frac{B^2}{8\pi K_0 \mu_r} \right) + \hat{n}_j x_i \varrho V^i V^j \right] d\sigma \tag{94}$$

$$= 2 k_{magnp} + U_s(\mathbf{B}, V_{magnp}^*) + \mathfrak{S}(V_{magnp}^*)$$

Note that the dynamic pressure term vanishes far downstream, where – asymptotically – the solar wind flows parallel to the magnetopause. In contrast, on the front-side of the magnetopause, this is the well-known dynamic pressure - which is computed by the assumption of single

between $S_{sc1||e}^*$ and S_{sc}^* (figure 13). Let us apply (93) to V_{magnp}^* . It is [by (75) and (76), and upon assuming that no particle is found immediately inside the magnetopause]

solar wind particles that strike on the magnetopause and are stopped by it (they are not reflected, otherwise a factor 2 ought to be introduced) (see, e.g., Poverlein, 1972 and Gregori and Leybourne, 2025m, or section 2 and figure 3).

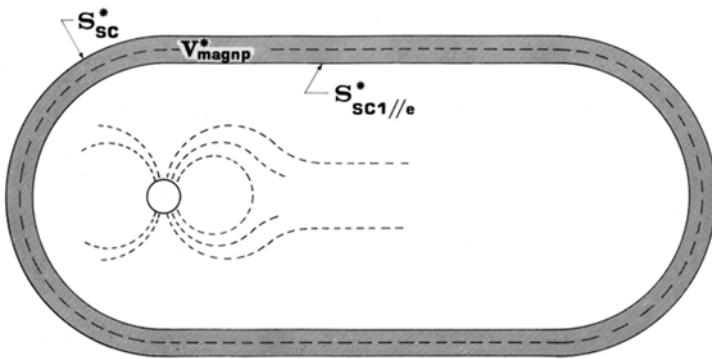


Figure 13. Definition of V_{magnp}^* as a volume comprised between S_{sc}^* , which is immediately outside the magnetopause, and $S_{sc1||e}^*$, which is immediately inside it. See text. Unpublished figure.

Let us suppose that the following approximations can be used:

- (i) no particles are found on the internal side of the magnetopause,
- (ii) \mathbf{B}_{int} vanishes outside the magnetopause,
- (iii) the thickness of the V_{magnp}^* layer tends to zero [thus $U_s(\mathbf{B}, V_{magnp}^*)$ and $\mathfrak{S}(V_{magnp}^*)$ are negligible],
- (iv) k_{magnp} is neglected.

Then (94) becomes the well-known pressure balance (in reality, its scalar product with \mathbf{r}) between an external pressure (dynamic plus thermal) and the internal (magnetic) pressure. This balance has been computed by several authors (Choe et al., 1973 and references therein; but see also Gregori and Leybourne, 2025m and section 2 and figure 3). In the final analysis, this is an important item of the present quantitative models of the magnetopause.

We can write relation (94) also when some “reconnection” and flow across the magnetopause is taken into account. However, the relation, which is thus obtained, is of little help, due to the difficulty while estimating, even approximately, the difference between the particle flows across S_{sc}^* and $S_{sc1||e}^*$. This is essentially the explanation of the difference between the present (92) and the analogous Siscoe's (1970) result, and this is related to the quantitative estimate of the plasma mantle (see figure 8).

Finally, note that if one considers V_{sc}^* instead of V_{magnp}^* he should obtain (89) in which the surface integral

coincides with the integral over S_{sc}^* that appears in (94) (always upon relying on the aforementioned assumption of no “reconnection” and so no particle flow). In this case, if $p_e \hat{n}$ is the external pressure on the magnetopause due to the solar wind, (89) becomes

$$\oint_{S_{sc}^*} p_e \hat{n} \times \mathbf{r} d\sigma = 2 k_{sc}^* + U_s(\mathbf{B}, V_{sc}^*) + \mathfrak{D} + \mathfrak{S}(V_{sc}^*) \tag{95}$$

In addition, note that, if it is assumed that $\mathbf{B}_{int} = 0$, then $U_s(\mathbf{B}, V_{sc}^*)$ is given by (26).

Expressions such as (95), i.e., in terms of a pressure $p_e \hat{n}$, are extensively used by Siscoe (1970), who also computes the power that is spent by the solar wind to cause time variations in the figure of the magnetopause. He uses expressions like $p_e \hat{n} \times \mathbf{V} d\sigma$, where \mathbf{V} is the velocity of the motion of the magnetopause (see also section 6).

This entire formalism is very helpful for the computation of the *DPS* ratio, of the forces and torques exchanged between different space domains of the magnetosphere, and finally also of their energy relations.

5.2.2 - The Dessler-Parker-Sckopke (DPS) ratio

The Dessler-Parker-Sckopke (*DPS*) ratio was named by Olbert et al. (1968) (but, see also Akasofu and Chapman, 1972). It is the ratio between $b_z(0)$, which is the \mathbf{b} component, at the origin, i.e., at Earth's center, along the direction $-\mathbf{M}$, and B_0 , which is the intensity at the equator at Earth's surface of the unperturbed \mathbf{B} . By (11) it is

$$U_j(\mathbf{B}_M, \mathbf{b}) = M \times \mathbf{b}(0) = -M b_z(0) \quad (96)$$

moreover, since it is (in the dipolar approximation, which is here used for the sake of simplicity; additional generalization is discussed in section 8)

$$U_s(\mathbf{B}_M, V_\infty - V_e) = \int_{V_\infty - V_e} \frac{B^2}{8\pi K_0 \mu_r} d\tau \quad (97)$$

$$= \frac{1}{3} M B_0$$

where V is the Earth's volume, it is found

$$\frac{b_z(0)}{B_0} = - \frac{U_j(\mathbf{B}_M, \mathbf{b})}{3 U_s(\mathbf{B}_M, V_\infty - V_e)} \quad (98)$$

The self-energy (97) is well-known (see, e.g., Verosub and Cox, 1971).

We can substitute for $U_j(\mathbf{B}_M, \mathbf{b})$ anyone of the previously given expressions [with the only exception of (11) and (96)], i.e., (27), (59), (63), (91) or (92) or any other expression obtained by combining (27), (63) and (91).

The ratio (98) has also been used to infer partial effects of single \mathbf{j} -systems. For instance, when dealing with VA, let us use (43), with $V = V_\infty$, while avoiding (as already mentioned) γ^{ij} and choosing $\mathbf{b}_1 = \mathbf{b}_{VA}$. Then, by (48), state that

$$\int_{V_\infty} \mathbf{r} \times \mathbf{j}_{VA} \wedge \mathbf{B}_1 d\tau = -\alpha U_j(\mathbf{b}_{VA}, \mathbf{B}_M) \quad (99)$$

where α is a constant that we can suppose close to 1, because the real \mathbf{B} field - in which the trapped particle move - is reasonably well described by the \mathbf{B}_M field. Moreover, if one neglects the solar wind, i.e., if sc \mathbf{j} -currents do not exist, the surface integral in (43) vanishes, and one gets [compare with Carovillano and Siscoe, 1973, eq. (35)]

$$U_j(\mathbf{b}_{VA}, \mathbf{B}_M) = \frac{1}{\alpha} [2 k_{VA} + U_s(\mathbf{b}_{VA}) + \mathfrak{S}(\mathbf{V}_{VA})] \quad (100)$$

where V_{VA} is the space domain that contains all VA orbits (note that, approximately, V_{VA} coincides with V_{VA}^* defined in figure 11).

When all these assumptions are avoided, a correct expression for (100) should be obtained by means of anyone of the aforementioned expressions for $U_j(\mathbf{B}_M, \mathbf{b})$, and by separating it in two parts

$$U_j(\mathbf{b}_{VA}, \mathbf{B}_M) = U_j(\mathbf{B}_M, \mathbf{b}) - U_j(\mathbf{b} - \mathbf{b}_{VA}, \mathbf{B}_M) \quad (101)$$

where

$$\mathbf{b} - \mathbf{b}_{VA} = \mathbf{b}_{tc} + \mathbf{b}_{to} + \mathbf{b}_{sc} \quad (102)$$

then, by computing the partial joint energies according to section 8. However, if only the particles exist that are trapped in the \mathbf{B}_M field, (100) is rigorous with $\alpha = 1$. Then, the coefficient α can be supposed to remain and considered a slight correction. Note that this statement cannot be generalized to \mathbf{j} -systems other than VA, because - in general - we cannot state that - while we neglect a few given \mathbf{j} -systems - the equilibrium state of the remaining currents \mathbf{j} is only slightly different compared to what is observed in natural reality.

Let us suppose that $\mathbf{b}(0) \approx \mathbf{b}_{VA}(0)$ (this seems to be what has to be expected, although it has not been properly shown), and insert (100) into (98). Thus, it is found

$$\frac{b_z(0)}{B_0} = - \frac{1}{3\alpha} \frac{2 k_{VA} + U_s(\mathbf{b}_{VA}) + \mathfrak{S}(\mathbf{V}_{VA})}{U_s(\mathbf{B}_M, V_\infty - V_e)} \quad (103)$$

Such a relation, with no $U_s(\mathbf{b}_{VA})$ and $\mathfrak{S}(\mathbf{V}_{VA})$ and by putting $\alpha = 1$, has been shown for axisymmetric \mathbf{j} -distributions by Dessler and Parker (1959), Parker (1962), Skopke (1966). Generalization to the asymmetric case (discussing also ionospheric effects) was given by Parker (1966a). See also the review by Parker and Ferraro (1971) and - for a few mentions - Rossi and Olbert (1970) and Poverlein (1972). The terms $U_s(\mathbf{b}_{VA})$ and $\mathfrak{S}(\mathbf{V}_{VA})$ have been taken into account, independently, by Baker and Hurley (1967), Carovillano and Maguire (1968), and Olbert et al. (1968).

Insert (92) into (98) and obtain a much more general and more correct expression, upon taking into account the entire \mathbf{b} perturbation (and not only \mathbf{b}_{VA}). This expression has been given the first time by Siscoe (1970) who neglects the σ_{tc} , σ_{to} and \mathfrak{S} terms and the last addendum in (92). Compare this with a formula in Carovillano and Siscoe (1973, p. 305).

Insert (27) into (98) and get

$$\frac{b_z(0)}{B_0} = \frac{2 [U_s(\mathbf{b}) - Q]}{3 U_s(\mathbf{B}_M, V_\infty - V_e)} \quad (104)$$

which is the generalized form of eq. (31) of Siscoe (1970) who neglects Q .

Let us investigate the variational principle that is satisfied by the DPS ratio. Define it in terms of $U_s(\mathbf{B}_M)$ instead of $U_s(\mathbf{B}_M, V_\infty - V_e)$. This cannot be achieved in the framework of the magnetostatic formalism. Thus, let us suppose that L_M is, e.g., a circular wire of radius R and cross-section of radius r with a current I_M flowing inside it (for a more general treatment see section 8). Owing to (11) let us state that it is

$$U_j(\mathbf{B}_M, \mathbf{b}) = I_M \Phi_M(\mathbf{b}) \quad (105)$$

$$= -[I_M \pi R^2] b_z(0)$$

$$= -[I_M f_1(R)] b_z(0)$$

where I_M is the current flowing in L_M and $f_1(R)$ is a proper constant, which depends only on the real geometry of the \mathbf{M} \mathbf{j} -system, which is πR^2 for a simple circular loop L_M . Upon comparing (105) with (96) it is concluded that

$$I_M f_1(R) \equiv M \quad (106)$$

where M is the intensity of the dipole moment of the Earth. We can therefore assume that $f_1(R)$ is positive. Moreover, if $a > R$ is the radius of the Earth and B_0 is the field at the equator at Earth's surface, pointing upward, it can be stated that

$$B_0 = f_2(R, a) I_M \quad (107)$$

where $f_2(R, a) > 0$ is a constant that depends on the geometry of the \mathbf{M} \mathbf{j} -system. Then, by I.7.19) it is

$$\begin{aligned}
 U_s(\mathbf{B}_M) &= \frac{1}{2} L I_M^2 & (108) \\
 &= -\frac{L}{2 f_1(R) f_2(R, a)} U_j(\mathbf{B}_M, \mathbf{b}) \frac{B_0}{b_z(0)} \\
 &= -f(a, R) U_j(\mathbf{B}_M, \mathbf{b}) \frac{B_0}{b_z(0)}
 \end{aligned}$$

where $f(R, a) > 0$ is a constant that depends on the geometry of the $\mathbf{M j}$ -system, and L is the self-inductance of the $\mathbf{M j}$ -system that, when it is a circular wire of radius R and cross-section radius r , is [as mentioned while dealing with comets (Gregori and Leybourne, 2025m), see, e.g., Durand (1968) or also Becker (1933) or Bruhat²⁹ (1963)]

$$L = 4\pi R \left(\log \frac{8R}{r} - \frac{7}{4} \right) \quad (109)$$

By (108) it follows

$$\frac{b_z(0)}{B_0} = -f(a, R) \frac{U_j(\mathbf{B}_M, \mathbf{b})}{U_s(\mathbf{B}_M)} \quad (110)$$

It is possible to attempt to “parameterize” - although in some oversimplified way - the natural system by considering the R, L, C parameters of an equivalent circular loop made like a toroid of some given simple geometry.

The self-inductance L of a toroid, which consists of N turns and has a rectangular cross-section with inner radius a , outer radius b , and height h (figure 14) is

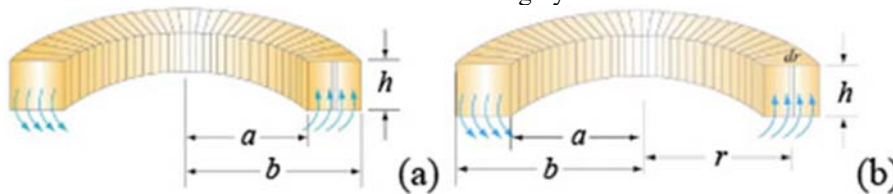


Figure 14. A toroid with N turns. After Liao et al. (2004, p. 11-7; figure 11.2.3). © 2004 Sen-ben Liao, Peter Dourmashkin, and John Belcher. With kind permission of *The MIT Press*.

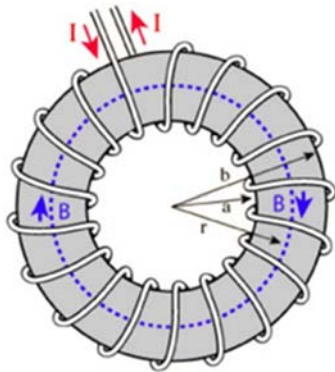


Figure 15. A circular toroid. After <https://www.quora.com/What-is-a-toroidal-electromagnet>, with kind free permission granted by *Quora*.

A slightly improved and more realistic “simple” terrella-model might be attempted, perhaps, (see details in Gregori and Leybourne, 2021) by constructing in the

²⁹ Georges Bruhat (1887-1945), French physicist.

$$L = \frac{N\Phi_B}{I} = \frac{\mu_0 N^2 h}{2\pi} \ln \frac{b}{a} \quad (111)$$

where Φ_B is the \mathbf{B} flux through the toroid.

The source is Liao et al. (2004, p. 11-7), i.e., the MIT study guide, or <http://web.mit.edu/8.02t/www/materials/StudyGuide/guide11.pdf>.

Another formula that seems, perhaps, better suited for the present case history is the approximate inductance of a circular toroid³⁰ (figure 15)

$$L \approx \frac{\mu_0 N^2 A}{2\pi r} \quad (112)$$

where A is the cross-section area, and r is the toroid radius to centerline. We can pose, e.g., r equal to the Earth’s radius and we can guess some conventional value for $N^2 A$. Thus, we can estimate L and its value can be put inside an L, R, C circuit, where R is some resistance, which is estimated according to some reasonable guess dealing with the Earth’s interior, etc. This should finally fit with some observed cyclic feature in the natural environment, including some climatic phenomenon that seems approximately periodical.

This is certainly a rough and approximate procedure, although it might, perhaps, lead to some indicative and roughly correct estimate of some order of magnitude.

laboratory some tentative model that ought to be representative of the MOR-“cage”, i.e., roughly a tetrahedron with edges suitably curved for matching Earth’s curvature. In addition, take into suitable account the related scaling factors dealing with cable resistance, cross-section, reduction to Earth’s radius etc.

Moreover, some inference can be intuitively guessed by means of some simple consideration of large scale morphological features. For instance, is it well-known that every auroral electrojet can be roughly described like a circular ring of electric currents “posed” over a polar cap. Since the MOR-“cage” includes a circular segment at constant negative latitude - which is extended almost along 360° in longitude - in this large region the MOR runs approximately roughly parallel to the southern auroral electrojet. Hence, these are two roughly parallel circular loops located at a reciprocal position suited to optimize their mutual e.m. induction. That is, this is likely to be a preferred “door” for the e.m. induction effects by the solar wind on the Earth’s circuits (maybe at periods $\gg 1$ day).

³⁰ After the *Georgia State University* website, <http://hyperphysics.phyastr.gsu.edu/hbase/magnetic/indtor.html>.

Differently stated, the two auroral electrojets, and the *MOR* “cage”, can be considered like windings of a transformer. On the other hand, air-earth currents are such that this is a leaking transformer. This entire perspective is more explicitly discussed in Leybourne et al. (2025) and in Gregori et al. (2025x). No additional detail is here given.

In any case, owing to the principle of magnetic energy variation (see section 1), equilibrium is attained by an increase of $U_j(\mathbf{B}_M, \mathbf{b})$ and by an equal decrease of $U_s(\mathbf{B}_M)$. Hence, it can be concluded that, at equilibrium, the *DPS* ratio is minimum (hence, in the case that it is negative, its absolute value is maximum).

The *DPS* ratio is negative if the currents \mathbf{j} alone of the ring current are taken into account, as it can be shown by (103) [as $\mathfrak{S}(\mathbf{V}_{VA})$ is in any case negligible]. In contrast, in the most general case, the sign of the *DPS* ratio can be inferred from expressions such as (104) or (110). From (110) it is inferred that the sign is opposite to the sign of $U_j(\mathbf{B}_M, \mathbf{b})$ or, by (63) and (64), it is the same as for \mathfrak{T}_M . By (64), \mathfrak{T}_M is composed of two positive addenda [i.e., $2k_M$ and $U_s(\mathbf{B}_M)$], $\mathfrak{S}(\mathbf{V}_M^*)$ is negative, and σ_M can be presumed to be negative (and, as it is shown in sections 6 and 8, it cannot be neglected). Thus, in the general case, no general statement can be made about the sign of the *DPS* ratio.

Note that the *DPS* ratio can be measured experimentally (see section 8), as $\mathbf{b}(0)$ can be inferred from measurements of \mathbf{b} at the Earth’s surface, which can be extrapolated to Earth’s center by means of a *SHE*. In any case, \mathbf{b} should not include storm or perturbed conditions, rather only very regular quiet time variations.

Previous attempts to evaluate the *DPS* ratio dealt with (103) (based on the aforementioned simplifications) in order to estimate the kinetic energy k_{VA} of the ring current, etc. That is, the experimental computation of *DPS*’ ratio, which is here discussed, is comparatively much more accurate.

This computation is rigorous as far as we can neglect air-earth currents. This is certainly incorrect, even though the present available evidences are insufficient for implementing an approximate geometrical model to be included in figure 11. A computation by assuming a negligible role of air-earth currents can be useful for an *a posteriori* evaluation of the role of air-earth currents in the energy processes that control magnetospheric phenomena.

5.2.3 – Forces

$$\mathbf{F}_{tc} = - \oint_{-S_M^* + S_{tc}^*} \hat{n}_j t^{ij}(M) d\sigma - \int_{V_M^*} \mathbf{j}_{tc} \wedge (\mathbf{B} - \mathbf{b}_{tc}) d\tau - \int_{V_M^*} \rho \mathbf{g} d\tau \quad (116)$$

where the two first addenda can be computed by means of the aforementioned experimental \mathbf{b} model, and by applying a formal separation of internal and external origin components of \mathbf{b} , thus obtaining a model for \mathbf{b}_{tc} and \mathbf{j}_{tc} (see, e.g., Matsushita, 1967).

The forces that are applied and exchanged between different magnetospheric domains can be evaluated as follows. Owing to (286), the potential energy (apart a constant quantity) equals $-U(\mathbf{b}, \mathbf{B}_M)$. Then, by (11) and (96) it follows

$$\mathbf{F}_M = \text{grad } U_j(\mathbf{B}_M, \mathbf{b}) = -M \text{grad } b_z(0) \quad (113)$$

that can be computed by means of the experimental values for \mathbf{M} and $b_z(0)$.

The result can be generalized by computing the gradients with respect to other independent co-ordinates. Moreover, the force \mathbf{F}_M was defined for (38) and (40). This result can be generalized by direct consideration of the momentum equation (30). That is, let us say that $\mathbf{b}_1 = \mathbf{B}_M$ and $\mathbf{B}_1 = \mathbf{b}$ and thus find

$$\mathbf{F}_M = \int_{V_M^*} \left\{ \frac{\partial}{\partial x^j} [p^{ij}(M) - t^{ij}(M)] - (\mathbf{I}_M \wedge \mathbf{b}) \right\} d\tau - \int_{V_M^*} \rho \mathbf{g} d\tau \quad (114)$$

where V_M^* is defined in figure 11 and the argument M for p^{ij} and t^{ij} means that reference is made to the \mathbf{M} \mathbf{j} -system alone. Apply Gauss’ theorem and, since the \mathbf{j} exchanges are neglected between M and tc , let us put $p^{ij} = 0$ over S_M^* and get

$$\mathbf{F}_M = - \oint_{S_M^*} \hat{n}_j t^{ij}(M) d\sigma - \int_{V_M^*} \mathbf{I}_M \wedge \mathbf{b} d\tau - \int_{V_M^*} \rho \mathbf{g} d\tau \quad (115)$$

The first addendum on the right hand side can be computed on the basis of any model for \mathbf{B}_M (however, the M currents must be supposed to be entirely contained inside S_M^*). The second addendum can be computed when the geometrical figure of L_M is assumed (e.g., a simple circular wire with current I_M) and \mathbf{b} is experimentally known inside V_M^* . The gravitational term must be extended to include all electrons (or charged particles) that enter into the \mathbf{M} \mathbf{j} -system [otherwise, let us claim that we compute $(\mathbf{F}_M + \int_{V_M^*} \rho \mathbf{g} d\tau)$]. In any case, it can be interesting to compare the values obtained by (113) and (115).

Similarly, let us apply (30) as in (114). However, the integral is over V_{tc}^* , and the result is (upon neglecting the \mathbf{j} exchanges between tc and io)

Similarly, let us extend the integration volume to V_{io}^* and get

$$\mathbf{F}_{io} = - \oint_{-S_{tc}^* + S_{io}^*} \hat{n}_j [p^{ij}(io) - t^{ij}(io)] d\sigma - \int_{V_{io}^*} \mathbf{j}_{io} \wedge (\mathbf{B} - \mathbf{b}_{io}) d\tau - \int_{V_{io}^*} \rho \mathbf{g} d\tau \quad (117)$$

However, unlike for (115) and (116), it is not easy to separate \mathbf{b}_{io} from $\mathbf{b}_{VA} + \mathbf{b}_{sc}$. For instance, this could be achieved by analyzing satellite measurements of quiet time \mathbf{B} over the external surface of V_{io}^* , although practically it results difficult to state what measurements are to be used. This difficulty can be avoided by integrating over larger volumes. Indeed, note that, when the integration is carried out over either V_{VA}^* or V_{psc}^* or V_{sc1}^* or V_{sc2}^* , it is (e.g., in case of V_{VA}^*)

$$\begin{aligned} & \int_{V_{VA}^*} \mathbf{j}_{VA} \wedge (\mathbf{B} - \mathbf{b}_{VA}) d\tau \\ &= \oint_{-S_{VA||i}^* - S_{VA\perp}^* + S_{VA||e}^*} \hat{n}_j [p^{ij}(VA) \\ & - t^{ij}(VA)] d\sigma - \int_{V_{VA}^*} \rho \mathbf{g} d\tau \end{aligned} \quad (118)$$

Note also that, owing the action-reaction principle, if a and b are two \mathbf{j} -system indices, it is

$$\int_{V_a^*} \mathbf{j}_a \wedge \mathbf{b}_b d\tau = - \int_{V_b^*} \mathbf{j}_b \wedge \mathbf{b}_{ba} d\tau \quad (119)$$

Integrate over V_{sc}^* and get

$$\begin{aligned} \mathbf{F}_M + \mathbf{F}_{tc} + \mathbf{F}_{io} \\ &= \oint_{S_{tc}^*} \hat{n}_j [P^{ij} \\ & - T^{ij}] d\sigma - \int_{V_{tc}^*} \rho \mathbf{g} d\tau \end{aligned} \quad (120)$$

where the first addendum on the right hand side can be computed whenever one assumes to know the amount of \mathbf{B} “reconnection” and particle flow across the magnetopause. For instance, if “reconnection” and particle flow are neglected, by (69) it follows

$$\oint_{S_{sc}^*} \hat{n}_j [P^{ij} - T^{ij}] d\sigma = \oint_{S_{sc}^*} \hat{\mathbf{n}} \frac{\mathbf{B}^2}{8\pi K_0 \mu_r} d\sigma \quad (121)$$

Note that the gravitational term includes also the gravitational integrals of (115), (116) and (117). Let us assume that we include the gravitational integral in the definition of \mathbf{F}_M , \mathbf{F}_{tc} and \mathbf{F}_{io} , and that we neglect the gravitational integrals over all volumes external to V_{io}^* . Thus, we can safely avoid to mention at all the gravitational terms in expressions such as (115) through (120). Note also that, in (121), $[\hat{\mathbf{n}} \mathbf{B}^2 / 8\pi K_0 \mu_r]$ is the internal pressure \mathbf{p}_i that acts on the magnetopause. Thus, express (120) in terms of \mathbf{p}_i , neglect the gravitational term, and also \mathbf{F}_{tc} and \mathbf{F}_{io} with respect to \mathbf{F}_M . By (113) the approximate expression is thus finally found

$$-M \text{grad } b_z(0) = \oint_{S_{sc}^*} \mathbf{p}_i d\sigma \quad (122)$$

that was given by Siscoe (1970).

5.2.4 – Torques

The same argument that leads to (113) can be applied to evaluate the torque

$$\int_{V_M^*} \mathbf{r} \wedge \mathbf{f}_M d\tau = \mathbf{M} \wedge \mathbf{b}(0) \quad (123)$$

which is a well-known result in the case of a pure dipole [when (11) applies].

If L_M is represented by some more complicated loop, one should compute the components of the torque by means of $\partial U_j(\mathbf{B}_M, \mathbf{b}) / \partial \vartheta$ and $\partial U_j(\mathbf{B}_M, \mathbf{b}) / \partial \varphi$ where ϑ and φ are two given polar coordinates.

A more formal and general approach can be carried out by means of the momentum equation (30) and by computing the vector product with \mathbf{r} of both sides

$$\begin{aligned} \varepsilon_{hik} x^h \frac{\partial}{\partial x^j} [p^{ij}(1) - t^{ij}(1)] \\ &= [\mathbf{r} \wedge (\mathbf{j}_1 \wedge \mathbf{B}_1)]_k \\ &+ \sum (\mathbf{r} \wedge \mathbf{f})_k \\ &+ \rho (\mathbf{r} \wedge \mathbf{g})_k \end{aligned} \quad (124)$$

Since ε_{hik} is antisymmetric it is possible to commute $\partial / \partial x^j$ with $(\varepsilon_{hik} x^h)$. Integrate over any given volume V and apply the Gauss’ theorem

$$\begin{aligned} \oint_S \varepsilon_{hik} x^h \hat{n}_j [P^{ij} - T^{ij}] d\sigma \\ &= \int_V \{ [\mathbf{r} \wedge (\mathbf{j}_1 \wedge \mathbf{B}_1)]_k \\ &+ \sum (\mathbf{r} \wedge \mathbf{f})_k \\ &+ \rho (\mathbf{r} \wedge \mathbf{g})_k \} d\tau \end{aligned} \quad (125)$$

The right hand side is the torque of all forces that are externally applied. The left hand side should be computed. For instance, in special case histories, one can use the simplified expressions (66), (69) etc. Owing to brevity purpose, formal details are not here given. However, one can compute the torque, which acts on every current loop. If it is chosen $V = V_{sc}^*$, one can express the torque in terms of \mathbf{p}_i or \mathbf{p}_e [as for (122)] and thus get another approximate result that was already given by Siscoe (1970).

5.2.5 - The work spent by the electric field (the energy equation)

The momentum equation (30) was used to infer forces, torques (by cross product with \mathbf{r}), and partial energies through the virial theorem (obtained by scalar product with \mathbf{r}). Additional energy relationships can be obtained directly by means of the energy equation.

For the sake of generality, let us separate \mathbf{J} and \mathbf{B} according to (28) and (29). Moreover, separate analogously also the electric field \mathbf{E}

$$\mathbf{E} = \mathbf{e}_1 + \mathbf{E}_1 \quad (126)$$

Represent \mathbf{j}_1 either by a peculiar \mathbf{j} -system, or by the ensemble of all particles inside a given volume V , or by any given subset of particles. Consider a stationary situation, treat \mathbf{e}_1 and \mathbf{b}_1 in terms of e.m. energy density and of Poynting vector, while \mathbf{E}_1 and \mathbf{B}_1 are likened to forces that are externally applied. It is

$$\begin{aligned} \text{div} [c^2 \mathbf{g}(1) + \mathbf{s}(1)] & \quad (127) \\ &= \mathbf{E}_1 \times \mathbf{j}_1 + \varrho(1) \mathbf{g} \times \mathbf{v}(1) \\ &+ \sum \mathbf{f} \times \mathbf{v}(1) \end{aligned}$$

where $\mathbf{g}(1)$ is the total momentum density of the particles that originate \mathbf{j}_1

$$\mathbf{s}(1) = \gamma_0 \frac{\mathbf{e}_1 \wedge \mathbf{b}_1}{4\pi} \quad (128)$$

is the Poynting vector, and $\sum \mathbf{f}$ represents the holonomic constraints (35). Note that, when the aforementioned simplifying assumptions are used, since \mathbf{f} is supposed to be perpendicular to the surface over which particles flow, it is $\mathbf{f} \times \mathbf{v}(1) = 0$.

Equation (127) can be written (in the non-relativistic case, see, e.g., Rossi and Olbert, 1970) also by substituting

$$\begin{aligned} c^2 g_i(1) = & \left\{ \frac{1}{2} \varrho(1) \mathbf{v}^2(1) \right. \\ & \left. + \varepsilon_T(1) \right\} v_i(1) + p_{ij}(1) \\ & + q_i^*(1) \end{aligned} \quad (129)$$

$$\int_V \mathbf{E} \times \mathbf{j} \, d\tau + \frac{\partial}{\partial t} \int_V [1/(8\pi)] (K_{el,0} \varepsilon_r \mathbf{E}^2 + K_0 \mu_r \mathbf{H}^2) \, d\tau + \int_S [\gamma_0/(4\pi)] \mathbf{E} \wedge \mathbf{H} \times \overline{d\sigma} = 0 \quad (132)$$

where $d\tau$ is the volume differential, $\overline{d\sigma}$ is the surface differential over S and it is defined in terms of a differential vector oriented outward (where the “internal” side is defined as that part of space with respect to S that is identified with V). This is the *Poynting theorem*. The first addendum in (132) is Joule heat; the second addendum is the time variation of the electric energy density

$$[1/(8\pi)] K_{el,0} \varepsilon_r \mathbf{E}^2 = [1/(8\pi)] \mathbf{E} \times \mathbf{D} \quad (133)$$

plus the magnetic energy density

$$[1/(8\pi)] K_0 \mu_r \mathbf{H}^2 = [1/(8\pi)] \mathbf{H} \times \mathbf{B} \quad (134)$$

The third addendum is the flux of the Poynting vector $[\gamma_0/(4\pi)] \mathbf{E} \wedge \mathbf{H}$ across S .

Refer to the first addendum in the Poynting theorem (132). When adopting the *MHD* assumptions, the total current is essentially the conduction current

$$\mathbf{j} = \sigma \left[\mathbf{E} + \frac{1}{\gamma_0} \mathbf{v} \wedge \mathbf{B} \right] \quad (135)$$

where \mathbf{v} is the bulk velocity of particles. Therefore

$$\begin{aligned} \int_V \mathbf{E} \times \mathbf{j} \, d\tau &= \int_V (\mathbf{j}^2/\sigma) \, d\tau \\ &+ (1/\gamma_0) \int_V \mathbf{v} \times \mathbf{j} \wedge \mathbf{B} \, d\tau \end{aligned} \quad (136)$$

where $\varepsilon_T(1)$ is the thermal energy density of the \mathbf{j}_1 system, and $q_i^*(1)$ is the heat flow vector. More precisely, one should add inside the square bracket in (129) the rest energy, i.e., $\varrho(1) c^2$, and delete $q_i^*(1)$. Then, by means of the continuity equation, the rest energy is transformed into heat flow vector (see, e.g., Rossi and Olbert, 1970). This ought to be recalled when $\mathbf{g}(1)$ is used in the time varying equations (see section 6). An alternative and much simpler expression for $\mathbf{g}(1)$ is

$$\mathbf{g}(1) = \varrho(1) \mathbf{v}(1) \quad (130)$$

Integrate (127) over V and apply Gauss’ theorem

$$\oint_S \hat{\mathbf{n}} \times [c^2 \mathbf{g}(1) + \mathbf{s}(1)] \, d\sigma \quad (131)$$

$$\begin{aligned} &= \int_V \mathbf{E}_1 \times \mathbf{j}_1 \, d\tau \\ &+ \int_V \varrho(1) \mathbf{g} \times \mathbf{v}(1) \, d\tau \\ &+ \sum \int_V \mathbf{f} \times \mathbf{v}(1) \, d\tau \end{aligned}$$

that is self-explanatory, and the $\mathbf{g}(1)$ flux includes (i) the net change of “thermal” and kinetic energy caused by the plasma flow across S , (ii) the work done by “pressure” forces, and (iii) the heat flow.

Let us consider the Poynting theorem, referring to an arbitrary pre-chosen volume V confined by a surface S ,

Hence, the first addendum in (136) is Joule heat, while the second addendum is the effective work done by \mathbf{B} over a sample of matter that has bulk velocity \mathbf{v} . In the case that σ is infinite, in order to keep \mathbf{j} finite, in (135) it must be $\mathbf{E} + (1/\gamma_0) \mathbf{v} \wedge \mathbf{B} = 0$. In this case the Joule term vanishes in (136).

Moreover, the total body-force acting on a sample of matter is

$$\varrho_{el} \mathbf{E} + (1/\gamma_0) \mathbf{j} \wedge \mathbf{B} \quad (137)$$

where ϱ_{el} is the net charge density. But in general the contribution by \mathbf{E} can be shown to be negligible. Thus, the second addendum in (136) is the power spent by the body force (e.g., for deforming the “flexible wires” of the “water-pipe” model of the water-pipe model (see sections 2 and 3).

As a particular case, apply the Poynting theorem (132) to the case of a stationary state (with infinite σ). Consider the model with perfectly flexible wires. From (136) it follows

$$\int_V \mathbf{E} \times \mathbf{j} \, d\tau = 0 \quad (138)$$

With reference to (131), note that the $\mathbf{E}_1 \times \mathbf{j}_1$ term cannot be simplified by means of (136), which deals with the whole \mathbf{E} . By means of (129) and (33) the purely dynamic term in (131) can be expressed as

$$\hat{n} \times c^2 \mathbf{g}(1) = \left[\frac{1}{2} \rho v^2(1) + \varepsilon_T(1) + \tilde{p}_\perp(1) \right] (\mathbf{v}(1) \times \hat{n}) + (\tilde{p}_\parallel - \tilde{p}_\perp) \frac{[\mathbf{B} \times \hat{n}] [\mathbf{B} \times \mathbf{v}(1)]}{B^2} + \hat{n} \times \mathbf{q}^* \quad (139)$$

Moreover, when $\mathbf{b}_1 = \mathbf{B}$ and $\mathbf{B}_1 = 0$, (131) becomes

$$\oint_S \hat{n} \times [c^2 \vec{\mathcal{E}} + \mathbf{S}] d\sigma = \int_V \rho \mathbf{g} \times \mathbf{v} d\tau + \sum \int_V \mathbf{f} \times \mathbf{v} d\tau \quad (140)$$

where $\vec{\mathcal{E}}$ is the momentum density vector and \mathbf{S} is the Poynting vector.

If the Poynting vector \mathbf{S} is not used, (140) can also be written as

$$\oint_S \hat{n} \times c^2 \vec{\mathcal{E}} d\sigma = \int_V \mathbf{E} \times \mathbf{J} d\tau + \int \mathbf{g} \times \mathbf{v} d\tau + \sum \int_V \mathbf{f} \times \mathbf{v} d\tau \quad (141)$$

When it is possible to refer to the frozen-in approximation, i.e., $\mathbf{E} + \mathbf{v} \wedge \mathbf{B} = 0$, such as, e.g., inside the solar wind, the $\hat{n} \times \mathbf{S}$ term in (140) can be expressed as

$$\oint_S \hat{n} \times \mathbf{S} d\sigma = -\frac{\gamma_0}{4\pi} \oint_S \hat{n} \times (\mathbf{V} \wedge \mathbf{B}) \wedge \mathbf{B} d\sigma = \frac{\gamma_0}{4\pi} \oint_S [\hat{n} \times (\mathbf{V}) B^2 - (\hat{n} \times \mathbf{B}) (\mathbf{V} \times \mathbf{B})] d\sigma \quad (142)$$

[equivalently, the simplification (136) can be used in (141)]. Moreover, when the “reconnection” across the magnetopause is neglected, it is $\hat{n} \times \mathbf{B} = 0$ in (139) and (142), etc.

In general, expressions like (131) can be used to compute the $\mathbf{E}_1 \times \mathbf{j}_1$ integrals. Indeed, the surface integral can be supposed to be evaluated on the basis of experimental models that represent physical conditions over S , while, compared to the work spent by \mathbf{E} , the holonomic constraints and gravity terms are likely to be less important. By (131), in principle, it is possible to evaluate the work spent over \mathbf{j}_1 by the \mathbf{E} generated by all other particles. By (141) it is possible to compute the total work spent by the total \mathbf{E} over the total ensemble of particles inside V (and the surface integral requires no experimental model for \mathbf{E}). If one knows a model for both \mathbf{B} and \mathbf{E} over S , by (140) it is possible to estimate how far the gravity and constraints terms can be neglected.

Let us consider the simplest case history. Let V be a huge box (as far as it can be physically defined) of solar wind that contains the whole magnetosphere, and let us assume that, over S , all quantities \mathbf{V} , \mathbf{B} , \mathbf{E} , ρ , $\tilde{\mathcal{P}}_\parallel$, $\tilde{\mathcal{P}}_\perp$, ε_T are constants. Evaluate the left hand side of (141). By means of (139), since $div \mathbf{V} = 0$ and $div \mathbf{B} = 0$ (and as long as also $div \mathbf{q}^* = 0$), it can be concluded that the left hand side of (141) is zero. This means that the total power spent by \mathbf{E} , \mathbf{g} and $\sum \mathbf{f}$ over all particles is zero. But, by (142), and by the same argument, it can also be shown that

$$\oint_S \hat{n} \times \mathbf{S} d\sigma = \oint_S \mathbf{E} \times \mathbf{J} d\sigma = 0 \quad (143)$$

that also implies

$$\int_V (\rho \mathbf{g} + \sum \mathbf{f}) \times \mathbf{v} d\tau = 0 \quad (144)$$

The same conclusion holds also when the huge box collapses into a smaller volume V , which always encloses

the magnetosphere, and such that the solar wind properties can be presumed constant all over its surface.

Consider a volume V defined by a surface S , which is just inside the magnetopause, and assume that no particle flows across S , except the particles that enter or leave the currents \mathbf{j} of the neutral sheet. Assume also that these currents \mathbf{j} have constant ρ , \mathbf{V} , ε_T , $\tilde{\mathcal{P}}_\parallel$, $\tilde{\mathcal{P}}_\perp$, and that \mathbf{B} is constant on both lateral borders of the neutral sheet (and that $div \mathbf{q}^* = 0$). By (139) it can be seen that (owing to the change in direction of \hat{n} on the two borders of the neutral sheet) the left hand side of (141) vanishes.

Relation (143) should be compared with (138) that had been obtained on a simpler basis of *MHD* and infinite conductivity hypotheses. Compared to (143), the relation (138) is much more compulsory. However, (143) allows for a comparably more detailed investigation of the influence of the approximations introduced in the description of magnetospheric plasmas and fields.

5.2.6 - Summary

Let us briefly summarize the results of the present section. Dissipative phenomena are neglected. The collisionless Boltzmann equation is considered, and a few of its moments: the momentum, the angular momentum, plus energy and virial equations.

The previous results available in the literature were essentially concentrated on the virial theorem and on the computation of *DPS* ratio. They are extensively reviewed by Siscoe (1970).

Substantial generalizations of the Siscoe’s (1970) results are here given. First of all, the Siscoe’s virial theorem approach is generalized. Several different expressions for the *DPS* ratio are given, and it is shown that, at equilibrium, the *DPS* ratio has to be minimum (relative value).

It is also shown that (i) the currents \mathbf{j} in the Earth’s core, (ii) the currents \mathbf{j} induced in the Earth’s crust and mantle,

and (iii) the ionospheric currents \mathbf{j} , all of them should flow, as far as possible, on their respective outermost layers, compatibly with local resistivity. Moreover, several other relationships are given that, potentially, can be applied to experimental measurements, and by which it is possible to evaluate the total kinetic plus thermal energy content inside every given sub-volume of the magnetosphere.

An additional generalization, similarly to the virial equation, relies on consideration of the momentum and angular momentum equations, which provide with relationships of the forces and of the torques produced by the solar wind on the ionosphere and on solid Earth. This can be useful, e.g., for the investigation of the anomalies of the astronomical motion of the Earth associated with solar activity, as it is discussed in better detail in section 8. However, a full discussion is outside the main scope of the present paper.

In addition, the energy equation provides with relationships on the total power that is spent by \mathbf{E} inside every given sub-volume.

6. The energy of the magnetosphere - Time varying conditions

The formal treatment of section 5.2 is here generalized to the case of time varying conditions. The result looks formally much more complicated. Hence, from the view point of numerical application to experimental measurements, they are practically less useful. However, they are required for the sake of completeness, and as a premise for subsequent theoretical treatment. In any case, as shown in section 7, it is possible to explain, by means of the approach that is here outlined, the laws that control the energy flux between different components of the magnetosphere.

A generalization is here made of a formulation originally appeared in Siscoe (1970) and dealing with the solar wind power (SWP), which is spent to modify the magnetosphere.³¹ The heuristic possibilities of the more general formulation that is here presented can be appreciated only by comparison with the case history of a steady state system.

Concerning the time variation - and as a premise for a first operative approach - one additional physical assumption is needed. Consider the role of the formal terms that must be added to the steady state formulas. In addition, for the time being let us first suppose that the physical system changes vs. time following a sequence of quasi-equilibrium states. This is not always correct. For instance, from a strictly rigorous viewpoint, a formal MHD modeling cannot justify \mathbf{B} "reconnection" in terms of changes of the

system through quasi-equilibrium states. Analogous limitations hold also for the phase-space approach.

In any case, as long as the physical system of the magnetosphere is arbitrarily represented - such as in figure 11 in terms of an approximate model where different spatial domains are distinguished - such an approximation is a simplifying assumption that unavoidably implies some loss of physical rigor.

On the other hand, even when formulas no more hold, it is possible to liken both the initial and the final states to approximately steady equilibrium states. Hence, the steady state formulas can be approximately applied to both states. Then, their energy contents can be compared with each other, and also the reciprocal forces and torques, the powers being spent, etc. In this way it is possible to infer some physical information about the system, either before or after the change. Section 7 contains some better discussion about the way by which such an approximation can be dropped.

Let us begin and refer to the current loop formulation. Call

$$\mathbf{B} = \mathbf{B}_M + \mathbf{b} + \mathbf{b}' \quad (145)$$

where \mathbf{B}_M is the field generated by the \mathbf{M} \mathbf{j} -loop, \mathbf{b} is the steady state "perturbation" field, i.e., generated by all other \mathbf{j} -loops, and \mathbf{b}' is an additional superimposed perturbation of period, say, shorter than a few decades. The system is also assumed to oscillate, always remaining in a quasi-steady or quasi-equilibrium state.

Owing to theorem (9), i.e., (19), it is

$$U_j(\mathbf{B}_M, \mathbf{b} + \mathbf{b}') = U_j(\mathbf{B}_M, \mathbf{b}) \quad (146)$$

that means that the joint energy, or the potential energy, of the system remains constant. This is obvious in (11), (96) and (63), while (27) implies that both \mathcal{Q} and $U_s(\mathbf{b} + \mathbf{b}')$ fluctuate in time, although their difference remains constant. The relations (91), (92), and other relations similar to them, which must be applied to derive (146), look comparatively much more intricate.

Consider the phase space approach, and generalize the energy, momentum, angular momentum, and virial equations to the case of time varying conditions.

The energy equation (127) becomes (see, e.g., Rossi and Olbert, 1970)

$$\begin{aligned} \frac{\partial}{\partial t} \left[\frac{1}{2} \rho(1) \mathbf{v}^2(1) + \varepsilon_T(1) + \varepsilon_{em}(1) \right] & \quad (147) \\ & + \operatorname{div} [c^2 \mathbf{g}(1) + \mathbf{s}(1)] \\ & = \mathbf{E}_1 \times \mathbf{j}_1 + \rho(1) \mathbf{g} \times \mathbf{v}(1) \\ & + \sum \mathbf{f} \times \mathbf{v}(1) \end{aligned}$$

where $\varepsilon_{em}(1)$ is the e.m. energy density associated with the electric and magnetic fields \mathbf{e}_1 and \mathbf{b}_1 produced by \mathbf{j}_1 , defined in (28). A corresponding integral must be added on the left hand side of (131), (140) and (141). When the

³¹ For completeness sake, also "simpler" models have sometimes been proposed. For instance, Bryunelli and Pudokin (1966) use a model in terms of two \mathbf{j} -loops. One \mathbf{j} -loop is supposed to represent the Earth's \mathbf{B} , and it is assumed to be steady in time. The other \mathbf{j} -loop is the ring current that, during a storm,

progressively intensifies vs. time. However, this kind of "simple" model is of no direct concern for the present discussion.

volume of integration is constant in time, the time derivation can be commuted with the integration.

The momentum equation (30) becomes

$$\frac{\partial}{\partial t} \left[\mathbf{g}^i(1) + \frac{\mathbf{s}^i(1)}{c^2} \right] + \frac{\partial}{\partial x^j} [p^{ij}(1) - t^{ij}(1)] \quad (148)$$

$$= (\mathbf{J}_1 \wedge \mathbf{B}_1)^i + \sum \mathbf{f}^i + \rho(1) \mathbf{g}^i$$

The corresponding integral of the time varying term extended over a suitable volume must be subtracted on the right hand side in equations (114), (115), (116), (117), (118) and similar equations, (120) and (122). The integration can be commuted with time derivation when the integration volume is constant in time.

$$\mathfrak{A} = \frac{\partial}{\partial t} \int_V \mathbf{r} \wedge \left[\mathbf{g}(1) + \frac{\mathbf{s}(1)}{c^2} \right] d\tau \quad (151)$$

$$= \frac{\partial}{\partial t} \left\{ \frac{1}{2} \int_V \text{div} \left[r^2 \left(\mathbf{g}(1) + \frac{\mathbf{s}(1)}{c^2} \right) \right] d\tau - \frac{1}{2} \int_V r^2 \text{div} \left[\mathbf{g}(1) + \frac{\mathbf{s}(1)}{c^2} \right] d\tau \right\}$$

\mathfrak{A} is the virial of the system. When V is a huge sphere of solar wind that contains the magnetosphere - and such that over its surface the solar wind parameters are constant - it can be shown, by (139) and (142), that the first integral on

$$-\frac{1}{2} \int_V r^2 \text{div} \left[\mathbf{g}(1) + \frac{\mathbf{s}(1)}{c^2} \right] d\tau \quad (152)$$

$$= \frac{1}{2} \frac{\partial^2}{\partial t^2} \int_V r^2 \frac{1}{c^2} \left[\frac{1}{2} \rho(1) \mathbf{v}^2(1) + \varepsilon_T(1) + \varepsilon_{em}(1) \right] d\tau$$

$$- \frac{1}{2} \frac{\partial}{\partial t} \int_V r^2 \frac{1}{c^2} \left[\mathbf{E}_1 \times \mathbf{j}_1 + \rho(1) \mathbf{g} \times \mathbf{v}(1) + \sum \mathbf{f} \times \mathbf{v}(1) \right] d\tau$$

and the first integral on the right hand side of (152) can be interpreted in terms of the moment of inertia of the system of particles that cause \mathbf{j}_1 in (28)

$$\mathfrak{I}_{ik} = \int_V x_i x_k \frac{1}{c^2} \left[\frac{1}{2} \rho(1) \mathbf{v}^2(1) + \varepsilon_T(1) + \varepsilon_{em}(1) \right] d\tau \quad (153)$$

$$\mathfrak{A} + \int_V x_i \frac{\partial}{\partial x^j} [p^{ij}(1) - t^{ij}(1)] d\tau = \int_V \left[\mathbf{r} \times \mathbf{j}_1 \wedge \mathbf{B}_1 + \sum \mathbf{r} \times \mathbf{f} + \rho(1) \mathbf{r} \times \mathbf{g} \right] d\tau \quad (154)$$

The expression

$$\mathfrak{A} = \frac{1}{2} \frac{\partial^2 \mathfrak{I}_i^i}{\partial t^2} - \frac{1}{2} \frac{\partial}{\partial t} \int_V r^2 \frac{1}{c^2} \left[\mathbf{E}_1 \times \mathbf{j}_1 + \rho(1) \mathbf{g} \times \mathbf{v}(1) + \sum \mathbf{f} \times \mathbf{v}(1) \right] d\tau \quad (155)$$

$$+ \frac{1}{2} \frac{\partial}{\partial t} \oint_S r^2 \hat{\mathbf{n}} \times \left(\mathbf{g}(1) + \frac{\mathbf{s}(1)}{c^2} \right) d\sigma$$

(where, as already mentioned, the last integral vanishes if S lies in the solar wind and the solar wind parameters can be assumed constant) must be added on the left hand side of (43), (52), (56), (58), (61), (62), (79), (89), (94) and (95) [the integration volume needed to define \mathfrak{I}_i^i and in the second addendum of (155) has to be properly and differently defined for every formula]. The addendum \mathfrak{A} must be added on the right hand side in equations (57), (59)

Concerning the angular momentum equation (124), an addendum must be added on the left hand side

$$\varepsilon_{hik} x^h \frac{\partial}{\partial t} [\mathbf{g}^i(1) + \mathbf{s}^i(1) c^2] \quad (149)$$

The corresponding volume integral to be added on the left hand side in (125) becomes (when V is constant in time)

$$\frac{\partial}{\partial t} \int_V \mathbf{r} \wedge \left[\mathbf{g}(1) + \frac{\mathbf{s}(1)}{c^2} \right] d\tau \quad (150)$$

In the virial theorem equation (36), an addendum, which is here called \mathfrak{A} , must be added on the left hand side, and it can be transformed in the following way (V is supposed constant in time)

the right hand side of (151) vanishes. The second integral, by (147), is

while the second integral in (152) can be interpreted as 1/2 the time derivative of the moment of inertia associated with the relativistic mass density, equivalent to the power spent by the external forces over the system. Finally, (36) is transformed into

$$\mathfrak{A} + \int_V x_i \frac{\partial}{\partial x^j} [p^{ij}(1) - t^{ij}(1)] d\tau = \int_V \left[\mathbf{r} \times \mathbf{j}_1 \wedge \mathbf{B}_1 + \sum \mathbf{r} \times \mathbf{f} + \rho(1) \mathbf{r} \times \mathbf{g} \right] d\tau \quad (154)$$

$$\mathfrak{A} = \frac{1}{2} \frac{\partial^2 \mathfrak{I}_i^i}{\partial t^2} - \frac{1}{2} \frac{\partial}{\partial t} \int_V r^2 \frac{1}{c^2} \left[\mathbf{E}_1 \times \mathbf{j}_1 + \rho(1) \mathbf{g} \times \mathbf{v}(1) + \sum \mathbf{f} \times \mathbf{v}(1) \right] d\tau \quad (155)$$

$$+ \frac{1}{2} \frac{\partial}{\partial t} \oint_S r^2 \hat{\mathbf{n}} \times \left(\mathbf{g}(1) + \frac{\mathbf{s}(1)}{c^2} \right) d\sigma$$

and (91); $\mathfrak{A}/2$ must be added on the right hand side of (63). In contrast, (92) and (93) are remarkably independent of \mathfrak{A} (but this does not mean that they are constant in time). Consider therefore explicitly

$$\mathfrak{A} + \mathfrak{S}(\mathbf{B}) = 2\mathfrak{K} + U_s(\mathbf{B}) + \mathfrak{D} + \mathfrak{E} \quad (156)$$

where, as we have shown, $\mathfrak{K}, U_s(\mathbf{B}), \mathfrak{S}(\mathbf{B}) > 0$, and $\mathfrak{D}, \mathfrak{E} < 0$, hence

$$\mathfrak{A} = [2\mathfrak{K} + U_s(\mathbf{B})] - [-\mathfrak{D} - \mathfrak{E} + \mathfrak{S}(\mathbf{B})] \quad (157)$$

where each square bracket is positive. Consider the case [as it is for (56)] that in (126) it is $\mathbf{E}_1 = 0$ and write (155) in the form

$$\mathfrak{A} = \frac{1}{2} \frac{\partial}{\partial t} \left\{ \frac{\partial}{\partial t} \mathfrak{S}_i^i - \int_V r^2 \left[\varrho(1) \mathbf{g} \times \mathbf{v}(1) + \sum \mathbf{f} \times \mathbf{v}(1) \right] d\tau + \oint_S r^2 \hat{\mathbf{n}} \times \left(\mathbf{g}(1) + \frac{\mathbf{s}(1)}{c^2} \right) d\sigma \right\} \quad (158)$$

Let us consider a plasma that is entirely contained inside a finite region of space. Assume that V contains this whole region. If the plasma is in equilibrium, by (157) [and (55)] it is

$$\mathfrak{A} = 2\mathfrak{K} + U_s(\mathbf{B}) - [-\mathfrak{D} - \mathfrak{S}] \equiv 0 \quad (159)$$

that is, the gravity and the holonomic constraint terms are essential in order to keep the plasma at equilibrium. This is a different way of stating the *Chandrasekhar-Fermi theorem* (Chandrasekhar and Fermi, 1953).

Suppose that the plasma is not in equilibrium, but it is contracting. In (158) it is, by definition, $(\partial/\partial t) \mathfrak{S}_i^i < 0$. We can safely assume also that $\mathbf{g} \times \mathbf{v}(1) > 0$ and $\sum \mathbf{f} \times \mathbf{v}(1) > 0$, because gravity and holonomic constraints are generally pointed towards the origin, where the source of the gravity field is located. The third addendum in curl brackets can also be supposed negative for a contracting plasma, because we can expect a contraction both of the momentum flow vector and of the Poynting vector. The virial A is still defined by (159), but it is no more $\mathfrak{A} = 0$. Hence, when $\mathfrak{A} > 0$, the negative bracket in (158) increases in value. Therefore, either it tends to some limiting asymptotic value, i.e., toward an equilibrium state, or it should change sign, and by some finite time lag it should become positive. However, a positive bracket in (158) means, in general, an expanding plasma. That is, in general, if $\mathfrak{A} > 0$ the plasma has to be expected to expand, and if $\mathfrak{A} < 0$ (as it occurs in the case of a collapsing star) the plasma has to be expected to contract.

As a conclusion, from (157) it follows that the plasma expands or contracts, respectively, when

$$2\mathfrak{K} + U_s(\mathbf{B}) > \quad \text{or} \quad < \mathfrak{S}(\mathbf{B}) - \mathfrak{D} - \mathfrak{S} \quad (160)$$

and, at equilibrium, $\mathfrak{S}(\mathbf{B})$, \mathfrak{D} and \mathfrak{S} are the external forces necessary to contain the plasma inside a limited region of space.

The larger are the energies \mathfrak{K} and $U_s(\mathbf{B})$ contained in V , the larger must be $|\mathfrak{D}|$, $|\mathfrak{S}|$ and/or $|\mathfrak{S}(\mathbf{B})|$ in order to contain them.

Moreover, let us suppose to switch off these external forces and to leave the plasma free to expand. Let us separate $\mathbf{B} = \mathbf{B}_1 + \mathbf{B}_2$ (\mathbf{B}_1 and \mathbf{B}_2 arbitrary). Owing to the principle of magnetic energy variation (see section 1), the potential energy $-U_j(\mathbf{B}_1, \mathbf{B}_2)$ decreases by $-\Delta U$, the kinetic plus thermal energy \mathfrak{K} increases by ΔU , and the self-energies $U_s(\mathbf{B}_1)$ and $U_s(\mathbf{B}_2)$ decrease, each one, by $U_s(\mathbf{B}_1)$, and

$$\Delta[2\mathfrak{K} + U_s(\mathbf{B})] = +\Delta U \quad (161)$$

or, which is the same, when we switch on again the external forces, the right hand side of (160) must be larger than it was before plasma expansion, or, which is the same, in general, we can state (even though not in a strictly proper

sense) that the external forces must be stronger after the plasma expansion (and the stronger they must be, the farther the plasma has expanded).

Actually, we can rigorously state that the right hand side in (160) must be larger, and in general (but not always) the larger $-\mathfrak{D}$, the stronger $\sum \mathbf{f}$ should be, etc. Then, if at a given time instant \mathfrak{D} and \mathfrak{S} are not sufficient to contain the plasma, it is unlikely that they are sufficient to contain it at any later time. An equivalent statement is that the farther the plasma has expanded, the lower is its potential energy. Similar consideration can be applied to every other expression that contains \mathfrak{A} .

Let us consider the case that also the surfaces, which define the different subdomains, change in time, i.e., consider how to deal with moving surfaces. The most obvious example is the displacement of the magnetopause under the influence of solar wind fluctuations. This theoretical approach leads to evaluate the solar wind power. Two possible methods can be envisaged.

The first method is to consider equations for time varying conditions with varying integration volumes V . Call $\vec{\mathfrak{V}}$ the velocity field of the surface S that envelopes V .

Hence, $\vec{\mathfrak{V}}$ is defined only over S . During a time lag Δt , the volume V changes by

$$\Delta V = \int_V \vec{\mathfrak{V}} \times \hat{\mathbf{n}} d\sigma \Delta t \quad d\tau \quad (162)$$

In general, we deal with expressions of the kind (where \mathfrak{C} is any arbitrary function or vector)

$$\int_V \frac{\partial}{\partial t} \mathfrak{C}(x, y, z) d\tau \quad (163)$$

$$= \frac{\partial}{\partial t} \int_V \mathfrak{C}(x, y, z) d\tau - \lim_{\Delta t \rightarrow 0} \frac{1}{\Delta t} \int_{\Delta V} \mathfrak{C}(x, y, z)$$

When \mathfrak{C} is a vector $\vec{\mathfrak{C}}(x, y, z)$, the first term on the right hand side of (163) is the time derivative of the total resultant of all vectors $\vec{\mathfrak{C}}(x, y, z)$ that are applied to V . The second term can be expressed in the following form

$$\lim_{\Delta t \rightarrow 0} \frac{1}{\Delta t} \int_{\Delta V} \vec{\mathfrak{C}}(x, y, z) d\tau \quad (164)$$

$$= \int_{S(t)} \vec{\mathfrak{C}}(x, y, z) (\vec{\mathfrak{V}} \times \hat{\mathbf{n}}) d\tau$$

where $S(t)$ is the position of S at time t . That is, (164) can be interpreted as the volume integral of $\vec{\mathfrak{C}}(x, y, z)$ over the volume (let us still call it ΔV) which is spanned by $S(t)$ during a unit time interval.

When $\mathfrak{C}(x, y, z)$ is a scalar quantity, if $\mathfrak{C}(x, y, z) = \text{div } \vec{\mathfrak{C}}_1(x, y, z)$, the second term on the right hand side of (163) can be rewritten as

$$\begin{aligned} & \lim_{\Delta t \rightarrow 0} \frac{1}{\Delta t} \int_{\Delta V} \mathfrak{C}(x, y, z) d\tau \\ &= \lim_{\Delta t \rightarrow 0} \frac{1}{\Delta t} \left\{ \int_{S(t+\Delta t)} \hat{n} \times \vec{\mathfrak{C}}_1(x, y, z) d\sigma - \int_{S(t)} \hat{n} \times \vec{\mathfrak{C}}_1(x, y, z) d\sigma \right\} \\ &= \int_{S(t)} \{ \text{div } \vec{\mathfrak{C}}_1(x, y, z) \} (\vec{\mathfrak{B}} \times \hat{n}) d\sigma \\ &= \int_{V(t)} \text{div} \{ [\text{div } \vec{\mathfrak{C}}_1(x, y, z)] \times \vec{\mathfrak{B}} \} d\tau \\ &= \int_{V(t)} \{ \text{grad div } \vec{\mathfrak{C}}_1(x, y, z) \times \vec{\mathfrak{B}} + \text{div } \vec{\mathfrak{C}}_1(x, y, z) \text{div } \vec{\mathfrak{B}} \} d\tau \\ &= \int_{V(t)} \{ \text{curl curl } \vec{\mathfrak{C}}_1(x, y, z) \times \vec{\mathfrak{B}} + \Delta_2 \vec{\mathfrak{C}}_1(x, y, z) \times \vec{\mathfrak{B}} \\ &+ \text{div } \vec{\mathfrak{C}}_1(x, y, z) \text{div } \vec{\mathfrak{B}} \} d\tau = \text{etc.} \end{aligned} \tag{165}$$

where $V(t)$ is the volume V at time t .

In the energy equation it is [by (147)]

$$\mathfrak{C}(x, y, z) = \frac{1}{2} \varrho(1) \mathbf{v}^2(1) + \varepsilon_r(1) + \varepsilon_{em}(1) \tag{166}$$

and the limit in (163) is the energy content inside the volume ΔV spanned by $S(t)$ in a unit time interval.

In the momentum equation, it is

$$\vec{\mathfrak{C}}(x, y, z) = \mathbf{g}(1) + \frac{\mathbf{s}(1)}{c^2} \tag{167}$$

$$\lim_{\Delta t \rightarrow 0} \frac{1}{\Delta t} \int_{\Delta V} \mathbf{r} \times \left[\mathbf{g}(1) + \frac{\mathbf{s}(1)}{c^2} \right] d\tau$$

$$\begin{aligned} &= \frac{1}{2} \oint_{S(t)} \text{div} \left[\mathbf{r}^2 \left(\mathbf{g}(1) + \frac{\mathbf{s}(1)}{c^2} \right) \right] (\vec{\mathfrak{B}} \times \hat{n}) d\sigma + \frac{1}{2} \lim_{\Delta t \rightarrow 0} \frac{1}{\Delta t} \frac{\partial \mathfrak{S}_i^i(\Delta V)}{\partial t} \\ &- \frac{1}{2} \lim_{\Delta t \rightarrow 0} \frac{1}{\Delta t} \int_{\Delta V} \frac{\mathbf{r}^2}{c^2} \left[\mathbf{E}_1 \times \mathbf{j}_1 + \varrho(1) \mathbf{g} \times \mathbf{v}(1) + \sum \mathbf{f} \times \mathbf{v}(1) \right] d\tau \end{aligned}$$

The first term on the right hand side of (169) can be transformed into

$$\begin{aligned} & \frac{1}{2} \oint_{S(t)} \text{div} \left[\mathbf{r}^2 \left(\mathbf{g}(1) + \frac{\mathbf{s}(1)}{c^2} \right) \right] (\vec{\mathfrak{B}} \times \hat{n}) d\sigma \\ &= \oint_{S(t)} \mathbf{r} \times \left[\mathbf{g}(1) + \frac{\mathbf{s}(1)}{c^2} \right] (\vec{\mathfrak{B}} \times \hat{n}) d\sigma + \frac{1}{2} \oint_{S(t)} \mathbf{r}^2 \text{div} \left(\mathbf{g}(1) + \frac{\mathbf{s}(1)}{c^2} \right) (\vec{\mathfrak{B}} \times \hat{n}) d\sigma \end{aligned} \tag{170}$$

Moreover, owing to the continuity equation, it is [in the non-relativistic approximation and assuming $\text{div } \mathbf{q}^*(1) = 0$]

$$\text{div } \mathbf{g}(1) = - \frac{\partial \varrho(1)}{\partial t} \tag{171}$$

Finally, the last addendum in (170), by taking into account (132), can be transformed into

(164) applies and it represents the total content of momentum flow vector and of Poynting vector within ΔV .

In the angular momentum equation, it is

$$\vec{\mathfrak{C}}(x, y, z) = \mathbf{r} \wedge \left[\mathbf{g}(1) + \frac{\mathbf{s}(1)}{c^2} \right] \tag{168}$$

and (164) applies.

In the virial theorem equation, the first term on the right hand side of (163) is what has been called \mathfrak{A} , i.e., (155). The second term in (163) becomes [by (151), (152), (153), and (165)]

$$\tag{169}$$

$$\begin{aligned} & \frac{1}{2} \oint_{S(t)} \mathbf{r}^2 \left[\frac{\partial \varrho(1)}{\partial t} + \frac{\varepsilon_{em}(1) + \mathbf{e}_1 \times \mathbf{j}_1}{c^2} \right] (\vec{\mathfrak{B}} \\ & \times \hat{n}) d\sigma \end{aligned} \tag{172}$$

The resulting total expression is somewhat intricate that must be added on the left hand side of the virial (36). Every term can be interpreted in terms of virial, moment of inertia, energies, etc. These lengthy expressions are useless until a specific choice of $S(t)$ and $\vec{\mathfrak{B}}$ has been made.

A second method of approach is: (i) to consider any differential equation for time varying conditions (i.e., momentum, energy, angular momentum, virial, or any other moment of the density function in phase space); (ii) to consider some smooth extrapolation to all space of the $\vec{\mathfrak{B}}$ function, which had been defined only over S (with the only condition that the extrapolated function coincides, over S , with the original function); and (iii) to multiply (scalar or vector product) both sides of the differential equation by any function of $\vec{\mathfrak{B}}$ (and, eventually, also of other variables).

$$\int_{V_{magnp}^*} \mathfrak{B}_i \frac{\partial}{\partial t} \left[g^i(1) + \frac{s^i(1)}{c^2} \right] d\tau + \int_{V_{magnp}^*} \mathfrak{B}_i \frac{\partial}{\partial x^j} [p^{ij}(1) - t^{ij}(1)] d\tau \tag{173}$$

$$= \int_{V_{magnp}^*} \mathfrak{B}_i \left[(\mathbf{J}_1 \wedge \mathbf{B}_1)^i + \sum f^i + \varrho(1) g^i \right] d\tau$$

The second term on the left hand side of (173) can be transformed into

$$\int_{V_{magnp}^*} \mathfrak{B}_i \frac{\partial}{\partial x^j} [p^{ij}(1) - t^{ij}(1)] d\tau \tag{174}$$

$$= \oint_{S_{Magnp}^*} \mathfrak{B}_i \hat{n}_j [p^{ij}(1) - t^{ij}(1)] d\sigma - \int_{V_{magnp}^*} [p^{ij}(1) - t^{ij}(1)] \frac{\partial \mathfrak{B}_i}{\partial x^j} d\tau$$

where S_{Magnp}^* is the surface that encloses V_{magnp}^* , which is formed [according to the treatment of (94)] by a surface immediately outside the magnetopause (S_{sc}^*) and by a surface immediately inside it ($S_{sc1||e}^*$) (see figure 13).

Let us consider only one example. We want to get the general, not approximate, expression equivalent to the Siscoe (1970) treatment by means of the virial equation - which was already mentioned in section 5.2 - of the solar wind power defined as $\oint_{S_{sc}} \mathbf{p}_c \times \vec{\mathfrak{B}} d\sigma$.

Let us consider the momentum equation (148), apply a scalar product with with \mathfrak{B} , and integrate over V_{magnp}^* (that can change in time)

The first addendum in (174) can be transformed, by (31), (32) and (33), into

$$\oint_{S_{Magnp}^*} \mathfrak{B}_i \hat{n}_j [p^{ij}(1) - t^{ij}(1)] d\sigma \tag{175}$$

$$= \oint_{S_{Magnp}^*} \mathfrak{B}_i \hat{n}_j \left\{ \tilde{\mathfrak{p}}_{\perp}(1) \delta^{ij} + [\tilde{\mathfrak{p}}_{\parallel}(1) - \tilde{\mathfrak{p}}_{\perp}(1)] \frac{B_i B_j}{B^2} + \varrho(1) v_i(1) v_j(1) \right.$$

$$+ \left. \frac{1}{8\pi K_0 \mu_r} [b^2(1) \delta^{ij} - 2 b^i(1) b^j(1)] \right\} d\sigma$$

$$= \oint_{S_{Magnp}^*} \left\{ (\vec{\mathfrak{B}} \times \hat{\mathbf{n}}) \left[\tilde{\mathfrak{p}}_{\perp}(1) + \frac{b^2(1)}{8\pi K_0 \mu_r} \right] + \frac{(\vec{\mathfrak{B}} \times \mathbf{B})(\hat{\mathbf{n}} \times \mathbf{B})}{B^2} [\tilde{\mathfrak{p}}_{\parallel}(1) - \tilde{\mathfrak{p}}_{\perp}(1)] \right.$$

$$+ \left. \varrho(1) (\vec{\mathfrak{B}} \times \mathbf{v}_1) (\hat{\mathbf{n}} \times \mathbf{v}_1) - \frac{1}{8\pi K_0 \mu_r} (\vec{\mathfrak{B}} \times \mathbf{b}_1) (\hat{\mathbf{n}} \times \mathbf{b}_1) \right\} d\sigma$$

Let us separate the integration surface S_{magnp}^* and distinguish its two contributions S_{sc}^* and $S_{sc1||e}^*$. Assume that $\mathbf{B}_{int} = 0$ in the interplanetary environment, and that,

close to the magnetopause, just inside it, the space is void of particles [moreover, let $\mathbf{b}_1 = \mathbf{B}$ inside (28)], thus (175) becomes (note also that in this case it is $\mathbf{B} \times \hat{\mathbf{n}} = 0$)

$$\oint_{S_{Magnp}^*} \dots d\sigma = \oint_{S_{sc}^* - S_{sc1||e}^*} \dots d\sigma \tag{176}$$

$$= \oint_{S_{sc}^*} [(\vec{\mathfrak{B}} \times \hat{\mathbf{n}}) \tilde{\mathfrak{p}}_{\perp} + \varrho(1) (\vec{\mathfrak{B}} \times \hat{\mathbf{v}}) (\hat{\mathbf{n}} \times \hat{\mathbf{v}})] d\sigma - \oint_{S_{sc1||e}^*} (\vec{\mathfrak{B}} \times \hat{\mathbf{n}}) \frac{B^2}{8\pi K_0 \mu_r} d\sigma$$

where the first term on the right hand side is the scalar product of $\vec{\mathfrak{B}}$ with the “thermal-like” pressure in the solar wind ($\hat{\mathbf{n}} \tilde{\mathfrak{p}}_{\perp}$), the second term [analogously to (94)] is the

scalar product of $\vec{\mathfrak{B}}$ with the dynamic pressure, and the third term is minus the scalar product of $\vec{\mathfrak{B}}$ with the internal magnetic pressure. Hereafter, let us assume that V_{magnp}^*

collapses, in a limit process, to a vanishing thickness. In analogy with Siscoe (1970), let us call solar wind power

$$\begin{aligned}
 SWP &= \oint_{S_{sc}^*} \mathfrak{B}_i \hat{n}_j [p^{ij}(1) - t^{ij}(1)] d\sigma \\
 &= \oint_{S_{sc1||e}^*} \mathfrak{B}_i \hat{n}_j [p^{ij}(1) - t^{ij}(1)] d\sigma \\
 &\quad + \int_{V_{magnp}^*} [p^{ij}(1) - t^{ij}(1)] \frac{\partial \mathfrak{B}_i}{\partial x^j} d\tau - \int_{V_{magnp}^*} \mathfrak{B}_i \frac{\partial}{\partial t} \left[g^i(1) + \frac{s^i(1)}{c^2} \right] d\tau \\
 &\quad + \int_{V_{magnp}^*} \mathfrak{B}_i \left[(\mathbf{J}_1 \wedge \mathbf{B}_1)^i + \sum \mathbf{f}^i + \varrho(1) g^i \right] d\tau
 \end{aligned} \tag{177}$$

The first term on the right hand side of (177) is the power spent against the internal pressure. The second term is connected to the strain/torsional properties of the interaction between $\vec{\mathfrak{B}}$ and $p^{ij}(1)$ and $t^{ij}(1)$. The third term is connected to the rate of change of the total momentum density inside V_{magnp}^* . The fourth term is the power spent by $\vec{\mathfrak{B}}$ against the “external” forces. These terms could be further transformed and discussed in detail, term by term.

Let us just mention the limit when the thickness of V_{magnp}^* vanishes. The time derivative of the total momentum density integral is concerned with changes in the structure of the magnetopause. As far as the term is concerned that deals with the external forces, when $\mathbf{B}_1 = 0$ [in (28)] and since the $\sum \mathbf{f}$ do not apply on the magnetopause, this term reduces to the power spent against the gravitational field. When $\vec{\mathfrak{B}}$ is constant, also the *grad* $\vec{\mathfrak{B}}$ (strain/torsional) term vanishes. The remaining expressions (i.e., integrals over S_{sc}^* or $S_{sc1||e}^*$ that, in the limit, coincide) can be further separated in dynamic, \mathfrak{P}_\perp and \mathfrak{P}_\parallel and magnetic pressure terms, as it is done by Siscoe (1970) (although according to his approximations).

Recall that k_{sc}^* [see (87)] is the total kinetic plus thermal energy of all particles inside S_{sc}^* (i.e., including k_{magnp}^*), and call $\varepsilon_{em}(V_{sc}^*)$ the total e.m. energy inside V_{sc}^* . As it has been here previously assumed, neglect \mathbf{E} and assume

$$\varepsilon_{em}(V_{sc}^*) \cong U_s(\mathbf{B}, V_{sc}^*) \tag{178}$$

The total energy inside V_{sc}^* is therefore

$$k_{sc}^* + U_s(\mathbf{B}, V_{sc}^*) \tag{179}$$

Since V_{magnp}^* (either with vanishing thickness or not) completely envelops all other parts (defined in figure 11), which are internal to the magnetopause, and since every energy change inside the magnetosphere must be supplied by the solar wind, every change of (179) must cross through V_{magnp}^* . Owing to the meaning of every addendum in (177), it is concluded that

$$\begin{aligned}
 SWP &= \oint_{S_{sc}^*} \mathfrak{B}_i \hat{n}_j [p^{ij}(1) - t^{ij}(1)] d\sigma \\
 &= \frac{d}{dt} [k_{sc}^* + U_s(\mathbf{B}, V_{sc}^*)]
 \end{aligned} \tag{180}$$

(SWP) the integral over S_{sc}^* , and insert it into (174), then into (173), and get

which is the generalized expression of formula (43) in Siscoe (1970).

Additional relations can be obtained by means of (89), but these developments are not here considered in detail.

In summary, in the present section the formal time-varying terms have been included into the formulas derived in section 5.2 that applied to steady state conditions. Compared to the steady state equations, the corresponding relationships deal with a larger number of terms, and are practically less useful for experimental application. Nevertheless, they are useful to enlighten the formal role in the entire theory of gravity and holonomic constraints in order to keep the M , tc and io \mathbf{j} -systems inside their respective regions of space. The entire physical rationale is much better outlined in section 7.

As far as the formal treatment is concerned that deals with arbitrary moving surfaces, no relevant result can be obtained on a very general basis. However, some concept, such as the solar wind power (SWP) that is spent while modifying the geometry of the magnetosphere and its structure, can be treated in full generality (this item was formerly introduced by Siscoe, 1970 under much more restricting hypotheses). These relationships can be applied to the time varying magnetosphere, but, at present, it is difficult to foresee the real practical usefulness of these time varying formulas from the viewpoint of a numerical application to experimental data. See some results reviewed in section 9.

7. The minimum potential energy of the magnetosphere

The formation of the neutral sheet, and the concept of “reconnection”, have been physically and briefly introduced in sections 1 and 2. Similarly, the earthward termination of the neutral sheet - and the Jupiter’s magnetodisk - have been explained in section 3 by means of the same physical rationale. Let us reconsider these same items according to the more complicated formal approach of sections 5.1 through 6.

When dealing with time-varying conditions, a distinction had to be made between quasi-steady state and “step-like” variations. In reality, every natural phenomenon is never “step-like”. Rather, it simply looks “step-like”

when the monitoring time resolution is not sufficiently detailed. Even an e.m. signal takes a physical time-lag to justify e.m. forces. The time-lag is not known for the gravitational interaction, and this is a great concern of present theoretical physics. Refer to Gregori et al. (2025w) and references therein.

A “quasi-steady state” variation occurs whenever one can suppose that equilibrium conditions are approximately attained at every intermediate instant of time. This definition is usually related to the specific kind of formulation that is adopted - and, in general, for every given formulation an upper limit for frequencies is usually specified, while for higher frequencies one must rely on a different approach.

In general, quasi-steady variations are not a frequent occurrence in the magnetosphere, because abrupt and very rapid changes in the solar wind affect the microstructure of the magnetopause. The effect is a change of the topology of the general \mathbf{B} , through “merging” or “reconnection” of \mathbf{B} field-lines, occurring either across the magnetopause or across the neutral sheet.

In the final analysis, this is a matter of application of the continuity approximation, by which the solar wind flow is supposed to occur according to *MHD*, which fundamentally relies on the continuity abstraction. In contrast, the real physical picture must be in terms of discrete particles (see, e.g., Willis, 1971 and 1972, or Gregori et al., 2025w, and references therein). That is, one must introduce the concept of “merging” or “reconnection” in order to keep the *MHD* formalism, even though - according to Maxwell’s laws - this concept *per se* is just absurd. Differently stated, “merging” or “reconnection” are an aspect of a mathematical concern, as they are raised when one wants to treat a physical system, which is composed of discrete particles, by means of an algorithm that refers to the continuity abstraction. Therefore, this item is of direct concern for books or reviews dealing with *MHD*, while it is not directly related to the fundamental physical discussion of the present study.

A conspicuous amount of studies have been concerned - and are still presently discussed - about the so-called microstructure of the magnetopause and/or “reconnection” phenomena. This kind of studies are not here considered, and the interested reader must refer to an extensive literature. We give here only a brief reminder of a few general properties that can be suitable for some aspects of the present discussion.

Let us briefly recall the concepts of *Alfvén’s layer* and *Dessler’s vacuum merging*.

An Alfvén’s layer occurs whenever two almost parallel layers occur, which are close to each other, each one with an electric charge of opposite sign to the other (Alfvén, 1968). For instance, in a region of space where the magnetic energy density is overwhelming, positive ions and electrons have different gyration radii, hence a separation occurs in space, generating distinct regions of positive and negative charge. Alfvén’s layers, synonymous of electric double

layers, are explicitly considered while dealing with the earthward termination of the neutral sheet (section 3). In addition, *Alfvén’s layers* are the logical key of the electrostatic hypothesis for the sunspot cycle (see section 1). The same mechanism was also hypothesized, e.g., for the magnetopause, although the magnetic energy density and the kinetic pressure of solar wind particles are, in that region of space, comparable to each other, and no overwhelming \mathbf{B} can be envisaged (see section 2).

The Dessler “*vacuum merging*” was formerly proposed by Dessler (1968) and later applied by Dessler (1971). The term “vacuum” reminds about the need to refer to regions characterized by a plasma pressure that is insufficient for keeping separated points with oppositely directed \mathbf{B} . That is, the concept is the same as in the case of a lack of particle supply, such as it occurs in the case of a “plasma cavity” in the solar wind. In the final analysis, from a strictly physical viewpoint, both concepts of “*vacuum merging*” and of “*reconnection*” refer to local differential features, independent of the behavior of the whole integral pattern of the physical system of concern, which is rather the viewpoint implied by every variational principle.

These concepts are therefore almost synonymous of “reconnection”, which can be eventually triggered by any phenomenon by which the particle supply has a gap (i.e., a “plasma cavity”). Differently stated, a particle gap is interpreted like a “step-like” phenomenon, as the primary composition of the physical system is changed, thus causing an inconsistency with the continuity abstraction. However, no smooth, although “fast”, transition occurs of any physical process, rather, just a change of physical system. That is, both the system before, and the system after, the “event” refer to objectively different and non-comparable objects. Therefore, *per se* no physical law can justify such a “transition”, as in fact no “transition” occurred.

One additional general remark is that particles are accelerated by “reconnection” of \mathbf{B} field-lines, and that \mathbf{B} energy is transformed into kinetic energy. This holds for every kind of plasma instability, as this is a simple consequence of the energy balance and of the formal algorithm that is used, which relies on the continuity abstraction (see, e.g., Hasegawa, 1971, 1975). Subsequently, the particle kinetic energy can be eventually back-transformed into \mathbf{B} energy, and this can occur in every suitable region of space. The balance between the two amounts of kinetic energy – which are produced and later back-transformed - affects the potential energy or of thermal and/or kinetic energy density of the system, etc.

Note that a false appearance of “reconnection” can be produced anywhere by a very rapid and true physical transition, whenever the system is monitored with an insufficient time resolution. This occurs, e.g., due to a violent Cowling dynamo, whenever a large thermal gradient is sufficient to generate an almost “impulsive” convective motion that supplies a dynamo effect - where “impulsive” means that the transformation happens during a time lag shorter than what can be detected by the available

monitoring device. However, in general, such a very rapid occurrence is rare inside a plasma of very low density; hence, in such a case, the aforementioned “plasma cavity” scenario is more realistic.

In any case, we must consider every given system in its whole integrity, while local “infinitesimal” phenomena are a prerequisite of “continuous” differential equations, which are *per se* inconsistent with the corpuscular nature of every electric current \mathbf{j} . That is, we must distinguish between every skillful *MHD* treatment, which in the final analysis mainly tackles a mathematical problem, and the objective physics in natural reality.

Refer to the “*principle of magnetic energy variation*” (see section 1). For the present purpose, according to the formalism of sections 5.2 and 6, the best suited form is by looking for maximum $U_j(\mathbf{B}_M, \mathbf{b})$. Different expressions have been proposed for $U_j(\mathbf{B}_M, \mathbf{b})$, i.e., (23), (27), (59), (63), (91), (92), (96) and several expressions similar to (91) and (92). The best suited expression is maybe (27). Concerning other forms, just note that (23) and (96) imply to maximize

$$U_j(\mathbf{B}_M, \mathbf{b}) = \mathbf{M} \times b(0) = -M b_z(0) \quad (181)$$

that means that $b_z(0)$ should be minimum (in relative value).

As far as (59), (63), (91), (92), and similar expressions are concerned, (59) and (63) seem to be of little help. Indeed, from (63) it is concluded that $2k_M + U_s(\mathbf{B}_M)$ should be minimum. However, at the same time, $v_M + \mathcal{G}(V_M)$ should be minimum, and this last expression in general must be negative, otherwise, as shown in sections 5.2 and 6, the M system cannot be constrained inside a limited volume of space. In reality, these four terms are not independent of one another. Owing to the same reason, the relations (91), (92) and similar ones, which contain a surface integral, are of little help, as they rely on several interdependent addenda.

The form (27) seems to be the most useful expression. Refer to the definition of \mathcal{Q} given by (25). As far as the *ns* (for neutral sheet) and *magnp* addenda are concerned, the separation has been here used, which indeed is more symbolic than formal,

$$I_{sc} \Phi_{sc}(\mathbf{B}) = I_{ns} \Phi_{ns}(\mathbf{B}) + I_{magnp} \Phi_{magnp}(B_{\perp}) \quad (182)$$

Note that, while considering $I_{sc} \Phi_{sc}(\mathbf{B})$, one is concerned with the whole set of all possible flux tubes of the actual total \mathbf{B} . Separate these flux tubes into smaller tubes. One set of these tubes goes across the neutral sheet and contributes with a term that is symbolically indicated by $I_{ns} \Phi_{ns}(\mathbf{B})$. The flux tubes of another subset merge with \mathbf{B}_{int} across the magnetopause, thus becoming part of \mathbf{B}_{int} flux tubes. This subset contributes with the term that is symbolically indicated with $I_{magnp} \Phi_{magnp}(B_{\perp})$. Therefore, every given \mathbf{j} -loop, which is part of the very intricate *sc* \mathbf{j} -system, can contribute several times, either to the *ns* contribution, or to the *magnp* contribution, or to both

of them, or it contributes every time when reference is made to every “elementary” \mathbf{B} flux tube.

Consider (27) and a huge box in the solar wind that contains the whole magnetosphere. In section 5.2 it has been shown that, when the huge solar wind box tends to include all space, according to the assumptions here used, both \mathcal{Q} and $U_s(\mathbf{b})$ tend to infinity. On the other hand, by (23) and (58) it is known that $U_j(\mathbf{B}_M, \mathbf{b})$ remains finite. The \mathcal{Q} addendum in (25) that tends to infinity [to compensate the infinite limit of $U_s(\mathbf{b})$ in (27)] is the *magnp* term, as shown in detail here below. Concerning $U_s(\mathbf{b})$, owing to the “*principle of magnetic energy variation*”, whenever equilibrium has not yet been reached, all joint energies tend to increase, and all self-energies tend to decrease.

These statements hold in the “quasi-steady” approximation. It is thus concluded (i) that $U_s(\mathbf{b})$ must be minimum, and this is well suited also for (27), and (ii) that at equilibrium \mathcal{Q} must be maximum.

The \mathcal{Q} contribution to $U_j(\mathbf{B}_M, \mathbf{b})$ takes into account “reconnection” across the neutral sheet and/or the magnetopause. This can be considered from *two different viewpoints*.

One viewpoint is consistent with the aforementioned case history of a “quasi-steady” phenomenon.

The *other viewpoint* deals with a formal treatment of an abrupt change in the solar wind. For instance, let us think about an abrupt decrease in solar wind conductivity σ . This causes, in general and locally, \mathbf{B} “reconnection” and particle acceleration. Let us describe this event in terms of a step function, and let us consider the total magnetic energy of the system before and after the step.

A step-like phenomenon must be considered as a local occurrence. However, it is possible to investigate whether the system is shifted - by the step - towards a state of lower total magnetic energy, or not. If the total magnetic energy is lower, we can presume that the process is somewhat favored by the system. If the total magnetic energy is increased by the step, it is likely that the system will try to avoid it - as far as possible - and to oppose the trend toward a higher energy, although the phenomenon is *per se* compulsory and forced by the solar wind. Indeed, this is the rationale of the “squeezing” of the plasmashet that supplies the earthward particle flux during the recovery phase of a magnetospheric substorm (see section 3). Consider, however, that this statement holds only as long as the assumption is accepted about the real physical significance of a “step-like” phenomenon.

The meaning of every term that enters in the definition in (25) can be highlighted as follows.

$$I_{ns} \Phi_{ns}(\mathbf{B})$$

According to the sign rule, this term is positive, as the I_{ns} loops are clockwise (as seen from the Earth) in the southern lobe of the tail, and counterclockwise in its northern lobe. In addition, the larger this term is, the longer the neutral sheet, and also the tail. According to the first

aforementioned view point, maximize $U_j(\mathbf{B}_M, \mathbf{b})$ and conclude that the neutral sheet expands as far as possible both earthward and downstream. Thus, also the tail must be as long as possible, compatibly with \mathbf{B} flux conservation.

Equivalently, one can also state that the larger is the “reconnection” across the neutral sheet, the shorter is the tail due to \mathbf{B} flux conservation in the tail. Thus, the lower $I_{ns} \Phi_{ns}(\mathbf{B})$, the lower $U_j(\mathbf{B}_M, \mathbf{b})$ is, and the higher the potential energy of the magnetosphere. Hence, there must be as less “reconnection” as possible across the neutral sheet. Equivalently, one can also state that the solar wind is injected inside the neutral sheet across the tail, in order to link as much \mathbf{B} flux as possible.

Consider the second aforementioned viewpoint. Consider one additional new “reconnection” of a \mathbf{B} flux tube across the neutral sheet. Suppose that, in all other regions of space, the state of the whole magnetosphere is unaffected by the “reconnection” of this additional \mathbf{B} flux tube.

Note, however, that this approximate argument can lead to a wrong conclusion. In fact, it is $\Delta U_s(\mathbf{B}_M) \cong 0$, $\Delta \Omega = \Delta[(1/2) I_{ns} \Phi_{ns}(\mathbf{B})] < 0$, and, by (23) and (27), $\Delta U_j(\mathbf{B}_M, \mathbf{b}) = 2\Delta \Omega - 2\Delta U_s(\mathbf{b}) = 0$. This implies that $\Delta U_s(\mathbf{b}) = \Delta \Omega$. Hence, $\Delta[U_s(\mathbf{B}_M) + U_j(\mathbf{B}_M, \mathbf{b}) + U_s(\mathbf{b})] = \Delta \Omega < 0$, which is a wrong conclusion, as it is known on the basis of the rigorous argument based on the first aforementioned viewpoint.

Therefore, it is incorrect to assume that the entire magnetosphere is unaffected by the “reconnection” of the \mathbf{B} flux tube across the neutral sheet.

Nevertheless, even with these approximations, the second viewpoint can lead to a correct result, if it is claimed that the “reconnection” of just one \mathbf{B} flux tube across the neutral sheet is equivalent to a collapse of that \mathbf{B} flux tube into a \mathbf{B} flux tube having a smaller flux. Indeed, in section 6, it was shown that the collapse of orbits and/or \mathbf{B} field-lines is, in general, equivalent to the collapse of whole plasma. In addition, a collapsed plasma has a higher potential energy. Hence, we can conclude that, in general, “reconnection” across the neutral sheet increases the potential energy.

However, note that this last conclusion, which holds only in general, is less compulsory than the inference implied by the first viewpoint.

$$I_{magnp} \Phi_{magnp}(\mathbf{B})$$

Let us call “loop 2” the set of all \mathbf{j} -currents that flow in the solar wind, magnetosphere, ionosphere and telluric currents (i.e., *sc*, *VA*, *io*, and *tc*), and let us call “loop 1” the Earth’s core, i.e., the M \mathbf{j} -currents that originate the internal origin geomagnetic field. Consider the form $U_j = I_1 \Phi(\mathbf{B}_2)$. It is concerned with the \mathbf{B} flux that reaches the Earth’s core, notwithstanding the screening by the Earth’s crust and mantle. This \mathbf{B} flux cannot vanish, due to a strict physical requirement of the action-reaction principle.³²

Consider a \mathbf{B}_2 flux tube that leaves the Sun and crosses through interplanetary space. Whenever a merging occurs across the magnetopause, this \mathbf{B}_2 flux tube links the I_1 currents in the Earth’s core - and the sign rule is always such that U_j is increased. Then, whenever this is possible by any kind of process, “merging” must occur.

From the second viewpoint, let us consider a step-phenomenon that leads to “reconnection”, across the magnetopause, of a \mathbf{B} flux tube that was formerly “reconnected” across the neutral sheet. Such a \mathbf{B} flux tube crosses through interplanetary space before closing on the opposite polar cap. This is equivalent to expand, abruptly, i.e., by a step-like process, a closed \mathbf{B} flux tube, eventually up to “infinity”. Since it has been here shown that in general this is equivalent to expand the plasma, it is inferred that the potential energy is decreased.

This is equivalent to the statement of classical electromagnetism that all \mathbf{j} -loops - and hence also their \mathbf{B} flux tubes (see, e.g., Bruhat, 1963) - tend to expand in space as much as possible.

It can therefore be concluded that as much “reconnection” as possible should occur across the magnetopause, because by this, in general, the potential energy of the magnetosphere is lowered. In the ultimate analysis, this is the detail of the argument behind the right panel of figure 3.

On the other hand, owing to the conceptual limitation of step-like phenomena, the physical system can lack the time to reach the ideal final condition of maximum \mathbf{B} “merging”. Owing to this reason, a limited occurrence of “merging” can be justified. Nevertheless, the most important inference is that, whenever any local phenomenon on the magnetopause can favor the occurrence of “reconnection”, “reconnection” must occur.

This agrees with the experimental evidence associated - in general, though not always - with the effects of the North to South flip of the vertical component of \mathbf{B}_{int} . This is related to the so-

³² An obvious objection is that the Earth’s mantle and lithosphere screens the Earth’s core from e.m. signal originated from the solar wind. In reality, the Earth has the structure with several sea-urchin spikes, which act like antennæ that ensure an

efficient e.m. connection with the external inducing signals. See, e.g., Gregori (2002) and Gregori and Leybourne (2021), and references therein.

cellaed “*open model*” of the magnetosphere, mentioned in section 4, by which it has become frequent and customary in the literature to assume (erroneously) that \mathbf{B}_{int} is perpendicular to the ecliptic plane - contrary to every observational evidence that \mathbf{B}_{int} lies in the ecliptic plane, apart at most a scatter of very few degrees. In fact, a slight change of the vertical component of \mathbf{B}_{int} causes a gentle change of the amount of “reconnection” across the magnetopause. This implies some observed effects, although in any case the correlation coefficient is always insignificantly low, between flip of the vertical component of \mathbf{B}_{int} and any given observed effect.

$I_{VA} \Phi_{VA}(\mathbf{B})$

Refer to (100). The larger (100), the larger k_{VA} and $U_s(\mathbf{b}_{VA})$, as it had to be intuitively expected. That is, the larger the kinetic and thermal energy of trapped particles, and the larger the self-energy of their \mathbf{B} , the lower the potential energy is of the magnetosphere. That is, the more the radiation belts are filled up, the lower the potential energy is of the magnetosphere.

Note that this is the physical justification of the plasmasphere. That is, as it is well known, the radiation belts are replenished by trapped particles as much as possible, compatibly with the temporarily available particle flux in the environment.

$I_{io} \Phi_{io}(\mathbf{B})$ and $I_{tc} \Phi_{tc}(\mathbf{B})$

These terms are quite similar, because two roughly spherical shells were assumed, even though - according to the present model - no other, even qualitative, pattern can be envisaged for them. Moreover, owing to the actual resistivity of the ionosphere and of the Earth’s mantle, in the case of a strictly steady state, Joule heat should quickly quench every \mathbf{j} . On the other hand, the observed temporal variations (e.g., even Sq) almost steadily induce new io and tc currents.

The energy, which is transformed into Joule heat, is taken from the selfenergy of the solar wind and of the M system. The self-energy of the M \mathbf{j} -system can be restored, in principle, by time variations in the solar wind of opposite sign, although this can occur only for very low frequency, due to the screening by the tc system. This low frequency constraint, however, is less compulsory than it ought to be expected, due to the

role played by the sea-urchin spikes that act like effective antennæ (see Gregori, 2002, and Gregori and Leybourne, 2021, and references therein) that ensure an excellent e.m. coupling between solar wind and deep Earth. In fact, the phenomenon occurs through the mechanism of the TD dynamo performance (see section 5.1).

In any case, consider some average condition. A reasonable guess is to assume that the induced currents (either in the ionosphere or in the Earth’s crust and mantle) should reflect the general trend of nature to decrease the potential energy of the system or, equivalently, to increase the magnetic joint energy. In fact, in the opposite case, these currents \mathbf{j} should not be triggered at all.

Thus, it can be concluded that the larger the number is of the free charges that are available to supply such a kind of \mathbf{j} -currents, the higher their positive contribution should be to \mathcal{Q} in order to lower as much as possible the potential energy of the magnetosphere.

As already stressed, the major drawback of this model is the incapability to give a model for air-earth currents that, in some way, are a cause of damping of the \mathbf{j} -currents below and above Earth’s surface.

Energy relationships can be formally considered also inside an Alfvén layer. Magnetospheric Alfvén’s layers were envisaged and supposed to be located either in the neutral sheet (Dessler, 1971), or at the magnetopause (Alfvén, 1968), or at the earthward termination of the plasmashet (Schield et al., 1969).³³

As far as the neutral sheet and the magnetopause case histories are considered, no remark is needed in addition to what has already been stressed above. The solar wind is continuously renewed due to the solar corona expansion. Thus, “reconnection” across the magnetopause and/or the neutral sheet is just the result of the continuous attempt by the magnetosphere to reach an equilibrium configuration. However, equilibrium is never attained, because the solar wind continuously flows and renews itself.³⁴

Some comments are needed about the earthward termination of the plasmashet. Consider that the direction of \mathbf{B} inside - and its direction outside - an Alfvén’s layer can or cannot be parallel to each other. In addition, while referring to the region downstream with respect to the layer, we can either suppose that the magnetic energy density is larger, or smaller, than the kinetic energy density. Wherever the magnetic energy density is larger, there is no reason to consider “reconnection” because \mathbf{B} dominates particle

³³ It is curious that no author applied this same concept to the Sun, and thus nobody envisaged the electrostatic hypothesis of the sunspot cycle (see section 1).

³⁴ In any case, upon considering a lengthy critical discussion of the fundamentals of physics (Gregori et al., 2025w), all natural

phenomena are a steady search for equilibrium that is never attained. Therefore, the never reached equilibrium of the solar wind flow is the correct occurrence, not an exceptional property.

motion both inside and outside the layer. In this case, we can hardly liken this pattern (i.e., the neutral sheet) to an Alfvén's layer. In contrast, wherever the magnetic energy density is lower than the kinetic energy density, magnetic properties are dominated by particle dynamics, and particles drive \mathbf{B} flux tubes. In this case, the argument is identical as for the magnetopause.

The result is a balance between the kinetic energy density of the particles, which flow earthward in the plasmashet, opposite to the internal pressure or magnetic energy density, etc. As long as the magnetic energy density is larger than the kinetic energy density, particles spiral along pre-existing \mathbf{B} field-lines. In this way, particles increase either the flux of quasi-trapped radiation, or the particle population inside the plasmosphere.

Whenever the kinetic energy density is larger than the magnetic energy density, plasmashet particles blow earthward the embedded \mathbf{B} field. Locally, the physical system is changed due to the input of a previously non-existing large number of particles. Hence, previously "reconnected" \mathbf{B} field-lines are "broken" and opened, compared to the previous (approximately) dipolar geomagnetic field-lines.

The result is a practical "stretching" of geomagnetic field-lines, and an increase of \mathbf{B} flux through both lobes of the tail. This is the same as to state that there is, locally, more availability of solar wind particles to be injected into the geomagnetic flux tubes, so that the neutral sheet can be further extended earthward.

Differently stated, there is a great similarity between the interaction (i) at the magnetopause and (ii) at the earthward termination of the neutral sheet, although the two phenomena are usually described in a different way. The magnetopause is usually explained in terms of a dynamically dominated solar wind flow, and by means of an *MHD* pressure balance. Viceversa, the same phenomenon which occurs at the earthward termination of the plasmashet is more commonly interpreted in terms of particles that spiral along approximately fixed \mathbf{B} field patterns. As already mentioned, the two view points are complementary to each other and, as a rule, they are equally wrong wherever, like in an Alfvén's layer, the two energy densities (magnetic and kinetic) are comparable to each other.

As far as the end of the tail is concerned, the tail must be as long as possible, in order to minimize the potential

energy of the magnetosphere. The end of the tail is controlled by instant \mathbf{B} "reconnection" across both neutral sheet and/or magnetopause. Owing to the fluctuations in the microstructure of the solar wind - including its transient micro-"plasma cavities" - the end of the tail will always result to be very far from any averaged and quiet condition. Or the tail has a filamentary structure, similar to Type I comet tails, and this feature has been observed experimentally since a long time (e.g., Mariani³⁵ and Ness,³⁶ 1969). Cometary tails, conceived like cometary magnetospheres (or "cometospheres") are specifically discussed in Gregori and Leybourne (2025m).

8. Energy contents, stresses and torques in magnetospheric subvolumes

The present section is concerned, first of all, with the evaluation of the hypothetical total energy of the geomagnetic field in the case that the solar wind had never been switched on, or - in the opposite case - when the solar wind would be hypothetically switched off. The next item is the experimental evaluation of $U_j(\mathbf{B}_M, \mathbf{b})$ and of its time derivative. Therefore, the concern is about the \mathbf{j} -currents of the Earth's core, including $U_s(\mathbf{B}_M)$ extended over all space, i.e., by avoiding to exclude any volume that envelops the dipole singularity (i.e., the so-called "characteristic" singularity at $\mathbf{r} = 0$ of Laplace' equation, see Courant and Hilbert, 1953) as it is usually done (e.g., by Verosub and Cox, 1971).

Independent of any choice of some specific model for the deep Earth's \mathbf{j} -currents, it is possible - on the basis of ground based geomagnetic data alone - to compute³⁷ the following quantities, except a constant factor C (or, equivalently, apart the arbitrary choice of I_M): (i) the self-inductance of the \mathbf{M} loop; (ii) its equivalent surface, which links the total \mathbf{b} flux, and (iii) the geometrical factor expressed by the ratio B_0/I_M , where, as already mentioned, B_0 is the intensity of \mathbf{B} at the equator at Earth's surface.

The same mathematical formalism is also applied to compute $U_s(\mathbf{b})$. In principle, its value is finite even though *a priori* it might even be $U_s(\mathbf{b}) \rightarrow \infty$, as it is shown section 5.2. However, $U_s(\mathbf{b})$ must be finite, as it is shown upon considering the energy of the real interaction between solar wind and geomagnetic field that, owing to physical requirements, involves only a limited portion of the

be changed of the treatment that is given in the present computations. In fact, the present treatment was implemented when the Gauss' working hypothesis seemed reasonably correct. On the other hand, the observational information about air-earth currents is still insufficient for improving the "simple" scheme that is here envisaged. In addition, the exploitation of the evaluations - which are here envisaged on the basis of actual observations - can be an indirect way the check the quantitative relevance of air-earth currents in the energy balance of geomagnetic phenomena.

³⁵ Franco Mariani (1927-), Italian physicist.

³⁶ Norman Frederick Ness (1933-2023), American geophysicist.

³⁷ This holds, however, only upon assuming the air-earth currents can be neglected. This is the standard and well assessed assumption dating back to Gauss. However, at present, we know that this formerly "reasonable" assumption is challenged by the huge e.m. effects associated with strong soil exhalation in tectonically active regions as inferred, e.g., by the Quinn's inversion analysis of 6 months of records by the magnetic satellite *CHAMP* (see Quinn et al., 2025). When this fundamental effect is taken into account, several details must

infinitely extended solar wind.³⁸ An eventual finite value obtained for $U_s(\mathbf{b})$ corresponds to this fact. On the other hand, it is impossible to guess the size of the volume that encloses the magnetosphere and that contains only this portion of solar wind.

The final step is the generalization of the same method for estimating the selfenergy of the tc \mathbf{j} -currents induced into crust and mantle and of all associated joint-energies U_j .

It is thus possible to get a complete picture of all self-energies U_s and joint energies U_j in the magnetosphere, with the only exception of the separation between ionospheric, trapped particle, and plasmashet's particles that precipitate on the ionosphere, because we lack any physical information capable to separate and distinguish their respective \mathbf{B} contribution. This completes the picture that can be inferred according to the discussion carried out in section 5.2.

It is also possible, by means of this same formalism, to evaluate the influence on the astronomical motion of the Earth caused by the e.m. interaction with the solar wind. This important and much complicated and multi-faceted item requires an extensive discussion that is outside the perspective of the present paper.

In any case, we assume that the electric field \mathbf{E} is negligible all over the Earth's surface. When suitable approximations are assumed, It is here shown how to evaluate the total force and relative torque that acts on the Earth. This ought to be carried out at least at three time instants, i.e., before an eventual perturbation occurring on the solar wind flow, at the time of maximum effect, and after its recovery.

The role of Joule heat is neglected - and its role should require an extensive discussion that cannot be here given..

8.1 - The geomagnetic field in absence of solar wind

Call $U_s(\mathbf{B}_{M\infty})$ the self-energy of the geomagnetic (dipole) field when, according to a hypothetical "Gedankenexperiment", the solar wind is at infinity. Then, progressively move the solar wind until its real location, apply the "principle of magnetic energy variation" (see section 1), and get

$$U_s(\mathbf{B}_{M\infty}) = U_s(\mathbf{B}_M) + U_j(\mathbf{B}_M, \mathbf{b}) \quad (183)$$

that can be evaluated experimentally, as it will be here shown. Moreover, substitute for $U_j(\mathbf{B}_M, \mathbf{b})$ any expression among (23), (27), (59), (63), (92), or (96), or any other expression obtained by combining (27), (63) and (91). The substitution of (23) or (96) is equivalent to insert the experimental value for $U_j(\mathbf{B}_M, \mathbf{b})$ (see below). The substitution with (63) gives

$$U_s(\mathbf{B}_{M\infty}) = \frac{1}{2} [U_s(\mathbf{B}_M) - 2 k_M - \varrho_M - \mathfrak{G}(V_M)] \quad (184)$$

where (i) k_M is the kinetic plus thermal energy of the particles that are responsible for the M \mathbf{j} -system; (ii) ϱ_M is related to the holonomic constraints that act on them; and (iii) \mathfrak{G} is the gravitational energy inside their volume V_M . If $[\varrho_M + \mathfrak{G}]$ is neglected, it is concluded that the intensity of the dipole of the Earth has been increased by the e.m. induction by the solar wind.

By (108) it also follows

$$U_s(\mathbf{B}_{M\infty}) = U_j(\mathbf{B}_M, \mathbf{b}) \left[1 - \frac{f(a, R)}{b_z(0)/B_0} \right] \quad (185)$$

The definition of the geometrical factor $f(a, R)$ is given in (108), where a is the Earth radius, and R is the radius of the M \mathbf{j} -circuit. Equivalently, as far as the magnetostatic formalism is concerned, it is [by (106), (108) and (110)]

$$\begin{aligned} \frac{|M_\infty|}{|M|} &= \frac{I_{M\infty}}{I_M} = \sqrt{\frac{U_s(\mathbf{B}_{M\infty})}{U_s(\mathbf{B}_M)}} \\ &= \sqrt{1 + \frac{U_j(\mathbf{B}_{M\infty}, \mathbf{b})}{U_s(\mathbf{B}_M)}} \\ &= \sqrt{1 - \frac{1}{f(a, R)} \frac{b_z(0)}{B_0}} \end{aligned} \quad (186)$$

that can also be evaluated experimentally on the basis of f and DPS ratio.

8.2 - $U_j(\mathbf{B}_M, \mathbf{b})$ and its time derivative

The joint-energy $U_j(\mathbf{B}_M, \mathbf{b})$ and its time derivative can be evaluated experimentally. $U_j(\mathbf{B}_M, \mathbf{b})$ can be computed in the dipolar approximation by means either of (23) or of (96), or, in the most general case, by standard *SHEs* of the geomagnetic potential (details are classical and cannot be here reported).

Owing to (146), its time derivative $\dot{U}_j(\mathbf{B}_M, \mathbf{b})$ can differ from zero only on the time scale of several decades (at least), i.e., let us say on the secular scale. Therefore, there is need to know the *SV* of both the internal origin Gauss elements of terrestrial magnetism, and also of $\mathbf{b}(0)$, i.e., of *Sq*.

Let us suppose that these data are available, hence also reliable estimates are available of $U_j(\mathbf{B}_M, \mathbf{b})$ and of $\dot{U}_j(\mathbf{B}_M, \mathbf{b})$. Note that (23), (96), or the standard classical formulas, are valid even for quasi-static time variations, as it can be shown by considering the way by which (105) has been derived. Moreover, note that, according to section A.6, it follows that

$$\dot{U}_j(\mathbf{B}_M, \mathbf{b}) = -\dot{U}_s(\mathbf{B}_M) = -\dot{U}_s(\mathbf{b}) \quad (187)$$

Consider expressions for $U_j(\mathbf{B}_M, \mathbf{b})$ other than (23) or (96). By (27), owing to the same reasons as for (23) and (96), it is

³⁸ In fact, the e.m. interaction is formally extended up to infinity, although this is a consequence of the continuity approximation. If the interaction is explained through photons

etc. the volume of the interaction is necessarily finite. The concept is analogous to the discussion on the meaning of "monad". See Gregori et al. (2025w).

$$\dot{\mathcal{Q}} = -\frac{1}{2} \dot{U}_j(\mathbf{B}_M, \mathbf{b}) \quad (188)$$

By (59) it is found, upon taking into account (187)

$$\frac{d}{dt} [\mathcal{S}(\mathbf{B}) - 2\mathcal{K} - \mathcal{G} - \mathcal{D}] = -\dot{U}_j \quad (189)$$

and by (63)

$$\frac{d}{dt} [2k_M + \sigma_M + \mathcal{S}(V_M)] = -\dot{U}_j \quad (190)$$

Similar expressions can be inferred by means of (91), (92) and (93). Finally, insert into (180) the expression (89) for $U_s(\mathbf{B}, V_{sc}^*)$, then insert (93), take into account (188) and (63), and get

$$\dot{U}_j = \frac{d}{dt} k_{sc}^* - SWP - \frac{d}{dt} U_s(\mathbf{B}, V_{sc}^*) \quad (191)$$

that is remarkably simple, even simpler than the more approximate expression used by Siscoe (1970) for his formula (46). Note that (191) can be more simply derived also from (180) and (187).

8.3 - The Earth's core

Reconsider (107) and write it, more properly, by means of Laplace' law in terms of \mathbf{j} density distribution, and by giving to B_0 the meaning of its average along the equator over all geomagnetic longitudes φ

$$B_0 = \frac{1}{2\pi} \int_0^{2\pi} d\varphi \int_{V_\infty} \frac{\mathbf{j}_M \wedge \mathbf{r}}{r^2} d\tau = I_M f_2 \quad (192)$$

Apply the average theorem in integration, and find the same expression as (107), which corresponds to the case of a single loop with a current I_M inside it.

Let us reconsider (108), where L is the self-inductance of the circuit. This can be considered to be derived from $U_s(\mathbf{B}_M) = (1/2) \int_{V_\infty} \mathbf{j}_M \times \mathbf{A}_M d\tau$, where \mathbf{A}_M is the vector potential for \mathbf{B}_M , which derives from the solution of Poisson's equation³⁹ (according to the approach in terms of the magnetostatics formalism). Thus, if the entire \mathbf{j} -distribution is multiplied by a constant, then \mathbf{A}_M increases also by the same factor, and $U_s(\mathbf{B}_M)$ by the square of this factor. However, in general, very little is known about the real \mathbf{j} -distribution in the Earth's core, and it is therefore reasonable to deal with (108) as a proper expression, where I_M is defined in (192), and where L is assumed to be independent of time. Differently stated, the geometry of the circuit is assumed constant, at least on a time scale smaller compared to the geological time range.

Insert L into (108), as it is derived from (192)

$$U_s(\mathbf{B}_M) = \frac{1}{2} \frac{L}{f_2^2} B_0^2 \quad (193)$$

This expression can be derived with respect to time, and written [by (187); let us skip the argument of U_j]

$$\frac{1}{2} \frac{L}{f_2^2} = -\frac{\dot{U}_j}{\frac{d}{dt} B_0^2} \quad (194)$$

Finally, insert (194) into (193) and get

$$U_s(\mathbf{B}_M) = \frac{\dot{U}_j}{\frac{d}{dt} \ln \frac{1}{B_0^2}} \quad (195)$$

which is rigorous, because (192) is rigorous.

Let us skip the hypothesis of time-invariance of f_2 and L . It can be shown that, at least in principle, it is possible to check experimentally their constancy in time. Indeed, there are sound reasons to believe that the internal structure of the Earth experiences relevant changes in time. Therefore, derive (193) with respect to time, take into account the "principle of magnetic energy variation" (see section 1), and get

$$-\dot{U}_j = \frac{d}{dt} \left[\frac{1}{2} \frac{L}{f_2^2} B_0^2 \right] \quad (196)$$

then, integrate (196) and find out

$$U_j = -\frac{1}{2} \frac{L}{f_2^2} B_0^2 + A \quad (197)$$

where A is a strictly constant and unknown quantity (such a statement holds in both cases, either that L/f_2^2 is constant in time or not). In contrast, U_j and B_0^2 are experimentally known, and also their time variation, while the form factor of the Earth L/f_2^2 is unknown, whether it is constant or a function of time.

In the case that it is a constant, (197) is the equation of a straight line in the (\hat{x}, \hat{y}) plane, where $x \equiv B_0^2$ and $y \equiv U_j$. Suppose that several measurements of U_j and B_0^2 are available, referring to different time instants. Plot them in the (\hat{x}, \hat{y}) plane. As long as they look aligned along a straight line, it is possible to get a least square estimate of both $-(1/2)(L/f_2^2)$ and A . The value of $-(1/2)(L/f_2^2)$ should coincide with the value of (194).

If they do not appear significantly aligned, fit them by assuming the following expression for the form factor

$$-\frac{1}{2} \frac{L}{f_2^2} = \xi_0 + \xi_1 t + \xi_2 t^2 + \dots \quad (198)$$

and find out, by the least square method, the constants ξ_0 , ξ_1 , ξ_2 , etc.

From a practical point of view, if the Earth's radius a did not change significantly in time (Hoppers and Van Andel, 1970; but a long devoted discussion should be needed that cannot be here given) it is easy to estimate

$$B_0 = \frac{M}{a^3} \quad (199)$$

as a function of time, on the basis of the known SV of M (see Merrill et al., 1996 and references therein). However, since the SV of $\mathbf{b}(0)$ is poorly known, this analysis is not straightforward.

In any case, it is possible to investigate the present trend of variation of the Earth's core structure, even though it is very unlikely that we will ever get information on the $\mathbf{b}(0)$ trend on the geological time scale.⁴⁰ Note also that the entire

³⁹ Baron Siméon Denis Poisson, FRS FRSE, (1781-1840), French mathematician, engineer, and physicist.

⁴⁰ This refers to the approach discussed in the present section, while much more detailed investigations should require a long devoted discussion that cannot be here given.

previous derivation is independent of the assumption of dipolar approximation.

Let us derive the analogous, although approximate, expression by means of (105) that, owing to (17), should be written (where \mathbf{a} is the vector potential of \mathbf{b})

$$U_j(\mathbf{B}_M, \mathbf{b}) = \int_{V_\infty} \mathbf{j}_M \times \mathbf{a} \, d\tau \quad (200)$$

Let us take off the integration sign, and refer to some mean current I^* (let us choose $I^* = I_M$) such that the remaining integral equals $1/I^*$ times the U_j value given according to the standard classical formalism of geomagnetism (not here shown in detail). Let us assume that the classical $\{g, h\}$ and $\{\alpha, \beta\}$ coefficients of geomagnetism, and I_M , all change in time, but g/I_M and h/I_M are constant in time, where $\{g, h\}$ are the Gauss elements of terrestrial magnetism, and $\{\alpha, \beta\}$ are the analogous coefficients for the SHE of \mathbf{b} .

All this is formally correct. Only the time independence of g/I_M and h/I_M must be explicitly assumed. In any case, since it is here shown how to evaluate I_M and its time derivative, it is possible to check, *a posteriori*, the self-consistency of the approximations that are introduced in the framework of any tentative formal model of the currents \mathbf{j} in the Earth's core.

There is need to state that every expression for U_j - which is expressed according to the standard classical formalism of geomagnetism - can be substituted by an expression with a single term, which is formally identical to the case of a pure dipole. Then (200) can be written like (105). In this case insert I_M - as obtained from (105) - into (108) and get the following relation [let us skip the argument of b_z , like in (193) and in subsequent formula]

$$U_s(\mathbf{B}_M) \cong \frac{1}{2} \frac{L}{f_1^2} \frac{U_j^2}{b_z^2} \quad (201)$$

where f_1 is a geometrical factor.

In the case that the form factor $(1/2)(L/f_1^2)$ is constant in time, it is possible to carry out the time derivative of (201). Then, take into account the "principle of magnetic energy variation" (as above), and find

$$\frac{1}{2} \frac{L}{f_1^2} = - \frac{\dot{U}_j}{\frac{d}{dt} \frac{U_j^2}{b_z^2}} \quad (202)$$

$$U_s(\mathbf{B}_M) = \frac{\dot{U}_j}{\frac{d}{dt} \ln \frac{b_z^2}{U_j^2}} \quad (203)$$

In case that the form factor is not constant in time, by (201) and by the "principle of magnetic energy variation", it is found

$$-\dot{U}_j \cong \frac{d}{dt} \left[\frac{1}{2} \frac{L}{f_1^2} \frac{U_j^2}{b_z^2} \right] \quad (204)$$

and, upon integration,

$$U_j \cong - \frac{1}{2} \frac{L}{f_1^2} \frac{U_j^2}{b_z^2} + A^* \quad (205)$$

Analogously to the previous procedure, plot the experimental values on a (\hat{x}, \hat{y}) plot, being $x \equiv U_j^2/b_z^2$ and

$y \equiv U_j$. If a straight line is found, the form factor $[-(1/2)(L/f_1^2)]$ is time invariant. In the opposite case, call

$$- \frac{1}{2} \frac{L}{f_1^2} = \xi_0^* + \xi_1^* t + \xi_2^* t^2 + \dots \quad (206)$$

A third derivation is obtained by inserting for I_M , into (108), once the value obtained by (107) and once that one obtained by (105), thus finding

$$U_s(\mathbf{B}_M) \cong - \frac{L}{2 f_1 f_2} U_j \frac{B_0}{b_z} = -f \frac{U_j}{D} \quad (207)$$

where

$$D = \frac{b_z}{B_0} \quad (208)$$

is the DPS ratio and

$$f = \frac{L}{2 f_1 f_2} \quad (209)$$

is a new form factor.

Assume that f is time invariant, carry out the time derivative of (207), take into account the "principle of magnetic energy variation", and get

$$f \cong \frac{\dot{U}_j}{\frac{d}{dt} \frac{U_j}{D}} \quad (210)$$

$$U_s(\mathbf{B}_M) \cong \frac{\dot{U}_j}{\frac{d}{dt} \ln \frac{D}{U_j}} \quad (211)$$

In case that f changes with time, by (207) and by the "principle of magnetic energy variation", it is found

$$-\dot{U}_j \cong - \frac{d}{dt} \left[f \frac{U_j}{D} \right] \quad (212)$$

and, upon integration,

$$U_j \cong -f \frac{U_j}{D} - A^{**} \quad (213)$$

Let us use an (\hat{x}, \hat{y}) plot with $x \equiv U_j/D$ and $y \equiv U_j$. When the plotted points appear aligned along a straight line, f is time invariant. In the opposite case, call

$$f \cong \xi_0^{**} + \xi_1^{**} t + \xi_2^{**} t^2 + \dots \quad (214)$$

etc. Note that the strictly constant quantities A , A^* , and A^{**} should satisfy the following equalities

$$A \cong A^* \cong A^{**} \quad (215)$$

because their definition and sign was chosen in such a way that

$$U_s(\mathbf{B}_M) = -U_j + \begin{cases} A \\ \text{or } A^* \\ \text{or } A^{**} \end{cases} \quad (216)$$

The procedure can be clearly generalized by defining additional form factors, everyone being associated with some quantity that can be measured experimentally (i.e., analogous to our treatment for B_0 , b_z , D , and U_j).

The eventual discrepancy between (203) or (211) and (195) is indicative of the reliability of the dipolar approximation used to derive (202) and (108).

If we accept the approximate description in terms of a single current loop with current I_M (or even in terms of several \mathbf{j} -loops but with the same current intensity I_M flowing inside them), it is possible to evaluate, on experimental basis, I_M , f_1 , f_2 and L , apart a unique

arbitrary constant C . In fact, insert (105) and (108) into (187), and get

$$f_2 f \frac{d}{dt} I_M^2 \cong \frac{d}{dt} (I_M b_z) \quad (217)$$

that can be integrated. Then, one should substitute (192) to give

$$I_M \cong \frac{C}{f B_0 - b_z} \quad (218)$$

where C is an arbitrary constant. Finally, f_1 is obtained directly by (105), L by (202), and f_2 by (194).

The constant C cannot be determined, because the available experimental information deals with products such as $[I_M f_1]$, $[I_M f_2]$, and $[L I_M^2]$ that are independent of C . Equivalently, we can state that we vary the geometrical dimension of the \mathbf{j} -loop and change correspondingly the intensity of I_M while leaving unchanged energies and the observed \mathbf{B} .⁴¹

The constant C can, however, be evaluated as explained in detail in Gregori (2002), according to a method that can be briefly summarized as follows. If the internal origin \mathbf{B} is represented by a spherical shell (ss) of arbitrary radius, the energy is finite only if this radius is larger than an asymptotic value, which results - as a matter of observational evidence - close to the ICB (inner core boundary) determined by seismological evidence. Hence, if the seismic radius is taken for granted, one can guess a reasonable value for the total energy, hence for C . That is, we feed into the aforementioned computation the additional observational evidence of seismology.⁴²

Moreover, independent of all these real physical implications, the previous formulas are consistent with the general treatment made in the preceding sections, dealing with magnetospheric energy contents and relationships. Therefore, their numerical evaluation is necessary in order to evaluate several other energetic processes in the magnetosphere.

Consider (216). It means that $U_s(\mathbf{B}_M)$ and U_j change by opposite amounts, consistently with the “*principle of magnetic energy variation*”, while A or A^* or A^{**} (hereafter briefly called A) remains constant in time. The “*principle of magnetic energy variation*” deals with e.m. induction process between two sets of \mathbf{j} -loops. The A contribution refers to every other source of \mathbf{B} that cannot be associated with simple e.m. induction.

Since $U_s(\mathbf{B}_M)$ and U_j can be quantitatively evaluated from observations, it is possible to check whether A is null or not, etc. In addition, if A is not constant in time, (198), (206) and (214) can be applied, etc. This item has some

additional implication. However, let us first note that, in principle, it is possible to carry out an experimental estimate of the aforementioned form factors of the Earth.

By (194) or (198), (202) or (206), and (18) or (214) we know experimental estimates of L/f_2^2 , L/f_1^2 , and f or $L/(f_1 f_2)$, respectively. That is, we know \sqrt{L}/f_1 and \sqrt{L}/f_2 , and we have one additional relation that can be used for a self-consistency check.

It is possible to evaluate I_M , f_1 , f_2 and L . By (214) it is

$$L = 2 f f_1 f_2 \quad (219)$$

hence, it is sufficient to compute I_M , f_1 , f_2 . From the “*principle of magnetic energy variation*” and by (105) it follows, respectively,

$$I_M f_2 = B_0 \quad (220)$$

$$I_M f_1 = -\frac{U_j}{b_z} \quad (221)$$

and by (108), after inserting (219), we get a self-consistency check for (220) and (221)

$$(I_M f_1) (I_M f_2) = \frac{U_s(\mathbf{B}_M)}{f} \quad (222)$$

Moreover, f_1 and f_2 are related by (222) [see below].

Thus, the problem is concerned only with the separation of I_M either from f_1 or from f_2 . Indeed, I_M is the result of an abstraction, i.e., of an arbitrary choice when we cut into small \mathbf{j} -loops the \mathbf{j} -distribution on the approximately ss layer of currents \mathbf{j} that flow on the ICB .⁴³ Then, I_M must be supposed to be unavoidably largely arbitrary, and f_1 and f_2 must be deduced from (220) and (221). Note that the smaller is I_M , the more intricate is the set of the aforementioned small \mathbf{j} -loops, and, as it has to be expected, the larger are f_1 and f_2 . In addition, it must be pointed out that the whole previous derivation requires no assumption on the time invariance of the form factors.

For the sake of completeness, note that a formally identical treatment can be applied to \tilde{f}_1 , \tilde{f}_2 , \tilde{f} , \tilde{L} and \tilde{I}_M , which are defined and briefly discussed at the next section 8.4(IV). But \tilde{I}_M is arbitrary; hence, it can be chosen, e.g., $\tilde{I}_M \equiv I_M$. On the other hand, there appears to be no advantage to know, e.g., the self-inductance of the magnetosphere, etc.

All these computations are feasible in principle. On the other hand, in general they request an observational database that very often is not yet available. Hence, this entire speculation remains only in the realm of an intriguing theoretical possibility.

In addition, as already stressed, the drawback must be taken into account of the relevant role played by air-earth currents that flow mainly across areas of high crucial

⁴¹ A more complete and systematic treatment is given in Gregori (2002).

⁴² For the sake of completeness, it should be mentioned that Zidarov and Petrova (1974) computed a simple model, including its secular variation (SV), in terms of a simple circular loop. They found a radius $\sim 1,500$ km. Several analogous computed models are reported in the literature, although they are not here of concern.

⁴³ This is according to the simple model here considered in terms of \mathbf{j} -loops. In reality, the IC ought to be in “magpol” state (see Gregori et al., 2025w). Hence, as far as the computation is concerned that is considered in the present section, this fact implies that the IC ought to appear to be the location of an approximately spherical body with permanent magnetization. The role of e.m. induced currents \mathbf{j} is an additional superposed time-varying effect.

fracturing, according to the evidence recently found by the late John M. Quinn (see Quinn et al., 2025). In principle, one can implement all aforementioned evaluations based on available observations, and one can thus check how far air-earth currents bias and enter into the whole previous computation of the energy balance of geomagnetic phenomena. An alternative approach can be, in principle, to exploit a theoretical derivation similar to the development that is here envisaged, while referring, however, to a geometry of \mathbf{j} -loops that is substantially other than the pattern that was here used. That is, the whole computation ought to be re-started since the beginning. However, present observations can allow for no realistic model, other than stating that some leakage \mathbf{j} -currents exist between \mathbf{j} -circuits below and above Earth's surface.

A substantially different discussion deals with the \mathbf{j} -distribution inside deep Earth, as it can be inferred upon combining the energy balance with the information derived from seismic evidence. This is the leading anthem in Gregori (2002), but this topic cannot be considered in the present paper.

Re-consider (216) and the aforementioned comment. If A is strictly constant - and if the deep Earth's structure does not change vs. time - every variation in $U_s(\mathbf{B}_M)$ must be ascribed to a corresponding variation of U_j , i.e., to a SV of the solar wind and of its e.m. induction into the Earth. In contrast, if a secular trend⁴⁴ exists in the deep Earth structure, the corresponding variation in $U_s(\mathbf{B}_M)$ causes a related variation in U_j , thus affecting the solar wind.

These phenomena can be investigated by the following mathematical treatment.

Since we are concerned with variations on a geological time scale, we can explicitly refer to the dipolar approximation (but this approximation could be easily dropped). We can suppose to know $U_s(\mathbf{B}_M)$ by (193), where the form factor is given either by (194) or by (198) [and we can suppose that ξ_0 coincides with (194)], and B_0 is given by (199). Let us insert them into (216), where also A is known, and solve with respect to b_z

$$b_z = \frac{1}{M} \left[\frac{1}{2} \frac{L}{f_2^2} \frac{M^2}{a^6} - A \right] \quad (223)$$

If a is supposed not to have significantly changed with time, by (223) we can infer the SV of b_z . Note that this one includes both the effects of e.m. induction by the solar wind and the variation of the deep Earth's structure. If we suppose that $(1/2)L/f_2^2$ is represented by ξ_0 alone [which should coincide with (194)], we should thus succeed, in principle, to distinguish the solar wind effect alone.

In reality, all these statements are tautological, because we need to know experimentally the SV of b_z in order to

estimate the form factors and A . Then, by (223), we compute again the SV of b_z .

On the other hand, (223) is useful for the following extrapolation vs. time. Suppose that the internal structure of the Earth does not change with time. Then, by means of the knowledge of the present trend of the SV of \mathbf{b} we can evaluate the form factors and A . In this way, (223) permits to estimate the SV of b_z on a much longer time lag, deriving from the knowledge of the SV of M . A similar argument applies if we suppose to know some explicit expression for the time variation of the form factor that appears in (223).

Finally, note that the secular change in $U_s(\mathbf{b})$ follows directly from (216) after applying the transformation (228). Hence, the SV of the total energy of \mathbf{B} can be expressed as

$$U_s(\mathbf{B}) = U_s(\mathbf{B}_M) + U_j(\mathbf{B}_M, \mathbf{b}) + U_s(\mathbf{b}) \quad (224)$$

$$= -U_j(\mathbf{B}_M, \mathbf{b}) + A + \tilde{A}$$

For the sake of completeness, note that if (203) or (207) are used instead of (193), the b_z formulas analogous to (223) are

$$b_z \cong \frac{1}{M} \left[\frac{1}{2} \frac{L}{f_1^2} M^2 - A^* \right] \quad (225)$$

$$b_z \cong \frac{1}{M} \left[f \frac{M^2}{a^3} - A^{**} \right] \quad (226)$$

Owing to (215), by comparing (223), (225) and (226) it is concluded

$$f_1 \cong a^3 f_2 \quad (227)$$

8.4 - $U_s(\mathbf{b})$ and the total magnetic energy of the magnetosphere

All \mathbf{j} -systems other than the $M\mathbf{j}$ -system, which deal with the geometry of the $tc + io + VA + sc\mathbf{j}$ -systems, produce \mathbf{b} , and can be formally treated in a perfectly symmetrical way as for \mathbf{B}_M .

This same formalism can therefore be applied, apart suitable changes, to the field \mathbf{b} instead than to \mathbf{B}_M . Consider $U_s(\mathbf{b})$. The entire previous treatment has been essentially concerned with the interaction of two sets of currents \mathbf{j} that flow, each one, on closed loops, i.e., the \mathbf{j} -currents of the Earth's core and the set of all other \mathbf{j} -currents. The Earth's core \mathbf{j} -currents are responsible for B_0 , the others for \mathbf{b} . In addition, the form factors f_1 , f_2 and L are relative to the Earth's core \mathbf{j} -currents.

Exchange the role of B_0 and b_z and define the analogous form factors for the second set of currents \mathbf{j} , which are called \tilde{f}_1 , \tilde{f}_2 , \tilde{f} , \tilde{L} . All previous formulas can be re-obtained by simple application of the following equivalence table

$b_z \Rightarrow B_0$	$U_s(\mathbf{B}_M) \Rightarrow U_s(\mathbf{b})$
$B_0 \Rightarrow b_z$	$\xi \Rightarrow \tilde{\xi}$
$I_M \Rightarrow \tilde{I}_M$	$\xi^* \Rightarrow \tilde{\xi}^*$
$f_1 \Rightarrow \tilde{f}_1$	$\xi^{**} \Rightarrow \tilde{\xi}^{**}$

(228)

⁴⁴ This really occurs on the secular and geological time scale, being the mechanism of the Earth's "battery". See Gregori (2002), and some mentions in Gregori and Leybourne (2021).

$$\begin{aligned} f_2 &\Rightarrow \tilde{f}_2 & A &\Rightarrow \tilde{A} \\ f &\Rightarrow \tilde{f} & A^* &\Rightarrow \tilde{A}^* \\ L &\Rightarrow \tilde{L} & A^{**} &\Rightarrow \tilde{A}^{**} \end{aligned}$$

A comment is required about the time variation of the form factors. When dealing with the \mathbf{j} -currents in the Earth's core, the concern was about the natural evolution of the deep Earth's interior, i.e., in any case about a slow process. In contrast, $\tilde{f}_1, \tilde{f}_2, \tilde{f}, \tilde{L}$ refer to \mathbf{j} -loops responsible for the external origin \mathbf{B} . Hence, we must expect that these form factors change very rapidly with time and that formulas such as (198), (206) and (214) are inadequate. On the other hand, since such a kind of magnetospheric-like phenomena are introduced in our theory only by means of $\mathbf{b}(0)$, reference is here made only to SV changes, i.e., to changes on a $\sim n \cdot 10$ years scale. Hence, the treatment here considered can be meaningful – and also (198), (206) and (214) appear therefore suited for our purposes.

As a conclusion, it is found

$$U_s(\mathbf{b}) \cong \frac{\dot{U}_j}{\frac{d}{dt} \ln \frac{1}{b_2^2(0)}} \quad (229)$$

$$U_s(\mathbf{b}) \cong \frac{\dot{U}_j}{\frac{d}{dt} \ln \frac{B_0^2}{U_j^2}} \quad (230)$$

$$U_s(\mathbf{b}) \cong \frac{\dot{U}_j}{\frac{d}{dt} \ln \frac{1}{DU_j}} \quad (231)$$

The $U_s(\mathbf{b})$ value, in general, is finite. It seems, however, impossible to envisage any criterion suited to define - inside the infinitely extended solar wind - a finite portion of it that actually interacts with the geomagnetic field. However, this finite $U_s(\mathbf{b})$ value, which directly derives from experiments, provides a finite and physical figure for such a separation.

The total magnetic energy of the physical system of the magnetosphere is given by $U_s(\mathbf{b}) + U_j(\mathbf{B}_M, \mathbf{b}) + U_s(\mathbf{B}_M)$, and it can be computed by means of the numerical values of every addendum.

8.5 - Other self- and joint energies and their respective currents and geometrical factors. Partial DPS ratios and their time derivatives

The process that was applied to $U_s(\mathbf{B}_M)$ can be generalized and applied to other \mathbf{j} -systems. Some preliminary remarks are that:

(i) $U_j(\mathbf{B}_M, \mathbf{b})$ and $U_s(\mathbf{b}_{tc})$ can be computed on the basis of the aforementioned ss \mathbf{j} -system for the tc \mathbf{j} -currents;

(ii) it is

$$\begin{aligned} U_j(\mathbf{B}_M, \mathbf{b}_{io} + \mathbf{b}_{VA} + \mathbf{b}_{sc}) \\ = U_j(\mathbf{B}_M, \mathbf{b}) - U_j(\mathbf{B}_M, \mathbf{b}_{tc}) \end{aligned} \quad (232)$$

(iii) $U_s(\mathbf{b}_{io} + \mathbf{b}_{VA} + \mathbf{b}_{sc})$ can be computed by the method that is described here below, and briefly called JS ;

(iv) it is

$$\begin{aligned} U_j(\mathbf{b}_{tc}, \mathbf{b}_{io} + \mathbf{b}_{VA} + \mathbf{b}_{sc}) \\ = U_s(\mathbf{b}) - U_s(\mathbf{b}_{tc}) \\ - U_s(\mathbf{b}_{io} + \mathbf{b}_{VA} + \mathbf{b}_{sc}) \end{aligned} \quad (233)$$

In contrast, it is impossible to separate either self- or joint-energies inside the composite system [$io + VA + sc$] unless it is possible to distinguish between \mathbf{b}_{io} , \mathbf{b}_{VA} and \mathbf{b}_{sc} .

The general method of computation - in addition to the simple aforementioned relations - can be formally applied in a way similar to the \mathbf{B}_M case. Suppose to deal with two \mathbf{j} -systems, call them h and k , and call

$$U_j(\mathbf{B}_h, \mathbf{B}_k) \cong -\tilde{f}_1 \tilde{I}_h B_k(0) \quad (234)$$

$$B_{h0} = \tilde{f}_2 \tilde{I}_h \quad (235)$$

$$U_s(\mathbf{B}_h) = \frac{1}{2} \tilde{L} \tilde{I}_h^2 \quad (236)$$

Express I_h by means either of (234) or of (235). Substitute these two expressions into (236). Take time derivatives, and get, analogously to (193), (194), (201), (202), (108) and (210)

$$U_s(\mathbf{B}_h) = \frac{1}{2} \frac{\tilde{L}}{\tilde{f}_2^2} B_{h0}^2 \quad (237)$$

$$\frac{1}{2} \frac{\tilde{L}}{\tilde{f}_2^2} = -\frac{\dot{U}_j}{\frac{d}{dt} B_{h0}^2} \quad (238)$$

$$U_s(\mathbf{B}_h) = \frac{1}{2} \frac{\tilde{L}}{\tilde{f}_1^2} \frac{U_j^2}{B_k^2(0)} \quad (239)$$

$$\frac{1}{2} \frac{\tilde{L}}{\tilde{f}_1^2} \cong -\frac{\dot{U}_j}{\frac{d}{dt} \frac{U_j^2}{B_k^2(0)}} \quad (240)$$

$$U_s(\mathbf{B}_h) \cong -\tilde{f} \frac{U_j}{\tilde{D}} \quad (241)$$

$$\tilde{f} \cong \frac{\dot{U}_j}{\frac{d}{dt} \frac{U_j}{\tilde{D}}} \quad (242)$$

where the DPS ratio is

$$\tilde{D} = \frac{B_k(0)}{B_{h0}} \quad (243)$$

When U_j is known, it is possible to evaluate (238), (240) and (242), hence also $U_s(\mathbf{B}_h)$ and $U_s(\mathbf{B}_k)$ by the same procedure as for $U_s(\mathbf{B}_M)$ and $U_s(\mathbf{b})$. This method is here called JS (acronym for "from joint- to self-energies").

In contrast, when $U_s(\mathbf{B}_M)$ is known, it is possible to compute $U_j(\mathbf{B}_h, \mathbf{B}_k)$. In fact, from (240), by (187) it is found

$$\dot{U}_s \cong -\frac{1}{2} \frac{\tilde{L}}{\tilde{f}_1^2} 2 \frac{U_j}{B_k^3(0)} [B_k(0) \dot{U}_s + \dot{B}_k(0) U_j] \quad (244)$$

and, by (239)

$$\dot{U}_s \cong -2 \frac{U_s}{U_s B_k(0)} [B_k(0) \dot{U}_s + \dot{B}_k(0) U_j] \quad (245)$$

that gives

$$U_j \cong -\frac{2 U_s B_k(0) \dot{U}_s}{\dot{U}_s B_k(0) + 2 U_s \dot{B}_k(0)} \quad (246)$$

Analogously, from (242), (241) and (187) it is easily found

$$U_j \cong - \frac{U_s \dot{U}_s \bar{D}}{\frac{d}{dt}(U_s \bar{D})} \quad (247)$$

These expressions permit to carry out a self-consistency check of the approximations introduced in the definition of to $\tilde{f}_1, \tilde{f}_2, \tilde{f}, \tilde{L}, \tilde{I}_h, \tilde{I}_k$, etc. If one wants to know the actual values of these geometrical parameters and of these j -currents, they can be computed, apart an arbitrary constant factor C , by means of a method that is strictly identical to the procedure applied to the aforementioned M case history. However, in general there is no equivalent way to estimate such a constant factor C .

Partial DPS ratios can be defined by (243), and can be expressed in terms of self- and joint-energies by (241)

$$\bar{D} \cong -\tilde{f} \frac{U_j}{U_s} \quad (248)$$

The equality is approximate according to the assumptions explicitly discussed for (201) ... (211). Their time derivatives can be estimated. Note that, owing to (146), (149) and (187), the classical DPS ratio $b_z(0)/B_0$ can vary in time only on a secular time scale (rapid changes might be considered only when one subtracts from \mathbf{b} the \mathbf{b}_{tc} contribution; these rapid changes are discussed by Siscoe, 1970).

8.6 - The electromagnetic drag of the Earth

The physics, the drivers, and the implications of the e.m. interaction of the solar wind with the Earth, and the associated effects on its astronomical motion (*l.o.d.* and pole motion, etc.), are the concern of an extensive discussion that cannot be given in the present paper. In particular, the treatment, which is here given, is a direct connection with the formalism of the present paper. It was prepared in the early 1970s, and it contains a review of the pre-existing state of the art available at that time. This is pertinent in the present framework. The more updated review, and its discussion, should require a long devoted discussion that, owing to brevity requirements, cannot be here given.

Gribbin and Plagemann (1973) (see figure 16) reported the anomalous change in the spin rate of the Earth, following the great solar storm of August 1972. They gave a tentative interpretation in terms of a variation of the general circulation of the atmosphere.

The Gribbin and Plagemann (1973) finding triggered a revival of interest on this topic. Hines (1974) confirmed that the drag on the polar ionosphere exerted by the interplanetary \mathbf{E} can give no significant contribution to this effect. Papagiannis (1973) calculated the torque on the magnetopause, while Carovillano and Siscoe (1973), Olson (1973) and Siscoe (1974) used the formula originally given by Siscoe (1970) (see section 5.2).

A simple Earth's dipole \mathbf{M} is supposed to be embedded in an external magnetic field \mathbf{b} , and the formalism of elementary magnetostatics is used. Olson (1973) calculated the effect, on the tilt angle of the dipole, of the torque that

acts on the Earth, and also of the total force that affects its orbital motion.

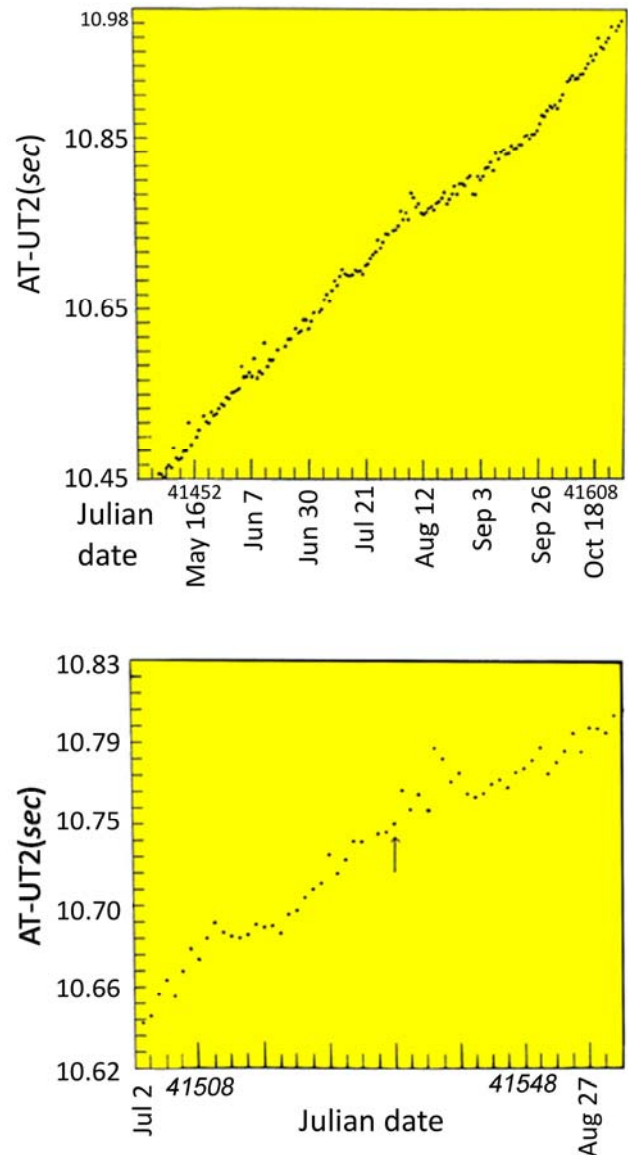


Figure 16. (a) *l.o.d.* vs. date in 1972, when a huge solar storm was observed. One datum every day is plotted, according to measurements carried out only at one site, i.e., at the *U. S. Naval Observatory*, Washington, as - unlike at present - at that time global averaged data were provided - as a standard - only once every 5 days. The Julian date is indicated. During the middle of August, the spin rate of the Earth abruptly slowed down. During a few subsequent days, the spin rate increased anew, in order to recover along the main unperturbed trend. This phenomenon is tentatively explained in terms of the concept intuitively represented in figure 17. Figure (b) shows a detail of figure (a). Unpublished figure, adapted after Gribbin and Plagemann (1973).

However, his estimates were based on a well-known mathematical model of the magnetosphere, which neglected the effects of the ring current, of radiation belts,

of the ionosphere, and of the telluric currents induced in the Earth. Moreover, since he used an averaged model of the magnetosphere, his evaluation can give only mean values for the torque and for the total force, while it is not suited to provide any instant value. Instantaneous effects ought to require to extrapolate \mathbf{b} , i.e., the external origin geomagnetic field, from Earth's surface to Earth's center. However, this raises problems concerning the e.m. screening by the Earth's interior.

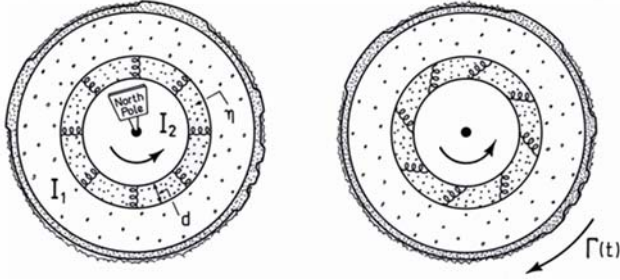


Figure 17. Principle idea for explaining the effect observed in figure 16. A temporary torque $\Gamma(t)$ operates on the crust acting like a brake on a wheel. The solid body is supposed to be composed of two solid components, having moment of inertia I_1 and I_2 , respectively, mutually linked by a viscoelastic coupling. As soon as the externally applied torque $\Gamma(t)$ fades off, the inner solid component re-accelerates the outer shell, and it brings it back along the unperturbed "regular" dynamic regime. Upon a formal least square fit on the data of figure 16(b) it is possible to estimate the thickness of this outer layer of the Earth. The result - in the order of magnitude of $\sim 100 \text{ km}$ - is perfectly consistent with the hypothesis that the outer shell is the lithosphere (see Gregori, 2002, and Gregori and Letbourne, 2021, unpublished figure, in cooperation with Bruno Alessandrini). Unpublished figure.

Hence, short time variations, such as the aforementioned August 1972 event, in principle cannot be accounted for by means of a point source, such as a dipole, and by neglecting telluric currents. On the other hand, such a warning is substantially avoided due to the role of the aforementioned sea-urchin spikes, which act like very effective antennas and permit a direct e.m. coupling between solar wind and deep Earth (see Gregori, 2002, and some mentions in Gregori and Leybourne, 2021). Note, however, that at present it appears difficult to compute any even approximate quantitative estimate of this effect.

A different method of computation is here envisaged of the e.m. drag on the Earth as a consequence of the e.m. interaction with the solar wind. This method is suited also for instantaneous events. It is here shown how to compute:

$$\int_V \mathbf{r} \wedge (\mathbf{j}_1 \wedge \mathbf{B}_1) d\tau = - \frac{1}{4\pi K_0 \mu_r} \oint_S (\hat{\mathbf{n}} \times \mathbf{b}_1)(\mathbf{r} \times \mathbf{b}_1) d\sigma = \frac{a}{4\pi K_0 \mu_r} \oint_S b_{1r}^2 d\sigma$$

$$= \frac{a}{4\pi K_0 \mu_r} \int_0^{2\pi} \int_0^\pi b_{1r}^2 \sin \vartheta d\vartheta d\varphi$$

(i) the torque that acts on the Earth at every given instant of time, and also (ii) the total force that acts on the Earth and affects its orbital motion.

The required observational information are the \mathbf{E} and \mathbf{B} fields measured at Earth's surface. Since \mathbf{E} is poorly known, it is here simply neglected, or, equivalently, it is formally assumed $\mathbf{E} = 0$ all over the globe. This is consistent with the present generally agreed belief.⁴⁵ Let us call

$$\mathbf{B} = \mathbf{B}_1 + \mathbf{b}_1 \quad (249)$$

$$\mathbf{b}_1 = \mathbf{B}_M + \mathbf{b}_{tc} \quad \mathbf{B}_1 = \mathbf{b}_{io} + \mathbf{b}_{VA} + \mathbf{b}_{sc}$$

and apply (125), where V and S are the Earth's volume and surface, respectively. It is, by (31) and upon assuming $\mathbf{B} = 0$ all over S

$$t^{ij}(1) = - \frac{1}{8\pi K_0 \mu_r} [\mathbf{b}(1)^2 \delta^{ij} - 2 b^i(1) b^j(1)] \quad (250)$$

and, by (32) and (33)

$$p^{ij}(1) = \tilde{p}_\perp(1) \delta^{ij} + [\tilde{p}_\parallel(1) - \tilde{p}_\perp(1)] \frac{B_i B_j}{B^2} + \varrho(1) v^i(1) v^j(1) \quad (251)$$

where $p(1)$ is the pressure tensor of the particles responsible for \mathbf{b}_1 , $\varrho(1)$ is their density, and $\mathbf{v}(1)$ is their bulk velocity. On the other hand, it is here supposed that all these particles flow either inside V , or at most - although by a smaller amount - over S . In any case, let us substitute (251) into (125). The first and third addenda on the right hand side of (251) give a vanishing contribution. The second addendum gives a contribution

$$\oint_S [\tilde{p}_\parallel(1) - \tilde{p}_\perp(1)] (\mathbf{B} \times \hat{\mathbf{n}}) (\mathbf{r} \times \mathbf{B}) d\sigma \quad (252)$$

that can be neglected, if - as already mentioned - only a negligible part flows over S of the particles that are responsible for \mathbf{b}_1 , so that $\tilde{p}_\parallel(1)$ and $\tilde{p}_\perp(1)$ can be assumed to be close to zero.

Moreover, the second and third addenda on the right hand side of (125) identically vanish, because, for a spherical Earth, both the gravitational acceleration \mathbf{g} and the holonomic constraints \mathbf{f}_{tc} are antiparallel to \mathbf{r} .

Summarizing, the torque of the e.m. drag that acts on solid Earth is

$$\int_V [\mathbf{r} \wedge (\mathbf{j}_1 \wedge \mathbf{B}_1)]_k d\tau = - \oint_S \varepsilon_{hik} x^h \hat{n}_j t^{ij}(1) d\sigma \quad (253)$$

Formally insert (250) into (253). Note that the δ^{ij} term vanishes (because its contribution is proportional to $\mathbf{r} \wedge \hat{\mathbf{n}} = 0$). Hence, the result is

$$\int_V [\mathbf{r} \wedge (\mathbf{j}_1 \wedge \mathbf{B}_1)]_k d\tau = \frac{a}{4\pi K_0 \mu_r} \oint_S b_{1r}^2 d\sigma \quad (254)$$

⁴⁵ An extensive critical discussion cannot be here given.

that is, the moment of the e.m. drag on solid Earth is equal to $1/4\pi K_0 \mu_r$ times the integral over S of the square of the radial component of \mathbf{b}_1 , multiplied by the Earth radius a . This moment can be evaluated by means of the available \mathbf{B} measurements. Just separate \mathbf{B} into \mathbf{B}_1 and \mathbf{b}_1 , i.e., into its external and internal part, respectively.⁴⁶ Then, (254) can be computed by means of the internal part \mathbf{b}_1 .

$$\int_V \frac{\partial}{\partial x^j} [p^{ij}(1) - t^{ij}(1)] d\tau = \int_V (\mathbf{j}_1 \wedge \mathbf{B}_1)^i d\tau + F_M^i + F_{tc}^i + \int_V \rho(1) g^i d\tau \quad (255)$$

Let us: (i) transform the left hand side into a surface integral, and (ii) neglect the contribution by $p^{ij}(1)$ because

$$\begin{aligned} & \frac{1}{8\pi K_0 \mu_r} \oint_S \mathbf{b}(1)^2 \hat{\mathbf{n}} d\sigma - \frac{1}{4\pi K_0 \mu_r} \oint_S [\hat{\mathbf{n}} \times \mathbf{b}(1)] \mathbf{b}(1) d\sigma \\ & = \int_V (\mathbf{j}_1 \wedge \mathbf{B}_1) d\tau + \mathbf{F}_M + \mathbf{F}_{tc} + \int_V \rho(1) \mathbf{g} d\tau \end{aligned} \quad (256)$$

The right hand side is, by definition, the total force that acts on the orbital motion of the Earth. The first addendum is the e.m. drag, and the second and third addenda are the result of the holonomic constraints. The final term is the resultant gravitational force that acts on all charged particles that are responsible for \mathbf{b}_1 and are distributed inside V with density distribution $\rho(1)$.

Note that, if the Earth is a sphere and $\rho(1)$ has spherical symmetry, this term vanishes. That is, the gravitational term is presumably negligible. In addition, owing to symmetry reasons, also the holonomic terms are presumably negligible. In summary, it is presumable that the main part of the total drag is the e.m. force. However, in any case, the computation of the left hand side of (256) gives the total force that acts on the orbital motion of the Earth.

It ought to be emphasized that the assumption $\mathbf{E} = 0$ all over the globe is the weak point of this entire derivation. Apart this concern, the total force that acts on the Earth can be easily computed by means of (254) and (256), respectively. There is only need (i) to separate⁴⁷ the external and internal components of \mathbf{B} , i.e., \mathbf{B}_1 and \mathbf{b}_1 , respectively, and (ii) to compute an interpolated value for \mathbf{b}_1 all over the globe. This method permits to compute instantaneous estimates.

A comparison with the Olson's results can give an indication on the influence of the approximations that are used either in the Olson's computation or in the method that is here proposed. Unfortunately, the normal magnetograms for these events, such as the aforementioned August 1972, are usually very confused and practically useless. Hence, a concrete evaluation of this e.m. drag is a quite a difficult job.

If the Gribbin and Plagemann (1973) result is interpreted according to the model of figure 17, this interpretation can be expressed in quantitative terms by means of the results of (254), evaluated before, during, and after the anomalous change of Earth's spin rate.

The total force of the e.m. drag that acts on the Earth can be computed as follows. Consider the formal splitting (249), use (30) and integrate over V . Thus, get

the charged particles responsible for \mathbf{b}_1 flow deep inside V , and only a negligible portion of them flows over S . As mentioned above, neglect \mathbf{E} and insert (250). The result is

At present, it is difficult to foresee all the heuristic possibilities of these theoretical methods. More detailed arguments and computations are possible, in principle, but they critically need for a particularly great care in data handling. For instance, there is need for a reliable knowledge of the secular trend of the Sq and L geomagnetic variations in order to carry out several aforementioned computations. It is very difficult to state *a priori* whether the presently available data are sufficient to get any significant result.

In principle, the theoretical methods that are here proposed are logically correct with the appropriate approximations, although they rely on the assumption of a negligible role played by air-earth currents. In any case, they can be applied only if suitable experimental data are available on some suitable space and time scales. The present available knowledge of air-earth currents does not permit to improve the formulation here envisaged in any "simple" way. Owing to this reason, such a kind of applications is possible in principle, although in practice their exploitation is often awkward, if possible at all.

8.7 – Conclusion

The analysis of the energy balance of the e.m. interaction between solar wind and Earth can be effectively carried out by means of a few simplifying abstractions.

The magnetostatic formalism is a historically classic approach to magnetism in terms of an unrealistic abstraction, which however simplifies the discussion of several observations, although it leads to an unrealistic divergence when dealing with energy relationships.

⁴⁶Note, however, that the aforementioned air-earth currents are such that we must seriously reconsider the separation of the geomagnetic field into internal and external origin components.

⁴⁷ We stress anew that this requires the aforementioned assumption of a negligible role of the air-earth currents, and – as already emphasized – this is the weakest point of the present whole derivation.

In contrast, by making reference to simple \mathbf{j} -loops rather than to magnetic dipoles etc., we can give a representation of natural reality, which is certainly not akin to the intrinsic physical details of the complication of natural phenomena, although it gives a realistic framework of the overall energy contents and exchanges between different magnetospheric sub-systems. Several relevant and important mutual relations can thus be shown, although the real numerical estimates are often hampered by an insufficient availability and/or reliability of historical geomagnetic data series.

On the other hand, the resulting properties highlight some fundamental relations, which provide some key constraints between different derived observational parameters. The treatment carried out in the present study can be considered as a lengthy discussion of what can - or cannot - be actually observed in the e.m. interaction between solar wind and Earth.

The general discussion of the energy relationships in magnetospheric phenomena must therefore be considered as some kind of general introduction to this whole problem. It is just an energetic framework - or an overall constraint - deriving from the fundamental laws of physics that, whether observable or not, whether feasible or not in terms of concrete numerical estimate, must be in any case always satisfied.

For sure, such a kind of energy relationships must be satisfied as an unavoidable constraint for every kind of a more or less "technical" model, or interpretation, or working hypothesis, or algorithm, such as, e.g., either the *MHD* formalism or the single particle dynamics, either with "reconnection" or not, etc.

9. Energy computations. Case histories reported in the literature

Only few authors attempted to evaluate the energy content inside some subvolumes of the magnetosphere. A list is here given of some papers in chronological order, however with no presumption for completeness. We apologize for eventually forgetting some other study.

Willis (1976) is concerned mainly with the possible influence on the atmosphere by the earthward flow of particles in the plasmashet. He considers magnetospheric convection and the coupling with the troposphere. Note, however, that the mention to convection in the magnetosphere must be suitably changed and re-interpreted according to the rationale for explaining particle flows in the plasmasphere (see section 7). He concludes that it is unlikely that magnetospheric processes can produce by direct mechanism any significant meteorological global change. He stresses that one should search for some indirect mechanism.

The evaluation of energy processes in the magnetosphere must consider that the magnetosphere is a unique entire physical system that can be identified with no

specific volume in space. Neither it is possible to define, on a strictly rigorous physical basis, any subsystem of the magnetosphere. One can define different types of energy contents in energy contents in different subvolumes of the magnetosphere and on the temporal changes during the development of geomagnetic disturbances of increasing strength. Different types of energy were thus defined.

Let us refer, e.g., to Baker et al. (2001). However, we have no presumption of completeness, because, owing to the aforementioned reason, no exhaustive treatment is conceptually possible. One energy is the kinetic energy flux rate E_k in the solar wind, another parameter is the so-called "solar wind energy coupling rate" ε , that they are defined as

$$E_k = \frac{1}{2} \rho V^3 A \quad (257)$$

$$\varepsilon = V B^2 l_0^2 \sin^4 \frac{\theta}{2} \quad (258)$$

where ρ is the solar wind mass density, V is its speed, A is the magnetospheric cross-section area, B is the strength of \mathbf{B}_{int} (more often denoted by *IMF*), $l_0 = 7R_E$ is a geometrical parameter, which is derived from the average figure of the magnetosphere (the earthward termination of the neutral sheet), and θ is the angle between the $\hat{\mathbf{z}}$ -axis in the so-called *GSM* solar-magnetospheric system (see Russell, 1971) and the projection of \mathbf{B}_{int} on the $\hat{\mathbf{x}} - \hat{\mathbf{y}}$ plane.

The parameter ε was defined upon considering some reasonable average geometries and physical model for the magnetosphere. Akasofu (1981) carries out an authoritative discussion, including an extensive treatment both of different case histories and of the role of different approximations. He defined this parameter and claims that the energy coupling of two systems A and B can be represented by an energy flux ε from A to B and an from energy flux \mathcal{U}_T as an output from B. That is, he considers the joint magnetic energy of two \mathbf{j} -loops. Refer to the aforementioned discussion of geomagnetic storms or magnetospheric substorms.

The reader who wants to deal with specific case histories ought to refer to the learned discussion by Akasofu's (1981).⁴⁸ These reasonable models were also used to estimate other energy contents inside subvolumes of the magnetosphere, including ring current, Joule heat, ionospheric absorption, etc. We cannot give here additional details, as they should require a devoted long and very specific discussion, which is not pertinent for the present paper.

Let us only report figure 18, which is a synthesis of the results, according to Baker et al. (2001). Table 14 (unpublished) is a numerical representation of figure 18, where the power and energy values are visually read on the figure, and are therefore affected by a consequent error bar.

Baker et al. (2001) describe these estimates as follows. Note that the definition of different geomagnetic

⁴⁸ See also Akasofu (1999).

disturbances is somewhat arbitrary, as - in reality – it is very difficult to distinguish different categories of phenomena. The solar wind input power (W) is claimed to be the highest estimated sustained level of input-power during an event as measured by an “ ϵ -like” parameter. However, they claim that every equivalent combination of solar wind speed and B_{int} parameters could, in principle, be used (Nishida, 1983; Baker et al., 1997). Every indicated energy referring to a given disturbance corresponds to the total energy dissipated during the course of an identifiable event of the given kind. No additional detail is here given.

As mentioned above, the physics and energy balance of magnetospheric phenomena, and of the associated geomagnetic disturbances, must be treated in a formal and rigorous general approach to the whole physical system of the magnetosphere, i.e., of the global interaction between solar wind and Earth. In fact, the use of reasonable physical approximations - although unavoidably implying a lack of sufficient formal logical rigor - was the origin of misconceptions, debates, controversies, sometimes contradictions, etc. For instance, remind about “reconnection”, about the physical justification of substorms and of storms, and, in general, about all items more or less directly related to energy balance (see sections 2, 3, 4).

The reader should now reconsider the severe judgement by Akasofu (1999) who states “... at a time, it was said that one could not be a magnetospheric physicist unless one tried to explain auroral substorms in terms of magnetic reconnection ... In this paradigm, it was said that magnetic reconnection must occur, since the theory is so trustworthy and that all observations will eventually be understood in

terms of it ... However, in a powerful paradigm, an observation contradictory to the accepted theory gets little attention and often gets ridiculed ... A powerful paradigm will delay the progress of its field. A high degree of agreement in a paradigm will suppress alternatives, so that researchers are lost when their paradigm is eventually found to be inoperative. During the period of a powerful paradigm, the progress of its field is actually retarded and sometimes it regresses. Much research time is lost as well. Indeed, we have lost about 30 year s by pursuing the hypothesis of magnetic reconnection by believing that it is the only theory to explain substorms.”

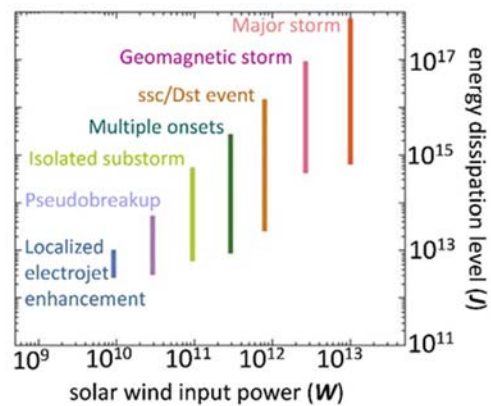


Figure 18. Magnetospheric energy dissipation. Progression of processes according to increasing solar wind energy input. Vertical bars show the range of typical physical processes, corresponding to input power levels. Figure redrawn and adapted after Baker et al. (2001).

Table 14. Energy dissipation level for geomagnetic disturbances, according to figure 18

Kind of disturbance	solar wind input power (W)	Minimum energy (J)	Maximum energy (J)
localized electrojet enhancement	9×10^9	2×10^{12}	1013
pseudobreakup	2×10^{10}	2×10^{12}	5×10^{13}
isolated substorm	10^{11}	6×10^{12}	5×10^{14}
multiple onsets	2×10^{11}	9×10^{12}	3×10^{15}
ssc/Dst event	9×10^{11}	2.5×10^{13}	1.05×10^{16}
geomagnetic storm	2×10^{12}	4×10^{14}	10^{17}
major storm	10^{13}	6×10^{14}	8×10^{17}

Stern (1984), in his authoritative review of the energy balance in the magnetosphere, concludes by stating that several unresolved controversies must be clarified concerning substorms and their mechanism, and also magnetic merging, and the storage of magnetic energy. Gonzalez et al. (1994) in a much authoritative paper discuss the “associated storm/substorm relationship problem” and claim that “the physics of this relationship does not seem to be fully understood ...”. To our knowledge, according to what can be found in the literature, very little changes (if any) occurred during the last few decades in the theory of substorms.

In the final analysis, a primary bias is the effort to represent the magnetosphere in a way that reminds about a

model-airplane in a wind tunnel - i.e., the effort to use the continuum approximation of the MHD formalism derived from a generalization of fluid dynamics and the introduction of the concept of “reconnection”. However, such an *a priori* assumption unavoidably leads to some physical compromise.

The most evident paradox implies “killing” Maxwell’s equations by introducing “reconnection” etc. However, since a substorm can be very effectively justified (as above) by means of an energy balance, depicted by means of the Hamilton’s variational principle, the aforementioned “wind tunnel” analogy is unsuited for dealing with such a very general energy argument and balance. Indeed, one should frankly claim that the “wind tunnel” model is misleading.

A comparatively more recent observation by the five satellite *THEMIS* spacecrafts, launched in February 2007 by NASA (Petrukovich, 2008), is shown in figure 19. On February 26th, 2008 the five satellites were aligned in such

a way that they detected the effect of an “explosion” occurred in the neutral sheet at $\sim 20 - 30 R_E$ from the Earth.

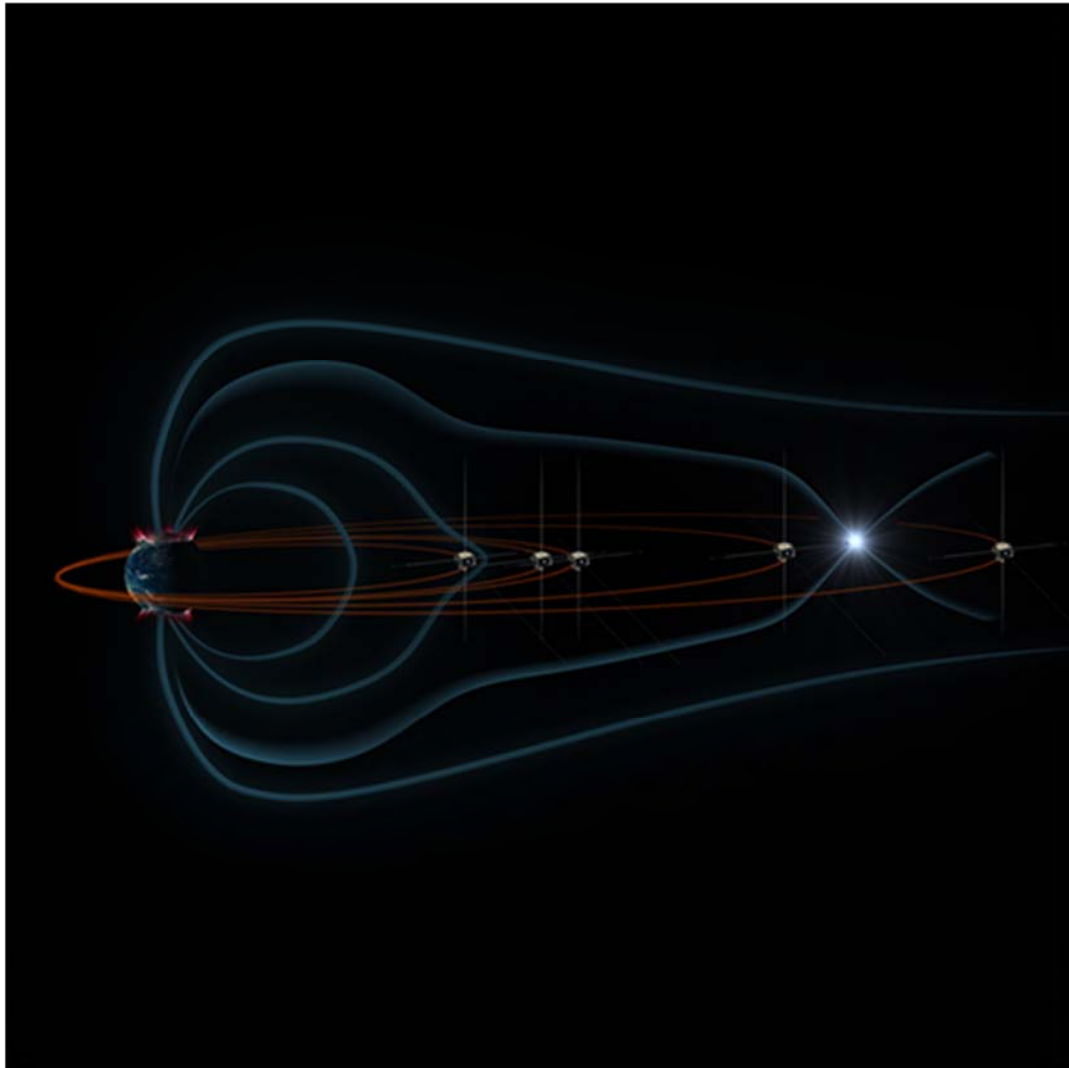


Figure 19. An artist's concept of the *THEMIS* satellites lined up inside the Earth magnetotail with an “explosion” observed to occur between the 4th and 5th satellites. Credit: NASA. After Steigerwald (2009a). NASA copyright free policy.

Figure 19, which is an artist cartoon, reminds about the interpretation according to Dungey's rationale mentioned in section 4 that, however, is just a conceptual model. Observations are matters-of-fact, and can be interpreted in different ways. The “point” is shown in figure 19 where the “explosion” occurred, that – according to the model here given - corresponds to the location, along the neutral sheet, which is instantaneously crossed by the “plasma cavity” resulting from the lack of particle-supply by the solar wind. Its energy was estimated to be of the order of $\sim 10^{15} J$. According to Dungey's rationale, this “point”, is called “*reconnection point*”, and its linear extension across the tail - perpendicularly to the plane of the figure - is called “*neutral line*”.

According to the rationale here used, this morphological feature corresponds to the varying downstream extension of the neutral sheet that can be instantaneously attained, compatibly with the available charged particle supply by the solar wind. This “*reconnection point*” moves downstream, consistently with the outward expansion of the solar corona, and typically by a matter of $\sim a\ few\ hours$ it runs along the entire length of the tail, i.e., say, up to $\sim 1,000 R_E$.

The earthward flow of charged particles - generated by this permanent “explosion” that moves downstream - results into an effective substitute for the lack of particles deriving from the “plasma cavity” inside the solar wind. Hence, the substorm displays its typical recovery that

elapses as long as the earthward flux of particles occurs. When the earthward flux exhausts, if the “plasma cavity” persists within the solar wind, a new substorm is triggered, etc. The time series of several successive substorms - more or less regularly repeated in time - composes a typical geomagnetic storm.

Akasofu (1981) is a remarkable and authoritative long study, which contains also several plots of the parameter ϵ [see (258)]. He discusses, with extensive details, several case histories that display different typical morphologies. The interested reader ought to refer to his paper that, however, cannot be likened to the discussion of the energy content that is here given.

The Akasofu (1981) approach relies on a substantially different viewpoint, shared by several authors. Their approach can be briefly called “differential”, in contrast with the viewpoint here adopted that can be called “integral” (or “variational”). That is, Akasofu (1981) attempts to infer specific details of the internal structure and dynamics of the magnetosphere. He relies on observational inferences, e.g., related to some geomagnetic indices, or measurements carried out by space platform on an instant and point-like basis, etc. Then, he tries to integrate the magnetospheric model that he can thus envisage, etc. In contrast, the approach that is here adopted directly deals with “integral” and “overall quantities” and energy contents - and the interpretation of observations is then exploited by means of Hamilton’s variational principle.

In addition, Akasofu (1981) relies on Dungey’s open model of the magnetosphere (see section 4) and on the concept of “drag” at the magnetopause. Hence, his consequent estimates derived from such a modeling cannot be compared with the treatment that is here considered. In general, he finds a substantial scatter. In fact, upon considering the intrinsic large scatter of the solar wind flow - and also the tiny fraction of expanding solar corona that can be monitored by the Earth’s magnetosphere (a fraction $\sim 0.45 \times 10^{-9}$; see section 1) - the system can hardly be framed into any “simple” scheme relying on a few typical case histories. Indeed, this scatter is what must be expected.

Akasofu (1981, p. 161) claims that “*the energy coupling function ϵ can be identified as the power generated by the solar wind-magnetosphere dynamo.*” This is correct if this interaction is considered as a phenomenon that transforms the kinetic energy (plus the frozen-in magnetic energy) of the solar wind into a variation of the magnetic energy content of the magnetosphere. Akasofu (1981, p. 162 and 169) relies on the theoretical development by Siscoe and Cummings (1969) and Gonzalez and Mozer (1974).

The ultimate concern of Akasofu (1981) deals with the starting hypothesis about the energy relations in the magnetosphere that - as he mentions - can be represented from either one of two conflicting viewpoints. One viewpoint is what he calls a “driven” system, where the input and the output ought to appear closely correlated, although eventually with a suitable time delay. The opposite viewpoint, which he seemingly formerly

preferred, is what he calls “unloading” system. Such a kind of approach is here called of “calorimetric” kind, by which a magnetospheric substorm, or a geomagnetic storm, is interpreted as the effect of some energy that, during some previous time, was stored inside the magnetosphere, and that is eventually released due to some solar wind perturbation. That is, this is the same principle that applies to the energy balance of a pressure cooker.

Akasofu (1981, p. 169) claims that his finding “*indicates conclusively ... that the magnetosphere is, as a first approximation, a directly driven system.*” He stresses also that “*this is an unexpected result. On the other hand, it is not difficult to realize that the concept of an unloading system was simply a hypothesis, since the relationship between energy input and output rates had not been known before.*”

On the other hand, Akasofu (1981, p. 176) warns that “*it should be emphasized that the magnetosphere is not strictly a driven system. It is only closer to a driven system than to an unloading system. This is because the magnetosphere has a large inductance $L \sim 100 - 500 H$. It will accumulate magnetic energy in the magnetotail and convert it into substorm energy ...*” That is, such an inference, which he derives from observational evidence, is related to the role played by the charged particles that are stored inside the plasmashet, while the plasmashet is progressively depleted of its particle content by the succession of substorms.

Let us emphasize that Akasofu has been one of the very few scientists of the magnetosphere that challenged the concrete and very difficult problem of the energy balance, according to a “top-down” viewpoint.

Gonzalez (1990) is mostly concerned with the theory for the evaluation of a most general model for the transfer of power from the solar wind to the magnetosphere through *MHD*. He expressively refers to the role of E at the magnetopause, which he considers large scale “reconnection”, etc. That is, his approach relies on the search for semi-empirical interpolated models derived from a fit on observational data. Hence, he applies a “bottom-up” perspective that is other than the general “top-down” rationale that is here considered. No additional mentions are therefore here given about the Gonzalez (1990) model.

Baker et al. (2001) give real quantitative estimates. They review previous attempts. However, in contrast with the more general and formal theoretical treatment here mentioned, i.e., of the kind given by Siscoe (1970), these quantitative computations rely on approximate models, based on a simple and intuitive geometry, and concerned with the physical interpretation of geomagnetic indices. Their consequent estimates rely on interpolation of satellite measurements. That is, they apply a “bottom-up” viewpoint. In fact, every model - proposed either by Baker et al. (2001) or others - is physically reasonable, although in general the specific details are not of direct concern for the present “top-down” discussion. Hence, for brevity purpose these models are not be here described in detail.

The interested reader ought to refer to the original papers, but mostly he should refer to Akasofu (1981). In addition, the relation between DPS ratio and magnetospheric modeling has been the object of specific studies (e.g., Liemohn, 2003).

Baker et al. (2001) refer to the magnetic storm occurred on 10-11 January 1997 that was well-modeled. This storm was analyzed by Lu et al. (1998). Baker et al. (2001) mention that Lu et al. (1998) relied on continuous upstream solar wind measurements carried out by the *WIND* spacecraft for estimating the solar wind kinetic energy (257) and the solar wind energy coupling rate (258). This is consistent with the aforementioned Akasofu (1981) analysis.

Lu et al. (1998) used also some ionospheric modeling aimed to compute “detailed estimates ... of the ionospheric Joule heating rates and ionospheric particle precipitation rates. An important outstanding issue ... is to calculate accurately the ring current energy dissipation. In the January 1997 event, Lu et al. (1998) did not have detailed measurements of the ring current ion populations. Therefore, they used the formulation of Akasofu (1981) to estimate the ring current energy injection rate

$$U_R = -4 \times 10^4 \left(\frac{\partial D_{st}}{\partial t} + \frac{D_{st}}{\tau} \right) \quad (259)$$

In this equation, D_{st} is the pressure-corrected index (in nT) based on 18 low-latitude stations computed specifically for this event and τ is the (variable) ring current particle lifetime (in sec).”

Baker et al. (2001) specify also that “it is usually the pressure-corrected D_{st} ($D_{st}^* = D_{st} - b\sqrt{P} + c$), where P is solar wind pressure and b and c are constants) that is used in quantitative work.”

Concerning the relation (259), it is derived by Akasofu (1981, p. 129) on the basis of the aforementioned semi-empirical approach, by speculating a model magnetosphere that ought to be suited to give in some way a physical explanation for the D_{st} index.

Figure 20 shows the result where, as Baker et al. (2001) specify, the value of ϵ for 10-11 January is shown by the solid line. The lighter dashed line illustrates the combination of auroral particle precipitation and Joule heating rate. This combination refers to the integral over both the Northern and Southern Hemispheres, plus adding the ring current injection rate (U_R). In contrast, the auroral particle precipitation power and Joule heating rates combined (U_I) is shown by the light dotted line.

Baker et al. (2001) comment also on previous estimates of storm-time energy dissipation. For instance, they mention Akasofu (1981) who guesses that perhaps 90% of solar wind-coupled energy enters into the ring current. On the other hand, Baker et al. (2001) point out that, according to figure 20, this is not confirmed in well-observed *CME*-driven events. In addition, they point out that during the January 10-11, 1997, according to the Lu et al. average estimates, the magnetosphere-ionosphere system dissipated $\sim 4 \times 10^{11}$ W, while 48% of this (i.e.,

$\sim 1.9 \times 10^{11}$ W) supplied Joule heat, 30% (i.e. $\sim 1.2 \times 10^{11}$ W) supplied the injection of the ring current, and 22% (i.e., $\sim 0.9 \times 10^{11}$ W) went into auroral precipitation.

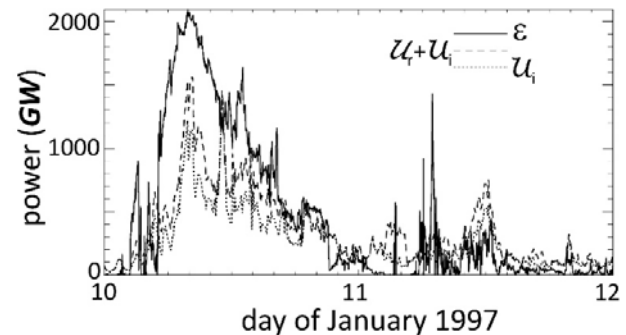


Figure 20. The ϵ (solid line) during 10-11 January 1997, compared with the magnetospheric energy dissipation rate ($U_R + U_I$; dashed line) and the ionospheric dissipation rate (U_I ; dotted line) (figure adapted from Lu et al., 1998; AGU copyright free policy.)” Figure after Baker et al. (2001).

Baker et al. (2001) carry out a detailed discussion on the meaning of the D_{st} index. They report their analysis of a geomagnetic event occurred in early May 1998, and finally conclude with figure 18.

A series of papers (Palmroth et al., 2001, 2001a, 2003, 2004; Huttunen et al. 2002; Palmroth, 2003) deals with the investigation of the energy relationships in the magnetosphere by means of a *MHD* model, and by making reference to the Akasofu ϵ parameter. In addition, they discuss the diagnostic implications associated with the location of the cusp. Their study is according to the aforementioned Akasofu’s viewpoint. Therefore no details are here given.

Also Rosenqvist et al. (2006) refer to the same viewpoint, but they combine simultaneous measurements by the *Cluster* spacecraft, and ionospheric observations from the *European Incoherent Scatter (EISCAT)* radars and magnetometers. “The *Cluster* spacecraft crossed the magnetopause at the duskward flank of the tail ... during a sequence of intense substorm-like geomagnetic activity in October 2003. [They] attempt to estimate the local and global energy flow from the magnetosheath into the magnetotail and the ionosphere under these extreme conditions ... The global power input based on *Cluster* observations was found to be between 17 – 40 TW at the onset of the substorm intensification. However, spacecraft observations and global modeling of the magnetotail suggest that it is most probably closer to 17 TW. This is more than two times lower than the predicted ϵ parameter value (37 TW).”

Energy deposition in the ionosphere has been estimated locally with *EISCAT* and globally with the assimilated mapping of ionospheric electrodynamics (*AMIE*) technique. The amount of the global solar wind power input (17 TW) that is dissipated via Joule heating in the ionosphere is found to be 30%. The corresponding ratio

based on empirical estimates is only 3%. However, empirical proxies seem to underestimate the magnitude of Joule heating rate as compared to AMIE estimates (- a factor 4) and the ϵ parameter is more than twice as large as the Cluster estimate.

In summary, the observational estimates provide a good balance between the energy input to the magnetosphere and deposition in the ionosphere. Empirical proxies seem to suffer from overestimations (ϵ parameter) and underestimations (Joule heating proxies) when pushed to the extreme circumstances during the early main phase of this storm period.”

The conspicuous amount of modeling is evident in this astute study, which is, however, substantially different compared to the approach discussed in previous sections. Hence, this is not pertinent for the present study, and no additional details are here reported.

Observations carried out by a new technique are reported by Phillips (2012). They deal with a large storm occurred on March 8th through March 10th, 2012. The observations were carried out by the SABER instrument onboard NASA’s TIMED satellite. TIMED is the Thermosphere Ionosphere Mesosphere Energetics and Dynamics satellite. “SABER monitors IR emissions from Earth’s upper atmosphere, in particular from CO₂ and NO ...”. These gases are opaque for IR radiation. On March 8th a CME was originated from an X5-class solar flare. “The action produced spectacular auroras around the poles and significant upper atmospheric heating all around the globe ...

For the three day period, March 8th through 10th, the thermosphere absorbed 26×10^9 kWh of energy. IR radiation from CO₂ and NO ... re-radiated 95% of that total back into space.” Phillips (2012) shows also figure 21.



Figure 21. “A surge of IR radiation from NO molecules on March 8-10, 2012, signals the biggest upper-atmospheric heating event in seven years. Credit: SABER/TIMED.” Figure and captions after Phillips (2012). NASA copyright free policy.

In summary, the magnetosphere system is very complicated and complex. Multiparametric diagnostic information is required to monitor different facets of phenomena, which display a great variability in space and time. No “simple” model can be sufficient to explain the great variety of the observed, and rapidly changing, morphological features.

The traditional “continuum” viewpoint, i.e., in terms of MHD, “reconnection”, “drag”, etc. - which is derived from a generalization of fluid dynamics and which is the historical Alfvén achievement - is suited to explain some relevant aspects of observations. However, it cannot explain all features, whenever the starting assumption (continuity of the medium) is manifestly violated.

The classical alternative approach in terms of integral (rather than of differential) quantities - that led to the Hamilton/Jacobi’s formulation of classical physics by means of variational principles - is certainly better suited for the “topdown” investigation of energy relations. On the other hand, it is *per se* unsuited to describe specific geometrical and dynamical details, such as the measurements carried out at a given instant of time by space probes and at a given point (or at a few points) alone.

Therefore, both viewpoints must be considered, and their respective achievements combined altogether. However, as far as the energy balance is concerned, the “continuum” approach certainly appears comparably less useful and less reliable.

In particular, to our understanding, the “continuum” viewpoint cannot give a physical (and not simply descriptive) explanation of the dynamics and evolution of the magnetosphere during a substorm and a storm. In contrast, according to the variational viewpoint, this appears to be the phenomenon that must be physically expected, in order that the system can reach its new equilibrium state, whenever the interplanetary environment changes by some large amount.

Appendix

It is impossible to report in a few pages the full set of standard formulas, conventionally used in geomagnetism. Owing to practical purposes, we mention here only some general formulas that re eventually used in this paper. However, a full treatment can be implemented inside a long textbook on geomagnetism. In any case, since many decades the symbols here used are standard in the literature, and every reader who is acquainted with the literature on these topics should easily afford to understand the present text.

The magnetic energy density is [from the Poynting theorem etc.]

$$\frac{K_0 \mu_r}{8\pi} \mathbf{H}^2 = \frac{1}{8\pi} \mathbf{H} \times \mathbf{B} = \frac{1}{8\pi K_0 \mu_r} \mathbf{B}^2 \quad (260)$$

Let us consider how it can be computed in different systems.

A.1. In terms of *c*-loops and of *m*-loops.

The dichotomy - or symmetrical representation - must be considered of *j*-current loops (or *c*-loops), and of loops of *B* field lines, or *B* flux tubes (or *m*-loops). See, e.g., Perucca⁴⁹ (1960). In addition, we refer to the vector

⁴⁹ Eligio Perucca (1890-1965), Italian physicist.

potential of \mathbf{B} , by which $\mathbf{B} = \text{curl } \mathbf{A}$. These concepts are here considered well assessed from college textbooks. It is

$$\begin{aligned} \mathbf{B}^2 &= \mathbf{B} \times \text{curl } \mathbf{A} = \text{div } \mathbf{A} \wedge \mathbf{B} + \mathbf{A} \times \text{curl } \mathbf{B} = \text{div } \mathbf{A} \wedge \mathbf{B} + \mathbf{A} \times \frac{4\pi K_0 \mu_r}{\gamma_0} \mathbf{j} + \frac{K_0 \mu_r}{\gamma_0} \mathbf{A} \times \frac{\partial \mathbf{D}}{\partial t} \\ &= \text{div } \mathbf{A} \wedge \mathbf{B} + \mathbf{A} \times \frac{4\pi K_0 \mu_r}{\gamma_0} \mathbf{j} + \frac{\gamma_0}{c^2} \epsilon_r \mu_r \mathbf{A} \times \frac{\partial \mathbf{E}}{\partial t} \end{aligned} \quad (261)$$

where the last term can be neglected, due to the factor (γ_0/c^2) [or, which is the same, whenever the quasi-stationarity (QS) approximation can be considered]. The total magnetic energy associated with a given \mathbf{B} field is

$$\begin{aligned} U_{s,total}(\mathbf{B}) &= \frac{1}{8\pi K_0 \mu_r} \int_{V_\infty} \mathbf{B}^2 d\tau \\ &= \frac{1}{8\pi K_0 \mu_r} \oint_{S_\infty} \hat{\mathbf{n}} \times \mathbf{A} \wedge \mathbf{B} d\sigma \\ &\quad + \frac{1}{2\gamma_0} \int_{V_\infty} \mathbf{A} \times \mathbf{j} d\tau \end{aligned} \quad (262)$$

However, when no singular points exist at a finite distance from the origin, the integral over S_∞ vanishes – i.e., the existence of magnetostatic dipoles or shells must be excluded. This will be here supposed.⁵⁰ Therefore,

$$U_{s,total}(\mathbf{B}) = \frac{1}{2\gamma_0} \int_{V_\infty} \mathbf{A} \times \mathbf{j} d\tau \quad (263)$$

This formula gives an expressive way to interpret the magnetic energy of a system in terms of \mathbf{j} -flux tubes linking \mathbf{B} -flux tubes (or briefly c -loops linking m -loops).

A.2. c -loops linking m -loops.

Consider (263) and perform the integration over V_∞ by integrating firstly along all c -loops. Since $\mathbf{B} = \text{curl } \mathbf{A}$, it follows

$$U_{s,total}(\mathbf{B}) = \frac{1}{2\gamma_0} \sum_l J_l \Phi_l(\mathbf{B}) \quad (264)$$

where J_l is the current that flows within the l -th c -loops and $\Phi_l(\mathbf{B})$ is the \mathbf{B} flux across this loop (it is positive when J_l is seen to flow counter-clockwise as observed from \mathbf{B}). The sum is extended over all c -loops and it should be eventually substituted by an integral.

Define the following notations: when

$$\mathbf{B} = \mathbf{B}_1 + \mathbf{B}_2 + \dots + \mathbf{B}_n \quad (265)$$

call

$$U_j(\mathbf{B}_l, \mathbf{B}_m) = U_j(\mathbf{B}_m, \mathbf{B}_l) = \frac{1}{\gamma_0} J_l \Phi_l(J_m) = \frac{1}{\gamma_0} J_m \Phi_m(J_l) = \frac{1}{\gamma_0^2} L_{lm} J_l J_m = \frac{1}{\gamma_0^2} L_{ml} J_m J_l \quad (271)$$

where $L_{lm} = L_{ml}$ is the mutual induction coefficients of the c -loops that generate J_l and J_m .

In (263) V_∞ strictly means entire space, i.e., it extends as far as infinity. In contrast, (264) extends strictly only over all c -loops that in general must be entirely supposed to be located and to close at some finite distance from the origin.

⁵⁰ Further insight related to this assumption can be derived from discussing the approximation of the magnetostatic limit. However, this classical item is not here treated.

$$\begin{aligned} \Phi_l(\mathbf{B}) &\equiv \Phi_l(\mathbf{B}_1 + \mathbf{B}_2 + \dots + \mathbf{B}_n) \\ &\equiv \Phi_l(\mathbf{B}_1) \\ &\quad + \Phi_l(\mathbf{B}_2) + \dots + \Phi_l(\mathbf{B}_n) \end{aligned} \quad (266)$$

where we know that the field \mathbf{B}_i is produced by a suitable current J_i . In the following it will be indifferently called

$$\Phi_l(\mathbf{B}_i) \equiv \Phi_l(J_i) \quad (267)$$

i.e., the argument of Φ_l can equivalently express either a magnetic field \mathbf{B}_i or the current J_i that originates it.

Suppose that the physical system being considered is composed either of a finite or of an infinite, but denumerable, set of c -loops. Therefore, decompose \mathbf{B} as for (265) (with n being either finite or infinite) and rewrite (264) as

$$U_{s,total}(\mathbf{B}) = \frac{1}{2\gamma_0} \sum_{l,m} J_l \Phi_l(J_m) \quad (268)$$

where the sum is extended over all c -loops and every addendum is the product of a current J_l flowing within the l -th c -loop, times the \mathbf{B}_m flux linked by it and that is produced by the m -th c -loop. When $l = m$ the addendum in (268) is called *self-energy* $U_s(\mathbf{B}_l)$ of the l -th c -loop. When $l \neq m$ the following quantity is called either *joint energy*, or *mutual energy*, or sometimes *superposition energy* (e.g., Perucca, 1960), of the l -th and m -th c -loops

$$\begin{aligned} U_j(\mathbf{B}_l, \mathbf{B}_m) &= U_j(\mathbf{B}_m, \mathbf{B}_l) \\ &= \frac{1}{2\gamma_0} J_l \Phi_l(J_m) \\ &\quad + \frac{1}{2\gamma_0} J_m \Phi_m(J_l) \end{aligned} \quad (269)$$

Owing to the action-reaction principle (following the application of the variational principles discussed, e.g., in Gregori et al., 2025e), it is

$$\frac{1}{2\gamma_0} J_l \Phi_l(J_m) = \frac{1}{2\gamma_0} J_m \Phi_m(J_l) \quad (270)$$

Hence, (269) becomes [see also (285)]

$$U_j(\mathbf{B}_l, \mathbf{B}_m) = U_j(\mathbf{B}_m, \mathbf{B}_l) = \frac{1}{\gamma_0} J_l \Phi_l(J_m) = \frac{1}{\gamma_0} J_m \Phi_m(J_l) = \frac{1}{\gamma_0^2} L_{lm} J_l J_m = \frac{1}{\gamma_0^2} L_{ml} J_m J_l \quad (271)$$

Whenever one is concerned with integration in space over sub-domains - and whenever all c -loops do not close inside a given sub-domain of integration - one can introduce some additional fictitious \mathbf{j} , which flow over the confining surface of this sub-domain, like in figure 22. Thus, it is

possible to get back to the case in which all c -loops close inside every given sub-domain.

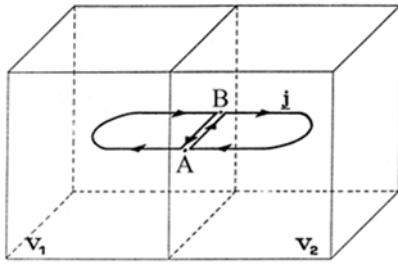


Figure 22. A closed c -loop embedded in a domain $V = V_1 \cup V_2$ is no more closed when V is separated into V_1 and V_2 . This difficulty can be avoided by introducing a current $(\mathbf{j} - \mathbf{j})$ along some arbitrary line between A and B. The physical effects remain unchanged, while a single c -loop in V has been separated into two closed c -loops, one contained inside V_1 and the other inside V_2 . Unpublished figure.

Strictly speaking, this argument has only a mathematical value as it implies to deal with a 2D \mathbf{j} -distribution, even when one deals with 3D \mathbf{j} -distributions (and, in this case, every 2D \mathbf{j} -distribution is only the result of a mathematical abstraction). In practice, the consequence of this drawback can be suitably handled, with full logical rigor, in terms of some appropriate mathematical treatment. Basically, this is analogous to a similar difficulty related to linear c -loops. In fact, in principle, every c -loop should be supposed to have a physical non-vanishing cross-section, i.e., every \mathbf{j} -distribution must be actually 3D and one should never deal with linear circuits depicted like c -loops. One can get rid of this difficulty by a suitable limit process (e.g., Perucca, 1960, or Durand, 1968).

A.3. m -loops linking c -loops.

An equivalent formulation can be obtained from (263) by considering closed flux tubes of \mathbf{B} (or m -loops) linking c -loops (instead than c -loops linking m -loops as in section A.2; see, e.g., Perucca, 1960). All m -loops can be considered closed, if the volume of integration is all space V_∞ . Whenever V_∞ is separated into several subdomains, all m -loops can still be considered closed, if one applies the same argument of figure 22 (and if the c -loops are there substituted by m -loops). However, in this case this argument requires some care, as over every surface - which divides every two sub-domains of integration - one must consider a 2D \mathbf{B} field, which is non-physical, when a most general 3D \mathbf{B} field is considered. This difficulty can be suitably handled, and all unwanted consequences avoided, by means of an appropriate limit process similarly to section A.3 when reference was made to c -loops.

The analogy between the viewpoint of c -loops linking m -loops and the viewpoint of m -loops linking c -loops - which will be henceforward briefly called c -loop/ m -loop duality - requires some additional comment. For the sake of clarity, let us consider first a finite set of m -loops. Associate with every c -loop - say with every C_k having a

current J_k flowing within it - its equivalent magnetostatic double layer. Divide this double layer into several "elementary" infinitesimal double layers, every one of them being equivalent to a very small infinitesimal "elementary" c -loop having a current J_k flowing inside it and enclosing an "elementary" \mathbf{B} flux tube, or m -loop. Every element of the integral in (263) can be represented as

$$\mathbf{j} \times \mathbf{A} d\tau = \mathbf{j} \mathbf{B} \times \hat{\mathbf{n}} d\sigma \quad (272)$$

where $\hat{\mathbf{n}}$ is a unit vector normal to the elementary double layer.

It can be shown that the vectors $\hat{\mathbf{n}}$ and \mathbf{B} are either parallel or anti-parallel. The argument is as follows. Consider the magnetostatic double layer equivalent to this "elementary" infinitesimal c -loop. Substitute this magnetostatic double layer by a very thin "magnetic condenser", in terms of its analogy with the electrostatic formalism. Each plate of this condenser is an equipotential surface, hence the proof.

The entire argument works also in the case of several c -loops, even in the case of c -loops linked with each other (just by applying the simple argument of figure 23).

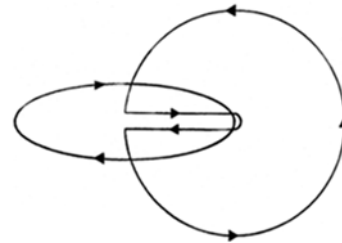


Figure 23. Unlinking two linked c -loops by means of the same argument of figure 22. Unpublished figure.

In summary, refer to (272) and remark that, apart at most the sign, it is

$$\mathbf{j} \mathbf{B} \times \hat{\mathbf{n}} d\sigma = d\vec{\Phi}(\mathbf{B}) \times \mathbf{j} \wedge \hat{\mathbf{n}} \quad (273)$$

Finally integrate (263) along all closed m -loops (call them $\{M_h\}$, $h = 1, 2, \dots$) and get

$$U_{s,total}(\mathbf{B}) = \frac{1}{2\gamma_0} \sum_{M_h} \Phi_h(\mathbf{B}) J_h^* \quad (274)$$

where J_h^* is the sum of the currents flowing within all c -loops that are linked by the m -loop M_h . The sign is defined by stating the rule that J_h is positive when it sees M_h having a \mathbf{B} that "flows" counter-clockwise (figure 24). Therefore it is

$$U_{s,total}(\mathbf{B}) = \frac{1}{2\gamma_0} \sum_{M_h} \left[\Phi_h(\mathbf{B}) \sum_k^{*h} J_k \right] \quad (275)$$

where $\sum_k^{*h} J_k$ means that the sum is limited only to all c -loops that are linked by the h -th m -loop M_h .

The argument has been applied to a finite set of m -loops $\{M_k\}$ ($k = 1, 2, \dots$). The argument must be generalized to an infinite set of m -loops. This can be easily done by dividing all space into a finite set of m -loops, i.e., by considering only infinitesimal \mathbf{B} flux tubes and by stating that any two of them partake to one and the same m -loop when - and only when - both of them link the same subset of c -loops.

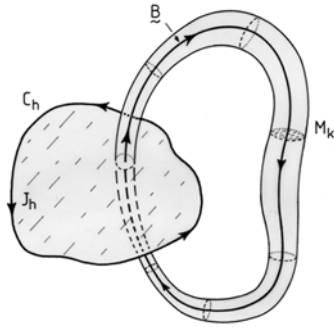


Figure 24. The c -loop C_h (which, strictly speaking should always have an actual non-vanishing cross-section, see text) links an m -loop M_h in a positive way in the case of the present figure. Namely, \mathbf{B} flows across C_h in such a way that \mathbf{B} sees J_h to flow counter-clockwise within C_h . Similarly, M_k links C_h in a positive way, because J_h sees \mathbf{B} to flow counter-clockwise within C_h . See text. Unpublished figure.

Obviously, one supposes that a finite set of c -loops exists; and in general they are also supposed to close at some finite distance from the origin. This condition, however, does not limit the validity of the argument, even when it is applied to a most general 3D \mathbf{j} -distribution. As a matter-of-fact, every 3D \mathbf{j} -distribution can be separated into a sum of a denumerable set of \mathbf{j} flux tubes or c -loops - or even better into a finite set of these loops (the number of loops becomes eventually infinite only in the limit of vanishing cross-section of every loop). In any case, one always considers a \mathbf{j} -distribution that is entirely contained inside a finite volume, while outside it is supposed $\mathbf{j} = 0$.

A.4. Computation of the magnetic self-energies for specific models.

The present section deals with the formal computation of the magnetic energy associated with specific sources of the magnetic field, modeled according to the geometrical patterns.

A magnetic field is produced by electric currents that can be represented by means of a distribution in space of an electric current density \mathbf{j} , which depicts closed loops of currents, here briefly denoted either as \mathbf{j} -loops or as c -loops. No isolated magnetic charge exists. The magnetostatic formalism - which was used in the history of physics before the discovery of the magnetic effect of electric currents - is just the result of a mathematical limit process, which in the past eventually gave some misleading results. One must rather refer to c -loops alone, and forget about the magnetic charges that will be here briefly denoted as m -loops (in terms of the Ampère's equivalence principle) in order to distinguish them with respect to c -loops.

Several different and simple geometrical configurations of c -loops can be considered. No extensive mathematical treatment of intricate geometrical configurations is here considered, as they are not here of concern. They can be found on specifically devoted papers or books, such as, e.g., Snow (1953), Binns and Lawrenson (1963), Garrett (1963),

Bonnevier (1964), and Hart (1967), while Williams and Cain (1975) and references therein discuss the generation of suitably homogenous fields within specific regions by means of multi-loop sources.

The most elementary structure is one c -loop having a total current J flowing inside it and a self-inductance L . The magnetic field is given by the Biot-Savart law

$$\mathbf{H} = \oint_C \frac{J}{\gamma_0} \frac{\mathbf{r}}{r^3} \wedge d\mathbf{l} \quad (276)$$

where C is the c -loop and \mathbf{r} is a vector oriented from the point where \mathbf{H} is evaluated to the element $d\mathbf{l}$ of C . The self-inductance L of the circuit is defined by means of the formal equality

$$\Phi(\mathbf{B}) = L \frac{J}{\gamma_0} \quad \text{or} \quad J = \gamma_0 \frac{\Phi(\mathbf{B})}{L} \quad (277)$$

where $\Phi(\mathbf{B})$ is the flux, linked by C , of the \mathbf{B} field produced by the current J flowing within C itself.

Blednov (1971) gives detailed computations of the magnetic vector potential of a circular loop, expanded in Taylor series up to $n = 7$, expressed by means of complete elliptic integrals of the I and II kind, while the derivatives of the total elliptic integrals of the III kind are computed up to the sixth order.

A.5. Loops.

The Ohm law for a c -loop C is

$$F_e - \frac{L}{\gamma_0} \frac{dJ}{dt} = J R \quad (278)$$

(F_e is the applied external e.m.f. and R is the resistance of C). The energy balance can be evaluated by means of

$$\int F_e J dt - \frac{L}{\gamma_0} \int \frac{dJ}{dt} J dt = \int J^2 R dt \quad (279)$$

or

$$\int U_{s,total}(\mathbf{B}) dt = F_e J dt - \int J^2 R dt \quad (280)$$

$$= \frac{L}{2\gamma_0^2} J^2$$

where the $[F_e J]$ integral is the work done by the external e.m.f., and the $[J^2 R]$ integral is the Joule heat term.

In this case, the c -loop/ m -loop duality can be evidenced as follows. Insert (277)b into (280) and get

$$U_{s,total}(\mathbf{B}) = \frac{1}{2\gamma_0^2} L J^2 = \frac{1}{2} \frac{[\Phi(\mathbf{B})]^2}{L} \quad (281)$$

where (280) and (281) can be interpreted by means of (264), i.e.

$$U_s(\mathbf{B}) = \frac{1}{2\gamma_0} J \Phi(\mathbf{B}) = \frac{1}{2\gamma_0^2} L J^2 \quad (282)$$

as, owing to the same definition of L [see (277)], it is

$$\Phi(\mathbf{B}) = \frac{1}{\gamma_0} L J \quad (283)$$

Similarly to this, (280) and (281) can be interpreted in terms of (274), i.e.

$$U_s(\mathbf{B}) = \frac{1}{2\gamma_0} J \Phi(\mathbf{B}) \quad (284)$$

which is identical to (282).

Consider a region V of space, which contains no electric power supply, i.e., consider any portion V of space where the relative permittivity (or dielectric constant) ϵ_r and the permeability μ_r are constant and homogeneous. Apply the Poynting theorem. It states that every eventual work being spent by the e.m. field inside V , i.e., the term $\mathbf{E} \times \mathbf{j}$ must be interpreted either by decreasing the electric and/or magnetic energy (i.e., the terms \mathbf{E}^2 and \mathbf{H}^2), or by a suitable incoming flux of the Poynting vector across S . The relationship with (279) relies on the fact that the integrals

$$\int F_{e1} J_1 dt - \frac{L_{11}}{\gamma_0^2} \int \frac{dJ_1}{dt} J_1 dt - \frac{L_{12}}{\gamma_0^2} \int \frac{dJ_2}{dt} J_1 dt = \int J_1^2 R_1 dt$$

$$\int F_{e2} J_2 dt - L \frac{L_{22}}{\gamma_0^2} \int \frac{dJ_2}{dt} J_2 dt - \frac{L_{21}}{\gamma_0^2} \int \frac{dJ_1}{dt} J_2 dt = \int J_2^2 R_2 dt$$
(285)

where one can easily recognize the terms associated with the work spent by the power supplies, the terms associated with the self-energies and with the joint energy, and with Joule heat. As well, it is possible to write explicitly the Poynting theorem for a region of space having ϵ_r and μ_r homogeneous, and to envisage the roles of - and the reciprocal exchanges between - different kinds of energy, etc.

A.6. Two rigid loops.

$$\text{Max} \quad U_j = \frac{1}{4\pi} \int_{V_\infty} \mathbf{H} \times \mathbf{B} d\tau = \frac{1}{\gamma_0} J_1 \Phi_1(\mathbf{B}_2) = \frac{1}{\gamma_0} J_2 \Phi_2(\mathbf{B}_1)$$
(286)

where $\gamma_0 = 1$ in SI units. Therefore, $-U_j$ behaves like a potential energy in the fact that $-U_j$ tends to become minimum and to transform itself into a different kind of energy.

$$\text{min} \quad U_{s1} = \frac{1}{8\pi} \int_{V_\infty} \mathbf{H} \times \mathbf{B} d\tau = \frac{1}{\gamma_0} J_1 \Phi_1(\mathbf{B}_1)$$
(287)

or the loop expands as much as possible in such a way as to get $\Phi_1(\mathbf{B}_1)$ as large as possible (this is a well-known experimental result from classical elementary electromagnetism; see, e.g., Bruhat, 1963, p. 457-458; or it can also be proven by application of the virial theorem to plasmas, see section 5.2-I, or, e.g., Rossi and Olbert, 1970).

Upon repeating 14 Gedankenexperimente with different properties of C_1 and C_2 , one can formally show the principle of magnetic energy variation (see section I).

A.7. Spherical shell.

$$W^{(-)}(r, \vartheta, \varphi) = R^* \sum_{n=1}^N \sum_{m=0}^n \left(\frac{r}{R^*}\right)^n P_n^m(\cos \vartheta) [u_n^{m(-)} \sin m\varphi + v_n^{m(-)} \cos m\varphi] \quad (\text{for } r < R^*) \quad (289)$$

$$W^{(+)}(r, \vartheta, \varphi) = R^* \sum_{n=1}^N \sum_{m=0}^n \left(\frac{R^*}{r}\right)^{n+1} P_n^m(\cos \vartheta) [u_n^{m(+)} \sin m\varphi + v_n^{m(+)} \cos m\varphi] \quad (\text{for } r < R^*) \quad (290)$$

in (279) are extended over all space V_∞ , and the flux of the Poynting vector takes into account the magnetic energy that must "migrate" across S to build up the energy density outside V .

The case of several loops leads to a similar conclusion. For the sake of simplicity, consider only the case of two loops C_1 and C_2 , with mutual inductance L_{12} , and with currents J_1 and J_2 , power supplies F_{e1} and F_{e2} , self-inductances L_{11} and L_{22} , and Ohmic resistances R_1 and R_2 , respectively. The equations analogous to (279) are

A system of two loops is, in several respects, the simplest case history. It is well-known from elementary electromagnetism that any two given loops C_1 and C_2 attempt to reorient themselves in such a way as to make maximum the magnetic flux that is originated by one loop and that is linked by the other. That is, call J_1, J_2, \mathbf{B}_1 and \mathbf{B}_2 , respectively, the electric currents that flow within, and the magnetic fields that are generated by, C_1 and C_2 . Physics states that their joint total magnetic energy must be maximum, i.e.,

Similarly to this, it is well-known that any one given loop, say C_1 , when it is considered alone, is such that its self-energy is minimum, i.e.,

The content of the present section deals with a straightforward application of a classical formal development. However, in the present section, we refer to a general spherical shell (ss) of radius R^* (instead of the Earth's radius a^*). Given a potential $W(r, \vartheta, \varphi)$, the magnetic field is defined in the QS approximation by

$$\mathbf{H}(r, \vartheta, \varphi) = -\text{grad } W(r, \vartheta, \varphi) \quad (288)$$

Sometimes, also the following symbols are used

where R^* is a suitable, arbitrary, and fixed radius. Most often, it is chosen $R^* \equiv a^*$, but sometimes a different choice may be used, e.g., $R^* = a$.

For clarity purposes, it ought to be emphasized that different radii can apply to (289) and (290): the radius a of the ss , the arbitrary fixed and pre-chosen radius R^* , the Earth radius a^* , and the varying radial distance r . These radii can eventually have values that coincide with one another, while their basic differences still remain important when considering, e.g., $grad W$, which implies to make a partial derivative with respect to r , and then to put r equal to either R^* , or a , or a^* . This point often results important in order to avoid misunderstanding while reading the literature.

$$u_n^{m(-)} = -\frac{4\pi}{R^*} \frac{n+1}{2n+1} \left(\frac{R^*}{a}\right)^n A_n^m \quad v_n^{m(-)} = -\frac{4\pi}{R^*} \frac{n+1}{2n+1} \left(\frac{R^*}{a}\right)^n B_n^m \quad (\text{for } r < R^*) \quad (291)$$

$$u_n^{m(+)} = \frac{4\pi}{R^*} \frac{n}{2n+1} \left(\frac{a}{R^*}\right)^{n+1} A_n^m \quad v_n^{m(+)} = \frac{4\pi}{R^*} \frac{n}{2n+1} \left(\frac{a}{R^*}\right)^{n+1} B_n^m \quad (\text{for } r > R^*) \quad (292)$$

or also

$$W(r, \vartheta, \varphi) = \sum_{n=1}^N \sum_{m=0}^n P_n^m(\cos \vartheta) [U_n^m \sin m\varphi + V_n^m \cos m\varphi] \quad (293)$$

where

$$U_n^{m(-)} = -4\pi \frac{n+1}{2n+1} \left(\frac{r}{R^*}\right)^n A_n^{m(-)} \quad V_n^{m(-)} = -4\pi \frac{n+1}{2n+1} \left(\frac{r}{R^*}\right)^n B_n^{m(-)} \quad (\text{for } r < R^*) \quad (294)$$

$$U_n^{m(+)} = 4\pi \frac{n}{2n+1} \left(\frac{R^*}{r}\right)^{n+1} A_n^{m(+)} \quad V_n^{m(+)} = 4\pi \frac{n}{2n+1} \left(\frac{R^*}{r}\right)^{n+1} B_n^{m(+)} \quad (\text{for } r > R^*)$$

The magnetic energy associated with this ss is given by integrating (260) over entire V_{∞} . Call S_{R^*} the surface of the ss of radius R^* , call V_{R^*} the volume of space confined by

Note that the observed field is always supposed to be measured at Earth's surface. Then, it is analytically continued through space. However, in the case of $R^* \neq a^* \neq a$, and in the case that the field is measured on a surface other than Earth's surface, this analytical continuation can be different within some layers comprised between these values with either $r = R^*$, or $r = a^*$, or $r = a$. This drawback, however, is physically irrelevant, as far as we deal only with magnetic field observations measured at Earth's surface.

With reference to some other standard symbols used in the geomagnetic literature, the following formal relationships can be shown

S_{R^*} and call \hat{n}_{R^*} the unit vector perpendicular to S_{R^*} at every point and oriented outward. Call $d\tau$ and $d\sigma$ the volume and surface differential, respectively. It is

$$\int_{V_{\infty}} \mathbf{H} \times \mathbf{B} \, d\tau = - \int_{V_{\infty}-V_{R^*}} grad W^{(+)} \times \mathbf{B} \, d\tau - \int_{V_{R^*}} grad W^{(-)} \times \mathbf{B} \, d\tau \quad (295)$$

$$= - \int_{V_{\infty}-V_{R^*}} div (W^{(+)} \mathbf{B}) \, d\tau - \int_{V_{R^*}} div (W^{(-)} \mathbf{B}) \, d\tau$$

$$= \int_{S_{R^*}} W^{(+)} \mathbf{B} \times \hat{n}_{R^*} \, d\sigma - \int_{S_{R^*}} W^{(-)} \mathbf{B} \times \hat{n}_{R^*} \, d\sigma = \int_{S_{R^*}} [W^{(+)} - W^{(-)}] \mathbf{B} \times \hat{n}_{R^*} \, d\sigma$$

$$= -K_0 \mu_r \int_{S_{R^*}} [W^{(+)} - W^{(-)}] grad W^{(-)} \times \hat{n}_{R^*} \, d\sigma$$

$$= -K_0 \mu_r \int_{S_{R^*}} [W^{(+)} - W^{(-)}] \left(\frac{\partial W^{(-)}}{\partial r}\right)_{r=R^*} d\sigma$$

$$= K_0 \mu_r \int_{S_{R^*}} \sum_{n=0}^N \sum_{n_1}^{N_1} (4\pi)^2 M_{n_1}(\vartheta, \varphi) \frac{n_1(n_1+1)}{2n_1+1} \frac{1}{R^*} M_n(\vartheta, \varphi) \, d\sigma$$

It is

$$\int_{S_{R^*}} M_{n_1}(\vartheta, \varphi) M_n(\vartheta, \varphi) \, d\sigma \quad (296)$$

$$= R^{*2} \sum_{n=0}^N \sum_{m_1=0}^{n_1} \int_0^{2\pi} d\varphi \int_0^{\pi} \sin \vartheta \, d\vartheta P_n^{m_1}(\cos \vartheta) P_{n_1}^{m_1}(\cos \vartheta) \cdot [A_n^m \sin m\varphi$$

$$+ B_n^m \cos m\varphi] [A_{n_1}^{m_1} \sin m_1\varphi + B_{n_1}^{m_1} \cos m_1\varphi] = R^{*2} \frac{4\pi}{2n+1} \sum_{m=0}^n [(A_n^m)^2 + (B_n^m)^2]$$

because of the orthogonality of $[P_n^m(\cos \vartheta) \sin m\varphi]$ and $[P_n^m(\cos \vartheta) \cos m\varphi]$ [details not here given]. Therefore, by (260), (295) and (296)

$$U_s(\mathbf{B}) = K_0\mu_r 8\pi^2 R^* \sum_{n=1}^N \sum_{m=0}^n \frac{n(n+1)}{(2n+1)^2} [(A_n^m)^2 + (B_n^m)^2] \quad (297)$$

This formula can be used for the practical evaluation of the self-energies of the geomagnetic field $U_s(\mathbf{B}^{(e)})$ and $U_s(\mathbf{B}^{(i)})$, respectively, associated with the field that is originated in the space either external or internal with respect to Earth's surface. Call a^* the Earth's radius, and R_{TC} and R_{IOM} the radii of the two *ss*, which are the "equivalent" source of the external and internal field, respectively. These R_{TC} and R_{IOM} can be computed independently. Let us therefore use a different symbol in the present computation. Call \tilde{R}_{TC} and \tilde{R}_{IOM} some real, and in general unknown, values, while R_{TC} and R_{IOM} are the

$$U_s(\mathbf{B}^{(e)}) = K_0\mu_r 8\pi^2 \tilde{R}_{IOM} \sum_{n=1}^N \sum_{m=0}^n \frac{n(n+1)}{(2n+1)^2} [(A_n^{m(e)})^2 + (B_n^{m(e)})^2] \quad (299)$$

$$U_s(\mathbf{B}^{(i)}) = K_0\mu_r 8\pi^2 \tilde{R}_{TC} \sum_{n=1}^N \sum_{m=0}^n \frac{n(n+1)}{(2n+1)^2} [(A_n^{m(i)})^2 + (B_n^{m(i)})^2] \quad (300)$$

that can be evaluated whenever \tilde{R}_{TC} and \tilde{R}_{IOM} are known.

The most conventional standard way to express the geomagnetic potentials is in terms of the Gauss elements of

$$W = W^{(e)} + W^{(i)} \quad (301)$$

$$W^{(e)} = a^* \sum_{n=1}^N \sum_{m=0}^n \left(\frac{r}{a^*}\right)^n [h_n^{m(e)} \sin m\varphi + g_n^{m(e)} \cos m\varphi] P_n^m(\cos \vartheta)$$

$$W^{(i)} = a^* \sum_{n=1}^N \sum_{m=0}^n \left(\frac{a^*}{r}\right)^{n+1} [h_n^{m(i)} \sin m\varphi + g_n^{m(i)} \cos m\varphi] P_n^m(\cos \vartheta)$$

hence $W^{(e)}$ is a potential of the kind $W^{(-)}$ by putting $a = \tilde{R}_{IOM}$, while $W^{(i)}$ is of the kind $W^{(+)}$ with $a = \tilde{R}_{TC}$. By comparing (301), (289), (290), (293), and by referring to other standard symbols in geomagnetism, it follows

$$A_n^{m(e)} = -\frac{1}{4\pi} \frac{2n+1}{n+1} a^* \left(\frac{\tilde{R}_{IOM}}{a^*}\right)^n h_n^{m(e)} \quad (302)$$

$$B_n^{m(e)} = -\frac{1}{4\pi} \frac{2n+1}{n+1} a^* \left(\frac{\tilde{R}_{IOM}}{a^*}\right)^n g_n^{m(e)}$$

$$A_n^{m(i)} = \frac{1}{4\pi} \frac{2n+1}{n} a^* \left(\frac{a^*}{\tilde{R}_{TC}}\right)^{n+1} h_n^{m(i)}$$

values that eventually can be even different compared to their respective \tilde{R}_{TC} and \tilde{R}_{IOM} values. Suppose that the geomagnetic field has been analyzed in terms of a *SHE* at Earth's surface, of the form (293) and (294). That is, the following quantities are known (where \tilde{R}_{TC} and \tilde{R}_{IOM} are unknown)

$$U_n^{m(e)}(a^*) = -4\pi \left(\frac{a^*}{\tilde{R}_{IOM}}\right)^n \frac{n+1}{2n+1} A_n^{m(e)} \quad (298)$$

$$V_n^{m(e)}(a^*) = -4\pi \left(\frac{a^*}{\tilde{R}_{IOM}}\right)^n \frac{n+1}{2n+1} B_n^{m(e)}$$

$$U_n^{m(i)}(a^*) = 4\pi \left(\frac{\tilde{R}_{TC}}{a^*}\right)^n \frac{n}{2n+1} A_n^{m(i)}$$

$$V_n^{m(i)}(a^*) = 4\pi \left(\frac{\tilde{R}_{TC}}{a^*}\right)^n \frac{n}{2n+1} B_n^{m(i)}$$

from which it is possible to evaluate $A_n^{m(e)}$, $B_n^{m(e)}$, $A_n^{m(i)}$, $B_n^{m(i)}$ that are used by (297), which thus gives the following expressions

terrestrial magnetism $\{g_n^m, h_n^m\}$ according to the expression

$$B_n^{m(i)} = \frac{1}{4\pi} \frac{2n+1}{n} a^* \left(\frac{a^*}{\tilde{R}_{TC}}\right)^{n+1} g_n^{m(i)}$$

$$U_n^{m(e)} = a^* \left(\frac{r}{a^*}\right)^n h_n^{m(e)}$$

$$V_n^{m(e)} = a^* \left(\frac{r}{a^*}\right)^n g_n^{m(e)}$$

$$U_n^{m(i)} = a^* \left(\frac{a^*}{r}\right)^n h_n^{m(i)}$$

$$V_n^{m(i)} = a^* \left(\frac{a^*}{r}\right)^{n+1} g_n^{m(i)}$$

by which (299) and (300) become

$$U_s(\mathbf{B}^{(e)}) = \frac{K_0\mu_r}{2} (a^*)^2 \tilde{R}_{IOM} \sum_{n=1}^N \sum_{m=0}^n \frac{n}{n+1} \left(\frac{\tilde{R}_{IOM}}{a^*}\right)^{2n} [(h_n^{m(e)})^2 + (g_n^{m(e)})^2] \quad (303)$$

$$U_s(\mathbf{B}^{(i)}) = \frac{K_0\mu_r}{2} (a^*)^2 \tilde{R}_{TC} \sum_{n=1}^N \sum_{m=0}^n \frac{n+1}{n} \left(\frac{a^*}{\tilde{R}_{TC}}\right)^{2(n+1)} [(h_n^{m(i)})^2 + (g_n^{m(i)})^2] \quad (304)$$

A.8. 2D current distribution of arbitrary shape (general shell).

The computation of the magnetic self-energy of an arbitrary 2D \mathbf{j} -distribution is analytically cumbersome, although it is numerically feasible by computer.

$$U_s(\mathbf{B}) = \frac{1}{8\pi} \int_{V_\infty} \mathbf{H} \times \mathbf{B} \, d\tau = -\frac{K_0 \mu_r}{8\pi} \int_{S_a} [W^{(+)} - W^{(-)}] \, \text{grad } W^{(-)} \times \hat{\mathbf{n}}_a \, d\sigma \tag{305}$$

where S_a is no more a spherical surface⁵¹; rather, it is the surface of the shell $a(\vartheta, \varphi)$ while $\hat{\mathbf{n}}_a$ is the unit vector perpendicular to it, at any point (ϑ, φ) and oriented outward [i.e., toward $r > a(\vartheta, \varphi)$]. The integral on the right hand side of (305) can be numerically evaluated and computed according to the following specifications

$$\begin{aligned} & (W^{(+)} - W^{(-)})_{r=a(\vartheta_0, \varphi_0)} \\ &= \int_0^{2\pi} d\varphi \int_0^\pi \sin \vartheta \, d\vartheta \, M(\vartheta, \varphi) \sum_{n_1=0}^{N_1} P_{n_1}(\cos \psi) \left\{ n_1 \left[\frac{a(\vartheta, \varphi)}{a(\vartheta_0, \varphi_0)} \right]^{n_1+1} + (n_1 + 1) \left[\frac{a(\vartheta_0, \varphi_0)}{a(\vartheta, \varphi)} \right]^{n_1} \right\} \end{aligned} \tag{306}$$

where it must be intended that $[W^{(+)} - W^{(-)}]$ is a function of ϑ_0 and φ_0 (which have not to be confused with ϑ and φ that are integrated on the right hand side). The ϑ_0 and φ_0 dependence enters through $a(\vartheta, \varphi)$ and $\cos \psi$, which is defined by generalizing figure 25 into figure 26. The integral on the right hand side in (306) is extended over S_a , i.e., over the surface $r = a(\vartheta_0, \varphi_0)$ over which a magnetic "strength" (or "power") $M(\vartheta_0, \varphi_0)$ is located at every ϑ_0 and φ_0 .

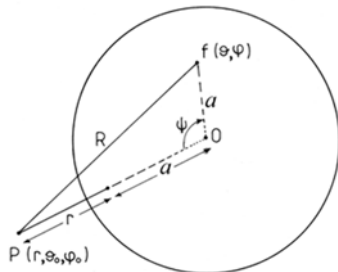


Figure 25. Given a spherical shell of radius a , with a magnetic density $f(\theta, \phi)$ at any given point on the spherical surface of spherical coordinates (θ, ϕ) , and given a point $P(r, \theta_0, \phi_0)$, define the angle ψ and the distance R . Unpublished figure.

Suppose that a varying radius of a ss is expressed as $a(\vartheta, \varphi)$ and is given in the most general way, which is, e.g., in terms a log of numerical values, i.e., one value of a for every ϑ and φ . Start from (260) and generalize (295) - which contains several identities that hold also in the present case - and get

(suppose that $d\sigma$ is expressed in terms of the angles ϑ_0 and φ_0).

The function $[W^{(+)}(r, \vartheta_0, \varphi_0) - W^{(-)}(r, \vartheta_0, \varphi_0)]$ for $r = a(\vartheta_0, \varphi_0)$ can be expressed accordingly, and thus formally find

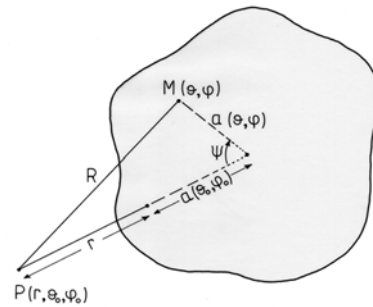


Figure 26. This is the same as figure 25, but for a general non-spherical shell $r = a(\vartheta, \varphi)$ over which either a magnetic charge density $f(\vartheta, \varphi)$ or a magnetic dipole density per unit surface $M(\vartheta, \varphi)$ is located, while $P(r, \theta_0, \phi_0)$ is used for defining the angle ψ and the distance R . Unpublished figure.

The term $[W^{(+)} - W^{(-)}] \, \text{grad } W^{(-)} \times \hat{\mathbf{n}}_a$ in (305) can be evaluated by considering that the components of $[\text{grad } W^{(-)}]$ and of $\hat{\mathbf{n}}_a$ are (in spherical coordinates) respectively (the computation is according to the standard mathematical treatment and symbols of geomagnetism)

$$\begin{aligned} & \left(\frac{\partial W^{(-)}}{\partial r} \right)_{\vartheta_0, \varphi_0, r=a(\vartheta_0, \varphi_0)} \\ &= - \int_0^{2\pi} d\varphi \int_0^\pi \sin \vartheta \, d\vartheta \sum_{n_1=0}^{N_1} n_1(n_1 + 1) P_{n_1}(\cos \psi) M(\vartheta, \varphi) \frac{1}{a(\vartheta, \varphi)} \left[\frac{a(\vartheta_0, \varphi_0)}{a(\vartheta, \varphi)} \right]^{n_1-1} \end{aligned} \tag{307}$$

⁵¹ In addition, S_n ought not to be confused with the symbol for a general spherical harmonic function.

$$\frac{1}{a(\vartheta_0, \varphi_0)} \left(\frac{\partial W^{(-)}}{\partial \vartheta_0} \right)_{\vartheta_0, \varphi_0, r=a(\vartheta_0, \varphi_0)} \quad (308)$$

$$= - \int_0^{2\pi} d\varphi \int_0^\pi \sin \vartheta d\vartheta \sum_{n_1=0}^{N_1} (n_1 + 1) M(\vartheta, \varphi) \left[\frac{a(\vartheta_0, \varphi_0)}{a(\vartheta, \varphi)} \right]^{n_1} \frac{1}{a(\vartheta_0, \varphi_0)} \frac{\partial P_{n_1}(\cos \psi)}{\partial \cos \psi} \frac{\partial \cos \psi}{\partial \vartheta_0} \frac{1}{a(\vartheta_0, \varphi_0) \sin \vartheta_0} \left(\frac{\partial W^{(-)}}{\partial \varphi_0} \right)_{\vartheta_0, \varphi_0, r=a(\vartheta_0, \varphi_0)} \\ + \frac{1}{a(\vartheta_0, \varphi_0) \sin \vartheta_0} \left(\frac{\partial W^{(-)}}{\partial \vartheta_0} \right)_{\vartheta_0, \varphi_0, r=a(\vartheta_0, \varphi_0)} \quad (309)$$

$$= - \int_0^{2\pi} d\varphi \int_0^\pi \sin \vartheta d\vartheta \sum_{n_1=0}^{N_1} (n_1 + 1) M(\vartheta, \varphi) \left[\frac{a(\vartheta_0, \varphi_0)}{a(\vartheta, \varphi)} \right]^{n_1} \frac{1}{a(\vartheta_0, \varphi_0) \sin \vartheta_0} \frac{\partial P_{n_1}(\cos \psi)}{\partial \cos \psi} \frac{\partial \cos \psi}{\partial \vartheta_0} \\ (\hat{n}_a)_r = const \quad (310)$$

$$(\hat{n}_a)_\vartheta = \frac{1}{a(\vartheta_0, \varphi_0)} \left(\frac{\partial a(\vartheta_0, \varphi_0)}{\partial \vartheta_0} \right)_{\vartheta_0, \varphi_0} \cdot const \quad (311)$$

$$(\hat{n}_a)_\varphi = \frac{1}{a(\vartheta_0, \varphi_0) \sin \vartheta_0} \left(\frac{\partial a(\vartheta_0, \varphi_0)}{\partial \varphi_0} \right)_{\vartheta_0, \varphi_0} \cdot const \quad (312)$$

$$const = \left\{ 1 + \left[\frac{1}{a(\vartheta_0, \varphi_0)} \left(\frac{\partial a(\vartheta_0, \varphi_0)}{\partial \vartheta_0} \right)_{\vartheta_0, \varphi_0} \right]^2 + \left[\frac{1}{a(\vartheta_0, \varphi_0) \sin \vartheta_0} \left(\frac{\partial a(\vartheta_0, \varphi_0)}{\partial \varphi_0} \right)_{\vartheta_0, \varphi_0} \right]^2 \right\}^{-1/2} \quad (313)$$

The factors $\partial \cos \psi / \partial \vartheta_0$ and $\partial \cos \psi / \partial \varphi_0$ can be easily evaluated by means of suitable formulas,⁵² where the symbols have to be changed as follows (see figure 25). That is, this is a particular case of a transformation of spherical

coordinates over S_a from latitude and longitude (λ_1, φ_1) into a new latitude and longitude (λ_2, φ_2) , where, however, φ_2 is not here of direct concern

$$\begin{aligned} \lambda_1^{(2)} &= \pi/2 - \vartheta_0 & \varphi_1^{(2)} &= \varphi_0 & \varphi_2^{(1)} &= 0 & (314) \\ \lambda_1 &= \pi/2 - \vartheta & \varphi_1 &= \varphi & \psi &= \pi/2 - \lambda_2 \end{aligned}$$

to give

$$\cos \psi = \cos \vartheta_0 \cos \vartheta + \sin \vartheta_0 \sin \vartheta \cos(\varphi_0 - \varphi) \quad (315)$$

thus providing, by using also (321) through (324) to express the same quantities also in the coordinate system (λ_2, φ_2)

$$\begin{aligned} \frac{\partial \cos \psi}{\partial \vartheta_0} &= -\sin \vartheta_0 \cos \vartheta + \cos \vartheta_0 \sin \vartheta \cos(\varphi_0 - \varphi) = & (316) \\ &= -\sin \vartheta_0 \cos \vartheta + \frac{\cos \vartheta_0}{\sin \vartheta_0} (\cos \psi - \cos \vartheta_0 \cos \vartheta) = \frac{1}{\sin \vartheta_0} (\cos \vartheta_0 \cos \psi - \cos \vartheta) \\ &= -\sin \psi \cos \varphi_2 \\ \frac{\partial \cos \psi}{\partial \varphi_0} &= -\sin \vartheta_0 \sin \vartheta \sin(\varphi_0 - \varphi) = -\sin \vartheta_0 \sin \varphi_2 \sin \psi \end{aligned}$$

In addition, the partial derivatives of $a(\vartheta, \varphi)$ with respect to ϑ and φ have to be evaluated numerically.

This whole computation deals with the evaluation of the self-energy of a general shell defined by means of a numerical log. One can also carry out the formal computation for a shell described by an analytical function.

The computation is cumbersome. The remaining part of this section deals with this computation.

The formal analytical development results more straightforward by changing the frame of reference according to (314). Refer to figure 26, where ϑ and φ are defined in any given pre-chosen and arbitrary way (e.g., by

⁵² The same procedure applies to the addition theorem for Legendre's polynomials, for the first derivative of Legendre's

polynomials, and for spherical harmonics. Details not here given.

geographic coordinates). Let us choose a new system of spherical coordinates having pole such that P has latitude $\lambda_2^{(P)} = \pi/2$. That is, $\psi = \pi/2 - \lambda_2 \equiv \vartheta_2$ is the colatitude

$$\sin \lambda_2 = \sin \lambda_1^{(2)} \sin \lambda_1 + \cos \lambda_1^{(2)} \cos \lambda_1 \cos(\varphi_1 - \varphi_1^{(2)}) \quad (317)$$

$$\sin \varphi_2 = -\frac{\cos \lambda_1}{\cos \lambda_2} \sin(\varphi_1 - \varphi_1^{(2)}) \quad (318)$$

$$\sin \lambda_1 = \sin \lambda_2^{(1)} \sin \lambda_2 + \cos \lambda_2^{(1)} \cos \lambda_2 \cos(\varphi_2 - \varphi_2^{(1)}) \quad (319)$$

$$\sin \varphi_1 = -\frac{\cos \lambda_2}{\cos \lambda_1} \sin(\varphi_2 - \varphi_2^{(1)}) \quad (320)$$

that, by the alternative symbols (314), can be written as

$$\cos \psi = \cos \vartheta_2 = \cos \vartheta_0 \cos \vartheta + \sin \vartheta_0 \sin \vartheta \cos(\varphi - \varphi_0) \quad (321)$$

$$\sin \varphi_2 = -\frac{\sin \vartheta}{\sin \psi} \sin(\varphi - \varphi_0) \quad (322)$$

$$\cos \vartheta = \cos \vartheta_0 \cos \psi + \sin \vartheta_0 \sin \psi \cos \varphi_2 \quad (323)$$

$$\sin \varphi = -\frac{\sin \psi}{\sin \vartheta} \sin \varphi_2 \quad (324)$$

When we have to carry out an integral over the entire general shell, it is

$$\begin{aligned} & \int_0^{2\pi} d\varphi \int_0^\pi \sin \vartheta d\vartheta \dots \quad (325) \\ &= \int_0^{2\pi} d\varphi_2 \int_0^\pi \sin \vartheta_2 d\vartheta_2 \dots \\ &= \int_0^{2\pi} d\varphi_2 \int_0^\pi \sin \psi d\psi \dots \end{aligned}$$

This completes the preset Appendix, which is an excerpt of a much longer and systematic formulary, and only one formula is here recalled that are needed for the present paper.

Acknowledgement

We acknowledge several friends and colleagues that, during several decades and in different and often indirect way, contributed with their comments to implement the present study.

Funding Information

The main funding was to the first author by CNR through institutional supply.

Author's Contributions

The first author exploited the main and leading concepts, and wrote the present draft. The other coauthors contributed with discussion and criticisms aimed to clarify different topics.

Ethics

No peculiar ethical issues concern the present paper.

References

in such a new coordinate system. The transformation formulas for transforming (λ_1, φ_1) into (λ_2, φ_2) , and viceversa are

Akasofu, Syun-Ichi, 1964. The development of the auroral substorm, *Planet. Space Sci.*, 12, (4): 273-282; DOI:10.1016/0032-0633(64)90151-5.

Akasofu, Syun-Ichi, 1968. *Polar and magnetospheric substorms*, D. Reidel Publ. Co., Dordrecht: 1-280.

Akasofu, Syun-Ichi, 1977. *Physics of magnetospheric substorms*, D. Reidel, Dordrecht, Netherlands: 1-599.

Akasofu, Syun-Ichi, 1981. Energy coupling between the solar wind and the magnetosphere. *Space Sci. Rev.*, 28, (2): 121-190; DOI:10.1007/BF00218810.

Akasofu, Syun-Ichi, 1999. The rise and fall of paradigms and some longstanding unsolved problems in solar-terrestrial physics. In S. Kokubun, and Y. Kamide, Eds, *Substorms-4-International Conference in Substorms-4, Lake Hamana, Japan, March 9-13, 1998*, Kluwer Academic Publs.: 21-25.

Akasofu, Syun-Ichi, and Sydney Chapman, 1972. *Solar-terrestrial physics - An account of the wave and particle radiations from the quiet and the active Sun, and of the consequent terrestrial phenomena*. Oxford, at the Clarendon Press: 1-901.

Alfvén, Hannes Olof Gosta, 1968. Some properties of magnetospheric neutral surfaces, *J. Geophys. Res.*, 73: 4379-4381.

Arley, N., and K.R. Buch, 1950. *Introduction to the theory of probability and statistics*. Science Editions, John Wiley and Sons, Inc., New York: 1-240.

Baker, Daniel N., N. E. Turner, and T. I. Pulkkinen, 2001. Energy transport and dissipation in the magnetosphere during geomagnetic storms, *J. Atmos. Solar-Terr. Phys.*, 63: 421-429; DOI:10.1016/S1364-6826(00)00169-3.

Baker, Daniel N., T. I. Pulkkinen, M. Hesse, and Robert L. McPherron, 1997. A quantitative assessment of energy storage and release in the Earth's magnetotail, *J. Geophys. Res.*, 102: 7159-7168.

Baker, J., and J. Hurley, 1967. A self-consistent study of the Earth radiation belts, *J. Geophys. Res.*, 72: 4351-4355.

Becker, Richard, 1933. *Theorie der Elektrizität, Band I, Einführung in die Maxwellsche Theorie der Elektrizität*,

- (IX ed., 1941), and *Band II, Elektronen Theorie* (VI ed.), Teubner. Leipzig. (Italian translation published by Sansoni, Firenze, 1949: pp. 1-313, and 1950: pp. 1-481 pp.).
- Biermann, Ludwig, 1941. Der gegenwärtige Stand der Theorie konvektiver Sonnenmodelle. *Vierteljahrsschrift der Astronomischen Gesellschaft, Leipzig*, 76, 194-200. [After 1950 the journal continued as *Mitteilungen der Astronomischen Gesellschaft, Hamburg*].
- Binns, K. J., and P. J. Lawrenson, 1963. *Analysis and computation of electric and magnetic field problems*, Pergamon Press, Oxford, etc.: 1-333.
- Blednov, V. A., 1971. Expansion of the magnetic vector potential, computed for a current-carrying loop, *Geomagn. Aeron.*, 10: 549-552.
- Bonnevier, B., 1964. On the early development of the metagalactic system, *Arkiv. Fysik*, 27, (21): 310-.
- Brandstatter, Julius J., 1963. *An introduction to waves, rays and radiation in plasma media*, McGraw-Hill Book Co., New York: 1-690.
- Bruhat, Georges, 1963. *Cours de physique générale. Electricité*. Masson, Paris: 1-911.
- Bryunelli, B. Ye., and M. I. Pudovkin, 1966. Energy of a magnetic storm, *Geomagn. Aeron.*, 6, (6): 844-848.
- Campbell, W. H., 1996. Geomagnetic storms, the *Dst* ring-current myth and lognormal distributions. *J. Atmos. Terr. Phys.*, 58, (10): 1171-1187; DOI:10.1016/0021-9169(95)00103-4.
- Carovillano, Robert L., and George L. Siscoe, 1973. Energy and momentum theorems in magnetospheric physics, *Rev. Geophys.*, 11: 289-353.
- Carovillano, Robert L., and J. J. Maguire, 1966. The energy of confinement of a shielded magnetic dipole field, *Geophys. J. Roy. Astron. Soc.*, 12: 23-28.
- Carovillano, Robert L., and J. J. Maguire, 1968. Magnetic energy relationships in the magnetosphere. R. L. Carovillano, J. F. Mc Clay, and H. R. Radoski, , Eds, *Physics of the magnetosphere*, Reidel Publ. Co., Dordrecht; 290-300.
- Chandrasekhar, Subrahmanyan, and Enrico Fermi, 1953. Problems of gravitational stability in the presence of a magnetic field. *Astrophys. J.*, 118: 116-141.
- Chapman, Sydney, 1964. The energy of magnetic storms, *Geophys. J. R. Astr. Soc.*, 8: 514-536.
- Choe, J. Y., D. B. Beard, and E. C. Sullivan, 1973. Precise calculation of the magnetosphere surface for a tilted dipole, *Planet. Space Sci.*, 21: 485-498.
- Courant, Richard, and David Hilbert, 1953. *Methods of mathematical physics. Vol. I: 1-561, Vol. II, Partial differential equations: 1-830*, Interscience Publishers, New York and London. First published in German, *Methoden der mathematischen Physik*, Berlin, 1924.
- Dessler, Alex J., 1968. Magnetic merging in the magnetospheric tail, *J. Geophys. Res.*, 73: 209-214; correction *J. Geophys. Res.*, 73: 1861.
- Dessler, Alex J., 1971. Vacuum merging: a possible source of the magnetospheric cross-tail electric field, *J. Geophys. Res.*, 76: 3174-3176.
- Dessler, Alex J., 1971. Vacuum merging: a possible source of the magnetospheric cross-tail electric field, *J. Geophys. Res.*, 76: 3174-3176.
- Dessler, Alex J., and Eugene N. Parker, 1959. Hydromagnetic theory of geomagnetic storms, *J. Geophys. Res.*: 64, 2239-2252.
- Dungey, James W., 1961. Interplanetary magnetic field and the auroral zones, *Phys. Rev. Lett.*, 6: 47-48.
- Dungey, James W., 1963. The structure of the exosphere or adventures in velocity space. In C., deWitt, J., Hieblot, and A., Lebeau, (eds.), *Géophysique extérieure-Geophysics, The Earth's environment*, Gordon and Breach, Science Publ., New York and London: 503-550.
- Durand, E., 1968. *Magnétostatique*, Masson, Paris : 1-673.
- Garrett, Milan Wayne, 1963. Calculations of fields, forces, and mutual inductances of current systems by elliptic integrals, *J. Appl. Phys.*, 34: 2567-.
- Gonzales, W. D., and F. S. Mozer, 1974. A quantitative model from the potential resulting from reconnection with an arbitrary interplanetary magnetic field, *J. Geophys. Res.*, 79: 4186-4194.
- Gonzalez, W. D., J. A. Joselyn, Y. Kamide, H. W. Kroehl, G. Rostoker, and V. M. Vasyliūnas, 1994. What is a geomagnetic storm, *J. Geophys. Res., Space*, 99, (A4): 5771-5792, [93JA02867]; DOI:10.1029/93JA02867.
- Gonzalez, Walter Demetrio, 1990. A unified view of solar wind-magnetosphere coupling function, *Planet. Space Sci.*, 38: 627-631; DOI:10.1016/0032-0633(90)90068-2.
- Gregori, G. P., 1968. On the origin of day-side auroras, *Annales de Géophysique*, 24, (1): 153-158.
- Gregori, G. P., 1991. Artificial generation of a magnetospheric substorm. In E. Sindoni, and A.Y. Wong (eds.), *Controlled active global experiments (C.A.G.E.)*, Proceedings of the International School of Plasma Physics "Piero Caldirola", Varenna (Como-Italy), September 5-12, 1989, Editrice Compositori, Società Italiana di Fisica, Bologna: 361-366.
- Gregori, G. P., 1998. Natural catastrophes and point-like processes. Data handling and prevision. *Annali di Geofisica*, 41, (5/6): 767-786.
- Gregori, G. P., 1999. Variational principles and geomagnetism. In W. Schröder, Ed., *Physics and geophysics (A compilation with special historical case studies)*, History Commission of the German Geophysical Society, Mitteilungen des Arbeitskreises Geschichte der Geophysik der DGG, Science Edition/DGG, Bremen, 18, Heft 1-3: 268-303.
- Gregori, G. P., 1999a. The external magnetic sources over the polar caps. Feasible modelling vs. unrealistic expectations. *Annali di Geofisica*, 42, (2): 171-189.
- Gregori, G. P., 2000. Geomagnetism and fundamental science. In W. Schröder, Ed., *Geomagnetism (research,*

- past and present*), *Newsletter of the IDCH of IAGA*: 12-50.
- Gregori, G. P., 2001. Self-consciousness in Earth's sciences - Some personal reflections. In W. Schröder, Ed., *Wege zur Wissenschaft, Gelehrte erzählen aus ihrem Leben – Pathways to science, Scientists tell of their life and work*, Beiträge zur Geschichte der Geophysik und Kosmischen Physik des Arbeitskreises Geschichte der Geophysik und Kosmischen Physik, W. Schröder, AKGGKP, Bremen-Roenebeck, (4): 123-133.
- Gregori, G. P., 2002. Galaxy – Sun – Earth relations. The origin of the magnetic field and of the endogenous energy of the Earth, with implications for volcanism, geodynamics and climate control, and related items of concern for stars, planets, satellites, and other planetary objects. A discussion in a prologue and two parts. *Beiträge zur Geschichte der Geophysik und Kosmischen Physik*, Band 3, Heft 3: 1-471 pp. [Available at <http://ncgtjournal.com/additional-resources.html>].
- Gregori, G. P., 2016a. The endogenous energy and the magnetic field of planetary objects: the Pluto/Charon binary system and its seasonal rejuvenation, *New Conc. Global Tect., J.*, 4, (3): 406-431.
- Gregori, G. P., and B. A. Leybourne, 2021. An unprecedented challenge for humankind survival. Energy exploitation from the atmospheric electrical circuit, *American Journal of Engineering and Applied Science*, DOI:10.3844/ajeassp.2021.258.291.
- Gregori, G. P., and B. A. Leybourne, 2025g. The physics of electrical discharges – 3. Sparks and lightning - electrostatics of the ionosphere – TLEs - plasma jets collimation – Birkeland currents & sea-urchin spikes - stellar and galactic alignments, pending publication on *Am. J. Engin. Appl. Sci.*
- Gregori, G. P., B. A. Leybourne, and J. R. Wright, 2025d. Generalized Cowling theorem and the Cowling dynamo, pending publication on *Am. J. Engin. Appl. Sci.*
- Gregori, G. P., B. A. Leybourne, Dong Wenjie, Gao Xiaoqing, 2025o. Energy release from ALB, CMB and ICB and secular variation. V – Results. *New Concepts in Global Tectonics Journal*, 13, (3).
- Gregori, G. P., B. A. Leybourne, W. Soon, and V. Straser, 2025e. The heuristic meaning of variational principles, pending publication on *Am. J. Engin. Appl. Sci.*
- Gregori, G. P., F. F. Bonavia, and B. A. Leybourne, 2024x. Geoelectrical geology in North America. In press on *New Concepts in Global Tectonics*.
- Gregori, G. P., M. T. Hovland, B. A. Leybourne, S. Pellis, V. Straser, B. G. Gregori, G. M. Gregori, and A. R. Simonelli, 2025w. Air-earth currents and a universal “law”: filamentary and spiral structures - Repetitiveness, fractality, golden ratio, fine-structure constant, antifragility and “statistics” - The origin of life, *New Concepts in Global Tectonics*, 3, (1): 106-225.
- Gregori, Giovanni P., and Bruce A. Leybourne, 2025m. Comets like probes of the solar wind. Magnetospheres and cometospheres. In press on *New Concepts in Global Tectonics*.
- Gribbin, John, and Stephen Plagemann, 1973. Discontinuous change in Earth's spin rate following great solar storm of August 1972. *Nature*, 243, (5401): 26-27.
- Hart, Philip J., 1967. *Universal tables for magnetic fields of filamentary and distributed circular currents*, American Elsevier Publ. Co., New York: 1-489.
- Hasegawa, Akira, 1971. Plasma instabilities in the magnetosphere, *Rev. Geophys. Space Phys.*, 9: 703-772.
- Hasegawa, Akira, 1975. Plasma instabilities and nonlinear effects, 217 pp., Springer-Verlag, Berlin, etc.
- Heikkila, W.J., 1972. Penetration of particles into the polar cap Regions of the magnetosphere. In E.R., Dyer, *Critical problems in magnetospheric physics*, Proceedings. of the Symposium, held 11-13 May, 1972 in Madrid, Spain, Ed., IUCSTP Secretariat, National Academy of Sciences, Washington D.C.: 67-82.
- Hines, Colin O., 1974. Solar wind torque as an inhibitor of terrestrial relation, *J. Geophys. Res.*, 79: 1543-1545.
- Hospers, J., and S. I. Van Andel, 1970. Statistical analysis of ancient Earth radii computed from palaeomagnetic data. In S. K. Runcorn, , Ed., *Palaeogeophysics*, Academic Press: 407-412.
- Hultqvist, B., 1969a. Auroral and polar substorms: observations and theory. *Rev. Geophys.*, 7, (1,2): 129-177.
- Huttunen, K. E. J., H. E. J. Koskinen, T. I. Pulkkinen, A. Pulkkinen, M. Palmroth, E. G. D. Reeves, and H. J. Singer, 2002. April 2000 magnetic storm: solar wind driver and magnetospheric response, *J. Geophys. Res.*, 107, 1440 [21 pp.]; DOI:10.1029/2001JA0009154.
- Larmor, Sir J., 1919a. Possible rotational origin of magnetic fields of Sun and Earth. *Electr. Rev.*, 85: 412 (or 512?).
- Larmor, Sir J., 1920. How could a rotating body such as the Sun become a magnet?, *Rep. Brit. Ass. Adv. Sci., Bournemouth Meeting, 1919*: 159-160, also in *Mathematical and physical papers*, Cambridge University Press, 1929, Vol. II: 611-612.
- Lassen, K., 1967. Polar cap aurora. In B.M. McCormac, Ed., *Aurora and airglow*. Reinhold Publ. Corp., New York etc.: 453-464.
- Lassen, K., 1969. Polar cap emissions. In B.M. McCormac and A. Omholt, Eds., *Atmospheric emissions*, Van Nostrand Reinhold Company, New York etc.: 63-71.
- Leybourne, B. A., D. W. Johnson, and G. P. Gregori, 2025. Arc-Blast as static electricity or interplanetary lightning short circuits in Stellar Transformers. A plausible North American scenario. *New Concepts in Global Tectonics*, 13, (2): 229-251.
- Liao, Sen-ben, Peter Dourmashkin, and John W. Belcher, 2004. *Physics 8.02 - Electricity & Magnetism* – MIT, Chapter 11.
- Liemohn, Mike W., 2003. Yet another caveat to using the Dessler-Parker-Sckopke relation, *J. Geophys. Res.*, 108, (A6): 1251, 20 pp.; DOI:10.1029/2003JA000939.

- Longmire, C. L., 1963. *Elementary plasma physics*, Interscience, New York: 1-296.
- Lu, G., D. N. Baker, Robert L. McPherron, C. J. Farrugia, D. Lummerzheim, J. M. Ruohoniemi, F. J. Rich, D. S. Evans, R. P. Lepping, M. Brittnacher, X. Li, R. Greenwald, G. Sofko, J. Villain, M. Lester, J. Thayer, T. Moretto, D. Milling, O. Troshichev, A. Zaitzev, V. Odintsov, G. Makarov, and K. Hayashi, 1998. Global energy deposition during the January 1997 magnetic cloud event, *J. Geophys. Res.*, 103, (A6): 11685–11694.
- Maguire, J. J., and Robert L. Carovillano, 1966. Energy principles of confinement of a magnetic field, *J. Geophys. Res.*, 71: 5533-5539.
- Maguire, J. J., and Robert L. Carovillano, 1968. Effects of the interplanetary field on the energy of geomagnetic disturbances, *J. Geophys. Res.*, 73: 3395-3405.
- Mariani, Franco, and Norman F. Ness, 1969. Observations of the geomagnetic tail at 500 Earth radii by Pioneer 8, *J. Geophys. Res.*, 74, 5633-5641.
- Matsushita, Sadami, 1967. Solar quiet and lunar daily variation fields. In S. Matsushita, and W. H. Campbell, Eds., *Physics of geomagnetic phenomena*. 2 vol., Academic Press, New York, etc.: 301-424.
- Mauersberger, Peter, 1964. *Theorie der elektromagnetischen Felder*, [Geomagnetismus und Aeronomie – Band I/1, herausgegeben von Prof. Dr. Gerhard Fanselau] Veb deutscher Verlag der Wissenschaften, Berlin: 1-248.
- Merrill, Ronald T., Michael W. McElhinny, and Phillip L. McFadden, 1996. *The magnetic field of the Earth. Paleomagnetism, the core, and the deep mantle*, Academic Press, San Diego, etc.: 1-527.
- Nishida, Atsushiro, 1983. IMF control of the Earth's magnetosphere, *Space Sci. Rev.*, 34: 185-200.
- Olbert, Stanislaw, George L. Siscoe, and V. M. Vasyliūnas, 1968. A simple derivation of the Dessler-Parker-Sckopke relation, *J. Geophys. Res.*, 73: 1115-1116.
- Olson, V. P., 1973. Forces and torques on the Earth produced by magnetospheric currents, *J. Geophys. Res.*, 79: 1128-1130.
- Palmroth, M., H. Laakso, and T. I. Pulkkinen, 2001. Location of high-altitude cusp during steady solar wind conditions, *J. Geophys. Res.*, 106: 21,109-21,122.
- Palmroth, M., P. Janhunen, T. I. Pulkkinen, and H. E. J. Koskinen, 2004. Ionospheric energy input as a function of solar wind parameters: global MHD simulation results, *Annales Geophysicae*: 22, 549–566.
- Palmroth, M., P. Janhunen, T. I. Pulkkinen, and W. K. Peterson, 2001a. Cusp and magnetopause locations in global MHD simulation, *J. Geophys. Res.*, 106, (A12): 29,435-29,450; DOI:10.1029/2001JA900132.
- Palmroth, M., T. I. Pulkkinen, P. Janhunen, and C.-C. Wu, 2003. Stormtime energy transfer in global MHD simulation, *J. Geophys. Res.*, 108; DOI:10.1029/2002JA009446.
- Palmroth, Minna M. E., 2003. Solar wind – magnetosphere interaction as determined by observations and a global MHD simulation, *PhD Thesis*, Finnish Meteorological Institute: 1-65.
- Papagiannis, M. D., 1973. The torque applied by the solar wind to the tilted magnetosphere, *J. Geophys. Res.*, 78: 7968-7977.
- Paparo, G., and G. P., Gregori, 2003. Multifrequency acoustic emissions (AE) for monitoring the time evolution of microprocesses within solids. In D. O. Thompson and D. E. Chimenti, Eds), *Reviews of Quantitative Nondestructive Evaluation*, 22, (AIP Conference Proceedings): 1423-1430.
- Parker, Eugene Newman, 1962. Dynamics of the geomagnetic storm, *Space Sci. Rev.*, 1: 62-99.
- Parker, Eugene Newman, 1966a. Nonsymmetric inflation of a magnetic dipole, *J. Geophys. Res.*, 71: 4485-4494.
- Parker, Eugene Newman, and Vincenzo C. A. Ferraro, 1971. Theoretical aspects of the worldwide magnetic storm phenomenon, *Hand. Physik*, XLIX/3: 131-205.
- Paschmann, G., N. Sckopke, and H. Grünwaldt, 1976. Plasma in the polar cusp and plasma mantle. In B.M. McCormac, Ed., *Magnetospheric particles and fields*, D. Reidel Publishing Co., Dordrecht, etc.: 37-46.
- Perucca, Eligio, 1960. *Fisica generale e sperimentale, II-Ottica, elettricità e magnetismo* (Tomo I and II, 7th ed.), U.T.E.T., Torino: 1-1229.
- Perucca, Eligio, 1966. *Des origines de la métrologie au Système International (SI)*, Unione Tipografica-Editrice, Torino: 1-171.
- Petrukovich, A. A., 2008. The elusive onset of geomagnetic substorms, *Science*, 321, (5891): 920-921. DOI:10.1126/science.1162426.
- Philipp, W., .G. Morfill, 1976. The plasma mantle as the origin of the plasmasheet. In B. M. McCormac, Ed., *Magnetospheric particles and fields*, D. Reidel Publishing Co., Dordrecht, etc.:55-66.
- Phillips, Tony, 2012. Solar storm dumps Gigawatts into Earth's upper atmosphere, *Science@NASA*, issued 03.22.2012.
- Poeverlein, H., 1972. The Earth's magnetosphere, *Hand. Phys.*, XLIX/4: 1-113.
- Quinn, J. M.,† G. P. Gregori, and B. A. Leybourne, 2025. Satellite monitoring of air-earth currents, pending publication in *American Journal of Engineering and Applied Science*.
- Reid, G.C., 1963. Polar cap absorption. In B. Landmark, Ed., *Advances in upper atmosphere research*. Pergamon Press, Oxford etc.: 309-316.
- Rosenqvist, L., S. Buchert, H. Opgenoorth, A. Vaivads, and G. Lu, 2006. Magnetospheric energy budget during huge geomagnetic activity using Cluster and ground-based data, *J. Geophys. Res.*, 111: A10211, 14 pp.; DOI:10.1029/2006JA011608.
- Rossi, Bruno, and Stanislaw Olbert, 1970. *Introduction to the physics of space*. McGraw-Hill Book Co., New York, etc.: 1-454.
- Russell, Christofer T., 1971. Geophysical coordinate transformations, *Cosmic Electrodynamics*, 2: 184-196.

- Schild, Milo A., J. W. Freeman and Alex J. Dessler, 1969. A source for field-aligned currents at auroral latitudes, *J. Geophys. Res.*, 74, 247-256: 1969.
- Schulz, M., 1991. The magnetosphere. In J. A. Jacobs, Ed., *Geomagnetism*, Academic Press, Harcourt Brace Jovanovich, Publ., London, etc. Volume 4: 87-293.
- Schwenn, R., 1981. Solar wind and its interaction with the magnetosphere: measured parameters, *Adv. Space Res.*, 1: 3-17.
- Scopke, Norbert, 1966. A general relation between the energy of trapped particles and the disturbance field near Earth, *J. Geophys. Res.*, 71: 3125-3130.
- Scopke, Norbert, 1972. A study of self-consistent ring current models, *Cosmic Electrodyn.*, 3: 330-348.
- Scopke, N., and G. Paschmann, 1978. The plasma mantle: a survey of magnetotail boundary observations, *J. Atmos. Terr. Phys.*, 40: 261-278.
- Siscoe, George L., 1970. The virial theorem applied to magnetospheric dynamics, *J. Geophys. Res.*, 75: 5340-5350.
- Siscoe, George L., 1974. Correction, *Rev. Geophys. Space Phys.*, 12: 135.
- Siscoe; G. L., and W. D. Cummings, 1969. On the cause of geomagnetic bays, *Planet. Space Sci.*, 17: 1795-1802.
- Snow, Chester, 1953. *Magnetic field of cylindrical coils and annular coils*, National Bureau of Standards, Applied Mathematics Series, (38), U. S. Government printing Office, Washington, D.C.
- Steigerwald, Bill, 2009a. "Singing" electrons protect and threaten your TV and GPS, *NASA News*, issued May 7, 2009.
- Stern, David P., 1984. Energetics of the magnetosphere, *Space Sci. Rev.*, 39: 193-213; DOI:10.1007/BF00173674.
- Stratton, Julius A., 1941. *Electromagnetic theory*. McGraw-Hill Book Co., New York: 1-615. Italian translation published by Einaudi, Torino, 1952: 1-838.
- Verosub, Kenneth L., and Allan Cox, 1971. Changes in the total magnetic energy external to the Earth's core, *J. Geomagn. Geoelectr.*, 23, (2): 235-242.
- Williams, V. L., and J. C. Cain, 1975. Uniform magnetic fields generated by circular current-carrying coils. *Geomagnetism and Aeronomy*, 15: 715-722.
- Willis, D. M., 1971. Structure of the magnetopause, *Rev. Geophys. Space Phys.*, 9: 953-985.
- Willis, D. M., 1972. The boundary of the magnetosphere: the magnetopause. In E. R. Dyer, Ed., *Critical problems in magnetospheric physics*, Proc. of the Symp. held 11-13 May, 1972 in Madrid, Spain, IUCSTP Secretariat, National Academy of Sciences, Washington D.C.: 17-34.
- Willis, D. M., 1976. The energetics of Sun-weather relationships: magnetospheric processes, *J. Atmosph. Terr. Phys.*, 38, (7): 685-698; DOI:10.1016/0021-9169(76)90107-0.
- Zidarov, D., and T. Petrova, 1974. Representation of the Earth's magnetic field as a field of a circular loop. *Dokl. Na Bolgarskata Akademiya na Naukite*, 27 (2): 203-206.

Acronyms

- AGU – American Geophysical Union
 AMIE - assimilated mapping of ionospheric electrodynamics (technique).
 AU – Astronomical Union
 CHAMP - magnetic satellite
 CME – coronal mass ejection
 DPS - Dessler-Parker-Scopke (ratio)
 EISCAT - European Incoherent Scatter
 HNS - heliospheric neutral sheet
 ICB – inner core boundary
 l.o.d. - length of the day
 MHD – magneto-hydro-dynamics
 MOR – mid.ocean ridged
 NASA – National and Aeronautics Administration
 PCA - polar cap absorption events
 SABER - instrument onboard NASA's TIMED satellite
 SHE – spherical harmonic expansion
 SIF – Società Italiana di Fisica
 SV – secular variation
 SWP - solar wind power
 TD dynamo . tide-drive dynamo
 THEMIS - NASA spacecrafts,
 TIMED Thermosphere Ionosphere Mesosphere Energetics and Dynamics satellite.
 UAF - University of Alaska Fairbanks

Solar and Earth's Geomagnetic Activity Related to the M6.2 Earthquake Recorded in Chile on November 8, 2024

Valentino Straser¹, Gabriele Cataldi², Daniele Cataldi²⁻³

¹ University of Makeni (Sierra Leone).

² Radio Emissions Project (I)

³ LTPA Observer Project (I)

Corresponding Author:
Valentino Straser, University of
Makeni (Sierra Leone).
valentino.straser@gmail.com

Abstract: This study highlights the close correlation that the authors have identified between solar activity, terrestrial geomagnetic activity and the M6.2 earthquake recorded in Chile on November 8, 2024 at 11:37 UTC, and at a depth of 10 km. This correlation was determined through the analysis of solar ion flux data provided by the Advanced Composition Explorer (ACE) Satellite, and through the Kp index data provided by the National Oceanic and Atmospheric Administration (NOAA).

Keywords: space weather, geomagnetic activity, proton density, Chile, M6+.

Introduction

On November 8, 2024, a M6.2 earthquake was recorded at 278 km WNW of Cochrane, Chile (Fig. 1).

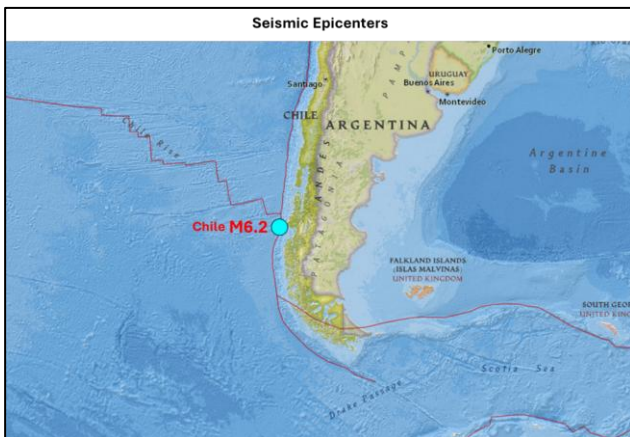


Fig. 1 – Seismic epicenter of the M6.2 earthquake recorded in Chile on November 8, 2024. The map above shows the seismic epicenter of the M6.2 earthquake recorded in Chile on November 8, 2024. Credits: USGS, Radio Emissions Project.

Chile is one of the most seismically and tectonic active regions on the planet, located along the convergent margin of the Nazca Plate and the South American Plate. This tectonic boundary is dominated by a highly dynamic subduction process, in which the Nazca Plate dives beneath the South American Plate at an average rate of about 68 mm/year. This interaction is responsible for the formation of the Andean volcanic belt, frequent high-magnitude earthquakes, and complex crustal deformation along the coastal region.

- **Subduction and Contact Zone.** The subduction zone off the coast of Chile is known as the Peru-Chile Trench, a major morphological and tectonic feature that marks the point of contact between the two plates. This convergent margin is characterized by a series of seismic rupture zones that have historically given rise to numerous devastating seismic events, including the 1960 Valdivia earthquake, the strongest ever recorded (M 9.5). [80-82].
- **Seismotectonic Segmentation.** The Chilean margin is divided into distinct tectonic segments, each with its own seismogenic characteristics and deformational behaviors. These segments are separated by seismic asperities and structural barriers that influence the propagation of seismic waves and the distribution of energy released during seismic events. In addition, the geometry of the subducting plate varies significantly along the margin, with subduction angles becoming steeper in the northern and central parts compared to the southern region. [78] [79].
- **Associated Volcanism.** Tectonic interaction is also responsible for intense volcanic activity along the South American Volcanic Belt. Chile is home to approximately 500 active and potentially active volcanoes, many of which are located within the Andean Volcanic Arc, which extends along the entire Andes Mountain range. This volcanism is fueled by the release of volatile-rich fluids from the subducted Nazca Plate, which triggers partial melting in the upper mantle. [83] [84].

- **Crustal Deformation.** In addition to subduction, the Chilean margin is subject to significant deformation along the coast-parallel transpressive fault system known as the Chilean Coastal Fault System. These faults accommodate the horizontal component of interplate motion and are often associated with shallow earthquakes of moderate magnitude. [85-87].
- **Seismic-tectonic Implications.** Plate convergence has important implications not only for the generation of subduction earthquakes but also for intraplate seismicity and back-arc deformation. Stresses accumulated along the subduction zone are released during large megathrust seismic events, with the potential for destructive tsunamis. In addition, oblique compression generates a transpressive tectonic regime, contributing to the formation of secondary deformational structures, such as folds and reverse faults, in the back-arc region. [88-91].

The Chilean tectonic margin represents a unique natural laboratory for the study of subduction dynamics and associated seismogenesis. The combination of frequent seismicity, active volcanism, and crustal deformation makes Chile an area of primary interest for researchers investigating global tectonic processes and associated geological hazard. A detailed understanding of the tectonic characteristics of this region is essential to develop predictive models that can improve seismic and volcanic hazard mitigation strategies. [1-3]

Methods and Data

The analysis method that allowed the authors to identify a close correlation between the M6.2 earthquake recorded in Chile on November 8, 2024, at 11:37 UTC consists of continuous monitoring of solar and terrestrial geomagnetic activity to track increases in the density of the solar proton flux. It has now been ascertained through the studies conducted by the authors from 2012 to today that every potentially destructive seismic event is always preceded by an increase in the proton density of the solar wind that is directed towards the Earth [4-46]. Following the impact between this dense flow of electrically charged particles and the Earth's magnetosphere, disturbances of the Earth's geomagnetic field occur which can precede earthquakes of significant magnitude. [4] [9] [11] [15] [17] [22-33] [47-50]. In this specific case, the Chilean earthquake was preceded by both an increase in the proton density of the solar wind and an increase in the Earth's geomagnetic activity. (Fig. 2).

By analyzing the variation curves present in Fig. 2 it was possible to calculate the time intervals recorded between the beginning of the proton increase and of the Earth's geomagnetic field that preceded the Chilean earthquake M6.2:

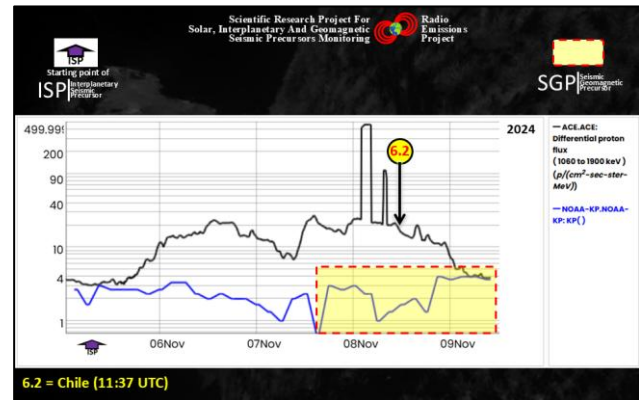


Fig. 2 – Variation of solar proton flux and terrestrial geomagnetic activity recorded between 5 and 9 November 2024. The graph above shows the proton variation curve (in black) recorded by the Advanced Composition Explorer (ACE) Satellite, located in L1 Lagrangian orbit, between 5 and 9 November 2024; and the Kp index curve (in blue) recorded between 5 and 9 November 2024. The yellow areas outlined by the dotted red line highlight the increase in the Earth's geomagnetic field that preceded the Chilean M6.2 earthquake recorded on 8 November 2024 at 11:37 UTC. The purple arrow (ISP) represents the time marker that identifies the beginning of the proton increase that preceded the M6+ earthquakes. The vertical black arrow represents the time marker of the Chilean earthquake. Credits: USGS, ISWA, Radio Emissions Project.

- Time interval recorded between the start of the solar wind proton increase and the M6.2 Chilean earthquake \approx 76 hours (Fig. 2).
- Time interval recorded between the beginning of the increase of the Earth's geomagnetic field and the Chilean earthquake M6.2 \approx 20 hours (Fig. 2-3).

The beginning of the proton increase was recorded on November 5, 2024, at approximately 07:00 UTC; while the maximum increase (of impulsive type) was reached on November 8, 2024, at 03:00 UTC. After this increase, the proton density began to decline, returning to baseline values on November 9, 2024. The Chilean M6.2 earthquake was recorded precisely during the phase of decrease in the proton density of the solar wind. This correlation is statistically supported by the analyses carried out by the authors by analyzing the distribution of potentially destructive seismic events with respect to the proton variation curve: 82.8 percent of potentially destructive earthquakes that are recorded on a global scale are recorded during the phase of increase or decrease in the proton density of the solar wind.

The authors first presented the results of this type of correlation in 2013 [48], highlighting how the study of solar and geomagnetic activity can represent an innovative and complementary approach to traditional seismic monitoring methodologies. The analysis of proton increments in the solar wind has highlighted their ability to directly influence the Earth's magnetosphere, causing measurable variations in the geomagnetic field. When the proton flux of the solar

wind increases significantly, the charged particles interact with the Earth's magnetosphere, generating geomagnetic perturbations that manifest as amplitude increments in measurements made with magnetometers.

The ability to identify these correlations provides a useful temporal framework for seismic monitoring, since proton increases, detectable by satellites, precede potentially destructive seismic events by ~99 hours (on average) [4-46]. This approach opens new perspectives for the development of early warning systems that, exploiting the combination of solar and geomagnetic data, can improve the accuracy in the prediction of potentially destructive earthquakes, reducing the risk for vulnerable populations and promoting mitigation strategies based on robust scientific evidence.

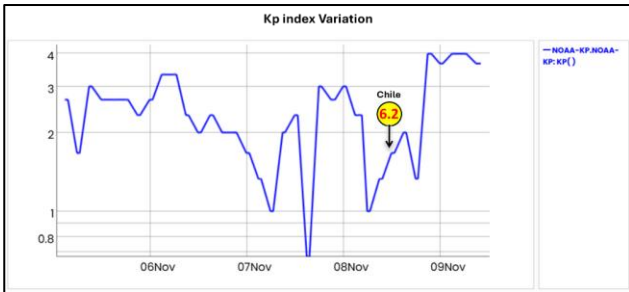


Fig. 3 – Kp index change recorded between 5 and 9 November 2024. The graph above shows the variation curve of the Kp index (blue line) recorded between 5 and 9 November 2024. The vertical black arrow represents the time marker of the Chilean M6.2 earthquake recorded on 8 October 2024 at 11:37 UTC. Credits: ISWA, Radio Emissions Project.

Fig. 3 shows that the Chilean M6.2 seismic event was recorded after an increase in the Earth's geomagnetic field that started on November 7, 2024, at 15:30 UTC, reaching its maximum intensity (Kp 4) between November 8 and 9, 2024 (**Fig. 3**). Before this increase in the Earth's geomagnetic field, another increase occurred that started right with the beginning of the increase in the proton density of the solar wind related to the Chilean earthquake, but which then ended on November 7, 2024, at 15:10 UTC (**Fig. 2-3**). The proton increase related to the Chilean M6.2 earthquake therefore caused two increases in the Earth's geomagnetic field.

By analyzing the variation of the Interplanetary Magnetic Field (IMF) the authors discovered that the Chilean earthquake M6.2 was also preceded by two perturbations of the Interplanetary Magnetic Field: the first one started on November 7, 2024 at 13:25 UTC and ended on November 8, 2024 at 03:34 UTC; the second one started on November 8, 2024 at 04:47 UTC and was still ongoing during the writing of this work that ended on November 10, 2024 (**Fig. 4**). By analyzing the variation curves of the Interplanetary Magnetic Field, it is evident that the Chilean earthquake M6.2 was recorded in proximity to the maximum variation recorded by the second perturbation of the Interplanetary Magnetic Field. Interplanetary Magnetic

Field perturbations are a direct consequence of increases in solar ion flux and were first correlated with potentially destructive seismic activity by the authors between 2010 and 2011.

The Chilean seismic event M6.2 was preceded by about 22 hours by the first perturbation of the Interplanetary Magnetic Field and by about 7 hours by the second perturbation of the Interplanetary Magnetic Field visible in **Fig. 3**.

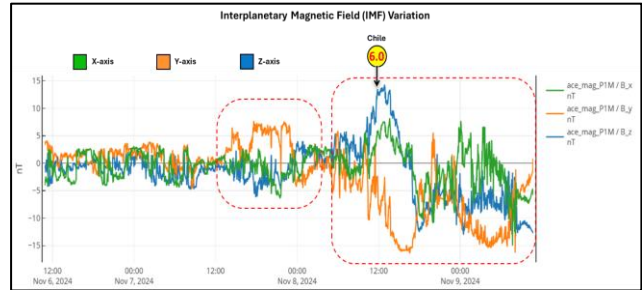


Fig. 4 – Interplanetary Magnetic Field (IMF) variation recorded between 6 and 9 November 2024. The graph above shows the variation (in nanoTesla – nT) of the Interplanetary Magnetic Field (IMF) recorded between 5 and 9 November 2024 by the Advanced Composition Explorer (ACE) Satellite, located in Lagrangian orbit L1. The recording occurred on three axes: X-axis (green curve), Y-axis (orange curve), Z-axis (blue curve). The black vertical arrow represents the time marker of the Chilean seismic event M6.2 recorded on 8 November 2024. The area of the graph highlighted in the area delimited by the red dotted line highlights a perturbation of the Interplanetary Magnetic Field (IMF) that preceded the Chilean earthquake. Credits: ISWA, Radio Emissions Project.

Discussion

The analysis presented in this study demonstrates a robust correlation between solar activity, geomagnetic disturbances and potentially destructive seismic events, as evidenced by the M6.2 earthquake that occurred in Chile on 8 November 2024. By integrating data from the Advanced Composition Explorer (ACE) satellite and geomagnetic indices, such as the Kp index, the authors have highlighted a consistent temporal relationship between the increase in solar proton flux and the subsequent terrestrial geomagnetic variations that preceded the earthquake. This discussion aims to contextualize these results in the broader framework of seismic precursor studies and to assess their implications for earthquake forecasting methodologies.

- **Geomagnetic disturbances as seismic precursors.** The data reveal that increases in solar proton flux, which began on November 5, 2024, caused detectable geomagnetic variations about 20 hours before the seismic event. These perturbations are related to the interaction of charged solar particles with the Earth's magnetosphere, generating measurable changes in the geomagnetic field, as evidenced by the Kp index. This temporal alignment supports the hypothesis that

geomagnetic perturbations induced by solar activity can act as non-local precursors to seismic events. These results are in line with previous studies conducted by the authors, who have consistently identified similar patterns before M6+ earthquakes on a global scale.

- **Mechanism linking solar activity and seismicity.**
The observed correlation is supported by a plausible geophysical mechanism: the interaction of geomagnetic variations with tectonic stress along faults. The influx of charged solar particles modifies the geomagnetic field, generating Lorentz forces that can influence the dynamics of electric particles present in stressed rocks. These forces can facilitate the final rupture process by altering the equilibrium state of tectonic stress, thus leading to the triggering of seismic events.
- **Statistical and temporal robustness.**
Statistical analysis of the study highlights the consistency of this phenomenon, with 82.8 percent of potentially destructive earthquakes recorded globally occurring during phases of proton flux variation (during increases and decreases in proton density). The time intervals identified in this case, ≈ 76 hours from the start of the proton flux increase to the earthquake, and ≈ 20 hours from the geomagnetic response, are within the range documented in previous studies. This strengthens the predictive potential of monitoring solar and geomagnetic activity as part of a comprehensive seismic forecasting strategy.
- **Integration with existing monitoring systems.**
One of the main advantages of this methodology is its ability to complement traditional seismic monitoring techniques. While terrestrial networks focus on local stress accumulation and micro-seismicity, satellite monitoring offers a global perspective. The integration of geomagnetic and solar data with terrestrial electromagnetic monitoring networks, such as the Radio Direction Finding (RDF) system used by the authors, has the potential to improve the resolution and accuracy of seismic forecasts [17] [51-77].
- **Limitations and future prospects.**
Despite these promising results, some limitations must be acknowledged. The variability of geomagnetic responses to solar activity, influenced by factors such as the orientation of the Interplanetary Magnetic Field (IMF) and regional geomagnetic conditions, introduces an element of uncertainty. Furthermore, the spatial resolution of this approach remains limited by the global nature of solar and geomagnetic phenomena. Future work should focus on refining the temporal and spatial correlation models, while exploring the integration of this methodology with high-resolution ground-based monitoring systems.

- **Implications for early warning systems.**

The ability to detect non-local seismic precursors represents a significant advance in earthquake preparedness. By exploiting the temporal predictability of solar-induced geomagnetic disturbances, it becomes possible to extend the warning time for seismic early warning systems. This could provide crucial minutes or hours for the adoption of safety measures, particularly relevant in high-risk regions such as Chile, where tectonic activity is intense and frequent.

In summary, the results presented in this study underline the crucial role of solar proton flux variations and terrestrial geomagnetic perturbations as precursor signals of earthquakes of significant magnitude. Statistical and temporal analyses demonstrate a robust and reproducible correlation, supported by a large data base collected over time. This approach represents an important step forward in the understanding of electromagnetic mechanisms preceding seismic events.

Although there are still limitations, such as the variability of geomagnetic responses and global spatial resolution, the potential for integrating this methodology with traditional seismic monitoring systems offers promising prospects. The inclusion of geomagnetic and solar data in forecasting models could significantly improve the ability to identify areas at risk, extending the time available for mitigation measures.

Finally, continued interdisciplinary research and further development of advanced technological tools, such as RDF digital receivers (which the authors are currently developing), are essential to refine the monitoring and forecasting capacity. This work represents a point of reference for future studies aiming to integrate heliophysics, seismology and electromagnetics into a single forecasting framework, contributing to the reduction of global seismic risk.

Conclusion

Monitoring and analyzing variations in the solar wind proton flux and terrestrial geomagnetic perturbations offers a significant advantage: the possibility of identifying non-local precursor signals, which consistently precede high-magnitude earthquakes.

This methodology stands out for its ability to provide a global context, exploiting satellite and geomagnetic data that are not limited by geographic factors or direct access to seismic areas. Furthermore, the integration with data from terrestrial electromagnetic monitoring networks allows obtaining a comprehensive view, combining non-local signals with local electromagnetic emissions, typically associated with the genesis of the earthquake [17] [51-77]. The use of these techniques not only increases the chances of identifying areas at risk before seismic events but also allows for the development of more accurate predictive

models. These models could represent a crucial step towards the implementation of more efficient early warning systems, capable of mitigating the social and economic impact of potentially destructive earthquakes. In an era in which natural disasters continue to cause extensive damage, the application of an interdisciplinary approach based on heliophysics and geomagnetics appears not only promising, but also necessary for the advancement of applied seismology.

This study consolidates the role of solar and geomagnetic activity as reliable indicators of seismic risk. By integrating space weather data into seismic monitoring systems, researchers can improve the predictive capacity of current methodologies. These findings underscore the need for continued interdisciplinary research to further elucidate the mechanisms linking solar activity, geomagnetic perturbations and seismicity, paving the way for more effective strategies for earthquake forecasting and risk mitigation.

References

- [1] Chile Margin and Triple Junction Geology – NOAA Ocean Exploration.
- [2] 3-D thermal structure and dehydration near the Chile Triple Junction – Geoscience Letters.
- [3] Eduardo Contreras-Reyes. (2018). Structure and Tectonics of the Chilean Convergent Margin from Wide-Angle Seismic Studies: A Review. The Evolution of the Chilean-Argentinean Andes – Springer Earth System Sciences series. Pp 3-29.
- [4] V. Straser, G. Cataldi. (2014). Solar wind proton density increase and geomagnetic background anomalies before strong M6+ earthquakes. Space Research Institute of Moscow, Russian Academy of Sciences, MSS-14. 2014. Moscow, Russia. pp280-286.
- [5] V. Straser, G. Cataldi. (2015). Solar wind ionic variation associated with earthquakes greater than magnitude M6.0. *New Concepts in Global Tectonics Journal*, V. 3, No. 2, June 2015, Australia. P.140-154.
- [6] G. Cataldi, D. Cataldi, V. Straser. (2015). Solar wind proton density variations that preceded the M6+ earthquakes occurring on a global scale between 17 and 20 April 2014. European Geosciences Union (EGU) General Assembly 2015, Vienna, Austria.
- [7] G. Cataldi, D. Cataldi, V. Straser. (2015). Solar wind ion density variations that preceded the M6+ earthquakes occurring on a global scale between 3 and 15 September 2013. European Geosciences Union (EGU) General Assembly 2015, Geophysical Research Abstract, Vol. 17, EGU2015-4581, Vienna, Austria.
- [8] G. Cataldi, D. Cataldi, V. Straser. (2015). Solar wind proton density variations that preceded the M6.1 earthquake occurred in New Caledonia on November 10, 2014. European Geosciences Union (EGU) General Assembly 2015, Geophysical Research Abstract, Vol. 17, EGU2015-4167, Vienna, Austria.
- [9] V. Straser, G. Cataldi, D. Cataldi. (2015). Solar wind ionic and geomagnetic variations preceding the Md8.3 Chile Earthquake. *New Concepts in Global Tectonics Journal*, V. 3, No. 3, September 2015, Australia. P.394-399.
- [10] G. Cataldi, D. Cataldi, V. Straser. (2016). Solar activity correlated to the M7.0 Japan earthquake occurred on April 15, 2016. *New Concepts in Global Tectonics Journal*, V. 4, No. 2, pp202-208, June 2016.
- [11] G. Cataldi, D. Cataldi, V. Straser. (2016). Tsunami related to solar and geomagnetic activity. European Geosciences Union (EGU) General Assembly 2016. Geophysical Research Abstract, Vol. 18, EGU2016-9626, Vienna, Austria.
- [12] G. Cataldi, D. Cataldi, V. Straser. (2017). SELF-VLF electromagnetic signals and solar wind proton density variations that preceded the M6.2 Central Italy earthquake on August 24, 2016. *International Journal of Modern Research in Electrical and Electronic Engineering*, Vol. 1, No. 1, 1-15. DOI: 10.20448/journal.526/2017.1.1/526.1.1.15.
- [13] G. Cataldi, D. Cataldi, V. Straser. (2017). Solar wind proton density increase that preceded Central Italy earthquakes occurred between 26 and 30 October 2016. European Geosciences Union (EGU), General Assembly 2017. Geophysical Research Abstracts Vol. 19, EGU2017-3774, 2017. Vienna, Austria.
- [14] V. Straser, G. Cataldi, D. Cataldi. (2017). Solar and electromagnetic signal before Mexican Earthquake M8.1, September 2017. *New Concepts in Global Tectonics Journal*, V. 5, No. 4, December 2017. pp600-609.
- [15] G. Cataldi, D. Cataldi, V. Straser. (2017). Solar and Geomagnetic Activity Variations Correlated to Italian M6+ Earthquakes Occurred in 2016. EGU General Assembly 2017. EGU2017-3681, Vol. 19. Vienna, Austria.
- [16] G. Cataldi, D. Cataldi, V. Straser. (2019). Solar wind ionic density variations related to M6+ global seismic activity between 2012 and 2018. European Geosciences Union (EGU) General Assembly 2019.

Geophysical Research Abstract, Vol. 21, EGU2019-3067, 2019, Vienna, Austria.

- [17] G. Cataldi. (2020). Precursori Sismici – Monitoraggio Elettromagnetico. Kindle-Amazon, ISBN: 9798664537970. ASIN Code: B08CPDBGX9.
- [18] G. Cataldi, D. Cataldi, V. Straser. (2019). Wolf Number Related To M6+ Global Seismic Activity. New Concepts in Global Tectonics Journal, Volume 7, Number 3, December 2019, pp178-186.
- [19] V. Straser, G. Cataldi, D. Cataldi. (2020). The Space Weather Related to the M7+ Seismic Activity Recorded on a Global Scale between 28 January and 25 March 2020. Acta Scientific Agriculture 4.12 (2020): pp55-62.
- [20] G. Cataldi, V. Straser, D. Cataldi. (2020). Space weather related to potentially destructive seismic activity recorded on a global scale. New Concepts in Global Tectonics Journal. Vol.8, No.3, pp233-253, December 2020. ISSN 2202-0039.
- [21] G. Cataldi. (2021). Radio Emissions Project – A new approach to seismic prediction. Kindle-Amazon, ISBN: 9798709593411.
- [22] G. Cataldi, D. Cataldi, V. Straser. (2021). Space weather and geomagnetic activity related to the Japan M7.1 earthquake recorded on February 13, 2021. New Concepts in Global Tectonics Journal, Vol. 9, No. 1, pp16-23. March 2021.
- [23] G. Cataldi, D. Cataldi, V. Straser. (2021). Space weather and geomagnetic activity related to the Chilean M6.7 earthquake recorded on February 3, 2021. New Concepts in Global Tectonics Journal, Vol. 9, No. 1, pp3-9. March 2021.
- [24] G. Cataldi, D. Cataldi, V. Straser. (2021). Space weather and geomagnetic activity related to M6+ global seismic activity recorded on February 7, 2021. New Concepts in Global Tectonics Journal, Vol. 9, No. 1, pp24-30. March 2021.
- [25] G. Cataldi, D. Cataldi, V. Straser. (2021). Space Weather and geomagnetic activity related to Ecuadorean M7.5 earthquake recorded on February 22, 2019. New Concepts in Global Tectonics Journal, Vol. 9, No. 2, pp79-86. June 2021.
- [26] G. Cataldi, D. Cataldi, V. Straser. (2021). Solar Activity and geomagnetic activity related to M6+ global seismic activity recorded on March 20, 2021. New Concepts in Global Tectonics Journal, Vol. 9, No. 2, pp87-93. June 2021.
- [27] G. Cataldi, D. Cataldi, V. Straser. (2021). Space weather and geomagnetic activity related to M6+ global seismic activity recorded on 3-4 March 2021. New Concepts in Global Tectonics Journal, Vol. 9, No. 2, pp94-98. June 2021.
- [28] G. Cataldi, D. Cataldi, V. Straser. (2021). Solar activity and geomagnetic activity related to M6.0 South Sandwich Islands region earthquake recorded March 14, 2021. New Concepts in Global Tectonics Journal, Vol. 9, No. 2, pp99-105. June 2021.
- [29] G. Cataldi, D. Cataldi, V. Straser. (2021). Space weather and geomagnetic activity related to the Vanuatu M6.3 earthquake recorded on March 20, 2019. New Concepts in Global Tectonics Journal, Vol. 9, No. 2, pp106-111. June 2021.
- [30] G. Cataldi, D. Cataldi, V. Straser. (2021). Space weather and geomagnetic activity related to M6+ earthquakes recorded between 7 and 20 November 2017. New Concepts in Global Tectonics Journal, Volume 9, Number 3, September 2021. pp137-144. ISSN 2202-0039.
- [31] G. Cataldi, D. Cataldi, V. Straser. (2021). Space weather and geomagnetic activity related to M6+ earthquakes recorded between 12 and 15 April 2012. New Concepts in Global Tectonics Journal, Volume 9, Number 3, September 2021. Pp145-154. ISSN 2202-0039.
- [32] G. Cataldi, D. Cataldi, V. Straser. (2021). Space weather and geomagnetic activity related to M6+ earthquakes recorded between 13 and 16 April 2016. New Concepts in Global Tectonics Journal, Volume 9, Number 3, September 2021. pp158-163. ISSN 2202-0039.
- [33] G. Cataldi, D. Cataldi, V. Straser. (2021). Space weather and geomagnetic activity related to M6+ earthquakes recorded between 17 and 19 July 2017. New Concepts in Global Tectonics Journal, Volume 9, Number 3, September 2021. pp164-169. ISSN 2202-0039.
- [34] G. Cataldi, D. Cataldi, V. Straser. (2021). Space weather related to M6+ earthquakes recorded on June 24, 2019. New Concepts in Global Tectonics Journal, Volume 9, Number 3, September 2021. pp132-136. ISSN 2202-0039.
- [35] G. Cataldi, V. Straser, D. Cataldi. (2021). Space weather related to M6.1 Indonesia earthquake recorded on June 3, 2021. New Concepts in Global Tectonics Journal. Volume 9, No 4, December 2021. Pp 185-193.

- [36] G. Cataldi, V. Straser, D. Cataldi. (2021). Space weather related to M6.0 Tonga earthquake recorded on March 17, 2020. *New Concepts in Global Tectonics Journal*. Volume 9, No 4, December 2021. Pp 206-214.
- [37] G. Cataldi, V. Straser, D. Cataldi. (2021). Space weather related to M8.2 earthquake recorded in Alaska on 29 July 2021. *New Concepts in Global Tectonics Journal*. Volume 9, No 4, December 2021. Pp 194-205.
- [38] V. Straser, G. Cataldi, D. Cataldi. (2022). Space weather related to M6+ potentially destructive seismic events recorded on a global scale between 13 and 16 March 2022. *New Concepts in Global Tectonics Journal*. Volume 10, Number 1, March 2022. ISSN 2202-0039. pp. 3-10.
- [39] V. Straser, G. Cataldi, D. Cataldi. (2022). Space weather related to M6+ potentially destructive seismic events recorded on a global scale between 2012 and 2021. *New Concepts in Global Tectonics Journal*. Volume 10, Number 1, March 2022. ISSN 2202-0039. pp. 11-21.
- [40] V. Straser, D. Cataldi, G. Cataldi. (2023). Weather Events Associated with Strong Earthquakes and Seismic Swarms in Italy. *Advances in Geological and Geotechnical Engineering Research*. Volume 05, Issue 03, Pp 39-54. July 2023.
- [41] V. Straser, G. Cataldi, D. Cataldi. (2023). Magnitude of potentially destructive earthquakes recorded in Mexico correlated to the extent of the solar proton flux. *New Concepts In Global Tectonics Journal*. Vol 11, N 4, December 2023. ISSN 2202-0039. Pp 261-266.
- [42] V. Straser, G. Cataldi, D. Cataldi. (2024). Space Weather related to destructive seismic activity that has been recorded globally between 2012 and 2023. *New Concepts In Global Tectonics Journal*. Vol 12, N 1, March 2024. Pp: 1-8.
- [43] D. Cataldi, G. Cataldi, V. Straser. (2024). Solar activity and Electromagnetic Signals that preceded the M7.5 Earthquake of January 1, 2024, in Japan. *New Concepts In Global Tectonics Journal*. Vol 12, N 1, March 2024. Pp: 9-25.
- [44] D. Cataldi, G. Cataldi, V. Straser. (2024). Earthquakes, Solar Activity, and Bright Meteors. *New Concepts In Global Tectonics Journal*. Vol 12, N 1, March 2024. Pp: 85-94.
- [45] V. Straser, G. Cataldi, D. Cataldi. (2024). Space weather linked to potentially destructive earthquakes between 2012 and 2023. *New Concepts in Global Tectonics Journal*. Volume 12, Number 3, September 2024. ISSN 2202-0039. PP248-257.
- [46] D. Cataldi, G. Cataldi, V. Straser. (2024). Space weather and pre-seismic radio frequency related to the Italian M5.1 earthquake recorded on August 1, 2024. *New Concepts in Global Tectonics Journal*. Volume 12, Number 3, September 2024. ISSN 2202-0039. PP240-247.
- [47] G. Cataldi, D. Cataldi. (2013). Reception of Natural Radio Emissions in the ELF Band. *The INSPIRE Journal*, Volume 20, Spring/Summer 2013. pp12-16.
- [48] G. Cataldi, D. Cataldi, V. Straser. (2013). Variations Of Terrestrial Geomagnetic Activity Correlated To M6+ Global Seismic Activity. EGU (European Geosciences Union) 2013, General Assembly, Geophysical Research Abstracts, Vol. 15. EGU2013-2617, Vienna, Austria.
- [49] G. Cataldi, D. Cataldi and V. Straser. (2014). Earth's magnetic field anomalies that precede the M6+ global seismic activity. European Geosciences Union (EGU) General Assembly 2014, Geophysical Research Abstract, Vol. 16, EGU2014-1068, Vienna, Austria.
- [50] T. Rabeh, G. Cataldi, V. Straser. (2014). Possibility of coupling the magnetosphere-ionosphere during the time of earthquakes. European Geosciences Union (EGU) General Assembly 2014, Geophysical Research Abstract, Vol. 16, EGU2014-1067, Vienna, Austria.
- [51] V. Straser, D. Cataldi, G. Cataldi. (2018). Radio Direction Finding System, a new perspective for global crust diagnosis. *New Concepts in Global Tectonics Journal*, V. 6, No. 2, June 2018. pp203-211.
- [52] D. Cataldi, G. Cataldi, V. Straser. (2019). Radio Direction Finding (RDF) - Pre-seismic signals recorded before the earthquake in central Italy on 1/1/2019 west of (AQ). European Geosciences Union (EGU) General Assembly 2019. Geophysical Research Abstract, Vol. 21, EGU2019-3124, 2019, Vienna, Austria.
- [53] V. Straser, D. Cataldi, G. Cataldi. (2019). Registration of Pre-Seismic Signals Related to the Mediterranean Area with the RDF System Developed by the Radio Emissions Project. *International Journal of Engineering Science Invention (IJESI)*, www.ijesi.org. Volume 8 Issue 03 Series. March 2019. PP 26-35. ISSN (Online): 2319 – 6734, ISSN (Print): 2319 – 6726.2019.
- [54] V. Straser, D. Cataldi, G. Cataldi. (2019). Radio Direction Finding (RDF) - Geomagnetic Monitoring

Study of the Himalaya Area in Search of Pre-Seismic Electromagnetic Signals. *Asian Review of Environmental and Earth Sciences*, v. 6, n. 1, pp16-27, 14 jun. 2019.

- [55] V. Straser, D. Cataldi, G. Cataldi. (2019). Electromagnetic monitoring of the New Madrid fault us area with the RDF system - Radio Direction Finding of the radio emissions project. *New Concepts in Global Tectonics Journal*, V7 N1, March 2019. pp43-62.
- [56] V. Straser, G. Cataldi, D. Cataldi. (2019). Namazu's Tail – RDF: a new perspective for the study of seismic precursors of Japan. *Lulu Editore*, 2019.
- [57] V. Straser, G. G. Giuliani, D. Cataldi, G. Cataldi. (2020). Multi-parametric investigation of pre-seismic origin phenomena through the use of RDF technology (Radio Direction Finding) and the monitoring of Radon gas stream (Rn222). *An international journal for New Concepts in Geoplasma Tectonics*, Volume 8, Number 1, May 2020, pp11-27.
- [58] D. Cataldi, G. G. Giuliani, V. Straser, G. Cataldi. (2020). Radio signals and changes of flow of Radon gas (Rn222) which led the seismic sequence and the earthquake of magnitude Mw 4.4 that has been recorded in central Italy (Balsorano, L'Aquila) on November 7, 2019. *An international journal for New Concepts in Geoplasma Tectonics*, Volume 8, Number 1, May 2020, pp32-42.
- [59] V. Straser, G. Cataldi, D. Cataldi. (2020). Radio direction finding for short-term crustal diagnosis and pre-seismic signals. The case of the Colonna earthquake, Rome (Italy). *European Journal of Advances in Engineering and Technology*, 2020, 7(7):46-59.
- [60] V. Straser, D. Cataldi, G. Cataldi. (2020). Radio Direction Finding (RDF) - Geomagnetic monitoring study of the Japanese area related to pre-seismic electromagnetic signals. *New Concepts in Geoplasma Tectonics Journal*. Vol. 8, No. 2, August 2020. pp119-141.
- [61] T. Rabeh, D. Cataldi, Z. Z. Adibin, G. Cataldi, V. Straser. (2020). International study Italy-Malaysia pre-seismic signals recorded by RDF – Radio Direction Finding monitoring network, before earthquakes: Mw 6.3, occurred at 111 km SW of Puerto Madero in Mexico and Mw 6.3, occurred at 267 km NW of Ozernovskiy in Russia, November 20, 2019. *New Concept in Geoplasma Tectonics*. Vol. 8, No. 2, pp105-118. August 2020.
- [62] D. Cataldi, V. Straser, G. Cataldi, G. G. Giuliani, Z. Z. Adibin. (2020). Registration of Pre-Seismic Radio Signals Related To The Russian And Jamaican Earthquakes With The RDF System Developed By The Radio Emissions Project. *International Advance Journal of Engineering Research (IAJER)*, Volume 3, Issue 9 (September – 2020), PP 01-30; ISSN 2360-819X.
- [63] V. Straser, D. Cataldi, G. Cataldi, G. G. Giuliani, J. R. Wright. (2020). Effects Of Hurricane Laura On The New Madrid Fault Area - Results Of Electromagnetic Monitoring Through The RDF Network - Radio Direction-Finding And Arkansas Electromagnetic Monitoring Station. *New Concepts in Global Tectonics Journal*. Vol.8, No.3, pp187-218, December 2020. ISSN 2202-0039.
- [64] V. Straser, D. Cataldi, G. Cataldi, G. G. Giuliani. (2021). Pre-Seismic Signals Recorded By The Italian RDF Network Before The Occurrence Of Some Earthquakes In Northern Italy. *International Journal of Software & Hardware Research in Engineering (IJSHRE)*, ISSN-2347-4890, Volume 9, Issue 1, pp63-76. January 2021.
- [65] V. Straser, D. Cataldi, G. Cataldi. (2021). Radio Direction Finding, A New Method For The Investigation Of Presismic Phenomena. The Case Of Japan. *International Journal Of Engineering Sciences & Research Technology (IJESRT)*. ISSN: 2277-9655, CODEN: IJESS7. 10(2): February, 2021, pp10-18. <https://doi.org/10.29121/ijesrt.v10.i2.2021>.
- [66] V. Straser, D. Cataldi, G. Cataldi, G. G. Giuliani. (2021). Electromagnetic monitoring of Italian volcanoes with the RDF Network, developed by the Radio Emissions Project. *iJournals: International Journal of Social Relevance & Concern (IJSRC)*. ISSN-2347-9698, Volume 9 Issue 7 July 2021. pp92-136. DOI: 10.26821/IJSRC.9.7.2021.9710.
- [67] D. Cataldi, V. Straser, G. Cataldi. (2021). Crustal relaxing - a new seismogenesis phenomenon associated with seismic trigger on a global scale. *iJournals: International Journal of Social Relevance & Concern (IJSRC)*. ISSN-2347-9698, Volume 9 Issue 7 July 2021. pp137-163. DOI: 10.26821/IJSRC.9.7.2021.9711.
- [68] V. Straser, D. Cataldi, G. Cataldi. (2022). Pre-seismic phenomena that preceded the M7.0 earthquake recorded in Acapulco (Mexico) on September 8, 2021. *iJournals: International Journal of Social Relevance & Concern (IJSRC)*, ISSN-2347-9698, Volume 10, Issue 1 January 2022. pp. 41-57.

- [69] D. Cataldi, V. Straser, G. Cataldi. (2022). "Terrestrial Flares" and presismic monitoring of the Radio Direction Finding network. Results of the experimentation carried out in Italy from 18 to 31 September 2021. *iJournals: International Journal of Social Relevance & Concern (IJSRC)*, ISSN-2347-9698, Volume 10, Issue 4 April 2022. pp. 72-90.
- [70] V. Straser, D. Cataldi, G. Cataldi, G. Giuliani. (2021). Electromagnetic Monitoring of Italian Volcanoes With the RDF Network. *Journal Emerging Environmental Technologies and Health Protection (JEETHP)*, vol. 4, issue 1, pp. 32-40, ISSN 2623-4874, e-ISSN 2623-4882.
- [71] D. Cataldi, G. Cataldi, V. Straser. (2023). Experimentation of The Italian RDF - Radio Direction Finding - Network, In The Search For Electromagnetic Seismic Precursors. *iJournals: International Journal of Social Relevance & Concern (IJSRC)*. Volume 11 Issue 1 January 2023. ISSN-2347-9698. Pp 1-9.
- [72] V. Straser, D. Cataldi, G. Cataldi. (2023). Radio Direction Finder Method to Mitigate Tsunami Risk in Sierra Leone. *Advances in Geological and Geotechnical Engineering Research*. Volume 05, Issue 02, pp 64-75. April 2023.
- [73] V. Straser, G. Cataldi, D. Cataldi. (2023). Analysis of possible electromagnetic seismic precursors related to the Turkish seismic sequence recorded on february 6, 2023. *New Concepts In Global Tectonics Journal Vol 11, N 3, September 2023*. Pp 213-232.
- [74] D. Cataldi, Z. Bin Z. Abidin, G. Cataldi, V. Straser, A. A. Siyad, M. S. Radzi, Z. Hassan, A. N. Zulkiplee, M. Abdullah, N. S. A. Hamid. (2023). Experimentation of the RDF network for research on pre-seismic electromagnetic signals. *New Concepts In Global Tectonics Journal Vol 11, N 3, September 2023*. Pp 233-249.
- [75] V. Straser, D. Cataldi, G. Cataldi. (2024). Comparison of Electromagnetic Signals Before an Earthquake Using the Radio Direction Finding Method. The Case of Po Plain Valley (Italy). *MedGU 2022. Recent Research on Geotechnical Engineering, Remote Sensing, Geophysics and Earthquake Seismology* pp 279-283. February 21, 2024. DOI: 10.1007/978-3-031-48715-6_60.
- [76] D. Cataldi, G. Cataldi, V. Straser. (2024). Electromagnetic signals that preceded the M4.8 magnitude earthquake that occurred between New Jersey and New York on April 5, 2024. *New Concepts in Global Tectonics Journal*. Volume 12, Number 2, June 2024. Pp. 154-162.
- [77] D. Cataldi, G. Cataldi, V. Straser. (2024). Electromagnetic signals that preceded the destructive earthquakes that occurred in Taiwan between April 2 and 3, 2024. *New Concepts in Global Tectonics Journal*. Volume 12, Number 2, June 2024. Pp. 132-141.
- [78] S. D. Comte. (1992). The 1960 Chile earthquake: National and international seismic data. *Bulletin of the Seismological Society of America*, Vol. 82, No. 4, pp. 1549-1562. ISSN: 0037-1106.
- [79] L. Contreras-Reyes, M. Carrizo. (2011). Control of high oceanic features and subduction erosion on plate coupling along the Chilean margin. *Journal of Geophysical Research*, Vol. 116, B10102. ISSN: 0148-0227.
- [80] S. Barrientos, S. N. Ward. (1990). The 1960 Chile earthquake: Inversion for slip distribution from surface deformation. *Geophysical Journal International*, Vol. 103, No. 3, pp. 589-598.
- [81] T. Lay, H. Kanamori. (1981). An asperity model of large earthquake sequences. *Journal of Geophysical Research: Solid Earth*, Vol. 86, No. B4, pp. 2853-2868.
- [82] J. Kelleher. (1972). Rupture zones of large South American earthquakes and some predictions. *Journal of Geophysical Research*, Vol. 77, No. 11, pp. 2087-2103.
- [83] S. Stern. (2004). Active Andean volcanism: its geologic and tectonic setting. *Revista Geológica de Chile*, Vol. 31, No. 2, pp. 161-206.
- [84] P. W. Francis. (1993). *Volcanoes of the Central Andes*. Springer-Verlag, Berlin Heidelberg, ISBN: 978-3-642-77356-1.
- [85] E. Jensen, J. Cembrano, D. Faulkner, E. Veloso, G. Arancibia. (2011). Development of a self-similar strike-slip duplex system in the Atacama Fault system, Chile. *Journal of Structural Geology*, Vol. 33, No. 10, pp. 1611-1626.
- [86] J. Cembrano, L. Lara. (2009). The link between volcanism and tectonics in the southern volcanic zone of the Chilean Andes: a review. *Tectonophysics*, Vol. 471, No. 1-2, pp. 96-113.
- [87] J. Cembrano, A. González, D. Arancibia, A. Ahumada, L. Olivares, H. Herrera. (2005). Fault zone development and strain partitioning in an extensional strike-slip duplex: A case study from the Mesozoic

Atacama fault system, northern Chile. *Tectonophysics*, Vol. 400, No. 1-4, pp. 105-125.

- [88] P. Bird. (2003). An updated digital model of plate boundaries. *Geochemistry, Geophysics, Geosystems*, Vol. 4, No. 3, 1027.
- [89] S. Lallemand, F. Funiciello. (2009). *Subduction zone geodynamics*. Springer-Verlag, Berlin Heidelberg, ISBN: 978-3-540-87974-9.
- [90] J. P. Avouac. (2007). Dynamic processes in extensional and compressional settings – Mountain building: From earthquakes to geological deformation. *Treatise on Geophysics*, Vol. 6, pp. 377-439.
- [91] K. M. Fischer, M. J. Fouch, D. A. Wiens, M. S. Boettcher. (1998). Anisotropy and flow in Pacific subduction zone back-arcs. *Pure and Applied Geophysics*, Vol. 151, No. 2-4, pp. 463-475.

Solar and Earth's Geomagnetic Activity Related to the M6+ Earthquake Recorded Between 12 and 18 November 2024

Valentino Straser¹, Gabriele Cataldi², Daniele Cataldi²⁻³

¹ University of Makeni (Sierra Leone).

² Radio Emissions Project (I)

³ LTPA Observer Project (I)

Corresponding Author:
 Valentino Straser, University of
 Makeni (Sierra Leone).
 valentino.straser@gmail.com

Abstract: Between 12 and 18 November 2024, two strong seismic events were recorded: M6.6 earthquake, recorded at 123 km ESE of Kokopo, Papua New Guinea on November 15, 2024, at 05:28 UTC; M6.1 earthquake, recorded at 155 km SSE of Koshima, Japan on November 17, 2024, at 12:16 UTC. The analysis conducted by the authors highlighted that the two strong seismic events were preceded by an increase in the proton density of the solar wind and by an increase in the Earth's geomagnetic activity.

Keywords: space weather, geomagnetic activity, proton density, Papua New Guinea, Japan.

Introduction

Two earthquakes of strong magnitude were recorded between 12 and 18 November 2024 (**Fig. 1**):

- 1) M6.6 earthquake, recorded at 123 km ESE of Kokopo, Papua New Guinea on November 15, 2024, at 05:28 UTC.
- 2) M6.1 earthquake, recorded at 155 km SSE of Koshima, Japan on November 17, 2024, at 12:16 UTC.

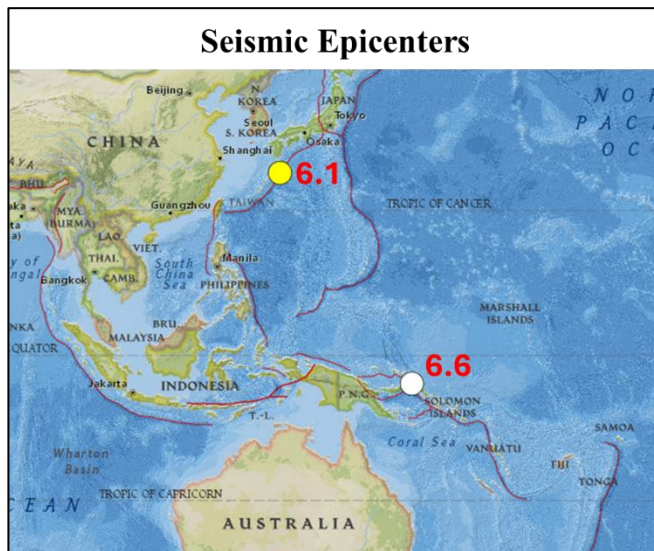


Fig. 1 – M6+ Seismic epicenters recorded between 12 and 18 November 2024. The map above shows the seismic epicenters of the two strong earthquakes recorded between 12 and 18 November 2024: M6.6 earthquake recorded in Papua New Guinea on November 15, 2024 at 05:28 UTC; M6.1 earthquake recorded in Japan on November 17, 2024 at 12:16 UTC. Credits: USGS, Radio Emissions Project.

Seismotectonics of the New Guinea Region and Vicinity

The Australia-Pacific plate margin extends for over 4,000 km, from the northern margin of the Australian plate at the Sunda Trench to the Solomon Islands. Northward subduction of the Australian plate dominates this region. Along the South Solomon Trench, the Australian plate converges with the Pacific plate at a rate of about 95 mm/yr, with high subduction-related seismicity. Since 1900, 13 earthquakes of magnitude 7.5+ have been recorded, including three events of magnitude 8.1 (1939, 1977, 2007). The 2007 earthquake generated a tsunami that caused at least 40 fatalities.

To the east, in the New Britain Trench, subduction is complex due to numerous microplates, such as the Woodlark Basin. Thirty-three earthquakes of magnitude 7.5+ have been recorded here since 1900, concentrated near New Ireland, including three magnitude 8.1 events in 1906, 1919 and 2007.

The western portion of the Australia-Pacific boundary, about 2,000 km long, is the most complex, with continental-arc collisions along New Guinea, convergent, translational and extensional deformation. This convergence generates uplifts of the New Guinea Highlands at rates of 2-8 mm/yr. The Pacific plate is slowly subducting southward along the New Guinea Trench, with a relative plate velocity of about 110 mm/yr.

In West Papua, near the Indonesia-Papua New Guinea border, there are microplates such as the Birds Head Peninsula, bounded to the south by the Seram Trench, a southward subduction zone. Since 1900, 22 earthquakes of magnitude 7.5+ have been recorded in the New Guinea region, mostly associated with strike-slip and thrust faulting. The largest, magnitude 8.2, occurred in 1996 in Papua, causing 166 fatalities.

The western portion of the boundary between the Australian and Eurasian plates, about 4,800 km long, includes subduction along the Sunda Trench and juvenile collisions between the Australian plate and the Eurasian volcanic arc. In the eastern section, from the Timor Trench to the Banda Sea, a disconnection of the subducting oceanic lithosphere from the continental crust has been observed, with an eastward propagating tear slab. The Timor region, according to GPS measurements, is currently moving at the same speed as the Australian plate.

Large earthquakes are common in eastern Indonesia, but interplate megathrust events are rare, due to the disconnection of the oceanic plate. Since 1900, 9 earthquakes of magnitude 7.5+ have been recorded from the Kai Islands region to Sumba. The strongest, with a magnitude of 8.5, was the 1938 Banda Sea earthquake, an intermediate depth thrust event that did not cause significant losses. [1].

Seismotectonics of the Philippine Sea and Vicinity

The Philippine Sea plate is bounded by the Pacific, Eurasian, and Sunda plates and is characterized almost exclusively by convergence zones. Subduction of the Pacific plate beneath the Izu-Bonin and Mariana Island arcs along the eastern margin generates high seismicity down to depths of over 600 km. However, megathrust earthquakes ($M > 8.0$) are rare due to weak plate interaction. These convergent margins are associated with back-arc extension, which separates the volcanic arcs from the rest of the plate (Karig et al., 1978; Klaus et al., 1992).

South of the Mariana arc, subduction continues along the Yap trench, creating the Izu-Bonin, Mariana, and Yap trenches and typical circum-Pacific Island arcs. To the northwest, the plate subducts beneath Eurasia along the Ryukyu Convergence Zone, manifested by the Ryukyu Islands and the Ryukyu Trench, associated with the Okinawa Basin Extension Zone. Near Taiwan, the boundary is marked by the collision between the Luzon Arc and the continental crust of Eurasia. Along the western margin, the plate is in oblique convergence with the Sunda Plate. Opposing subduction systems are found east and west of the Philippines, crossed by the Philippine Sea Fault, an active transform fault associated with volcanism and high seismicity. On the eastern margin, the plate subducts along the Philippine Sea Trench and its northern extension, the East Luzon Trench, considered a subduction in the making (Hamburger et al., 1983). To the west, subduction of the Sunda Plate generates the Manila, Negros, Sulu, and Cotabato Trenches. Subduction in the Manila Trench is interrupted by arc-continent collisions, such as that between the northern Philippine arc and the Eurasian margin in Taiwan.

The Philippine Sea Fault, over 1,200 km long, is seismically active and has generated significant historical earthquakes, including the 1990 M7.6 Luzon event. Other

active intra-arc fault systems include the Cotabato Fault and the Verde Passage-Sibuyan Sea Fault (Galgana et al., 2007). Relative plate velocities (about 80 mm/yr) cause orthogonal convergence along the trenches and nearly pure translational motion along the Philippine Sea Fault (Barrier et al., 1991).

Active seismic zones are distributed along plate boundaries and follow volcanic arcs, such as the Izu, Mariana, Ryukyu and main Philippine islands, parallel to the Manila, Negros, Cotabato and Philippine trenches. The region has produced seven large earthquakes ($M > 8.0$) and 250 significant events ($M > 7$), including disasters such as the 1923 Kanto earthquake (99,000 fatalities), the 1999 Chi-Chi earthquake (2,500 fatalities) and the 1976 Moro Gulf earthquake, which generated a tsunami with over 5,000 fatalities [1].

Methods and Data

The analysis method developed by the authors in 2011 involves the continuous monitoring of solar activity and terrestrial geomagnetic activity to track perturbations of the solar ion flux or of the terrestrial geomagnetic field that precede the $M6+$ seismic activity that is recorded on a global scale. This innovative approach in the field of seismic forecasting has allowed the authors to identify a seismic precursor that always precedes potentially destructive earthquakes that are recorded on a global scale: the increases in the proton density of the solar wind [2-44]. In this study the analysis was conducted with reference to the two strong seismic events recorded between 12 and 18 November 2024 (Fig 1-2).

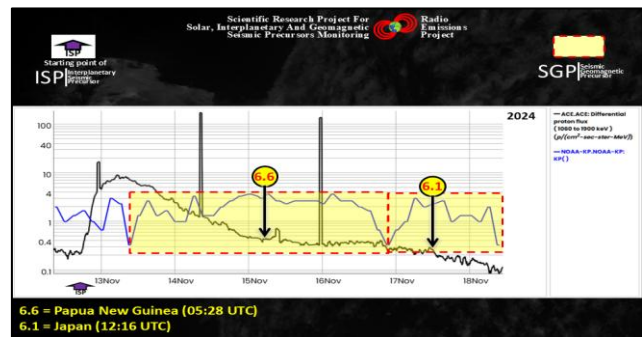


Fig. 2 – Variation of solar proton flux and terrestrial geomagnetic activity recorded between 12 and 18 November 2024. The graph above shows the proton variation curve (in black) recorded by the Advanced Composition Explorer (ACE) Satellite, located in L1 Lagrangian orbit, between 12 and 18 November 2024; and the Kp index curve (in blue), provided by the National Oceanic and Atmospheric Administration (NOAA), recorded between 12 and 18 November 2024. The yellow areas outlined by the dotted red line highlight the increase in the Earth's geomagnetic field that preceded the two $M6+$ earthquakes recorded between 12 and 18 November 2024. The purple arrow (ISP) represents the time marker that identifies the beginning of the proton increase that preceded the $M6+$ earthquakes. The vertical black arrows represent the time markers of the $M6+$ earthquakes recorded between 12 and 18 November 2024. Credits: USGS, ISWA, Radio Emissions Project.

The analysis of the solar wind proton density variation curve is performed in real time by the authors thanks to data provided by the Advanced Composition Explorer (ACE) Satellite, located in Lagrangian orbit L1. In fact, on November 12, 2024, at 17:15 UTC the authors had identified the beginning of the proton increase visible in **Fig. 2** and were waiting for a resumption of M6+ seismic activity that on average occurs within 99 hours from the beginning of the proton increase. The authors, therefore, knew with certainty that this new proton increase identified on November 12, 2024, would certainly be followed by at least one potentially destructive seismic event (on average, a proton increase is followed by 2.6 seismic events: this data was obtained by analyzing the solar proton flux and the M6+ seismic activity between 2012 and today). In fact, about 60 hours later the M6.6 earthquake was recorded at 123 km ESE of Kokopo, Papua New Guinea on November 15, 2024, at 05:28 UTC; while 115 hours later the M6.1 earthquake was recorded at 155 km SSE of Koshima, Japan on November 17, 2024, at 12:16 UTC (**Fig. 2**).

Both seismic events occurred during the phase of reduction of the proton density of the solar wind, confirming the distribution of seismic events with respect to the proton variation curve that the authors identified already in 2012 (**Fig. 3**).

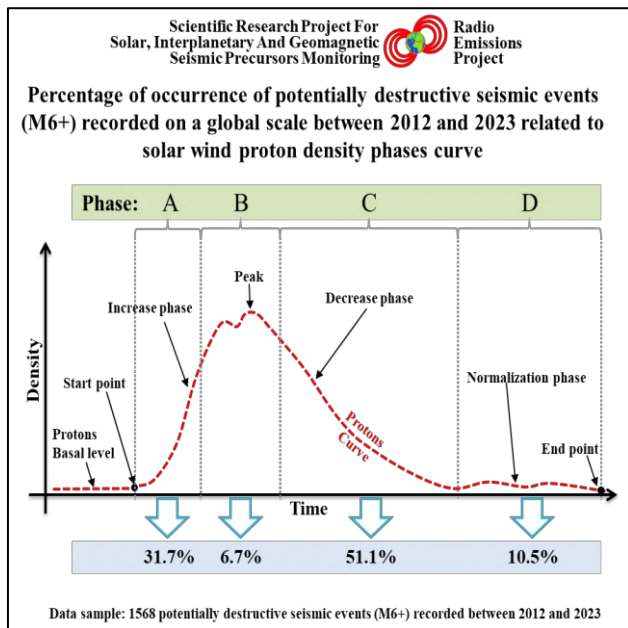


Fig. 3 – Distribution of M6+ seismic events versus the proton variation curve of the solar ion flux. The image above schematically represents the distribution of M6+ seismic events recorded on a global scale with respect to the solar wind proton density increase curve (rough dashed line). 31.7 percent of seismic events are recorded during the proton density increase phase; 6.7 percent of seismic events are recorded during the maximum density reached by the proton increase (± 6 hours). 51.1 percent of seismic events are recorded during the proton density decrease phase while 10.5 percent of seismic events are recorded during the phase of reduction of the proton increase to baseline values. Credits: Radio Emissions Project.

The percentage distribution of seismic events with respect to the variation curve of the proton density of the solar wind has established that the majority of potentially destructive seismic events that are recorded on a global scale occur during the phase of decrease of the proton density (51.1 percent). In fact, the two M6+ earthquakes recorded between 12 and 18 November 2024 occurred precisely during the phase of decrease of the proton density of the solar wind, confirming the statistical trend observed by the authors already in 2012 (**Fig. 3**).

The onset of the proton increase that preceded the M6.6 earthquake recorded at 123 km ESE of Kokopo, Papua New Guinea on November 15, 2024, at 05:28 UTC, and the M6.1 earthquake recorded at 155 km SSE of Koshima, Japan on November 17, 2024, at 12:16 UTC, was recorded on November 12, 2024, at 17:15 UTC. The maximum density was reached on November 13, 2024, at 05:30 UTC although some impulsive increases of higher density were recorded on:

- 1) November 12, 2024, at 23:05 UTC.
- 2) November 14, 2024, at 08:25 UTC.
- 3) November 15, 2024, at 23:30 UTC.

Following the proton increase, two increases in the Earth's geomagnetic field were recorded (**Fig. 2**) measured through the variation of the Kp index provided by the National Oceanic and Atmospheric Administration (NOAA):

- 1) The first recorded between 13 November 2024 at 09:15 UTC and 16 November 2024 at 21:00 UTC, preceded the earthquake recorded in Papua New Guinea by ~44 hours.
- 2) The second recorded between 16 November 2024 at 21:00 UTC and 18 November 2024 at 09:15 UTC, preceded the earthquake recorded in Japan by ~15 hours.

Each increase in the Earth's geomagnetic activity overlapped with one of the two potentially destructive seismic events recorded between 12 and 18 November 2024 (**Fig. 2**). This confirms what the authors have observed since 2012 [10] [12] [19] [44-52]. The hypothesis formulated by the authors, presented in other international scientific publications, is that the increases in the solar proton flux influence the Earth's magnetosphere, inducing perturbations of the geomagnetic field that interact with tectonic processes. Studies conducted by the authors since 2012 show that each seismic event of high magnitude (M6+) is preceded by an increase in the proton density of the solar wind and by geomagnetic variations that can reach significant values. The observed perturbations include fluctuations in the Earth's magnetic field, which could facilitate the release of energy along tectonic faults, contributing to the triggering of earthquakes. Added to this is the hypothesis that magnetostriction and electrostriction

phenomena, induced by geomagnetic variations, can cause microscopic deformations in rocks. These effects, combined with the action of the Lorentz force on the electric charges present along the faults, can alter their static equilibrium.

The origin of these electric charges is linked to tectonic stress, which causes phenomena of piezoelectricity, triboelectricity and gas release. During the deformation of rocks, microfractures generate accumulations of electric charges, which, under the action of geomagnetic perturbations, are set in motion again. This complex set of physical processes could explain how geomagnetic variations are able to directly influence the dynamics of faults, bringing them to the breaking point.

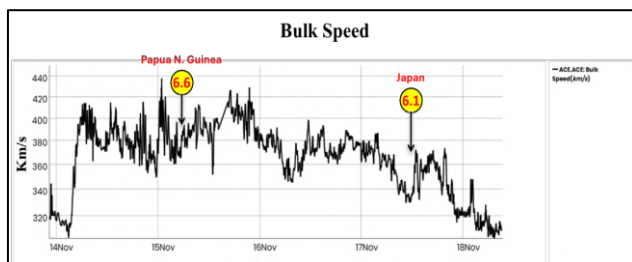


Fig. 4 – Average speed of the solar wind directed towards the Earth. In the image above you can observe the variation of the average speed of the solar wind directed towards the Earth recorded between 13 and 19 November 2024. The increase in the speed of the solar wind underwent a rapid acceleration on 4 November 2024 at 03:00 UTC reaching the maximum speed (438 km/s) on 15 November 2024 at 00:58 UTC. Credits: iSWA.

Further confirmation of the magnitude of the proton increase observed between 12 and 18 November 2024 is represented by the average speed of the solar wind visible in **Fig. 4**. Also, in this case the data were provided by the Advanced Composition Explorer (ACE) Satellite, located in Lagrangian orbit L1. The graph (**Fig. 4**) shows that the two M6+ seismic events recorded between 12 and 18 November 2024 occurred during an increase in the average speed of the solar wind directed towards the Earth.

Discussion

The results of this study further strengthen the relationship between increases in solar wind proton density and geomagnetic disturbances preceding significant seismic events. The identification of these correlations, observed in the seismic events of 12–18 November 2024, provides compelling evidence to support the hypothesis that Sun-Earth interactions can serve as reliable indicators for earthquake prediction.

The M6.6 earthquakes recorded in Papua New Guinea and M6.1 in Japan occurred during the phase of solar wind proton density decrease. This result is consistent with previous studies indicating that more than 50 percent of global M6+ seismic events occur during this phase. Furthermore, the timing of proton density increases,

followed by peaks in geomagnetic activity measured by the Kp index, closely align with the observed seismic events. These correlations highlight a consistent temporal relationship between solar wind perturbations and tectonic activity, confirming the results already documented by the Radio Emissions Project.

This study supports the hypothesis that solar wind perturbations, influencing the Earth's geomagnetic environment, can interact with pre-existing tectonic stress conditions. Geomagnetic variations are hypothesized to generate Lorentz forces on electric charges present along tectonic faults, charges that originate from tectonic stress processes through phenomena such as piezoelectricity, triboelectricity and gas release. Furthermore, magnetostriction and electrostriction phenomena, induced by geomagnetic variations, are thought to further contribute to the process. Magnetostriction and electrostriction can cause microscopic deformations of rocks, amplifying the effects of geomagnetic variations. These mechanisms, operating in combination with Lorentz forces, could alter the static equilibrium of tectonic faults, accelerating the release of energy and favoring the triggering of earthquakes.

The results of this analysis are in line with observations conducted since 2012, according to which each seismic event of high magnitude (M6+) is preceded by an increase in the proton density of the solar wind and by significant variations in geomagnetic activity [2-52]. The uniformity of these observations over more than a decade strengthens the validity of the method used to identify seismic precursors. Despite the encouraging results, some limitations remain. The generalization of this model requires further verification, especially in different geodynamic contexts. Furthermore, the automation and expansion of electromagnetic monitoring stations designed to detect pre-seismic electromagnetic sources following the release of electric charges by piezoelectric, triboelectric and gas release effects could significantly improve data collection and analysis, allowing for more accurate seismic forecasting on a global scale that also includes the possibility of performing crustal diagnosis. This research represents a crucial step forward in the understanding of the interactions between solar activity and seismic phenomena, opening new possibilities for seismic risk mitigation.

Conclusion

The results presented in this study further confirm the link between solar wind proton density increases and geomagnetic perturbations as reliable pre-seismic indicators. The M6.6 earthquakes in Papua New Guinea and M6.1 in Japan, which occurred between 12 and 18 November 2024, were preceded by significant changes in proton density and geomagnetic activity, consistent with observations conducted since 2012. These results demonstrate the reliability of the proposed analysis method,

which successfully identified electromagnetic and geomagnetic precursors for earthquakes of significant magnitude. The hypothesis that geomagnetic perturbations influence tectonic stress conditions through electromagnetic forces, such as Lorentz forces, magnetostriction and electrostriction, finds further support. These phenomena, combined with piezoelectric and triboelectric effects in tectonic stressed rocks, contribute to earthquake triggering by altering the static equilibrium of faults. The temporal distribution of seismic events with respect to the proton density variation curve shows that more than 50 percent of M6+ earthquakes occur during the proton density decrease phase. This statistical pattern further strengthens the validity of the adopted approach, which proves useful not only to identify global seismic precursors, but also to improve the understanding of the physical processes that precede earthquakes.

Despite the progress achieved, some limitations need to be addressed, including the need for a global network of electromagnetic monitoring stations to improve data collection and analysis. The automation of the detection and triangulation processes of local electromagnetic sources is a crucial objective to optimize the effectiveness of this approach.

Furthermore, future studies could further investigate the physical mechanisms linking geomagnetic perturbations to seismogenesis, with a focus on their applicability in different geodynamic settings. These developments could not only enable more accurate seismic forecasting, but also a better understanding of seismic hazards, thus contributing to the mitigation of impacts associated with large earthquakes.

This research represents an important step towards a new paradigm in earthquake forecasting, based on the integrated analysis of electromagnetic, geomagnetic and solar variations, paving the way for a future where seismic forecasting could become a viable reality on a global scale.

References

- [1] United States Geological Survey (USGS) – Tectonic Summary
- [2] V. Straser, G. Cataldi. (2014). Solar wind proton density increase and geomagnetic background anomalies before strong M6+ earthquakes. Space Research Institute of Moscow, Russian Academy of Sciences, MSS-14. 2014. Moscow, Russia. pp280-286.
- [3] V. Straser, G. Cataldi. (2015). Solar wind ionic variation associated with earthquakes greater than magnitude M6.0. *New Concepts in Global Tectonics Journal*, V. 3, No. 2, June 2015, Australia. P.140-154.
- [4] G. Cataldi, D. Cataldi, V. Straser. (2015). Solar wind proton density variations that preceded the M6+ earthquakes occurring on a global scale between 17 and 20 April 2014. European Geosciences Union (EGU) General Assembly 2015, Vienna, Austria.
- [5] G. Cataldi, D. Cataldi, V. Straser. (2015). Solar wind ion density variations that preceded the M6+ earthquakes occurring on a global scale between 3 and 15 September 2013. European Geosciences Union (EGU) General Assembly 2015, Geophysical Research Abstract, Vol. 17, EGU2015-4581, Vienna, Austria.
- [6] G. Cataldi, D. Cataldi, V. Straser. (2015). Solar wind proton density variations that preceded the M6,1 earthquake occurred in New Caledonia on November 10, 2014. European Geosciences Union (EGU) General Assembly 2015, Geophysical Research Abstract, Vol. 17, EGU2015-4167, Vienna, Austria.
- [7] V. Straser, G. Cataldi, D. Cataldi. (2015). Solar wind ionic and geomagnetic variations preceding the M8.3 Chile Earthquake. *New Concepts in Global Tectonics Journal*, V. 3, No. 3, September 2015, Australia. P.394-399.
- [8] G. Cataldi, D. Cataldi, V. Straser. (2016). Solar activity correlated to the M7.0 Japan earthquake occurred on April 15, 2016. *New Concepts in Global Tectonics Journal*, V. 4, No. 2, pp202-208, June 2016.
- [9] G. Cataldi, D. Cataldi, V. Straser. (2016). Tsunami related to solar and geomagnetic activity. European Geosciences Union (EGU) General Assembly 2016. Geophysical Research Abstract, Vol. 18, EGU2016-9626, Vienna, Austria.
- [10] G. Cataldi, D. Cataldi, V. Straser. (2017). SELF-VLF electromagnetic signals and solar wind proton density variations that preceded the M6.2 Central Italy earthquake on August 24, 2016. *International Journal of Modern Research in Electrical and Electronic Engineering*, Vol. 1, No. 1, 1-15. DOI: 10.20448/journal.526/2017.1.1/526.1.1.15.
- [11] G. Cataldi, D. Cataldi, V. Straser. (2017). Solar wind proton density increase that preceded Central Italy earthquakes occurred between 26 and 30 October 2016. European Geosciences Union (EGU), General Assembly 2017. Geophysical Research Abstracts Vol. 19, EGU2017-3774, 2017. Vienna, Austria.

- [12] V. Straser, G. Cataldi, D. Cataldi. (2017). Solar and electromagnetic signal before Mexican Earthquake M8.1, September 2017. New Concepts in Global Tectonics Journal, V. 5, No. 4, December 2017. pp600-609.
- [13] G. Cataldi, D. Cataldi, V. Straser. (2017). Solar and Geomagnetic Activity Variations Correlated to Italian M6+ Earthquakes Occurred in 2016. EGU General Assembly 2017. EGU2017-3681, Vol. 19. Vienna, Austria.
- [14] G. Cataldi, D. Cataldi, V. Straser. (2019). Solar wind ionic density variations related to M6+ global seismic activity between 2012 and 2018. European Geosciences Union (EGU) General Assembly 2019. Geophysical Research Abstract, Vol. 21, EGU2019-3067, 2019, Vienna, Austria.
- [15] G. Cataldi. (2020). Precursori Sismici – Monitoraggio Elettromagnetico. Kindle-Amazon, ISBN: 9798664537970. ASIN Code: B08CPDBGX9.
- [16] G. Cataldi, D. Cataldi, V. Straser. (2019). Wolf Number Related To M6+ Global Seismic Activity. New Concepts in Global Tectonics Journal, Volume 7, Number 3, December 2019, pp178-186.
- [17] V. Straser, G. Cataldi, D. Cataldi. (2020). The Space Weather Related to the M7+ Seismic Activity Recorded on a Global Scale between 28 January and 25 March 2020. Acta Scientific Agriculture 4.12 (2020): pp55-62.
- [18] G. Cataldi, V. Straser, D. Cataldi. (2020). Space weather related to potentially destructive seismic activity recorded on a global scale. New Concepts in Global Tectonics Journal. Vol.8, No.3, pp233-253, December 2020. ISSN 2202-0039.
- [19] G. Cataldi. (2021). Radio Emissions Project – A new approach to seismic prediction. Kindle-Amazon, ISBN: 9798709593411.
- [20] G. Cataldi, D. Cataldi, V. Straser. (2021). Space weather and geomagnetic activity related to the Japan M7.1 earthquake recorded on February 13, 2021. New Concepts in Global Tectonics Journal, Vol. 9, No. 1, pp16-23. March 2021.
- [21] G. Cataldi, D. Cataldi, V. Straser. (2021). Space weather and geomagnetic activity related to the Chilean M6.7 earthquake recorded on February 3, 2021. New Concepts in Global Tectonics Journal, Vol. 9, No. 1, pp3-9. March 2021.
- [22] G. Cataldi, D. Cataldi, V. Straser. (2021). Space weather and geomagnetic activity related to M6+ global seismic activity recorded on February 7, 2021. New Concepts in Global Tectonics Journal, Vol. 9, No. 1, pp24-30. March 2021.
- [23] G. Cataldi, D. Cataldi, V. Straser. (2021). Space Weather and geomagnetic activity related to Ecuadorean M7.5 earthquake recorded on February 22, 2019. New Concepts in Global Tectonics Journal, Vol. 9, No. 2, pp79-86. June 2021.
- [24] G. Cataldi, D. Cataldi, V. Straser. (2021). Solar Activity and geomagnetic activity related to M6+ global seismic activity recorded on March 20, 2021. New Concepts in Global Tectonics Journal, Vol. 9, No. 2, pp87-93. June 2021.
- [25] G. Cataldi, D. Cataldi, V. Straser. (2021). Space weather and geomagnetic activity related to M6+ global seismic activity recorded on 3-4 March 2021. New Concepts in Global Tectonics Journal, Vol. 9, No. 2, pp94-98. June 2021.
- [26] G. Cataldi, D. Cataldi, V. Straser. (2021). Solar activity and geomagnetic activity related to M6.0 South Sandwich Islands region earthquake recorded March 14, 2021. New Concepts in Global Tectonics Journal, Vol. 9, No. 2, pp99-105. June 2021.
- [27] G. Cataldi, D. Cataldi, V. Straser. (2021). Space weather and geomagnetic activity related to the Vanuatu M6.3 earthquake recorded on March 20, 2019. New Concepts in Global Tectonics Journal, Vol. 9, No. 2, pp106-111. June 2021.
- [28] G. Cataldi, D. Cataldi, V. Straser. (2021). Space weather and geomagnetic activity related to M6+ earthquakes recorded between 7 and 20 November 2017. New Concepts in Global Tectonics Journal, Volume 9, Number 3, September 2021. pp137-144. ISSN 2202-0039.
- [29] G. Cataldi, D. Cataldi, V. Straser. (2021). Space weather and geomagnetic activity related to M6+ earthquakes recorded between 12 and 15 April 2012. New Concepts in Global Tectonics Journal, Volume 9, Number 3, September 2021. Pp145-154. ISSN 2202-0039.
- [30] G. Cataldi, D. Cataldi, V. Straser. (2021). Space weather and geomagnetic activity related to M6+

- earthquakes recorded between 13 and 16 April 2016. *New Concepts in Global Tectonics Journal*, Volume 9, Number 3, September 2021. pp158-163. ISSN 2202-0039.
- [31] G. Cataldi, D. Cataldi, V. Straser. (2021). Space weather and geomagnetic activity related to M6+ earthquakes recorded between 17 and 19 July 2017. *New Concepts in Global Tectonics Journal*, Volume 9, Number 3, September 2021. pp164-169. ISSN 2202-0039.
- [32] G. Cataldi, D. Cataldi, V. Straser. (2021). Space weather related to M6+ earthquakes recorded on June 24, 2019. *New Concepts in Global Tectonics Journal*, Volume 9, Number 3, September 2021. pp132-136. ISSN 2202-0039.
- [33] G. Cataldi, V. Straser, D. Cataldi. (2021). Space weather related to M6.1 Indonesia earthquake recorded on June 3, 2021. *New Concepts in Global Tectonics Journal*. Volume 9, No 4, December 2021. Pp 185-193.
- [34] G. Cataldi, V. Straser, D. Cataldi. (2021). Space weather related to M6.0 Tonga earthquake recorded on March 17, 2020. *New Concepts in Global Tectonics Journal*. Volume 9, No 4, December 2021. Pp 206-214.
- [35] G. Cataldi, V. Straser, D. Cataldi. (2021). Space weather related to M8.2 earthquake recorded in Alaska on 29 July 2021. *New Concepts in Global Tectonics Journal*. Volume 9, No 4, December 2021. Pp 194-205.
- [36] V. Straser, G. Cataldi, D. Cataldi. (2022). Space weather related to M6+ potentially destructive seismic events recorded on a global scale between 13 and 16 March 2022. *New Concepts in Global Tectonics Journal*. Volume 10, Number 1, March 2022. ISSN 2202-0039. pp. 3-10.
- [37] V. Straser, G. Cataldi, D. Cataldi. (2022). Space weather related to M6+ potentially destructive seismic events recorded on a global scale between 2012 and 2021. *New Concepts in Global Tectonics Journal*. Volume 10, Number 1, March 2022. ISSN 2202-0039. pp. 11-21.
- [38] V. Straser, D. Cataldi, G. Cataldi. (2023). Weather Events Associated with Strong Earthquakes and Seismic Swarms in Italy. *Advances in Geological and Geotechnical Engineering Research*. Volume 05, Issue 03, Pp 39-54. July 2023.
- [39] V. Straser, G. Cataldi, D. Cataldi. (2023). Magnitude of potentially destructive earthquakes recorded in Mexico correlated to the extent of the solar proton flux. *New Concepts In Global Tectonics Journal*. Vol 11, N 4, December 2023. ISSN 2202-0039. Pp 261-266.
- [40] V. Straser, G. Cataldi, D. Cataldi. (2024). Space Weather related to destructive seismic activity that has been recorded globally between 2012 and 2023. *New Concepts In Global Tectonics Journal*. Vol 12, N 1, March 2024. Pp: 1-8.
- [41] D. Cataldi, G. Cataldi, V. Straser. (2024). Solar activity and Electromagnetic Signals that preceded the M7.5 Earthquake of January 1, 2024, in Japan. *New Concepts In Global Tectonics Journal*. Vol 12, N 1, March 2024. Pp: 9-25.
- [42] D. Cataldi, G. Cataldi, V. Straser. (2024). Earthquakes, Solar Activity, and Bright Meteors. *New Concepts In Global Tectonics Journal*. Vol 12, N 1, March 2024. Pp: 85-94.
- [43] V. Straser, G. Cataldi, D. Cataldi. (2024). Space weather linked to potentially destructive earthquakes between 2012 and 2023. *New Concepts in Global Tectonics Journal*. Volume 12, Number 3, September 2024. ISSN 2202-0039. PP248-257.
- [44] D. Cataldi, G. Cataldi, V. Straser. (2024). Space weather and pre-seismic radio frequency related to the Italian M5.1 earthquake recorded on August 1, 2024. *New Concepts in Global Tectonics Journal*. Volume 12, Number 3, September 2024. ISSN 2202-0039. PP240-247.
- [45] D. Cataldi, G. Cataldi and V. Straser. (2014). Variations of the Electromagnetic field that preceded the Peruvian M7.0 earthquake occurred on September 25, 2013. *European Geosciences Union (EGU) General Assembly 2014, Geophysical Research Abstract, Vol. 16, EGU2014-1075.*
- [46] G. Cataldi, D. Cataldi. (2014). Sismicità – Gas Radon – Elettromagnetismo – Radioattività. Reti di monitoraggio ufficiali e amatoriali. Stato dell'arte nella ricerca di segnali possibili precursori sismici. Regione Autonoma Friuli Venezia Giulia, Protezione Civile. Comune di Pozzuolo Del Friuli, F.E.S.N. 2014. pp. 44-49; 97-99.
- [47] V. Straser, G. Cataldi, D. Cataldi. (2015). Radio-anomalies: tool for earthquakes and tsunami

forecasts. European Geosciences Union (EGU) General Assembly 2015, Natural Hazard Section (NH5.1), Sea & Ocean Hazard - Tsunami, Geophysical Research Abstract, Vol. 17, Vienna, Austria.

- [48] V. Straser, G. Cataldi, D. Cataldi. (2016). SELF and VLF electromagnetic signal variations that preceded the Central Italy earthquake on August 24, 2016. *New Concepts in Global Tectonics Journal*, V. 4, No. 3, September 2016. pp473-477.
- [49] D. Cataldi, G. Cataldi, V. Straser. (2017). SELF and VLF electromagnetic emissions that preceded the M6.2 Central Italy earthquake occurred on August 24, 2016. European Geosciences Union (EGU), General Assembly 2017. *Geophysical Research Abstracts Vol. 19, EGU2017-3675*, 2017.
- [50] G. Cataldi, D. Cataldi, R. Rossi, V. Straser. (2017). SELF-ELF Electromagnetic signals correlated to M5+ Italian Earthquakes occurred on August 24, 2016 and January 18, 2017. *New Concepts in Global Tectonics Journal*, V. 5, No. 1, March 2017. pp134-143.
- [51] V. Straser, G. Cataldi, D. Cataldi. (2017). Seismic signals detected in Italy before the Nikol'skoye (off Kamchatka) earthquake in July 2017. *New Concepts in Global Tectonics Journal*, v. 5, no. 3, September 2017. pp391-396.
- [52] D. Cataldi, E. Cavina, G. Cataldi, V. Straser. (2022). Reverse Migration of the Wood Pigeons and electromagnetic emissions, before the Mw 3.7 earthquake occurred in Visso-Macerata, Central Italy on October 18, 2021. *iJournals: International Journal of Social Relevance & Concern (IJSRC)*, ISSN-2347-9698, Volume 10, Issue 1 January 2022. pp. 24-40.

Plate Tectonic Issues, The Influence of Electricity in Rock Forming Processes and a Coherent Connection Between Science, Mythology and History of Finland - Part III

Stefan Ahmala

Natural Philosopher and Independent Researcher, A3 Anomalies, Year 2023 Finland

Corresponding Author: Stefan Ahmala, Joensuu, Finland
Email: stefan.ahmala@outlook.com

Abstract: **Abstract:** Part III of the Plate Tectonic Issues series takes a look at peat from a new perspective. We will explore its genesis and possible role in the environment. As has been the case in this series, we will touch on a rather wide range of topics, from history to chemistry and from mythology to space weather.

Keywords: Electromagnetism, sun cycles, geology, transmutation of elements, shockwaves, induced currents, Earth is a capacitor, amorphous and crystalline silica, EZ-water, zeolitic water, alkalinity, acidity, hydrogen anion, daisy chains, mineral facies, craters

*“They say that a little knowledge is a dangerous thing,
but it is not half so bad as a lot of ignorance.”*

Terry Pratchett



Fig. 1 .1. For those who have eyes to see. A coffee mug with petroglyphs made by Pentik in the middle. To the left, a Finnish brimstone and to the right we see a beautiful example of mineral facies.

Content

1. Introduction
2. Comparison of different theories about peat and other contradictions in modern science
3. Creation and accretion of peat from a new perspective
4. Peat's active role in the environment and in the end of the last ice age
5. Cultural rituals and Mythological stories revolving around peat
6. Conclusions
7. References

1. Introduction

Many of the modern sciences exist within the uniformitarianism notion, that is, except for the Big Bang, everything happened at a steady pace over millions of years. Every now and then, an asteroid falls on Earth, sometimes with devastating consequences like the extinction of the dinosaurs. Most often they just burn in the atmosphere without anyone noticing it. But otherwise, things happen generally very slowly. When reading or watching something about ancient people, it cannot be overheard, how often it is expressed that not only the hominids/humans but also the animals, seem always to struggle to survive. Since the author realized this repetitive pattern, he got sensitive to this topic. In the author's opinion, this assumption is a totally empty phrase and seems to have only one purpose: Lifting modern men even higher in a strange hierarchy of living beings. "We have conquered nature" or "Science is settled" are expressions some seem to believe and take them as absolute truths, without understanding their own lack of critical thinking. Many things which are used to keep our modern society going are not very well understood. Often it is more known about how to use something, than about its origins, most people simply don't care. Many people are also not really aware of what they are saying in terms of everyday language, for example, everyday sayings used by the people. What does it actually mean? Where does it come from? Why is the sun reinderring? There is a big possibility that the animals and peoples of ancient times thrived in an exceptionally fertile environment where food, water, warmth and light was much more abundant than many could imagine. It might have been a totally different world and stories about the old sun, or the good sun, only undermine these possibilities. On the other hand, we also have evidence that the past wasn't a "forever-stable" time. Many things have changed over the years, and it is foolish to believe that nothing is going to change anymore. Many species went extinct, but also new ones formed. Every now and then archeologists find new evidence that ancient people were more advanced than previously assumed, which sometimes poses problems with their interpretations of certain patterns. Geology is also full of contradictions, assumptions and unprovable claims which are often explained away by using extremely long timelines. Sometimes they just seem to care too much about the contradictions, and they just move on with a "Oh, look! A bird!" kind of an attitude. Birds are dinosaurs, they didn't go extinct, they just got smaller.

Peat is something most of us are familiar with, at least to some degree. It is found all over the globe and usually related to water. Despite the huge amount of literature about peat, bogs, fens or wetlands in general, the origins and creation of it are not well understood, and it is classified as a

geomorphological phenomenon. In other words: They don't really know how it got created or where it came from. When talking about wetlands, we have "still" water, not flowing, as a key component which is usually "stored" in lakes and ponds. According to mainstream scientific theory, some of these water bodies are seen as meteor impact craters, often they are seen as a result of plate tectonics but also glaciers might have carved them out. The end of the last ice age seemed to have happened rather quickly in terms of melting. The author thinks that peat might have played a crucial role in some of the melting processes due to its electromagnetic properties. Peat will be the main topic of this paper, but other topics will be discussed as well. Not only because they are interesting, but also to show how, at first glance seemingly unrelated things are surprisingly similar with each other. Earth provides an ever-changing environment for life in a cyclical manner. It, and all the other planets with all their moons, are contained within the sun's magnetosphere. The sun is nowadays not only geographically the center of our solar system but also energy-wise, this implies that it might have been different in the past. All the planets are constantly connected to the sun by interplanetary Birkeland currents. The sun, and therefore all the planets of our solar system, are constantly connected to the center of our galaxy with intergalactic Birkeland currents. Birkeland currents are strings of electricity which have many recognizable patterns. It is important to understand that electric currents are creating the magnetic fields, they are the easiest to see with bare eyes because matter accumulates magnetically. Every electric current has a magnetic field (sphere) and every magnet has electric currents flowing around and through it, the magnetic flux. Every living being is electromagnetic by nature, and every natural process can be explained with electromagnetism. It is scalable from the atomic realm up to the cosmic size. Peat or turf is known to most people around the world. It can be found on every continent on Earth. Peatlands, which also includes mires, bogs, muskogs and moors, are easily recognizable since they have a distinct look, as well as from ground level as from above. They often have brownish or reddish color and water bodies. It has been used by people for centuries in different ways. Some preserved their food in it, others used it for leather processing and people were even buried in it. Nowadays, peat is still used in different ways, that is mostly by the industrial sector. Two main uses make it still somewhat important for modern society. One is through burning it for electricity production or as fertilizer in agriculture. The use of peat for industrial purposes is not without contradiction due to its impact on the environment. Peatlands are usually wetlands, which means they must be drained in order to make it accessible to

machines. This includes deforestation, the excavation of drainage channels, construction of roads and other facilities. Flora and fauna will suffer greatly. When water bodies are altered artificially, usually the influence of these changes comes to light in extreme conditions such as drought or flood conditions. In dry conditions peat can get lifted aloft by winds, and the very fine dust produces problems in respiratory systems of the population in the vicinity. Another aspect of dried out peatlands, either artificially or naturally, is the danger of long-lasting, subsurface fires, which are very hard to distinguish. There are different kinds of peatlands but their origin or forming processes remain largely unknown. On one hand, it is believed that peats accumulate very slowly over a long time period, approximately 1 mm per year. This kind of explanation fits perfectly into the uniformitarianism paradigm where everything happens very slowly and gradually, so slow that it is almost impossible to see or even to reproduce the theory in a laboratory in order to prove or disprove the theory. It is impossible to re-create a scientific laboratory experiment which lasts, for example, 5432 years. Totally impossible. Nonetheless, the use of very long-time scales in science is rather common and used in different branches of mainstream science such as geology and cosmology. Furthermore, certain agreements made upon scientific consensus, which do not allow any new information to penetrate the already agreed theory, "gate-keepers" in peer-reviewing processes make sure that nothing new will enter the established paradigm. It is ignorance towards new perspectives and ignorance is the opposite of nescience, the very word, from which the word science is derived from. This alone is very ironic by itself, but the reason for this is quite likely the dogmatization and commercialization of science, in other words: Modern/mainstream science doesn't search for the ultimate truth, its goal is ultimate profit, assure funding, and therefore is keen to keep all the mysteries alive, from who has the biggest money is expected through political agendas. These processes of scientific agreement on theories which are based more on assumptions than on actual facts, nor reproduction in laboratories, have no or very few repetitive patterns and often lacks the ability of prediction, is known as a belief system. The theory falls apart at the moment it is not believed in anymore. Facts don't care about anyone's beliefs or feelings; they all stand on their own. In this paper, the author brings forward a new theory about peat and its creation, and its role in our environment. The author lives in Finland, the peat-richest country in the world. The Finnish name of Finland is Suomi, "suo" means swamp/wetland, so it seems to be a place which identifies itself with it. The internet is full of texts, chemical analyses and economic calculations about peats. It also became part of the climate change conversation as a source of CO₂. Which is one of the

main reasons why it works as a fertilizer, provided by nature itself. You can find really accurate maps and all sorts of things related to peats. Many scientific papers have been written about the topic but nowhere is explained how exactly it came into existence. It remains also rather unclear what it is, in terms of biology and/or geology, so it is seen as a "geomorphological phenomenon". Quite much like metamorphosed rock, it is just there, and people figured out how to make use of it. We know quite accurately what it is made of and that there are differences between different peatlands. A holistic explanation of what is missing. It remains a geomorphological phenomenon, which might sound very scientific, but the words used to describe it, reveal also that it isn't understood. The only agreed consensus about it is that it is a phenomenon.

Several questions about peat must be asked:

What is it?

Where did it come from?

How did it form?

Why is something like peat found on Earth?

Could its dielectric properties have an influence on its environment?

Why is it dielectric in the first place?

Are there indications of peat interacting with its environment?

The end of the last ice age, approximately 12 '000 years ago, was a very significant event. It made it possible for life to spread all over the globe, again. Life didn't disappear during the ice age, it got reduced in quantity and confined in places where it was possible to survive, near the equator. Several theories exist about how the great melting occurred. They agree more or less on one specific topic, which is that the melting seems to have happened rather quickly. What else than the sun could have provided the energy for it? The question remains about how it happened. The albedo effect of white surfaces, such as snow and ice, pose somewhat of a problem. Geothermal heat must be taken into consideration, it is a part of volcanism. This on the other hand implies yet another mystery: How is the heat beneath our feet produced? Some propose that Earth's core is a molten ball of iron, and the heat is produced by nuclear processes due to the immense pressure. How is it then possible that Earth's thermosphere, which starts about 85 km over the surface of Earth and extends to about 500 km altitude, can exhibit temperatures of 2000 degrees Celsius or more, if the heat of Earth is supposed to come from its core? Something really doesn't match in many common things still taught in schools or even universities. The following text tries to bring some new viewpoints to this topic, in a fresh way. Common sense, a holistic view and interdisciplinary scientific evidence are

crucial points of attitude which will guide us throughout this text.

2. Comparison of different theories about peats, and other contradictions in modern science

We will start this chapter with two quotes in order to show some basic contradictions within the topic:

Quote Nr. 1 from the FAO Bulletin (1) (Food and Agriculture Organization of the United Nations):

"Peats are generally considered to be partly decomposed biomass (vegetation). They show a wide range in degree of decomposition. Kurbatov (1968) briefly summarizes 35 years of research into the formation of peat as follows: "The formation of peat is a relatively short biochemical process carried on under the influence of aerobic microorganisms in the surface layers of the deposits during periods of low subsoil water. As the peat which is formed in the peat-producing layer becomes subjected to anaerobic conditions in the deeper layers of the deposit, it is preserved and shows comparatively little change with time". (2)

Quote Nr. 2 from Wikipedia.org (3):

"Peat is a renewable source of energy in theory, but not in practice, due to its extraction rate in industrialized countries far exceeding its slow regrowth rate of 1 mm (0.04 in) per year."(4)

There seems to be some contradiction between those two quotes, timewise. It also is hard to distinguish between "formation" and "accumulation". The first quote refers to a rather short process, but the second quote refers to a slow process. For some reason the author hasn't been able to find any satisfying explanation of how peat got or gets formed. There is evidence in literature that the peat forms in certain times in history like 12000 years (5), 6000 years (6) or maybe even 3500 years ago. It is obvious the creation dates correlate to some degree with sun cycles (7, 8), but we also need to take into account what our ancestors recorded for us to decipher. The author thinks it is possible that peat forms more or less in a cyclical pattern. Also, it should be taken into account, that the creation of peats might have happened regionally. In other words: Plants, and other biological mass from a certain time period at a certain place might have persisted, whilst in another location of the same aged biomass, turned into peat. Eventually it got mixed up by winds or other meteorological processes and functioned as a fertilizer. Quite like it is still used in modern society. It is a natural process, so it shouldn't be a surprise that nature works this way. In the first quote a biochemical (9) process

is mentioned. So, we must talk about the meaning of the word "biochemical", which is obviously constructed of two words. It is a very interesting word because it forces us to think about life itself. Somewhere a distinction must be made between dead matter, and matter which is alive. The two parts of living and nonliving things are called biotic/alive and abiotic/not alive (10). Somewhere "the line" between living and not living must be drawn (11). It is something which has been done already many times throughout history and is one of the most fundamental questions of all, and of course the discussion is not over yet (12). In the author's opinion, a form of distinguishment could be made by defining the amount, and the relative amount to each other, of "closed" and "open" electric circuits in a being or entity. Closed circuits are processes which are happening within the entity. Things like our blood circuitry, muscle movement or the movement of water within a plant, from the roots all the way up/out to the leaves are measurable processes, which cease to exist if the process inheriting entity cannot maintain a certain energy flow within itself. They are more or less confined within the being, they have often a physical form, are measurable and are in some cases also visible with the naked eye. In many cases they also exhibit certain patterns which are also seen in nature's electric display. For example, our vein network has the shape of lightning, they are an energy circuit after all. We are made of things like blood plasma (13) which, besides other functions, contributes heat throughout our bodies. Our blood contains iron (14) which is a very important part of our blood energy circuit, and it also undermines the electric nature of life itself. Every living being needs to have a certain amount of "closed" circuits in order to be an entity. No entity can exist without interacting with its environment, but the environment doesn't need the entity. All chemical processes are electrical in nature (15) and therefore we have to understand that changes in the electromagnetic environment can either slow down or speed up those processes. If the charge increases, and reaches a certain intensity threshold, we notice rapid changes. In an electrical environment change can happen lightning fast (16), literally. Earth is a capacitor in space (17) in which everything is connected, and therefore no islands are to be found (18). Earth has not only geographic poles (19), but also magnetic poles (20). This is something everybody knows, but the deeper meaning of it doesn't seem to be part of mainstream science. By deeper meaning I mean the fact that wherever there is a magnetic field, there is also an electric current and vice versa (21), this has been discovered accidentally already in 1820 by Oersted (22). Earth's magnetosphere (23), and its magnetic poles existence has to be considered as undeniable proof of an electric current flowing through planet Earth. But electricity is very often ignored as being a part of natural processes, especially in

cosmology. It even seems that the use of the word ELECTRICITY is consciously avoided.

Gravity is not understood by mainstream science. Sometimes it even gets mystified, like in this article from the "New Scientist" where 7 things which don't make sense about gravity" (24) are listed. The author doubts that this article was written by someone in his free time, so we must understand it, as either something written in a state of nescience or, as purposely made disinformation. It is not surprising to find many mysteries in science, like mysteries about the aforementioned gravitational "force", because it is simply not a force itself. It is only an effect of electromagnetism (25). The electrical force is 10-38 (the value varies from 10-36 to 10-39) times stronger than gravity (26). Einstein's theory of gravity has been debunked several times (27). This has to be taken very seriously; it will change the perception of reality and many mysteries will cease to exist. Pieces will "fall" naturally into place through a natural understanding of attraction and repulsion, frequency, resonance and geometry of the mechanics on every scale. Nature doesn't waste anything, ever, and peat is a great example of this. It is not only peat but also metamorphosed rock (28), volcanism (29), weather (30), history (31),

- **Kristian Birkeland** (1867-1917) 7 times (!) Nobel Prize nominee
https://www.apollon.uio.no/english/articles/2017/birkeland_english.html
- **Hannes Alfvén** (1908-1995) Winner of the Nobel Prize for physics in 1970
H. Alfvén, "Double Layers and Circuits in Astrophysics," in *IEEE Transactions on Plasma Science*, vol. 14, no. 6, pp. 779-793, Dec. 1986, doi: 10.1109/TPS.1986.4316626.
- **Nikola Tesla** (1856-1943)
<https://www.teslasociety.com/index.html>
<https://teslauniverse.com/>
- **Immanuel Velikovsky** (1895-1979) Psychoanalyst
<https://www.velikovsky.info/3>.
- **Ralph Juergens**
<https://www.kronos-press.com/juergens/>
- **Halton Arp**
<http://www.haltonarp.com/>
- **Anthony Peratt**

Peat and its properties, which sometimes also includes its electrical nature (37), is studied all around the world. It is partially decayed organic matter, but; Quote from the International Peatland Societies web page with the title; What is peat?: "Definitions of peat vary across disciplines and between authorities for different purposes and there is no universal agreement that is applicable in all

mythology (32), religion (33) and astronomy (34) which is poorly understood, but also soil (soil organic matter SOM) in general (35). In other words: According to common theory, most things are unknown or mysterious, a proven fact, since they admit it by themselves. Despite this fact, all kinds of rules and laws are implied in regard to the use of peat, conservation and protection of peat lands. The arising question is: Is there a possibility that this also happens in other realms and topics than peat related? Is answered with a YES (36). In order to prove the ignorance of mainstream science towards certain scientific discoveries and paradigms, which could have changed the path of humanity for the better, decades ago, through a better understanding of our environment, history and mythology. I listed a few important names and their works, who didn't get, and still are not getting the attention, acknowledgement and respect they would have deserved, and still deserve:

The author is aware this is not the "correct" way to present names and works in a scientific paper, but by doing it this way, the author makes sure that these names are noticed by the reader.

- <https://plasmauniverse.info/>
Peratt, Anthony. (2004). *Characteristics for the Occurrence of a High-Current, Z-Pinch Aurora as Recorded in Antiquity*. *Plasma Science, IEEE Transactions on*. 31. 1192 - 1214.
[10.1109/TPS.2003.820956](https://doi.org/10.1109/TPS.2003.820956).
- **Michael Steinbacher** (RIP)
<http://www.eu-geology.com/>
<https://www.youtube.com/@n0ble0bserver37>
- **David Talbott**
<https://www.thunderbolts.info/wp/author/david-talbott/>
- **Wal Thornhill** (RIP)
<https://www.holoscience.com/wp/>
<https://www.thunderbolts.info/wp/>
- **C. J. Ransom**
Ransom, C.J., & Thornhill, W. (2007). Plasma-Generated Craters and Spherules. *IEEE Transactions on Plasma Science*, 35, 828-831.
- **Viktor Schaubert** (1885-1958)
<https://pks.or.at/en/>

circumstances."(38) The international Peatland Society was founded in Canada 1968 but is nowadays a registered NGO in Jyväskylä, Finland. The scientific investigation into the mystery of peat is a vast field, with many different approaches. One of the newer viewpoints on the topic of peat, has become the climate change discussion. Joseph Fourier might be the first who proposed CO2 to be the main

driver behind climate change in the year 1827 (39). The whole discussion about the role of CO₂ as the main driver of terrestrial climate change, tied to the industrial revolution, doesn't make any sense at all. It is instrumentalized as a political tool and not based on logic, nor evidence. Nature doesn't and can't work in such a self-destructible way. No life could ever emerge. We only have to look at what plants need to grow: Light, Water and CO₂. Quote from Oklahoma State University: "Photosynthesis is the process which involves a chemical reaction between water and carbon dioxide (CO₂) in the presence of light to make food (sugars) for plants, and as a by-product, releases oxygen in the atmosphere" (40). This means that CO₂ is a very important part of Earth's atmosphere, without it, life couldn't exist. "Back in the days" when dinosaurs roamed the Earth, the CO₂ content of the atmosphere was much higher than it is

nowadays (41). Some of the dinosaurs were very big and they conclusively also needed a lot of food, which obviously was provided (Fig 1.2.). Only with a much higher level of CO₂ in the atmosphere could plants provide enough food for the dinosaurs. The overall charging potential of planet Earth also had a big influence on the size of the species. A higher charge potential means a stronger gravitational pull. This indicates that planet Earth seems to grow (43) and the species are getting smaller (44). As demonstrated above, many topics in mainstream science are still "largely unknown", "mysterious" or even "enigmatic", despite science being announced to be "settled" (45), an obvious contradiction. We now have the possibility, finally, to go into a new interpretation, concept or theory about the "geomorphological phenomenon" called peat.

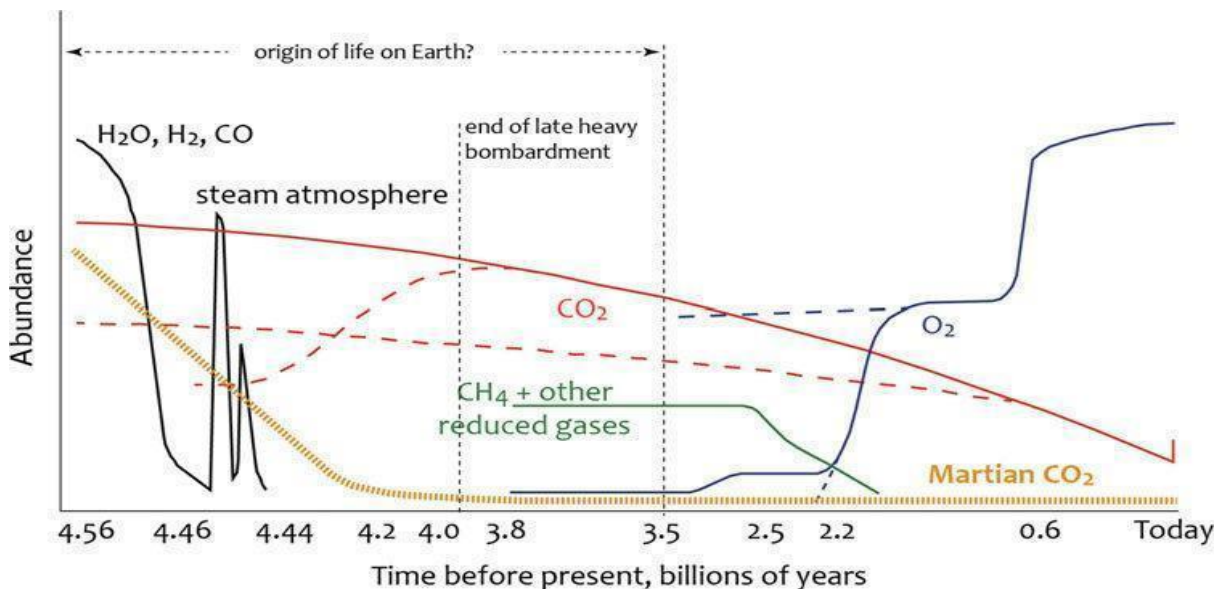


Fig. 1. 2. A simple diagram, which shows how the CO₂ content of Earth's atmosphere declined over time, and it also could give some people headaches. The presented timelines should be taken with a grain of salt. (42)

The overall charging potential of planet Earth also had a big influence on the size of the species. A higher charge potential means a stronger gravitational pull. This indicates that planet Earth seems to grow (43) and the species are getting smaller (44). As demonstrated above, many topics in mainstream science are still "largely unknown", "mysterious" or even "enigmatic", despite science being announced to be "settled" (45), an obvious contradiction. We now have the possibility, finally, to go into a new interpretation, concept or theory about the "geomorphological phenomenon" called peat.

3. Creation and accretion of peat from a new perspective

Let's go back in time, let's say, 17000 years or so. Some parts of Earth were covered by ice and snow, but there were also vast forests and grasslands that covered the surface of the Earth (1). Huge herds of animals fed on the abundant food sources. Some settlements of people were found rather sparsely contributed over the landscape (2). This assumption could be totally wrong. The amount of people, the size and amount of settlements could have been much bigger than anyone ever could imagine! It is mainly based on archeological findings within the paradigm of consensus theory, but it is not a crucial part of this paper to discuss whether there were many sophisticated cultures present or not. We are treating all animals, people and plants equally as biomass, because all biomass on Earth is based on carbon (3). In a study of the inorganic chemistry of peat in the

Okavango delta system in Botswana, is stated about the origin of inorganic matter: Quote "*allochthonous kaolinite (40%) and quartz (20%), and both allochthonous and autochthonous phytolith silica (30%). Several inorganic components (Fe, K, P, Na, Ca and Mg) which make up the remaining 10% are associated with the organic fraction*" (4). It is important to understand what the words allochthonous and autochthonous mean, in order to point out something significant. Autochthonous means that the minerals were found at the same place as they were formed, they were created in-situ. Allochthonous on the other hand, means that they were formed "somewhere else", in other words: They don't know where they came from. The term for something in between is parautochthonous, despite this not being relevant, the author likes to mention it here, for the sake of completeness, and it is a funny word after all (5). Phytolith silica (6) is still an unsolved problem in botany. Plants "somehow" create cell-sized, or even several cells combined-sized, silica deposits, that also have the form of a cell. The reason exactly why or how it happens remains unclear. These parts of plants have CO₂ and other chemical compounds stored within this piece of silica. Because it is silica, it does not decay. As earlier mentioned, we have 30% silica and 20% quartz in peat, at least in this particular case. Quartz and silica are the same material, so why are they mentioned this way? The difference between the two lies in the arrangement of the atoms, silica is amorphous and quartz crystalline (7). The easiest way to explain the difference between the two is to talk quickly about the production of glass (8). Quartz rich sand, or quarried quartz (rock quartz) gets heated up to about 1700 C degrees, the melting point of quartz, by which the crystalline structure disappears and gets clear. Otherwise, you wouldn't be able to watch out of the window due to the refraction of the crystalline structure of quartz. Of course, the process of making glass is much more complex, many other things take place, like taking out impurities and adding chemicals (which is basically just changing the impurities), in order to make the melting point lower. The final properties of glass can also be influenced by the cooling process, either slow or fast. Some glass is also chemically treated in order to get a very hard surface, this process is called "ion-exchange process", which exchanges sodium ions with potassium ions in a salty solution (9). Most glass produced is a mixture of three main ingredients and therefore called soda-lime glass or "waterglass". Commonly the mixture is 75% silica (Rock quartz is used more often than sand), 10% lime (Calcium oxide, CaO) and 15% soda (Na₂CO₃)(10). The fact that peat contains amorphous silica indicates that it must have experienced some kind of extreme heating, at least some 700 C degrees. When searching for sources of heat, common theory refers usually to volcanic activity, geothermal

activity, or heat which occurs deep underground, in order to provide an explanation. Sometimes asteroid impacts are also used as a source of heat, which could be possible (11) on very rare occasions. We know that Earth is a capacitor in space (12). So, we have to take fluctuations in Earth's electric circuitry into account and remember the scalability of them. The amount of energy the universe could provide is immense and hard to imagine. All the different layers of Earth contain energy, the atmosphere with its many layers is no exception. Everybody has experienced lightning. It is an atmospheric discharge event, except it is positive lightning, rising up from the ground, which can be seen as a ground discharging event (13). A lightning bolt has an approximate heat of 50,000 degrees Fahrenheit or 27,760 degrees Celsius (14). This amount of heat would easily evaporate silica and many other materials. Silica changes its state from liquid to gas at 2900 C degrees (15). Until 1414 C degrees it is solid. Polar-lights or aurora borealis/australis (16) produce up to 1400 K (1126.85 C) temperatures (17). It might also be much higher. Earth's magnetic field is weakening, the poles are on the move (18) and we are experiencing already many kinds of changes in weather (19), seismicity (20) and volcanic activity (21), not only on Earth but also on almost every planet in our solar system (22, 23), the sun included (24, 25). With this said, it is clear that the atmosphere can produce heat sufficient enough to melt silica. With more and more recurring "rare" events, such as the "rare pink aurorae" (26), we can only imagine what happens when the aurora actually touches the ground. Some of the indigenous people of Australia associate aurorae with fire, death and destruction (27), their ancestors have survived such an event. One of the best-known ancient stories from the Aborigines, is the story of the rainbow serpent (28), which is very closely related to water. It is said that it connects from water body to water body, and it is the reason why some water holes never dry out, even in extreme drought conditions. In other words: A plasma discharge, either ground to cloud, cloud to ground (positive and negative lightning) or a ground-to-ground arc discharge, from water source to water source. Some remnants of these events are still visible today: water holes (29), kimberlite pipes (30) and mountains (31). This might be the origin of the saying "at the end of the rainbow is a treasure", kimberlite pipes are places where diamonds are found. These kinds of events must have produced unimaginably powerful shock waves and winds of biblical proportions. The shockwave pulverized and heated up all biological creatures on the surface of Earth in the vicinity of the shock. In an instant, some of the material evaporated (gas), some of it burned (ash, coal) and a fair part of it got vitrified. These events happened rather regionally but we need to understand that these electrical discharge events were just a part of the overall weather instability. Some of

these events may have occurred several times with different magnitudes, at the same place due to the geological pre-setting of the ground. We have to remember that these events didn't take place on a sunny day. In other words, the weather was bad. Very bad. Water has been everywhere, clouds, rain and different kinds of water bodies. The process got cooled by the water present in the atmosphere, and like in glass production, where different styles of cooling processes are used, the melted silica went through many stages of heat processing with all kinds of results. The presence of water in the atmosphere might have fluctuated greatly from place to place. Biological life forms contain water all by themselves, which means that water was always present but maybe not in an amount that would have been sufficient for having a cooling effect. Material could have undergone several electromagnetic transmutations and due to the fluctuations of the events themselves, some material could have undergone some changes in its chemical composition, whilst other materials didn't change at all due to their chemical composition and therefore electric circuitry i.e. geometry and charge potential, platonic solids. Things like heat, strength of the induced currents, polarity of the event, AC or DC, hence the magnitude and nature of the event, has had a very great influence on the outcome. Biomass got instantaneously pulverized and vitrified, then carried away by the winds. The vitrified biomass got further pulverized as the already small particles collided constantly in the air. Due to its biological origin, it might be lighter than common stone dust. The grains are also very small, so they might have stayed aloft much longer in the winds of the events. Maybe for months or even years and settled as the last layer. That could be the reason why it is often found as a top layer. Peat is heavier than water, so it will accumulate in places with water, where wind doesn't carry it away, such as the bottoms of the seas. This also means that peat found in certain places might have had its origins somewhere else and could be seen as a meteoritic deposit. The relatively high content of metals in peat (32) is also a very important factor to notice as a factor of electromagnetic separation according to their magnetic properties in different temperatures. The accumulation of peat in certain areas is quite likely linked to surface conductivity-, magnetic features and other things which could have influenced the accumulation of the "peat-cloud". After its first accumulation on the ground, it experienced a secondary accumulation process. Either water carried it away or if it dried up, wind could have carried it again to other places. As we speak now of winds after the event, we can use the word in a "normal" sense. The ionization of the atmosphere has decreased significantly, and electromagnetic properties of the atmosphere on dust don't have the influence as they had in a strongly ionized environment. If peat accumulated in places with water

bodies, it started to accumulate in ponds and lakes. Further accumulation into standing water bodies happened and still happens through drainage mechanisms from precipitation. The process of petrification is called permineralization (33) that can be divided into three subgroups: Carbonate mineralization, silification, and pyritization. As earlier discussed, we have silica in its crystalline and its amorphous state in peat. This is an important point to take into further consideration about the formation of peat, the petrified biomass, because it is an indicator of heat being present at the time of its formation. In the paper "Rapid pyritization in the presence of a sulfur/sulfate-reducing bacterial consortium" (34), published in 2020, the influence of sulfur in petrifying processes was investigated. Also, the possible origin of sulfur was in debate as it is generally assumed that sulfur is produced either by microbes or volcanism. The author explained in part two of this previously published paper how it seems to be likely that some of the sulfur on Earth seems to have come from the heavens (Venus), and that these processes included heat, pressure and electric currents. Things needed to create minerals and metals. Their experiments did not lead to any significant forming of pyrite (35). No heat or electrical currents were used in their experiments. When considering chemical processes, like stated earlier, it is all about valence transfer (36) of the different ingredients, a natural establishing of a charge equilibrium between electron donors and receivers. Increasing the overall environmental charge by inducing electricity, not only speeds up processes, but it might change specific properties of the involved materials, so that the outcome will be very different compared to a "cold" (no induced electricity, no application of heat etc.) experiment. The author thinks that they might have left out something of their experiment, something very important but also very obvious. Heat. Nature provides heat in two ways: Either from below through volcanic activity or from above, let's call it atmospheric activity. There are no hot volcanoes in Finland, nor plate boundaries, but all sorts of minerals and metals which need very high pressure and temperatures for formation, such as diamonds. We are left with atmospheric activity. The scientists who did the experiments probably should have looked up the etymology of their main topic in focus, pyrite. The mineral's name comes from the Greek word "pyr", which means fire. It is said that pyrite got its name because it sparks when hit with iron. The possibility of the origin of the word being only partially true comes from the thought that the creation process of pyrite might have included fire. Simply explained: No fire, no pyrite. The process of pyritization involves sulfur. Pyrite occurrence is linked, according to geologyscience.com (37) to three geological processes: Hydrothermal-, sedimentary- and metamorphic processes. The hydrothermal process is

explained by hot and mineral rich fluids in rocks which eventually form pyrite. The sedimentary process is explained by organic matter releasing sulfur which turns into a sulfide and then combines with iron. The third, and in the case of Finnish pyrite, the most likely pyrite forming process, is metamorphism. Quote from Geologyscience: *“Pyrite can form during metamorphism, which is the process of changes in mineralogical, chemical, and textural characteristics of rocks due to high temperature and pressure. Pyrite can form during regional or contact metamorphism, where existing iron-rich minerals are subjected to heat and pressure, leading to the formation of pyrite.”* The metamorphism changes basically everything of the material, an explanation of what provided the heat and pressure is not given. Peat contains sulfur, mostly in the form of pyrite which usually occurs as very tiny crystals. Quote from “Characteristics of sulfide bearing soil materials in peat extraction areas in N-Finland” published in the Journal of Geochemical Exploration (38): *“These concentration peaks in peat show that substantial amounts of elements are introduced not only by weathering and/or capillary and lateral groundwater flow of the underlying geological material, but also by atmospheric deposition.”* The very last part of this quote is the most interesting, atmospheric deposition. Despite the paper lacking an explanation of what exactly is meant by atmospheric deposition, in the author’s opinion, something like the earlier mentioned “peat cloud” that was created by atmospheric discharge events, would fit perfectly as an explanation of atmospheric deposition. There are still further clues which support the peat cloud theory. It is not only about the layering, but also about the bedrock. Generally, a muddy/silty and sulfur containing layer was found just below the peat layer, often it is referred to as silt. Silt is

considered a glacial deposit (39) which occurs in all kinds of different constituencies, layering patterns and different grain sizes. From very fine-grained powder up to boulders. There is no doubt that glaciers wouldn’t have influence on the ground on which they are and produce their own kind of erosion. Referring to the Mountain Water paper, the author thinks that there is much more to the picture than just gradual abrasion through the glacier’s movement over time. There have been glaciers in Finland, too. They have, according to common theory, carved out all the lakes and rivers, but also left behind a glacial silt. In the aforementioned paper about the sulfides in peat lands in Finland, the researchers’ focus seems to be somehow on one specific type of bedrock: Black Schist (40). Schist rocks are generally considered medium-grade metamorphic rock. The “original” material, also called protolith, contains clays. The topic of clay is under investigation by the author and will be possibly processed in a following paper. Nonetheless, whatever clay turns out to be, we need to assume that clay is strongly related to groundwater. The protolith in the case of schist, was quite likely a very watery environment. This indicates that the term protolith doesn’t really fit the picture. In order to get schist, we need to take a look at the different stages of metamorphism of schist. The basic materials from which we can build up the different stages are clay, silt and other fine-grained materials. Clay seems to be a very important ingredient which is always present, but the constituency of the rest varies greatly. With this being said, we must recognize already, what a wide variety of “end results” through different kinds and different strengths of metamorphological processes we will end up with.

Here is a short list of the metamorphological stages of schist (41):

- shale, protolith
- slate, low-grade metamorphism
- schist, high-grade metamorphism
- gneiss, high-grade metamorphism

We have a very large variety of different kinds of rocks that are classified as schist, slate, shale or gneiss. They can look very different, have different ingredients and properties, but they also share an alignment to a certain direction of the minerals. The alignment increases with the amount of metamorphism, this is not just a random occurrence. The author believes that the same force or process which provided the heat and pressure, has also been involved in the alignment process of minerals. The force in question is electromagnetism, i.e. weather. Again, the author wants to emphasize that the term weather includes not only

“our” weather, tropospheric weather. The term weather includes all layers, from deep below, from the core-plasmoids up to the crust and further out to the magnetosphere. The alignment of the minerals suggests strongly that the mechanism behind those alignments is a strong magnetic field during the creation of the rocks. Only electric currents produce magnetic fields. The minerals align according to their magnetic properties and the prevailing direction of current. Magnetic fields are always perpendicular to the current flow. We must consider mixing weather patterns, which includes of course vortex structures.

The intermixing of atmospheric and ground currents. Black schist is, in the opinion of the author, basically “very badly burnt” schist. A little bit more heat and/or time of induced electricity, and therefore also an increased heating up of the mass would have turned it into graphite. Graphite, besides kimberlite, is investigated by many, not only because graphite is a very good conductor, but also often associated with diamonds. It is not only the diamonds which are associated with the black schist but also many metals, of which some have been “always” of interest, and some gained interest on a larger scale only in recent years. The Outokumpu region in eastern Finland is a very interesting place, as is once more mentioned in the paper ‘Geochemistry of Proterozoic metamorphosed black shales in eastern Finland, with implications for exploration and environmental studies’ (42) Quote: “*The Outokumpu rock assemblage (serpentinite - calc-silicate rock - cherty quartzite - black schist) contains a black schist type not*

known to occur anywhere else in the Proterozoic of Finland: black schist with greenish grey tremolite-rich layers.” There has been quite something going on, once upon a time in Finland, and it was electrical in nature. As a side note on the contradictions and other unclarities in so-called settled science, the author would like to bring forth the quartzite problem (43). There are disagreements on whether quartzite is a metamorphic rock or a sedimentary rock. This seems to indicate that there are also difficulties with the origin and creation of quartzite. That the mineral is very hard but also can contain metal inclusions is familiar to the author, because he found a piece of quartzite (Fig. 3.1.) at a relatively random location, near the Plasma Rocks Site, at the parking place. So, the origin of the piece is impossible to tell, it might be from the Plasma Rocks Site itself, after all, but we don’t know, and it doesn’t really matter because it’s found within the region of the minerals occurrence.



Fig. 3.1. The author spent quite some time trying to get this piece as smooth as his patience allowed it. In other words: This is a very hard stone! The metal inclusion’s surface is lower than the surrounding material, which means the metal is softer than the mineral around it, and got grinded away,

More clues of electricity being the main player in the events, not volcanism nor random meteorite impacts are shown in the figures following (Fig. 3.2., 3.3. 3.4.). In the

aforementioned paper about the black schist there are some very interesting pictures for people with an electric eye, i.e., pattern recognition of electric (discharge) mechanisms.

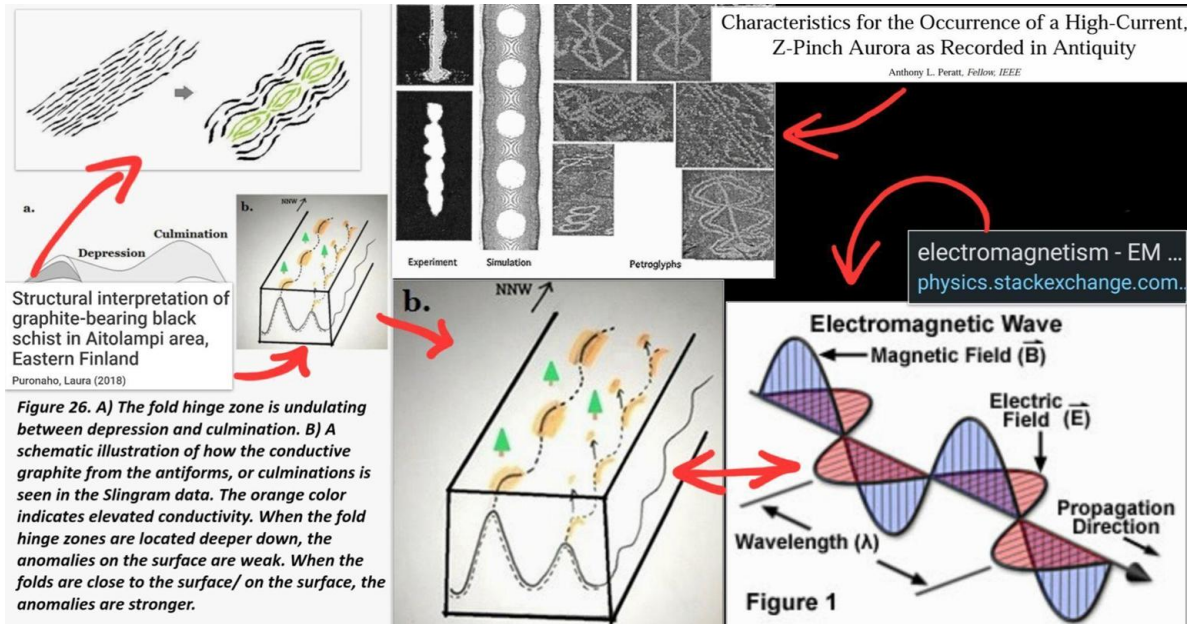


Fig. 3.2. Graphite is a very good conductor and so we could take the correlations between the graphite deposits and a propagating electromagnetic wave not only as proof of electricity being the main force of the creation of these geological features. Super enhanced Geomagnetically induced currents coupled with atmospheric currents seem to be quite likely the cause of these rock formations. There is also a plasma discharge laboratory experiment in the picture, because plasma is an electromagnetic phenomenon and obviously can produce somewhat similar features as are found within the rocks.

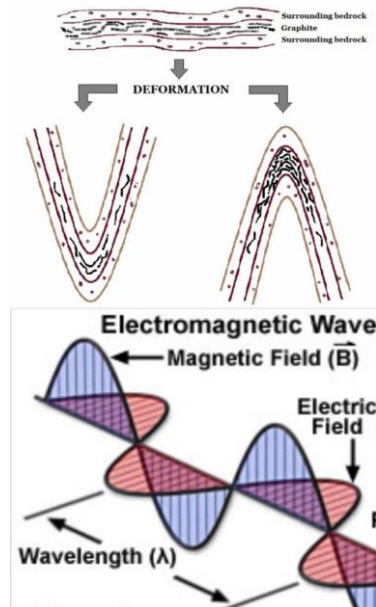




Fig. 3.4. A slice of a rock sample, made by the author, which exhibits a similar pattern as explained in the black schist paper. The most important thing to note is that the pattern is visible on both sides of the stone which means that there was not up or down at the moment of creation of this pebble. Remember: Gravity, on which usually the up or down is based, is only a side effect of the electromagnetic force. Another proof as an explanation these kinds of patterns might be wrong for plate tectonics. (Picture by the author, the piece was also found, cut (circular saw) and polished (by hand) by the author)

In order to emphasize nature's electric way to get things done, the author wants to bring forward a very amazing and intriguing paper about a 3-D modeling of ores in Finland. As explained in Part II of this paper, energy always goes both ways and not everything gets physically pushed but also pulled, either directly by magnetic forces or it gets pulled up by winds, which are expressions of electrical currents whilst spin direction is defined by polarity, i.e., magnetic-vortex spin direction. The earlier discussed kimberlite rocks and their associated kimberlite pipes make yet another appearance in this paper, the topic is very interesting! Kimberlite pipes are poorly understood and generally it is assumed that they are ancient volcanoes which erupt only once. Furthermore, they are often in places with no fault lines or other significant volcanic activities, a very good example for such a place is Finland. Not only do we find kimberlite in Finland, but we also find some other, in a way similar geological occurrence. Most are familiar with Fulgurites (44). They are petrified, lightning strikes, if the lightning strikes a sandy environment they can be easily

excavated. The immense heat fused the materials in the ground together. A somewhat similar process might not only have created the sandstones on Earth, induced electricity fused the silica grains together, but also created the Outokumpu copper hill, another very interesting geological feature of Finland (45). The knowledge about this feature was only possible to accrete in recent times, because without a very high standard of technical know-how and a lot of money, these features of geological formations would have never been discovered. The author would like to express his admiration and respect towards engineers of all kinds, because they are the ones making these kinds of discoveries (Fig. 3.5.) possible in the first place. Thank you! This great technical achievement also reflects the impossibility ancient people would have known about such mineral or metal occurrences. Still, their tales match the creation process of the geological features better than the prominent geological theory. Just think about the "Revontulet", the "Fox-Fires", aka Aurorae. The ancient knew about static electricity and the heat of aurorae, at least.

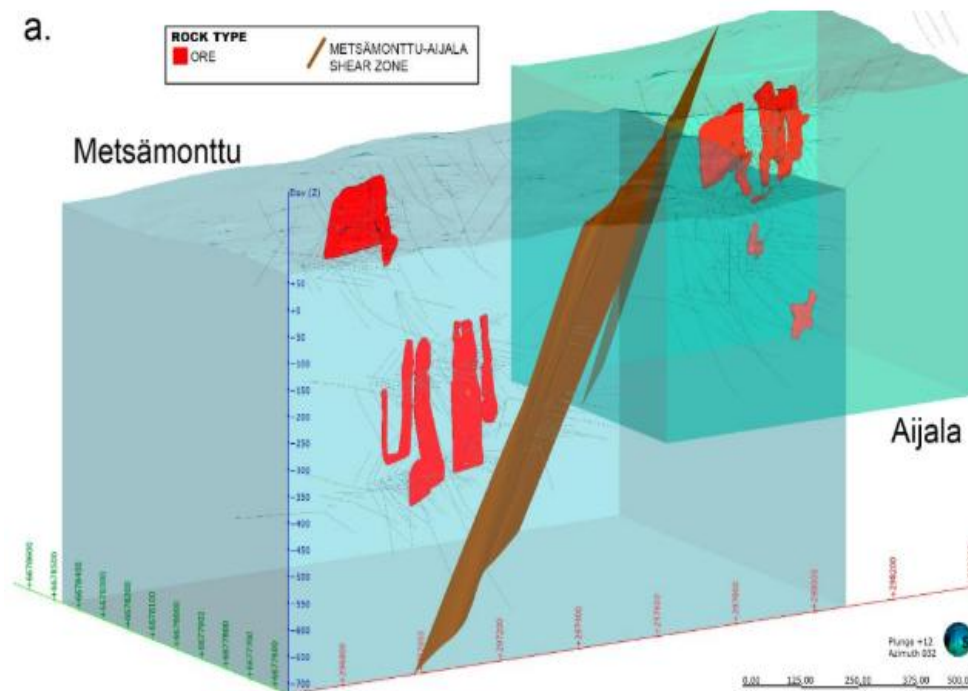


Fig. 3.5. Results of modern day technology are amazing, no question. Being able to see giant fulgurites in the ground is even more amazing! (source: Geological 3D Modelling of Aijala-Metsämonttu Cu-Zn-Au-Ag-Pb deposits, Joonas Sandström, 12/2021, Master's Programme in Geology and Geophysics, University of Helsinki)

There are many other geological features in Finland which are under investigation, not only by the author but also by experts. Many examples of electricity playing a very large role in the creation process of the landscape are being brought forward and compared to conventional geologic theory. Considering rapid petrification as a mechanism in the

creation of peat, the author would like to point out that this has been achieved in a laboratory (46). We must consider that nature is capable of doing such things much faster and on a much larger scale. Also, the possibility of such events having occurred already more than once, cannot be ruled out.

4. Peats active role in the environment and in the end of the last ice age

Peatlands are often wetlands. Water is very abundant on Earth, even more than previously thought (1) and it has specific electrical properties (2). Pure water is a very good insulator (3) but very rare to be found as such in nature, because it is also a “universal solvent” (4) due to its hydrogen bond variability (5). A wetland environment contains a large amount of “impurities”, which can dissolve in water, in other words: the water is charged. We also have to remember that water pouring out of the ground has its own charge, which can immediately change as it comes to the surface and gets in contact with air. For example, calcareous Tufa depositing systems (6) which are found in many places in the world. Very calcium rich water comes out of the ground, and it experiences an immediate change. It releases CO₂ in the air and calcium gets deposited. I think that raised bogs (7) or also called ombrotrophic bogs may have a somewhat similar process which makes them grow, the

emitted gas or element might also be different. Peat has the ability to store or capture an enormous amount of water (8). It is a very porous material which means the actual surface of it is rather great, relatively. When talking about surface interactions of water, we have to take into account the effect it has on the water itself. Water close to surfaces exhibits a charge differential within the water itself; it is much more organized than bulk water. It is the so-called “exclusion-zone”, EZ-water (9). Since water in nature is always charged to some degree, we need to assume that these exclusion zones might be either smaller and weaker as expected, or much bigger, stronger and more influential than previously thought. PhD G. H. Pollack did experiments about the water’s exclusion zones reacting to metal plates, the results were unexpected but also very interesting. It turned out that water establishes connections between different metals and it also transfers charge. Water also charges metals. In one of

the experiments where zinc and platinum were used, zinc is highly reactive whereas platinum is not. Zinc had immediately a strong EZ layer but the platinum, as expected, did not. Zinc made the water also more alkaline. After connecting the two electrically with a wire, the platinum also showed EZ water layer (10, 11). In the paper about peat, from the Journal of physics where heavy metals were studied “Geochemical Distribution of Heavy Metals in Peat Soil

Profile and Estimation of Water Table Patterns in Peatland at Klias Peninsula, Sabah.” (12) are several diagrams shown about the metal content, and it becomes clear that iron is by far the most abundant element. Zinc plays an important role too, but it seems that at least one diagram is strangely manipulated (I am suspicious enough to think that this is not a mistake). The following picture/diagram is from the mentioned paper.

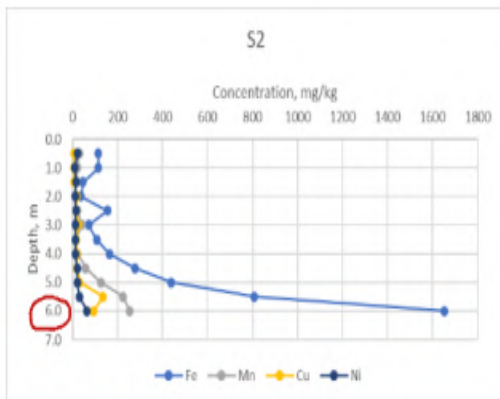


Figure 6a The chemical concentration of Fe, Mn, Cu & Ni in S2 profile, Klias Peninsular, West Coast of Sabah.

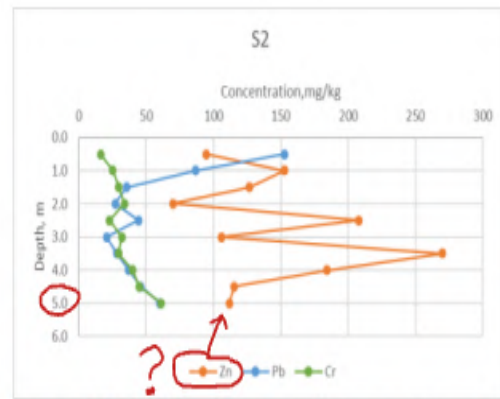


Figure 6b The chemical concentration of Zn, Pb, & Cr in S2 profile, Klias Peninsular, West Coast of Sabah.

Fig. 4.1. Figures from the paper mentioned above. Note how the depth of the samples differs by one meter, from 6 m to 5 m. Also note how the iron concentration spikes upward from 5 to 6 meters. Why are there no measurements from the depth from 5 to 6 meters available from zinc? We can only guess... The author thinks it spikes upwards too. Furthermore, we have to note that the concentration scale is not the same either. The one on the right is six times smaller than the one on the right, so the spike in iron content would be much better visible if they would be similarly scaled. (source: S N M Zamri et al 2022 J. Phys.: Conf. Ser. 2314 012024)

In the author's opinion, water plays a much bigger role in the peat world than previously thought, this conclusion is a straightforward logical assumption, based on a more holistic view of the environment which includes electromagnetism. In peatlands, in its liquid state, it is only present in its unclean form, so it works as conductor. We have a great abundance of metals with their own charges and electromagnetic properties, and quartz, mixed together as very tiny pieces and soaked in a conductive medium, water. Just the fact alone that peat is highly hydrophilic (13), implies that peatlands are charged waters, because soaked water is basically “only surface water”, or, better said, EZ water. This, combined with all the metals included, already makes up a great mix of natural electricity circuits and charge potentials. Some peatlands are in regions with clay (14) occurrences, other peat regions are in limestone/karst (15) regions. Both are alkaline environments, and both are strongly associated with water.

Let's talk first about clay. I think that clay is an intrusive material which originates from the interior of Earth and

should be seen as a volcanic element from mud volcanoes (16). It doesn't need heat to get liquefied (17), it needs water, gases or vibration. In other words: a mudflow made of clay isn't necessarily hot, but the water in it will eventually evaporate and the clay will get harder over time. Often the groundwater level in “clay-lands” is rather high, since it has been once a “very dirty waterflow” by itself. Over time, thousands of years, such as sun cycles and by planetary or asteroidal encounters, coupled with energy surges in Earth's circuitry itself, some of the clay got vitrified (18) by electrical discharge events and turned into rock which is commonly known as schist (19). The abundance and importance of water correlate well between peat and clay. Without it, they couldn't “perform” their nature and therefore their role in nature. This could explain the abundance of peatland in clayish environments, peats are heavier than water but lighter than clay, and where you find clay, you also have water. Of course, some aquifers might dry up because of Earthquakes destroying the connection to the waters below (20), changing weather patterns, or even

excessive use by humans (21), so the layer of clay dries up very deep into the ground. If it dries up, it can form an almost impenetrable barrier for water, as well for water from above as for water from below. The water from below will break through the barrier when the pressure is high enough. If the supply from the waters above is sufficient enough, it will soften the ground gradually until it's all muddy again. Again, no heat needed, only water. Earthquakes will have a great influence on the aspect of liquefaction, too. Clay can get very liquid, very quickly. As some incidents of "quick-clay" landslides in Norway have shown (22). When assuming that volcanic activity at the time of the events, in this case the focus is on "waterbased" volcanic eruptions, such as the aforementioned mud volcanoes or cryptodomes (23), was at much higher levels, anyway. Then we also have to assume that the abundance of surface water and wet ground was also much greater, also without rain.

Karst regions (24) are mostly limestone (25), and are known for the abundance of caves and gorges but also the great amount of wells and good groundwater circulation, an alkaline environment. The formation of karst regions remains a mystery in common theory of geology (26) despite attempts to bring up a new explanation (27), the role of electricity in rock forming processes is not taken into account. Let me bring forth my own, brief and therefore incomplete explanation about the genesis of karst: Limestone consists to a great degree of calcium which has

only one electron more than potassium. I think with an increased electromagnetic potential, different pressure and heat in the environment, potassium gets "charged" i.e. it gains an electron and is thereby transformed into calcium. The chemical does not undergo an oxidation or a reduction process, it undergoes elemental transmutation which also includes a change in its geometry. It is alkaline, which is a very important similarity with the kinds of minerals we find in peat. In a study about the mineral content of peat (28) were listed several minerals which were identified.

In the paper: "Effect of pH on the stability of quartz in a multi-phase system of kaolinite, hydrous Al hydroxide and quartz" (29) is shown how the PH affects chemical reactions. Again, all chemical reactions are electric events and therefore PH has to be seen as the charge and its polarity of the environment. An acidic environment is positively charged whilst an alkaline environment is negatively charged (30). At the end, it all comes down to the amount of positively charged hydrogen ions relative to the amount of negatively charged hydrogen ions, but basically, hydrogen is charged negatively, the hydrogen anion has a net negative charge (31). Hydrogen is the most abundant chemical substance in the universe (32), therefore we have to assume it is so also on Earth. It shouldn't come as a surprise that the mentioned minerals in (Fig. 2) are all alkaline and mainly made from the same "stuff", in different configurations.

Table 1. Loadings of the reference minerals in the PCA for bulk peat (pCp1 to pCp5) and ash (aCp1 to aCp5) samples (their spectra were included in both cases).

Mineral	Bulk Peat					Ash Samples				
	pCp1	pCp2	pCp3	pCp4	pCp5	aCp1	aCp2	aCp3	aCp4	aCp5
quartz	0.30	0.47	0.12	0.79	0.09	0.83	0.15	0.45	0.12	-0.02
microcline	0.26	0.87	0.26	0.31	0.10	0.42	0.27	0.86	0.09	0.02
orthoclase	0.27	0.85	0.27	0.31	0.16	0.42	0.29	0.85	0.15	-0.01
albite	0.29	0.84	0.28	0.28	0.17	0.37	0.32	0.85	0.16	0.04
anorthite	0.32	0.50	0.37	0.17	0.69	0.23	0.45	0.53	0.69	0.02
muscovite	0.38	0.38	0.75	0.27	0.20	0.35	0.81	0.40	0.19	-0.02
biotite	0.33	0.27	0.86	0.19	0.13	0.27	0.90	0.29	0.10	-0.10

Fig. 4.2. Interesting is, that quartz is listed, but silica is not, despite the similarity of the difference being in the amorphous or crystalline structure of the mineral. Much like it makes the difference between microcline and orthoclase. Something must have altered some of the materials with heat. Induced electrical currents can do that easily. (Source: Martínez Cortizas A, López-Merino L, Silva-Sánchez N, Sjöström JK, Kylander ME. Investigating the Mineral Composition of Peat by Combining FTIR-ATR and Multivariate Analysis. *als*. 2021)

- Quartz: SiO_2 silicate, oxygen (33)
- Microcline: KAlSi_3O_8 potassium, aluminum, silicate, oxygen (34)
- Orthoclase: KAlSi_3O_8 potassium, aluminum, silicate, oxygen (35)
- Albite: $\text{NaAlSi}_3\text{O}_8$ sodium, aluminum, silicate, oxygen (36)
- Anorthite: $\text{CaAl}_2\text{Si}_2\text{O}_8$ calcium, aluminum, silicate, oxygen (37)

Ph interaction with silica is an important factor, its variability is a nice example of the dynamic nature of charge exchange (valence), because they can have huge influence on the environment. For example, this statement from a study about engineered nano silica particles for oil recovery, from the King Abdullah University of Saudi Arabia: Quote “*The silica nanoparticles have a high negative charge in alkaline conditions and become slightly positively charged as $pH \leq 4$* ” (38). Another very interesting valence-process which includes silica is so-called “concrete cancer” or ASR (alkali-silica-reaction) (39). Concrete cancer is a process where the alkaline ingredients of cement/concrete start to react with the amorphous silica content if sufficient moisture is available. The result is an expansion in volume. Through the force and magnitude of the expansion it produces cracks and weakens the construction. We have concrete construction, which is the solid and stable part of the interaction, and we have the fluctuating part, the moisture. Moisture is provided by the atmospheric conditions, so it fluctuates a lot, compared to the state of the concrete. The main driver behind this process is in the fluctuating element containing hydrogen in different states of charge, hence, ion exchange. I think the process of ASR also happens in nature, maybe invisible, inside Earth. It could make mountains bulge or create land uplift. Silica collects water which also can be released to the environment, maybe this could happen rather quickly too. The aspect of hygroscopy (40) is yet another important part of the energy circuitry evolving water; it might be something similar to EZ water, but the author isn’t sure about this. Hygroscopy takes place when water molecules get suspended between the molecules of materials. It charges the material and changes therefore also their properties, such as volume, temperature, viscosity and other properties. Zeolites (41, 42) are also something to take into account. They are “water-trapping” solids made of silica, aluminum, oxygen and alkaline Earth compounds such as magnesium, potassium, sodium, plus the water molecules trapped in them. They can be produced for industrial use in order to process oil into gasoline, for example. Not only can they be re-used due to their self-cleaning properties, but they are also very heat resistant. We must assume that something similar exists in nature and possibly plays an important role in natural environments. It might be one of the reasons why peat can hold so much water.

The “peat-cloud” settled in places with water, and opposite polarity relative to the peat-cloud. As described, calcareous rock and clays are alkaline, but peats are acidic, so they may have had a natural magnetic attraction towards each other. Another reason why peats accumulated in certain areas more than in others might be the geological imprints in Earth’s crust. Meaning, those areas with a positive charge

create naturally counterclockwise vortices (northern hemisphere), which in terms of weather means a high-pressure weather system, i.e. not much wind. The material ionized by the shockwave, traveled through the atmosphere as an ionized cloud and pulled in iron from the environment when it was in liquid state. The environment might have been enriched with iron, such as Mars’ encounters with Earth. Maybe the deposition process was similar to an industrial process called: Plasma-enhanced chemical vapor deposition (PECVD) (43). Peat contains quite a lot of iron, which is usually present in an oxidized form. The importance of iron has also been recognized in several studies about peats (44), and it is also seen as a source of iron for the lifeforms of the seas. What I find very interesting is the fact that peat contains Fe (III), iron in its 3rd oxidation state. It is the only form of iron, which is useful for organisms, from algae to humans. We should recognize this as something very important, it might be as important for Earth as it is for us. Earth is a huge organism, too. A further source of iron, besides the initial aggregation through electromagnetism and ionization, could be groundwater sources with great iron content. It might have been transformed from its “original” state, when coming out of the ground Fe (II), into Fe (III). A somewhat similar process as we see in growing tufa ditches. There are many examples of how limestone and iron “go well together”. Here are two, both from Switzerland: The “iron-well” or “place of power” Grimmiwasser (45) in the canton of Bern, near St. Stephan, and the oolitic iron (spherulites) ore occurrence in the Jurapark in canton Aargau (46, 47). Not only the accumulation of the ore in layers of limestone, but also its creation happened quite likely through electrical discharge events and included a lot of water. The spherical iron deposits looked like someone was welding with an arc-welding machine, it sputtered, the iron sparks fell into water, where they preserved their spherical shapes. It should not come as a surprise that in the Jurapark there are also peatlands present. Not big ones, but there are a few. The magnetic properties of iron (48) change from ferromagnetic to paramagnetic at the curie-point which is 770 C degrees, which is about the same temperature which is used in glass production. Not only was electromagnetism involved in the creation and accretion of peats, but it also plays an active role in the electromagnetic environment today. Peatlands are storages for water, and they also can store thermal energy, such as heat and cold. Usually, the release of the stored energy happens through water vapor and CO₂. Which is, once again, essential for plant growth. CO₂ is a greenhouse gas which gets pumped into greenhouses for a better yield (49). And speaking of plant food, light might play a very important role in some of the chemical reactions happening in peat lands. Light has many different wavelengths and intensities, so we have to think also about

the influence of sunlight on peatlands. It is well known that Siberia has very vast peatlands, and it is very cold in the winter and very hot in the summer. The author thinks that the Siberian traps with their high metal content have an influence on the regional weather. Positive ground charges seem to attract high pressure systems and are therefore “responsible” for the clear skies. Sunlight might charge up peatlands, elemental transmutation takes place at a more rapid pace which might also explain the bigger CO2 emissions. Some radiation coming from the Sun or even further away penetrates quite deep into the surface, and as earlier shown, some materials like zinc are more abundant in deeper layers of peat that could experience charging. An example of how light with a specific wavelength can trigger a chemical reaction, is an experiment made by Chris Cramer which has the name “Hydrogen Chloride Cannon” (50). The first thing which came to the author's mind when he saw this Hydrogen Chloride Cannon, were the mysterious craters in Siberia (51). The region where those craters form is within the auroral oval. The author thinks it is possible that strong atmospheric disturbances can create such strong magnetic fields that daylight, not only auroral light emissions, could be funneled or pinched into certain wavelengths, in such a way that it could trigger an ignition. Solar activity and fluctuations in Earth's weakening magnetic field only enhance such possible mechanisms. A sudden peak in telluric current intensity and a brief establishment of a strong connection between the ground and heavens, is probably the best way to find out what is behind the mystery of these craters. A big problem investigating the relationship between solar activity and crater formation is that those structures are in very remote areas, no one really knows when the explosion happened. If we had an eye witness report or some

satellite observations about the exact time of such an explosion, we possibly could make a significant step forward in order to prove or disprove the theory of the author. It also needs more investigations into the atmospheric processes the author tried to express. Visual pattern recognition is an important part of science, which also the University of eastern Finland practices while making research about peat (52). The focus in the research is more or less focused on the amount of water and plant growth. When watching peatlands from an electric point of view it is easy to recognize them as a charged fluid interacting with its environment. If we take geological formations, their composition, hence the charge potential of them as a “stable factor”, into account, we also should expect some visible electromagnetic separation taking place. Different parts of rock formations have different charges and when they are connected, a current will flow between them. In calm conditions like we have experienced in modern times, the current is rather weak, but I think it is sufficient to produce patterns. Like in the above-mentioned article, where the focus of the patterns is on the moss growth, it is the easiest way to see them. Different mosses prefer different kinds of nutrients, and I think they are separated by electric currents and their magnetic fields within the wetland, so the mosses grow where they find nutrition. The following picture shows exactly this (Fig. 4.3.). The water level plays a big role too, not only because of the volume but also because it could change the connections between the bedrocks and therefore change the visible pattern.



Fig. 4.3. A comparison between peatland from Finland and a laboratory experiment including electricity and iron dust. Similar patterns are visible. It seems that in some peatlands the floating particles are forming daisy chains (53). The youtube channel from Billy Yelverton has many very interesting electric discharge experiment videos (54).

Wetlands are often craterous regions (**Fig 4.4**) associated with limestone (**Fig. 4.5**). Common theory has only meteorite impacts as an explanation for craters. There is quite much evidence that electrical discharges might be a

way better explanation for most of the craters found on Earth and elsewhere in the universe. The following pictures are examples of this.

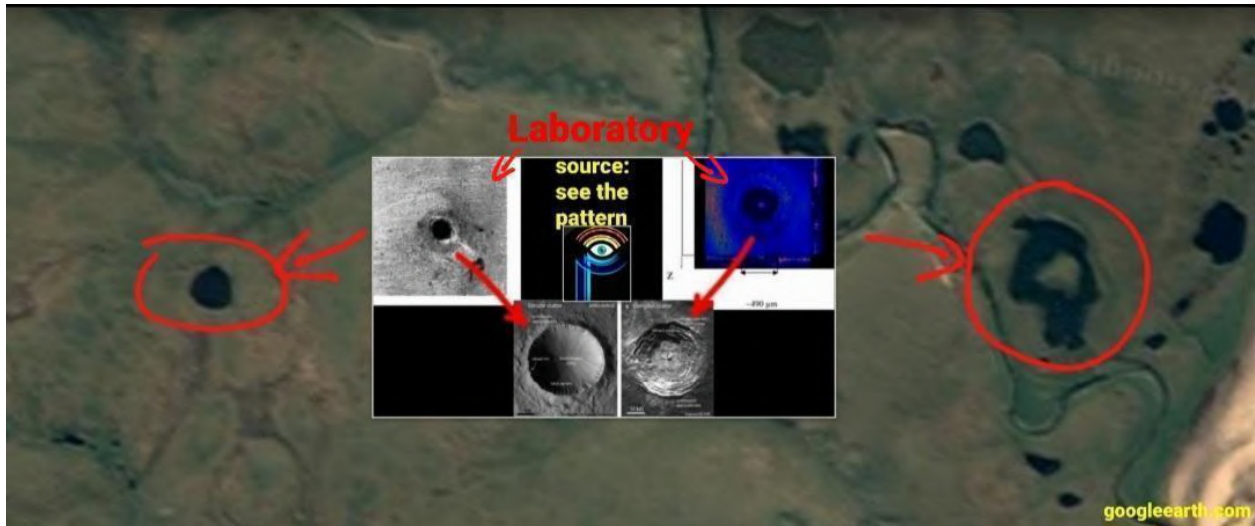


Fig. 4.4. A Comparison of craters made in a laboratory and similar craters in peatlands somewhere in Russia. Note that the satellite picture is one picture which means those craters are neighbors. The youtube channel “See the pattern” made a very nice video about craters from electric discharges (55).



Fig. 4.5. This image shows peat in a craterous region somewhere in Russia. It is easy to see that the ground beneath the peat layer is white. (picture credit: GoogleEarth.com)

Our modern society is very reliant on electricity, the invention of batteries was a further step into the age of mobility, and portable electricity was something that made many new things possible. The modern alkaline battery was invented in 1950 by the Canadian engineer Lewis Urry (56).

An alkaline battery produces electricity by a chemical reaction between potassium, zinc and manganese (57). Other versions with different materials are also available. We have the same “ingredients” in batteries as we have in many peatlands. So, we also have to expect similar reactions

happening in peatlands. The analogy between alkaline batteries and peatlands underlines probably in the best way that they are a crucial part of Earth's electrical circuitry. The drainage of peat lands has possibly a much greater influence on weather, flow of telluric currents and the general circuitry of Earth, than is anticipated. Lack of water reduces counterclockwise spin, which would keep the moisture conductivity significantly. Local weather patterns will be coming in, through rain or creating the foggy environment, influenced greatly in a short amount of time when a peat land could switch into a clockwise spin which creates a high is dried out. The author thinks the main reason is that the pressure system and therefore dries out the area even more.

5. Cultural rituals and Mythological stories revolving around peat

Modern western society has certain annual festivals, some are tied to Christian beliefs, but some are of pagan origin. Whatever the case may be, they all share one thing: They are heavily monetized. Their original meaning or purpose got lost a long time ago. The story got re-invented and changed to fit certain religious paradigms. This also functions for wiping out ancient knowledge for common people. A further tool to achieve a similar result is education. Uniformitarianism has its origins in England. It is the cradle of settled science on which mainstream "science" is based upon. Oxfordian science is very tightly connected to Christian beliefs. The origin of the peer-review process also originates, at least partially, in England. It was invented to make sure the results of scientific discoveries don't give any possibility to question Christianity, the King, Queen or whatever other authority. Still, as kids we are awaiting Christmas time, in spring we celebrate Easter and occasionally other "days off school" because the Church. The author hasn't been raised in any specific religious frame, and only due to certain rules of authorities, time in churches

was spent. It always felt strange to participate in these rituals because they didn't seem to be from "this world." Stories got told, rules explained, and ritualistic procedures were performed. Over time, the author learned that there are also other religions. Later, it turned out that they have fought with each other, basically since the day they were founded until today, despite promoting that peace is the ultimate thing to achieve. For the author, the amount of contradictions, "outer worldly stories" and the rigorous defense system of each religion towards "the others", always posed a very big problem. It simply didn't make any sense. Discovering the Electric Universe, with all the people and their works which were leading up to the point where it is now, opened a whole new way of looking at things. It is such a unifying theory that it seems too much, for too many. There seems to be a deep-rooted fear to let go of old beliefs, and embrace new ones. Almost no amount of contradictions are enough to let go. Many rather believe in something that was taught in school as an absolute truth, rather than in something which is understood, proven and thought about.



Fig. 5.1. Everybody knows that a Halloween pumpkin should look scary, and that it should glow in the dark. But why? Yet another example of how modern society seems to have lost at least part of its memory.

Let's take Halloween as an example of an ancient cult embraced by capitalism, and maybe even kept alive by it. Many people don't really know what Halloween is about (1). They know that at that time of the year, scary faces are carved into pumpkins (Fig. 5.1.), and that there should be a candle burning in the pumpkin, in order to make it visible in the dark. The only time of the year when you can see witches. But why? A scary pumpkin glowing in the dark? Witches? Most people never took the time to actually think about things like this. Too many don't even want to know, and they will have an excuse for it, which, after all, could quite likely be rooted in fear. They lack the ability to be honest to themselves, and admitting that they were wrong, and/or the new knowledge would partially destroy their world view. It is important to understand that the "old knowledge" doesn't go away. It will remain, and it can be processed in new and different ways. Once you start to see, you can't unsee it anymore, because the forms and patterns, visual or literal, are omnipresent. As explained in part II, light phenomena in nature might have been much more common in ancient days, and very often they seem to be related to plasma. 50% of swamps in Finland are drained. This number could be much bigger in other countries. Considering water as a universal conductor and therefore as something very important for the energy to flow, we will have a chance to try to understand

the importance of wetlands for the electrical environment. They are batteries, they provide energy for processes which include Earth and Heaven. Taking the water away will break the battery. Wetlands, peatlands, bogs and such, are considered mythical places, often misty, and going there can be dangerous. The ground might look stable, but it isn't, and the possibility of drowning in an unknown wetland is a real danger. In the past, several hundred years ago, wetlands were probably much more abundant than they are nowadays. This could mean that the overall charge in the environment was much bigger than it is today. Huge areas of wetlands were doing their thing, they created such an environment of charge that they had their own micro-climate. The net-negative charge, possibly due to acidity, created water vapor in the area, and winds carried the vapor into regions with less water. Wetlands are not only important themselves, but also for the surrounding areas. In other words, a dried-up wetland will affect all the ecosystems surrounding it. When we think about the wetlands of the past and the huge amount of water they bore, we probably also understand that the energy confined to and produced by such areas was by far bigger than it is nowadays. This is a very important point to recognize because the author thinks that the jack-o'-lantern (the pumpkin) is a representation of plasma phenomena. They occurred in peatlands probably much more often than

they do nowadays. It might be something similar to St. Elmo's fire (2) which was described by sailors. Their appearance must have been a rather frightening experience for the onlookers, especially when the lights emitted some sound. It is not known to the author if there has been any relation to solar activity, but it would only make sense. GIC's traveling through the crust, of which peatlands are a part of, could have charged the environment even more than usual. At a certain height above the ground, an atmospheric charge differential got naturally established, geological features including metals or other conductive materials, and gas emissions from the moor, created a brief accumulation of charge in the air. So much so, that it started to glow. We can call them plasmoids. There might be a very wide variety of plasmoids. Some of them probably "burn cool". Plasma has different stages, and we might look at a phenomenon which goes into the realm of "glow-mode". The position of those ominous lights in peatlands might in certain cases be almost the same. The author thinks that it has something to do with the geological setting like the bedrock itself, which as earlier explained, seems to form daisy-chains reminiscent patterns. Other factors, like temperature differences, amount of sunlight, moisture content of the atmosphere and the ground etc., will have effects on the occurrence of lights. They might move around, hover up and down and change size, shape and color, too. Something like a discharge upwards, as described in part II (the streamers in Fig. 21) could probably also be expected. We also need to recognize that, depending on the atmospheric conditions, hence; gas

mixture, it might not need very much of a current in order to get something ignited. In this case (Fig. 5.2.), we are looking more at something burning instead of glowing. The paper "Minimum Values of Voltage, Current, or Power for the Ignition of Fire" (Vytenis Babrauskas)(3) states (Quote): "No electrical ignition will occur under conditions of zero voltage, current, power, or energy. Conversely, ignitions can occur when substantial amounts of voltage, current, power, or energy are available. This leads one to consider that there may be some lower limits for ignition to be possible. This is consistent with the general observation that for ignition to occur of substances which are not self-heating or exothermically reacting, some finite amount of external energy must be provided." There is no reason why the environment, which needs to be understood on all scales and as a whole, like the Earth-sun-galaxy and beyond for example, and not just locally (Earth or even just a specific area), couldn't provide unprecedented amounts of energy. Considering this thought, we should expect these kinds of phenomena to ignite fires. But since they were presumably happening in wetlands, we could imagine that fires didn't spread very far, maybe just one burning bush. Nowadays, as we have so many dried out wetlands, and the water level seems generally lower than back in the days, the possibility of underground fires, ignited by induced currents, which are very hard to extinguish, is much higher. Also, common lightning strikes can ignite places which were formerly wetlands, much easier.

Figure 1. The effect of fuel/air mixture on the MIE for alkane-series hydrocarbons [6,10].

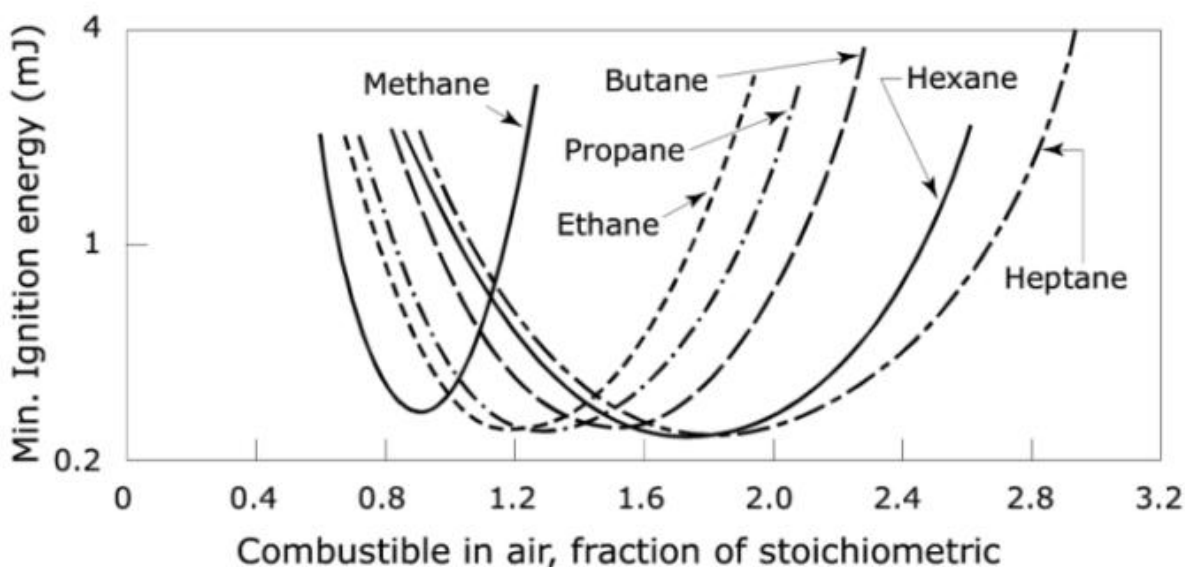


Fig. 5.2. As this graph shows, the amount of energy to ignite certain gases doesn't need much energy. The energy to make something glow, might be even less. Source: "Minimum Values of Voltage, Current, or Power for the Ignition of Fire" (Vytenis Babrauskas)

Considering also energy peaks in telluric currents, which could also be understood as underground lightning, the possibility of fires breaking out many meters below the surface shouldn't come as a surprise. It is, after all, a similar mechanism which could have melted the ice and snow at the end of the last ice age. Induced energy travels underground and heats up the ground. Considering that in many places there was a lot of water, rarely things ignited, nor could the fire spread very far. Nonetheless, we have a charged environment and strongly fluctuating telluric currents which easily can make stuff light up, in different ways. The fact alone that there are several ways to have something glowing in the dark, is a rather strong argument for an electrical explanation of the Jack-o'-Lantern phenomenon.

Let's still go quickly to something considered very Finnish, the Kalevala. In the first part of this paper (4), the author quoted a part of the Kalevala (Fig. 5.3.). A few

sentences described the theory of the formation of peat already then. That the aurorae might have played an important role in the events, is a conclusion made by the author rather recently. It is not known to the author, in scientific terms or by experiments, what actually would happen if the aurora touched the ground. We can assume that the hot material (if the heat is maintained all the way down to the surface) would trigger some rather fast reactions in materials present on, or in the ground. Things like water could experience rapid expansion, much like a phreatic volcanic eruption, that could produce massive shockwaves. The emitted noise of such an event should be taken into consideration, too (5). Acoustic shock waves also carry current (6). The abundance of water on Earth must be taken into the thinking of shock waves propagating through the environment.

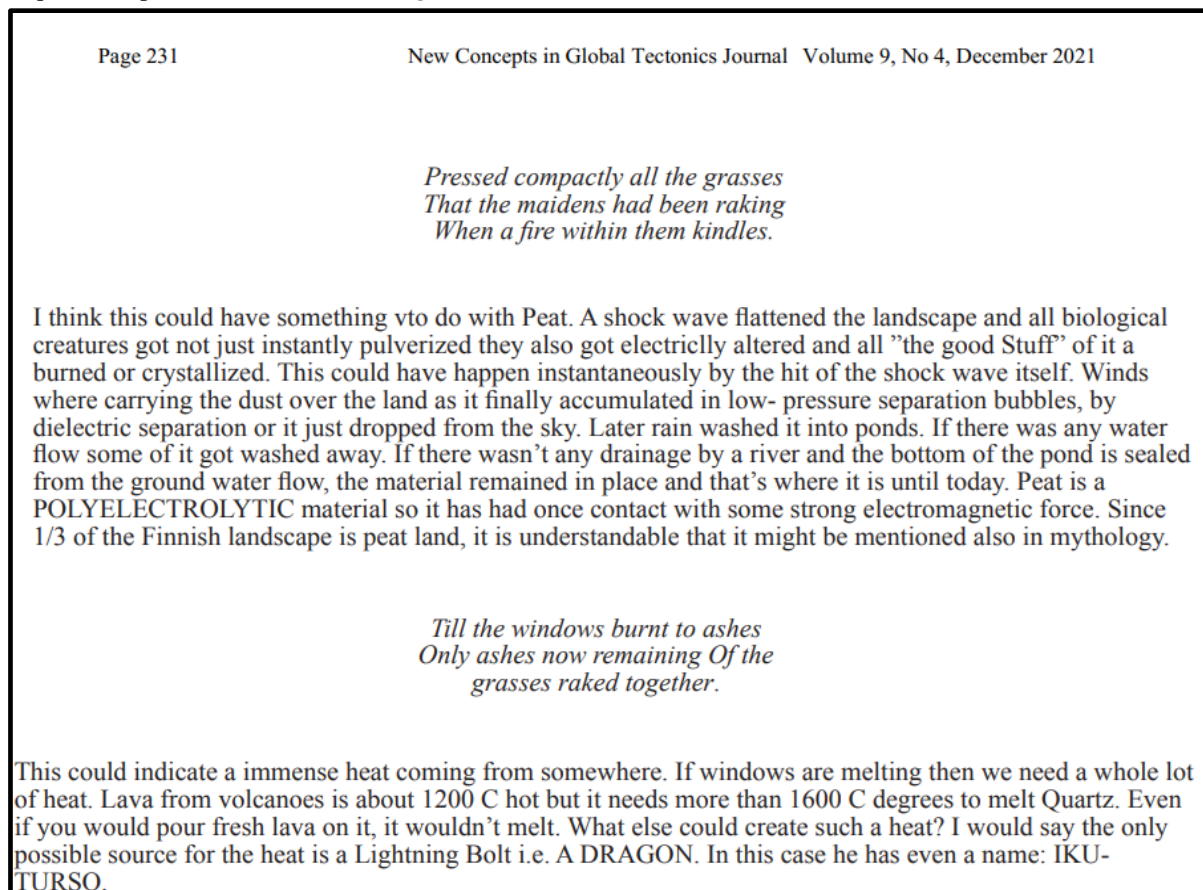


Fig. 5.3. A screen grab from Part 1 of this paper. The theory remains more or less the same. We might have to add the aspect of aurorae playing a role in the process. Adding something to an existing theory only makes it stronger.

It is not only Finnish mythology that has something like sea monsters or dragons living in the water or rising from the ocean. One example is the mythological tale from the Ojibwa (Ojibwe, Sauteaux, Chippewa) Indians from the Ontario region (7, 8). The correlations between the

mythological tales don't end with having a sea monster, usually with horns, but also copper plays an important role in those stories. We should take these stories from our ancestors much more seriously than the consensus scientific view suggests. Ancient people were serious about what they

were telling, and as a fact they spoke the truth, we only have to look at the large sulfide and copper ore deposits in Finland, and in the Ontario region (9)(Fig. 5.4.). There is no doubt that the ancients didn't invent these stories, they described what they witnessed. When reading these ancient stories, one might understand that these events were

extraordinary, and many people lost their lives. What remains for us from these times are not only the stories, but also the materials in Earth's crust. Often the ore deposits are literally the top layer, which only undermines their proposed origination from above, described in Part II.

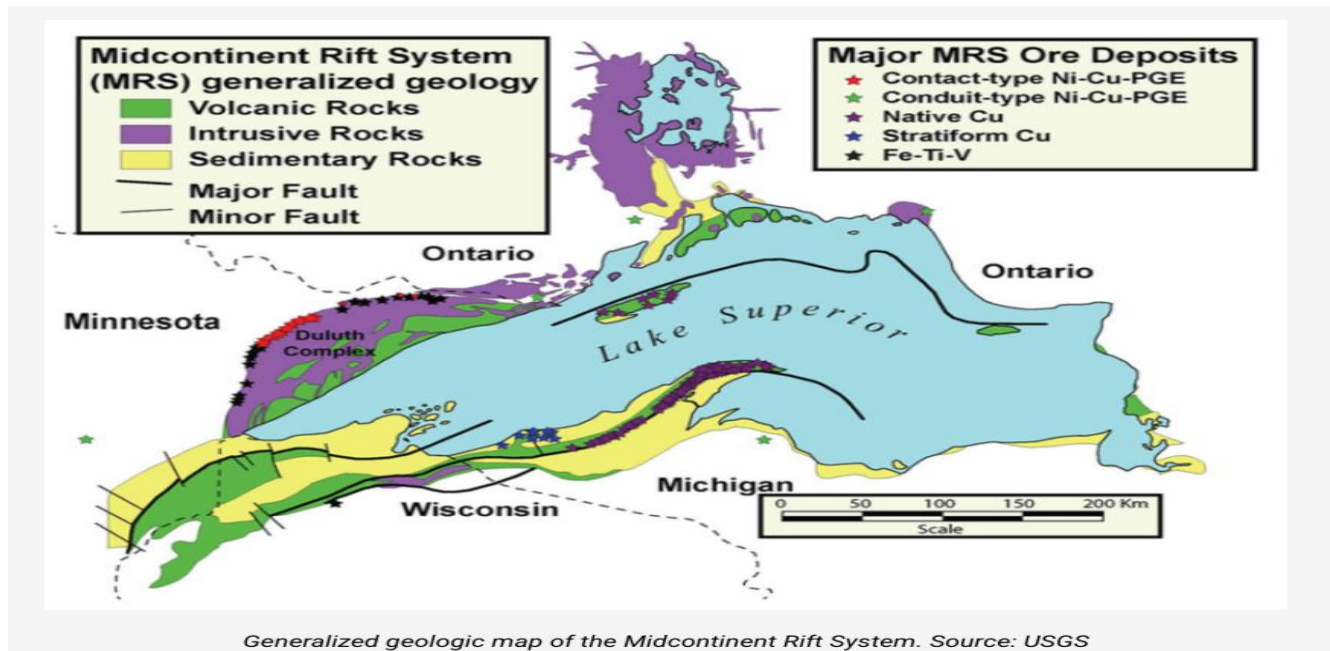


Fig. 5.4. A map of ore deposits in the Ontario region, taken from a scientific paper published in 2021 “Prospectivity modelling of Canadian magmatic Ni (±Cu ± Co ± PGE) sulfide mineral systems” showing banded structures of ore occurrences.

As another example of possible proof that the aurorae once touched the ground, the author wants to show a collage (Fig. 5.5.) of aurorae and metallogenic occurrences in Finland. It is easy to see the band structures of the aurorae. What may not be so easy to identify are the vortices. People who have never seen aurora with their own eyes probably don't know how fast these beautiful structures in the sky can

move. Even more fascinating is the fact that the vortex-like structures of auroral sub-storms are actual vortices and apparently do always spin in a counterclockwise direction (10). Because a geomagnetic substorm is caused by Earth's own magnetotail, we might think of it as an energy release of Earth's electrical circuitry, and therefore a counterclockwise spin direction is logic.

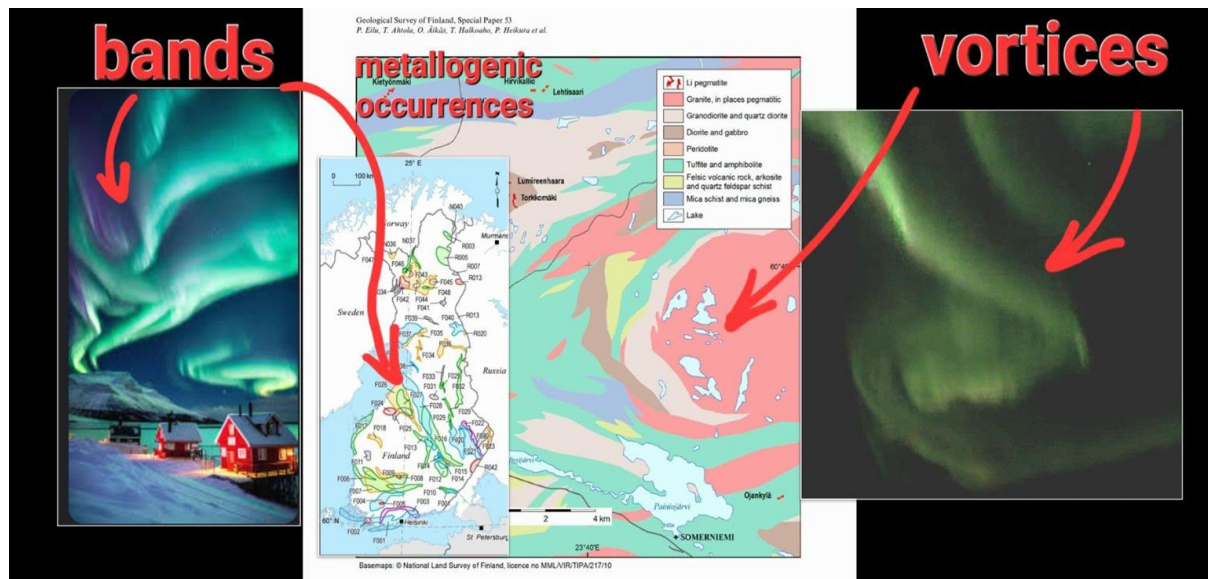


Fig. 5.5. A self-made collage of metallogenic occurrences in Finland and auroral displays. The visual similarities between the two are striking, especially when volcanoes or plate tectonic boundaries are totally absent. (Picture credits from left to right: auroracourses.eu, gtk.fi, mbl.is)

The Finnish saying “aurinko porottaa”, “the sun is reindeering” seems to refer to something getting burned. This conclusion is derived from several clues. First, an explanation of the saying itself. Especially in springtime or early summer, the “sun reindeers” more often, that basically just means that you hear the saying more often. This is due to lower ozone levels in the atmosphere which lets more UV radiation through and our skin needing to adapt to higher UV levels after winter (11). That has the effect that the radiation feels like it burns your skin, it actually does, and the consequence can be severe, like the emergence of skin cancer. In order to make sure if the sun is reindeering or not, you only need to go into a shadow. If the burning stops immediately, you know it is solar radiation and not the air temperature that makes you feel hot. What electromagnetic radiation can do to things like pebbles is easily visible in the author’s microwave experiments. As a second example of why the author thinks the saying is related to something burnt, is the existence of another saying that includes reindeer. “Palaa poroksi” meaning: “Burning into reindeers”. It is rather hard to translate this more accurately due to the differences between the English and Finnish language. Maybe it could be translated or explained also by something like: Through the process of burning the material turns into a reindeer. Admittedly, this sounds very strange. A third everyday saying including reindeers is that used coffee in the filter (or pan) is called “kahvin porot”, the coffee’s reindeers.

The author has been pondering about these sayings, their origin and the association with fire for more than 15 years. Without the discovery of the Electric

Universe/Thunderbolts Project (12, 13), the author would still wander in the dark. So many doors would have been unopened, and realizations never could have occurred. Equipped with more knowledge and understanding, acquired also through self-made experiments, the author proposes a possible explanation for these sayings. They belong together, not only because they all include reindeers but also a certain association to fire. Whilst in the Finnish speaking part of Finland aurorae are called “revontulet”, the fox fires; in northern Finland, where people speak Sami, the aurorae are associated also with reindeers.

“Many of the indigenous Sami people of Lapland are semi-nomadic reindeer herders. One of their traditional stories describes a glowing, golden-horned reindeer, who, if caught by a hunter, will cause chaos to engulf the world.” Quote from East of the Sun and West of the Moon: The Folklore of Arctic Animals (14).

From a PEMC (Plasma-electromagnetic Cosmology) (15) point of view, this could be interpreted as a plasma event, either happening rather far away (between Mars and Venus) or rather close (between Venus and Earth). Or, much more laterally thought: The catching of the golden horned reindeer means ground-touching aurorae. Ground-touching aurorae might be very hot, and depending on the area where they touch the ground, even a shockwave might be generated. Heat, as earlier explained, can be “produced” with invisible radiation from a distant source, in this case the sun. It is a form of electromagnetic radiation, after all. The reason or source for the aurorae, which are charged particles, don’t necessarily need to come from the sun. Basically, whatever planetary or cometary body, or its tail of dust, will do it. The

author would like to refer, once again, to the theory of “auroral precipitation”, the copper, the sulfur and their possible connection to the planet Venus. Probably the authors You Tube Playlist “Finnish Copper” is the only source available (16). At this point we need to talk a little bit about the polar configuration by David Talbott (17). In a nutshell: Only a few thousand years ago, our solar system was very different. At one time, the configuration was such that the planets Earth, Venus, Mars, Saturn and Jupiter were aligned in one line by their poles. A cosmic daisy chain. From this alignment, and its configuration into our modern solar system emerged all the archetypes of mythology and religions, because people from all over the world saw the events. The visual perspective on the events in the sky varied due to the different geographic location of the onlookers. Similar petroglyphs are found all over the world, and often they depict similar forms and shapes. As shown in Part I of this paper, where the focus rested for a while on the owl pattern. We see the same pattern repeated here again. This is

a strong indicator that this is not a coincidence. In figure Nr. 10 (Fig. 5.6.), on the upper left side, we have two pictures with a similar “core-pattern”, quote: “the graphical solution of the chandraskhar-fermi equations”. The author proposes that the “reindeer” emerging out of the “chandraskhar-fermi equation pattern” could be an electrical discharge, a lightning bolt, coming out of the plasma instability. Or explained in another way, something modern people might have actually seen: Imagine a volcanic ash cloud, that would be a plasma instability. Then, imagine lightning strikes emerging out of the volcanic ash plume, that would be the reindeer, or the golden horns of it. These kinds of lightning bolts could have happened repeatedly and on a much bigger scale, also the duration of such a lightning bolt could have been significantly longer than what we are experiencing today. Certain places could have been hit much more often than others, due to geological properties of the ground, such as metal ore occurrences. These might be places where you can find diamonds nowadays.

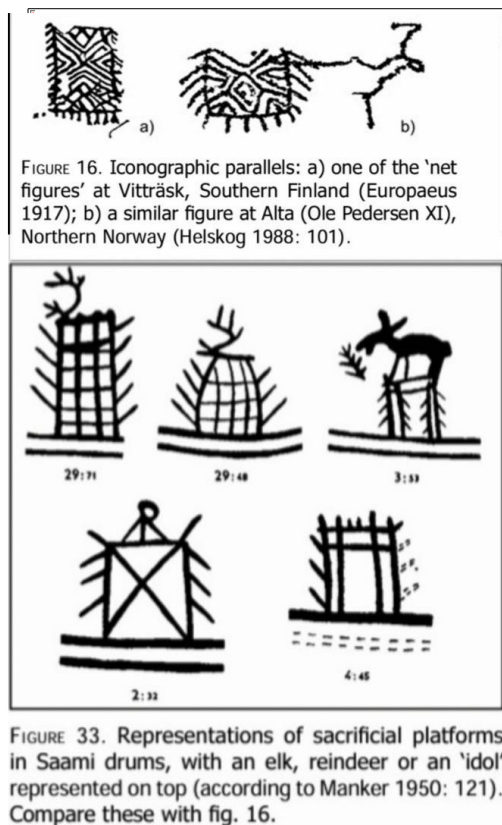


FIGURE 16. Iconographic parallels: a) one of the 'net figures' at Vitträsk, Southern Finland (Europaeus 1917); b) a similar figure at Alta (Ole Pedersen XI), Northern Norway (Helskog 1988: 101).

FIGURE 33. Representations of sacrificial platforms in Saami drums, with an elk, reindeer or an 'idol' represented on top (according to Manker 1950: 121). Compare these with fig. 16.

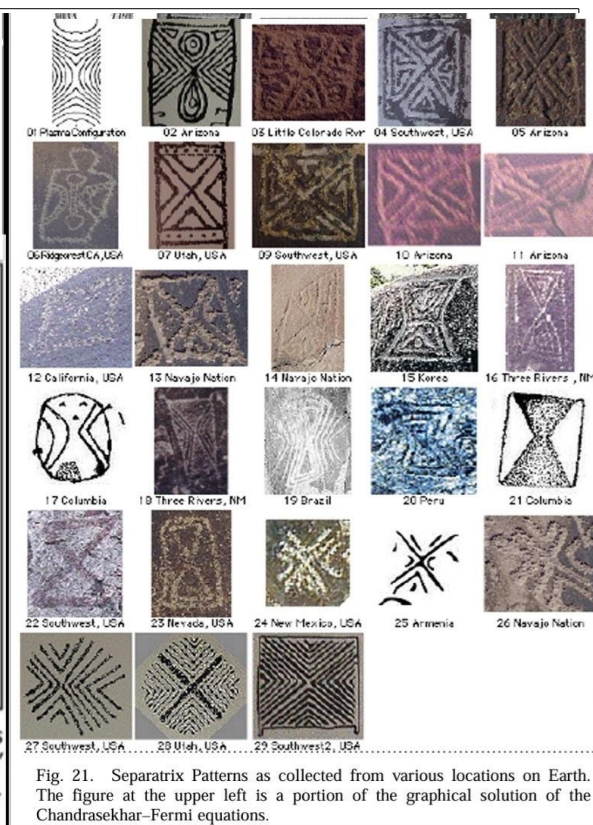


Fig. 21. Separatrix Patterns as collected from various locations on Earth. The figure at the upper left is a portion of the graphical solution of the Chandrasekhar-Fermi equations.

Fig. 5.6. A comparison between petroglyphs and their interpretations. Interpreting the reindeer/caribou glyph as a lightning bolt is probably rather new. Picture credits: Left, Lahelma (18). Right, Peratt (19)

The new interpretation of these glyphs as lightning strike-like discharge events would explain the reason for why the reindeer is associated with things burnt. The author has no doubt that some of the reindeer/caribou/elk petroglyphs are actual representations of reindeers/caribou's and elks. But some of the glyphs seem to be something

completely different. Plasma discharges emit occasionally very strong radiation, such as synchrotron radiation (20) which can be very harmful for biological life forms. In other words, you don't need to be at the epicenter of such an event to get hurt. This is why the author thinks how and why the reindeer is linked to something burnt.

6. Conclusions

Peat is instantly vitrified and pulverized biological mass that got churned up into even finer dust in very strong winds. The winds carried the material to other places and due to its small particle size, stayed a loft longer, therefore settled the last and therefore became the top layer. The main driver behind this process, which occurred in a short time, is electromagnetism. Whether it was a CME from our Sun, or interactions with other planets, the basic principles of the

formation of peat stay the same. Together with its water, peatlands seem to be like a "real", Sun charged, natural battery, and therefore the role in the environment could be much more important than previously thought. Wetlands are very active regions that could exhibit much stronger activities with stronger geomagnetically currents than previously assumed. With Earth's weakening magnetic field, we might also need to expect increased activity in and around wetlands. The author continues his investigations on this topic.

Stefan Ahmala

This paper is dedicated to my parents.

They have left their physicality and are now part of all the circuits.

7. References

2. Comparison of different theories about peat, and other contradictions in science

1. <https://www.fao.org/publications/en> (no author listed)
2. <https://www.fao.org/4/x5872e/x5872e05.htm>
3. <https://en.wikipedia.org/wiki/Peat>
4. Keddy, P.A. 2010. Wetland Ecology: Principles and Conservation (2nd edition). Cambridge University Press, UK. Cambridge. 497 p. Chapter 7.
5. Vitt, D.H., L.A. Halsey and B.J. Nicholson. 2005. The Mackenzie River basin. pp. 166–202 in L.H. Fraser and P.A. Keddy (eds.). The World's Largest Wetlands: Ecology and Conservation. Cambridge University Press, Cambridge. 488 p.
6. The 6000 Year Old Wood from the AONB North Pennines – Salmon Jam Press, December 18, 2019
7. Nicola Scafetta, Empirical evidence for a celestial origin of the climate oscillations and its implications, Journal of Atmospheric and Solar-Terrestrial Physics, Volume 72, Issue 13, 2010, Pages 951-970, ISSN 1364-6826 <https://doi.org/10.1016/j.jastp.2010.04.015>.
8. Douglas Vogt <https://youtu.be/WAlyvbt8Nlk>
9. Biochemistry | Definition, History, Examples, Importance, & Facts | Britannica, Elmer H. Stotz, Birgit Vennesland, Feb 12, 2025
10. Balasubramanian, A.. (2008). ECOSYSTEM AND ITS COMPONENTS.
11. Victoria State Government, Departement of Education, Skamp (2004)
12. <https://www.frontiersin.org/articles/10.3389/fspas.2020.00007/full> / Front. Astron. Space Sci., 18 March 2020 Sec. Astrobiology Volume 7 - 2020 | <https://doi.org/10.3389/fspas.2020.00007>
13. Yawn, David H.. "plasma". Encyclopedia Britannica, 12 Jan. 2023, <https://www.britannica.com/science/plasma-biology>. Accessed 20 January 2023.
14. Abbaspour N, Hurrell R, Kelishadi R. Review on iron and its importance for human health. J Res Med Sci. 2014 Feb;19(2):164-74. PMID: 24778671; PMCID: PMC3999603.
15. Markgraf, Bert. "What Happens To Atoms During A Chemical Reaction?" [sciencing.com, https://www.sciencing.com/what-happens-to-atoms-during-a-chemical-reaction-13710467/](https://www.sciencing.com/what-happens-to-atoms-during-a-chemical-reaction-13710467/). 19 March 2018. Read More: <https://www.sciencing.com/what-happens-to-atoms-during-a-chemical-reaction-13710467/>
16. Lightning Strike, NASA, Glenn Research Center, Nancy Hall, May 13 2021
17. Leybourne, Bruce & Gregori, Giovanni. (2020). Introduction to Plasma Tectonics & Electric Geology: Solar Wind Coupling to Planetary Circuits Lightning Tells The Stellar Transformer Story.
18. <https://www.holoscience.com> Wal Thornhill: No Islands in Our Electric Universe | Space News, November 30th, 2019

19. Archinal, B. A.; A'Hearn, M. F.; Bowell, E.; Conrad, A.; Consolmagno, G. J.; Courtin, R.; Fukushima, T.; Hestroffer, D.; Hilton, J. L.; Krasinsky, G. A.; Neumann, G.; Oberst, J.; Seidelmann, P. K.; Stooke, P.; Tholen, D. J.; Thomas, P. C.; Williams, I. P. (February 2011). "Report of the IAU Working Group on Cartographic Coordinates and Rotational Elements: 2009". *Celestial Mechanics and Dynamical Astronomy*. 109 (2): 101–135. Bibcode:2011CeMDA.109..101A. doi:10.1007/s10569-010-9320-4
20. Regi, M., Di Mauro, D., & Lepidi, S. (2021). The location of the Earth's magnetic poles from circum-terrestrial observations. *Journal of Geophysical Research: Space Physics*, 126, e2020JA028513. <https://doi.org/10.1029/2020JA028513>
21. Cotton, H. (1973). *The Magnetic Fields Produced by Electric Currents*. In: *Basic Electrotechnology*. Palgrave, London. https://doi.org/10.1007/978-1-349-01705-8_9
22. <https://www.aps.org/apsnews/2008/07/1820-oersted-electromagnetism> American Physical Society, July 1, 2008, Alan Chodos
23. Borovsky, Joseph & Valdivia, J.. (2018). The Earth's Magnetosphere: A Systems Science Overview and Assessment. *Surveys in Geophysics*. 39. 10.1007/s10712-018-9487-x.
24. Seven things that don't make sense about gravity | New Scientist, [newscientist.com](http://www.newscientist.com)
25. Electric Gravity in an Electric Universe by Wal Thornhill | Aether Force, www.aetherforce.energy, August 22nd, 2008 Wal Thornhill
26. Electromagnetic Force vs. Gravitational Force | www.nuclear-power.com
27. <http://www.sjcrothers.plasmareources.com/papers.html> GEOMETRY AND APPLICATIONS - RIGA 2008 Serious anomalies in the reported geometry of Einstein's gravitational field, Stephen J. Crothers Queensland, Australia 25 April 2008
28. <http://www.ncgtjournal.com/journals.html> NCGT Journal Vol. 9, Nr. 4, December 2021, Plate tectonic issues, the influence of electricity in rock forming processes and a coherent connection between science, mythology and history of Finland, Stefan Ahmala
29. <http://www.ncgtjournal.com/journals.html> NCGT Journal Vol. 11, Nr. 1, March 2023, (Page 78-111) Mountain Water, Stefan Ahmala
30. www.scienceabc.com Kavya Nambiar, Last Updated On: 19 Oct 2023, Published On: 22 Jan 2022
31. The Great Unconformity or Great Unconformities? www.eos.org Alka Tripathy-Lang 23 December 2022
32. Ways of Interpreting Myth, <https://faculty.gvsu.edu> (no author, no year of publishing found)
33. Why religion is a widely misunderstood doctrine - Global Village Space, globalvillagespace.com Shah Fahad, May 3, 2021
34. 8 Modern Astronomy Mysteries Scientists Still Can't Explain, *Space.com* By Space.com Staff, published May 31, 2012
35. Schmidt, M., Torn, M., Abiven, S. et al. Persistence of soil organic matter as an ecosystem property. *Nature* 478, 49–56 (2011). <https://doi.org/10.1038/nature10386>
36. 7 Answers to Climate Contrarian Nonsense - *Scientific American*, John Rennie November 30, 2009
37. Gulistan Amalia Rahman, Mimin Iryanti, Siti Inna Zainab, Aldi Rijaldi, Dwi Putri Desti Utami, Amalia Nurfitriani, Ahmad Aminudin, Yuyu Rahmat Tayubi, Rossie Wiedya Nusantara, Year: 2020, Analysis of Physical and Electrical Properties on Peat Soils in Longan Plantations in West Kalimantan Region, MSCEIS, EAI, DOI: 10.4108/eai.12-10-2019.2296302
38. What is peat? - International Peatland Society, Main page, (no author, nor date of publishing found)
39. James R. Fleming, Joseph Fourier, the 'greenhouse effect', and the quest for a universal theory of terrestrial temperatures, *Endeavour*, Volume 23, Issue 2, 1999, Pages 72-75, ISSN 0160-9327, [https://doi.org/10.1016/S0160-9327\(99\)01210-7](https://doi.org/10.1016/S0160-9327(99)01210-7).
40. Greenhouse Carbon Dioxide Supplementation | Oklahoma State University, Published Sep. 2023|Id: HLA-6723 By Bruce Dunn, Megha Poudel
41. Earth Systems Through Time – Historical Geology, opengeology.org, (no author nor time of publishing found)
42. ten Kate IL, Reuver M. PALLAS: Planetary Analogues Laboratory for Light, Atmosphere, and Surface Simulations. *Netherlands Journal of Geosciences - Geologie en Mijnbouw*. 2016;95(2):183-189. doi:10.1017/njg.2015.19
43. NCGT Journal, Volume 10, Number 1, March 2022. ISSN 2202-0039. James Maxlow, Expansion Tectonics: Archaen to Present-day Small Earth Modelling
44. A prehistoric revolution, *Laboratory News*, Brian J Ford, April 03, 2012

45. 10 Examples of Settled Science that Are 'Controversial' - Big Think, bigthink.com, August 30, 2013 (no author listed)

3. Creation and accretion of peat from a new perspective

1. Ray, N. and J. M. Adams. 2001, " A GIS-based Vegetation Map of the World at the Last Glacial Maximum (25,000-15,000 BP). Internet Archaeology 11. " Source: http://intarch.ac.uk/journal/issue11/rayadams_toc.html
2. Alia J. Lesnek *et al.* ,Deglaciation of the Pacific coastal corridor directly preceded the human colonization of the Americas, *sci.Adv.*4.eaar5040 (2018). DOI:10.1126/sciadv.aar5040
3. What is the importance of carbon in living beings by Maria Anderson, Curiosities of nature, August 27, 2021, agrocorn.com
4. Mccarthy, Terence & McIver, J.R. & Cairncross, Bruce & Ellery, William & Ellery, Karen. (1989). The inorganic chemistry of peat from the Maunachira channel-swamp system, Okavango Delta, Botswana. *Geochimica et Cosmochimica Acta.* 53. 1077-1089. 10.1016/0016-7037(89)90212-3.
5. Difference Between Allochthonous Autochthonous and Parautochthonous, February 6, 2020. Posted by Dr. Samantha, differencebetween.com
6. Kameník, J., Mizera, J. & Řanda, Z. Chemical composition of plant silica phytoliths. *Environ Chem Lett* 11, 189–195 (2013). <https://doi.org/10.1007/s10311-012-0396-9>
7. Glass 101: Fused Silica vs. Quartz Mo-Sci Corporation, Krista Grayson, July 27, 2021
8. René Gy, Ion exchange for glass strengthening, *Materials Science and Engineering: B*, Volume 149, Issue 2, 2008, Pages 159-165, ISSN 0921-5107, <https://doi.org/10.1016/j.mseb.2007.11.029>. (<https://www.sciencedirect.com/science/article/pii/S0921510707006599>)
9. Glass | Definition, Composition, Material, Types, & Facts | Britannica, Written and fact-checked by the editors of Encyclopedia Britannica, Last Updated: Apr 6, 2025
10. Baderttinov, A.R. & Churkin, B.S. & Milyaev, V.M. & Gushchin, V.A. & Khoruzhenko, V.I., (2002). Water glass making by single-state method and using it in green sand molding.
11. Electromagnetic pulses generated by meteoroid impacts on spacecraft - Close - 2010 - *Journal of Geophysical Research: Space Physics* - Wiley Online Library, S. Close, P. Colestock, L. Cox, M. Kelley, N. Lee
First published: 21 December 2010
<https://doi.org/10.1029/2010JA015921>
12. Stellar Transformer Concepts: Solar Induction Driver of Natural Disasters Forecasting with Geophysical Intelligence, Bruce Leybourne – Research Director Institute for Advance Studies on Climate Change (IASCC), SYSTEMICS, CYBERNETICS AND INFORMATICS, VOLUME 16 - NUMBER 4 - YEAR 2018, ISSN: 1690-4524
13. Nag, A., and V. A. Rakov (2012), Positive lightning: An overview, new observations, and inferences, *J. Geophys. Res.*, 117, D08109, doi:10.1029/2012JD017545.
14. Li, X., Zhang, J., Chen, L. *et al.* Measuring Method for Lightning Channel Temperature. *Sci Rep* 6, 33906 (2016). <https://doi.org/10.1038/srep33906>
15. Ptable, Michael Dayah. Updated Oct 3, 2024.
16. N. Østgaard, S.B. Mende, H.U. Frey, J.B. Sigwarth, A. Åsnes, J.M. Weygand, Auroral conjugacy studies based on global imaging, *Journal of Atmospheric and Solar-Terrestrial Physics*, Volume 69, Issue 3, 2007, Pages 249-255, ISSN 1364-6826, <https://doi.org/10.1016/j.jastp.2006.05.026>.
17. A. G. McNamara *Canadian Journal of Physics* September 1969 <https://doi.org/10.1139/p69-242>
18. ESA - Swarm probes weakening of Earth's magnetic field, www.livescience.com, Kelly Dickerson published July 8, 2014
19. The whole atmosphere response to changes in the Earth's magnetic field from 1900 to 2000: An example of "top-down" vertical coupling, Ingrid Cnossen, Hanli Liu, Hua Lu, First published: 27 June 2016 <https://doi.org/10.1002/2016JD024890>
20. Lei, Y., Jiao, L. & Chen, H. Possible correlation between the vertical component of lithospheric magnetic field and continental seismicity. *Earth Planets Space* 70, 179 (2018). <https://doi.org/10.1186/s40623-018-0949-7>
21. Changes in Earth's Magnetic Field are a main cause of Volcanism, Earthquakes, HGFA-seismicity&

- Global Warming, Harry K. Hahn, 15.7.2023, vixra.org
22. Subseasonal Variation in Neptune's Mid-infrared Emission Michael T. Roman, Leigh N. Fletcher, Glenn S. Orton, Thomas K. Greathouse, Julianne I. Moses, Naomi Rowe-Gurney, Patrick G. J. Irwin, Arrate Antuñano, James Sinclair, Yasumasa Kasaba Published 2022 April 11 2022Published by the American Astronomical Society The Planetary Science Journal, Volume 3, Number 4 Citation Michael T. Roman *et al* 2022 *Planet. Sci. J.* 3 78, DOI 10.3847/PSJ/ac5aa4
 23. O'Donoghue, J., Moore, L., Bhakyaipabul, T., Johnson, R., Melin, H., and Stallard, T.: A planetary-scale heat wave in Jupiter's mid-latitude upper atmosphere, Europlanet Science Congress 2022, Granada, Spain, 18–23 Sep 2022, EPSC2022-373, 2022.
 24. Evidence for distinctive changes in the solar wind helium abundance in solar cycle 24 Yogesh, D Chakrabarty, N Srivastava Monthly Notices of the Royal Astronomical Society: Letters, Volume 503, Issue 1, May 2021, Pages L17–L22, <https://doi.org/10.1093/mnrasl/slab016>
 25. McIntosh, S.W., Chapman, S., Leamon, R.J. *et al.* Overlapping Magnetic Activity Cycles and the Sunspot Number: Forecasting Sunspot Cycle 25 Amplitude. *Sol Phys* 295, 163 (2020). <https://doi.org/10.1007/s11207-020-01723-y>
 26. Super rare pink and orange auroras surprise Norwegian skywatchers again | Space, Tereza Pultarova published December 16, 2022, space.com
 27. Fire in the sky: The southern lights in Indigenous oral traditions, April 1, 2015, 9.09pm, Duane Hamacher, theconversation.com
 28. Bird, Stephanie Rose (2006). "Australian Aborigines". In William M. Clements (ed.). *The Greenwood Encyclopedia of World Folklore and Folklife*. Westport, CT: Greenwood Press. pp. 292–299
 29. Crater Orgins, Barry Setterfield, July 28, 2012, www.barrysetterfield.org
 30. The Electrical Origin of Kimberlite Pipes, Jan 25, 2010, Louis Hissink, M.Sc, www.thunderbolts.info
 31. Electric Discharge - Not an Impact Caused Formation Of Upheaval Dome, Canyonlands National Park , Utah, Robert Hawthorne Jr. Undergraduate School of Science, Mathematics, and Engineering, Salt Lake Community College, SYSTEMICS, CYBERNETICS AND INFORMATICS, VOLUME 18, NUMBER 3 - YEAR2020,ISSN:1690-4524, www.iiisci.org/journal
 32. Novosyolova, E & Shikhova, Lyudmila & Lisitsyn, Eugene. (2021). Content of heavy metals (Zn, Pb, Cu and Cd) in peat and plants of cutover peatlands. IOP Conference Series: Earth and Environmental Science. 862. 012106. 10.1088/1755-1315/862/1/012106.
 33. Mustoe, G. E. (2017). Wood Petrification: A New View of Permineralization and Replacement. *Geosciences*, 7(4), 119. <https://doi.org/10.3390/geosciences7040119>
 34. Berg, J.S., Duverger, A., Cordier, L. *et al.* Rapid pyritization in the presence of a sulfur/sulfate-reducing bacterial consortium. *Sci Rep* 10, 8264 (2020). <https://doi.org/10.1038/s41598-020-64990-6>
 35. Pyrite, Hobart M. King, Ph.D., GIA GG, <https://geology.com>
 36. Murrel, JN, Kettle, SF Tedder, JM "The Chemical Bond", John Wiley & Sons (1985) ISBN 0-471-90759-6
 37. <https://geologyscience.com/minerals/pyrite/?amp;04/09/2023> (no author given)
 38. Miriam I. Nystrand, Mirikka Hadzic, Heini Postila, Anneli Wichmann, Anssi Karppinen, Raimo Ihme, Peter Österholm,
 39. Characteristics of sulfide bearing soil materials in peat extraction areas in N-Finland, Journal of Geochemical Exploration, Volume 220, 2021, 106640, ISSN 0375-6742, <https://doi.org/10.1016/j.gexplo.2020.106640>.
 40. The Engineering Properties of Glacial Tills, B. G. Clarke, School of Civil Engineering, University of Leeds, Leeds, UK, 04 July 2018, doi: 10.1680/jgere.18.00020
 41. STRUCTURAL INTERPRETATION OF GRAPHITE- BEARING BLACK SCHIST IN AITOLAMPI, EASTERN FINLAND, Geology and mineralogy Faculty of Science and Engineering Åbo Akademi University, spring 2018 Laura Puronaho, 37615
 42. Loukola-Ruskeeniemi, Kirsti. (1992). Geochemistry of Proterozoic metamorphosed black shales in eastern Finland, with implications for exploration and environment studies.
 43. Howard, J. L. (2005). The Quartzite Problem Revisited. *Journal of Geology* 113(6), 707-13. <https://doi.org/10.1086/449328>.

44. Elmi, Chiara & Chen, Jiangzhi & Goldsby, David & Gieré, Reto. (2017). Mineralogical and compositional features of rock fulgurites: A record of lightning effects on granite. *American Mineralogist*. 102. 1470-1481. 10.2138/am-2017-5971.
45. Geological 3D Modelling of Aijala-Metsämonttu Cu-Zn-Au-Ag-Pb deposits, Joonas Sandström, 12/2021, Master's Programme in Geology and Geophysics, University of Helsinki
46. Syntesis of SiC Ceramics by the Carbothermal Reduction of Mineralized Wood with Silica, Yongsoon Shin, Chongmin Wang, Gregory J. Exarhos, Pacific Northwest National Laboratory, Richland, *Advanced Materials* 2005, 17, No. 1, January 6, DOI: 10.1002/adma.200400371

4. Peat's active role in the environment and in the end of the last ice age

1. Brandon Schmandt *et al.* Dehydration melting at the top of the lower mantle. *Science* 344, 1265-1268 (2014). DOI: 10.1126/science.1253358
2. de Sousa, F. F., da Silva, L. D. P., & Freitas, K. H. G. (2017). Electrical and dielectric properties of water. *Scientia Plena*, 13(1). <https://doi.org/10.14808/sci.plena.2017.012722>
3. Gerasimov, A.I. Water as an insulator in pulsed facilities (*Review*). *Instrum Exp Tech* 48, 141–167 (2005). <https://doi.org/10.1007/s10786-005-0029-7>
4. Water, the Universal Solvent | U.S. Geological Survey. Water Science School June 9, 2018
5. Y.S. Djikaev, Eli Ruckenstein, The variation of the number of hydrogen bonds per water molecule in the vicinity of a hydrophobic surface and its effect on hydrophobic interactions, *Current Opinion in Colloid & Interface Science*, Volume 16, Issue 4, 2011, Pages 272-284, ISSN 1359-0294, <https://doi.org/10.1016/j.cocis.2010.10.002>.
6. Geochemical Insights Into an Active Calcareous Tufa Depositing System in Southern Germany, *Procedia Earth and Planetary Science*, Volume 17, 2017, Pages 328-331, ISSN 1878-5220, <https://doi.org/10.1016/j.proeps.2016.12.083>
7. COUWENBERG, J. and JOOSTEN, H. (2005), Self-organization in raised bog patterning: the origin of microtope zonation and mesotope diversity. *Journal of Ecology*, 93: 1238-1248. <https://doi.org/10.1111/j.1365-2745.2005.01035.x>
8. Greenhouse Management online, Dr. Michael R. Evans, Department of Horticulture University of Arkansas, 2014
9. Chai B, Pollack GH. Solute-free interfacial zones in polar liquids. *J Phys Chem B*. 2010 Apr 29;114(16):5371-5. doi: 10.1021/jp100200y. PMID: 20369860; PMCID: PMC2865192.
10. INFLUENCE OF ELECTRICAL CONNECTION BETWEEN METAL ELECTRODES ON CONTIGUOUS SOLUTE-FREE ZONES, Binghua Chai, et al., Influence of electrical connection between metal electrodes *Contemporary Materials*, IV 1 (2013), UDK 66.017/.018, doi: 10.7251/COMEN1301001C
11. UNEXPECTED PRESENCE OF SOLUTE-FREE ZONES AT METAL-WATER INTERFACES, B. Chai, A. G. Mahtani, G. H. Pollack, Unexpected presence of solute-free zones at metal-water interfaces, *Contemporary Materials*, III, 1 (2012), UDK 669.334+669.295.571:[626.8, doi: 10.7251/COM1201001C
12. S N M Zamri et al 2022 *J. Phys.: Conf. Ser.* 2314 012024
13. Definitions for Hydrophilicity, Hydrophobicity, and Superhydrophobicity: Getting the Basics Right | *The Journal of Physical Chemistry Letters*, Kock-Yee Law *The Journal of Physical Chemistry Letters* 2014 5 (4), 686-688, DOI: 10.1021/jz402762h
14. What is clay? A new definition of “clay” based on plasticity and its impact on the most widespread soil classification systems, *Applied Clay Science*, Volume 161, 2018, Pages 57-63, ISSN 0169-1317, <https://doi.org/10.1016/j.clay.2018.04.011>
15. Hartmann, A., N. Goldscheider, T. Wagener, J. Lange, and M. Weiler (2014), Karst water resources in a changing world: Review of hydrological modeling approaches, *Rev. Geophys.*, 52, 218–242, doi:10.1002/2013RG000443.

16. Briceag, Andrei. (2019). MUD VOLCANOES FROM ROMANIA: GEOLOGICAL AND GEOCHEMICAL APPROACHES. 10.5593/sgem2019/1.1/S01.045.
17. LIQUEFACTION STUDIES: A REVIEW, Ali A. Mahmood, Catherine N. Mulligan, Annual Conference of the Canadian Society for Civil Engineering, Montréal, Québec, Canada 5-8 juin 2002 /June 5-8, 2002
18. Ojovan, M. I.; Lee, W. E. (2010). "Connectivity and glass transition in disordered oxide systems". *Journal of Non-Crystalline Solids*. **356** (44–49): 2534–2540. Bibcode:2010JNCS..356.2534O. doi:10.1016/j.jnoncrsol.2010.05.012
19. Seyed Zanyar Seyed Mousavi, Hossein Tavakoli, Parviz Moarefvand, Mohammad Rezaei, Micro-structural, petro-graphical and mechanical studies of schist rocks under the freezing-thawing cycles, *Cold Regions Science and Technology*, Volume 174, 2020, 103039, ISSN 0165-232X, <https://doi.org/10.1016/j.coldregions.2020.103039>
20. Der Sauerbrunn - Heilwasser aus Ladis seit 1212 | Blog, www.serfaus-fiss-ladis.at, (no author found)
21. United States Department of the Interior. 2002. Hydrologic impacts of mining. Chapter 1. In: Permitting hydrology, a technical reference document for determination of probable hydrologic consequence (PHC) and cumulative hydrologic impact assessments (CHIA) (PDF) Washington, DC. Accessed November 8, 2003.
22. Quick Clay Landslides in Norway, May 12, 2021 by David Nikel, www.lifeinnorway.net
23. <https://de.wikipedia.org/wiki/Kryptovulkanismus> (no other resource found)
24. Belay Zerga, Karst topography: Formation, processes, characteristics, landforms, degradation and restoration: A systematic review, *Watershed Ecology and the Environment*, Volume 6, 2024, Pages 252-269, ISSN 2589-4714, <https://doi.org/10.1016/j.wsee.2024.10.003>
25. May-Crespo, J. & Quintana, Patricia & Alvarado-Gil, Juan & Juárez-de la Rosa, B. Alejandra & May Pat, Alejandro & Aviles, Francis. (2012). Physical, Petrographic, and Mineralogical Properties of Limestone Rocks from the Peninsula of Yucatán. *Materials Research Society symposia proceedings*. Materials Research Society. 1373. 53-58. 10.1557/opl.2012.295.
26. The Mysterious Minevre Karst Feature: Know 10 things About This natural wonder - Geotourism, March 6, 2022, sutikshan.thejerker.com
27. Radulović MM (2013) A new view on karst genesis. *Carbonates and Evaporites* doi:10.1007/s13146-012-0125-2
28. Martínez Cortizas A, López-Merino L, Silva-Sánchez N, Sjöström JK, Kylander ME. Investigating the Mineral Composition of Peat by Combining FTIR-ATR and Multivariate Analysis. *Minerals*. 2021; 11(10):1084. <https://doi.org/10.3390/min11101084>
29. Ali, A.M., Padmanabhan, E., Mijinyawa, A. *et al.* Effect of pH on the stability of quartz in a multi-phase system of kaolinite, hydrous Al (hydr)oxide and quartz. *SN Appl. Sci.* 1, 388 (2019). <https://doi.org/10.1007/s42452-019-0398-3>
30. Ivan Sekerka, Josef F Lechner, Determination of Alkalinity and Acidity of Water by Conductometric Acid-Base Titration, *Journal of Association of Official Analytical Chemists*, Volume 67, Issue 5, 1 September 1984, Pages 893–895, <https://doi.org/10.1093/jaoac/67.5.893>
31. Proof that the H⁻ Ion Has Only One Bound State, Robert Nyden Hill, *Phys. Rev. Lett.* 38, 643 – Published 21 March, 1977, DOI: <https://doi.org/10.1103/PhysRevLett.38.643>
32. Wildt, R., "Negative Ions of Hydrogen and the Opacity of Stellar Atmospheres.", *The Astrophysical Journal*, vol. 90, IOP, p. 611, 1939. doi:10.1086/144125.
33. Götze J. Chemistry, textures and physical properties of quartz — geological interpretation and technical application. *Mineralogical Magazine*. 2009;73(4):645-671. doi:10.1180/minmag.2009.073.4.645
34. McLaren, A.C. (1984). Transmission Electron Microscope Investigations of the Microstructures of Microclines. In: Brown, W.L. (eds) *Feldspars and Feldspathoids*. NATO ASI Series, vol 137. Springer, Dordrecht. https://doi.org/10.1007/978-94-015-6929-3_10
35. Chao SH, Hargreaves A, Taylor WH. The structure of orthoclase. *Mineralogical Magazine and Journal of the Mineralogical Society*. 1940;25(168):498-512. doi:10.1180/minmag.1940.025.168.05
36. Hwang, G.C., Hwang, H., Bang, Y. *et al.* A role for subducted albite in the water cycle and alkalinity of subduction fluids. *Nat Commun* 12, 1155 (2021). <https://doi.org/10.1038/s41467-021-21419-6>
37. Lei Xu, Yuxuan Wang, Xubiao Li, Yang Liu, Min Chen, Sintering, microstructure and mechanical properties of anorthite-based ceramics prepared from iron-extracted steel slag, *Journal of Alloys*

- and Compounds, Volume 1005, 2024, 176221, ISSN 0925-8388, <https://doi.org/10.1016/j.jallcom.2024.176221>
38. Qi Liu, Zhonghao Sun, and J. Carlos Santamarina *Energy & Fuels* 2019 33 (5), 4009-4016 DOI: 10.1021/acs.energyfuels.9b00057
 39. L.F.M. Sanchez, B. Fournier, M. Jolin, D. Mitchell, J. Bastien, Overall assessment of Alkali-Aggregate Reaction (AAR) in concretes presenting different strengths and incorporating a wide range of reactive aggregate types and natures, *Cement and Concrete Research*, Volume 93, 2017, Pages 17-31, ISSN 0008-8846, <https://doi.org/10.1016/j.cemconres.2016.12.001>
 40. Pranav Shukla, Tejas Jagdhari, Andrew P. Fugaro, and Jonathan B. Boreyko *Langmuir* 2020 36 (8), 1871-1877 DOI: 10.1021/acs.langmuir.9b02840
 41. Eduardo Pérez-Botella, Susana Valencia, and Fernando Rey *Chemical Reviews* 2022 122 (24), 17647-17695 DOI: 10.1021/acs.chemrev.2c00140
 42. Meng Wang, Nicholas R. Jaegers, Mal-Soon Lee, Chuan Wan, Jian Zhi Hu, Hui Shi, Donghai Mei, Sarah D. Burton, Donald M. Camaioni, Oliver Y. Gutiérrez, Vassiliki-Alexandra Glezakou, Roger Rousseau, Yong Wang, and Johannes A. Lercher *Journal of the American Chemical Society* 2019 141 (8), 3444-3455 DOI: 10.1021/jacs.8b07969
 43. Hamedani, Yasaman & Macha, Prathyushakrishna & Bunning, Timothy & Naik, Rajesh & Vasudev, Milana. (2016). Plasma-Enhanced Chemical Vapor Deposition: Where we are and the Outlook for the Future. 10.5772/64654.
 44. Zhang Y, Liu C, Li Y, Song L, Yang J, Zuo R, Li J, Teng Y, Wang J. Spectroscopic Characteristics and Speciation Distribution of Fe(III) Binding to Molecular Weight-Dependent Standard Pahokee Peat Fulvic Acid. *Int J Environ Res Public Health*. 2022 Jun 26;19(13):7838. doi: 10.3390/ijerph19137838. PMID: 35805509; PMCID: PMC9266197.
 45. Bergwanderung Kraftort Grimmiwasser, www.diemtigital.ch
 46. Jurapark Aargau, <https://jurapark-aargau.ch/>
 47. Jeannet, A. (1951): Stratigraphie und Palaeontologie des oolithischen Eisenerzlagers von Herznach und seiner Umgebung (1. Teil). Beiträge zur Geologie der Schweiz. Geotechnische Serie, 13. Lieferung, 5. Band, 240 pp., 107 pls.
 48. Suraj D. Serai, Hansel J. Otero, Janet L. Kwiatkowski, Chapter 26 - Physical and Physiological Properties of Iron, Editor(s): Nicole Seiberlich, Vikas Gulani, Fernando Calamante, Adrienne Campbell-Washburn, Mariya Doneva, Houchun Harry Hu, Steven Sourbron, *Advances in Magnetic Resonance Technology and Applications*, Academic Press, Volume 1, 2020, Pages 681-693, ISSN 2666-9099, ISBN 9780128170571, <https://doi.org/10.1016/B978-0-12-817057-1.00028-7>.
 49. Wang, A., Lv, J., Wang, J., & Shi, K. (2022). CO2 enrichment in greenhouse production: Towards a sustainable approach. *Frontiers in plant science*, 13, 1029901. <https://doi.org/10.3389/fpls.2022.1029901>
 50. Hydrogen Chloride Cannon, Chris Cramer, prof. 27.1.2016, <https://youtu.be/BoC8LrNdnOc?si=c3pC1FHk7paUp4E2>
 51. Zolkos, S., Fiske, G., Windholz, T., Duran, G., Yang, Z., Olenchenko, V., Faguet, A., & Natali, S. M. (2021). Detecting and Mapping Gas Emission Craters on the Yamal and Gydan Peninsulas, Western Siberia. *Geosciences*, 11(1), 21. <https://doi.org/10.3390/geosciences11010021>
 52. eRepo - Vegetation and GIS data examined in the paper "Ongoing fen-bog transition in a boreal aapa mire inferred from repeated field sampling, aerial images, and Landsat data", Kolari, Tiina Hilkkä Maria, University of Eastern Finland, Sallinen, Antti, UEF, Wolff, Franziska, UEF, Kumpula, Timo, UEF, Tolonen, Kimmo, UEF, Tahvanainen, Teemu, UEF, 2021-06-01T08:55:16.758462+00:00, DOI 10.5281/zenodo.4889009.
 53. Z. Zheng, Y. Chen, J. Ding, C. Wang and J. Wu, "An EMI Immune Daisy Chain Interface for Battery Management System Communication," 2024 *IEEE Joint International Symposium on Electromagnetic Compatibility, Signal & Power Integrity: EMC Japan / Asia-Pacific International Symposium on Electromagnetic Compatibility (EMC Japan/APEMC Okinawa)*, Ginowan, Okinawa, Japan, 2024, pp. 501-504, doi: 10.23919/EMCJapan/APEMCOkinaw58965.2024.10585068.
 54. Billy, Yelverton, *Magnetohydrodynamics Part 2*, 13.2.2014. <https://youtu.be/gG1tDnvCo84?si=nY7dtxaeN2ISMsjM>

55. See, the, pattern, 29.5.2022, PlasmaRayCraters, <https://youtu.be/pD69C7bAfis?si=FyB25ail6MtjdNwh>
56. Lewis Urry a powerful man, Richard Jansen-Parkes, 26th January 2018, www.thechemicalengineer.com
57. Klaus Schmidt-Rohr Journal of Chemical Education 2018 95 (10), 1801-1810 DOI: 10.1021/acs.jchemed.8b00479

5. Cultural rituals and Mythological stories revolving around peat

1. Lori Dorn October 26, 2022, Randall Carlson, <https://laughingsquid.com/randall-carson-halloween/>
2. The Fire Of St. Elmo 1998, Keith C. Heidorn, PhD, www.heidorn.info
3. Babrauskas, V. (2022). Minimum Values of Voltage, Current, or Power for the Ignition of Fire. *Fire*, 5(6), 201. <https://doi.org/10.3390/fire5060201>
4. Plate tectonic issues, the influence of electricity in rock forming processes and a coherent connection between science, mythology and history of Finland, Stefan Ahmala, NCGT Journal, Vol. 0. Nr. 4. 2021, ISSN 2202-0039 (Page 45-70)
5. Robinet, Jean-Christophe & Casalis, Grégoire. (2001). Critical interaction of a shock wave with an acoustic wave. *Physics of Fluids - PHYS FLUIDS*. 13. 10.1063/1.1351548.
6. Study of the Electrical Characteristics, Shock-Wave Pressure Characteristics, and Attenuation Law Based on Pulse Discharge in Water, Dong Yan, Decun Bian, Jinchang Zhao, Shaoqing Niu, First published: 2016 <https://doi.org/10.1155/2016/6412309>
7. Great Lynx, the Thunder, and the Mortals - Mii Dash Geget, February 24, 2019, wordpress.com
8. CHIPPEWA BURIAL AND MOURNING CUSTOMS, Sister M. Inez Hilger, First published: October-December 1944, <https://doi.org/10.1525/aa.1944.46.4.02a00240>
9. Christopher J.M. Lawley, Victoria Tschirhart, Jennifer W. Smith, Sally J. Pehrsson, Ernst M. Schetselaar, Andrew J. Schaeffer, Michel G. Houllé, Bruce M. Eglinton, Prospectivity modelling of Canadian magmatic Ni (\pm Cu \pm Co \pm PGE) sulphide mineral systems, *Ore Geology Reviews*, Volume 132, 2021, 103985, ISSN 0169-1368, <https://doi.org/10.1016/j.oregeorev.2021.103985>
10. Haerendel, G., & Partamies, N. (2024). On the formation of auroral spirals. *Journal of Geophysical Research: Space Physics*, 129, e2024JA032413. <https://doi.org/10.1029/2024JA032413>
11. Nishimura, K., Ikehata, H., Douki, T., Cadet, J., Sugiura, S., & Mori, T. (2021). Seasonal Differences in the UVA/UVB Ratio of Natural Sunlight Influence the Efficiency of the Photoisomerization of (6-4) Photoproducts into their Dewar Valence Isomers. *Photochemistry and photobiology*, 97(3), 582–588. <https://doi.org/10.1111/php.13361>
12. The Electric Universe, Wallace Thornhill & David Talbott, May 24, 2007, Mikamar Publisher
13. The Thunderbolts Project™ Trademark of T-Bolts Group Inc. a 501(c)(3) non-profit organization, www.thunderbolts.info
14. Emily Goodheart | Feb 3, 2018, <https://www.nathab.com/blog/folklore-arctic-animals/>
15. Tables to Correct Eyes and Quickly Answer Differences in Cosmologies, Sf. R. Careaga, BSEE, MSTOM June 2023 www.academia.edu/103064184/PEMC
16. A3Anomalies/ Stefan Ahmala Finnish Copper Playlist https://youtube.com/playlist?list=PLLWZrQb_ZJzX9gB7e7dc9ZxRMW-tGXIEL&si=NAVBqGuc1hQR_9D1
17. Talbott, David N., *The Saturn Myth* ISBN: 0-385-113376-5 Library of Congress Catalog Card Number 76-51986 1980
18. Lahelma, Antti, University of Helsinki Open Repository, Suomen Muinaismuistoyhdistys r.y., *A Touch of Red : Archaeological and Ethnographic Approaches to Interpreting Finnish Rock Paintings*, <http://urn.fi/URN:ISBN:978-952-10-4845-6>, URN:ISSN:0355-3108
19. Peratt, Anthony. (2004). Characteristics for the Occurrence of a High-Current, Z-Pinch Aurora as Recorded in Antiquity. *Plasma Science, IEEE Transactions on*. 31. 1192 - 1214. 10.1109/TPS.2003.820956.
20. Lobachevsky, P., Forrester, H. B., Ivashkevich, A., Mason, J., Stevenson, A. W., Hall, C. J., Sprung, C.

N., Djonov, V. G., & Martin, O. A. (2021).
Synchrotron X-Ray Radiation-Induced Bystander
Effect: An Impact of the Scattered Radiation,
Distance from the Irradiated Site and p53 Cell
Status. *Frontiers in oncology*, *11*, 685598.
<https://doi.org/10.3389/fonc.2021.685598>

INTERPRETATION OF THE DATA ON THE KURSK MAGNETIC ANOMALY BASED ON RECORDINGS BY ARTIFICIAL EARTH SATELLITES

Vadim V. Gordienko¹ and Victor N. Tarasov²

¹S.I. Subbotin Institute of Geophysics, Kiev, Ukraine.

²National Academy of Sciences of Ukraine, Kiev, Ukraine.

Vadim V. Gordienko: S.I.
Subbotin Institute of Geophysics,
Kiev, Ukraine.
gordienkovadim39@gmail.com

Abstract: The article presents the results of a study of the Kursk magnetic anomaly (KMA) based on satellite data. The first such data were the subject of many publications, and although they are not currently in use, the authors believe that dismissing them entirely is not actually justified. The displacement of the anomaly observed after new-generation satellites provided new information is indisputable; however, other parameters may be interpreted together with the data acquired in recent years. Thus, five anomalies are recorded by satellites of altitudes of 300, 325, 350, 400, and 485 km can be studied. The available examples of interpreting absolute values of the vertical component (Z) of the magnetic field by fitting magnetization values do not inspire confidence in the prospects of that approach. The analysis is therefore performed using relative values. A source in the shape of a vertical cylinder of limited depth with a radius of 200 km was employed. It was also established in terms of gravimetric, geothermal, and seismic data that this cylinder is located in a zone of recent activation. Temperature calculations indicate that at a depth of about 25 km the Curie temperature of magnetite is exceeded, which suggests that the base of the anomaly source is located just there. Given such parameters, calculations were conducted to determine the distribution of relative magnetic field values at various altitudes. The results were compared with those observed. The agreement was quite acceptable despite the error in the experimental data. The said error is, however, quite significant, so that it is virtually impossible to improve the accuracy of the anomaly source parameters. The anomalous magnetization of rocks within the source is estimated at about 3 A/m.

Keywords: Kursk magnetic anomaly, satellite data, parameters of the anomaly source

Introduction

The regional Kursk magnetic anomaly (KMA), observed on the territories of Ukraine and Russia, has long attracted attention of researchers due to its high intensity, vast area, and complex structure [Abramova et al., 2016; Baysarovich et al., 2002; Geophysical ..., 1987; Gordienko, 2000; Pashkevich et al., 1990; Rotanova et al., 2005; Heines, 1985; Hemant et al., 2005a, 2005b, etc.]. The anomaly is territorially linked to iron ore deposits hosted in Precambrian quartzites, which were naturally believed to be its source. However, over time, data emerged, indicating a deeper source responsible for part of the anomaly. Those data became increasingly more evident once magnetic observations began to be employed from artificial Earth satellites at altitudes of hundreds of kilometers. It is

precisely an attempt to contribute to determining the origin of such elements of the anomaly source that this article addresses.

Previous studies of the distribution of magnetic properties of crustal rocks in the KMA zone — coordinated with the observed field — were reported in the publications mentioned above [Baysarovich et al., 2002; Pashkevich et al., 1990; etc.]. The data recorded on the Earth's surface and those computed for relatively high altitudes (tens of kilometers) were used, but no significant results were achieved through that approach. Later, after satellite records began to include more than just scalar values of the field, there appeared additional versions of the interpretation of the MAGSAT satellite data [Pashkevich et al., 1990; etc.]. This led to efforts to reconcile known values of crustal rock's magnetization with the observed

anomaly. However, it had long been known [Primdahl et al., 1992; etc.] that magnetometers on satellites of this type could *have a significant tren*). For that reason, in recent years new data from CHAMP satellites have been used. A better orbit configuration has been achieved, and both the accuracy and duration of observations have improved significantly [Abramova et al., 2016; etc.]. In this study, preference was given to the data recorded by CHAMP, although these authors believe that some information from MAGSAT can also be utilized (see Fig. 1).

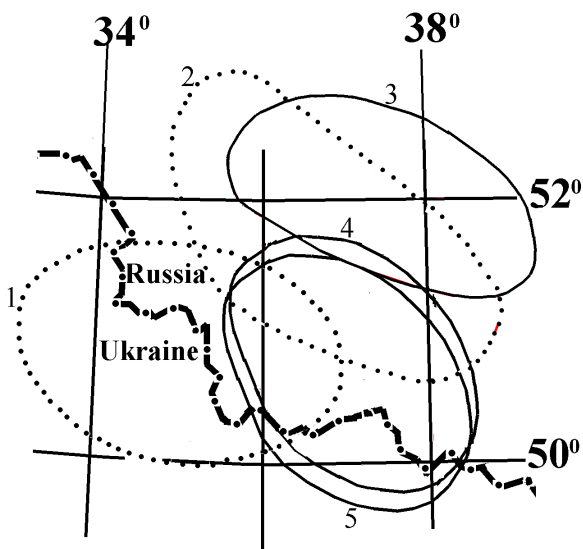


Fig. 1. Outlines of the central part of the KMA are recorded at different observation altitudes and according to various authors. 1 – 350 km, MAGSAT [Heines, 1985], 2 – 350 km, MAGSAT [Rotanova et al., 2005], 3 – 450 km, CHAMP [Rotanova et al., 2005], 4 – 400 km, CHAMP [Hemant et al., 2005b], 5 – 400 km, CHAMP [Abramova et al., 2016].

The territorial displacement of the anomaly is indisputable. Even though the absolute values (over roughly equal areas) agree well at the same observation altitudes. The general shapes of the KMA isometric part at the altitudes in question are also similar with the only notable difference being the orientation of the long axis. The relative change in the intensity of anomalies 1 and 2 with distance from the center coincides, so that interpretation results should also coincide. Similarly, the shapes of anomalies 4 and 5 are also in agreement, but they differ from the shape of anomaly 3. The latter is clearly asymmetric and was therefore excluded from further consideration.

In further discussion, the location of the KMA's central portion is assumed to conform to the outlines of anomalies 4 and 5 as shown in Fig. 1.

Information Used

Let us first coordinate the maximum intensity of the anomalous magnetic field vertical component (Z) with observation altitudes (Table 1) .

In addition to the data listed in the table, in the case of two anomalies determined by [Rotanova et al., 2005] the observation altitudes and maximum Z values agree to the same extent (at an altitude of 350 km with MAGSAT, $(H_{300}/H)^2=0.73$ and $Z_{max}/Z_{max 300}=0.70$ and at an altitude of 450 km with CHAMP, $(H_{300}/H)^2=0.44$, and $Z_{max}/Z_{max 300}=0.45$).

The following significant results of comparisons can be pointed out:

1. The anomaly parameters at an altitude of 350 km, as determined from MAGSAT data, fall into the same series as those established by the CHAMP satellite, just like the data recorded by both satellites and processed in [Rotanova et al., 2005], in which the anomalies are displaced larger (information from that article is not used further).

2. An inverse proportionality exists between the relative intensity values and the squared distance. This indicates that the anomaly source is not located at a large depth regarding the observation altitude, and its thickness is not high either.

Attempts to determine the magnetization (J) of the KMA source proceeding from the data of surface rocks' magnetization did not yield any positive results. Models were also employed in which the data on local rocks' magnetization applied only to the upper crustal layer. For the lower crustal layer, the magnetization needed to explain the satellite anomaly was selected randomly. In the case of a three-dimensional source, unrealistically high J values would be required [Pashkevich et al., 1990; etc.]. Taking into account the Earth's sphericity does not have any significant effect on the calculation results. In the authors' opinion, the approach used for interpreting anomalies in terms of the global distribution of crustal rocks' parameters [Hemant et al., 2005b; etc.] does not take into account dissimilar geological history of various regions. By way of example, a detailed comprehensive study of crustal composition in the Ukrainian Shield [Gordienko, 2000; Gordienko et al., 2005; etc.] produced results that differ markedly from those cited in [Hemant et al., 2005b]. It seems, therefore, reasonable to leave the determination of

Table 1. Observation altitudes and intensity of anomalies

H, km	300	325	350	400	485
$(H_{300}/H)^2$	1	0.85	0.73	0.56	0.38
Z_{max} , nT	33	29	24	18	14
$Z_{max}/Z_{max 300}$	1	0.88	0.73	0.54	0.42

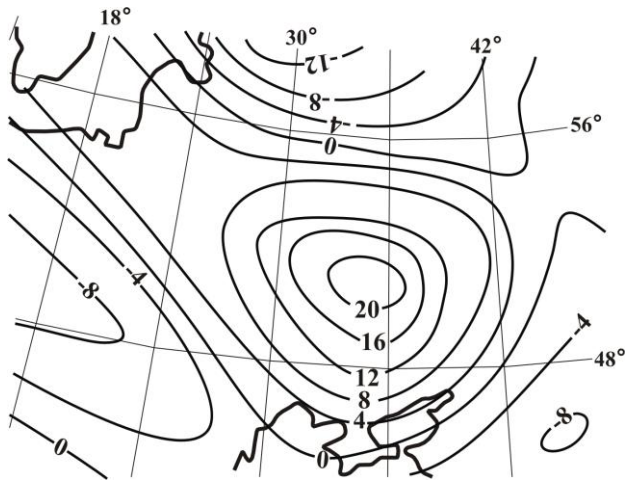


Fig. 2. Distribution of magnetic field anomalies over part of Europe at an altitude of 350 km according to the data from the MAGSAT satellite [Heines, 1985]. The numbers on the Z isolines denote intensities in nT.

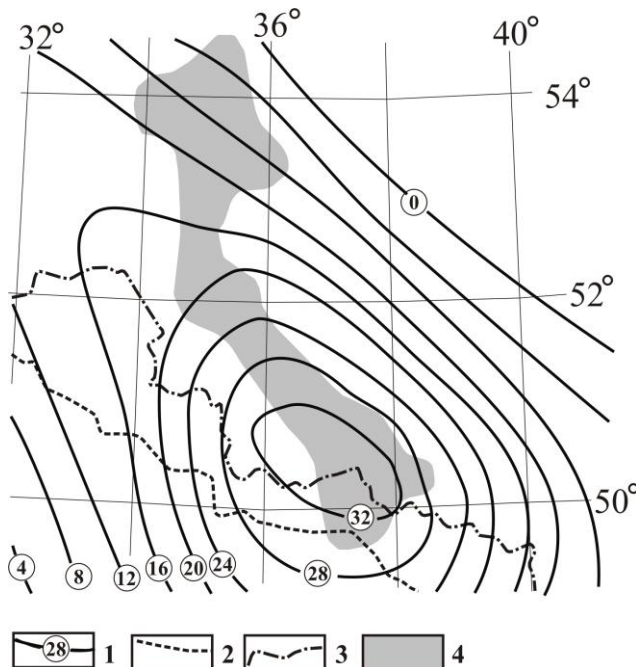


Fig. 3. A fragment of the CHAMP 300-km anomaly [Abramova et al., 2016] and the surface magnetic anomaly of the KMA. 1 – isolines of the anomaly recorded by the satellite; 2 – northeastern marginal faults of the Dnieper–Donets Depression (DDD) and Donbass; 3 – the border between Ukraine and Russia; 4 – a band of sharply variable anomalies with intensities of up to 10,000 nT [Maus et al., 2009].

the anomaly source rocks' magnetic properties until the final stage of the research. Studies of the shape of the anomaly which may hold information on the depth of its anomaly source appear to be quite promising. This could, however, only be true provided that we use a model reflecting the real situation. In our specific case, we have to admit that full conformity is impossible to achieve:

Apart from the effect of the KMA's major source, the map of European magnetic field anomalies clearly contains a “complementary” field stretching from the Voronezh Massif to the Baltic Shield (Fig. 2).

If we compare the anomaly with what looks like the reflection of the iron-ore regional zone on the Earth's surface (Fig. 3), we will see that its effect on the KMA shape should not be overrated. A band of high Z extends in the northeastern part of the KMA center, whereas north of the 54° latitude changes its strike to the northern. The anomaly recorded by the satellite is clearly due to deeper sources.

For the calculation of the magnetic anomaly the following formula for a vertical cylinder with a circular horizontal cross-section is used [Gershanok et al., 2007; etc.]:

$$Z = J \cdot S \left(\frac{h_1}{(h_1^2 + x^2)^{3/2}} - \frac{h_2}{(h_2^2 + x^2)^{3/2}} \right)$$

where J is the magnetization, S is the area of the cylinder's horizontal cross-section, h_1 and h_2 are the vertical distances from the calculation point to the top and bottom of the cylinder, respectively, and x is the horizontal distance from the cylinder's axis.

It was preliminarily established that the distribution of field intensity within the KMA does not match that expected for a source in the shape of a sphere. A similar discrepancy was found for the case of a vertical layer with an unlimited bottom depth [Gershanok et al., 2007], and so on.

Lines of northeastern orientation across the anomaly center were chosen as profiles for deriving information on the anomaly shape. Naturally, when using MAGSAT or CHAMP data, the orientation of those lines differed in geographic coordinates (Fig. 4).

For the calculation of the magnetic anomaly the following formula for a vertical cylinder with a circular horizontal cross-section is used [Gershanok et al., 2007; etc.]:

$$Z = J \cdot S \left(\frac{h_1}{(h_1^2 + x^2)^{3/2}} - \frac{h_2}{(h_2^2 + x^2)^{3/2}} \right)$$

where J is the magnetization, S is the area of the cylinder's horizontal cross-section, h_1 and h_2 are the vertical distances from the calculation point to the top and bottom of the cylinder, respectively, and x is the horizontal distance from the cylinder's axis.

It was preliminarily established that the distribution of field intensity within the KMA does not match that expected for a source in the shape of a sphere. A similar discrepancy was found for the case of a vertical layer with an unlimited bottom depth [Gershanok et al., 2007], and so on.

Lines of northeastern orientation across the anomaly center were chosen as profiles for deriving information on the anomaly shape. Naturally, when using MAGSAT or CHAMP data, the orientation of those lines differed in geographic coordinates (Fig. 4).

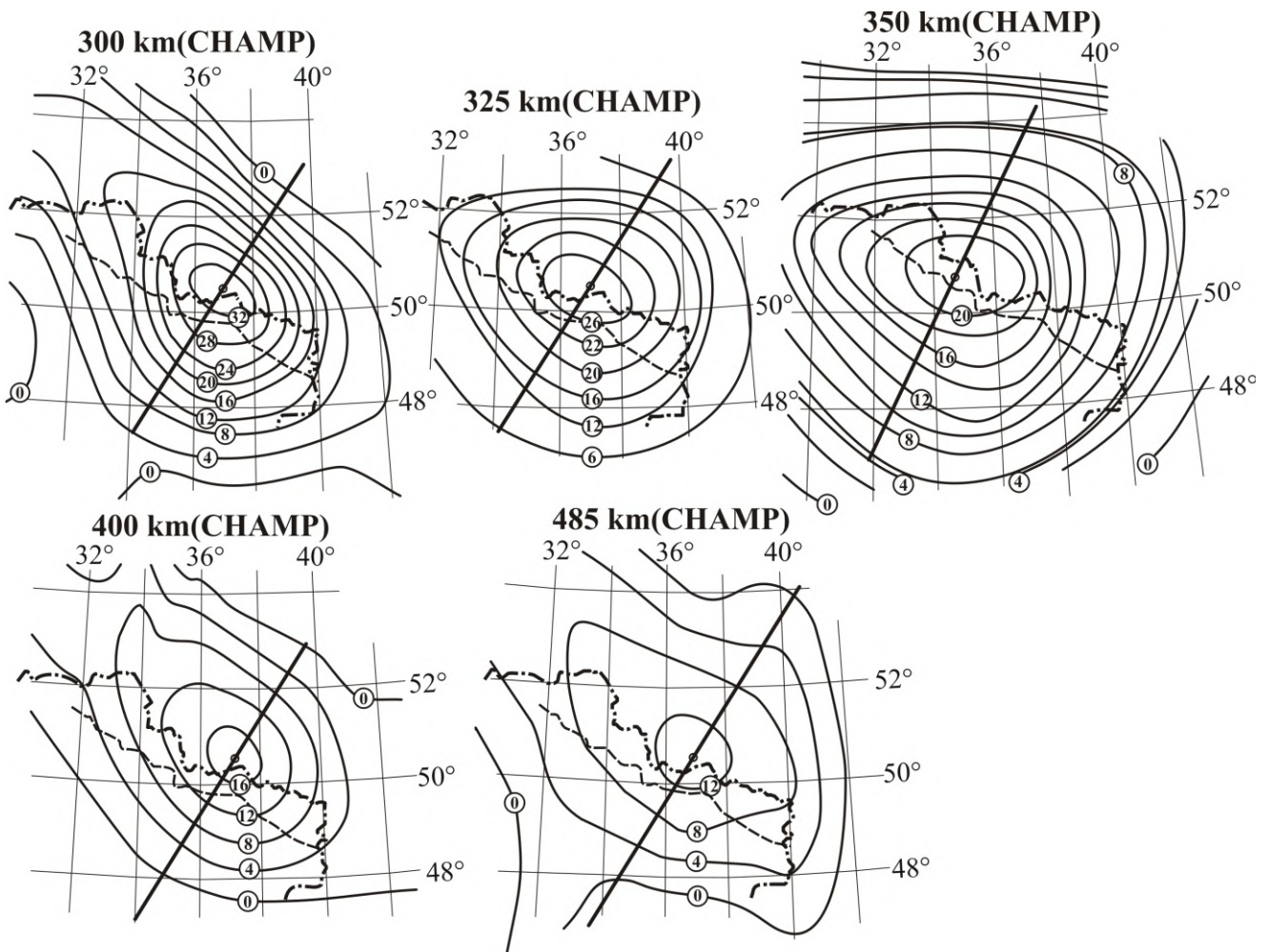


Fig. 4. Intensity isolines for anomalies recorded by satellites at various observation altitudes in nT

It is logical to assume that the anomaly source does not include the territory of the Dnieper-Donets Depression and Donbass, where crustal structure and geological history differ markedly from those of the Voronezh Massif, which is the main location of the anomaly source. It is unlikely that the very thick (over 10 km) sedimentary layer in the basins could contain highly magnetized material. It should, however, be taken into account that when selecting sufficiently deep sources, their boundaries tend to occur at field values equal to about half of the maximum intensity. It is of course not a precise criterion for delineating the area occupied by the anomaly-causing source.

In all anomalies detected by satellites, the distance to such a point from the center is virtually the same (at the level of $50 \pm 7\%$ of maximum intensity). Considering this fact and the location of the anomaly center, we can estimate the anomaly source radius to be about 200 km (Fig. 5).

The depth of the anomaly source can be estimated proceeding from information on the endogene regime in its area. The recent activation of the platform territory might have occurred just there. This was concluded from the data of gravity modeling along the Urals — Black Sea profile, although the accuracy of the results was not too high [Gordienko, 2022]. However, other information regarding the deep-seated process in question is also available for the Voronezh Massif and adjacent Donets Basin (as well as the transitional zone to the Dnieper-Donets Basin). This is exemplified by heat-flow anomalies. They do not necessarily prove the existence of recent activation. On the larger part of the Dnieper-Donets Depression, despite its ubiquitous distribution (beyond the Desna River Basin), the heat flow almost never exceeds values typical for the platform (43 mWt/m^2) for the reason that the heat wave from the lower crust has not yet reached the depth where temperatures were measured.

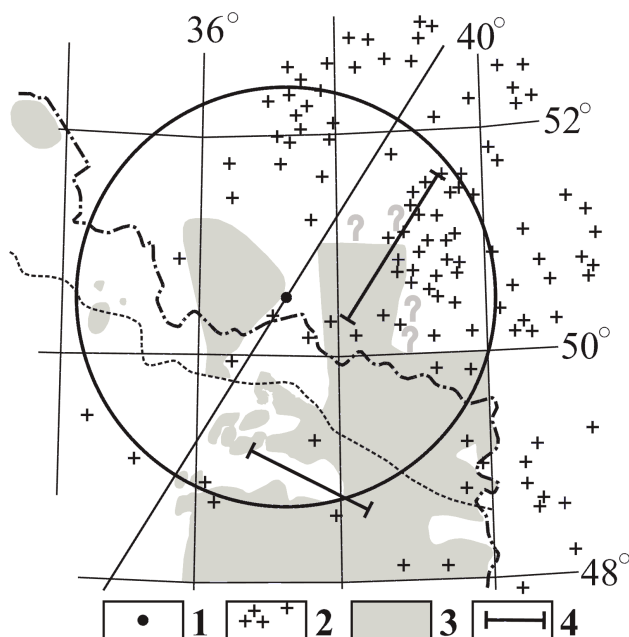


Fig. 5. Evidence pointing to recent activation in the area of the hypothetical KMA source. 1 – outlines of the magnetic anomaly source; 2 – earthquake epicenters; 3 – outlines of zones with elevated heat flow (50–60 mW/m²). The question marks indicate areas in which high heat-flow zones could not be located with certainty due to the absence of relevant data; 4 – segments of deep seismic sounding (DSS) profiles where the velocity inversion zone is observed at depths of about 20–25 km.

It is only in the vicinity of faults bringing hot fluids out of the depth that the heat flow increases sharply. In the event of anomalous heat flow on a vast territory activation is beyond doubt [Varentsov et al., 2013; and so on]. Moreover, quite noticeable seismicity is recorded in the area of the anomaly source and around it [Yefremova et al., 2010; Nikonov, 1999; and others] (Fig. 5). Fig. 5 shows some earthquake epicenters of class 6 and higher at depths ranging from 1 to 5 km. Many of those earthquakes took place over just three years.

Geoelectric data might make a certain contribution to efforts in determining the depth of the magnetized crust bottom [Varentsov et al., 2013; and others]. High electric-conductivity bodies have been detected in the region of recent activation on the Voronezh Massif within the crust and in the upper mantle. They may hold evidence on the state of partial melting in crustal rocks. Some of them are situated at the depth of 20 to 30 km, which conforms to the level established above. This information, however, pertains largely to the territory beyond the area of the hypothetical magnetic anomaly source. Within it, almost exclusively vertical bodies have been detected. It is only in the center and at the northeastern border of the Dnieper-Donets Depression between 34 and 39° eastern latitude that

conductive beds with the top at the depths of 20±8 km were identified [Kovachikova et al., 2016].

Some indications of recent activation could also be observed in velocity cross sections along the deep seismic sounding profiles on the Voronezh Massif (profile **G111**, inversion zone depths ranging from 20 to 30 km) and in the central part of the Donets Basin (Poltava-Lugansk profile, inversion zone depths 15-20 km) [Pavlenkova, 1980, and others]. Further northwest of the Poltava-Lugansk profile, in the central part of the Dnieper-Donets Depression, traces of a discontinuous velocity inversion zone were detected at the depth of 20 km.

A special methodology has already been developed for determining temperatures at crustal depths in zones of recent activation, although it does not resolve all problems [Gordienko et al., 2023; etc.]. Errors in the calculation results depend on the reliability of the data concerning the age of the process. Nevertheless, it can be stated with confidence that in the case under consideration the temperature will reach the Curie point of magnetite at a depth of approximately 25 km. This lower boundary of the source can therefore be used in the calculations.

Calculations and Results

The effect of the source will be compared with the relative change in the anomaly's intensity at different altitudes, measured along the specified profiles and averaged in terms of the data from both slopes of the curve.

First, it is desirable to assess the quality of the experimental material which is compared with the calculated results. This can be done by comparing two anomalies derived from the CHAMP satellite data by different authors using different methods [Abramova et al., 2016; Hemant et al., 2005a] (Fig. 6).

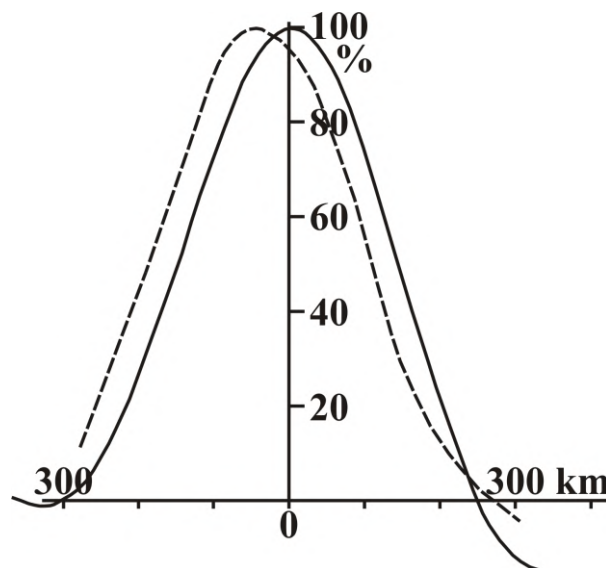


Fig. 6. Comparison of two versions of the distribution of relative values of the anomalous field along the KMA cross-section at an altitude of 400 km (CHAMP).

The average differences amount to approximately 15% of the maximum. According to [Abramova et al., 2016], this points to the virtual identity of the results of satellite data processing. Nevertheless, some discrepancies (suggesting that each method may contain an error of about 10%)

point to limitations of any further operations using such material. A comparison of the calculated source effects (according to the accepted model) with the observed distribution of anomalous Z for various altitudes is shown in Fig. 7.

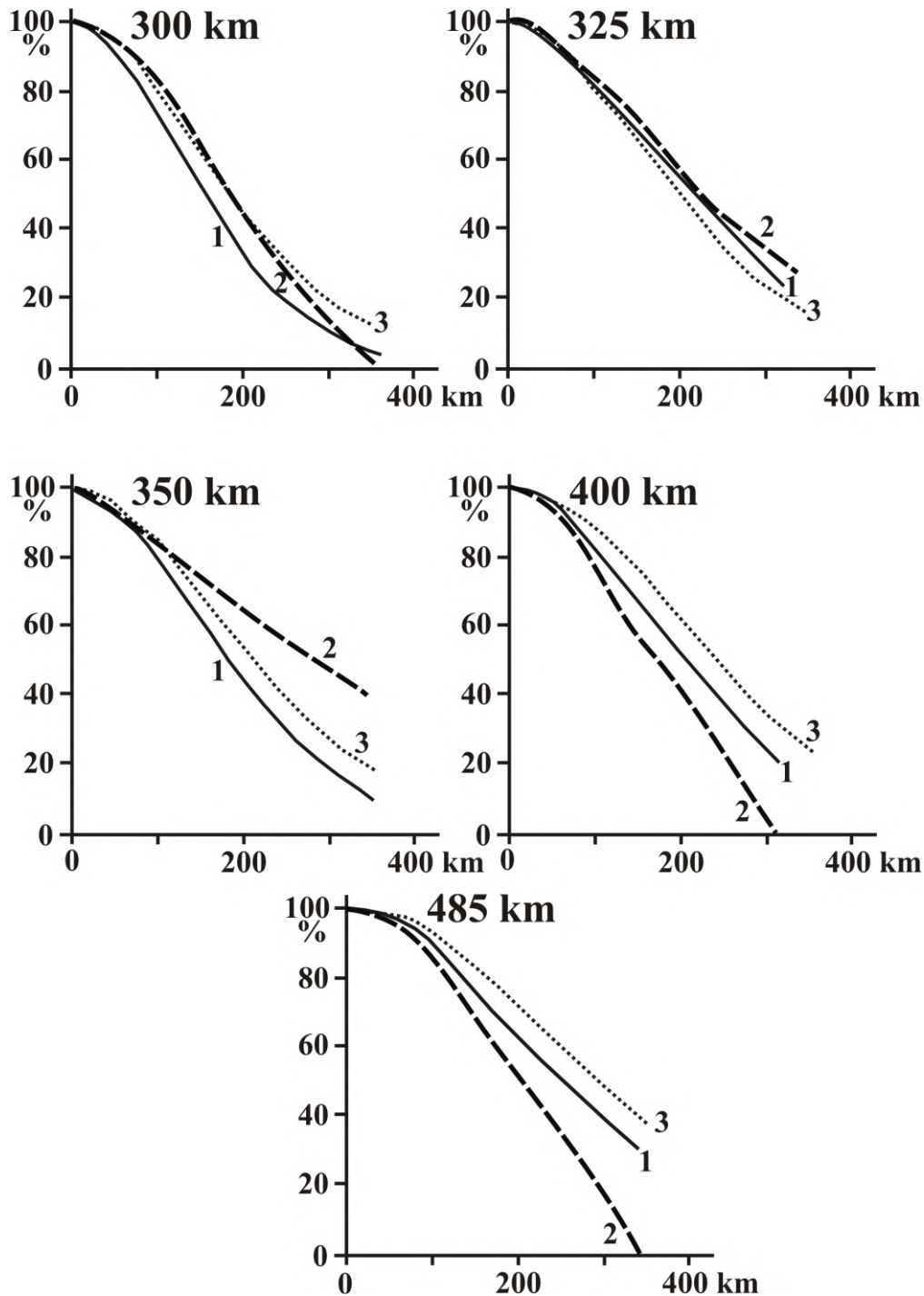


Fig. 7. Calculated (1) and observed (2) relative changes in the KMA anomalous field with distancing from the center for different altitudes of satellites; 3 – calculation results for the anomaly source in the depth range of 50–100 km (see below).

The size of the anomaly source was not used in the calculations. Nevertheless, its edge is located at points where the intensity is $46 \pm 10\%$ of the maximum (see above). On average, the discrepancies between calculated and experimental data are practically equal to the error in constructing the satellite anomaly. It might have been concluded that the hypothetical anomaly source corresponds to the KMA; however, calculation results obtained using other depths for the anomaly source bottom remain unchanged. For the depth of 40 km, they differ by only about 1%. With an alternative hypothesis regarding the anomaly source origin — convective flow in the asthenosphere at depths of 50–100 km beneath the zone of modern activation — the agreement between the curves would remain unchanged (Fig. 8).

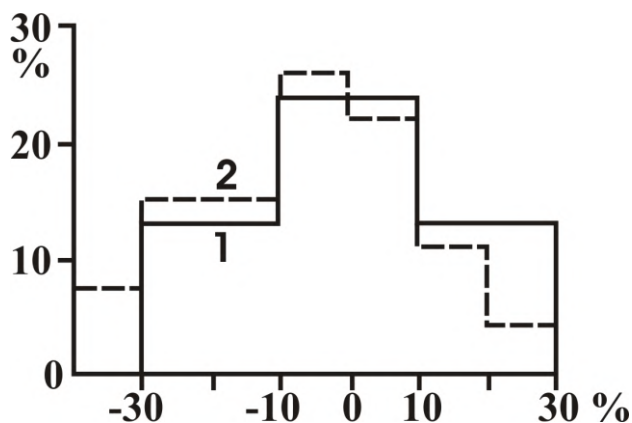


Fig. 8. Histograms showing the distribution of differences between observed anomalies at different altitudes and the calculated anomaly source effects at depths of 0–25 km (1) and 50–100 km (2).

Regions where the asthenosphere is currently observed at depths of 50–100 km are quite widespread (e.g., the Carpathians or the Scythian Plate) but are not accompanied by any significant magnetic anomalies. In other words, the accepted nature of the KMA source, namely, its bottom depth of around 20–25 km, appears to be most likely.

Thus, it must be acknowledged that the method applied here offers very limited possibilities for interpreting satellite anomalies. With the current error in the initial data and the very low sensitivity of the calculated effect to changes in the source parameters, any adjustment does not produce a hard-and-fast result.

However, it is still possible to determine the average magnitude of the anomalous magnetization of the source in terms of maximum Z disturbances at different altitudes (see above). The computed magnetization increases with observation altitude and is, on average, 2 ± 0.3 A/m. In the Dnieper-Donets Depression and Donbass, the upper 10 km of the crust are regionally

nonmagnetic. In the Voronezh massif, at these depths, rocks that form another part of the KMA are located. If the upper 10 km are excluded from the source, the calculated magnetization will increase to 3.5 A/m. It can be noted that such is the magnetization of serpentinized intrusions into the middle and upper crust [Gordienko, 2019]. They occur in large quantities during the modern activation of oceanic plates. Of course, such a model of the KMA source is purely hypothetical.

The data available to the authors do not make it possible to provide a well-founded explanation of the origin of any specific regional magnetization anomaly within the depth interval in question. Further special studies are required to resolve this problem. It must be pointed out that in the case of the Voronezh massif the database for such studies is abundant (unlike in many other areas of the East European Platform). This applies to both geophysical and geological data accumulated over many years of studying this ore-rich mega block of the continental crust.

Conclusions

Formally, the study has achieved its goals. This was, however, only owing to the use of information from other geophysical sources. The point is that calculated anomalies are actually invariable in the wide range of depths of the anomaly source bottom. Moreover, it is possible to coordinate with them parameters of the anomaly source at a completely different depth (and, accordingly, of a different nature). Therefore, there is no doubt that this study should continue, once we obtain more accurate experimental data.

Acknowledgements

The author wishes to express special thanks to Mrs. Rita Schneider for translating this paper from Russian.

References

- Abramova D. Yu., Filippov S. V., Abramova L. M., Varentsov I. M., Lozovsky I. N.* 2016. Changes in lithospheric magnetic anomalies with altitude (according to the CNAMR satellite data) *Geomagnetizm and Aeronomiya*, v. 56, no. 2, pp. 254–264 (in Russian)
- Baysarovich M. M., Mitropolsky O. Yu., Chuprina Sh. S.* 2002. Atlas. Depth structure of the lithosphere and ecogeology of Ukraine. Kyiv; *IGS NASU*. 38 p. (in Russian)

Comets like probes of the solar wind Magnetospheres and cometospheres

Giovanni Pietro Gregori¹, Bruce Allen Leybourne²

¹IDASC-Istituto di Acustica e Sensoristica O. M. Corbino (CNR), Roma, now merged into IMM-Istituto per la Microelettronica e Microsistemi (CNR); and ISSO-International Seismic Safety Organization, Italy, at present retired.

²GeoPlasma Research Institute-(GeoPlasmaResearchInstitute.org), Aurora, CO, USA

Corresponding Author: G. P. Gregori, IDASC-Istituto di Acustica e Sensoristica O. M. Corbino (CNR), Roma, now merged into IMM-Istituto per la Microelettronica e Microsistemi (CNR);
Email: giovannipgregori38@gmail.com

Abstract: A myriad of comets cross the Solar System from its outer fringes through some very short heliocentric distance. If we afford to calibrate cometary morphology, comets are a unique natural probe for an efficient 3D monitoring inside the entire Solar System. This is the target of the present paper. A comet is a dirty ball of ice, evaporating due to solar radiation. The evaporated matter is ionized, i.e., it is a plasma that generates a magnetic field. The interaction with the solar wind develops a magnetosphere that, for brevity, can be called cometosphere. A cometosphere is a miniature model of the Earth's magnetosphere. Therefore, we must understand the physics of the processes that occur in the Earth's magnetosphere. On the other hand, the present generally agreed model of the Earth's magnetosphere largely relies on observational inputs, even though the concern is often forgotten about understanding the physics that explains some crucial details. Therefore, there is need to begin and discuss some features of the Earth's magnetosphere. In particular, refer to the explanation of the formation of the neutral sheet, to reconnection of magnetic field lines, to the plasma mantle, to convection in the magnetosphere, to the role of the "vertical" component of the interplanetary magnetic field, etc. All these items must be clearly assessed and discussed - sometimes paradoxically - before dealing with the discussion of cometospheres. The second part of the present paper specifically addresses the processes that control the morphology of comets, depending on their distance from the Sun. Some key observational checks are envisaged that help to assess what morphological features of comets look comparatively more significant for monitoring the solar wind parameters and their variation vs. heliocentric distance. Some concrete case histories are critically considered in detail. A first draft of the present paper was written in 1974 - and it received quite a positive private feedback by a few authoritative scientists. However, the entire topic seemed excessively speculative. New observations became later available, and at present a better observational database permits to exploit a more significant discussion.

Keywords: solar wind and heliospheric neutral sheet (*HNS*) - Cowling dynamo - origin of the magnetic field of celestial objects - magnetosphere of planetary objects - comet tail - filaments, streamers, knots, kinks, puffs, "forelocks" - coma size - double-lobe tail and "*black axis*" - sungrazing comets - an independent check of comet's parameters

1. Introduction

Comets are natural probes for monitoring several features through the extended range of the Solar System. Comets are characterized by clouds of plasma; hence, they develop features that resemble a magnetosphere. Hence, we can talk about a cometary magnetosphere, or shortly a "*cometosphere*". The concern is about discussing the physical mechanisms that permit correlation of cometary morphologies with

some parameters of the environment that they cross.

On the other hand, the discussion was quite fashionable until a few decades ago concerning the magnetosphere of the Earth and of other large planetary objects. Conversely, at present, the morphology of a magnetosphere is taken for granted, based on a large amount of observational data, even though the interpretation of the physical features is eventually incomplete. Therefore, if one wants to discuss the physics of a cometosphere one must first discuss some

presently less fashionable aspects of the magnetosphere, both of the Earth and of other large planetary objects.

The first target of the present paper is to present a physical explanation of several well-known, even though generally unexplained, features of a magnetosphere. The present discussion will not deal with items that are already extensively reported in the literature. In contrast, some innovative concepts and analysis are here illustrated - and the reader is asked to forgive while dealing with magnetospheric phenomena in a sometimes unconventional way. These items are strictly necessary for a physical discussion of cometospheres. In addition, the reader must refer to several physical items that are already reported in recently published papers by the author and coworkers (Gregori, 2002; Gregori et al., 2021, 2025a), and that are not here repeated in detail.

Differently stated, the present paper deals with a revival of some topics that at present are already part of the history of Earth science. However, the focus is here on some still essentially unexplained issues - and sometimes misconceptions. Indeed comets certainly display features that can be indicative of the state of the solar wind, but the key issue is to implement a suitable calibration.

The plan of the present paper begins with a few key issues dealing with sunspot cycle and with the solar wind. The next topic is the origin of the magnetic field B of celestial objects.

The next topic is a potpourri of several items dealing with the Earth's magnetosphere. The focus is on some well-known morphological features that - however - are often unexplained by the present generally agreed models. Some basic misconceptions are highlighted and contended - as these items are fundamental for a correct understanding of the cometosphere. Then, the magnetospheres of large planetary objects are briefly discussed, as a premise for the key topic of the present paper, i.e., the magnetosphere of small planetary objects with particular emphasis on comets.

Comets are considered according to different case histories, and to different observed morphological features. Specific checks are proposed concerning linear trends between peculiar observational parameters. The linear trends must be observed if the approximations and discussion is correct that are to be exploited. Comets are discussed according to the following items:

- 1) a rationale for physical interpretation
- 2) large-scale possible evidence, a double-lobe tail, and filamentary patterns
- 3) sungrazing comets
- 4) quantitative dependence of the size of the coma vs. heliocentric distance
- 5) quantitative dependence of the cross-section of the tail vs. heliocentric distance
- 6) interaction with planetary atmospheres, and some proposed active experiments.

2. Sunspot cycle and solar wind

A likely explanation of the sunspot cycle relies on consideration of the electrostatics of the expansion of the solar corona (Gregori et al., 2025b). In fact, the Sun - like every star - is a huge dynamo, consistently with a former proposal by Larmor.¹ Field lines of the solar magnetic field B keep trapped electrons, and - on much larger gyration radii - also protons and ions. Hence, owing to a different trapping efficiency, the thermal exhalation of the solar corona involves more protons and ions than the more strongly trapped electrons. Thus, the Sun progressively loses positive charge, while its total negative charge increases.

For completeness, we should stress that sometimes it has been stated that electrons escape more easily from the Sun, because they have less mass and more energy, thus making the Sun positively charged. However, in this respect one must clearly distinguish three drivers: gravitational, electromagnetic (e.m.), and thermal.

The strongest driver is certainly thermal, as it derives from the huge thermonuclear energy that is steadily produced inside the Sun. The next driver is e.m., due to the huge solar Larmor's dynamo. Hence, the huge associated solar magnetic field B keeps trapped electrons, much more effectively than protons and positive ions. Protons and positive ions - being captured on larger radius spirals than electrons - can therefore exhale more freely from the Sun, due to the overwhelming role of the thermal driver.

In fact, as stressed below, if the e.m. driver is leading, the Larmor's dynamo should cause a full blocking of the whole solar body. In addition, in principle - with a solar wind of strictly infinite electrical conductivity σ - we should not even see the Sun, due to the total screening by e.m. blocking.

That is, in any case, the gravitational driver is by far the least relevant, or just a negligible, driver. The e.m. driver attempts to block all plasma inside the volume of

¹ Sir Joseph Larmor FRS (1857-1942), Irish physicist and mathematician.

the Sun. This, however, should forbid the energy balance of the Sun, which is a huge thermonuclear stove that must therefore steadily and explosively disrupt the e.m. blocking. By the way, this is the reason of the transient pattern of the observed Sun magnetic field B , because B does not afford to get any regular pattern, being continuously violently disrupted. In summary, the Sun progressively loses positive charge, while total solar negative charge increases. In any case the gravitational driver is certainly negligible, compared to the e.m. driver.

In summary, the Sun steadily acquires a total negative charge, but the process cannot progress indefinitely. When the total negative charge of the Sun gets above some threshold (depending on the intensity of the solar B), some mechanism must get rid of the electrostatic unbalance. Thus, huge van de Graaff accelerators launch violent electron jets that break through the photosphere. Thus, the photosphere displays dark sunspots. Huge

clouds of electrons precipitate on the Earth and on other planetary objects, causing most spectacular electron auroræ, while a violent perturbation crosses every magnetosphere through the whole Solar System.

The regular expansion of the solar corona generates the solar wind – and in an analogous way every star generates a stellar wind. Key physical features are the filamentary structures, which are observed, e.g., in several splendid *James Webb Space Telescope* images (Fig. 1). Indeed, the physical explanation relies on the Cowling dynamo (Gregori et al., 2025d) that can be briefly illustrated as follows – which also explains the filamentary structures that are a leading feature in comets (better details are given in Gregori et al., 2025d, even though we cannot repeat here the extensive discussion; only some mentions are given below).



Fig. 1. "NASA's James Webb Space Telescope dissected the Crab Nebula's structure, aiding astronomers as they continue to evaluate leading theories about the supernova remnant's origins. (Image credit: NASA, ESA, CSA, STScI, Tea Temim - Princeton University)." Figure and captions after Kuthunur (2024). NASA free copyright policy.

The Cowling dynamo (the reader *must* refer to Gregori et al., 2025d, and references therein) is a universal mechanism that holds all over through the whole universe, on every scale size – much like a universal rigorous theorem, almost like the Pythagoras theorem. The Cowling dynamo derives from a rigorous proof of the old-fashioned - and formerly unsolved - classical Cowling theorem, which since the 1930s is a nightmare for solar physicists and astrophysicists. The *rigorous* generalized Cowling dynamo claims that, under very general conditions, every system of charged particles with an

internal dynamics - such as, e.g., a convection cell - is an effective dynamo that, in general, can display only either one of the two patterns shown in Fig. 2. Fig. 2a has poloidal magnetic field B and toroidal electric field E , while Fig. 2b has poloidal E and toroidal B . The theorem states that the case of Fig. 2a is *unstable*, hence never observed, while the case of Fig. 2b is *stable*. However, the argument shows that, in the case of ideal cylindrical symmetry, the stable case of Fig. 2b has null energy - hence, this particular last statement is in close agreement with the old-fashioned classical Cowling theorem.

The Cowling dynamo applies to several natural systems, on every scale size (Gregori and Leybourne, 2025e; Gregori et al., 2025f, 2025g), from small-scale phenomena - such as fog, atmospheric precipitation, ball lightning (*BLs*), sparks and lightning - through other specific effects, such as runaway breakdown (*RB*), terrestrial gamma flashes (*TGFs*) and the Gurevich and Karashtin (*GK*) effect, up to larger scale-size phenomena including clouds and the electrostatics of the ionosphere, transient luminous events (*TLEs*), Birkeland currents (i.e., field aligned currents or *FACs*, inside the magnetosphere), stellar wind collimation, and even alignments of stellar, galactic, and galactic superclusters. In addition, inside the deep Earth, the same process is responsible for the shrinking and collimation of sea-urchin spikes (see below).

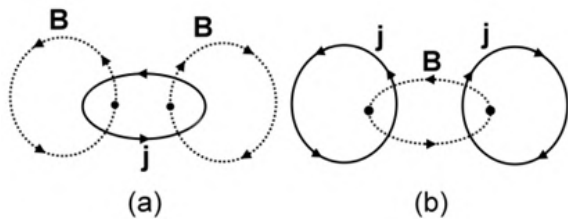


Fig. 2. Idealized scheme of every most general dynamo composed of charge matter with some internal dynamics. Only two configurations are possible. Case (a) has a mere poloidal B and toroidal j or E . Case (b) has a mere toroidal B and poloidal j or E . The generalized Cowling theorem states that case (a) is unstable while case (b) is stable. In addition, it is shown that, in either case, the perfect cylindrical symmetric configuration attains the maximum possible dynamo performance, even though the total energy of the stable dynamo of case (b) is null, and this is in agreement with the classical Cowling's theorem. In contrast, with no cylindrical symmetry the energy for case (b) is not null. For instance, no cylindrical symmetry occurs when the axis of symmetry of figure (b) is not the same as the rotation axis of the system. After Gregori (2002), also in Gregori et al. (2025d), with kind permission of the late Wilfried Schröder.

Concerning the solar wind (see Gregori et al., 2025g), consider a flow of an ionized fluid. Owing to local thermal heterogeneities, the fluid contains some small convection cells. Owing to the Cowling dynamo, these heterogeneities are responsible for an extra amount of self-confinement - due to toroidal B - which is not explained by standard magneto hydro-dynamic (*MHD*) models of the solar corona expansion. When the electrical conductivity σ of the solar wind is supposed infinite, one gets the classical Alfvén's "frozen in" concept. In fact, inside the solar wind, in general the kinetic energy always overwhelms the magnetic field energy. Hence, the

magnetic field B is dominated by the kinetic energy. Therefore, in a "frozen in" state, there is no need for Cowling dynamo, because the confinement is total - much like when the convection cell becomes a zero-radius cell.

The same effect of alignment due to the Cowling dynamo is operative, and explains the deadly *TGFs*, the filamentary patterns of Fig. 1, the stellar alignments inside galaxies, and the analogous impressive alignments of galaxies inside galactic superclusters.

For the time being, let us begin and consider the case of solar wind with infinite σ . The classical Alfvén's "frozen in" theorem is related to the concept of "mirror" (see Gregori et al., 2022d for better details). In fact, the abstract idea of "mirror" implies (i) an ideal infinitely thin surface, and (ii) an ideal "reflecting" surface. That is, we arbitrarily claim that a natural system behaves like a "mirror" when it reflects something much like according to the intuitive reflection law of college-optics.

For instance, refer first to the classical "skin depth" effect. Consider a region D of space, being some kind of "surface" - or more properly of a layer of physical thickness $k \neq 0$, i.e., D is a layer of any shape, which is not necessarily planar. This layer D has an "external" and an "internal" side, and is composed of material with a given mean σ . Consider a planar and homogenous e.m. wave impinging on D from "outside". Owing to e.m. induction, some electrical currents j are generated inside D . The impinging e.m. signal, while penetrating deeper through the medium of D , is damped off, according to an exponential law characterized by the "skin depth" of penetration, which is a function of the frequency ν (i.e., a higher ν has a shallower skin depth). Therefore, the e.m. field monitored by an observer, who is located externally to D , believes that the result looks the same as a reflection occurred by D of the impinging e.m. signal. At last, carry out a limit process, i.e., let $\sigma \rightarrow \infty$ and $k \rightarrow 0$, and in this way - by means of a simple abstraction - one defines an ideal "mirror", having infinitesimal thickness, which mimics the behavior of the system when it is observed from "outside".

As far as the solar wind is concerned, suppose that it can be conceived like an ionized medium with approximately $\sigma \rightarrow \infty$. Owing to Alfvén's theorem, one claims that B is "frozen-in" the solar wind. The physical reason is that the $\sigma \rightarrow \infty$ approximation implies an immediate cancellation - and total screening - of every externally impinging e.m. disturbance. That is, according to the aforementioned "skin depth" lexicon, the "skin depth" is perfectly null - and, in fact, the e.m. state is just "frozen-in" as nothing can change inside it, which is originated by an external impinging perturbation. Therefore, if this property is assumed to hold inside the solar wind at every frequency, we should be completely

forbidden from observing every e.m. emission released from the Sun, including every light ray, or every radio emission, etc. That is, we should not even see the Sun - such as we cannot see its interior, as it is completely screened by the conductive outer layers of the Sun. Differently stated, the Sun would look perfectly dark and invisible to us. That is, according to Alfvén's theorem, the solar wind is speculated to act as a perfect "mirror", i.e., just like an approximately infinitely thin and ubiquitous reflecting surface, although such an approximation does not hold for visible light or for radio waves, etc. Therefore, the solar wind is a perfect mirror, although only when referring to some given frequency band.

A more realistic - and less extreme - abstraction claims that the solar wind is characterized by micro-convection cells, of non-vanishing gyration radii, which are associated to small Cowling dynamos, which operate like effective collimation drivers that can ensure an otherwise unexplained filamentary structure, like in stellar phenomena (Fig. 1). The same phenomenon certainly occurs inside cometary tails.

Before dealing with other items concerning the solar wind, for the time being consider a different scenario, such as inside the magnetosphere, where the B energy density largely overwhelms the kinetic energy density. This typically occurs inside radiation belts. In this case, one considers *FACs*, also called Birkeland currents. Conversely, one cannot talk about *FACs* inside the solar wind, where B is passive and is transported by the solar wind, because the kinetic energy density overwhelms the B energy density. *FACs* precipitate on top of the atmosphere and are composed of spiraling electrons associated with their gyration radii. Here, a new phenomenon happens, due to thermal heterogeneities - on the micro-scale - that determine micro-Cowling dynamos (see Gregori et al., 2025g, 2025u, 2025v). Thus, a large beam of *FACs* splits into several micro-beams. These micro-beams interact one another and finally attain an equilibrium that can be attained only when the cross-sections of the micro-*FACs* are aligned along the edges of an exact polygon, with higher concentration at the vertices of the polygon. Very nice pictures are reported of polygonal patterns observed of polar auroras observed from the *International Space Station (ISS)* (Gregori et al., 2025u).

In addition, the phenomenon is similar to what happens inside the Earth, where sea-urchin spikes interact with one another to determine the exact tetrahedron pattern (Gregori et al. (2021). Thus, the Earth's surface signature is characterized by the planetary distribution of mid-ocean ridges (*MORs*), while the rotation of South America - and the formation of Scotia arc - seem to be originated by the kingpin in the Gulf of Mexico, which is

evidenced by magnetic anomaly maps.

Upon referring to the solar wind, a reminder is needed about two key phenomena: (i) one phenomenon deals with the well-known spiral pattern of the interplanetary magnetic field B_{int} - more frequently called *IMF* - including the heliospheric neutral sheet (*HNS*); (ii) the other phenomena concerns the corpuscular, i.e., discrete, non-continuous, solar wind composition.

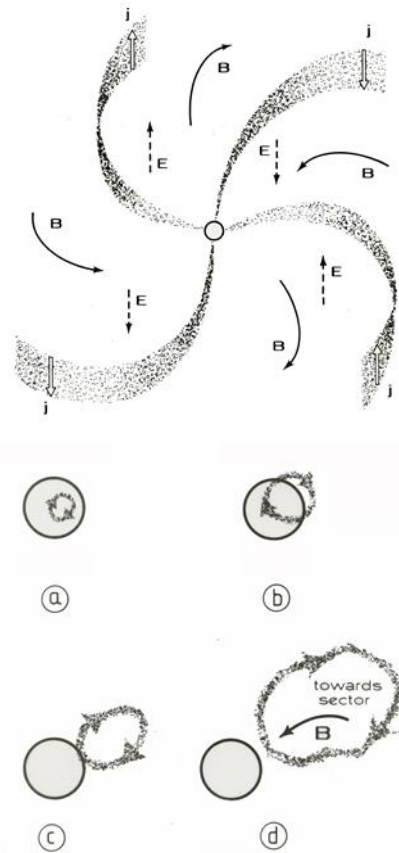


Fig. 3a. (top) 3D pattern of the solar wind observed in the ecliptic plane. The best-known image is the 2D pattern in terms of B_{int} alone. The four-sector pattern eventually collapses into a two-sector pattern. See text. After Fig. 2 of Gregori et al. (2025b). Fig. 3b. (bottom) A loop of currents is transported by the expanding solar corona inside the solar wind, while the geometrical size progressively expands. The case is here shown of a huge j -loop containing a "toward" sector of the well-known spiral pattern (i.e., B_{int} is towards the Sun). See text. After Fig. 3 of Gregori et al. (2025b).

The spiral pattern of B_{int} is well known, even though sometimes - when sunspots seem to coalesce at only one cluster - the better known four-sector structure pattern (in the ecliptic plane, as in Fig. 3, top) shifts to a two-sector pattern (Gregori et al., 2025c; Gregori and Leybourne,

2025c). In this respect, a key phenomenon, which is of concern for cometary investigation, is the pattern of the interplanetary electric field E . The concept can be illustrated by a few figures.

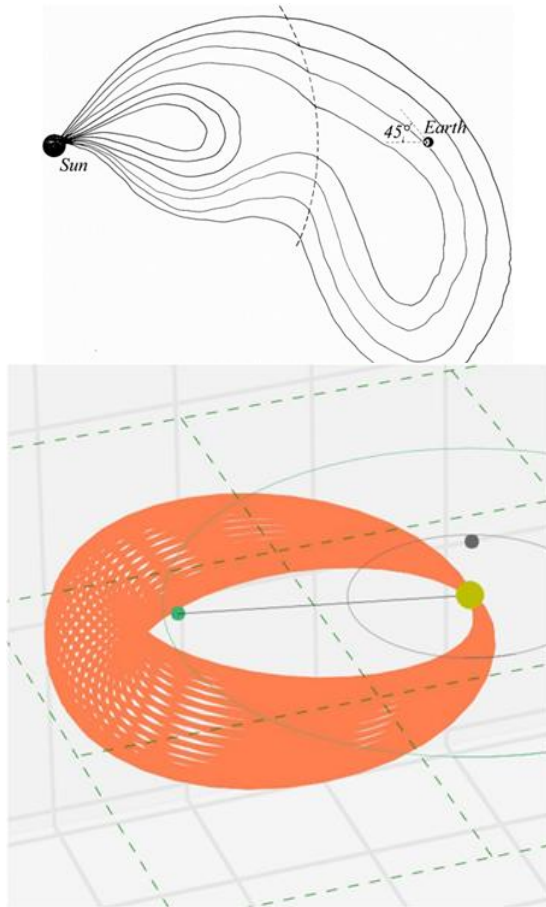


Fig. 4. Some kind of magnetic “tongue” or “ropes” are expelled from the Sun, and are transported by the solar wind, with the “frozen-in” B_{int} . Compared to the ideally simple case histories qualitatively sketched in Fig. 3, the resulting spiral structure of B_{int} field-lines through interplanetary space is very different. The top figure is unpublished. The bottom figure is borrowed after (Möstl et al., 2018), with captions: “3D Coronal ROPE Ejection prototype geometry. The model envelope (orange) consists of a tapered torus that is attached to the Sun at all times. The global shape as well as the cross section are circular. The Sun is shown as a yellow circle (not to scale), and the Earth is shown as a green dot.” Reproduced by kind “Open Access” license, and free copyright policy of AGU.

Fig. 3a shows the presence of intense currents j that are approximately perpendicular to the ecliptic plane. In

reality, one must consider that huge j -loops expand with the solar corona (Fig. 3b), transporting - due to the “frozen-in” field - some features that one can call “tongues” of B_{int} (Fig. 4). In reality, these patterns have a 3D shape (i.e., the “ballerina model” according to Alfvén; Fig. 5). The huge 3D sheet of j -currents is named *HNS*. The literature often reports fanciful 3D patterns of *HNS*, (see, e.g., Fig. 4 of Gregori et al., 2025b). The *HNS* is fundamental for the investigation of the morphology of comets.

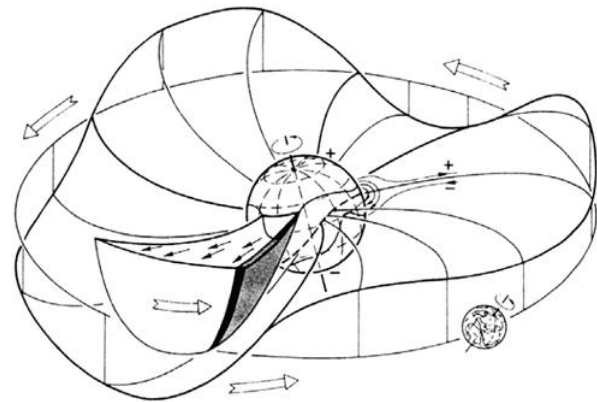


Fig. 5. “The heliosphere around solar activity minimum, in terms of the ‘ballerina’ model as proposed by Alfvén (1957). From Schwenn (1981).” Figure and captions after Schwenn (1988). Reproduced by kind “Public Domain” permission according to ICSUWDS free use policy.

The other key physical item deals with the corpuscular, i.e., discrete composition of the solar wind. According to the most popular model in terms of *MHD*, the solar wind is treated like an ideal fluid, where - whenever needed - the electric charge of every electron - or every proton or other charged particle - can even split into smaller infinitesimal fragments, according to the assumption of “perfect continuity” of the medium. Thus, the solar wind flow is conceived analogously to air flow in a wind tunnel, where, for every air molecules that leaves the tunnel, a new air molecule enters the tunnel on the opposite terminal of the tunnel.

Conversely, the solar wind has a corpuscular structure. Whenever a gap occurs in the availability of particles, the physical system changes composition. Therefore, since $\text{curl } \mathbf{B} \propto \mathbf{j}$, whenever \mathbf{j} is missing, the pattern of \mathbf{B} field-lines must change.

In any case, it has become customary to save the *MHD* formalism, and to claim that \mathbf{B} field-lines are “cut” and “reconnected” with a different geometry (Fig. 6). Such a phenomenon, named “reconnection”, is certainly a violation of Maxwell laws, as it implies that $\text{div } \mathbf{B} \neq 0$.

In any case, this approximation is presently fashionable in the literature.

Note that “reconnection” is a way to describe the discontinuous composition of the solar wind - which is the needed requirement for avoiding the aforementioned argument that paradoxically implies that the perfect “frozen-in” assumption must be associated with a completely invisible Sun.

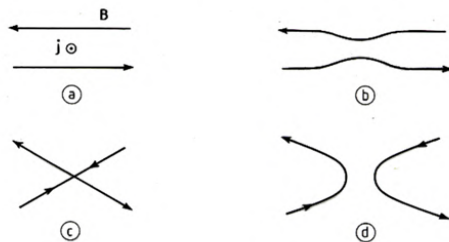


Fig. 6. *Reconnection*. A lack of supply of the current j [figure (a)], associated, e.g., with a “plasma cavity” in the solar wind, compels the system to change its geometry [figure (b)], because $\text{curl } \mathbf{B}$ can no more be sustained by j . On the occasion of some extreme case history, the topology of the \mathbf{B} field-lines can even be drastically changed [figure (c)], eventually evolving into some new pattern [figure (d)]. This process is mathematically described by stating that the former \mathbf{B} field-lines were “cut” and “reconnected”. However, this is a mathematical fiction, because it must always be $\text{div } \mathbf{B} = 0$. Hence, no \mathbf{B} field-line can be “cut” unless one violates the Maxwell laws. After Gregori (1991, 2000, 2001). With kind permission of *SIF*.

Differently stated, the Sun is visible due to the corpuscular structure of the solar wind – because the solar wind reflects the breaking of the e.m. blocking of the Sun. “Reconnection” is also appealed to (see below) for the formation of the neutral sheet of a magnetosphere, or for explaining the “friction” between solar wind and magnetopause, or the formation of “forelocks” of a magnetosphere, or the filamentary structure of comet rails, etc.

For future reference, recall a frequent mistake that - as a standard - is reported almost in every present paper on the Earth magnetosphere. Indeed, the actually measured \mathbf{B}_{int} is *always* observed to lie approximately *in the ecliptic plane* - apart some lesser scatter inside very few degrees. In contrast, following a systematic discussion of all possible speculated directions of \mathbf{B}_{int} - carried out by Dungey² (1961 and 1963) - Dungey proposed the “*open model*” of the Earth’s magnetosphere, which apparently explained several observed phenomena, although it assumed that the measured \mathbf{B}_{int} must be approximately

perpendicular to the ecliptic plane. This incorrect assumption had serious consequences, which still unfortunately bias a large fraction of the literature, as follows:

- The belief – very often reported in several papers - that the inversion of the tiny “vertical” (North/South) component of \mathbf{B}_{int} is crucial in solar-terrestrial relations.
- The formation of a unique “neutral line” crossing the night side of the Earth magnetosphere inside the neutral sheet.
- The assumption of “convection” inside the magnetosphere - i.e., the magnetosphere is conceived like a closed system, with anti-sunward flow of particles along the lobes of the magnetosphere, and earthward flow inside the plasmashet.

These three “beliefs” must be here contended in the following – for application to the discussion of cometspheres. Our criticisms rely on physical arguments that are only briefly outlined here, as these items are now “classical” and well known to everybody who has some confidence with the magnetospheric literature. A more detailed discussion is suited for a monograph on the Earth magnetosphere, and is outside the perspective of the present study on comets.

Indeed, as an unquestionable matter of fact, the actually measured \mathbf{B}_{int} approximately almost exactly always lies in the solar equatorial plane. Hence, the often claimed correlation of phenomena, with a tiny “vertical” component of the observed \mathbf{B}_{int} , generally has a very low correlation coefficient - thus raising a serious concern about the significance of any such a claimed correlation.

In addition, no physical reason requests that the magnetosphere is a closed system. In fact, the flow of particles detected inside the magnetopause is part of the flow of the solar wind, which is perturbed by the presence of the Earth. The particles detected inside the magnetopause are associated to the “forelocks” mentioned below - and mostly they share the same fate of other particles of the expanding solar corona. Hence, no return flow of particles must be expected to occur inside the magnetosphere, and no “convection” can occur inside the Earth’s magnetosphere. The well-known earthward flow of particles in the plasmashet, observed during magnetospheric substorms and geomagnetic storms, is easily explained in a different way. In fact, this concept is better highlighted in the following when dealing with the j -loops in the magnetosphere, and with magnetospheric substorms (see below).

² James Wynne Dungey (1923-2015), British space scientist, of the *Imperial College* in London, who in

1961 pioneered “reconnection” in the Sun–Earth system.

3. The origin of the magnetic field of celestial objects

Different mechanisms can originate the \mathbf{B} of celestial objects. That is, in addition to the obvious case of an iron meteorite, which is a remnant of a disruption of a larger magnetized object, four mechanisms can be envisaged:

- A Larmor dynamo, which correctly applies to stars.
- A tide-driven (*TD*) dynamo that applies to large objects, significantly smaller than stars, and that are composed of unbound components that can move relative to one another due to tidal pull.
- Orbital motion of objects of non-null electric charge.
- Generation of toroidal \mathbf{B} by Cowling dynamo.

3.1. Larmor dynamo

Following the discovery by Hale³ of the \mathbf{B} of the Sun, Larmor (1919a, 1920) envisaged the existence of a dynamo inside every star. The violent endogenous thermonuclear reactions determine a huge dynamics of the strongly ionized medium. At present, this is called an *MHD* process. That is, in this way the thermal energy supplies a strong dynamo process that transforms kinetic energy into e.m. energy. However, it is found that this dynamo unavoidably runs towards full blocking (called Biermann's⁴ blocking). See Gregori (2002). On the other hand, a star is dominated by the primary physical requirement of its thermodynamic energy balance, rather than by the e.m. interaction, which is, rather, a secondary effect.

Therefore, a star must be in a continuous state of steady thermonuclear explosion, just in order to ensure energy balance, and in this way the Biermann's blocking is continuously broken. That is, the Larmor dynamo exists inside a star only as a transient and steadily re-born phenomenon, being continuously disrupted as soon as the \mathbf{B} of the star is generated, because the newly born \mathbf{B} rapidly leads to blocking. Hence, in general, the \mathbf{B} of the Sun - or of a star - can display no "regular" dipole field - as in fact all available observations confirm.

This mechanism is certainly correct when dealing with objects with a huge source of endogenous energy. In contrast, this blocking argument contends the present generally accepted Elsasser⁵-Bullard⁶ dynamo, which relies on the application of the Larmor dynamo also to a planet like the Earth. For clarity purposes, the physical meaning must be specified of the concept of Biermann's

blocking (Gregori, 2002).

Begin and refer to the simple case history of a man-made dynamo that is constructed by engineers for a hydroelectric power -plant. It is well known that, depending on the power absorption by the user network, the operator of the power-plant must modulate the water flux, which is allowed to impinge on the turbines. For instance, the water flow must be reduced during nighttime. The purpose of the operator is to ensure an approximately steady power supply to the network, for balancing in some way the fluctuations of the user absorption.

Suppose that no user network is connected to the dynamo that is powered by the turbine - and suppose that Joule dispersion is negligible inside the circuit where the e.m. induction occurs that produces the dynamo output. Therefore, the induced currents inside the dynamo circuits must continue to increase up to infinity, because no energy-sink whatsoever can exist - while a steady and uninterrupted energy input is supplied to the system. Therefore, the forces always increase vs. time that attract to each other the different dynamo components, because these forces are originated by the ever increasing \mathbf{B} . Ultimately, the result is that all mechanical components of the dynamo must be firmly locked with one another. Hence, no relative movement can occur. The eventual addition of water flux - even with some very large kinetic energy - will be strictly incapable of moving the turbine. This is the Biermann's blocking. The dynamo must unavoidably stop producing additional electric current. The stop will last until some user takes off some electric current from the dynamo circuits, and thus lowers their tremendously large \mathbf{B} .

Differently stated, the dynamo blocking is a state where the magnetic energy density largely overwhelms the available kinetic energy density. A full blocking of the system is caused by the generated \mathbf{B} . Biermann (1941) first envisaged this paradoxical condition in 1941 while studying the cooling of sunspots.

3.2. Tide-driven (*TD*) dynamo

The Elsasser-Bullard dynamo is the application of the Larmor *MHD* dynamo to the case of the Earth, and this is the present fashionable explanation of the Earth's \mathbf{B} . The Biermann's blocking (Gregori, 2002), however, soon stops this kind of dynamo. This drawback applies to every celestial object that lacks a suitable endogenous process

³ George Ellery Hale (1868-1938), American solar astronomer.

⁴ Ludwig Franz Benedikt Biermann (1907-1986) German astronomer.

⁵ Walter Maurice Elsasser (1904-1991) German-born American physicist.

⁶ Sir Edward "Teddy" Crisp Bullard, FRS (1907-1980), British geophysicist.

capable to break the blocking.

The Earth is composed of movable components, such as, e.g., inner core (*IC*), outer core (*OC*), mantle and lithosphere (see, e.g., Fig. 4 of Gregori et al., 2025a). These components are ionized and must move relative to one another due to the different effect by the lunar and solar tide. This is an effective and unbelievably powerful dynamo, driven by tidal interaction. The total energy balance is impressive (see, e.g., Fig. 3 of Gregori et al., 2025a), or better details in Gregori et al., 2021, or in Gregori, 2002). This *TD-dynamo* can justify all geodynamic phenomena, including a tremendous impact on climate change.

It is possible to envisage whether a similar argument can apply to other objects, e.g., in the Solar System. In this respect, a crucial parameter is the size (diameter) of a given object *O* times the local gradient of gravitation, originated either by the Sun or by other objects, or even by other small objects although orbiting somewhere not far from *O*. This criterion is applied to compute Tables 2 and 3 of Gregori et al. (2025a), and the result looks consistent with the present known observational records of the ***B*** of planetary objects.

Note that, in general - when dealing with an intricate planetary system composed of a large number of satellites, such as it typically occurs for the large gaseous outer planets of the Solar System - in general every satellite can have its own endogenous *TD-dynamo*. In addition, whenever the object is electrically charged, the orbital motion of every object can generate a ***B***. That is, the whole planetary system of a large external planet can have a really composite structure of the mechanisms that generate ***B***. See below.

3.3. Orbital motion of objects of non-null electric charge

Since the solar wind has a non-null electrical charge (see above and Gregori et al., 2025b), a planetary object - not to be confused with a single electron or elementary particle - acquires a surface non-null charge. Hence, this object is a source of ***B*** simply deriving either from its orbital motion, or from its spinning - while the resetting of the electrostatic charge of the object occurs with the sunspot cycle, when interplanetary space is crossed by huge electron clouds.

In this respect, a surprising and most impressive case history is represented by the Pluto-Charon binary system, which has 4 rocky mini-satellites, rapidly spinning, hence characterized by a magnetic moment derived from their electric charge and from their rapid spin. Therefore, they mutually repel one another, and are located at a roughly identical reciprocal distance in their respective orbit. In addition, the mutual orientation of their spin axis is

accordingly precisely determined (see Fig. 10 of Gregori et al., 2025b, and for additional more extensive discussion see Gregori, 2016a). No other explanation was ever proposed for this specific morphology of dynamics of these 4 rocky mini-satellite. In fact, the system composed of the binary system Pluto/Charon plus the 4 mini-satellites is a typical set of small objects orbiting around their barycenter, often reported in asteroids or draft planets, and can be called "Pluto effect". The fate of every such a set of small objects is to collapse into a unique celestial object. See Gregori (2016^a) for additional details.

3.4. Generation of toroidal ***B*** by Cowling dynamo

The aforementioned Cowling dynamo process (Gregori et al., 2025d) is ubiquitous and is responsible for some large-scale and most important effects (Gregori and Leybourne, 2025e; Gregori et al., 2025f, 2025g), such as, e.g., in the case of the Earth, for the positive electrostatic charge of the ionosphere. In addition, an anomalous particle precipitation on the atmosphere of every large outer gaseous planet supplies a huge and anomalous convection cell, with a feedback on the solar wind, which is usually correlated with an observed gigantic storm in the atmosphere of that planet (Gregori and Leybourne, 2025c).

A most peculiar effect of the Cowling dynamo, however, deals with the generation of toroidal ***B***, which confines the surrounding plasma, being responsible either for the formation of "forelocks" inside magnetospheres (see below), or for the collimation of the solar wind, or of stellar wind, or for the galactic ***B***, or for the alignment of stars inside galaxies, or of galaxies inside superclusters of galaxies, etc.

4. The Earth's magnetosphere

For future reference, we must briefly mention some phenomena in the Earth's magnetosphere, which are required for the discussion of the magnetospheres of other planetary objects, including the cometspheres. Since the standard magnetospheric literature does not mention these items, a detailed description must be specified.

The present generally accepted model - which relies mostly on observational evidence independent of physical interpretation - is believed to have been first proposed by Walter John Heikkila (1972), a nice gentleman, Professor Emeritus at the *University of Texas* at Dallas, TX., who synthesized the most current beliefs of that time.

Begin with a well-known energy balance argument. As mentioned above, inside the solar wind the kinetic energy density overwhelms the magnetic energy density, hence ***B*** is "frozen-in" the solar wind.

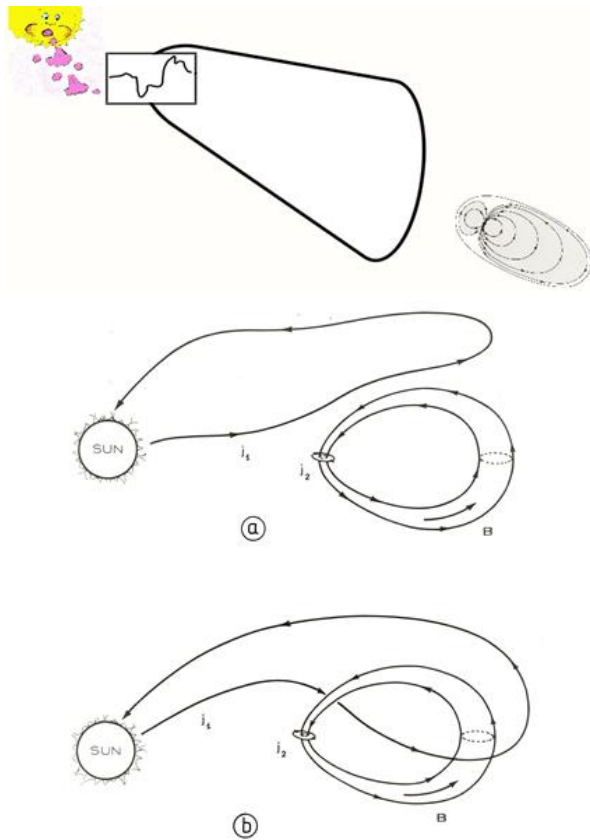


Fig. 7, (top) A j -loop of the solar wind approaches the j -loop that symbolizes the j currents that originate the B of the Earth. The solar wind j -loop contains a j -generator, i.e., a generator of electric current - not of voltage - indicated by the top-left rectangle. Historically, only the gravitational interaction was first considered, and only later also the thermodynamic and e.m. implications. After Gregori (2002). With kind permission of the late Wilfried Schröder. (bottom) The solar wind is here symbolized (with no loss of generality) only by one loop of electric current j_1 and the source of the Earth B only by one loop j_2 . Within a "drop" magnetosphere [Figure (a)] j_1 flows all outside the magnetopause and it links no flux Φ_2 of the magnetic field B_2 generated by j_2 . However, whenever some physical cause makes j_1 link as much Φ_2 as possible, such as it occurs in Figure (b), the Hamilton's principle states that - by this and only by this - stable equilibrium can be attained. Thus, (a) and (b) can be considered as physically possible and meaningful states of equilibrium, although (a) is unstable, while (b) is stable. After Gregori (1991, 1998, 1999a), also after Fig. 1 of Gregori et al. (2025e). With kind permission of SIF.

In contrast, close to the Earth the magnetic energy density overwhelms the kinetic energy density of particles, which are therefore trapped and form the radiation belts. The argument is classical. The region where the two kinds of energy density approximately balance each other is called "magnetopause". This is emblematically represented by a closed surface and is the basic rationale for defining the "drop-model" magnetosphere (Fig. 7, left panel). See additional details also in Gregori (1999).

It must be stressed that this concept should not consider the magnetosphere as a closed volume in space, separated from the interplanetary environment. In fact, several phenomena occur that cross the magnetopause where the corpuscular nature of the solar wind plays a crucial role - related to an intricate set of phenomena named in different ways, and observed by space probes by means of different sensors (see below).

Space probes later discovered the "neutral sheet", and - at present - the literature generally refers to the aforementioned Heikkila model of the magnetosphere, which relies on an interpolation of the several available observations - while, however, no real physical justification is given for the formation of the neutral sheet. In fact, the unique explanation seems to be illustrated by the cartoon of Fig. 7. In fact, if the solar wind is a "continuous" flow of particles, no change can occur of the topology of the B field lines - which are eventually only deformed, while the basic topology remains the same. In contrast, whenever a lack of particles occurs in the solar wind - which is generally called "plasma cavity" - the topology of the B field lines changes in Fig. 7 (right panel) from Fig. 7a to Fig. 7b. In the ultimate analysis, the system searches for a minimum energy of the system (Gregori et al., 2025e).

A key concept for the present discussion deals with the Maxwell law $div \mathbf{j} = 0$, by which all currents \mathbf{j} can be expressively imagined, e.g., as a flow of water inside a water-pipe of varying cross-section, whereby a comparably more intense \mathbf{j} corresponds to a smaller cross-section of the pipe, etc. The role of particle gaps (or "plasma cavities") in the solar wind can be intuitively treated as a secondary effect, which causes a perturbation of the main pattern (like an air bubble) of the "water-pipe" analogy.

Another key concept deals with another classical Maxwell's relation (in the non-stationary approximation), i.e., $curl \mathbf{H} = (4\pi/\gamma_0)\mathbf{j}$. Therefore, if we know the

7

⁷ The constant γ_0 refers to the need to refer to every kind of different units. Historically, different systems of units were used. Therefore, when dealing with historical papers, a basic concern is that we must use a

correct interpretation of the information and we must always refer to a correct unit system. This concern is quite intricate and is discussed in detail by Gregori et al. (2025o). No brief mention can be given here.

observed pattern of \mathbf{B} (or \mathbf{H}), we can map the field of \mathbf{j} and thus derive the intricate topological patterns of the \mathbf{j} -loops.

A 3D model, made in the late 1960s, is shown in Fig. 8. It should be stressed that no “exotic” hypothesis was necessary for interpreting this 3D model. These wooden model is roughly one meter long, and during two weeks of trials and suitable reflection, using only pencil and eraser, the *unique possible* results was found that is here explained. In fact, upon a close and detailed analysis, one affords to clearly infer that the whole \mathbf{j} -system is surprisingly composed of three loops (Fig. 9).

One \mathbf{j} -loop, denoted by J_1 , is shown in the bottom



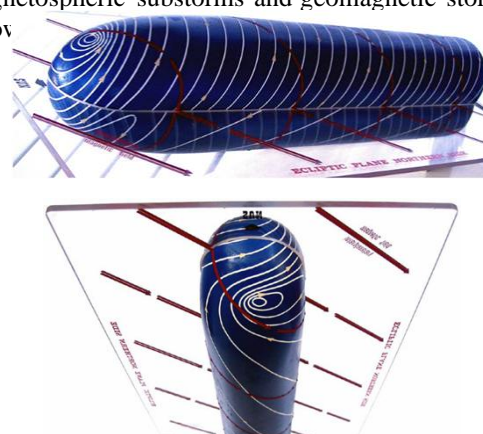
Fig. 8. 3D model of the Earth’s magnetosphere (not to scale), aimed to investigate the topology of \mathbf{j} currents, in the case of an “away” sector of \mathbf{B}_{int} . The two top photographs show the model observed from the Northern side, while the lower right photograph shows the model seen from the Southern side and the lower left photograph from the Eastern side. The \mathbf{B}_{int} field lines are shown by red arrows, which are tracked on a plastic transparent slab that represents the ecliptic plane. Note the substantial asymmetry between the Northern and Southern lobes of the magnetosphere. See text. Unpublished figure.

A third \mathbf{j} -loop, partially shown in the top panel of Fig. 9 by a red arrow, has a curious and certainly unexpected character of “trapped” radiation, which is shown by the bottom panel of Fig. 9. It must be pointed out that only two, *not* three, \mathbf{j} -loops are shown the bottom panel of Fig. 9. One \mathbf{j} -loop, denoted by a black circuit, has a unique winding around both lobes of the magnetosphere. The other \mathbf{j} -loop, shown by grey arrow, winds twice each lobe of the magnetosphere, while crossing the neutral sheet once earthward and once tailward, with respect to the crossing of the black \mathbf{j} -loop. That is, these are closed tracks, almost like curious trapping orbits for electrons, protons and ions.

Note that the anti-sunward flow of \mathbf{j} -currents

Reference to Gregori et al. (2025o) must be made also when dealing with other formulas mentioned below.

panel of Fig. 9 by a green arrow. It flows away from the Sun, and – when seen from the side of the Sun – it confines the Northern lobe of the magnetosphere by a clockwise current. Since the solar wind - in normal conditions - has a prevalence of positive charges, this loop is normally mainly composed of protons and He ions. Symmetrically, a similar \mathbf{j} -loop, denoted by J_2 , shown in the top panel of Fig. 9 by a blue arrow, must envelop the Southern lobe by a clockwise current – when seen from the side of the Sun – although the current must flow towards the Sun. This loop is dominating when intense clouds of electrons are ejected from the Sun. Therefore, this loop is typically much intensified during magnetospheric substorms and geomagnetic storms (see below



determines the formation of the *neutral sheet*, according to the energy rationale expressed by Fig. 7. Differently stated the natural system looks for the minimum energy of the system, consistently with a general variation principle (Gregori et al., 2025e).

Consider what happens when the Earth’s magnetosphere crosses through the *HNS*. The tail of the magnetosphere is directed in the radial direction away from the Sun. In contrast, the \mathbf{B}_{int} spiral structure is bent, approximately (at 1 AU) by $\sim 45^\circ$ with respect to the sunward direction, and the *HNS* contains \mathbf{j} -currents that, almost like a blade, impinge on the Earth’s magnetosphere. The Earth moves comparably slower along its orbit around the Sun, while the spiral pattern of

As far as the present application is concerned, the reader – if he likes - can put $\gamma_0 = 1$.

B_{int} rotates with a period of the order of ~ 27 days. The HNS j -currents merge with the magnetospheric J_1 and J_2 loops, and progressively - although “quietly” and regularly - reverse the asymmetry between the j -loops that twist around the two lobes of the magnetosphere.

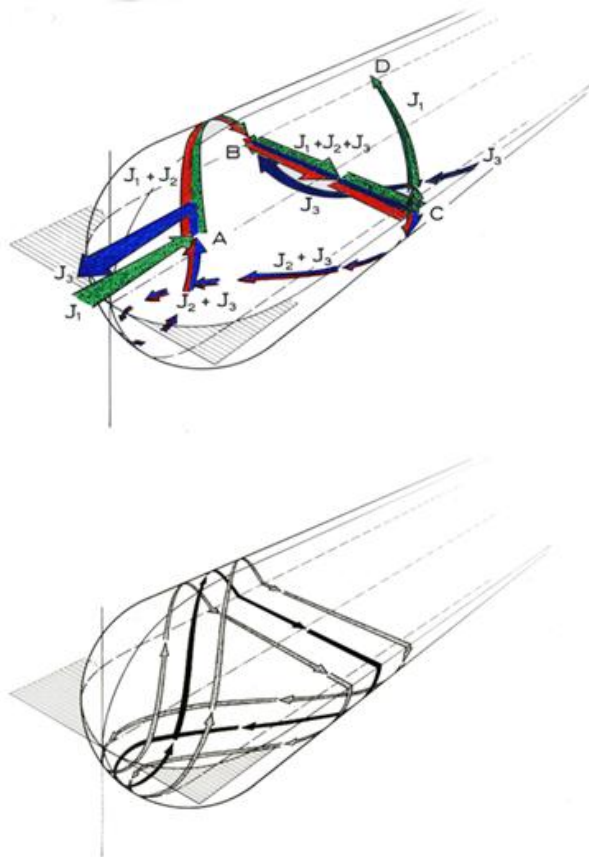


Fig. 9. (top) The whole j -system is composed of three loops. One j -loop, denoted by J_1 , is shown by a green arrow. It flows away from the Sun, and - when seen from the side of the Sun - it confines the Northern lobe of the magnetosphere by a clockwise current. A similar j -loop, denoted by J_2 , shown by a blue arrow, confines the Southern lobe of the magnetosphere by a clockwise current - when seen from the side of the Sun - although the current flows towards the Sun. A third j -loop, partially shown by a red arrow, has a curious and unexpected character of “trapped” radiation. This third j -loop is shown in more complete detail by the bottom panel, where we stress that only two, not three, j -loops are shown. One j -loop, denoted by a black circuit, has a unique winding around both lobes of the magnetosphere. The other j -loop, shown by grey arrows, winds up twice each lobe of the magnetosphere, crossing the neutral sheet once earthward and once tailward with respect to the crossing of the black j -loop. There is one unique loop like the black circuit, and an infinite number of loops similar to the grey arrows circuit. See text for better details. Unpublished figure.

Now, we must consider what happens whenever a small or large amount of particles is missing in the solar wind flow. The magnetospheric J_1 and J_2 loops abruptly experience an either small or large “plasma cavity”. The relation $curl \mathbf{H} = (4\pi/\gamma_0)\mathbf{j}$ requests a change of topology due to a lack of j supply.

Consider the aforementioned intuitive water-pipe model - and imagine that an air-bubble propagates along the water-pipes that represent the J_1 and J_2 j -loops. The physical system is substantially changed. It is formally claimed that “reconnection” occurs wherever the air-bubble is located. In terms of a variational principle (Gregori et al., 2025e), the system attempts to obviate to the missing particle supply by the solar wind, and it appeals to all available particles from other sources.

The result is that particles available downstream are accelerated both earthward and downstream in the neutral sheet. The result is the observed *plasmashet*, which is a layer a few R_E (Earth’s radii) thick with earthward flowing particles that are observed - like an almost permanent feature - to flow around the neutral sheet. It should be stressed that this argument shows that, in contrast with the aforementioned present general belief, no “convection” occurs in the magnetosphere.

It is reasonable to enquire how far the flow of particles in the plasmashet can penetrate earthward. In fact, one must refer to a balance between the kinetic energy density of the particle flow in the plasmashet, and the magnetic energy density of the geomagnetic field. That is, the argument is identical to the aforementioned definition of the magnetopause (Fig. 7), although it is now applied in 2D in the approximate plane of the plasmashet, rather than in 3D. Differently stated, just consider the formal balance between the kinetic energy density of the particle flow in the plasmashet - which is intensified during magnetospheric substorms and geomagnetic storm (see below) - and the magnetic pressure of the geomagnetic field, i.e., with the energy density of the geomagnetic field. In terms of simple direct geometrical arguments, the result is of two types, illustrated in the cartoon of Fig. 10.

When the plasma cavity is substantially more intense, the earthward flow of particles in the plasmashet becomes more relevant - because the aforementioned “reconnection” process along the tail persists for a longer time. Note that the anomalous flow of particles in the plasmashet occurs both earthward and downward, even though - on the Earth - we detect the effect of the earthward plasma flow. Thus, as far as the effect is concerned that is observed from the Earth, polar auroras display the typical morphology that Syun-Ichi Akasofu (1964) named “auroral substorm”, to be later interpreted (Akasofu, 1968, 1977) like a facet of a more general

magnetospheric substorm.⁸

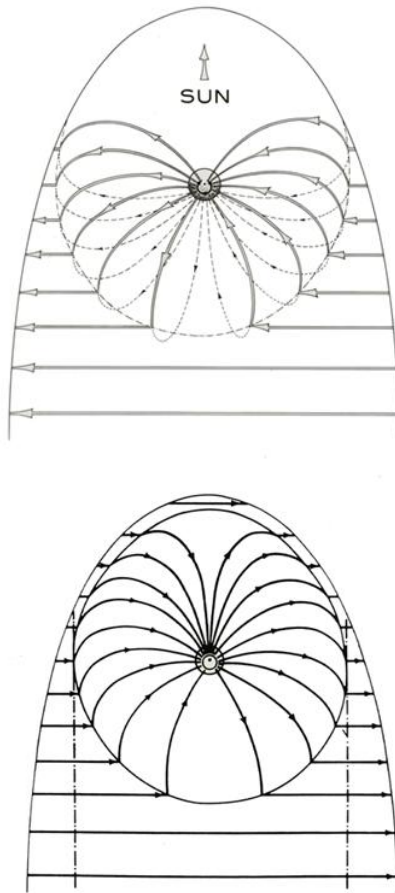


Fig. 10. Earthward termination of the earthward influx of particles in the plasmashield. The top figure (out of scale) shows the typical standard morphology observed in the case of the Earth. However, when the pressure by the particle inflow in the plasmashield is more intense, the earthward termination of the plasmashield affords to surround the Earth, even on the noon side. Indeed, this pattern is the standard observed in the case of the Jupiter magnetosphere, where this is called “magnetodisk”. See text for details. Unpublished figure.

The observed typical duration of an auroral substorm is $\sim 2 - 3$ hours. This entire phenomenon is consistent

with the propagation downstream of a plasma cavity at the mean speed of the solar wind ($\sim 400 \text{ km sec}^{-1}$), along the tail of the magnetosphere (that has a typical length of the order of $\sim 1,000 R_E$), and this corresponds to an earthward flow in the plasmashield lasting ~ 4.4 hours. It must be stressed that, before the onset of the substorm, the magnetic energy density is responsible for the balance between internal and external pressure across the magnetopause along the tail. When the electric currents of the magnetospheric system (as per Fig. 9) fade off due to the plasma cavity, the magnetosphere squeezes the tail, almost like a toothpaste tube, for using the particles available in the plasmashield in order to compensate the lack of internal magnetic pressure.

However, as a standard, a large plasma cavity in the solar wind typically persists much longer than a few hours. Hence, according to what can be detected by an observer located on the Earth, a magnetospheric substorm exhausts when the plasma cavity (or the “air-bubble” in the water-pipe) gets out of the last fringes of the magnetospheric tail. Therefore, the particle supply should exhaust, which is manifested by the earthward flow of particles in the plasmashield. However, if the plasma cavity still persists inside the solar wind, a new substorm starts. This, indeed, is what is observed. In fact, several substorms are triggered in sequence, while a new substorm eventually starts when the previous substorm is not over. This peculiar behavior depends on the irregularity of the composition of the impinging plasma cavity within the solar wind. Summarizing, a sequence of several substorms represents altogether the well-known classical phenomenon named “geomagnetic storm”, with a typical duration of a few days.

According to what seems available in the literature, this is the *unique available physical* explanation for the occurrence of substorms and of geomagnetic storms. As a curiosity, the typical morphology - depicted by the recorded horizontal component H of the observed geomagnetic field - has the reversed shape of a lognormal distribution (Campbell, 1996), consistently with the requirement of statistics, whereby the occurrence of an event is proportional to the number of already occurring similar events. In fact, this is the logics of every rush-hour

⁸ Syun-Ichi Akasofu (1930-), founding Director of the *International Arctic Research Center of the University of Alaska Fairbanks (UAF)*, served in that position from the center's establishment in 1998 until January 2007. Previously he had been Director of the University's *Geophysical Institute* from 1986. He discovered auroral substorms by exploiting a visual, empirical, analysis of the whole set of all-sky cameras

picture collected during the *International Geophysical Year* (1957-1959). This has been an absolutely impressive achievement, reminding about the old-fashioned Romantic investigations carried out with no computer aids. Professor Syun-Ichi Akasofu will be remembered in the history of Earth sciences for this great and almost unbelievable achievement.

phenomenon (i.e., of the Kapteyn⁹ class distributions; Arley and Buch, 1950, or Paparo and Gregori, 2003). That is, while looking at a geomagnetic storm, the probability of the start of a new substorm is proportional to the number of substorms that are already in progress.

After considering what happens across the neutral sheet - due to either lesser or large plasma cavities in the solar wind - the effect can be considered of all phenomena that occur across the magnetopause. Fig. 11 shows a single case history. Some secondary neutral sheet is developed on the pole. In fact, the missing particles determine “reconnection”, while particles propagate downstream. They twist, due to the internal micro-Cowling dynamos (see Gregori et al., 2025g, 2025u, 2025v), which determine the collimation of the particles that flow downstream at the mean speed of the solar wind. That is, a phenomenon occurs that can be illustrated like a “forelock”¹⁰ of B flux tube.

Differently stated, some *filamentary patterns are permanently observed* inside the magnetopause above both polar caps. This phenomenon is crucial to explain several filamentary patterns that are typical of cometary tails, and of cometspheres. In fact, observations are reported, which are much more extended in space, and in the case of the Earth the result was named “*plasma mantle*”¹¹ as shown in the cartoon of Fig. 12.

A related concept is the so-called *polar wind*, which represents a steady leakage of a tiny fraction of the Earth’s atmosphere, by which some earthly air is lost by an anti-sunward flux of air ions over both polar caps. At present, this topic is classical, and observations are available by which also the solar sunspot cycle dependence is well known. No details are here needed.

A closely related – and generally not well acknowledged – concept deals with the palaeovariations of the total mass of the atmosphere, which is manifested as variations of the *palaeodensity of the atmosphere*. In fact, consider that a depletion of the atmosphere occurs whenever a geomagnetic field reversal (*FR*) occurs. The explanation of a *FR* relies on the principal idea that occasionally the Solar System encounters a dense cloud of interstellar matter, which compresses the heliosphere inside the Earth’s orbit. Thus, the Earth detects a temporary disappearance of the solar wind. Hence, the Earth’ magnetosphere temporarily “disappears”. Following the huge environmental magnetic disorder, the geomagnetic field eventually decays. When the solar wind is reset, the Earth eventually lacks a significant shield by a magnetosphere, and is therefore spoiled by interaction

either with interstellar matter, or with the restored solar wind. The result is a reduction of the Earth’s atmospheric density.

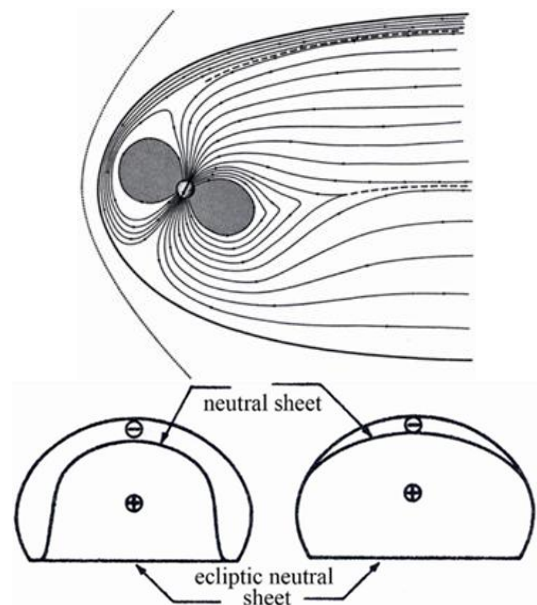


Fig. 11. Noon-midnight meridional cross-section [top panel] and tail cross-section [bottom panel] showing (out of scale) the formation of “forelocks” of B flux tubes caused by missing particles in the solar wind flow. Every “forelock” is collimated by a twisting B due to the toroidal B generated by micro-Cowling dynamos. This phenomenon typically occurs also in cometary tails. See text. This forerunning sketch is loaned after Gregori (1968) with permission by *Annales de Géophysique*, licensed under “Open Access” CC BY 4.0.

Summarizing, when a *FR* occurs – and consider that normally several *FR*s can happen clustered within some comparably “short” time lag - the Earth’s atmosphere is not protected by the magnetospheric shield. Hence, the atmosphere is temporarily spoiled. In any case, it is well-known that the solar wind exploits an effective spoiling action on every planetary object, whenever the object is not shielded by a magnetosphere. During every *FR* the Earth supposedly remained without magnetosphere for some time. The typical duration of a *FR* is estimated to be, maybe, a few thousand years or less, and its progression (i.e., whether the field vanishes and re-grows, or rather it flips) is not yet clear, even though the term “reversal” is a common usage implying a change in orientation or flip of the dipole.

⁹ Jacobus Cornelius Kapteyn (1851–1922), Dutch astronomer.

¹⁰ The term “forelock” is not found in the literature.

¹¹ See, e.g., Paschmann et al. (1976), Philipp and Morfill (1976), [Scopke and Paschmann (1978) and Schwenn (1981).

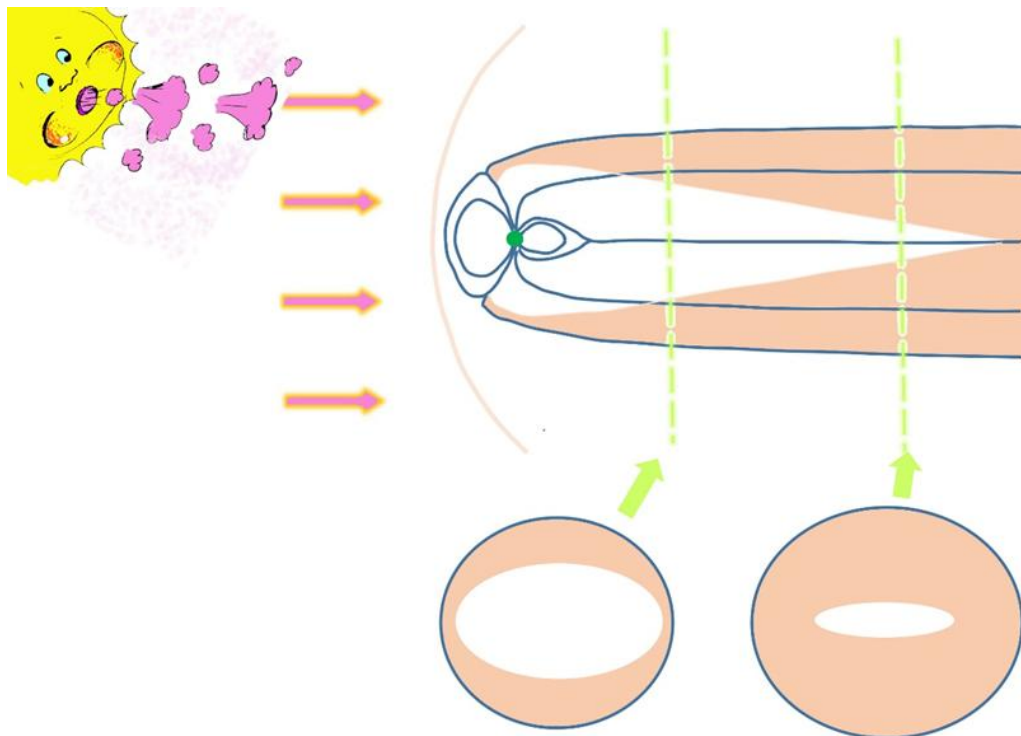


Fig. 12. Rough hand-made sketch showing what is called “*plasma mantle*”, i.e., a region (pink) where some diffuse flux of particles is observed by space probes, resulting from penetration of particles through the magnetopause, or - according to the interpretation here given - being associated with temporary “forelocks” of B flux tubes. A meridional cross-section is shown, with two transversal cross-section along the tail. See text. The sketch is based on an idea after Schulz (1991, p. 157, Fig. 26). Unpublished figure.

On the other hand, during every *FR* an excess production occurs of endogenous energy, through a direct modulation on the efficiency of the *TD*-dynamo. This causes an anomalous excess of soil exhalation.

Therefore, the density of the atmosphere varies depending on the balance between the spoiling action by the solar wind and the opposing increased soil exhalation. In any case, in general it is reasonable to expect that the palæodensity of the Earth’s atmosphere changed in some seemingly erratic - although relevant - way depending on the timing of *FR*s. Furthermore, no reason requires that the palæodensity of the Earth’s atmosphere varied according to any smooth or monotonic trend.

Among a conspicuous literature, recall the important papers by Levenspiel¹² (2000) and Levenspiel et al., (2000). The large flying animals (dinosaurs etc.) had a large Archimedean support by a denser atmosphere, etc. They extinguished when the atmospheric density

decreased. Palæontology gives several interesting suggestive evidences. No additional details are here needed.

In any case, all these inferences support the role of the solar wind in determining the shape of a cometary tail.

Concerning Fig. 8, particle gaps - and the consequent “reconnection” process - involve some temporary, varying, and more or less extended area around both “*singular points*” over both polar caps - which are clearly shown in Fig. 8 being characterized by closed j -loops encircling them. When “reconnection” occurs, direct precipitation of solar wind particles impinges directly over the high polar atmosphere. The term used in the literature for this phenomenon is “*cleft*” that penetrates on the atmosphere, directly from the front side of the magnetosphere.

A typical observed morphological feature is represented by *PCA* (polar cap absorption events)¹³

¹² Octave Levenspiel (1926-2017), Professor of chemical engineering at *Oregon State University (OSU)*.

¹³ Some old reviews are, e.g., Reid (1963), Lassen (1967, 1969) and Hultqvist (1969a).

detected by the abrupt disappearance of the observed radio-signals impinging from a natural celestial source. The disappearance derives from enhanced ionization in the upper atmosphere, whereby the impinging radio-signal is reflected outward by the increased ionization in the ionosphere. Thus, the radio-signals observed at Earth's surface abruptly disappear from radio telescope records.

A related concern is probably associated with noon-side auroræ. In fact, the instant location of polar auroræ is named *auroral oval*, while the statistical, time integrated, distribution of auroral ovals is called *auroral zone*. The

auroral *zone* displays a maximum in the midnight sector, and a secondary maximum in the noon sector, while the appearance of auroræ is comparably less frequent in the sunrise and sunset sectors.

The noon maximum of the auroral zone could be associated, maybe, to the "cleft". However, another possibility is that the earthward penetration of the plasmashet does not stop on the flanks of the magnetosphere. Rather, it penetrates until the noon side, thus forming a temporary "*magnetodisk*" (as shown in Fig. 10, bottom panel). This is shown, e.g., in Fig. 13.

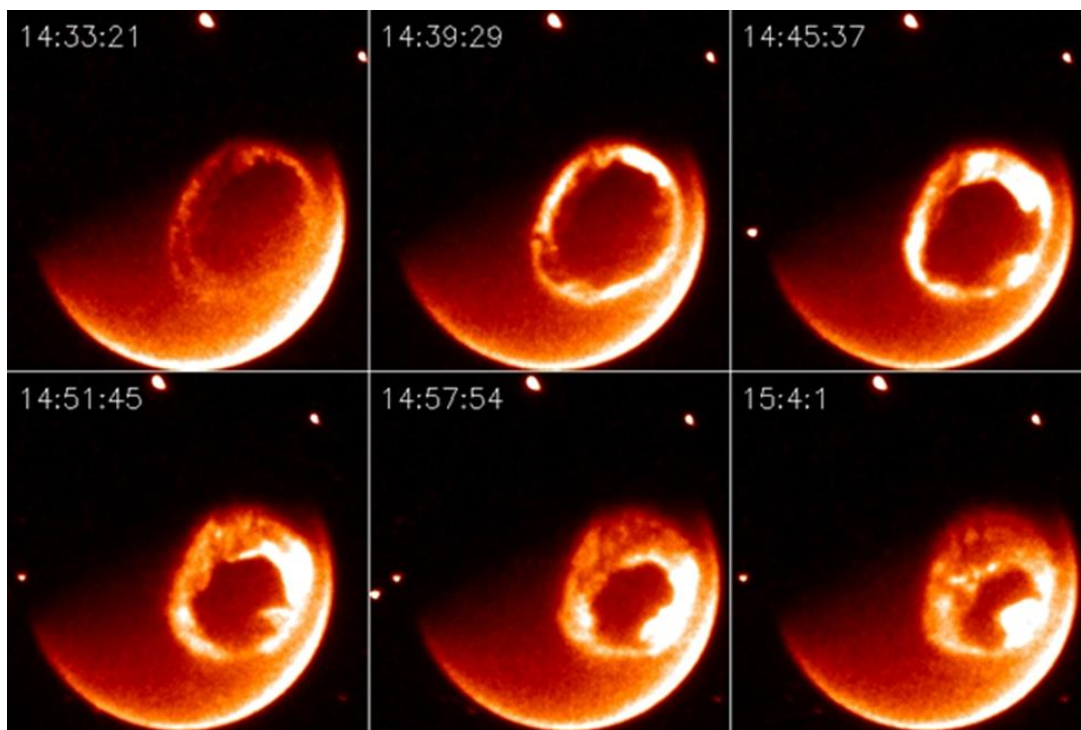


Fig. 13. Auroral substorm observed by the FUV (Far Ultraviolet) photometers on IMAGE (Imager for Magnetopause-to-Aurora Global Exploration). After <http://sprg.ssl.berkeley.edu/imagel>. Credit: NASA. NASA copyright free policy.

A different discussion deals with the so-called " Θ -auroræ", which are directly related to the discussion of the electric field \mathbf{E} inside the magnetosphere (Gregori, 1992, 1998a, 1999a). This item, which is related also to the Svalgaard¹⁴ vortex, to the distinction between the classical DP1 and DP2 systems of \mathbf{j} -currents in the ionosphere – and indirectly also to the aforementioned false concern about the "vertical" component of \mathbf{B}_{int} and to "convection" in the magnetosphere - is not here of concern and is not discussed in detail.

Another item, which is only occasionally considered

in the literature - although in terms of naïve and simple concepts - deals with the energy content in various sub-volumes of the magnetosphere. A much more general and physically significant discussion should request a long devoted paper, and this item is not here considered.

All these additional details are not here discussed, being not relevant for the present discussion, other than for envisaging the intricate nature of phenomena that must be considered when dealing with a cometsphere, which – in several respects - is a miniature model of the Earth's magnetosphere.

¹⁴ Leif Svalgaard, at present at *Stanford University, Departement of Physics*.

5. The magnetosphere of large planetary objects

As mentioned above, one can reasonably expect that several large objects in the Solar System have an internal *TD*-dynamo. This fact is crucial for the generation of a magnetosphere. See Tables 2 and 3 of Gregori et al. (2025a).

In addition, while dealing with several planets that have a large number of satellites, the presence of an electrically non-neutral solar wind (Gregori et al., 2025b) is such that every satellite is electrically charged. Hence, both its orbital motion and its spin generate a **B**. Thus, the magnetosphere of a planet is more correctly associated to an intricate system, which is the sum of the endogenous *TD*-dynamo of the planet and of every satellite, plus the **B** originated by the orbital motion and by the spin of the satellites.

As already mentioned, the Pluto-Charon binary system is a peculiar natural laboratory. The highly eccentric orbit around the Sun (aphelion at 4.931 *AU* and perihelion at 2.9667 *AU*) is such that the *TD*-dynamo mechanisms play a different role depending on the distance from the Sun of the Pluto-Charon system. This implies some mysterious morphological features, such as the presence of H_2O icebergs apparently floating and drifting in a frozen ocean of N_2 . The most obvious explanation is that during some time of the Hadean year – which is equivalent to ~ 248 *Earth years* – the endogenous energy generated by the *TD*-dynamo is such as to melt the N_2 oceans, and the H_2O icebergs can drift. When the endogenous energy – which is released by the *TD*-dynamo – diminishes, the N_2 oceans are frozen and the H_2O icebergs remain as a witness of the previous floating and dynamics.

Another impressive evidence is provided by the aforementioned 4 rocky micro-satellites of the Pluto-Charon binary system (see Fig. 10 of Gregori et al., 2025b, and additional more extensive discussion in Gregori, 2016a). Their location in space, and spin axis orientation, envisage a clear effect that can be explained only by considering that the solar wind is not electrically neutral. Hence, the spinning of the rocky micro-satellite is such that they develop a magnetic moment, by which they interact with one another. To our knowledge, no other explanation was ever proposed for these observed features.

No additional details are given here. However, another mysterious feature is the observation of tectonic and endogenous dynamic activity in some small objects (such as in small asteroids, or dwarf planets, etc.). Their small size is such that they cannot have an internal *TD*-dynamo, neither can one envisage any other energy source. A possible explanation is that these small objects are the

results of a former multi-objects composed of several different small objects orbiting comparably close to each other. A system of this kind is expected to generate a temporary and significant *TD*-dynamo also inside every small object, thus originating volcanic and/or tectonic activity. Thus, the system finally evolves – and small objects collapse into a unique larger object. Hence, the morphological features of the surface of previous small objects are partially maintained. Several case histories of this kind of multiple small objects orbiting around each other are reported. This process can be partially active in the Pluto-Charon binary system, and – owing to this reason – this general and seemingly widespread effect can be briefly called “*Pluto effect*” (Gregori, 2016a).

These details, however, are not directly relevant for the discussion of cometspheres. In contrast, a relevant topic of concern deals with the so-called *pole-on magnetospheres*, i.e., when the magnetospheres dipole axis of the internal object has an orientation almost lying in the ecliptic plane (Fig. 14). A typical case history is represented by Uranus. A large literature is available and is not here reported. The inclination of the neutral sheet is such that the orbital motion of eventual satellites can interfere – by a relevant amount – with the trapped radiation. Pole-on magnetospheres can frequently occur in the case of cometspheres.

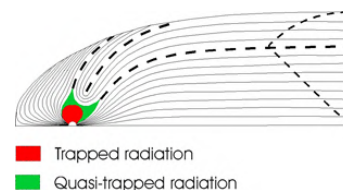


Fig. 14. Pole-on magnetosphere. The large asymmetric is evident between the two lobes. After Gregori (2001a). Unpublished figure.

The interaction of planetary objects that have no endogenous **B** deserves a short mention. Typically, this is the case history of the Moon and of Mars. At the time of their formation during the planetesimal process, the Moon and Mars contained a fluid inner portion. Hence, the tidal action in their environment originated a *TD*-dynamo, with endogenous energy that caused volcanic and tectonic activity – in addition to the formation of an atmosphere that was shielded by a magnetosphere. Thus, sea-urchin spikes were developed (Gregori, 2002, Gregori et al., 2025a). However, the endogenous energy was eventually totally released. In that case, the object’s interior completely solidified. No new *TD*-dynamo could thus be started, and the object lost its **B**, altogether with its magnetosphere, volcanism, tectonism, and atmosphere.

The Moon has clear remnant features of an ancient

volcanic and tectonic activity, similarly to Mars, where the Olympus Mons was probably the last great outburst of endogenous energy before the “death” of its internal *TD*-dynamo. Magnetic phenomena on Mars are well-known to be associated with local features related to crustal magnetization, etc. (Fig. 18). For completeness sake, let us mention that the anomalous behavior of Venus is possibly explained by hypothesizing an internal nuclear reactor (see Gregori and Leybourne, 2025c, and references therein).

These items, however, have little relevance for the present discussion of cometspheres, which is devoted to consideration of the plasma released by an evaporating comet, caused by solar radiation.

6. The magnetospheres of comets and other small planetary objects

6.1. A rationale for physical interpretation

A realistic possibility is that a small planetary object (asteroid, meteoroid, or comet) can have a magnetic field **B**, either permanent or transient, hence a time-varying magnetosphere. This feature, however, can be observed only when dealing with a fraction of all planetary objects, although - in general - these objects can also have no **B**. Every final assessment must therefore rely on *in situ* monitoring. In general, only very seldom we can expect to have the possibility to get a direct *in situ* check. Therefore, we rely on some indirect, even though eventually speculative, inference.

Comets are excellent natural probes, because light emission is a gauge of the environment that they cross along their often highly eccentric orbit. The concern is about a correct calibration. The calibration is speculative – although certainly less speculative than several other items in planetary science. In any case, comets are “free” natural probes that more or less frequently monitor a very wide range of spatial domains, at varying heliocentric distances.¹⁵

Ramanjooloo (2014) reports about a project in progress to use available cometary pictures for measuring the solar wind speed. The principle supposes that the ion tail is composed of multiple plasma bundles that travel at the solar wind speed. In every picture, some features are singled out - by visual inspection - inside every bundle, corresponding to the crossing of the bundle across the

comet’s ecliptic plane. Conversely, the analysis, which is here discussed and proposed, relies on some speculated more detailed physical model of the cometsphere - whether or not it is associated with a possible **B** of the comet’s core.

The same origin of meteoroids and comets, as well as the origin of asteroids, are items for speculative discussion, similarly to every discipline, whenever no direct *in situ* observation is available. For instance, refer to the authoritative brief review by Brownlee (2008). In any case, cometary observations are seldom available, if one relies only on records from Earth’s surface. Conversely, after the advent of space telescopes a huge number of cometary observations are available, which are undetectable from ground. This myriad of very small planetary objects is an ensemble of natural space probes for monitoring the expanding solar corona with an unprecedented detail both in space and time. *SOHO* is reported to have spotted over 2100 comets, which graze the solar atmosphere. Most of them are of the so-called Kreutz family (see below).

A reminder is as follows about the feeling concerning comets, and about how it evolved during the centuries, even in comparatively recent times. The seemingly erratic appearance of comets was a real mystery for ancient observers, and astrologists had a great chance to “investigate” the “sensational” influence of comets on human events. In 1577, Tycho Brahe (1546-1601) carried out accurate measurements on a comet, thus proving an astronomical origin. Edmund Halley (1656-1742) discovered the periodic character of comets, by means of the famous comet that was named after him. He used historical files that had been collected by Newton - who was very depressed after the hostile acceptance of his studies on optics. During the Enlightenment, Buffon believed that the origin of planets might have been caused by a comet precipitated on the Sun (Fig. 15). Fig. 15 is still reported by Sapper (1903), which is a learned German encyclopedia of the beginning of the 20th century.

This same concept survived during the 19 century in a cartoon dated 1857 (see Yeomans 1991, p. 351). The impact of a comet on the Sun is now directly observed by space probes. For instance, Yeomans (1991, p. 319) shows a sequence of photos of the collision of comet *SOLWIND 1* with the Sun occurred on August 30-31, 1979. The sequence was collected by the *Naval Research Laboratory*.

¹⁵ In this same respect, also the stormy features of the outer planets can be used like natural probes suited to monitor the behavior of the solar wind at a large heliocentric distance. Refer to Gregori and Leybourne (2025c).

¹⁶ Karl Theodor Sapper (1866-1945), German traveler, explorer, antiquarian and linguist, known for his research, around the turn of the 20th century, into the natural history, cultures and languages of Central America.



Fig. 15. Impact of a comet with the Sun. After the "Histoire naturelle" by Buffon, published in 1785, and here reproduced after Sapper (1903). The author of Sapper (1903), K. T. Sapper, died in 1945, hence the copyright lasted until December 31, 2015, although the original source of the image is much older. Note the representation of clouds of matter that are ejected by the Sun, anticipating a subconscious feeling that was shared until around 1958, when the solar wind was discovered.

Several case histories are mentioned below. Consider, however, that - in principle - there is no need that the cometary nucleus always remains a strictly solid iced body. Very little is known about the processes that occur during a dramatic cometary perihelion transit. Perhaps, the comet can even fully evaporate, although - maybe - it can be kept compact by a magnetic confinement inside a comatosphere, as a response to some internally generated **B**. The detailed mechanism of such a speculated process is unknown. Later, while going much far away from the Sun, the cometary matter can freeze anew, etc. On the other hand, at present, this is mere speculation that ought to be proven or disproved. This whole guess is discussed below in detail.

On October 3rd, 1828, Johann Wolfgang von Goethe (1749-1832) "told his secretary Eckermann, that the

Grand Duke had asked him whether the tails of comets interacted with the Earth's atmosphere" (Schröder, 2008).

Sensationalistic alarms about a forthcoming end of the world - eventually with great social concern - were repeatedly reported in the past, such as (in comparatively recent and documented times) on May 20th 1773, and on June 13th, 1857. At the end of 1843, according to a belief by William Miller (and his followers, the Millerites), they expected the end of the world on the basis of some interpretation of the *Bible*, and they progressively updated the date until October 22nd, 1844. Details on these items are given by Yeomans¹⁷ (1991).¹⁸ Some concern also existed in 1910 when the Earth passed through a region of space that had been crossed by Halley's comet. The comet made a relatively close approach at $\sim 0.15 AU$. On 19th May the Earth passed through the tail. Spectroscopic analysis had discovered the toxic gas cyanogen in the tail. Camille Flammarion (1842-1925; French astronomer) claimed that the gas "would impregnate the atmosphere and possibly snuff out all life on the planet". This vague statement was exaggerated by mass media. Panic led to "gas masks", "anti-comet pills", "anti-comet umbrellas", "bottles of pure air" suited to breath during the tail transit that was estimated to last ~ 8 hours, etc. However, astronomers had claimed that the event was harmless (see also below).

Even in a comparably recent time (Vsekhsvyatskii, 1964) the possibility was guessed that comets could be originated by volcanism on Jupiter.

When accurate observations became available - including spectroscopic information - the astronomers finally envisaged that a cometary nucleus is a very small object, only a few kilometers in size, mostly composed of ice - the so-called "dirty snowball" or "dirty iceberg", hypothesized in the 1950s by Fred Lawrence Whipple (1906-2004; American astronomer). Different kinds of ices (of H_2O , CH_4 , and/or NH_3) were soon believed to be a very common occurrence in the Solar System.

Meteorites, comets, and asteroids - which altogether are very frequent although eventually non-observed objects in the Solar System - are likely related to one another according to specific rules. A crucial role is played by the changing more or less temporary content of water inside every given object. According to the evidence provided by the different space probes of cometary missions, comets contain a relevant amount of material that typically occurs in the inner part of the Solar

event - was always considered everywhere, in many cultures and societies, an object of dread, fear, and awe. See, e.g., Goldman (2017) and references therein.

¹⁷ Donald K. Yeomans, American astronomer, specialist in celestial mechanics, presently retired.

¹⁸ In any case, since the beginning of human history, a comet appearance - like every unusual and mysterious

System. That is, a comet is not simply a “dirty snowball” or “dirty iceberg”. These items are reviewed, e.g., by Brownlee (2008). The concern is therefore about justifying the survival of a comet after several crossings at perihelion. For instance, the Halley’s comet was reported for the first time in 240 BC (according to Yeomans, 1991, p. 255), and in 466 BC (in China, according to Vsekhsvyatskii, 1964), and its period is 76 years.

According to Brownlee (2008, p. 30), most comets encounter planets in the inner Solar System, and this limits their lifetimes to $\sim 10^6$ years. Close to the Sun sublimation drives cometary activity with an estimated mass loss to $\sim 0.1\%$ per orbit. Brownlee (2008, p. 30) comments that “surprisingly, the major life-limiting factor for many comets is splitting or even severe fragmentation ... a process whose cause remains mysterious.” This mysterious aspect is reconsidered in detail in the following. An active comet has a $\sim 1\%$ chance of splitting in a given year, and it can fragment several times during its active lifetime. Fig. 16 is an impressive picture that shows how a comet is eventually fragmented into a huge number of fragments, everyone displaying an eventually different interaction with the interplanetary environment. Moreover, fragmentation “... a process whose cause remains mysterious ...”, starts when the comet is still very far from perihelion. This fact must be stressed for future reference.

A mass loss can cause a sensible perturbation on the orbit of the comet. According to Brownlee (2008, p. 32), cometary orbits are always somewhat slightly different than pure gravitational orbits. The reason is the rocket effect originated by the anisotropic ejection of matter. The ejection from the solar-heated regions has a component parallel to the orbital path and the effect is either an addition or a subtraction of kinetic energy of the comet. Halley’s comet has never been on time, even though returned as predicted. In 1910 it crossed at closest point to the Sun > 3 days later than expected.

An important morphological feature is the length of a cometary tail, which is impressively and unexpectedly longer than its visible segment. This fact is clear when computing a model of a comet, whether the comet has a magnetic nucleus or not. Jones et al. (2000) report about an accidental measurement carried out by a spacecraft. The plasma tail of comet Hyakutake (C/1996 B2) was unexpectedly crossed at a distance of > 3.8 AU (550×10^6 km) from its nucleus, where a cross-section of the tail was at least 7×10^6 km. This tail length is larger than the 2 AU estimated for the Great March Comet of 1843 (C/1843 D1).

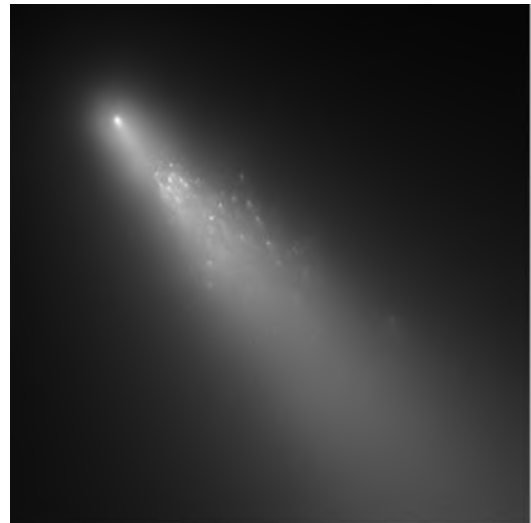


Fig. 16. “Crumbling comet - This false-color mosaic of crumbling comet Schwassmann-Wachmann 3 spans $\sim 6^\circ$ (12 full moons) along the comet’s orbit. Recorded on May 4-6th, 2006, by an IR camera on board the Spitzer Space Telescope, the picture captures about 45 of the 60 or more alphabetically catalogued large comet fragments. The brightest fragment at the upper right of the track is Fragment C. Bright Fragment B is below and left of center. Looking for clues to how the comet broke up, Spitzer’s IR view also captures the trail of dust left over as the comet deteriorated during previous passes. Emission from the dust particles warmed by sunlight appears to fill the space along the cometary orbit ...” This remarkable comet began to break up in 1995, i.e., 11 years before this image (Brownlee, 2008, p. 32). Credit: William Reach (SSC/Caltech), et al., JPL, Caltech, NASA. Figure and comments (with NASA copyright free policy) after <http://apod.nasa.gov/apod/ap060513.html>.

If the comet has no comatosphere, this effect must be explained by means of the obstacle represented by its nucleus against the flow of solar wind. However, the tiny cross section (typically at most only a few km size) of the cometary nucleus should thus justify an effect observed > 3.8 AU downstream. For comparison purpose, consider, e.g., the tail of Mercury (see Baumgardner et al., 2008) that, compared to a meteoroid or to a comet, has an endogenous tenuous **B** and a much larger radius.

In contrast, if the comet has a comatosphere, the effect at such a huge distance downstream must be associated with the filamentary structure at the end of the comatospheric tail, consequent to the aforementioned Cowling dynamo collimation (Fig. 17; Gregori et al., 2025d).



Fig. 17. Two screenshot images after Anonymous (2015bd). ESA copyright free policy. “This 3D simulation models the plasma interactions between comet 67P/Churyumov-Gerasimenko and the solar wind. The simulated conditions represent those expected at 1.3 AU from the Sun, close to perihelion, where the comet is strongly active - a gas production rate of 5×10^{27} molecules sec^{-1} is assumed here. The solar wind approaches from the left at $\sim 400 \text{ km sec}^{-1}$, carrying with it the embedded IMF with a strength of $\sim 5 \text{ nT}$. The material from the comet’s nucleus forms an extensive envelope, the coma, several million km in size (not shown here). Part of the neutral gas molecules in the coma gets ionized by solar UV radiation or by charge exchange with the solar wind particles. These cometary ions are picked up by the approaching solar wind, a process known as mass loading, and cause it to slow down. In the model simulation enough ions are produced and picked up by the solar wind to slow it down from supersonic speed to subsonic speed, causing a bow shock to form in front of the comet.” Figure and captions after Anonymous (2015bd). ESA copyright free policy.

The historical evolution of observations and concepts about comets is reviewed by Yeomans (1991). Shortly after the publication in 1873 of the Maxwell’s *Treatise on electricity and magnetism*, Svante August Arrhenius (1859-1927; Swedish physicist, Nobel Prize for Chemistry in 1903) proposed that light pressure may be responsible for the repulsiveness on cometary tails. This hypothesis raised some long-lasting debate, as the effect looked insufficient, until 1951 when Ludwig Biermann (1907-1986) proposed a continuous outflow of ionized particles from the solar corona. In 1957, Alfvén (1957),

owing to his frozen-in **B** concept, proposed that these ionized particles must bend the **B** field-lines until they become perfectly anti-sunward. Alfvén (1957) claims that “the interaction between such a beam and the head of the comet produces an amplified **B** which determines the shape of the tail.” This can explain the high accelerations observed in the tails.

These concepts are already akin to a cometsphere, although - even as recently as 1991 (Yeomans, 1991, p. 237 and 282) - the interplanetary **B** field-lines are drawn perpendicular to the ecliptic plane (see above for the substantial criticism to this untenable hypothesis). In general, it is therefore always speculative to envisage whether either one small planetary object or another has an intrinsic **B** or not. Concerning the previous literature, the hypothesis of an eventual **B** of the cometary nucleus seems to have been only seldom mentioned (e.g., Malaise, 1966). However, essentially relying on no sound argument, this possibility was always apparently considered “exotic” - and in general all models always referred to a direct interaction of a non-magnetized object with interplanetary environment. The related literature is very large, and it is not pertinent for the present discussion.

In any case, the role of magnetism in the interaction between solar wind and comets is seldom - or only occasionally - considered in the previous literature, and up to some limited extent. For instance, Forsyth et al. (2010) while reporting on a meeting about magnetotails throughout the Solar System, state that most magnetotails are detected by sparse remote sensing techniques, mainly at high time resolution. They add “although comets tend to be unmagnetized”. To our knowledge, there is no sound reason for such a statement. However, they agree that matter exhalation from the comet can be ionized, thus originating a plasma coma that interacts with **B**_{int}. Therefore, they comment that the orientation and length of cometary tail is a tool for carrying out remote sensing of the solar wind.

The feeling later changed. For instance, Koenders et al. (2015) carried out a modeling simulation aimed to achieve “a global 3D hybrid simulation model of the cometary plasma interaction.” A cometary bow shock, and a small diamagnetic cavity around the nucleus, can be originated close to perihelion, as the gas production by the comet is sufficiently large. They envisage a cometary ionopause and a recombination layer, thus being in general agreement with MHD simulations. For additional details see the original paper (Koenders et al., 2015), where they also computed a video of the simulation, presented by Anonymous (2015bd). Figs 17a and 17b are two screenshots of their video.

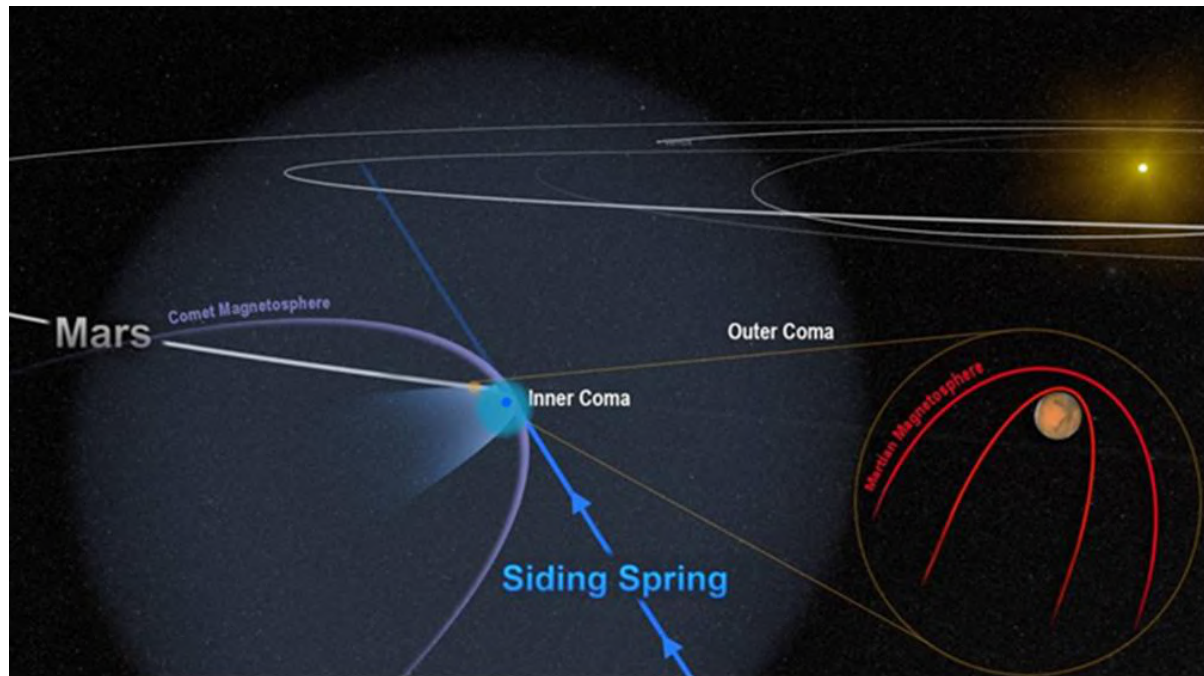


Fig. 18. “The close encounter between comet Siding Spring and Mars flooded the planet with an invisible tide of charged particles from the comet’s coma. The dense inner coma reached the surface of the planet, or nearly so. The comet’s powerful **B** temporarily merged with, and overwhelmed, the planet’s weak field, as shown in this artist’s depiction. Credits: NASA/Goddard.” Figure and captions after [Zubritsky \(2016, 2016a\)](#). NASA copyright free policy.

Also X-rays emitted by comets envisage the existence of a cometary **B** field. Bingham et al. (1996), reporting observations of comet C/Hyakutake 1996 B2, claim that electrons of energy in the *keV* range can be accelerated by the instability, which is a consequence of the motion of newly picked-up cometary photoions relative to the solar wind. Lower hybrid waves are thus generated that accelerate electrons. Thus, Bingham et al. (1996) explain in this way the X-rays released by comet C/Hyakutake 1996 B2 and observed by the *Röntgen X-ray Satellite*. The *keV* electrons contribute a photon power two orders of magnitude greater than 100 *eV* electrons, and this power ought to justify the observed X-rays. In any case, Bingham et al. (1996) stress that these peculiar phenomena ought to help to get a better insight of the composition of the comet.

The same topic is reconsidered by [Rigby et al. \(2018\)](#) from the viewpoint of plasma physics. An experiment was carried out by scientists from 15 institutes. According to Byrd (2018c), who interviewed a few co-authors of the experiment, “... when comets travel through the Solar System they interact with solar radiation, the solar wind and the solar **B**. This produces a visible atmosphere or coma as well as the observed cometary tail, and in some cases, X-rays. These are generated on the sunward side of the comet where the solar wind impacts the cometary atmosphere, forming a bow shock ...

... experimental results provide direct laboratory evidence that objects moving through magnetized plasmas can be sites of electron heating. This process is common in astrophysics and can take place not only in comets, but also in planetary magnetospheres (as of our own Earth), or even in supernova remnants where the ejected material sends a shock wave into the interstellar gas ... “

That is, [Rigby et al. \(2018\)](#) deal with the formal approach from the viewpoint of plasma physics, which is outside the general algorithms and tools considered in the present study. In their experiment (from their abstract), they “show, using laboratory laser-produced shock experiments, that, in the presence of a strong **B**, significant electron pre-heating is achieved. [They] demonstrate that the key mechanism in producing these energetic electrons is through the generation of lower-hybrid turbulence via shock-reflected ions. [Note that the Cowling dynamo process is very effective in the transformation of kinetic energy of any origin, e.g., related to turbulence, into the generation of e.m. energy and **B** that causes self-collimation.] Our experimental results are analogous to many astrophysical systems, including the interaction of a comet with the solar wind (Bingham et al. 1996), a setting where electron acceleration via lower-hybrid waves is possible.”

The relevant and leading role must be stressed played by the Cowling dynamo (see Fig. 2 and Gregori et al.,

2025d), particularly upon taking into account the great thermal gradient. The strong convection inside a highly ionized medium determines a self-confinement - the phenomenon is similar to what occurs inside a *BL* (see Gregori and Leybourne, (2025e). However, the phenomenon of a *BL* is feeble and can last from a few seconds to several ten seconds. In the case of an explosion, the phenomenon is violent and persistent in time. That is, the experiment finds (Rigby et al., 2018) the generated plasma is strongly self-collimated, thus enhancing the effects of the interaction with the target-ball. In addition, concerning X-ray emission, an expected mechanism may be analogous to the generation of *TGF* (see Gregori et al., 2025f).

According to our understanding, the Rigby et al. (2018) experiment can be interpreted in terms of a turbulence caused by the laser beam within a plasma jet. Owing to the Cowling dynamo, the turbulence transforms kinetic energy into an e.m. field - that must have a given orientation due to the constraint represented by the ***B*** of the magnetized *Nd* sphere used in the experiment. Electrons are thus rapidly accelerated and, owing to Bremsstrahlung, they release X-ray radiation. Since the phenomenon is observed also with a non-magnetized soda-glass sphere, the orientation constraint caused by the magnetized *Nd* sphere is not crucial. In fact, every accidentally occurring environmental ***B*** plays the role of the magnetized *Nd* sphere, and the phenomenon must always occur.

It must be emphasized that the discussion here focuses on the (eventual) heuristic possibilities associated with comets, and mostly on their several seemingly “exotic”, unexplained and unexpected, although frequent features, among a variety of cometary behavior. However, this discussion is independent of the existence, or not, of any ***B*** associated with any given small planetary object. Rather, it is here claimed that the existence of a ***B*** within a comet - or within a small planetary object - is just one realistic possibility that cannot be simply ruled out. Sometimes it is found to “explain” some observations that seem to be justified in no other way.

The present paper relies on some short excerpts - with updating - of a paper prepared in 1974 but never published.¹⁹ The key role of Cowling dynamo (Gregori et al., 2025d) emphasized in the present argument relies on the proof of the generalized Cowling theorem that was

achieved only almost three additional decades after 1974 (Gregori, 2002) Hence, in 1974 the present argument seemed excessively speculative, and GPG did not pursue on this investigation until later evidence came forth.

Now, owing to the proof of the Cowling dynamo, a comet can be identified with a plasma-cloud, or plasma-ball, characterized by a strong internal Cowling dynamo, which originates an effective and strong confinement of plasma, etc. Note that the term plasma-ball is more expressive, and emphasizes the self-confinement features of plasma, inside a toroidal ***B***, i.e., just inside a plasma bottle. Thus, several previously unexplained cometary features can be easily explained, and the whole model seems sound, and it can be effectively checked in several ways by suitable observations. This is the target of the discussion on comets here given.

Concerning the 1974 aborted draft, some old - although still relevant - literature is here sometimes mentioned. However, to our knowledge, according to the present generally shared feeling and agreement that is found in the most recent literature, such a viewpoint seems to be still considered a seemingly “exotic” hypothesis. The present brief discussion is not directly concerned with cometary studies *per se*. The purpose is, rather, to show how suitable cometary observations can support some key arguments that are here envisaged, and that deal with the possibility of an unprecedented and highly detailed monitoring of the solar wind.

Only a few old cometary pictures are here mentioned, based on the 1974 draft. Recently, new important facilities became available suited to carry out either observations outside the Earth’s atmosphere or *in situ* cometary observation by space probes. Some additional fascinating comet pictures are now included.

The origin of the ***B*** of a celestial object is discussed above. In any case - as far as a small planetary object is concerned - the conclusion is in terms of three possibilities, i.e., either (i) the object has a permanent magnetization, or (ii) a temporary ***B*** is originated by e.m. induction by the solar wind, or (iii) a *TD*-dynamo can be eventually operative if suitable conditions are satisfied, whenever the entire physical system - which is identified with the small object - is composed of conducting parts that can move relative to one another.

As far as the permanent magnetization is concerned, consider the iron meteorites. It is impossible to guess

¹⁹ GPG feels deeply indebted for very kind comments on this old draft by the late Murray Dryer (1925-2022; American scientist, emeritus in space physics and space weather), and for some authoritative and learned inputs by H. U. Schmidt from *Max-Planck-Institut für Astrophysik* (see below). GPG also feels deeply

indebted to the late Professor Reimar Lüster (1923-2020; German astrophysicist), who triggered the contact with H. U. Schmidt. GPG wants to express sincere gratitude to H. U. Schmidt, even though, at present, after several decades, unfortunately it seems impossible to rekindle this contact.

whether they have a \mathbf{B} before their interaction with the Earth's atmosphere. They suffer a dramatic transformation following both the stress while they cross through the atmosphere, and their impact at Earth's surface. Nevertheless, their composition is such that, maybe, it is probable that they have an intrinsic permanent magnetization. Therefore, in general we cannot exclude that - at least - some fraction of small planetary objects eventually has a permanent magnetization. In addition, their \mathbf{B} can be either mainly dipolar, or multipolar. Hence, their magnetosphere can eventually display a neutral sheet, or rather a much more complicated structure with "forelocks" of \mathbf{B} flux tubes (see above and Fig. 11). However, their magnetosphere cannot be observed.

The case history is very different in the case of a \mathbf{B} originated by e.m. induction from the solar wind. This \mathbf{B} is only a temporary phenomenon, which however experiences great changes due to the very large heliocentric variation of a small planetary object, and due to the consequent dramatic variation of its kinetic energy. Indeed, the kinetic energy variation is crucial in the control of the energy balance that determines the amount of induced electric currents \mathbf{j} , hence also the intensity of its temporary \mathbf{B} . At the same time, however, also a large variation occurs of the solar wind density, and of the embedding \mathbf{B}_{int} .

The aforementioned energy balance of an e.m. induction process is quantitatively expressed by the "principle of magnetic energy variation" (see Gregori et al., 2025e, 2025f) that can be briefly summarized as follows. Call C_1 and C_2 any two given circuits or \mathbf{j} -loops, which symbolically represent, respectively, the currents \mathbf{j} of the solar wind and the currents \mathbf{j} induced into the small planetary object. Call $U_s^{(1)}$ the self-magnetic energy of C_1 , and $U_s^{(2)}$ the self-magnetic energy of C_2 , and call $U_j^{(1,2)}$ their joint-magnetic energy. If Joule heat is neglected, which is released inside either one C_1 and C_2 , it is found that

$$\delta U_s^{(1)} = \delta U_s^{(2)} = -\delta U_j^{(1,2)} = -\delta W \quad (1)$$

where δW is the variation of kinetic energy of the whole C_1 plus C_2 system.

Conversely, if Joule heat is taken into account, it is shown that the $\delta U_s^{(2)}$ variation inside C_2 , which is caused by its Joule heat, produces a transfer of the same amount of energy $\delta U_j^{(1,2)}$. Hence, $U_j^{(1,2)}$ decreases, while $U_s^{(1)}$ increases by an identical amount $\delta U_s^{(1)}$. Similarly, an eventual loss by Joule heat inside $\delta U_s^{(1)}$ causes a transfer of energy from $U_j^{(1,2)}$ to increase $U_s^{(2)}$, etc. The process stops whenever both $U_s^{(1)}$ and $U_s^{(2)}$ are null.

In the case of a small planetary object, and mostly

when it has a highly eccentric orbit - such as it typically occurs for a comet - the object experiences a very large $\delta U_s^{(2)}$. Hence, owing to (1), it experiences a large $\delta U_s^{(2)}$. That is, the induced currents \mathbf{j} certainly always generate a conspicuous temporary \mathbf{B} that causes the consequent formation of a relevant cometosphere.

For instance, an unusual event was observed in 10th and 23rd September 2013 (Fig. 19) as reported by Phillips (2013d), with details in Jewitt et al. (2013). Phillips (2013d) specifies that "... its tail structures change dramatically in just 13 days as it belches out dust ...

P/2013 P5 has been ejecting dust periodically for at least five months. Astronomers believe it is possible the asteroid's rotation rate increased to the point where its surface started flying apart. They do not believe the tails are the result of an impact with another asteroid because they have not seen a large quantity of dust blasted into space all at once ...

Careful modeling by team member Jessica Agarwal of the Max Planck Institute for Solar System Research in Lindau, Germany, showed that the tails could have been formed by a series of impulsive dust-ejection events. She calculated that dust ejection events occurred April 15th, July 18th, July 24th, August 8th, August 26th and September 4th ...

... it appears P/2013 P5 is a fragment of a larger asteroid that broke apart in a collision roughly 200 Ma ago. There are many collision fragments in orbits similar to P/2013 P5's. Meteorites from these bodies show evidence of having been heated to as much as ~ 800 °C. This means the asteroid likely is composed of metamorphic rocks and does not hold any ice as a comet does."

This interpretation, however, is substantially other than the e.m. induction process that is here envisaged. In fact, they claim that "radiation pressure could have spun P/2013 P5 up. Jewitt said the spin rate could have increased enough that the asteroid's weak gravity no longer could hold it together. If that happened, dust could slide toward the asteroid's equator, shatter and fall off, and drift into space to make a tail. So far, only ~ 100 – 1,000 tons of dust, a small fraction of the P/2013 P5's main mass, has been lost. The asteroid's nucleus, which measures ~ 427 m wide, is thousands of times more massive than the observed amount of ejected dust."

However, if an abrupt increase of the spin rate was the driver of this phenomenon, which lasted ~ 5 months, what was the cause of the spin rate change? The concern is, rather, about the persistence in time of the transient induced currents, because the persistence depends on the amount of Joule heat released per unit time.

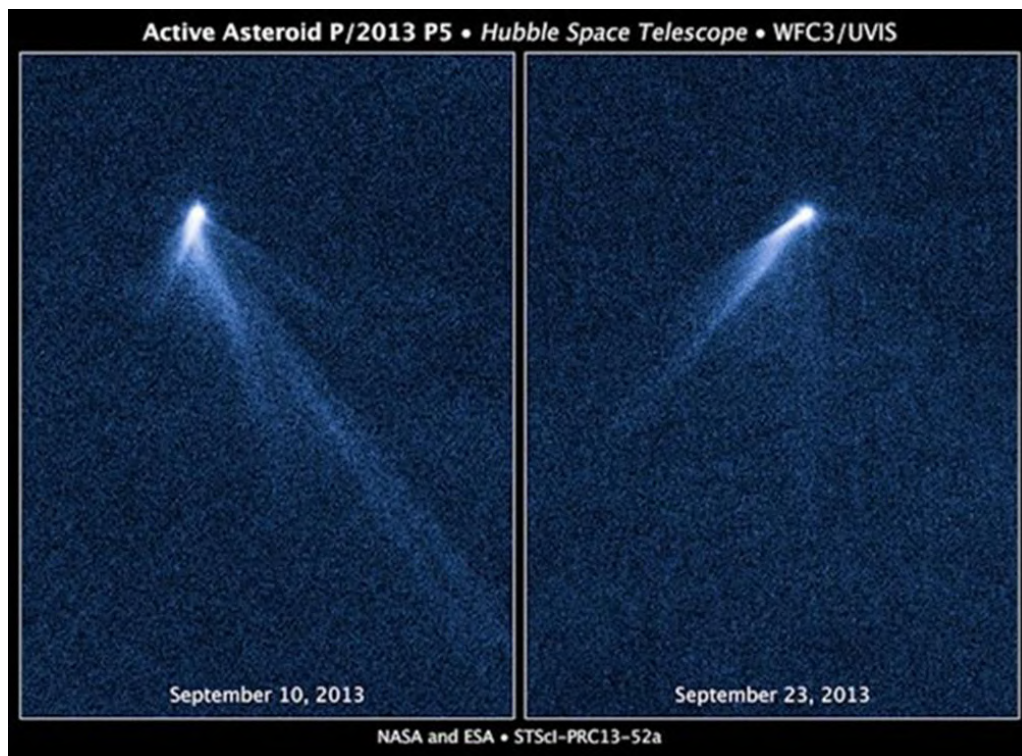


Fig. 19. “This NASA Hubble Space Telescope set of images reveals a never-before-seen set of six comet-like tails radiating from a body in the asteroid belt, designated P/2013 P5.” Figure and captions after Phillips (2013d). NASA copyright free policy.

However, even a transient short-lived effect - if it is sufficiently intense - can determine a repulsive force that disrupts the planetary object. It is well known that, owing to the Hamilton’s principle (see Gregori et al., 2025e), every loop of electric current must attempt to expand in space as much as possible. If the stretching force is large - and the mechanical cohesion is insufficient of the material that composes the circuit - the loop breaks. The intensity of the effect depends therefore on the orbit eccentricity, and on the local time-variation state of the solar wind. In fact, in the ultimate analysis, the variation of the solar wind flow implies a set of different phenomena, and all of them can be interpreted in terms of different mechanisms that, in reality, are often only a different way to look at the same occurrence. It is always a matter of e.m. interaction, i.e., induction and Cowling dynamo and Joule heat, plus mechanical cohesion of cometary materials.

In general, even with no direct indication - about the electrical conductivity σ of the material that composes a small planetary object, or a comet etc. - in principle, the concern is realistically twofold, as σ must refer either to the cometary nucleus, or to the volatiles, which are likely to play the most relevant role in the interaction with the

solar wind (see below).

As far as the cometary nucleus is concerned, we know that it certainly contains several different kinds of ice. Water ice is an excellent insulator, similarly to pure water. However, if water is polluted by some dust or other elements, σ can be conspicuous. In fact, salted water has a σ that is $\sim 40,000$ times the σ of dry rock (Lanzerotti and Gregori, 1986), although one should take into account the particular temperature of a comet. Hence, it is fully speculative to make any guess about the σ of a small planetary object. Rather, we must allow for every σ .

For instance, in a stone meteoroid - or in a body like the Moon, with no internal origin B - Joule heat of every induced (“telluric”) current rapidly damps off, due to the very poor σ of the composing material. Sometimes, temporary “mushroom” or “umbrella” of magnetic features can be developed, such as it occurs on Mars. On the other hand, these transient features cannot justify the persistence of a cometary tail.

The case history of a comet or meteoroid can perhaps be different if σ is substantially large, and if one considers the often-great eccentricity of a cometary orbit. A large eccentricity implies an enormous variation of the gravitational potential energy along the orbit, compared to

other planetary objects that move on orbits with low eccentricity. For instance, the dramatic role of the orbit eccentricity is shown by means of the guessed, although quite reasonable, huge seasonal dependence of Pluto's and Charon's tectonism (see Fig. 10 of Gregori et al., 2025b, and for additional more extensive discussion see Gregori, 2016a).

In addition, one must consider the volatiles typically released by a comet. They are a plasma, and plasma experiences a dynamics similar to a convection pattern. Hence, the Cowling dynamo process is very efficient. Its role becomes more relevant the closer the comet approaches to the Sun as the comet's evaporation becomes larger. Hence, a magnetic self-collimation is generated, by which ionized volatiles are constrained inside some limited volume.

In other words, consider that a Cowling dynamo generates a toroidal \mathbf{B} that confines plasma inside an effective "plasma bottle". Hence, if a space mission performs a flyby exploration of a comet (such as, e.g., the well-known *GIOTTO* mission to Halley's comet), no \mathbf{B} will be detected, unless the probe enters into the plasma confinement region (i.e., likely inside the coma, see section below).²⁰ That is, compared to a similar meteoroid that has no volatile exhalation, the role of volatiles makes the crucial difference of a comet, due to the crucial role played by the Cowling dynamo.

Furthermore, it appears that a cometary object, or an asteroid, etc., is not kept compact by gravitation alone. According to Heins (2014) - who reports about an investigation by [Rozitis](#) et al. (2014) on the near-Earth asteroid 1950 DA - they "*discovered that the body, which rotates so quickly it defies gravity, is held together by cohesive forces, called van der Waals, never before detected on an asteroid ... the rotation is so fast that at its equator, 1950 DA effectively experiences negative gravity ... The presence of cohesive forces has been predicted in small asteroids, but definitive evidence has never been seen before.*" That is, the real amount and mechanisms are still poorly known of the forces that hold compact an asteroid, or a comet, or a meteorite.

However, the role must be emphasized that sometimes is played by a *TD*-dynamo. This role can even be very important. In fact, the cloud of conducting volatiles around a cometary nucleus is composed of different parts, which can move with respect to one another. Therefore, the comet is almost like a fluid ball of plasma. The total

mass is extremely feeble, the space size is very small, the electrical conductivity σ is very large, but - when the orbit has a large eccentricity - the gradient of gravitation can be extremely large. Basically, gravitation determines the cometary orbit, according to the standard Newtonian formulation,²¹ while e.m. induction operates through the Cowling dynamo inside the plasma evaporated from the comet when it approaches the Sun.

Tables 2 and 3 of Gregori et al. (2025b) show that the effectiveness of a *TD*-dynamo inside a comet can be represented by the product of the cross-section S of the plasma-ball - which is identified with the comet - times the gradient (absolute value) of the gravitation of the Sun. That is, the reference parameter is $[S \times (1/2)GM_{\odot}/r]$, where M_{\odot} is the solar mass, and r is the heliocentric radial coordinate of the comet. Therefore, S is very small, and the mass of movable plasma is also very small, but the gravitation gradient can even diverge almost to infinity when r decreases. Hence, *a priori* one cannot exclude that, when a comet gets very close to the Sun, a *TD*-dynamo process can be eventually overwhelming. In fact, some numerical constraints can be perhaps specified (not here given) - upon making an estimation about the size for the plasma-ball, and about the plasma density that is needed in order to sustain the electric current intensity that is triggered by the *TD*-dynamo. That is, every estimation (much like the estimation of mass for gravity) is unavoidably speculative. On the other hand, in principle, we cannot exclude that perhaps the *TD*-dynamo effect can be sometimes operative, at least in the case of comets with very small perihelion and high eccentricity.

Summarizing, a *TD*-dynamo process can affect, maybe, only some sungrazing comets. Indeed, at least on some rare occasions, this phenomenon can be an important effect that, maybe, can justify some mysterious and presently unexplained features. Differently stated, a comet is a plasma-ball that is self-confined, almost like a huge and persistent *BL*. The phenomenon is steady, as the heat source is represented by solar radiation that causes sublimation of the cometary nucleus. In addition, σ is large, and - whether the resulting \mathbf{B} is generated by simple e.m. induction by the environmental \mathbf{B}_{int} , or by a *TD*-dynamo, or both - the cometary plasma-ball is very efficiently self-confined, just like inside a huge and steady *BL*. When the cometary plasma-ball goes far away from the Sun, the confined plasma can re-condense on the icy

²⁰ The concept is analogous to the case history of Figure 8 through 11 of Gregori and Leybourne (2025e), where a *BL* is simulated in the laboratory by the Fußmann's experiment (see below). A temporary toroidal \mathbf{B}

confines a plasma that is very hot inside it, while its boundary is practically cold.

²¹ An extensive discussion of the relationship between gravitation and e.m. interaction is not pertinent in the present paper (see Gregori et al., 2025w).

nucleus, and the comet can thus survive to several crossings at perihelion.

A concern, however, deals with the strict confinement of plasma inside a “box” locked by a strong toroidal \mathbf{B} , just like in a giant BL . Therefore, no \mathbf{B} is observed outside the plasma-ball. Hence, the interaction with the solar wind is certainly other than the interaction with a magnetized planet such as the Earth. This seems a paradox.

Indeed, a paradox occurs if the solar wind is hypothetically composed of neutral gas, because the interaction with the plasma-ball ought to be similar to the case history of air that interacts with an aircraft-model - or with a solid ball - inside a wind tunnel. In contrast, the solar wind is composed of electrons and ions. The interaction is therefore between a single charged particle and a plasma-ball. Nothing forbids a charged particle to strike on the plasma-ball (e.g., see Figs 17a and 17b). Therefore, the final effect is that some electrons and ions of the solar wind enter inside the plasma-ball, and become an additional component of the plasma, thus contributing to the electric currents \mathbf{j} . That is, the result looks like in the case that the plasma-ball has an expanded volume and total mass. The crucial driver is always the internal energy due to sublimation supplied by solar radiation.

Therefore, the cometsphere looks like a composite physical system, where the volatiles that are sublimated from the cometary nucleus combine with solar wind and constitute a unique large cometsphere. In addition, e.m. induction occurs inside the whole composite system. Differently stated, the plasma-ball is identified with the cometsphere, and we observe photons released from the whole cometsphere, which we call “comet”.

Consider, therefore, according to (1), the effect of an induced \mathbf{j} that can even become very intense while the small planetary object approaches the Sun, due to the dramatic variation δW , hence also $\delta U_s^{(2)}$. Owing to the Hamilton’s variational principle (Gregori et al., 2025e), every \mathbf{j} -loop must expand in space as much as possible. This means that the currents \mathbf{j} , which are induced in the object, tend to disrupt it, due to the outward violent pull of the \mathbf{j} -circuits. Indeed, this is what is observed in comets, mainly when their orbit gets very close to the Sun, where the time gradient is larger of the inducing e.m. field. That is, the plasma confinement can be a very effective and a safe obstacle against comet evaporation, while the mechanical stress on the solid nucleus can be destructive.

In this respect, a mere effect - caused by solar radiation alone - ought to produce a surface heating of the comet, and its evaporation, until its disappearance, almost like a flash. In contrast, comets are often seen to disrupt into a discrete set of a few pieces that eventually re-emerge on the opposite side of the Sun, after crossing through perihelion. Certainly, one can introduce *ad hoc*

assumptions, and - in this way - one can try to explain this feature also by means of solar radiation alone. Everything is always speculative. However, the explanation in terms of currents \mathbf{j} and of the Hamilton’s principle seems to be, maybe, less *ad hoc* and possibly more credible than other guessed explanations. Such an observational multiple disruption morphology is comparatively frequent and is discussed below.

In some way, a cometary \mathbf{B} , whether it has a permanent component or not, must be considered like a transient phenomenon, which is an essential ingredient of the entire set of phenomena that are involved in the overall interaction of the cometary nucleus with the interplanetary environment, including both solar e.m. and corpuscular radiation. That is, the speculation about a possible transient \mathbf{B} of a cometary nucleus cannot to be considered an “exotic” hypothesis. It is rather the physically most reasonable guess, i.e., it would be really surprising if this phenomenon does not exist. The concern is rather about assessing the quantitative role and contribution in the overall interaction comet-environment - and about assessing whether and how it can be clearly detected by observation of cometary morphology. Consider also that a transient magnetopause protects the cometary nucleus from direct impact with the solar wind, maybe resulting (perhaps) in a large reduction of the nucleus erosion also in terms of dust depletion, hence favoring a longer life for the comet.

In addition, owing to the Chandrasekhar-Fermi theorem (Gregori and Leybourne, 2025e), a plasma cannot be self-contained. However, the Chandrasekhar-Fermi theorem holds when *no internal heat source* is operative. Thus, e.g., a BL ends its ephemeral lifetime when the internal heat source has exhausted. In contrast, solar radiation causes the evaporation of the cometary nucleus and is thus a relevant heat source that supplies the Cowling dynamo associated to plasma convection due to volatile evaporation. Hence, the plasma originated from the nucleus is reasonably supposed to be confined around the nucleus by an e.m. effect, while the gravitational attraction by the nucleus is very feeble or even negligible at all. The implications - dealing with the need to save in some way the mass of the nucleus during several crossing of a comet at its perihelion - are briefly discussed below.

It should be pointed out that this discussion refers to the so-called “Type-I” tails, i.e., the plasma tails that point perfectly anti-sunward. Instead, the present discussion cannot deal with the dust (“Type-II” and “Type III”) tails (with particles claimed to be $\sim 1 \mu m$ size), which are a less permanent feature, and look curved. They normally disappear after the transit of the comet at perihelion. Therefore, the aforementioned reduction of nucleus depletion - through direct interaction with the solar wind

- which is represented by a cometosphere, is only operative during the early flyby of the comet to the Sun.

This fact envisages that, compared to dust tails, the plasma tails are associated with a definitely less destructive phenomenon either in terms of erosion of the nucleus, or, more likely, due to e.m. effects, i.e., either by an e.m. screening from a transient cometary magnetopause, or by the plasma confinement due to the Cowling dynamo, which protects the sublimated volatiles. Indeed, both phenomena are the same occurrence considered from a different viewpoint.

“Type I” tails display remarkable fine structures that remind about a self-collimation effect caused by the Cowling dynamo inside a plasma (Gregori et al., (2025d). They are called filaments, or streamers, or knots (-pinch), or kinks, or puffs, which move along the tail. Or they also display comparably more violent phenomena such as anomalous outbursts, “wagging tails”, etc. These phenomena envisage a disruption due to e.m. induction. Streamers appear sometimes to begin in the nucleus, with a large angle with respect to the Sun-comet line. Then, they bend downstream. Compared to the outbursts etc., a streamer might be a disruptive event of smaller scale size, i.e., it might involve only a smaller volume of matter.

The thinness of streamers has been interpreted as being suggestive of **B** field lines - or more correctly of thin **B** “forelocks” - that trap plasma along their very thin structures. This is an old hypothesis, dating back, e.g., to Dobrovolskij (1961), Richter (1963, p. 88), Öpik (1964a), Vsekhsvyatskii (1964, p. 7), Ness and Donn (1965, 1966), Brandt (1962, 1968), ... However, Beard (1966) gives a different explanation for these streamers.

In addition, if a comet has a temporary **B** of prevailing dipolar character, it develops a neutral sheet. If we are located, relative to the comet, in such a way that we can observe from a side the cometosphere tail, we must expect to observe some optical feature that ought to be determined by the presence of the neutral sheet. A few features of this kind are discussed below.

Furthermore, maybe, we have two possibilities to check whether all this is mere speculation or not, by means of a quantitative evaluation of suitable morphological features of comets.

A first possibility relies on the size of the coma. Suppose - as a tentative working hypothesis to be later confirmed or not - that the size of the coma is an index of the size of the plasma-ball, or of the cometosphere (which is the same). On a speculative basis, such a property could derive from the fact that the coma is somewhat representative of the size of the magnetopause, where the ions, which are evaporated from the nucleus, are permitted to interact with the solar wind particles, and are thus excited. In fact, the Cowling dynamo can be active

only inside the evaporated and ionized volatiles. A coma can be, perhaps, the volume that contains the sublimated volatiles, hence it is the location of the Cowling dynamo - or the coma is the visual manifestation of the volume of confinement by the Cowling dynamo through the toroidal **B**, i.e., much like it happens in a **BL**. Differently stated, comets are huge-size and persistent case histories of mysterious **BLs**.

The size of the coma can therefore depend on the nature and composition of the nucleus that might even be different when comparing different comets. However, the *relative* variation of the size of the coma - when we refer just to *one and the same comet* - ought to follow a specific law *vs.* the heliocentric distance along its orbit. This item is discussed below.

An analogous law represents a second possibility, and it ought to monitor the relative changes of the cross-section of the tail *vs.* heliocentric distance of the comet. Also, this item is discussed below.

We can therefore try and test these possible laws - and this is the purpose of the remaining following discussion of cometary items. However, an eventual agreement, or disagreement, with either one of these laws, when dealing with one specific case history, does not necessarily mean that this fact either proves, or disproves, the existence of a cometosphere for that specific comet. It is rather an observational constraint, by which we can guess whether some case histories seem consistent with the hypothesis of a cometosphere, or not. On the other hand, as already mentioned, we must reasonably expect that magnetic phenomena can sometimes occur on small planetary objects. The concern is about the occurrence frequency and about the quantitative relevance of this effect in the control of the observed cometary morphology. Therefore, we can appreciate the real physical significance and implication of this working hypothesis only after having carried out a series of attempts by referring to specific case histories.

In general, if the cometosphere hypothesis is credible and satisfies all possible reasonable checks, comets are important tools for the study both of the Earth’s magnetospheric processes and, more generally, also of solar-terrestrial relations. Therefore, comets must be considered experimental models on different scales of the Earth’s magnetosphere. They can be monitored by remote sensing and they scan regions of interplanetary space that otherwise could never be reached by manmade probes - except at most only by some very seldom available probes. This same concept is clearly stressed by Saito et al. (1987).

In this same respect, remind about the Mercury tail,²² which is monitored by ground-based observations of *Na* radiation, including its variation during a sunspot cycle. In fact, the length and breadth of the tail are important parameters for monitoring the properties of solar radiation. This holds for the Mercury tail, as well as for all other "tails" – eventually monitored by *Na* emissions (or others) - referring to every other planetary object, including comets.

Moreover, a quantitative estimate of the processes that justify mass conservation, or decay, of a comet is also related to the unsolved aforementioned problem dealing with the palæodensity of the Earth's atmosphere. In fact, during a *FR*, the Earth's atmosphere, owing to its direct interaction with the solar wind, is partially depleted of some total net amount of mass, much like it has to be expected to occur in comets with an insufficiently strong **B**. That is, the atmospheric density could have decreased all along the Earth's history on the occasion of every *FR*, being, however, eventually balanced by an increased fluid exhalation from soil (see above).

In any case, consider that, maybe, some experiments could be carried out that reproduce in some way - although on a reduced space size - an "artificial comet". That is, some kind of a peculiar manmade experiment could be carried out in the natural "space laboratory", aimed to check the occurrence of some phenomena that are speculated to occur (maybe) in a real comet. This item is discussed below.

6.2. Comets: large scale possible evidence, a double-lobe tail, and filamentary patterns

A curious case history is represented by comet 12P/Pons-Brooks, nicknamed the "Devil Comet", discovered in 1812. This comet "*is known for its violent eruptions, during which a powerful blast of ice and gas creates a glowing halo resembling devil horns. The fourth, and largest outburst, occurred on November 14th, 2023, and was photographed by amateur astronomer Eliot Herman, who witnessed a 100-fold increase in the comet's brightness*" (Fig. 20; Mathewson, 2023; but see also Baker, 2024). The comet headed toward Earth, and the violent outburst generated the glowing halo that, however, did not afford to enter the cometsphere, which looks like the black spot that generates the "devil horns".

Another clear evidence is possibly related to the double-lobe tail. It is reasonable to expect that some evidence suggests that the currents **j**, which flow over the magnetopause of the cometsphere, are composed of ions

that are excited by solar radiation. In contrast, the currents **j** that cross through the neutral sheet of the cometsphere should be comparatively less excited, as they are screened by the magnetopause of the cometsphere. If this guess is correct, the tail ought to display some kind of "black axis".

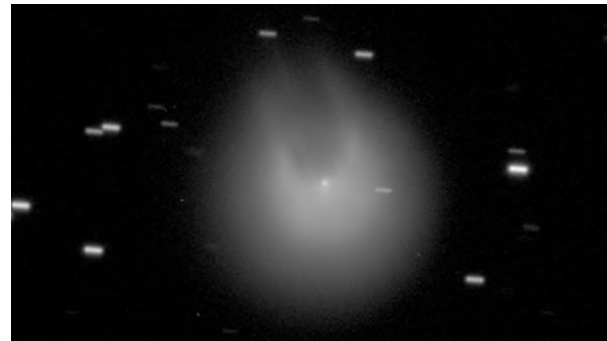


Fig. 20. Comet 12P/Pons-Brooks, nicknamed the "Devil Comet", photographed on November 14th, 2023, by amateur astronomer Eliot Herman. After Mathewson (2023). See text. NASA copyright free policy.

Fig. 21 refers to the Halley's comet, which has no permanent **B** – as we know by direct *in situ* observation by the *GIOTTO* mission that approached its nucleus at a distance of 596 km. On the other hand, as mentioned above, if a comet is a huge **BL**, the **B** is toroidal. Thus, plasma and **B** are confined inside the plasma-ball, and no **B** must be detected surrounding the cometsphere. Fig. 21 displays a feature that can be interpreted as a "black axis". On the other hand, it appears reasonable that the "black axis" is only seldom observed, even in the case that it really displays a cometsphere's neutral sheet (which is in any case always a speculative hypothesis). In fact, the location of the observer must be specifically oriented with respect to the neutral sheet in order to detect the "black axis". In addition, if the **B** of the comet is a transient phenomenon, we can observe such a feature only occasionally.

It is interesting to refer to a series of photographs made from the SAAO (South African Astronomical Observatory, Cape Town) during the Halley passage in 1985-1986. They used a Schmidt camera of 25/30 cm aperture, 80 cm focal length, with plate scale 258 arcsec mm⁻¹. The exposure times were generally around ~ 15 min, sometimes shorter as much as 1 min, sometimes longer as much as 64 min.

²² Some references are Potter et al. (2002, 2007), Baumgardner et al. (2008), Killen et al. (2008), McClintock et al. (2008), Potter and Killen (2008).

These observations were carried out during March 1st, 1986 - June 8th, 1986 as a part of the *International Halley Watch*. A selection of them, 44 pictures, was published in Cosmovici et al. (1993).²³ They range between March 1st, 1986 - May 16th, 1986. The *GIOTTO* flyby occurred on March 13th-14th.



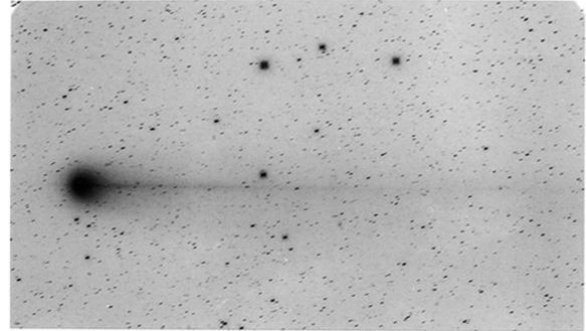
Fig. 21. "Head of Halley's comet as seen on May 8th, 1910. (Mt. Wilson Obs. photograph)." Figure and captions after Brandt et al. (1980). NASA copyright free policy.

Every picture was scanned for plotting the isophotes, as "the use of this technique shows many structures that are over - or under - exposed and not visible in the photographic reproduction" (Cosmovici et al., 1993, p. 18). A clear feature, which can be interpreted like a "black axis" (appearing white in a negative isophote picture), is observed in all published photographs (they are 3) between March 1st - March 9th. Then, it is no more observed in the 32 photographs between March 13th - April 21st and it is observed anew - and more clearly - in the remaining 9 photographs between April 27th - May 16th. Only one picture is here shown in Fig. 22, where the "black axis" is the white pattern in the bottom (isophote) picture. Note that the shrinking of the cross-section of the tail ought to be indicative of the progressive decrease of light intensity downstream along the tail.

This series of photographs shows that, if Halley really has a transient **B**, the transient **B** ought to be originated by e.m. induction, consistently with the direct flyby observation by *GIOTTO*. In any case, as already stressed, the observer can detect such a "black axis" only if he is located on a side of the tail, and not far from the plane of the hypothetical cometary neutral sheet. In any case, the "black axis" evidence is only a hunch, not a proof.

In principle, another - maybe better - possibility can be achieved by means of a spectral analysis of a comet tail, with the slit of the spectrometer perpendicular to the tail extension. Owing to a Doppler distortion, the spectral lines should be deformed like a parenthesis, i.e., like { or

} depending on the relative motion of ions with respect to the observer, i.e., depending on the sunward or anti-sunward orientation of **B** in the comet's tail, consistently with the **j**-loop pattern of Figs 8 and 9. The most favorable relative position of the Earth is when the line of sight is close to the plane of the cometary neutral sheet, and when the angle Earth-comet-Sun is roughly 90°. However, in this respect, two comments are deserved.



Frame N. 68 1986 May 12.89375; $\Delta = 1.18$; $r = 1.81$; $\beta = 31.4$
 Exp. 40 minutes, Observer: RMC

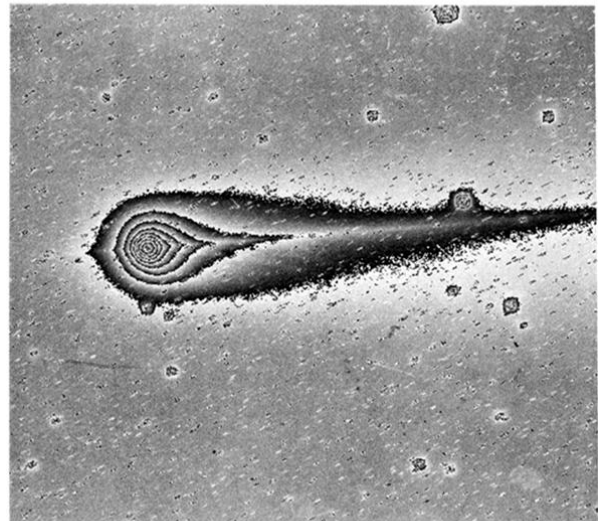


Fig. 22. "Frame no. 68 - 1986 May 12.89375, ... Exp. 40 min . Observer RMC." Figure and captions after Cosmovici et al. (1993, p. 166). With CNR/IFSI permission.

Firstly, at present it is difficult - or practically impossible - to estimate the quantitative amount of the Doppler shift deformation that must be expected, because: (i) Figs 9a and 9b represent currents **j**, not ion drift velocities; (ii) Figs 9a and 9b were drawn by assuming a

²³ Cristiano B. Cosmovici is kindly acknowledged for providing this very interesting material.

magnetopause represented by a 2D current sheet. In reality, the “magnetopause” is a layer with a finite non-null thickness.

A few authoritative estimates are reported here concerned with this target. They were kindly provided by H. U. Schmidt (private communication, 1974). GPG expresses once more deep thanks, and considers a true honor having an evaluation carried out by a distinguished and learned specialist. We are not specialist and we cannot be aware whether more recent estimates are possible, or not. In any case, the following estimate is concerned only with orders of magnitude. Hence, it is likely that these estimates hold independent of any lesser more recent refinement.

An estimate of the currents that flow on the magnetopause far downstream can be carried out by assuming that the intensities of the internal and external \mathbf{B} are identical, as their magnetic pressures must balance each other (as shown above). Then, the total current $\mathbf{J}_1 + \mathbf{J}_2 + \mathbf{J}_3$ (in Fig. 9a) that flows far downstream in the neutral sheet is determined by the intensity of the internal \mathbf{B} , which we suppose is identical to the intensity of \mathbf{B}_{int} . Hence, $[\mathbf{J}_1 + \mathbf{J}_2 + \mathbf{J}_3] \sim 10^{-5} (r_E/r_C)A$.

This H. U. Schmidt’s estimate can be explained as follows (but, every eventual mistake is only our responsibility). Consider the Maxwell relation $curl \mathbf{H} = (4\pi/\gamma_0)\mathbf{j}$ (for quasi-stationary approximation; see above and Gregori et al., 2025o) and apply it to a circuit that encloses, downstream, a unit area of the magnetopause. Suppose that the physical thickness of the electric currents that flow on the magnetopause is $D \sim 500 m$. Hence,

$$\mathbf{j} = curl \mathbf{H} \frac{\gamma_0}{4\pi} \sim \frac{1}{2D} \frac{2B}{4\pi K_0} \sim \frac{B \cdot 10^{+4}}{4\pi} \quad (2)$$

Therefore, if $\mathbf{B} \sim 6 nT$, one finds $j \sim 10^{-5} A$, which is the aforementioned estimate. The factor (r_E/r_C) refers, respectively, to the heliocentric distances r_E of the Earth and r_C of the comet. In fact, the current system of a cometosphere can be supposed to have a self-inductance L . If \mathbf{J} is an indicative electric current that flows in the circuit, the energy of the circuit is $LJ^2/2$. The local energy density, inside the expanding solar corona, decreases with $1/r^2$. Hence, $LJ^2/2$ decreases with $1/r^2$, or \mathbf{J} decreases as $1/r$. This approximation implies that L does not depend on r , and this ought to be tested. In any case, as far as orders of magnitude are concerned, this is a reasonable assumption.

The remaining H. U. Schmidt’s computation relies on his astute and learned specialized knowledge of spectroscopy of comets, which is outside our expertise and background. We just report our notes on this item. A magnitude is suggested by H. U. Schmidt of several $10^7 km sec^{-1}$ for the observable Doppler

velocities in the cometary plasma, because the CO^+ and other bands have no sharp lines. Hence, if these currents \mathbf{j} in the neutral sheet are carried by ions of unit charge, and if these ions move at the speed quoted by Schmidt, say at $\sim 10^8 km sec^{-1}$, the ion density should be $\sim 0.6 \times 10^2 (r_E/r_C) ions cm^{-3}$.

If the diameter of the cross-section of the tail is of the order of $10^5 km$, and the thickness of the plasmashet is of the order of magnitude of $10^4 km$, there are $\sim 0.6 \times 10^{21} (r_E/r_C)^2$ ions per unit length in the neutral sheet. If these ions flow downstream at the solar wind speed ($\sim 400 km sec^{-1}$) an evaporation ought to occur of $\sim 2.4 \times 10^{28} (r_E/r_C)^2$, which is reasonably close to the order of magnitude of $\sim 10^{30} gas particles sec^{-1} sterad^{-1}$ expected for a comet (H. U. Schmidt, private communication, 1974). In any case, in general, these currents \mathbf{j} are mainly due to electrons. Therefore, even a much lower ion evaporation rate can be sufficient.

To conclude, according to the aforementioned general estimates exploited by an authoritative specialist - whom we thank very much - perhaps this Doppler effect sometimes can be detected.

A second remark deals with the filamentary structure, or with the assessment of the distance - downstream along the tail - where one should point the spectrometer slit. In the case of the Earth, the question should be at what distance downstream the lobes of the tail begin to appear filamentary. In general, the irregularities in the solar wind flow can play a different role at different radial distances from the Sun, although the intensity and stability must be considered of the internal \mathbf{B} . In fact, compared to the Earth, the \mathbf{B} of a cometary nucleus, in general, ought to be substantially weaker, and its intensity could also be different for different comets. On the other hand, the basic mechanism is essentially different - because in the case of the Earth the currents \mathbf{j} of the magnetopause are more or less directly supplied by solar wind particles. Conversely, in the case of a comet they are mainly supplied by plasma evaporation from the nucleus (or, at least, this is true for the evaporated chemicals that we detect).

Moreover, consider that, even in the case of the Earth, the same concept of “merging” of \mathbf{B} flux across the magnetopause implies an environment that displays a filamentary structure, such as “forelocks” or fringes, which surround the magnetopause both downstream and close to the Earth (see Figs 11 and 12). In the case of a comet, this kind of fringes can be eventually monitored, thus suggesting a filamentary structure of the tail. Such a structure can begin even very close to the coma, where the cometary tail is not yet really filamentary. Maybe, an excellent available image (Fig. 23) is the “accidental observation” of comet Lovejoy (C/2014 Q2) when it was

at 82×10^6 km from the Earth (Howell, 2015b).

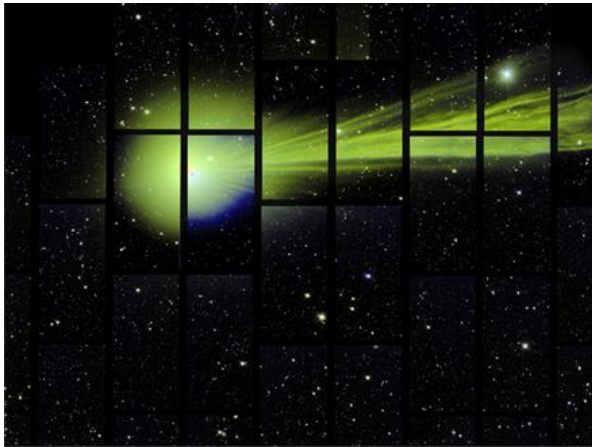


Fig. 23. “The 570-megapixel Dark Energy Camera in Chile captured this photo of Comet Lovejoy on December 27, 2014. Credit: Fermilab’s Marty Murphy, Nikolay Kuropatkin, Huan Lin and Brian Yanny.” Figure and captions after Howell (2015b). NASA copyright free policy.

According to the aforementioned argument, Fig. 23 envisages that the comet has no internal well-organized **B**. Rather, different fragments of various size detached from the core, and everyone developed an internal origin **B** caused by e.m.-induction from the solar wind, and also by the Cowling dynamo effect associated with ionized volatiles. Such a mechanism generated the observed **B** “forelocks”, through self-collimation of **B** flux.

On an intuitive - although pictorially effective - basis, one can claim that the physical condition $\text{div } \mathbf{B} = 0$ is such as to concentrate all available free charges towards the final common target of conservation of **B** flux tubes. In fact, this is the physical meaning of the e.m. induction process that determines the effectiveness of the Cowling dynamo. Thus, ions are trapped by these **B** flux tubes, and they are eventually visible like filamentary patterns of the comet tail.

Yagi et al. (2015) studied the motion of lesser knots inside a cometary tail through repeated observations by means of a surface-based telescope. They report short-time variations in the plasma tail of C/2013 R1 (Lovejoy) observed by means of a series of short (2 – 3 min) exposure images with the 8.2 m *Subaru* telescope. They detected faint details of filaments, displaying motions over 24 min observing duration, and rapid movements, of two knots in the plasma tail near the nucleus ($\sim 3 \times 10^5$ km). The measured speeds were 20 and 25 km sec⁻¹ along the tail and 3.8 and 2.2 km sec⁻¹ across it, respectively. “These measurements set a constraint on an acceleration model of plasma tail and knots as they set the initial speed just after their formation. We also found a rapid narrowing of the tail. [Such a

narrowing is indicative of a weakening of light emission .] After correcting the motion along the tail, the narrowing speed is estimated to be ~ 8 km sec⁻¹... “

According to one of the co-authors (Jin Koda), as reported by Howell (2015c), “The filaments were made up of H₂O and CO, indicating that they emanated from the comet itself. How they moved so fast afterward is still poorly understood ... The filaments of gas erupt from the comet at low speeds due to heating from the Sun, then are quickly accelerated - somehow - to the speed of the solar wind as the wind ‘blows’ against them ... “

According to the general rationale that is here envisaged, this acceleration can be explained by considering that the interaction between solar radiation (e.m. and/or corpuscular) and cometary material causes an abrupt ionization and temperature increase, also including a mixing with solar wind inside the intricate pattern of the cometsphere. The consequent particle dynamics implies a Cowling dynamo effect. The acceleration of electrons eventually experiences an additional conspicuous acceleration due to the “runaway breakdown” (RB) process (see Gregori et al., 2025f). Hence, the rapidly increased e.m. field enhances a self-focusing effect of the filament, which is observed simultaneously with a relevant acceleration of every charge particle, hence also of knots. This process finally explains both the appearance of sharp filaments inside the comet tail, and also sometimes an abrupt detachment of knots.

On the other hand, all comets are not identical. Maybe, sometimes a comet eventually has some reasonably intense internal origin **B**, whether **B** derives from a magnetized cometary core or from some peculiar e.m. induction by the solar wind. In either case, sometimes a cometspheric pattern can develop, which is characterized - as a first order approximation - by two large **B** flux tubes, similar to the two large lobes of the Earth’s magnetosphere (see Figs 9a and 9b). In this case, the comet tail, when it is observed with a suitable geometric orientation, can display a “black axis”.

In summary, we cannot state whether the simple Doppler shift deformation of spectral lines into a parenthesis-like shape can be observed or not. This can occur only for a cometsphere composed of two lobes, i. e., similar to the Earth’s magnetosphere – i.e. unlike a pole-on magnetosphere (see Fig. 14). In any case, the parenthesis-like shape should occur not too far downstream along the tail, and in any case only depending on a very critical location of the observer.

In addition, a few additional facts imply substantial observational and theoretical difficulties.

First, in general it cannot be assumed that the cometary **B** (or better the most important **B** component, i. e., the dipole **B**) is oriented, as it occurs for the Earth, at some

large angle relative to solar wind velocity. For instance, consider the case of a cometary **B** axis parallel or anti-parallel to the solar wind flow, i.e., this is the case history of a pole-on magnetosphere (see Fig. 14). Intuitively, we can expect a ring-shaped belt of trapped particles surrounding a funnel-shaped region on the front, through which the solar wind penetrates deep inside, towards the cometary nucleus. On the opposite side, i.e., at cometary midnight, a strong outflow can be expected, analogous to (and stronger than) the Earth's polar wind (see above). However, no neutral sheet will be observed. On the contrary, the solar wind particles spiral along numerous small flux tubes (i.e., "forelocks") contained in the two previously mentioned huge funnel-shaped flux tubes, located at cometary noon and midnight (e.g., remind about Fig. 23).

Second, the shape of the tail is sometimes indicative of strong turbulence in the solar wind.

Third, a super-Alfvénic shock accompanies the comet, although (perhaps) it is likely to be mainly concerned with solar wind particles alone, and not with volatiles released from the nucleus.

Fourth, from a practical point of view - compared to the standard spectroscopic measurements on comets - the Doppler deformation, which is here proposed, is only a tiny detail. In addition, it should be observed only when proper locations and orientations occur of Earth, Sun, comet and the comet's **B** axis.

Notwithstanding all these difficulties, the "black axis" pattern has often been observed.

In general, comets look regular, such as, e.g., comet Bennett (1969 i) (Brandt et al., 1971). In contrast, in some cometary pictures one can suppose, on a tentative basis, that the dark axis - which divides the tail all along its length into two lobes - could correspond to the neutral sheet. As a matter-of-fact, as already mentioned, when ions flow within the tail, i.e., inside the neutral sheet, they are not directly excited by direct interaction with the interplanetary environment; i.e., it is reasonable to expect that there is no light emission coming from the neutral sheet.

Some examples are the drawing of Donati's comet (1858 e) reproduced in Wurm (1959) and Sekanina (1968), the picture of Halley's comet (1909 c) in Sekanina (1968), the picture of Arend-Roland comet (1956 h) in

Porter (1960), and the picture of Morehouse comet (1908 III) in Wurm (1959, p. 502).

Several drawings of the Donati's comet are comparatively popular in books that deal with historical items about comets.²⁴ They show a "black axis", although with a regularity that is suggestive of some arbitrary interpretation by the artist. A less known picture is shown in Fig. 24 and seems credible and perhaps objective.



Fig. 24. "Hand drawn sketch of Donati's Comet by C.W.M., dated 9th October 1858. It is not apparent who C.W.M. was, as does not match staff or volunteers at Williamstown Observatory or Flagstaff Observatory. Made in Victoria, Australia. Transfer from Melbourne Observatory, 1945." At present the picture is at *Museums Victoria*. Figure and captions are after *Drawing - Sketch of Donati's Comet, 9th October 1858 - Museum Victoria.htm*. With kind permission of *Museums Victoria*.

Another drawing shows, perhaps, the standard double-tail pattern, rather than a black axis. It is the Donati's comet as seen at Melbourne, on October 11th, 1858. The image can be found on the website of the *National Gallery of Australia*.

Even older drawings - as far as they can be reliable - seem to have an analogous property (see, e.g., Vsekhsvyatskii, 1964, p. 115). Obviously, these are only tentative speculations to be confirmed by additional investigation. In this respect, Figs 25a through 25e show a "synthesis" of knowledge about cometary morphology according to Johannes Helvetius (Jan Heweliusz, 1625-1709, Polish astronomer, councilor and mayor of Danzig). Even more detailed examples are shown in Figs 25f and 25g, dated ca. 168 BC - and seemingly they look like almost an attempt to organize in some way, and with great accuracy, the several different types of observed comets. In addition, Fig. 25h shows the accurate drawings by

in Marseille by Wilhelm Temple (1821-1889). His drawing was probably used for a figure in his paper in *Astronomische Nachrichten* appeared on 10th August 1864. The first original Donati's drawing, which is still available at the *Historical Archive* of the Arcetri *Astrophysical Observatory*, is published by Galli et al. (2016).

²⁴ Giovanni Battista Donati (1826-1873; Italian astronomer, prematurely died from cholera) is known for his spectroscopic studies of stars, and for his role in the building of the *Arcetri Observatory* in Florence. He discovered 5 comets, the best known discovery was in 1828, but he also drew, on 5th-6th August 1864, the first spectrum of a comet, which had been discovered

Maria Clara Eimmart (1676-1707, German astronomer, precise engraver and designer), who was daughter and assistant of Georg Christoph Eimmart, the younger (1638-1705, German draughtsman and engraver). A more

quantitative and more objective evaluation of several ancient photographs of comets (between 1902-1967) was carried out by measuring the isophotes and published by Högner and Richter (1979).²⁵

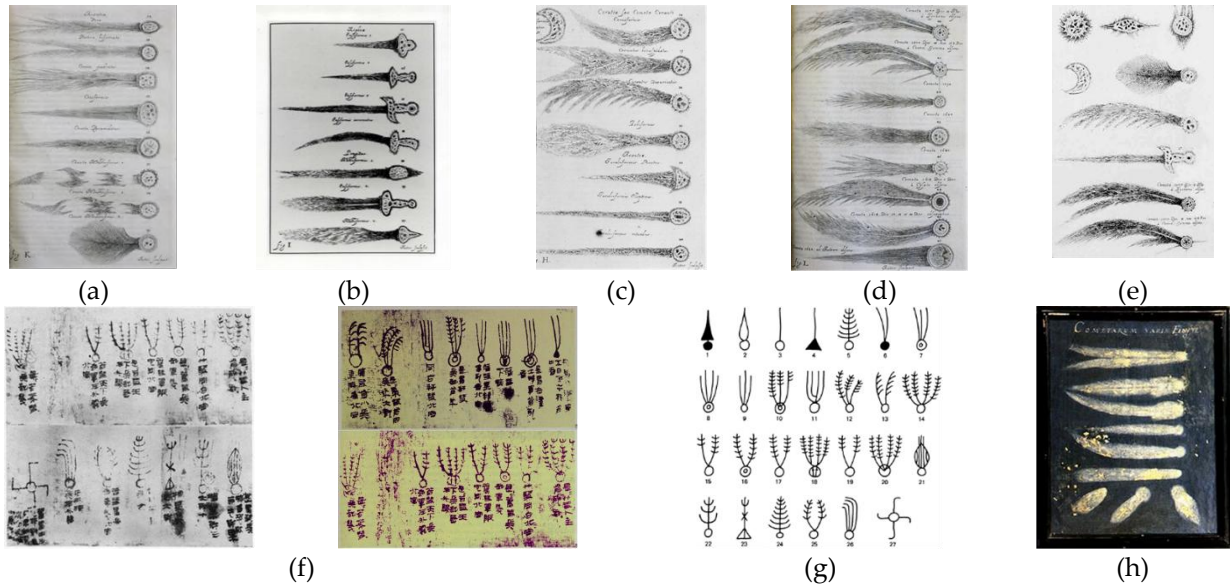


Fig. 25. (a),(b),(c),(d),(e) Images from Johannes Helvetius's *Cometographia* (Danzig, 1668), shown in Yeomans (1991). Copyright decayed. (f),(g) "Some examples of the cometary types displayed in the silk book of the Han tomb (ca. 168 BC ...)" After *Silk Atlas of Comets from the Hunan Provincial Museum* (Anonymous, 1980) (8, 57). "The Mawangdui silk, a 'textbook' of cometary forms and the various disasters associated with them, was compiled sometime around 300 BC, but the knowledge it encompasses is believed to date as far back as 1500 BC" (Goldman, 2020, who also shows the present image). See also comments in Yeomans (1991). Comets with a possible two-lobe structure may be easily recognized, and comets with more complicated structures of filaments or streamers, or **B** "forelocks". Figure after Yeomans (1991, p. 46, 47). Copyright decayed. NASA copyright free policy. (h) Accurate astronomical illustration by the astronomer Maria Clara Eimmart (1676-1707). Permission kindly granted by Tumblr, via Wikipedia.

Consider the implications of the "magnetic" model - which is here proposed - concerning the conservation of the total mass of the comet vs. decay by evaporation. Compared to other models, the "magnetic" model presumably implies a smaller loss of mass by evaporation. Indeed, the currents J_1 , J_2 , J_3 and $-J_1$ in Fig. 9a are mainly composed of electrons - because, in general, electrons have a much higher mobility than ions. In any case, the electrons are likely to supply the main responsible current that cause self-collimation. The currents J_1 and $-J_1$ are originated by solar wind particles (and leave the magnetosphere far downstream, when either the magnetosphere closes or, more realistically, when it ends into filamentary patterns). The currents J_2 and J_3 , in principle, flow on closed loops, hence the ions that flow along them ought to be partially conserved. In

reality, J_3 does not flow on a closed loop, and - up to some extent - in Fig. 9a the currents J_1 , J_2 and J_3 eventually mix up. They sum up at point B, then they split again at point C. However, when they split, they do not remember whether a charged particle originally belonged to either one j or another. Hence, this argument can be applied only up to a limited extent. On the other hand, the magnetic confinement must be considered, which is originated by the Cowling dynamo that finally results into a collimation of particles inside some kind of huge "magnetic bottle".

In any case, consider mass conservation inside the region of space - confined by a magnetopause, i.e., by a layer of some non-vanishing thickness, even though it is represented in Fig. 9a as a 2D distribution of j . The most important effect is the need to assume no mass loss inside

²⁵ Not available to us.

this region of space, apart the amount that is required to supply either (i) the loss from the outermost layer, or (ii) by the “polar wind” flow. In contrast, inside this region, charged particles must be expected to be trapped on closed orbits, similarly to the Earth’s radiation belts, although with a very different geometry. Phenomena are thus to be expected to occur, which are similar to what is observed inside the Earth’s magnetosphere.

If we tentatively assume that the coma is the domain of trapped radiation similar to the Earth’s radiation belts (i.e., the Earth’s *plasmosphere*), we can easily expect that the coma contracts when the comet approaches the Sun, because, owing to the increased solar wind pressure, the whole magnetosphere must contract. This is the argument of the D_{co} vs. r_c variation discussed below.

In contrast, in contradiction with this, some authors (e.g., Brandt, 1962, and references therein) claim that a coma ought to contain mainly neutral constituents. This is what ought to occur when the thermal evaporation plays the leading role, rather than the scattering of the molecules of cometary volatiles with solar wind and with its frozen-in \mathbf{B} . This is just a matter of the choice of the starting viewpoint, and of the consequent attempt to fit a pre-chosen model with available observations. It is likely that both effects occur, and that the presence should be considered of both neutral and ionized constituents. In fact, the different tails (“Type I”, “Type II” and “Type III”) are a clear confirmation of a twofold phenomenon.

According to this same viewpoint, some pictures of comets can sometimes appear suggestive of curious hypotheses, similar to the previously mentioned “*black axis*” that, perhaps, can be indicative of a possible neutral sheet. For instance, let us recall some old pictures, and consider the comet Whipple-Fedtke (1942 g) shown in Wurm (1959, p. 498), in the *CN* band $\lambda = 3883 \text{ \AA}$. The coma, perhaps, can be interpreted as being composed either (i) of ions or of molecules that evaporate from the nucleus and have an approximately spherical symmetry, or alternatively (ii) of quasi-trapped ions, hence the coma ought to display a toroidal shape. A possible coma with a clear toroidal shape is comet Humason (1961 e) (see Whipple, 1974).

However, sometimes the streamers seem to be originated from a nucleus, reminding about “forelocks”. Compared to the size of the coma, the streamers display a narrower cross-section. They ought to be likened to the “polar wind” of the Earth. Should this type of shape be displayed only at a few particular wavelengths, one can presume that what is observed at a given wavelength is actually trapped radiation and “polar wind”, rather than magnetopause currents.

On the other hand, such a kind of filamentary structures can lie, perhaps, outside the magnetopause,

being the consequence of “merging” between cometary \mathbf{B} field lines and \mathbf{B}_{int} . Should this type of shape be displayed at all wavelengths (see Öpik, 1964a and references therein), the comet should be interpreted as having a \mathbf{B} with dipole axis roughly parallel or antiparallel to the velocity of the solar wind, i.e., the cometosphere ought to be similar to a pole-on magnetosphere (Fig. 14).

All this is speculative, qualitative, and *ad hoc*, except – maybe – the spectral lines deformation like a parenthesis, i.e., like { or } depending on the relative motion of ions with respect to the observer. In any case, the “*black axis*” hypothesis is an interesting curiosity. The eventual \mathbf{B} associated with a comet must be quantitatively inferred from some sound observational check, based on the size of the coma and on the tail. This is the focus of the next subsections.

6.3. Comets: evidence from sungrazing comets

Comets can be considered from a twofold perspective. On the one hand, they look like a stony meteorite, with an amount of ice - or of any other easily vaporizable component - that should be sufficient to originate a detectable trail. That is, there is no difference between a stony meteorite and a comet, other than the availability of volatile substances for tracking. However, when a stony meteorite gets closer to the Sun, it warms up. Hence, unless it gets very close to it, no really dramatic consequence is expected to occur to its body. In contrast, a sungrazing comet is potentially subjected to evaporate a large percent of the icy nucleus. It eventually disappears. However, before disappearing, some peculiar phenomena occur inside the huge plasma-ball that results from its evaporation. In fact, ionized volatiles are certainly associated with a Cowling dynamo (Gregori et al., 2025d), hence with a magnetic confinement. Compared to the case history of a stony meteorite, this is likely to be the most relevant physical difference.

The discussion in the present section begins therefore by addressing the first viewpoint, i.e., what phenomena must be expected in a stony meteorite with tracing chemicals on it. Then, the second viewpoint - dealing with a plasma-ball of volatiles - is considered in some detail, including a discussion of some laboratory experiments that can help to model processes and mechanisms.

Sungrazing comets are a comparatively frequent occurrence. An interesting short review is Mazzucato (2007), who claims that, until 1979, only 9 case histories had been observed by ground observation. These comets have a very small perihelion. Instead of evaporating and smoothly fading off, they disrupt into a few to several fragments before reappearing, after crossing behind the opposite side of the Sun. In this same respect, several

historical records are also reported of comets observed close to the Sun during solar eclipses (Vaquero and Vázquez, 2009; Vaquero, 2014), beginning from ²⁶ Seneca's "*Naturales quaestiones*" [7.20.4].

At present, the generally reported interpretation is in terms of tidal forces. In contrast, the interpretation that is here envisaged relies on the Hamilton's variational principle (Gregori et al., 2025e), by which the \mathbf{j} -circuits - which are caused by the e.m. induction by the solar wind - tend to expand in space until eventually breaking the cometary nucleus. The quantitative treatment of this model is described below, although no formal quantitative check seems possible by means of cometary observations. That is, since we do not know the real ultimate strength of the materials of the comet nucleus, this evidence can be only qualitative.

The interpretation in terms of gravitational tide relies on the intensity of the gradient of gravitation, times the diameter of the cometary nucleus. The rationale is the same applied for the computation of Tables 2 and 3 of Gregori et al. (2025b). Note, however, that if the e.m. induction occurs inside the plasma-ball, no breaking occurs, as plasma is fluid. In contrast, e.m. induction

inside the solid cometary nucleus requires that the cohesion forces inside the nucleus afford to oppose the stress due to the induced \mathbf{j} .

Stefanik (1966) discussed 13 similar examples, i.e., either the 9 case histories of sungrazing comets in a strict sense, plus a few other similar comets. He concluded that tidal forces are not sufficient to justify this phenomenon. On the other hand, some more recent literature exists on this item (but, we carried out no systematic search). In any case, the typical very small diameter of a cometary nucleus ought to require a very strong - and perhaps unrealistic - gravitational gradient in order to explain such a phenomenon. Conversely, the interpretation in terms of e.m. induction and Hamilton's principle relies on the huge variation of kinetic energy of the cometary nucleus along the orbit. The maximum effect occurs close to perihelion, where, therefore, the maximum happens of induced currents \mathbf{j} . The phenomenon can occur when the cometary orbit is reasonably close to the Sun, or also close to Jupiter (see Fig. 26). In both cases, the primary cause can be either gravitational or e.m. induction, due to the large Jovian mass and due to its intense \mathbf{B} .



Fig. 26. "A NASA Hubble Space Telescope (HST) image of comet P/Shoemaker-Levy 9, taken on May 17th, 1994, with the Wide Field Planetary Camera-2 (WFPC-2) in wide field mode. This required 6 WFPC exposures spaced along the comet train to include all the nuclei. The image was taken in red light." Copyright ©1994 by H. A. Weaver and T. E. Smith (Space Telescope Science Institute), and NASA. Figure and captions after <http://cometography.com/pcomets/1993f2.html>. NASA copyright free policy. See also Weaver (1997).

For instance, some old case histories are the sungrazing comet 1882 II ("September comet" or "string of pearls" comet), which, after passage at perihelion, broke into 6-8 comet-like pieces (Vsekhsvyatskii, 1964). Two similar examples are the 5-comet set, which resulted after the breakup of comet Brooks 2 (1989 d), or the sungrazing comet Ikeya-Seki (1965 f) that on October 21st, 1965 broke into 3 comets (Sekanina, 1968).

A compilation of sungrazing comets is given in Table 1, borrowed after Mazzucato (2007),²⁷ who also briefly reviews the history of this concept and observations. *SOLWIND* was an instrument onboard the satellite *P78-1*, and during 1979-1984 it discovered 6 case histories. During 1987-1989 the *SMM* (*Solar Maximum Mission*) observed other 10 case histories by means of the *CP Coronagraph*. Shanklin (2003) claims that "by 1989 the

²⁶ Lucius Annæus Seneca (or Seneca, or Seneca the Younger; ~3 BC - AD 65), famous Latin philosopher and scientist.

²⁷ Reproduced with kind permission of *Il Giornale di Astronomia*.

SMM had added 10 more [which are the same aforementioned comets], and since 1996 SOHO had found a startling 465 ... “

Table 1. The sungrazing comets discovered by naked eye, and by probes SOLWIND and SMM

comet name	date of perihelion	perihelion distance (AU)
Naked-eye discovered		
371 BC Aristotle and Ephorus or Ephoros	?	?
1106	1106.02.??	?
1668	1668.03.01	?
1689	1689.09.??	?
1695	1695.10.23	?
1702	1702.02.13	?
C/1843 D1 Great March comet	1843.02.27	0.0055
C/1880 C1 Great Southern comet	1880.01.28	0.0055
X/1882 K1 Eclipse comet, or Tevfik comet (‡)	1882.05.17	?
X/1882 C1 Great September comet	1882.09.17	0.0077
C/1887 B1 Great Southern comet	1887.01.11	0.0048
C/1945 X1 du Toit	1945.12.28	0.0075
C/1963 R1 Pereyra	1963.08.24	0.0051
C/1965 S1 Ikeya-Seki	1965.10.21	0.0078
‡ - Ahmed Tevfik Pasha (1845-1936), khedive of Egypt, last Ottoman grand vizier.		
Discovered by SOLWIND		
C/1979 Q1 (SOLWIND 1)	1979.08.30	0.0048
C/1981 B1 (SOLWIND 2)	1981.01.10	0.0079
C/1981 O1 (SOLWIND 3)	1981.07.20	0.0061
C/1981 V1 (SOLWIND 4)	1981.11.04	0.0045
C/1984 O2 (SOLWIND 5)	1984.07.28	0.0154
C/1983 S2 (SOLWIND 6)	1983.09.23	0.0075
Discovered by SMM		
C/1987 T2 (SMM 1)	1987.10.06	0.0054
C/1987 U4 (SMM 2)	1987.10.18	0.0063
C/1988 M1 (SMM 3)	1988.06.27	0.0052
C/1988 Q1 (SMM 4)	1988.08.21	0.0059
C/1988 T1 (SMM 5)	1988.10.12	0.0051
C/1988 W1 (SMM 6)	1988.11.18	0.0059
C/1988 U1 (SMM 7)	1988.10.24	0.0058
C/1989 L1 (SMM 8)	1989.06.02	0.0056
C/1989 N3 (SMM 9)	1989.07.08	0.0046
C/1989 S1 (SMM 10)	1989.09.28	0.0048

These comets are also called “Kreutz sungrazer comets” after the German astronomer Heinrich Carl Friedrich Kreutz (1854-1907). He found that all sungrazing comets have a similar orbit. Therefore, he guessed that all of them are the remnant fragments of a unique large comet that broke during its first crossing through the Solar System. That is, the event was a giant rupture of a huge sungrazing comet. “Kreutz sungrazers are typically small (~ 10 m wide) and numerous. SOHO sees one falling into the Sun every few days” (Phillips, 2011a). According to studies by Brian Geoffrey Marsden (1937-2010), a likely candidate for this primitive large comet might have been observed in 371 BC by Aristotle (384-322 BC), and by the ancient Greek historian Ephorus

or Ephoros of Cyme (ca. 400-330 BC).

Mazzucato (2007, p. 19) comments as follows.²⁸ “The two fragments referred to by Ephoros ought to have an orbital period of ~ 350 and ~ 800 years, respectively. The object with short period had already returned in the 1st, 4th, 8th, and 11th century, and it can be identified with the 1847 comet. During the 11th century transit it had been additionally fragmented, forming the group that today is called Kreutz I, which should include the C/1843 D1 Great March comet, the C/1963 R1 Pereyra comet, and the comets discovered by probes SOLWIND and SMM.

Instead, the long period object had returned during the 4th century and in AD 1106 when it experienced a new fragmentation forming the presently called Kreutz II

²⁸ Our English translation.

group, which ought to include the C/1882 R1 Great September comet and comet C/1965 S1 Ikeya-Seki. The Kreutz I group represents the largest part of the objects discovered by SOHO.

Sungrazing comets have [typical longitudes and] ... a distance at perihelion $q < 0.007$ UA, with a mean $q \sim 0.005$ UA (or $\sim 750,000$ km). The Kreutz II group [has different typical longitudes at perihelion and] ... a distance at perihelion $q > 0.007$ UA. The larger objects - that also have $q > 0.005$ UA - survive at their transit at perihelion, while the smaller objects - that have $q < 0.002$ UA - dissolve through the solar atmosphere, hence they are also called 'suicidal comets'."

Also other groups, analogous to Kreutz I and II, have been recognized. Concerning the cometary size, Mazzucato (2007, p. 21) claims that a standard comet has a size comparable to a mountain, while a sungrazing comet has the size of a small house or even smaller. In contrast, the great primary unique sungrazing comet was estimated to have a size of the order of ~ 100 km. In addition, owing to gravitational perturbations, the distance at perihelion ought to be reduced at every transit. "... comet C/1995 O1 Hale-Bopp has 15% possibility to become a sungrazer comet."

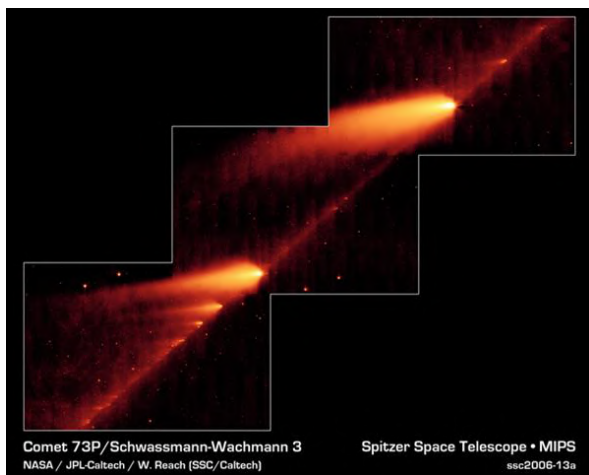


Fig. 27. Comet 73P/Schwassmann-Wachmann 3, fragment B, April 19th, 2006. *Hubble Space Telescope*. NASA, ESA, H. Weaver (JHU/APL), M. Mutchler and Z. Levay (STScI). NASA copyright free policy.

In addition, the total number of sungrazing comets was estimated to be several ten thousand. They occur with a

varying frequency, depending on month, etc. and sometimes they can be associated with the so-called "cometary storms". Several pictures are now available of sungrazing comets. Just recall Fig. 16. Fig. 27 shows several fragments altogether.

Calvin J. Hamilton comments as follows.²⁹ "Sequential Hubble images of the B fragment, taken a few days apart,³⁰ suggest that the chunks are pushed down the tail by outgassing from the icy, sunward-facing surfaces of the chunks, much like space-walking astronauts are propelled by their jetpacks. [Consider, however, the relevant role played by the Cowling dynamo due to ionization of volatiles.] The smaller chunks have the lowest mass, and so are accelerated away from the parent nucleus faster than the larger chunks. Some of the chunks seem to dissipate completely over the course of several days.

Deep-freeze relics of the early Solar System, cometary nuclei are porous and fragile mixes of dust and ices. [In reality, they are refilled periodically into the Solar System.] They can be broken apart by gravitational tidal forces when they pass near large bodies (e.g., Comet Shoemaker-Levy 9 [see Fig. 26] was torn to pieces when it skirted near Jupiter in 1992, prior to plunging into Jupiter's atmosphere two years later). [The role must rather be stressed of the intense Jovian **B** that causes a violent e.m. induction into the comet's nucleus. Hence, the disruption occurs due to e.m. force. In contrast, the tidal deformation is the product of the gradient of gravitation times the diameter of the comet's nucleus. The size of the nucleus is very small. Hence, tidal rupture can occur only with a particularly large gravitational gradient.] They can also fly apart from rapid rotation of the nucleus, break apart because of thermal stresses as they pass near the Sun, or explosively pop apart like corks from champagne bottles due to the outburst of trapped volatile gases ...

German astronomers Arnold Schwassmann³¹ and Arno Arthur Wachmann³² discovered this comet during a photographic search for asteroids in 1930, when the comet passed within 10^7 km of the Earth (only 24 times the Earth-Moon distance). The comet orbits the Sun every 5.4 years, but it was not seen again until 1979. The comet was missed again in 1985 but has been observed every return since then. During the fall of 1995, the comet had a huge outburst in activity and shortly afterwards four separate nuclei were identified ... "

²⁹ Comet 73P/Schwassmann-Wachmann 3, Views of the Solar System, <http://www.solarviews.com/eng/wachmann.htm>.

³⁰ See some images in *Astronomy and Geophysics*, 47, (3), p. 3.12. Our added note.

³¹ Friedrich Karl Arnold Schwassmann (1870–1964), discoverer of 22 minor planets and 4 comets.

³² Arno Arthur Wachmann (1902–1990), discoverer of comets and minor planets.

An unexpected and surprising behavior was found in comet Lovejoy, which was discovered on 27th November 2011 by Terry Lovejoy (1967-, engineer and amateur astronomer of Thornlands, Queensland, Australia). The comet was designated C/2011 W3 (Lovejoy). It appeared to be a member of the Kreutz family. The perihelion was at 0.0055 AU just after midnight on 16th December (Kronk, 2011; Williams, 2011), ~ 140,000 km above the Sun's surface (Anonymous, 2011c; Malik, 2011).

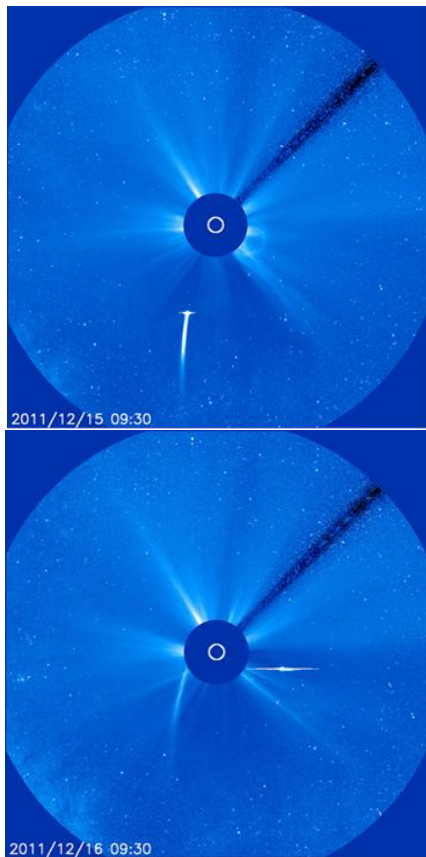


Fig. 28. “These two images were taken by SOHO and show comet Lovejoy heading in toward the Sun (top) and then emerging back out the other side (bottom). Credit: NASA/SOHO.” Figure and captions after Phillips (2011a). NASA copyright free policy.

“The comet's close encounter was recorded by at least five spacecraft: NASA's SDO and twin STEREO probes, Europe's Proba2 microsatellite, and the ESA/NASA SOHO. The most dramatic footage so far comes from SDO, which saw the comet go in (below) and then come back out again (above)” (Phillips, 2011a). See Figs 28a and 28b. A better composite photograph is given by Schrijver et al. (2013) (Fig. 29).

Another example is comet C/2011 N3 (note that the Lovejoy comet is C/2011 W3). Comet Lovejoy was not

expected to survive the encounter, due to extreme environmental conditions (temperatures $> 10^6$ K ; exposure time of nearly one hour). See Fig. 30. However, the comet C/2011 N3 was observed to emerge intact from the corona (Phillips, 2011a, 2012f; Wall, 2011a, 2011b). The nucleus diameter was formerly estimated ~ 100 – 200 m. Since it survived perihelion, it was later guessed having been perhaps up to 500 m (Phillips, 2012a).

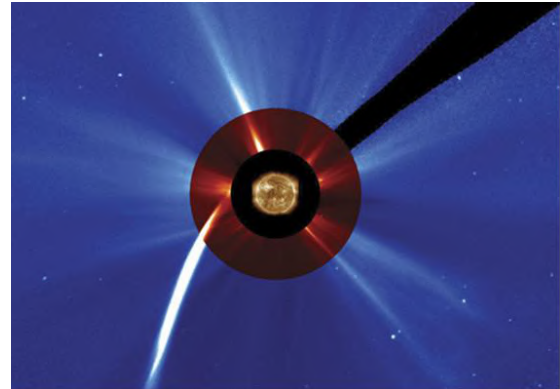


Fig. 29. “A composite photograph of the Sun and inner heliosphere taken at 01:30 UT on 16th December 2011. The center exposure, taken by NASA's SDO spacecraft, shows a false-color image of extreme UV radiation from gases in the corona at ~ 1.5 M K°. Surrounding that central image are images made using the Large-Angle and Spectrometric Coronagraph (LASCO) aboard the ESA's SOHO spacecraft. Two different LASCO telescopes (with image segments shown in red and blue) reveal structures known as streamers, which outline relatively dense coronal regions shaped by **B**, against a backdrop of stars. The arc reaching toward the Sun from the lower left is comet Lovejoy's tail as it approached perihelion. The bright mark near 2 o'clock at the inner edge of the red image shows post-perihelion Lovejoy just beginning to regrow a dust and gas tail after having lost it while closer to the Sun. Within three days from these images, Lovejoy's nucleus completely sublimated and ceased to exist.” Figure and captions after Schrijver et al. (2013). NASA/ESA copyright free policy.

“In the SDO movies, the comet's tail wiggles wildly as the comet plunges through the Sun's hot atmosphere only 120,000 km above the stellar surface. This could be a sign that the comet was buffeted by plasma waves coursing through the corona. Or perhaps the tail was bouncing back and forth off great magnetic loops known to permeate the Sun's atmosphere. No one knows.” (Phillips, 2011a).

A more recent case history deals with comet ISON (Fig. 31). It came within 1.1 M km of the Sun's surface. However, it was no more seen by SDO after perihelion transit. Hence, it was believed that it broke up and evaporated before reaching perihelion.

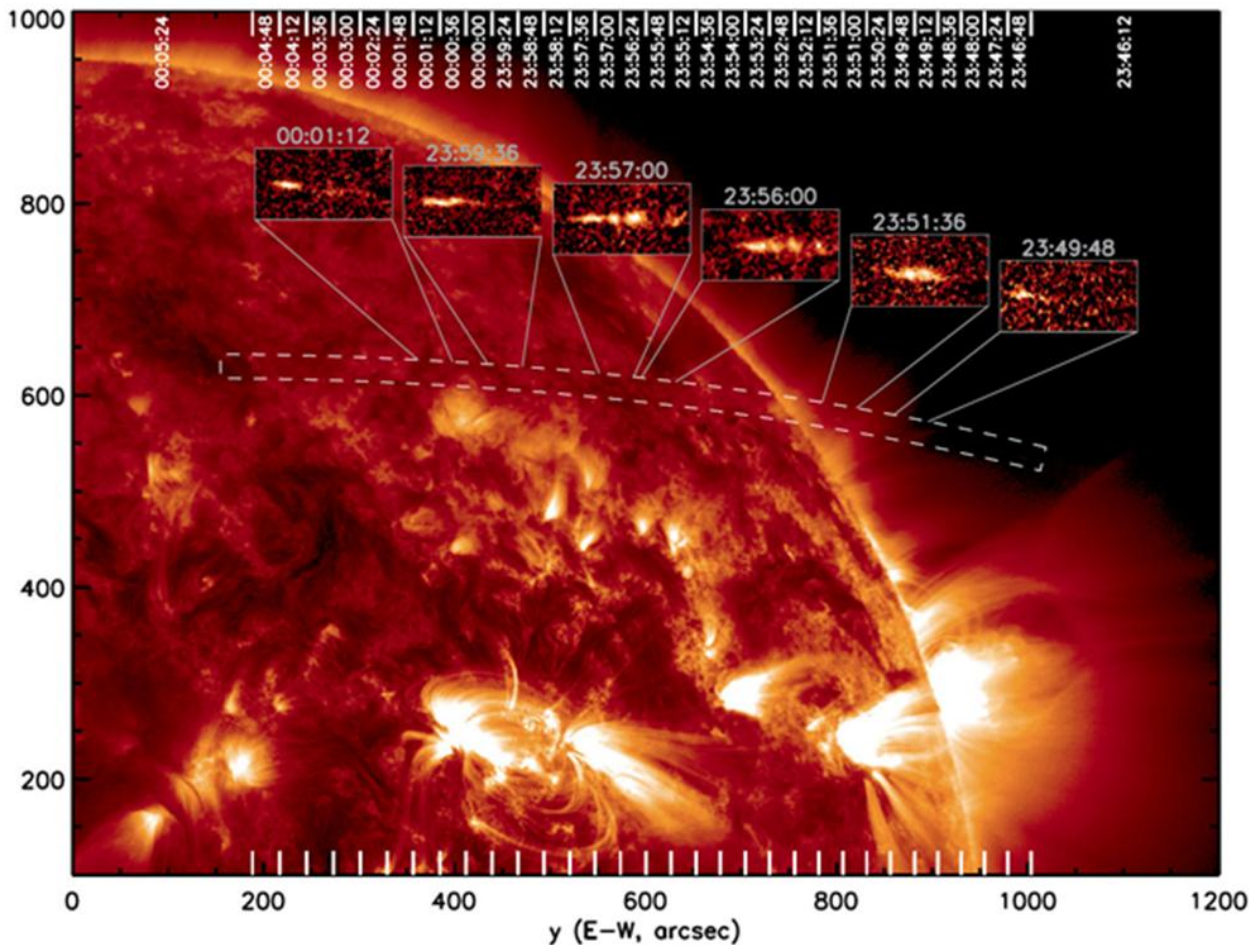


Fig. 30. “Comet C/2011 N3 fragments as it passes through the Sun’s atmosphere on July 6th, 2011. Credit: Solar Dynamics Observatory/K. Schrijver et al.” Figure and captions after [Phillips](#) (2012f). See also [Schrijver](#) et al. (2012, 2013). NASA copyright free policy.

“On the morning of November 28th, expectations were high as ISON neared perihelion ... The icy comet already had a riotous tail 20 times wider than the full Moon and a head bright enough to see in the pre-dawn eye with the unaided eye ...

... they watched live images from a fleet of solar observatories including the twin STEREO probes, the SDO, and SOHO. As comet ISON approached the Sun it brightened and faded again. That might have been the disintegration event ... Cameras onboard the SDO followed the comet all the way down to perihelion and saw ... nothing ... The researchers were surprised again when a fan-shaped cloud emerged from the Sun’s atmosphere. No one knows for sure what was inside. Possibilities include a remnant nucleus, too small for SDO to detect, or a ‘rubble pile’ of furiously vaporizing fragments. By the end of the day, comet ISON was nothing but a cloud of dust ... “ (Phillips, 2013e).

However, subsequent images - by a camera called LASCO C3 onboard the NASA/ESA’s SOHO - detected something rounding the Sun (Malik, 2013, and Wall, 2013). This appeared therefore like something that began to gradually brighten up again, but it soon faded off

“Recent observations by NASA’s Mars Reconnaissance Orbiter (MRO) suggest that ISON’s nucleus was between 100 – 1,000 m wide ... It was probably smaller than maybe 600 m in diameter ... and from past sungrazing comets, those smaller than about half a kilometer ... don’t survive” (Wall, 2013).

A recent case history is comet Nishimura, also known as C/2023 P1, which survived a close encounter with the Sun on September 17th, 2023, when it passed within only 33 Mkm of the Sun. The bright comet was observed by one of two STEREO spacecraft, i.e., STEREO-A. The images suggest the comet remained intact (Mathewson, 2023).

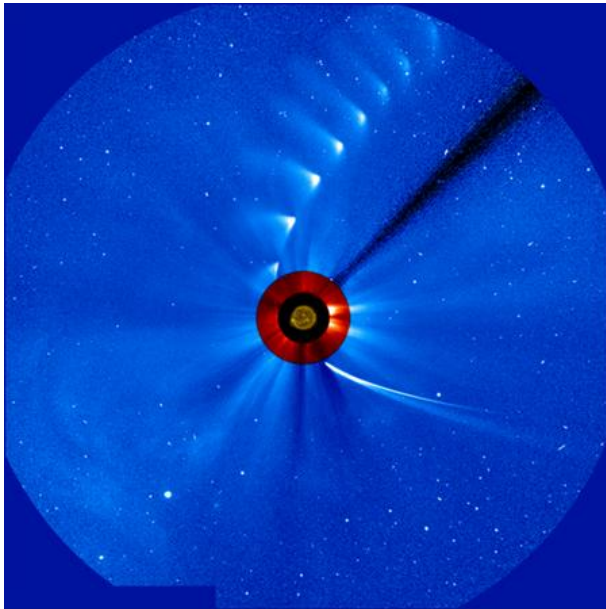


Fig. 31. “Comet ISON comes in from the bottom right and moves out toward the upper right, getting fainter and fainter, in this time-lapse image from the ESA/NASA SOHO on November 28th, 2013. The image of the Sun at the center is from NASA’s SDO. Credit: ESA/NASA/SOHO/SDO/GSFC.” Figure and captions after Wall (2013). NASA copyright free policy.

An unexpected hint recently derived from the observation and interpretation of the asteroid ‘Oumuamua (11/2017 U1), which [Sekanina \(2019\)](#) looks like “a piece of debris of a dwarf interstellar comet ... The rest of the parent dwarf comet’s debris is expected to have escaped detection after perihelion . [In fact, in principle a large amount of matter can move through the Solar System, although it can be detected only whenever suitable conditions exist so that it can release photons. This is the difference between an asteroid and a comet. Hence, the debris of a comet are eventually no more detectable.] It is pointed out that the unknown timing of the disintegration event, in the course of which the non-gravitational acceleration began to affect the orbital motion of ‘Oumuamua , may compromise investigations of the stellar system from which the object had arrived. The pre-perihelion brightness of ‘Oumuamua ’s parent remains unknown, but one cannot entirely rule out the possibility that it was serendipitously detected near, or during, the putative outburst ... “

Summarizing , a great variety is observed of different behaviors of sungrazing comets, and the explanation of their morphology can be tackled according to the twofold aforementioned perspective.

Let us first refer to the viewpoint of a comet that is likened to a stony meteorite with some tracing chemicals

in it.

According to the rationale of the present study , the crucial role must be considered of the e.m. induced currents j , and of the Hamilton’s principle (Gregori et al ., 2025 e), by which the currents j tend to expand - thus causing fragmentation of the cometary nucleus , independent of either tidal or thermal effects. All effects (e.m., tidal , thermal) can contribute and sum up altogether, although all drivers play comparable roles mainly when the comet is far away from the Sun. In fact, consider : (i) the very small size, hence the very small gravitation gradient across the nucleus ; (ii) the limited mass, hence the comparably limited thermal response ; (iii) the large electrical conductivity of the evaporated material ; and (iv) the large orbital eccentricity that implies a huge e.m. induction [as per (1)]. Hence, - it is reasonable to guess, at least intuitively, that - in general - the e.m. contribution is likely to be often overwhelming . In addition , the role of the Cowling dynamo (Gregori et al., 2025 d) is very likely to be the dominant confining effect resulting into self-collimation and filamentary patterns.



Fig. 32. Enki Catena crater chain on Ganymede. North is to the bottom of the picture and the Sun illuminates the surface from the left. The image was taken on April 5th, 1997 at a range of 27,282 km by the Galileo spacecraft. Credit: Galileo Project, Brown Univ., JPL, NASA. NASA copyright free policy.

This same argument applies to every comet, even other than sungrazer comets. Sometimes, when a comet is observed - and also even when it is still far away from the Sun - occasionally large discrete disruptive events are observed, envisaging that the comet lost a large piece of its nucleus. Hence, the same aforementioned argument can apply to every event of this kind.

For instance, a phenomenon of this kind can be, perhaps, the explanation of the Enki Catena, a 161.3 km

crater chain on Ganymede (Fig. 32³³). The 13 observed craters were probably formed by the impact of a comet that passed close to Jupiter. Then, either the Jovian gravity, or e.m. induction by the Jovian **B**, disrupted the cometary body. Then, the 13 fragments crashed onto Ganymede in rapid succession. On the other hand, the gravitational disruption - i.e., the tidal deformation caused by Jupiter - is directly related to the product of the space gradient of gravitation times the size of comet's core, which is very small. In contrast, the e.m. induction effect depends on the surface of the cross-section of the comet's core (for a known electrical conductivity σ of the comet) times the time variation of the Jovian **B**.

6.4. Comets: evidence plasma tail structure

Fig. 33 refers to the Halley comet. We know that *in situ* records (by the *GIOTTO* flyby mission) measured no **B** for Halley's. Consider, however, that the Cowling dynamo generates a toroidal field. Hence, **B** is null outside the confining "plasma bottle". This is the same phenomenon observed for *BLs* in Fig. 8 through Fig. 11 of Gregori and Leybourne (2025e). In addition, **B** has an essentially transient character, with an unknown persistence-time. That is, the induced **B** even rapidly decays, although after having eventually caused the more or less partial disruption of the nucleus.

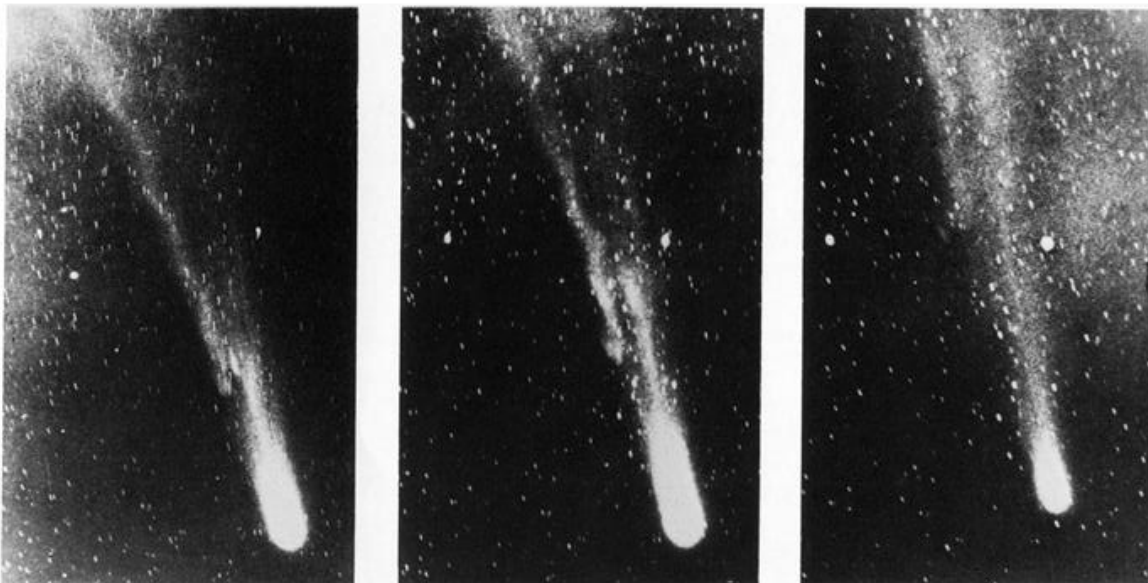


Fig. 33. "Photographic time sequence of Halley's comet, June 6th-7th, 1910. The sequence was constructed by E. E. Barnard from plates taken at (left to right) Yerkes Obs. (June 6th, 15.8 h GMT), Hawai'i (June 6th, 18.5 h GMT), and Beirut (June 7th, 7.0 h GMT). The photographs show rapid changes in the form of a receding plasma tail which disconnected late on June 5th and whose mean recession speed during the duration of this sequence was 57 km sec⁻¹ (Yerkes Obs. photograph)." Figure and captions after Brandt et al. (1980). NASA copyright free policy.

Vourlidas et al. (2007) report about a direct observation of the interaction between comet 2P/Encke and a *CME* (coronal mass ejection), which led to a complete plasma tail disconnection. "The observations were obtained by the Sun-Earth Connection Coronal and Heliospheric Investigation (SECCHI) Heliospheric Imager-1 (HI-1) aboard the STEREO mission. They reveal the extent of the plasma tail of comet 2P/Encke to unprecedented lengths and allow us to examine the mechanism behind a spectacular tail disconnection event ... the observations offer strong support to the idea that

large-scale tail disconnections are magnetic in origin. The online movie reveals a wealth of interactions between solar wind structures and the plasma tail beyond the collision with the CME ... "

On the other hand, the interaction of a comet with the *HNS* (see Figs 3 and 4) seems to have no relevant effect on the cometary tail. Indeed, Saito et al. (1986) report on an astute study of Halley's comet. The magnetometer aboard the Japanese spacecraft *Sakigake* clearly detected multiple crossings of a nearly horizontal *HNS* during 10th-12th March 1986. Saito et al. (1986) were concerned with

³³ <http://antwrp.gsfc.nasa.gov/apod/ap011215.html> (page in NASA Photojournal).

the absence, during 11th-14th March, of any apparent disconnection event (*DE*) in the ion tail of comet Halley. Therefore, they proposed a model for the interaction between the comet and \mathbf{B}_{int} at the crossing with a quasi-parallel *HNS*. Also some *MHD* wave enhancement was observed, almost at the closest approach to the comet. They guess that these waves can be interpreted as being excited by neutral particles of cometary origin (ionized O^+ or H_2O^+). These ions had been previously detected at $\sim 7 \times 10^6$ km upstream of the comet.

The Saito et al. (1986) study shows the great heuristic potential of a comet as a natural probe for monitoring the interplanetary environment. Saito et al. (1986) is one of several published papers dealing with the *Sakigake* mission. Let us focus on their specific analysis of Halley's comet. The great difficulty must be stressed of their data analysis. They used the instant and point-like magnetic records carried out during the closest approach achieved by *Sakigake* on 11th March 1986 at 04:18 UT. Saito et al. (1986) had available data spanning over ~ 13 hours - during the time lag 19:40 UT of 10th March through 8:37 UT of 11th March. They also correlated their measurements with the records by the *Stanford* solar magnetogram (provided by T. Hoeksema) and with the interplanetary scintillation data (provided K. Kojima and K. Kakinuma).

Saito et al. (1986) discussed different types of occurrences. They introduced some protocol and criteria to be satisfied in order to distinguish between different typical phenomena. There is no need to enter here into details. They claim having thus recognized several crossing of the *HNS* (see Figs 3 through 5). They show a detailed figure not here shown that they discuss in detail. They suppose that a radial expansion characterizes the *HNS*, and claim that during 10th-11th March *Sakigake* crossed several times the *HNS*. Also the disturbances were taken into account that affected \mathbf{B}_{int} , and they afforded to distinguish 4 categories of disturbance.

They supposed that, consistently with the Parker spiral, the *HNS* is transported radially, at the solar wind speed v_{sw} . Suppose that the cross-section with the *HNS* can be represented by a vertical plane (remind about Fig. 3a) where the *Sakigake* orbit is located. Such a cross-section seems therefore to move in the vertical plane, anti-sunward, at the apparent velocity component - of the *HNS* along the *Sakigake* orbit - that is given by $v_N = v_{sw} \tan \chi$, where χ is the angle between the plane and the Parker spiral. The orbital velocity of *Sakigake* was $v_{sk} \sim 70$ km sec⁻¹, anti-sunward. However, $v_{sk} < v_N \sim 450$ km sec⁻¹. Hence, *Sakigake* crossed the *HNS* moving sunward. Saito et al. (1986) state that, for at least 4 times, *Sakigake* certainly crossed the *HNS*. However, at a closer inspection, they report about additional evidence of

multiple crossings. Note that, in fact, these multiple crossings are consistent with the fluctuations of the solar wind flow and of the frozen-in \mathbf{B}_{int}

Saito et al. (1986) remind about Niedner and Brandt (1978) who proposed that every time a comet crosses through a (perpendicular) sector boundary, i.e., through *HNS*, a former ion tail is substituted, through a *DE*, by a newly-grown ion tail. To our understanding, this means that since 1978 cometologists already considered the possibility of a cometosphere.

In fact, Saito et al. (1986) apply the Niedner and Brandt (1978) model to the *Sakigake* crossings occurred during 10th-11th March 1986. They had available precise information dealing with the day of the closest *Sakigake* approach, concerning the sector boundary at 7×10^6 km upstream of Halley's comet. At that time, according to Yeomans (1981), the solar wind speed was 450 km se c⁻¹. If the length of Halley's ion tail is 0.3 AU, the solar wind spent therefore 28 hours to run through the whole length of the ion tail.

In this respect, it is important to refer to the aforementioned discussion concerning the transition of the Earth's magnetosphere while crossing through *HNS*. The effect is simply a smooth exchange of the role played by the \mathbf{j} in the two solenoids that are identified, respectively, with the two lobes of the tail (Fig. 9). The unique detectable effect ought thus to be only a gentle morphological disturbance of the *Sq* geomagnetic variation. On the other hand, the effect is probably hidden by the large disturbances that are usually associated with ionospheric activity. Therefore, owing to a similar argument, identical phenomena must be expected to occur inside a cometosphere.

Hence, Saito et al. (1986) searched for ground-based observations, during 11th-14th March 1986, of any possible *DE* in Halley's ion tail. However, no evidence was found in observations carried out from Asia, Australia and the United States. They noticed only two distinct streamers, and remark the helical structure observed close to the coma that - they note - ought to be related to the wavy structure of the *HNS*. They also show a sketch (not here shown) of the cometosphere before and after *HNS* crossing

Hence, no *DE* affected the Halley's ion tail. Therefore, Saito et al. (1986) propose a model, and suppose that *Sakigake* approached to the comet along an orbit quasi-parallel to *HNS*. They draw 3D patterns of the cometosphere, entering in the detailed description of the different angles between *HNS*, *Sakigake* orbit, \mathbf{B}_{int} , etc. No additional information is here given.

Let us only show Fig. 34 that represents the two-lobe pattern of Halley's cometosphere that is proposed in the model computed by Saito et al. (1986). The comet was in

a “toward” B_{int} sector. Remind about the transition of the Earth’s magnetosphere between interplanetary sectors of opposite polarity, as discussed with reference to Fig. 9.

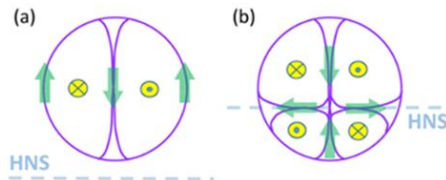


Fig. 34. Two cross-sections downstream of Halley’s comet tail, according to the model derived from the *Sakigake* observations during 10th-12th March 1986. Both cross-sections of the tail are observed from the comet head, looking towards the tail. *Sakigake* was in a “toward” sector of B_{int} , with an orbit above and slightly inclined with respect to *HNS*. During the few days of available observation, *Sakigake* crossed several times the *HNS*. One final state, after one crossing, is shown in figure (a) in terms of a 2-lobe cometosphere. In contrast, figure (b) refers to what occurs while the comet tail intercepts the *HNS*. A transition thus occurs of the 2-lobe pattern, in order to reverse the B direction in the 2-lobes. Every transition is expected to be smooth, and minor perturbations are associated only to the eventual non-uniformity of the solar wind flow. See text. Unpublished figure.

Saito et al. (1986) remind also a related study (Slavin et al., 1986) referring to comet Giacobini-Zinner. The interested reader ought to refer for better details to the original paper Saito et al. (1986). All these statements are in close agreement with the general discussion here proposed about the existence of more or less transient or permanent cometospheres. Therefore, also the speculated “black axis” feature, which is discussed above, seems realistic. This whole discussion also envisages the great heuristic potential of the huge population of cometary objects that can now be observed by space telescopes and that are natural probes of the interplanetary environment.

Saito et al. (1986) carried out also an investigation of the neutrals released from the cometary nucleus. They carried out dynamic spectrograms of the observed component of B_{int} . They considered the local cyclotron frequency for O^+ (or H_2O^+), estimated by means of 20 min averages of the total B_{int} . They found a correlation between some enhanced oscillations of B_{int} and the local O^+ (or H_2O^+) frequencies. By this, they found long-period waves, linearly polarized and in transverse mode, which are correlated with the local O^+ (or H_2O^+) cyclotron frequencies.

Fig. 34a shows the down-tail cross-section of a regular 2-lobe pattern of the cometosphere. The clockwise or anti-clockwise j direction must reverse while crossing through *HNS*. Fig. 34b shows the down-tail cross-section, during

the crossing stage from one Parker spiral sector to the other, consistently with the aforementioned discussion of Fig. 9.

Saito et al. (1986) discuss the previous literature concerned with *MHD* waves caused even by a very small amount of newly generated ionized particles. They believe that the long-period *MHD* waves - that were observed $7 \times 10^4 km$ upstream of comet Halley - ought to have been excited by ions originated from the comet (O or HO).₂ +

Saito et al. (1986) conclude with the following historical remark. They refer the two-hemisphere model to the solar-cycle variation of the 3D heliosphere, related to geomagnetic activity indices. Thus, the *HNS* configuration of the past can be approximately estimated, and the interaction can be studied of Halley’s comet with the *HNS* during the 13th May 1910 event (Saito and Saito, 1986). In general, it is therefore possible to use old photographs of comets to investigate the cometosphere interaction. In particular, Saito et al. (1986) mention a famous *DE* of comet Morehouse during September-October 1908.

Concerning the 13th May 1910 event of Halley’s comet, Saito and Saito (1986a) specify what follows. “Surveying 26 plates of comet Halley during the apparition in 1910, the ion tail with a distinct kink on May 13th is concluded to be one of the most specific events throughout the last apparition. The heliosphere was deduced from the analysis of its solar cycle variation to be in excursion phase. From the analysis of 27 day recurrence time pattern of geomagnetic activity index *C9* during 1909-1911, the inclination and the position of the *HNS* on the day is obtained and expressed on the two-hemisphere diagram. Superposition of the Earth and the comet on the diagram reveals that the comet was just on the neutral sheet on 13th May 1910. Considering the observation by *Sakigake* on the deflection of the solar wind near the neutral sheet, it is concluded that the kink of the ion tail is caused by a sector boundary crossing ...”

The Earth crossed through the tail of Halley’s comet in the early morning of May 19th, 1910. In addition to the aforementioned *C9* index (an old approximate geomagnetic index), some ground-based magnetograms are available, although they seem to provide with no better evidence other than the expected asymmetry of the cometary bow shock (Ivanov and Shevnin, 1966).

Let us point out that the former classical viewpoint - by which a comet is a simple dirty ice ball, which evaporates due to solar radiation - has been thus completely substituted by a new viewpoint, where the e.m. interaction between solar wind and cometosphere plays the dominant role.

The other comment by Saito et al. (1986) is that - as already mentioned - they showed the possible effect of Halley's comet ions (O^+ or H_2O^+) at 7×10^6 km ahead of the comet, by means of the dynamic spectrograms of *Sakigake* B_{int} records. Thus, they conclude that it is reasonable to expect that Halley's comet originates effects that can be detected over a much wider domain than formerly expected. In fact, note that the process that leads to the formation and evolution of a cometosphere has a spatial range much behind the mere observed extension of the comet.

In any case, these *Sakigake* records, and their discussion, clearly show the complication of the comet's interaction with interplanetary environment. Compared to the old fashioned and naive concept of simple thermodynamic evaporation of some dirty ice due to solar radiation, such a process is much more intricate. In fact, a cometosphere cannot be conceived like a planetary magnetosphere where a central solid object is the B source, which opposes the action by solar wind thus generating a magnetopause etc. Compared to other planetary objects, a comet is generally much smaller, and can release chemicals and/or ions. In addition, the most important difference is the presence of a Cowling dynamo, supported by ion evaporation, which generates an intense toroidal B that acts as an efficient self-confinement of the plasma.

A part of the plasma is supplied by the direct contribution of electrons and ions from the solar wind. The physical system of the cometary object is therefore a plasma-ball intimately composed of its nucleus plus the cloud of its surrounding neutral atoms, ions, and electrons. We identify the whole cometosphere with the object that we call "comet".

The e.m. induced currents j flow within the whole cometary system, and the currents result into the generation of a total B , which varies in time and also dramatically in space, along the much elongated cometary orbit. A fundamental role is played by the Cowling dynamo that transforms the kinetic (thermal) energy of the evaporation process into e.m. energy. The generated toroidal B results into a confining action. In addition, self-collimation of transient features leads to the formation of linear patterns (streamers and comet's tail). The cometosphere is the response to the total process.

For clarity purpose, remind, e.g., about two simple and clear sketches shown by Yeomans (1991, p. 237 and 282) due to the wrapping of B_{int} field lines around the comet. The sketches are drawn in the plane of B_{int} field lines, i.e., approximately in the ecliptic plane. Yeomans (1991) also considers the effect of the crossing of a comet through the *HNS*.

A more detailed sketch, which refers to the

aforementioned "reconnection", is shown by Niedner and Brandt (1978), which they claim "*outlines the key features of Alfvén's theory (Alfvén, 1957) of plasma tails*" and that is supposed to explain a *DE*. It must be stressed, however, that the concept of "reconnection" is used for cometary physics with the same approximation applied when dealing with the Earth's magnetosphere (see Fig. 6). That is, "reconnection" is a way to represent, by means of the continuous formalism of *MHD*, a phenomenon that is rather intrinsically related to a discrete variation of the small number of available charged particles in the solar wind, i.e., of solar wind density, of "plasma cavity", etc.

However, according to Saito et al. (1986, 1986a), this model is not confirmed by *Sakigake*'s observations. Rather, they interpret a *DE* as the effect of a sudden increase of the dynamic solar wind pressure. Saito et al. (1987) envisage also a primary cause of a different kind, always associated with a possible perturbation crossing through interplanetary space. They show Fig. 35, and consider the case history of an abrupt rotation of B_{int} (Fig. 36). All this is perfectly consistent and in agreement with the interpretation that is here proposed.

In any case, always upon likening comets to stony meteorites with a sufficient amount of tracing chemicals, the heuristic value of comets can be even better illustrated in terms of a quantitative analysis of the visual morphological variations of every one given cometary object along its orbit. This is discussed in the following subsections.

In summary, compared with the scenario of the former 1974 draft of the present study, a large amount of new measurements - also by space telescopes and/or space probes - led to a substantial improvement in our understanding of this fascinating show of Nature. All evidence and proposed interpretations clearly seem to be suggestive of a leading role of the e.m. aspects of the interaction between a cometary object and the interplanetary environment. In contrast, the gravitational and thermal effects give a significant contribution in terms of energy supply through sublimation of the iced nucleus. In addition, in terms of cometary structure, i.e., of cometosphere, the gravitational and thermal effects play only a complementary role, except that for sustaining the Cowling dynamo effect.

In fact, from the conceptual viewpoint, the assessment of the Cowling dynamo, dating to 2002 (Gregori, 2002, see Gregori et al, 2025d), is fundamental due to its role in the generation of a toroidal B supplied by kinetic and thermal energy. These closed B field-lines play a crucial role for plasma confinement and self-collimation, thus permitting the survival of comets even when they transit at some comparatively small perihelion.

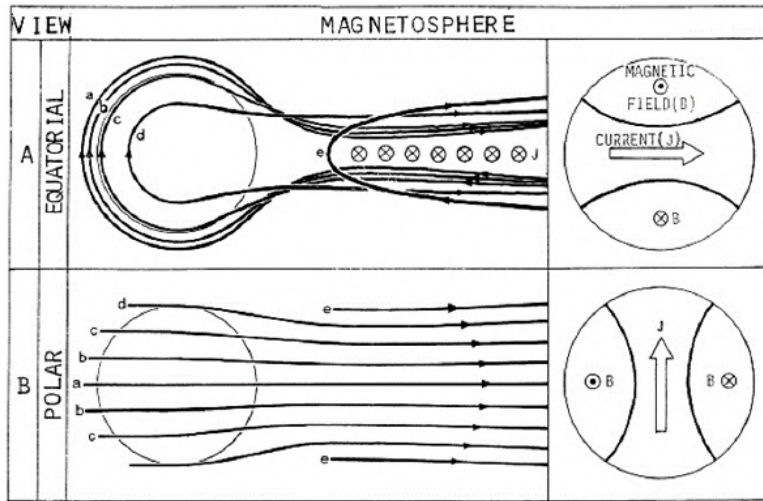


Fig. 35. “3D general model of cometary magnetosphere. The overdrafted field-lines are considered to be slipped from a, via b, c, d, to e. The equatorial and polar views are conventionally named by considering the case of the Earth’s magnetosphere.” Figure and captions after Saito et al. (1987). © ESO, through *Astronomy and Astrophysics*, kindly granted under a CC BY 4.0 International License.

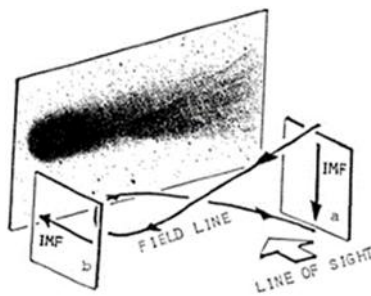


Fig. 36. “Rotating IMF model for the fan-shaped plasma tail. The photograph of comet Halley taken at the Kiso Astronomical Observatory on March 16th, 1986 is used here as an example. The comet is considered to be changing from the equatorial view to the polar view (cf. Fig. 35) owing to the change of the IMF direction from a to b.” Figure and captions after Saito et al. (1987). © ESO, through *Astronomy and Astrophysics*, kindly granted under a CC BY 4.0 International License.

6.5. Summary

Maybe, for clarity purpose, it is worthwhile - even at the expense of some repetition - to briefly summarize and reconsider critically our present understanding of cometary phenomena.

Some key inferences can be seemingly derived by considering specifically the behavior of a sungrazing comet, in particular when reference is made to the intense and comparatively “abrupt” large amount of vaporization when the comet approaches perihelion. The large eccentricity of the orbit is such that comets are very useful natural laboratories aimed to test the behavior of one and the same physical system inside an extremely different and changing environment.

According to a simple and straightforward analysis in

terms of college thermodynamics, a large icy body - which is suddenly warmed up by some very intense heat source - must rapidly evaporate through its “vacuum” environment. Neither such a conclusion has to be changed if the environment is filled up with some gas as some comparatively low density. The case of a sungrazing comet, however, cannot be treated according to such a simple rationale. Evaporation is comparatively very rapid, and generates a cloud of largely ionized plasma, characterized by an intense internal dynamics supplied by the evaporation process. In addition, such a cloud of plasma interacts with the solar wind that - compared to the outer fringes of the Solar System, where the comet was originated - is much denser the closer the comet is to the Sun.

The cometary plasma cloud, with intense internal dynamics, owing to the generalized Cowling theorem (see Gregori et al., 2025d), i.e., owing to Maxwell’s laws, strictly must (at least temporarily) generate a Cowling dynamo, i.e., a pattern like Fig. 2b, with a toroidal \mathbf{B} and a poloidal \mathbf{E} . The intensity of the generated e.m. field is directly related to the kinetic energy of the dynamics inside the cometary plasma nucleus.

The Cowling dynamo generates a “plasma bottle” that confines, and tightly contains, the cometary plasma. This phenomenon is certainly effective and operative, although only as long as the internal plasma dynamics provides with the needed energy supply. This condition is satisfied as long as the cometary nucleus captures solar radiation and thus evaporates. That is, if the original nucleus of the comet is sufficiently large, this condition persists all along the orbit of the comet around perihelion, and the closer the comet gets to the Sun, the stronger the Cowling dynamo is.

Indeed, this same process is observed on the Earth, in

several systems. For instance, refer to the seldom occurring - although well-known - *BL* phenomenon (see Gregori and Leybourne, 2025e). A *BL* is typically and occasionally observed inside some fireplace at home. It appears like a ball of light, a few tens of centimeters in diameter, which survives for several tens of seconds, i.e., as long as some amount of warmer (and ionized) air generates some small-scale convection that supplies an internal Cowling dynamo. A *BL* was previously considered as a mysterious phenomenon. Its explanation, which is here given, is original (Gregori et al., 2025e). In addition, some laboratory experiments are reported in the literature, and they are perfectly consistent with the expectation according to this physical explanation. These experiments, suitably improved, are also pertinent for comets investigations. Therefore, refer to one former experiment, shown in the Fußmann's experiment (Fig. 8 through Fig. 11 of Gregori and Leybourne, 2025e). Other subsequent experiments, also described in Gregori and Leybourne (2025e), are not needed for the present discussion.

This Fußmann's experiment produced transient "light balls" that elapsed typically only ~ 0.3 sec. They measured temperatures internal to the "light ball" of $\sim 2,000 - 5,000$ K for electrons and $\geq 1,300$ K for neutral particles, while the "light ball" surface was cool (a newspaper-sheet posed on top of it did not burn). That is, the plasma is very hot, but it is tightly confined inside the "plasma bottle" that is generated by the Cowling dynamo. In that experiment, the Cowling dynamo survived as long as the source was operative that generated plasma. Then, the *BL* faded off. The experiment was carried out by means of rapid-run movie techniques, etc. In principle, one could also repeat the experiment while flashing a huge amount of e.m. radiation aimed to warm up the *BL*. Rapid-run movies ought then to monitor the survival and behavior of the *BL*.

For the time being, suppose that this physical explanation is sound and correct. Consider the case history of a comet composed of a sufficiently large icy nucleus, which shortly evaporates while crossing through some part of the cometary orbit that is close to perihelion. Suppose that a "plasma bottle" is generated, which confines the cometary plasma. Suppose that this confinement eventually persists for a time lag sufficient to allow for a complete crossing of the comet at perihelion. As the comet later moves away from the Sun, the plasma eventually re-transforms into gas-liquid-solid phase, and the comet gets back to its original state of an icy object that moves through space. This whole process requires a balance between the original volume of the icy nucleus, the time spent close to perihelion, the minimum distance from the Sun's photosphere, and the amount of plasma

that is lost across the boundary of the "plasma bottle". Therefore, in general, it is possible to envisage also the possibility that on some (or several?) occasions a comet can surprisingly survive after its crossing at perihelion.

Concerning the extravagant behavior of comet ISON (Fig. 31), maybe, its new gradual appearance, while displaying anew a cometary tail, can be guessed to be the consequence of some internal process of progressive reorganization of its solid and icy nucleus, and of the tracing chemicals that inform us about the ongoing resetting. The final fading off, however, means that its fragments did not afford to "organize" a new cometary body of sufficient size in order that it can be detected.

Differently stated, according to such a guess, a sungrazing comet should be depicted like a frozen icy body during the largest part of its orbit. However, when it gets close to perihelion, it is transformed into a "plasma bottle", of a "ball of plasma", or a "light ball", or a persistent huge *BL*, to be later back-transformed into the former frozen icy body when it moves far from the Sun.

According to Cofield (2015) "NASA researchers think they understand why comets have a hard, crispy outside and a cold but soft inside just like fried ice cream. Two NASA spacecraft have interacted with a comet surface, and both found a crunchy exterior and somewhat softer, more porous interior ... researchers using a ... cryostat instrument have re-created the conditions on the surface of a comet ... Scientists suspect that the very coldest comets and icy moons in the Solar System contain a special kind of ice called amorphous, or porous, ice. To create amorphous ice, water vapor molecules must be flash-frozen at a temperature of ~ 243 °C ... Amorphous ice is extremely cold, but relatively soft, like cotton candy ... When the comet makes its way toward the Sun, the temperatures on the outside become too hot for amorphous ice to survive ..."

Also the *D/H* (deuterium -to-hydrogen) argument is consistent with such an evaporation /condensation hypothesis. In this respect, one must remind about a possibly related item dealing with the *Rosetta* spacecraft observation of Comet 67P/Churyumov-Gerasimenko (Kramer, 2014d). "An instrument called ROSINA ... has found that the molecular makeup of the water on Comet 67P/C-G is very different from the water found in Earth's oceans. This *D/H* ratio throws a hitch into the theory that comets from Comet 67P/C-G's region of space brought water to the Earth not long after the Solar System formed If even a small number of comets like 67P/C-G impacted Earth in the early days of the Solar System, it still would have greatly changed the molecular composition of the planet's water today ... Therefore, it seems unlikely that these kinds of comets brought water to Earth ... it's more probable that asteroids brought water

to Earth

Scientists have measured the D/H ratio in meteorites from asteroids and found that the water content in these tiny samples is comparable to Earth's water composition ... Thanks to Rosetta, scientists now think that Kuiper Belt comets are much more diverse than expected. In other words, not all comets are the same. Although Comet 67P/C-G has a 6.5 year orbit that brings it near Jupiter, researchers still think that it originated in the Kuiper Belt.

Scientists measured the comet Hartley 2's D/H ratio in 2011 and found that it was very close to that of Earth's, leading scientists to conclude that comets like Hartley 2 (a Kuiper Belt comet) may have delivered water to the early planet. But, because the ratio for Comet 67P/C-G is so off, it doesn't seem like the comets from the Kuiper Belt could have seeded the planet with water.

Comet 67P/C-G's D/H ratio is much higher than even comets found in the Oort Cloud ... Comets in the Oort Cloud were ruled out as possible water deliverers long ago because of their different ratio. This surprising finding could indicate a diverse origin for the Jupiter-family comets - perhaps they formed over a wider range of distances in the young Solar System ... ”

The same items are stressed also by Anonymous (2014r), who shows Fig. 37. The complete scientific paper

is Altwegg et al. (2015) who show a detailed plot (not here shown) of all measured D/H ratios.

[Schrijver](#) et al. (2013) appeal also to the role of the solar **B** in the control of the shape of the tail of a sungrazing comet. This is certainly in agreement with a speculated cometosphere, while the comet crosses very close to the Sun. In contrast, if the comet is a non-magnetized icy object, it simply evaporates when it gets close to the Sun. In this case, the solar **B** interacts with the unconfined gases that are released from the cometary nucleus and that generate the so-called plasma tail (Fig. 38). However, if the evaporated gases are ionized, e.m. interaction must enter into play, hence also the Cowling dynamo, and a cometosphere must be formed. That is, the old fashioned model forgets about the key role of Maxwell's laws.

[Schrijver](#) et al. (2013) propose the explanation of the disappearance of comet Lovejoy (see Figs 28, 29 and 30) according to a detailed figure (not here shown),³⁴ which is consistent with the mechanism that is here proposed, as it appeals to a crucial role played by solar **B**. Therefore, the explanation proposed by [Schrijver](#) et al. (2013) is seemingly much better than the standard interpretation that cannot agree with the confinement by a cometosphere.

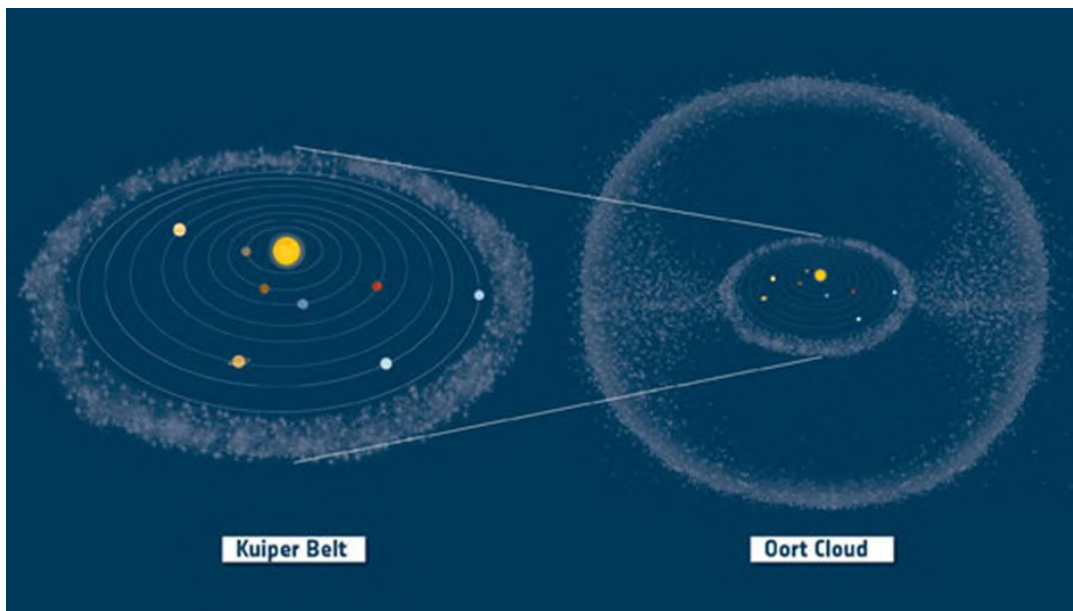


Fig. 37. "Kuiper Belt and Oort Cloud in context." Figure and captions after Anonymous (2014r). ESA copyright free policy.

³⁴ This and a few following figures are here reported for completeness sake, although the untenable - although very common and generally agreed - assumption has to be contended by which **B_{int}** is generally and incorrectly represented perpendicular to the ecliptic

plane (see above). In the comet case, the reference is the comet's ecliptic plane - unlike in the case of the Earth's magnetosphere where the reference is the Earth's ecliptic plane.

In the final analysis, there is no contradiction between the explanation given by [Schrijver et al. \(2013\)](#), and the explanation that is here proposed. The model here proposed involves just one additional effect. That is, every time that any micro- or macro-convection pattern occurs,

a Cowling dynamo is triggered that generates a toroidal **B**. This acts like a true “magnetic bottle” that confines plasma - at every respective spatial scale - just like in the aforementioned Fußmann’s experiment.

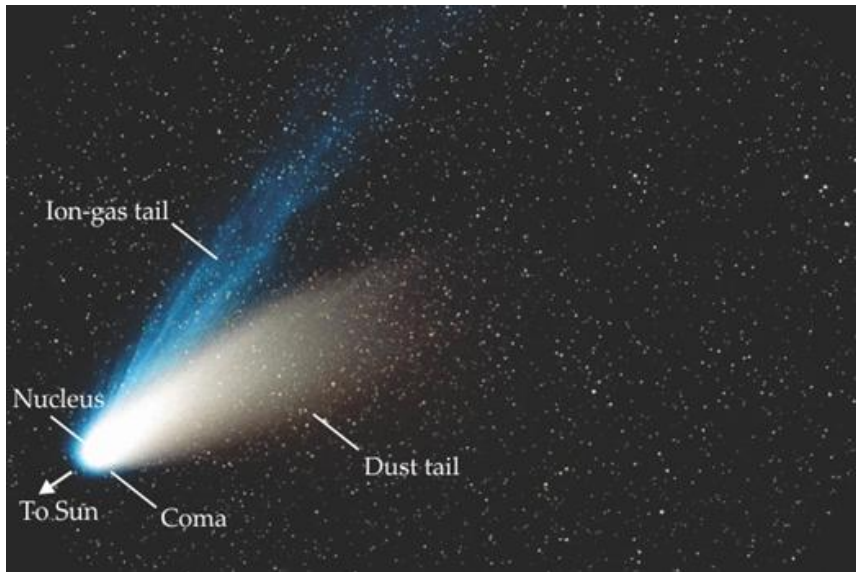


Fig. 38. “An image of comet Hale-Bopp in March 1997 when the comet was ~ 1.01 AU from the Sun. The nucleus of Hale-Bopp was unusually large, with a radius of 25 – 50 km; by comparison, a typical comet nucleus is 1 – 10 km in radius. The Hale-Bopp nucleus is here surrounded by a 100,000 km haze known as the coma. Two tails stretch away from the haze. The gray dust tail, pushed back from the coma by the pressure of sunlight, stretches over 33 Mkm. The bluish ion tail is pushed away from the Sun by the solar wind and its embedded **B**.” Figure and captions after [Schrijver et al. \(2013\)](#). Credit: ESO/E. Slawik. ESO copyright free policy, granted through CC BY-04 license (also Wikipedia license).

The present standard model relies on the mostly gravitational processes - which are believed to characterize the planetesimal aggregation of planets, of comets and of other planetary objects. Such an approach is one additional example of the unconscious strong bias in favor of gravitation compared to e.m. interaction. This bias has profound “historical” roots, because Newton proposed universal gravitation much earlier than the Maxwell’s synthesis of electromagnetism. Hence, planetologists continued to refer to gravitation, almost forgetting about e.m. interaction. And the general rationale still unconsciously survives inside a self-referencing scientific environment. The Alfvén’s theoretical setting of plasma physics, “Alfvén’s layers”, etc., are very recent - and often insufficiently exploited - algorithms. The interested reader can appreciate the following authoritative synthesis given by [Schrijver et al. \(2013\)](#).

They first remind about the so-called aggregational barrier in the formation of planetesimals (Wada et al., 2009, Güttler et al., 2010). In fact, upon suitable

consideration of all physical parameters, it is concluded that - in the “equatorial” plane of the Solar System - the aggregation of gas and dust can lead to centimeter-sized objects. On the other hand, such particles ought to disintegrate when colliding one another at speeds of at least a few kilometers per second. When this “barrier” is over, subsequent accretion is relatively straightforward up to planet-sized objects (Canup, 2004).

Reference to sungrazing comets is then made in order to inspect the size of bodies that contributed to form the parent cometary object. Reference is usually made to standard solid and icy solids. The considered temperature regime is of the order of 500–2000 °K, which is an unusual condition in the Solar System. By means of remote-sensing spectroscopy of the fragments of sungrazing comets, it is then believed that it is possible to investigate the size distribution of the least volatile components (see Brownlee, 2008). Note, however, that this argument relies on the standard old-fashioned concept of cometary structure, in contrast with the plasma-ball cometsphere. In fact, [Schrijver et al. \(2013\)](#) complain

that, at present, no model exists that specifies the details of the processes that affect the chunks of matter that leave a cometary nucleus. Evaporation ought to ensure, hopefully, a sublimation temperature of water ice ~ 200 °K. In contrast, when cooling is insufficient, matter rapidly heats even to thousands of degrees. Tiny pieces of dust and ice are thus produced by explosion. Then, the pieces of dust and ice rapidly dissociate, due to interaction with sunlight and solar wind. In particular, [Schrijver](#) et al. (2013) remind about C/2011 N3 (sometimes abbreviated N3) shown in Fig. 29, which is an image that displays nucleus, coma and debris tail. The mass loss near the Sun was also estimated ([Schrijver](#) et al., 2012) as $1 - 100 \text{ tons sec}^{-1}$. In contrast, telescope observations could monitor gases ejected from debris fragments, which were $< 400 \text{ m}$ in diameter, and were observed on the background of a bright star that had a size about two million times the fragment size. The observations were carried out - concerning N3 - by the *Atmospheric Imaging Assembly* aboard NASA's *SDO* and - concerning Lovejoy - by the *AIA* and the *SECCHI* telescopes aboard NASA's *STEREO* spacecraft. [Schrijver](#) et al. (2013) show also Fig. 39 of Lovejoy comet.

Such a relevant observed discrepancy, compared to expectation, supports the Cowling dynamo process that is here proposed. [Schrijver](#) et al. (2013) specify also the processes that permit to exploit these observations. In fact, the solar corona composition is $> 99.9\%$ *H* and *He* ions by number. In contrast, a comet previously lost almost all volatile species - and is now composed mainly of water ice and rock, with $> 40\%$ *O* atoms and $\sim 5\%$ *Fe* atoms by number. Hence, the solar coronal plasma is locally enriched with *O* and *Fe* atoms. These atoms are formerly neutral, then are ionized. The EUV emitted photons can be detected by instruments aboard *SDO* and *STEREO*. Intuitively, also the maintenance of a significant amount of *O* and *Fe* atoms - even with strong evaporation - seems to support the possible role of confinement, such as the "magnetic bottle" that is here envisaged. This is the same basic mechanism that ought to ensure a conservation of the sublimated plasma that, subsequently, can re-condense on the cometary nucleus.

[Schrijver](#) et al. (2013) compare also the response of a cometary nucleus to the solar wind interaction at different locations along the orbit. At perihelion, the free-fall speed is in the range of speed that is typical of the same solar wind speeds ($300 - 800 \text{ km sec}^{-1}$), which comets experience when they are far from the Sun. Therefore, the speed relative to the solar atmosphere - of a sungrazing comet close to perihelion - is comparable to the speed that the comet experienced far from the Sun relative to the solar wind. The difference is mainly concerned with the rate of molecular dissociation that follows sublimation,

and with the collision rate of atoms with the surrounding environment. For comparison purpose, the solar wind density at Earth's orbit is $\sim 3 - 10 \text{ atoms cm}^{-3}$, and on the order of $\sim 108 \text{ atoms cm}^{-3}$ for the solar corona near the perihelion either of N3 or of Lovejoy.

When considering the distant heliosphere (e.g., see Fig. 38) the leading driver is radiation pressure both on gas and dust, while it is claimed that ionization is responsible for the formation of the plasma tail. In contrast, closer to the Sun, the leading drivers are the collisions of monoatomic gases with the solar atmosphere. [Schrijver](#) et al. (2013) stress the role played by the solar *B*. However, dust and molecular gas have a brief survival time and cannot be detected. The ion tail quickly decelerates while it interacts with the coronal plasma and with the solar *B*. Therefore, concerning Lovejoy, all dust disappeared during about 2 days (or 0.17 AU) on either side of its perihelion passage. Even gas molecules were quickly dissociated. For instance, water molecules dissociated by 3 sec, followed in $< 0.1 \text{ sec}$ by ionization of its atoms (Bryans and Pesnell, 2012).

The complete aforementioned explanation, however, does not take into account the crucial role of the Cowling dynamo that determines self-collimation and self-confinement of plasma. The consequent effect is determinant for mass conservation in the interaction, both with the solar atmosphere and with solar radiation in general. However, the explanation that is here proposed is evidently speculative, at least as long as no dedicated laboratory experiments are available - and as long as some better quantitative models and estimates are exploited by means of direct measurements of several real sungrazing comets. Nevertheless, this speculation is worthy of careful consideration.

Furthermore, consider that the Cowling dynamo is a ubiquitous process - everywhere - from the spatial scale of a supercluster of galaxies, through a galaxy, through the acceleration of ionized particles inside the Sun, through the "micro"-scale of a spark, or of a cloud, where it is also responsible either for the electrification of the ionosphere, or for the generation of *TGFs*, or for making possible water condensation and precipitation (a phenomenon that otherwise is well-known to be completely unexplained). See Gregori and Leybourne (2025e), Gregori et al. (2025f, 2025g). In addition, also the self-collimation process of the solar wind - which is not fully explained - can be fully understood in terms of a micro-scale Cowling dynamo process. That is, the old-fashioned and classical "Cowling theorem" - when it is suitably and rigorously expanded to the "generalized Cowling theorem" - results to be the missing link that can justify several previously unexplained phenomena (Gregori et al., 2025d).

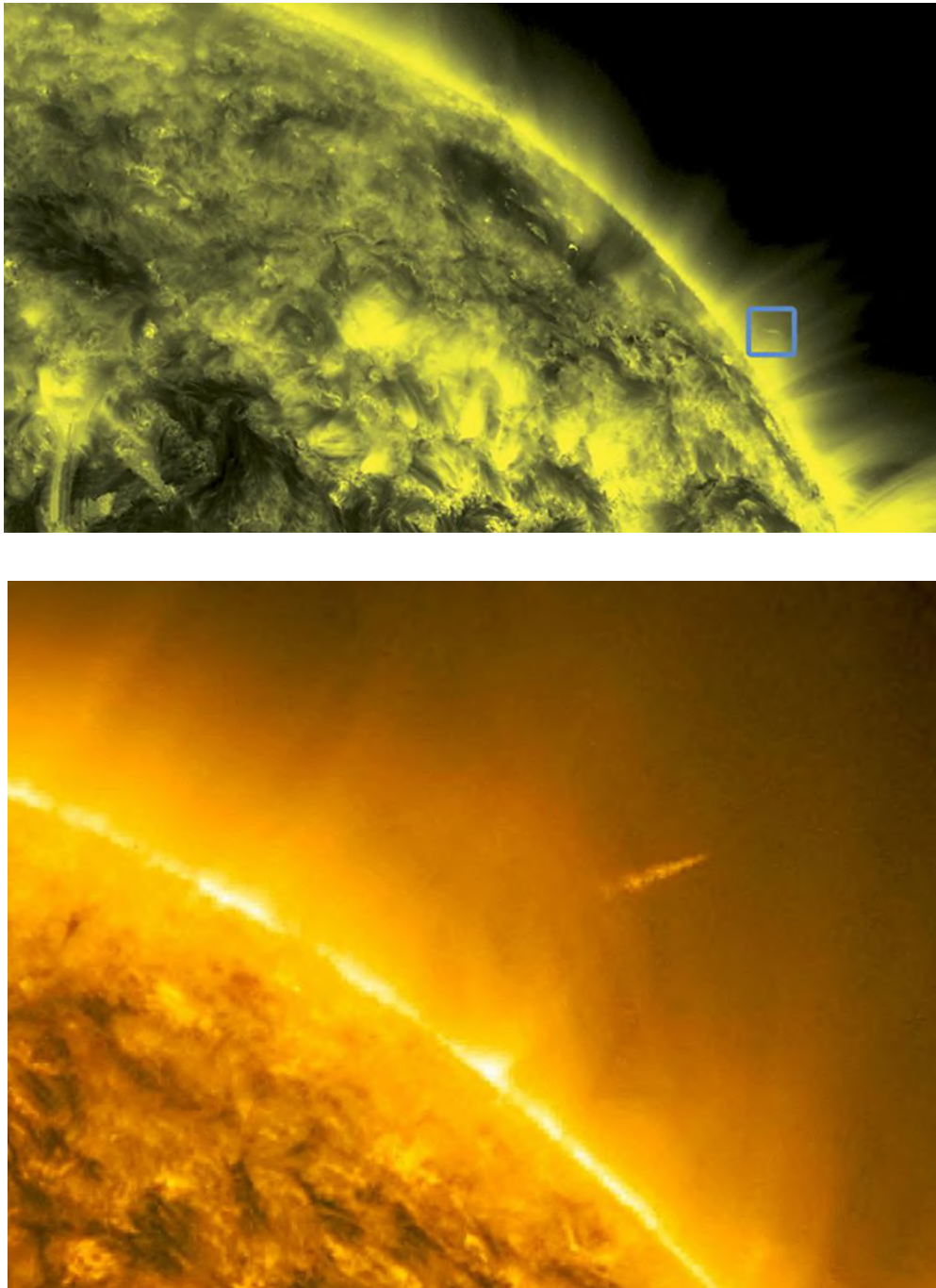


Fig. 39. A comet Lovejoy image. Credit: *NASA/SDO* and the *AIA*, *EVE*, and *HMI* science teams. After [Schrijver et al. \(2013\)](#).
[bottom figure] Comet C/2011 W3 (Lovejoy) re-emerging from behind the Sun on December 15th, 2011. Credit: *NASA/SDO*. *NASA* copyright free policy.

Therefore, the possibility is not “exotic” that this same Cowling dynamo mechanism can play a crucial role also for justifying the definitely surprising survival of a small body, such as a cometary nucleus, while it transits close to the Sun - and, in addition, even when it eventually survives also

after several repeated crossing close to the Sun. Comets are certainly intriguing probes of the interplanetary environment. In addition, much richer information can perhaps be inferred as follows, by means of simple direct monitoring of the morphology of every single comet.

6.6. Comets: dependence of the coma size vs. heliocentric distance

Some old literature must to be recalled. When a comet approaches the Sun, the coma is seen to contract (Lyttleton, 1972).³⁵ The coma can be used, independent of the tail, to monitor the solar wind (Sekanina, 1966; Whipple and Douglas-Hamilton, 1966). In addition, the magnitude of the cometary nucleus was reported to be seemingly correlated with changes in total sunspot area (Churyumov et al., 1972). That is, the changes in the solar wind seemingly affect the size of the image of a comet. In fact, maybe, this “magnitude of the cometary nucleus” is rather the apparent size of the image of the comet, and this ought to be just the size of a cometsphere – or, in any case, the “magnitude of the cometary nucleus” can be related to it.

Therefore, simply represent the comet by means of its “equivalent” \mathbf{j} -loop. Call it C . It has a surface S , defined as some kind of indicative cross-section of the comet interaction with the solar wind, and C has a self-inductance L . As a first order approximation, for simplicity, suppose that both S and L change by no significant amount along the comet’s orbit, although at a second time such an assumption must be suitably reconsidered.

Refer to a very simple treatment, in terms of the “principle of magnetic energy variation”, which refers to two general loops of currents C_1 and C_2 , respectively. A full proof is given in Gregori et al. (2025l), with reference also to previous literature. A brief summary is as follows.

Given any two general loops of currents C_1 and C_2 , producing, respectively, a field \mathbf{B}_1 and \mathbf{B}_2 , the magnetic energy (according to college physics) can be expressed as follows

$$U = U_{s1} + U_{s2} + U_j \quad (3)$$

$$U_{s1} = \frac{1}{8\pi} \int_{V_\infty} \mathbf{H}_1 \times \mathbf{B}_1 \, d\tau \quad (4)$$

$$U_{s2} = \frac{1}{8\pi} \int_{V_\infty} \mathbf{H}_2 \times \mathbf{B}_2 \, d\tau \quad (4)$$

$$U_j = \frac{1}{4\pi} \int_{V_\infty} \mathbf{H}_1 \times \mathbf{B}_2 \, d\tau \quad (5)$$

$$= \frac{1}{4\pi} \int_{V_\infty} \mathbf{H}_2 \times \mathbf{B}_1 \, d\tau$$

where $d\tau$ is the volume differential and V_∞ is all space, and U_{s1} and U_{s2} are called self-energies of C_1 and C_2 , respectively, while U_j is their joint (magnetic) energy. When these C_1 and C_2 are at an infinite reciprocal distance (hence the subscript infinity) it is

$$U_{s1\infty} = \frac{1}{2\gamma_0} L_{11} J_1^2 \quad U_{s2\infty} = \frac{1}{2\gamma_0} L_{22} J_2^2 \quad (6)$$

$$U_{j\infty} = 0$$

where L_{11} and L_{22} are their respective self-inductances.

Let C_1 and C_2 to approach each other, down to some finite distance, through a sum of reversible (hence, ideal) infinitesimal steps of *equilibrium* states. Then, C_1 and C_2 eventually move back at their original location. Consider the case of deformation of C_1 and C_2 , and later consider their reshaping to the original form and orientation, etc. Let C_1 and C_2 have infinite conductivity σ or not, hence an internal Joule heat dispersion or not. All these case histories can be discussed in detail in terms of 13 Gedankenexperimenten.

The result illustrated below can be called “principle of equal variations of the magnetic self-energies and opposite to that of the joint magnetic energy”, or, more concisely, “principle of magnetic energy variation”. This principle can be briefly summarized as follows.

Three case histories must be distinguished, i.e., whether Joule heat enters into play or not. The first two case histories deal with the e.m. interaction between \mathbf{j} -loops. In addition, a third key case history must be considered, which involves a “magpol” source for \mathbf{B} (see below and Gregori et al., 2025w).

Refer to any two most general distributions (in 2D or 3D) of electric current, or two loops, call them C_1 and C_2 , respectively.

I) - When Joule heat can be neglected either it is

$$\delta U_{s1} \equiv \delta U_{s2} \equiv -\delta U_j \equiv -\delta W \quad (7)$$

or either one of the following conditions hold

$$\text{Max } U_j \quad \text{min } U_{s1} \quad \text{min } U_{s2} \quad (8)$$

being

$$\delta U_{s1} + \delta U_{s2} + \delta U_j + \delta W = \delta E \quad (9)$$

where U_{s1} and U_{s2} are, respectively, the magnetic self-energies of C_1 and C_2 , U_j is their joint magnetic energy, W is their kinetic energy, and E includes all other forms of energy that are eventually either supplied to the system (when positive), or released by it (when negative).

II) - Whenever Joule heat cannot be neglected, U_{s1} and U_{s2} progressively damp off, while U_j is transferred step-by-step into either U_{s1} or U_{s2} , where it later decays by Joule heat. That is, U_{s1} decays, while an equal amount of energy is transferred from U_j into U_{s2} where it later decays by Joule heat. The symmetrical behavior occurs in U_{s2} . The process stops when both U_{s1} and U_{s2} vanish.

III) - In the third case one \mathbf{j} -loop is substituted by a “magpol” source. A “magpol” object is composed of “naked” atomic nuclei, i.e., with no electrons captured on atomic shells. Hence, a “magpol” object has zero electrical conductivity σ , as it has no free electrons that can move through it. However, a “magpol” state has a high mechanical performance. In fact, its rheology is different compared to a “solid”. Its structure is fibrous, where every fiber is along the direction of all nuclear magnetic moments that must be strictly and firmly aligned with one another. Therefore, every applied mechanical deformation is

³⁵ Raymond Arthur Lyttleton, FRS (1911-1995) English astronomer.

irrelevant when a displacement is triggered along the fiber direction. In contrast, the applied mechanical deformation is strongly opposed in the case of every external stress that is applied transversally with respect to the fiber alignment.

Note that this is the case of the *IC* of the Earth or of other large planets, and the direction of the fibrous structure is the direction of the dipole **B**. Owing to this reason, shear waves (S waves) can propagate through the *IC*, which is in a “*magpol*” state – in contrast with the generally reported incorrect statement that the *IC* is “solid”, which is inconsistent with all what we about solid state physics.

Since σ is null, no induced currents enter into play, and no transfer of magnetic energy can occur, just due to the assumption of perfect ideal magnetostatic source. That is, this a strict logical requirement implied by the basic, and generally unanimously accepted, present axiomatic formulation of particle physics (for a more general discussion see Gregori et al., 2025w).

The comet is one loop *C*, the ambient solar wind is symbolically represented by the other loop. Call *A* the total energy of *C*, which is the sum of its self-magnetic energy U_s and of the joint-magnetic energy U_j that results by the e.m. interaction with the solar wind. Therefore, consider the simplest case history of one *j*-loop, and by (7) it is

$$\frac{d}{dt} U_s = - \frac{d}{dt} U_j \quad (10)$$

and when we take into account also Joule heat, (10) should be read as

$$\frac{d}{dt} U_s = - \frac{d}{dt} U_j - \frac{I^2}{\sigma} \quad (11)$$

where σ is the conductivity of the loop, and *I* is the current that flows inside it.

Formally integrate (10) and get

$$\frac{1}{2} L \frac{I^2}{\gamma_0^2} + \frac{I}{\gamma_0} \Phi = A \quad (12)$$

where *A* is the integration constant, which expresses the total energy of the system, *L* is the inductance of the *j*-loop, and Φ is the **B** flux linked by it. The energy balance (12) states that the sum of U_j and of U_s is constant in time and it is equal to *A*. It can be interpreted graphically by means of Figs 40, 41 and 42.

We can suppose that the comet - when it begins the interaction with the solar wind - has either a vanishing **B** (hence, $A = 0$), or a non-vanishing **B** (hence $A \neq 0$). Nevertheless, the increase ΔU_s originated by the e.m. induction produced by B_{int} can be estimated by referring to the simpler case $A = 0$. An estimate of the order of magnitude of the effect can be given by means of Fig. 43.

³⁶ As already stressed in a previous footnote, the somewhat unusual constants (e.g., γ_0 and K_0) used in these formulas are required when referring to every kind of different units. In fact, historically, different systems of units were used. Therefore, when dealing with historical papers, a key concern is about a correct interpretation of the information by making reference to a correct unit

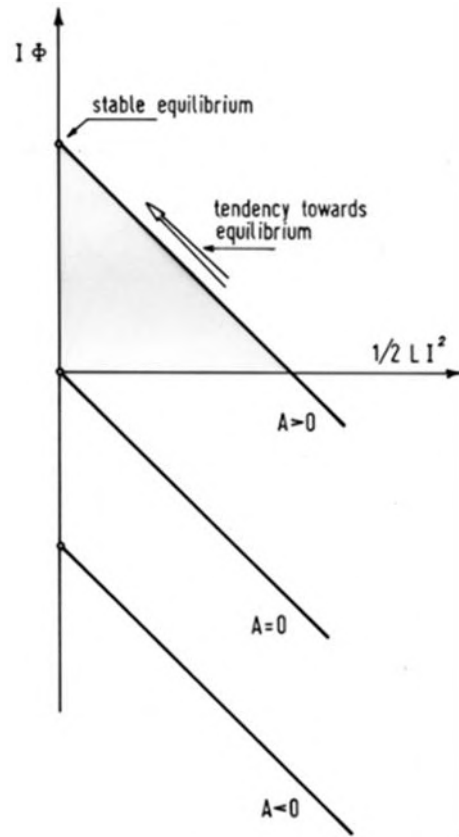


Fig. 40. Plot of U_j vs. U_s , according to (12), when Joule heat is neglected. A non-dissipative system sweeps up and down along the given line characterized by the total energy *A*. Stable equilibrium is attained when $U_s = 0$. If Joule heat is taken into account, the physical trend tends to move vertically the line, by decreasing the total energy *A*, according to (11). Final equilibrium is attained when $A = 0$. See text. Unpublished figure.

As mentioned above, call ϕ the flux of B_{int} that is linked by the effective surface *S* of the comet, which is symbolically represented by a loop *C* with current *I* and self-inductance *L*. Assume that the Φ vs. *I* relationship is simply given by the asymptote³⁶

$$\Phi \approx - \frac{1}{2} L \frac{I}{\gamma_0} \quad (13)$$

hence, since the comet has an effective surface *S* that links a flux of B_{int} , it is

$$\Phi \sim S B_{int} \quad (14)$$

where B_{int} is the intensity of B_{int} at the site where the comet is located. Therefore it is

system. This concern is quite intricate and, for the interested reader, this is discussed in every detail by Gregori et al. (2025o). However, when no historical paper is of concern, there is no need to refer to Gregori et al. (2025o)

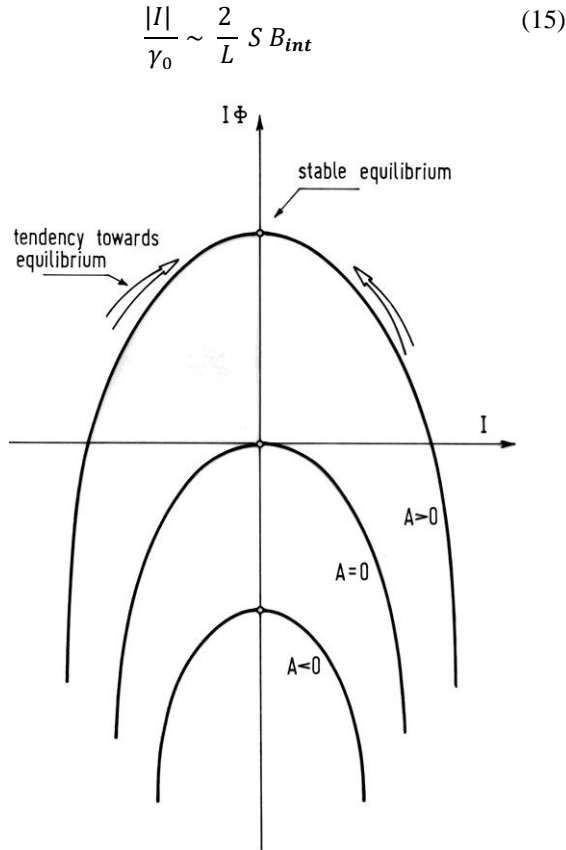


Fig. 41. Plot of U_j vs. I_s , according to (12), when Joule heat is neglected. A non-dissipative system sweeps between states with positive or negative I along one parabola characterized by the total energy A , thus tracking the j oscillation inside the loop. Stable equilibrium is attained when $I = 0$. If Joule heat is taken into account, the observed trend tends to move vertically the parabola, by decreasing the total energy A , according to (11). Final equilibrium is attained when $A = 0$. See text. Unpublished figure.

Note that (15) is only an indicative order of magnitude. The cometary magnetic moment M_c is therefore

$$\frac{|M_c|}{K_0} \sim \frac{|I|}{\gamma_0} S \sim \frac{2}{L} S^2 B_{int} \sim \frac{2}{L} S \Phi \quad (16)$$

Consider that B_{int} must satisfy flux conservation, and its flux depends on the surface through which it is computed. Hence, owing to the surface increase³⁷ vs. heliocentric distance r , the field intensity $B_{int} \equiv |B_{int}|$ ought to decrease vs. r like $1/r^2$. Similarly, the space

³⁷ Consider a spherical surface of radius r that represents an instant state of the solar corona expansion (see, e.g., Gregori et al., 2025b). Half of this spherical surface is crossed by B_{int} oriented outward, and the other half by B_{int} oriented inward. Since the total B_{int} flux must be conserved, the mean $|B_{int}|$ must decrease vs. r as $1/r^2$. As far as energy conservation is concerned, the energy density must decrease as $1/r^2$ in order to compensate the increase as r^2 of the spherical surface. Consider that

density $\rho(r)$ of the solar wind decreases vs. r like $1/r^2$.

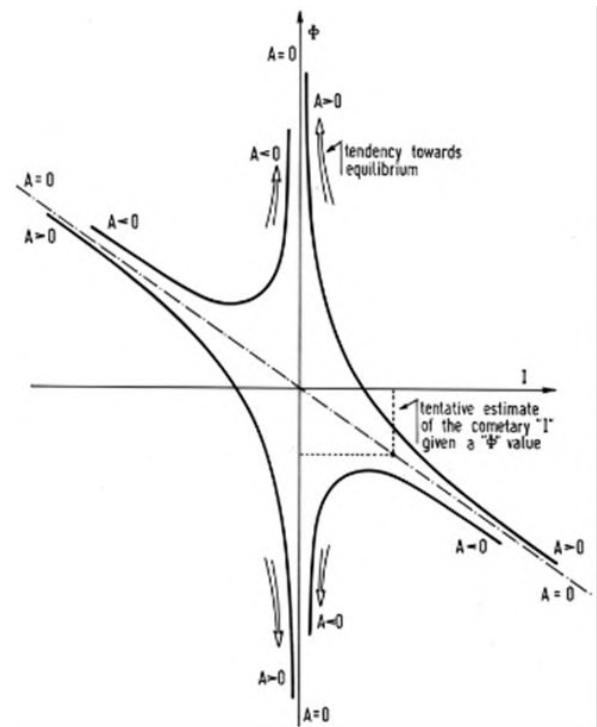


Fig. 42. Plot of Φ vs. I , according to (12), when Joule heat is neglected. A non-dissipative system sweeps between states with positive or negative I along both arms of the hyperbola characterized by the total energy A , thus tracking the j oscillation inside the loop. Stable equilibrium is attained when $I = 0$ and $\Phi \rightarrow \infty$. If Joule heat is taken into account, the observed trend tends to stretch the hyperbola, by decreasing the total energy A , according to (11). Final equilibrium is attained when $A = 0$. See text. Unpublished figure.

Consider the speed v of the comet relative to the solar wind. For simplicity, only the modulus $v \equiv |v|$ is considered. The dependence of $v(r)$ vs. r occurs because $v(r)$ is the vector sum, of a constant heliocentric radial component $v_{int}(r)$ of the solar wind, plus the comet's heliocentric velocity $v_c(r)$. In general, reference is made to comets with a highly eccentric orbit. Hence, the comet - at least during the largest fraction of its orbit - has a velocity $v_c(r)$ with a prevailing radial component. Since the present computation is only an order of magnitude estimate, for simplicity it can be assumed that $|v(r)| = |v_{int}(r) + v_c(r)| \sim |v_{int}(r) + v_c| = v_{int}(r) + v_c(r)$.

the total energy conveyed by the solar wind is kinetic (which is prevailing) and also magnetic. The magnetic energy density is proportional to B_{int}^2 , hence it decreases vs. r as $1/r^4$. That is, the role played by the magnetic energy density decreases more rapidly vs. r than the role of the kinetic energy density. For the present computation, reference is made to the mean value of $|B_{int}|$ that, therefore, decreases vs. r as $1/r^2$.

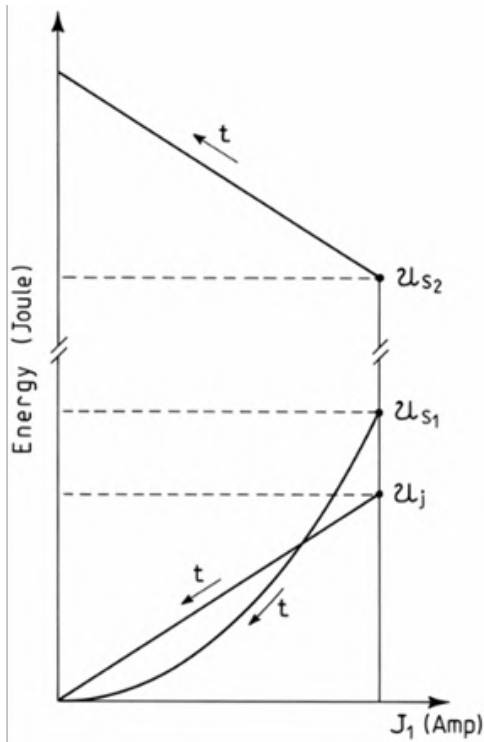


Fig. 43. The magnetic energy variation according to the “principle of magnetic energy variation” (see text). The self-energy U_{s1} decreases by Joule heat being $U_{s1} = (1/2\gamma_0) L_{11} J_1^2$, i.e., a quadratic relation of J_1 . Correspondingly, $U_j = (1/\gamma_0) L_{12} J_1 J_2$ varies linearly vs. J_1 (when it is supposed that J_2 remains constant), while U_{s2} has a variation equal and opposite to U_j . This figure is approximate, as it is assumed that J_2 remains constant. Since J_2 is actually increased, U_j decreases by a smaller amount than what appears in the present plot, and therefore also the increases of U_{s2} is less than the linear trend here shown. After Gregori (1999). Additional details are in the text and in Gregori et al. (20251). Figure also shown as Fig. 2 of Gregori et al. (20251). With kind permission of the late Wilfried Schröder.

The dependence of $v_{int}(r)$ on r can be computed by considering that the solar wind is released by the Sun at an initial mean radial speed $v_{int}(r_\odot) \equiv v_0$ conventionally referred, e.g., to the radius $r_\odot \equiv r_0$ of the photosphere. Then, $v_{int}(r)$ decreases vs. r due to the solar gravitational attraction. This effect can be quantitatively computed by considering the conservation of kinetic plus potential energy (while, as a first order approximation, the role is neglected of the magnetic energy density).

Consider a spherical shell of solar wind, of total mass m , contained inside a layer of radius r and thickness dr . It is (G is the gravitational constant and M_\odot is the Sun’s mass)

$$\frac{1}{2} m v_{int}^2(r) - \frac{GM_\odot}{r} m = \frac{1}{2} m v_0^2 - \frac{GM_\odot}{r_0} m \quad (17)$$

that can be solved with respect to $v_{int}(r)$ giving

$$v_{int}(r) = \sqrt{v_0^2 - 2GM_\odot \left(\frac{1}{r_0} - \frac{1}{r} \right)} \quad (18)$$

Consider the self-energy of the comet that can be computed as follows. The Ohm law for a loop C is

$$F_e - \frac{L}{\gamma_0^2} \frac{dJ}{dt} = J R \quad (19)$$

(F_e is the applied external *e.m.f.* and R is the resistance of C). The energy balance can be evaluated by means of

$$\int F_e J dt - \frac{L}{\gamma_0^2} \int \frac{dJ}{dt} dt = \int J^2 R dt \quad (20)$$

$$\text{or} \quad \int U_{s,total}(\mathbf{B}) = F_e J dt - \int J^2 R dt \quad (21)$$

$$= \frac{L}{2\gamma_0^2} J^2$$

where the $[F_e J]$ integral is the work done by the external *e.m.f.* and the $[J^2 R]$ integral is the Joule heat term.

In this case the duality between \mathbf{B} originated by a current loop C and \mathbf{B} originated by a magnetostatic source can be evidenced as follows. Insert (15) into (21) and get

$$U_{s,total}(\mathbf{B}) = \frac{1}{2\gamma_0^2} L J^2 = \frac{1}{2} \frac{[\Phi(\mathbf{B})]^2}{L} \quad (22)$$

where (21) and (22) can be interpreted as

$$U_s(\mathbf{B}) = \frac{1}{2\gamma_0} J \Phi(\mathbf{B}) = \frac{1}{2\gamma_0^2} J^2 L \quad (23)$$

as, owing to the same definition of L , it is

$$\Phi(\mathbf{B}) = \frac{1}{\gamma_0} L J \quad (24)$$

Similarly to this, (21) and (22) can be interpreted in terms of (23).

Therefore, by (22) the self-energy of the comet is

$$U_{s,c}(\mathbf{B}_{int}, r_c) = \frac{1}{2} \frac{[\Phi(\mathbf{B}_{int}(r_c))]^2}{L} \quad (25)$$

However

$$\Phi(\mathbf{B}_{int}(r_c)) \approx S \cdot v(r_c) \cdot B_{int}(r_c) \quad (26)$$

$$\approx S \cdot [v_{int}(r_c) + v_c(r_c)] \cdot \frac{r_c^2}{r_E^2} B_{int}(r_E)$$

where $v_{int}(r_c)$ is given by (18), r_E is the mean heliocentric distance of the Earth, and by (16)

$$\frac{|M_c|}{K_0} \sim \frac{2}{L} S \Phi \sim \frac{2}{L} S \cdot [v_{int}(r_c) + v_c(r_c)] \frac{r_c^2}{r_E^2} B_{int}(r_E) \quad (27)$$

An eventual cometsphere has therefore a subsolar point at a distance r_{css} that can be expressed as

$$r_{css} \approx r_{Ess} \sqrt[3]{\frac{M_c}{M_E} \frac{r_c}{r_E}} \quad (28)$$

$$\sim \frac{r_{Ess}}{\sqrt[3]{M_E}} \sqrt[3]{K_0 \frac{S^2}{L} \frac{r_E}{r_c} \cdot 10 \gamma}$$

where γ is the \mathbf{B} unit, $r_{Ess} \sim 11 R_E$ is the geocentric distance of the Earth’s subsolar point (and R_E is the Earth’s

radius), and $M_E = 8.01 \times 10^{25} \text{ e.m.u.}$ is the magnetic dipole moment of the Earth.

Relation (28) is deduced by equating the internal magnetic pressure and the external kinetic pressure (analogously to the aforementioned computation of the magnetopause, or of the earthward termination of the plasmashet, see above). In the case of the Earth, it is

$$\frac{1}{8\pi K_0 \mu_r} \left(\frac{M_E}{r_{Ess}^3} \right)^2 \approx \eta K_E \quad (29)$$

where η is a suitable constant factor, and K_E is the kinetic pressure (or the energy density in the solar wind) at 1 AU. Solve (29) with respect to the constant factor η and substitute it into the corresponding relationship that holds in the case of a comet, i.e.,

$$\frac{1}{8\pi K_0 \mu_r} \left(\frac{M_E}{r_{Ess}^3} \right)^2 \approx \eta K_c \approx \eta K_E \left(\frac{r_E}{r_c} \right)^2 \quad (30)$$

where K_c is defined similarly to K_E , and where energy conservation has been taken into account in the expanding solar wind. The result is (28).

Suppose that the cometary nucleus can be symbolically represented by a ring of radius R and cross-section radius $s \ll R$. Then, L is given by³⁸

$$L = 4\pi R \left(\log \frac{8R}{s} - \frac{7}{4} \right) \quad (31)$$

It is well known - and assessed - that the order of magnitude of a cometary nucleus has the typical size is of a few kilometers. Consider therefore a very simple model in order to evaluate in some way a few additional orders of magnitude. For instance, refer to the case of a ring with $R = 10 \text{ km}$ and $s = 1 \text{ km}$. It is $S = \pi 10^8 \text{ m}^2$ and $L \simeq \pi 10^{-3} \text{ Henry}$. Therefore, by (16) it is $M \sim 2\pi 10^{18} \mathbf{B}_{int} (\text{Am}^2)$ (SI units), which gives, at 1 AU an $M_c \sim 10^{-12} M_E$.

Consider that, when the comet approaches the Sun, according to (27) M_c increases as $[\mathbf{v}_{int}(r_c) + \mathbf{v}_c(r_c)] (r_c^2 / r_E^2)$. The factor $\sim (r_c^2 / r_E^2)$ decreases with decreasing (r_c / r_E) , but the factor $[\mathbf{v}_{int}(r_c) + \mathbf{v}_c(r_c)]$ contributes a substantial amplification, because both addenda increase while the comet approaches its perihelion, i.e., $\mathbf{v}_{int}(r_c)$ and most dramatically $\mathbf{v}_c(r_c)$.

Note that the entire aforementioned approximate computation relies on the assumption that S and L do not change along the orbit of the comet. In contrast, one should consider that the eventual cometsphere ought to be associated to the ionized cloud resulting from cometary evaporation. This phenomenon should therefore depend on the heliocentric distance of the comet. On the other hand, all previous formulas hold also with varying S and L . One should therefore measure the size of the coma vs. heliocentric distance of the comet. Then, one should check what assumptions seem to fit observations, in terms of

suitable correcting terms and assumptions that *a priori* cannot be foreseen.

The case histories of several so-called sungrazing comets - that typically have a very small perihelion - are mentioned above. In general, by (26) it is

$$U_j \sim \frac{I}{\gamma_0} \Phi \sim \frac{I}{\gamma_0} S \mathbf{B}_{int} \sim \frac{2}{L} (S \mathbf{B}_{int})^2 \quad (32)$$

$$\sim \frac{2}{L} \left\{ S \cdot [\mathbf{v}_{int}(r_c) + \mathbf{v}_c(r_c)] \cdot \frac{r_c^2}{r_E^2} \mathbf{B}_{int}(r_E) \right\}^2$$

The ring is stretched by a radial force per unit length measured along the ring

$$\left| \frac{\partial U_j}{\partial R} \right| \quad (33)$$

$$\sim 2 \left\{ S \cdot [\mathbf{v}_{int}(r_c) + \mathbf{v}_c(r_c)] \cdot \frac{r_c^2}{r_E^2} \mathbf{B}_{int}(r_E) \right\}^2 \cdot \frac{\partial}{\partial R} \frac{1}{L}$$

that, since $R \gg 1$, is equivalent to a tension along the ring

$$t_0 = \frac{1}{2 \sin(1/2R)} \left| \frac{\partial U_j}{\partial R} \right| \sim R \left| \frac{\partial U_j}{\partial R} \right| \quad (34)$$

$$= 2 \left\{ S \cdot [\mathbf{v}_{int}(r_c) + \mathbf{v}_c(r_c)] \cdot \frac{r_c^2}{r_E^2} \mathbf{B}_{int}(r_E) \right\}^2 \cdot R \frac{\partial}{\partial R} \frac{1}{L}$$

The ultimate strength of different materials ranges between $n \times 10^7$ (ice) and $10^{10} \text{ dyne cm}^{-2} = 10^9 \text{ N m}^{-2}$ (steel). In the case of the aforementioned ring-shaped nucleus with $R = 10 \text{ km}$ radius, a ring with cross section $s = 1 \text{ km}$ should break at a tension between $\sim n \pi 10^{10}$ and $\pi 10^{20} \text{ dyne cm}^{-2} \sim n \pi 10^9 - \pi 10^{18} \text{ N m}^{-2}$. This is roughly indicative, because there is no reason to believe that cometary nuclei are ring-shaped, although this evaluation refers to a fraction of the cometary nucleus where the relevant induced currents \mathbf{j} flow, which is therefore the part of the nucleus that is subject to a comparatively larger tension.

These approximate and (perhaps) indicative estimates can be used for additional evaluations. For instance, as mentioned above, the coma is observed to contract as it approaches the Sun. We have therefore to consider two possibilities.

One possibility is that the comet develops its cometsphere, in which case the interaction with the solar wind is fundamental, and eventually even much more important than the interaction with solar e.m. radiation. The other possibility is that the comet is a dirty "snowball" that "evaporates" due to the interaction with the solar e.m. radiation, essentially with a comparatively much lesser role

³⁸ See, e.g., Durand (1968), or also Becker (1933), or Bruhat (1963). The self-inductances of a few other more complicated \mathbf{j} -loops are given by Durand (1968).

played by the solar wind.

Let us infer the law of dependence of the size D_{co} of the coma vs. r_c according to either one of these two possible mechanisms.

If the comet has a cometsphere, we can tentatively suppose that the transversal dimension D_{co} of the coma is proportional to r_{css}

$$D_{co} \sim \alpha_0 r_{css} \quad (35)$$

where α_0 is a suitable and unknown coefficient. Then, from (28) it follows that

$$M_c \sim \alpha_1 \frac{D_{co}^3}{r_c} \quad (36)$$

and from (16)

$$I \sim \frac{\gamma_0}{K_0 S} \frac{M_c}{S} \sim \alpha_2 \frac{D_{co}^3}{r_c} \quad (37)$$

where α_1 and α_2 are suitable coefficients. For future reference, it is

$$\alpha_1 \sim \frac{1}{\alpha_0^3 r_{ESS}^3} M_E r_E \quad (38)$$

$$\alpha_2 \sim \alpha_1 \frac{1}{K_0 S} \sim \frac{1}{\alpha_0^3 r_{ESS}^3} M_E r_E \frac{1}{K_0 S} \quad (39)$$

Insert (14), (18), (26) and (37) in (12) and find

$$\alpha \frac{D_{co}^6}{r_c^2} \quad (40)$$

$$+ \beta \left\{ D_{co}^6 \cdot r_c \cdot \left[\sqrt{v_0^2 - 2GM_\odot \left(\frac{1}{r_0} - \frac{1}{r_c} \right)} + v_c(r_c) \right] \right\} \sim A$$

where

$$\alpha = \frac{1}{2} \frac{L}{\gamma_0^2} \alpha_2^2 \quad \beta = 1 \gamma_0 \frac{\alpha_2}{r_E^2} B_{int}(r_E) \quad (41)$$

That is, since it is possible to perform experimental measurements of D_{co} at different radial distances r_c from the Sun, it is possible to plot on a diagram the observed experimental points with coordinates

$$\frac{D_{co}^6}{r_c^2} \quad (42)$$

$$D_{co}^6 \cdot r_c \cdot \left[\sqrt{v_0^2 - 2GM_\odot \left(\frac{1}{r_0} - \frac{1}{r_c} \right)} + v_c(r_c) \right]$$

If the comet is really driven by phenomena related to B , these plotted points should appear located along a straight line. One can simplify the algorithm, and write, respectively, (40) and (42) as

$$\alpha \frac{1}{r_c^2} + \beta \left\{ r_c \cdot \left[\sqrt{v_0^2 - 2GM_\odot \left(\frac{1}{r_0} - \frac{1}{r_c} \right)} + v_c(r_c) \right] \right\} \sim \frac{A}{D_{co}^6} \quad (43)$$

$$\frac{1}{r_c^2} \quad (44)$$

$$r_c \cdot \left[\sqrt{v_0^2 - 2GM_\odot \left(\frac{1}{r_0} - \frac{1}{r_c} \right)} + v_c(r_c) \right]$$

that is, the linear relation (43) is independent of the measurements of D_{co} and there is no need to measure D_{co} , as the linear relation involves only parameters related to the Sun and to the source of the solar wind. The cometsphere hypothesis enters into play only through r_c and $v_c(r_c)$. That is, (44) is a self-consistency check of the hypothesis of cometsphere that can be applied to every comet on the basis of the cometary orbit alone. The measurement of D_{co} can be useful to derive estimates of other parameters of the comet, as per the previous relations.

In either case, the intersection with the ordinate axis - apart an arbitrary constant factor - is proportional to A . In addition, since we know the experimental errors of r_c and of the solar wind parameters, it is possible to try and check whether experimental data are consistent with the hypothesis $A \sim 0$ or not, even though the entire previous formulation relies on some substantial simplifying assumptions.

The physical parameters that enter in (43) refer to the Sun (i.e., M_\odot , r_0 and v_0), and to a given comet [i.e., r_c and $v_c(r_c)$].

Concerning the Sun, M_\odot is well-known apart the error-bar, r_0 can be any conventional choice, with the only constraint that it has to be smaller than the perihelion of the comet to be considered. For instance, one can choose the radius of the Sun, i.e., $r_0 = 700,000 \text{ km}$ (NASA website). As far as v_0 is concerned, v_0 is here defined as the speed of the solar wind at the surface of radius r_0 .

The solar wind speed decreases vs. heliocentric distance due to solar gravitation as per (17) or (18). Hence, if a mean value v_E is known for the solar wind speed at 1 AU, i.e., at Earth's orbit, one can put $v_{int}(r) \equiv v_E$ in (18), and solve with respect to v_0 . Thus, all needed physical parameters for the Sun are known.

As far as the comet's data are concerned, one should feed into (43) or (44) all available data for r_c and $v_c(r_c)$ referred to the whole comet's orbit. The final plot ought to be a linear trend that, however, is expected to have some scatter, due both to error-bars of observations, and to the approximations of the derivation of (43). Hence, such a plot can be made only by a specialist of cometary orbits.

However, a simpler plot can be carried out if one is not concerned with the scatter of points. Hence, one assumes that a linear plot must be found, which can be defined by two points alone, to be suitably chosen along the orbit of the comet, e.g., at perihelion and at aphelion. However, every couple of points is suited for this check.

Therefore, let us characterize the orbit of the given comet by means of 2 parameters, i.e.,

$$p = \text{perihelion distance} \quad q = \text{aphelion distance} \quad (45)$$

Sometimes also the eccentricity e is given

$$e = \text{eccentricity} = \frac{a^2 - b^2}{a^2} \quad (46)$$

where a and b are the semi-major and semi-minor axis, respectively, of an ideal elliptical orbit, and the two foci of the ellipse are, respectively, at a distance $\pm \sqrt{a^2 - b^2}$ from the center of the ellipse. The Sun is located at one focus, where the origin is located of a spherical coordinate system. But an ellipse is fully represented by 2 *d.o.f.s* (degrees of freedom), and - in fact - in the present computation there is no need for e . Suppose therefore that p and q are known concerning the comet of interest.

However, it is convenient to refer to p, q , and to the tangential velocity $u = v_{c,aph}$ of the comet at aphelion - and u can be derived from p and q as shown below.

Consider first that the radial velocity at both aphelion and perihelion is zero.

Call m_c the mass of the comet, plus - as usually done - call $\mu = GM_\odot$ the standard gravitational parameter, and - at a given location along the orbit - call E_p and E_k , respectively, the potential and kinetic energy of the comet, and in addition respectively, v_{rc} and v_{tc} the radial and tangential component of velocity. It is

$$E_p(p) = -2\mu/p$$

$$E_p(q) = -2\mu/q$$

$$E_k(p) = (1/2)mc v_{tc}^2(p) = (1/2)m_c v_{tc}^2(p) \quad (47)$$

$$E_k(q) = (1/2)mc v_{tc}^2(q) = (1/2)m_c u^2$$

where

$$E_k(p) = E_k(q) + E_p(q) - E_p(p) \quad (48)$$

Thus, from (47)c

$$v_{tc}(p) = \sqrt{\frac{2E_k(p)}{m_c}} \quad (49)$$

Now, apply the classical *vis-viva* equation - which is derived from energy conservation along the orbit - and, since $a = (p + q)/2$, get

$$v_{c,aph} = v_{tc}(q) = u = \sqrt{\mu \left(\frac{2}{q} - \frac{1}{a} \right)} \quad (50)$$

$$= \sqrt{\mu \left(\frac{2}{q} - \frac{2}{(p + q)} \right)}$$

In summary, it is

$$v_{cr}(q) = 0$$

$$v_{ct}(q) = v_{c,aph} = u = \sqrt{\mu \left(\frac{2}{q} - \frac{2}{(p + q)} \right)}$$

$$v_{cr}(p) = 0 \quad (51)$$

$$v_{ct}(p) = v_{c,p} = \sqrt{\frac{2E_k(p)}{m_c}}$$

Refer now to (44) applied at two points, i.e., at perihelion and at aphelion. That is, one has to draw a line through two points of coordinates $\{x_1, y_1\}$ and $\{x_2, y_2\}$, where

$$\begin{aligned} x_1 &= (1/p) \\ y_1 &= r_c \cdot \left[\sqrt{v_0^2 - 2GM_\odot \left(\frac{1}{r_0} - \frac{1}{p} \right)} + \sqrt{\frac{2E_k(p)}{m_c}} \right] \\ x_2 &= (1/q) \\ y_2 &= r_c \cdot \left[\sqrt{v_0^2 - 2GM_\odot \left(\frac{1}{r_0} - \frac{1}{q} \right)} + \sqrt{\mu \left(\frac{2}{q} - \frac{2}{(p + q)} \right)} \right] \end{aligned} \quad (52)$$

where $E_k(p)$ is given by (48), altogether with (47).

Therefore, (43) gives the result

$$\alpha x + \beta y = \text{const} \cdot A \quad (53)$$

$$\alpha = y_2 - y_1$$

$$\beta = x_1 - x_2$$

$$\text{const} \cdot A = (y_2 - y_1) x_1 - (x_2 - x_1) y_1$$

and the final check is how far ($\text{const} \cdot A$) deviates from zero, as this ought to be indicative of a permanent magnetization inside the cometary nucleus when the comet is at aphelion.

In summary, the identical somewhat intricate formula must be applied to a large set of comets, everyone associated to a respective couple of values p and q . For every comet compute ($\text{const} \cdot A$) and analyze the distribution of all results. Maybe, some indication can be inferred.

However, a better analysis can be carried out by considering the whole orbit of every comet, and by checking the scatter with respect to the expected linear trend. In addition, specific consideration of D_{co} can help to guess some additional physical parameters for the cometsphere.

A priori it is impossible to foresee how far this whole analysis can be physically significant or not. One must just try.

The same argument identically applies when one considers, instead of D_{co} , the size of the cross-section of the tail. This is concerned with the process of formation of the neutral sheet, and it is discussed quantitatively above (see Fig. 7 and the related discussion). The concern is therefore about the assessment of the way by which we can estimate D_{co} and/or the cross-section of the tail. Space telescope facilities are important in order to reduce error-bars originated by light absorption through the atmosphere.

A comet is known only by its image, hence we must make reference to the isocontour lines of photometric intensity measured at a given spectral line. The point with absolute maximum light intensity is identified with the cometary nucleus or barycenter. Then, we can choose, arbitrarily, an isocontour line that defines the "outer border" of the comet (e.g., say where the photometric intensity drops to a given percent of its maximum, e.g., to 1%). The closest point of this "outer border" to the cometary nucleus defines the cometo-centric distance of the subsolar point,

i.e., r_{CSS} , which is expressed as an arc. When we know the distance of the comet from the Earth, this angular distance can be transformed into a length unit. Finally, according to (35), it is reasonable to speculate that $D_{co} \propto r_{CSS}$.

As far as the cross-section of the tail is concerned, its transversal dimension D_T should be measured at a location downstream where the tail is practically cylindrical (i.e., “far downstream” where the internal and external pressures to the magnetopause can be presumed to be approximately purely magnetic). However, this location of the \mathbf{B} flux inside the tail should refer to a location not yet considerably eroded by “merging” across the magnetopause. Hence, a reasonable recommendation for the measurement of D_T is to refer the maximum apparent transversal extension of the tail.

On the other hand, since the tail is not perfectly cylindrical, we have to choose, arbitrarily, a conventional distance downstream where D_T is measured. Such a conventional distance can be chosen, e.g., by means of a given and fixed multiple of r_{CSS} . In fact, the entire geometrical figure of the comet and of its tail can be reasonably supposed to transform - while moving along its orbit - approximately according to a scale transformation, while keeping some rough geometrical self-similarity. In addition, the size D_T of the cross-section of the tail is thus an angular distance that can be transformed into a length distance, etc.

As already stressed, comet tails are often affected by anomalous outbursts, knots, kinks and irregularities, which are suggestive of a detachment from the nucleus of some large objects. They are some kinds of more or less large “stones”, compared to a tiny and more “regular” steady release either of dust or of plasma. In the final analysis, every object of “large size” can be likened to the nucleus of a newly born short-lived “comet” of comparably smaller size, which looks superposed on the tail of the “mother” comet.

The trigger for the occurrence of an event of this kind is certainly related to an increased tension inside the “mother” nucleus. An extensive literature obviously appeals, e.g., to shock-waves that occasionally cross through interplanetary environment. We cannot deal here with this topic. In any case, a shockwave in the solar wind implies both (i) large transient variations of the mass density of the solar wind, and also (ii) e.m. phenomena that originate induced currents \mathbf{j} , hence temporary transient tensions, according to a mechanism that - in terms of energy balance - is essentially of the same kind as the aforementioned simplified model. The mechanical effect, however, which is due to mass-density variations, is (maybe) unlikely upon considering the huge difference in mass density between solar wind and cometary nucleus. In contrast, the e.m. interaction is certainly much more credible. However, in the final analysis, the e.m. interaction of a cometary nucleus with the solar wind always implies induced currents \mathbf{j} . Hence, it is only a matter of semantics to claim, or not, that a temporary cometosphere is thus formed, as the final physical

phenomenon (i.e., an increased tension) is just one and the same, independent of the way by which it is described and computed.

In either case - whether this is a mechanical effect (i.e., similar to an aerodynamic effect inside a wind tunnel), or rather (more likely) it is an e.m. effect - the phenomenon is normally handled by means of the *MHD* expansion model of the solar corona, etc. In this way, some transient large tension eventually determines the rupture of a fraction of the cometary nucleus.

Consider, rather, the alternative case history of a comet with no cometosphere, and search for the law satisfied by D_{co} (or by the cross-section D_T of the tail) when the light emission by the comet is excited by the interaction with the solar e.m. radiation, while only a negligible role is played by the solar wind.

Since the intensity of solar radiation decreases as $(1/r_c)^2$, it has to be expected

$$D_{co} \propto (1/r_c)^2 \quad (54)$$

Suppose that in this case we (erroneously) hypothesize that a comet has a cometosphere, while in reality this is not correct. Therefore, we (erroneously) carry out the check expressed by plotting the observational points (42). However, if the comet has no cometosphere, in this way we (erroneously) plot, according to (54), two observational quantities that have a physical dependence on r_c expressed as two quantities proportional, respectively, to

$$\propto \frac{1}{r_c^{14}} \quad (55)$$

$$\propto \frac{1}{r_c^{11}} \cdot \left[\sqrt{v_0^2 - 2GM_\odot \left(\frac{1}{r_0} - \frac{1}{r_c} \right)} + v_c(r_c) \right]$$

It is very difficult to envisage the role of error-bars while drawing this diagram. However, a linear trend of the kind (40) and a trend of the kind (55) should be clearly distinguished.

The possible devastating consequences of the observational error-bars are, however, to be always considered, and also the eventually wrong assumptions that deal with the observational measurements of D_{co} .

One must just try and carry out these attempts by applying this whole and identical rationale to different comets.

6.7. Comets: quantitative dependence of the cross-section of the tail vs. heliocentric distance

Another complementary quantitative check - and estimate of the intensity of the cometary field - can be inferred by means of the transversal dimension D_T of the tail, according to the following argument. This argument works only for “magnetic” comets that have their dipole axis not parallel or anti-parallel to the solar wind velocity, i.e., their cometosphere should not be “pole-on” (see Fig. 14). That is, the present argument applies only to the comets that have a neutral sheet.

Suppose that a given comet satisfies the tests carried out

by means of the D_{co} vs. r_c dependence discussed above. In addition, suppose that the image of the comet is not suggestive of a cometary magnetic axis approximately parallel or anti-parallel to the solar wind velocity (see above). Then, apart a proper scaling, the cometosphere ought to be similar to the Earth's magnetosphere. Therefore, let us consider the structure of a general magnetosphere.

For simplicity, in the case of the magnetosphere of the Earth, state that all \mathbf{B} field-lines³⁹ with $L \leq L_E$ span the region of space that contains the radiation belts (i.e., the plasmasphere), while all \mathbf{B} field-lines with $L > L_E$ are completely "stretched" to form the Earth's tail. Indeed, owing to the minimum energy requirement that justifies the formation of the neutral sheet (see above the argument associated with Fig. 10), \mathbf{B} "reconnection" across the neutral sheet must be minimum. Hence, in the following assume an approximately vanishing "reconnection" across the neutral sheet.

Moreover, remind about the pressure balance that explains the location of the magnetopause when the argument is applied to the sunward side of the magnetopause (see above). Similarly, when the pressure balance is applied to the earthward termination of the plasmashet, the larger is the particle density available from the plasmashet, the closer to the Earth is L_E . On the other hand, the particle density, inside the plasmashet, reasonably ought to be proportional to the particle density in the solar wind. Hence, the larger is the particle density in the solar wind, the closer is L_E to the Earth.⁴⁰

That is, if the Earth would be located at a different distance r_E from the Sun, we can reasonably presume that the mean L_E should be increased or decreased according to the density variation of solar wind particles. The argument relies on the fact that the boundary between the trapping region and the outer or "stretched" region of space can be described in terms of a (mostly magnetic) pressure that is active from the interior, i.e., from the side of the trapping region, which balances an external pressure caused by the solar wind particles that flow in the plasmashet. These particles, owing to the aforementioned minimum energy requirement, attempt to "stretch" as much \mathbf{B} flux as possible, but when their pressure is not sufficient to overcome the internal pressure, they no more succeed to "stretch" additional \mathbf{B} flux.

The internal pressure is given by magnetic pressure plus

the pressure of trapped particles. However, since - compared to the kinetic energy density of particles - the magnetic energy density in the trapping region is larger, the particle pressure can be approximately neglected. Hence, the internal pressure is proportional to the square of the Earth dipole moment M_E . The external pressure is proportional to the available solar wind particle density. Then, in the case of the Earth, the pressure balance is

$$\left(\frac{M_E}{L_E^3}\right)^2 = \eta \kappa_E \quad (56)$$

where κ_E is the particle density in the solar wind that is available at 1 AU, and η is a proper (even though unknown) constant [not to be confused with the constant defined in (29)]. Owing to the general formal definition of η , there is no concern about the unit system that is used.

In the case of a comet, call⁴¹ L_c , M_c , and κ_c the corresponding quantities, and it is

$$\left(\frac{M_{Ec}}{L_c^3}\right)^2 = \eta \kappa_c = \eta \kappa_E \left(\frac{r_E}{r_c}\right)^2 \quad (57)$$

where r_E is 1 AU, and where particle conservation in the expanding solar wind has been taken into account. Compute η from (56) and insert it in (57) and get

$$L_c = L_E 3 R \sqrt[3]{\frac{M_c r_c}{M_E r_E}} \quad (58)$$

Consider a perfectly dipolar field and compute the total flux that crosses through the equatorial plane in the region outside a circle of radius L^* . It is

$$\begin{aligned} \Phi_{r>L^*} &= \frac{1}{K_0} \int_0^{2\pi} \int_{L^*}^{\infty} \frac{M}{r^3} r dr d\varphi \\ &= \frac{1}{K_0} 2\pi \frac{M}{L^*} \end{aligned} \quad (59)$$

where M is the dipole moment, and φ is the longitude. If we assume that the \mathbf{B} "reconnection" across the cometary neutral sheet is negligible, we must conclude that the \mathbf{B} flux inside half a cometary tail (or inside one lobe of the cometosphere) must be equal to $\Phi_{r>L_c}$.

Let us assume that the cometary tail is cylindrical, with a circular cross-section of diameter D_T . Let us also assume that the \mathbf{B} intensity inside the tail is identical to the intensity of \mathbf{B}_{int} . Then, the flux within a lobe of the cometosphere is

$$\Phi_c = \frac{1}{2} \pi \left(\frac{D_T}{2}\right)^2 B_{int,E} \left(\frac{r_E}{r_c}\right)^2 \quad (60)$$

argument in the present computation refers to "normal" or "quiet" "mean" state of the tail of the magnetosphere or cometosphere.

⁴¹ Note that L_c is the McIlwain parameter inside the cometosphere that separates trapped particles from the comet's magnetic tail. It should not be confused with the self-inductance L of the model-circuit that should represent a comet's nucleus.

³⁹ Where L is the classical McIlwain parameter. Carl E. McIlwain (1931-), a learned American space scientist, since 1992 Professor emeritus of the *University of California, San Diego*.

⁴⁰ Note, however, that this is certainly wrong during a substorm or geomagnetic storm event, because the particle flux in the plasmashet responds to the availability of particles in the plasmashet reservoir, which is available all along the tail, according to the argument referring to Figure 13. Conversely, the

where $B_{int,E} \equiv B_{int}(r_E)$ is the intensity of \mathbf{B}_{int} at 1 AU. Then, put $\Phi_c = \Phi_r > L_c$, insert (58), and thus find

$$M_c = \frac{K_0^{3/2}}{64} \sqrt{\frac{B_{int,E}^3 L_E^3}{M_E}} D_T^3 \left(\frac{r_E}{r_c}\right)^{5/2} \quad (61)$$

We know that $M_E = 8.01 \times 10^{25}$ (e.m.u.) = $8.01 \times 10^{22} \text{ Am}^{-2}$, $L_E \sim 10 R_E$, $B_{int,E} \approx 5 \gamma$. Then, we can estimate M_c from a measurement of D_T .

It has been shown [see (16) and the related discussion] that

$$M_c \sim const + 2K_0 \frac{S^2}{L} B_{int,E} \left(\frac{r_E}{r_c}\right)^2 \quad (62)$$

where the first addendum is the constant magnetic moment that pre-existed when the comet had not yet begun to interact with the outer fringes of the solar wind, and the second addendum is an order-of-magnitude estimate of the induced \mathbf{B} . By equating (61) and (62) it is found

$$\begin{aligned} \left[\frac{K_0^{3/2}}{64} \sqrt{\frac{B_{int,E}^3 L_E^3}{M_E}} \right] D_T^3 \left(\frac{r_E}{r_c}\right)^{5/2} & \quad (63) \\ \sim const & \\ + \left[2K_0 \frac{S^2}{L} B_{int,E} \right] \left(\frac{r_E}{r_c}\right)^2 & \end{aligned}$$

that is, if we plot on abscissa and ordinates, respectively

$$D_T^3 \left(\frac{r_E}{r_c}\right)^{5/2} \quad \left(\frac{r_E}{r_c}\right)^2 \quad (64)$$

we should find a linear relationship. By it, we can get an experimental estimate of the orders of magnitude of “const” and of (S^2/L) . We can therefore insert their values into (62), and thus we know M_c .

We can guess a reasonable value for L_E . Hence, by (58) we can estimate also L_c .

Then, by means of (28) and (35), it is possible to compute, respectively, r_{css} and α_0 , and by (38) and (39) also α_1 and $\alpha_2\sqrt{L}$ and by (37) also $I\sqrt{L}$. Finally, by (40) we can compute also the order of magnitude of A , which is the total magnetic energy of the comet before the solar wind interaction. This estimate can be combined with the check carried out by means of (43). The knowledge of an approximate estimate of A is equivalent to estimate the eventual endogenous \mathbf{B} of the comet’s nucleus before the entry in the solar wind.

6.8. Comets: interaction with planetary atmospheres, and some proposed active experiments

After implementing the whole previous discussion a direct measurement became available of the interaction of the tenuous Mars’ atmosphere with the close flyby of comet C/2013 A1 (Siding Spring), as reported by Harada et al. (2016). The description, however, must be mentioned that is given of Harada et al. (2016) in a NASA announcement (Zubritsky, 2016, 2016a). Everything seems in agreement with the guess here proposed, although there is a substantial difference in terms of cross-section of the cometsphere. It is worthwhile to report here their proposed model, just for

comparison purpose with the discussion here given.

Zubritsky (2016, 2016a) claims that “in October 2014, NASA’s Mars Atmosphere and Volatile Evolution (MAVEN) spacecraft entered orbit around the Red Planet ... a few instruments, including MAVEN’s magnetometer, remained on, conducting observations from a front-row seat during the comet’s remarkably close flyby. The one-of-a-kind opportunity gave scientists an intimate view of the havoc that the comet’s passing wreaked on the magnetic environment, or magnetosphere, around Mars. The effect was temporary but profound (Fig. 18).”

The emphasis must be on the “comet’s powerful magnetic field”, in contrast with the discussion that has been here carried out that considered an eventual weak cometary field temporarily generated by e.m. induction. In addition, the qualitative pattern envisaged in Fig. 18 depicts a cometsphere with a huge cross-section, compared to the model here intuitively roughly likened to the tail monitored by light emission.

Either one choice or the other is just a matter of speculation until an actual check can be carried out by observations. Zubritsky (2016, 2016a) also comments as follows. “ ‘Comet Siding Spring plunged the \mathbf{B} around Mars into chaos,’ said Jared Espley, a MAVEN science team member at NASA’s GSFC. ‘We think the encounter blew away part of Mars’ upper atmosphere, much like a strong solar storm would.’ ... Comet Siding Spring’s nucleus - ... measuring no more than half a kilometer - is small, but the coma is expansive, stretching out a million kilometers in every direction ...

When comet Siding Spring passed Mars, the two bodies came within ~ 140,000 km of each other. The comet’s coma washed over the planet for several hours, with the dense inner coma reaching, or nearly reaching, the surface. Mars was flooded with an invisible tide of charged particles from the coma, and the powerful \mathbf{B} around the comet temporarily merged with - and overwhelmed - the planet’s own weak one. ‘The main action took place during the comet’s closest approach,’ said Espley, ‘but the planet’s magnetosphere began to feel some effects as soon as it entered the outer edge of the comet’s coma.’

At first, the changes were subtle. As Mars’ magnetosphere, which is normally draped neatly over the planet, started to react to the comet’s approach, some regions began to realign to point in different directions. With the comet’s advance, these effects built in intensity, almost making the planet’s \mathbf{B} flap like a curtain in the wind. By the time of closest approach - when the plasma from the comet was densest - Mars’ \mathbf{B} was in complete chaos. Even hours after the comet’s departure, some disruption continued to be measured.

Espley and colleagues think the effects of the plasma tide were similar to those of a strong but short-lived solar storm. And like a solar storm, the comet’s close passage likely fueled a temporary surge in the amount of gas escaping from Mars’ upper atmosphere ... “

The use of comets like natural probes of the solar wind,

and inside a huge space domain, appears therefore a fascinating challenge, but also other kinds of observations can be envisaged.

In principle, some active experiments can be carried out in space, suited to simulate either an “artificial comet” or some processes that are involved in the hypothetical model of a comet that has a **B** field. Experiments in cometary physics have, however, been focused on space missions for cometary encounters. A few proposed active experiments remained therefore only the object for hypothetical discussion. A few mentions are here recalled – with no presumption for completeness – about these intriguing proposals, in order to show how they match the hypothesis of a **B** comet and its cometosphere.

Olson (1974) suggested to launch a superconducting magnet into the solar wind in order to build up a miniature magnetosphere.

Krimigis (1973) proposed to make a chemical release immediately outside the front of the Earth’s magnetosphere. He expected that chemicals ought to diffuse inward into the magnetosphere. This process, when properly monitored, should help to understand the microstructure of the (so-called) magnetopause.

In contrast, according to the rationale of a comet with **B** field, an alternative – and maybe even more probable – effect is that the chemicals enter the J_1 and $-J_1$ currents of Fig. 9. The objective competing roles of these two possibilities cannot be predicted, because – for such a purpose – the present knowledge is insufficient of the microstructure of the magnetopause.

A substantial drawback in the Krimigis’ argument is the limited amount of chemicals that can be practically evaporated by one release. This difficulty can be overcome by releasing the chemicals in front of an Olson miniature magnetosphere. This experiment ought to consist in launching a space probe on a circumsolar orbit, which carries a superconducting magnet with a current within it and capable to produce a large chemical release starting at a given time instant, and lasting for some given time lag. In principle, this appears to be what should resemble a **B** comet.

This experiment could also be simplified by using a permanent magnet, instead of a superconducting magnet. However, a superconducting magnet can permit to change magnetic moment, thus allowing – by means of just one experiment – to investigate different comets, different tail shapes and lengths, filamentary structures, etc. In addition, one could be able also to change the probe orientation in order to study **B** comets with dipole axis with a given orientation with respect to the solar wind.

Several previous theories of comets claim that a miniature comet ought to be made even with no **B** (owing to brevity purpose, no specific list is given here). The general idea is to use some icy conglomerate. However, they request a strong gravitational field, otherwise the chemicals that are released rapidly diffuse through interplanetary space.

In contrast, the model that is here proposed strictly requires, as a crucial ingredient, the presence of the **B** of the comet – because, in naturally occurring comets, the **B** should either be present, or increase when the comet enters into the expanding solar wind and it approaches the Sun. On the contrary, it is very probable that a naturally induced **B** in an artificial comet should be excessively weak, and chemicals should thus rapidly run out and exhaust.

On the other hand, in principle, before carrying out the comet experiment, the superconducting magnet ought to remain – and ought to be monitored – inside the solar wind, while the currents **j** should be monitored that are induced inside it. Moreover, when the probe has exhausted all the chemicals to be released, the current within the superconducting magnet should be reduced or canceled. Then, the probe should be injected into a highly eccentric orbit around the Sun. At the same time, the e.m. induced **j** within the superconducting magnet should be monitored. The experiment could even be more complete if the orbit perihelion is not excessively close to the Sun, in order that the probe can work even after transit at perihelion.

As a conclusion, in some respects, it is very unlikely that any manmade and expensive space probe is really similar to a natural comet. However, we can succeed to simulate some fundamental processes, which reasonably ought to control both cometary and/or magnetospheric physics.

7. Conclusion

According to the present available evidence, comets seem to be efficient natural probes for monitoring the solar wind through the extended Solar System. A list of observational checks can be summarized as follows. In any case, use photometer-scanned images.

Check whether a comet tail, when observed from a suitable location, displays a likely “black axis”.

In the case of a “black axis”, search – as far as possible – for a deformation of spectral lines like a parenthesis, i.e., like { or } depending on the **B** orientation on the upper and lower lobe of the cometosphere.

Check the behavior of sungrazing comets (“Type I” tail), as every case history is a different event, with a peculiar morphology.

Refer to (43) and (44). A simple check can be made of the entire approximate order-of-magnitude estimate here carried out. For this preliminary step, there is need to use only solar parameters, with no need to appeal to cometary parameters.

If one uses also cometary parameters, one can estimate the total energy of the comet, i.e., one can check whether the comet nucleus has a **B** or not, independent of the **B** caused by the evaporated plasma cloud. That is, one must feed into (43) or (44) all available data for r_c and $v_c(r_c)$ referred to the whole comet’s orbit.

The resulting plot must hopefully display a linear trend that, however, is expected to have some scatter, derived from error-bars of observations, and from the

approximations in the derivation of (43). This plot can be made only by a specialist of cometary orbits. However, if one is not concerned with the scatter of points, a simpler check can be carried out by assuming that a linear plot must be found - which can be defined by two points alone, to be suitably chosen along the orbit of the comet, e.g., at perihelion p and at aphelion q . Refer to (53) and the related discussion.

This identical somewhat intricate formula must be applied to a large set of comets, everyone associated to a respective couple of values p and q . For every comet compute ($const \cdot A$) and analyze the distribution of all results. Maybe, some indication can be inferred. However, if the whole orbit of every comet is considered, one can check the scatter with respect to the expected linear trend.

In addition, specific consideration of D_{co} can help to guess some additional physical parameters of the cometsphere. In fact, the alternative possibility is expressed by (55) including the associated discussion. However, one must always consider the possible devastating consequences of error-bars, and the eventually wrong assumptions that deal with the observational measurements of D_{co} . One must just try and carry out these attempts by means of an identical rationale applied to different comets.

In addition, with reference to the transversal dimension D_T of the tail, one can carry out an additional analysis that, however, holds only for "magnetic" comets, i.e., comets that truly have a cometsphere. A linear trend must be found according to the parameters given by (64), and related discussion.

By this it is shown how one can derive the magnetic moment and the total magnetic energy of the cometary nucleus, independent of the phenomenon associated to the plasma cloud of the comet.

It is impossible to foresee *a priori* whether this entire analysis makes a sense or not. If it works - even only for a limited set of comets - the result is of paramount importance both for understanding cometary phenomena, and for a free monitoring the solar wind through the whole Solar System, with a relevant impact on a better understanding of solar terrestrial relations. Therefore, it is certainly worthwhile to attempt to carry out this investigation.

Acknowledgement

Only a few scientists are here mentioned, as specified in the main text of the paper. Special thanks are expressed to the late Murray Dryer (1925-2022) for a warm and great encouragement concerning the former 1974 draft of the present study. Some authoritative and learned inputs were given by H. U. Schmidt from *Max-Planck-Institut für Astrophysik*. We feel also deeply indebted to the late Professor Reimar Lüst (1923-2020), who triggered GPG's contact with H. U. Schmidt. GPG expresses sincere gratitude to H. U. Schmidt, even though, at present, after several decades, unfortunately we do not know how to

rekindle this contact. GPG feels also indebted to a dear friend, the late Professor Wilfried Schröder (1941-2011) for his steady, always enthusiastic and warm support.

Funding Information

This research received no direct external funding. Originally this research was funded by CNR, through the salary paid to GPG, who, however, since November 2005 retired. BAL is a semi-retired self-funded independent researcher.

Author's Contributions

The entire study relies exclusively on a several decade study by the GPG, while BAL contributed to the revised final discussion and shape of the present entire study.

Ethics

No peculiar ethical issues are related to the paper.

Abbreviations

The following abbreviations are used in this manuscript:

AGU	American Geophysical Union
AIA	Atmospheric Imaging Assembly telescope aboard NASA's STEREO mission
AU	Astronomical Unit
BL	ball lightning
Caltech	California Institute of Technology
CME	coronal mass ejection
CNR	Consiglio Nazionale delle Ricerche
CP	Coronagraph/Polarimeter
CSA	Canadian Space Agency
D/H	deuterium-to-hydrogen ratio
DE	disconnection event
e.m.	electromagnetic
ESA	European Space Agency
ESO	European Southern Observatory
EVE	EVE Audio reveal true sound
FAC	field aligned current, also called Birkeland current
FR	field reversals (geomagnetic)
FUV	(Far Ultraviolet) photometers
GIOTTO	a European robotic spacecraft mission from ESA
GK	Gurevich and Karashtin (effect)
GSFC	Goddard Space Flight Center (NASA)
HI-1	Heliospheric Imager-1 of SECCHI aboard the STEREO mission
HMI	Helioseismic and Magnetic Imager onboard SDO
HNS	heliospheric neutral sheet
ICSUWDS	International Conference on Statistics and Data Science

<i>IFSI</i>	<i>Istituto di Fisica della Spazio Interplanetario (of CNR)</i>
<i>IMAGE</i>	<i>Imager for Magnetopause-to-Aurora Global Exploration</i>
<i>JHU/APL</i>	<i>Johns Hopkins Applied Physics Laboratory</i>
<i>JPL</i>	<i>Jet Propulsion Laboratory</i>
<i>LASCO</i>	<i>Large-Angle and Spectrometric Coronagraph aboard the ESA's SOHO spacecraft</i>
<i>MAVEN</i>	<i>Mars Atmosphere and Volatile Evolution (NASA)</i>
<i>MHD</i>	magneto hydro-dynamics
<i>MOR</i>	mid-ocean ridge
<i>MRO</i>	<i>Mars Reconnaissance Orbiter (NASA)</i>
<i>NASA</i>	<i>National Aeronautics and Space Administration</i>
<i>OSU</i>	<i>Oregon State University</i>
<i>PCA</i>	polar cap absorption (event)
<i>RB</i>	runaway breakdown (mechanism)
<i>SAAO</i>	<i>South African Astronomical Observatory (Cape Town)</i>
<i>SDO</i>	<i>Solar Dynamics Observatory</i>
<i>SECCHI</i>	<i>Sun-Earth Connection Coronal and Heliospheric Investigation telescope aboard the STEREO mission</i>
<i>SIF</i>	<i>Società Italiana di Fisica</i>
<i>SMM</i>	<i>Scanning Microwave Microscopy</i>
<i>SMM</i>	<i>Solar Maximum Mission</i>
<i>SOHO</i>	<i>Solar and Heliospheric Observatory</i>
<i>SOLWIND</i>	<i>a United States satellite SSC/ - Spitzer Space Telescope (Caltech)</i>
<i>STEREO</i>	<i>Solar TERrestrial RELations Observatory</i>
<i>STScI</i>	<i>Space Telescope Science Institute</i>
<i>TD</i>	tide driven (dynamo)
<i>TGF</i>	terrestrial gamma flash
<i>TLE</i>	transient luminous event
<i>UAF</i>	University of Alaska Fairbanks

Gasc, T. I. Gombosi, K. C. Hansen, M. Hässig, A. Jäckel, E. Kopp, A. Korth, L. LeRoy, U. Mall, B. Marty, O. Mousis, E. Neefs, T. Owen, H. Rème, M. Rubin, T. Sémon, C.-Y. Tzou, H. Waite, and P. Wurz, 2015. 67P/Churyumov-Gerasimenko, a Jupiter family comet with a high D/H ratio, *Science*, 347, (6220): 1261952 [3 pp.]; DOI:10.1126/science.1261952.

Anonymous, 2011c. [C/2011 W3 \(Lovejoy\)](#). *JPL Small-Body Database Browser*. NASA.gov. 14 December.

Anonymous, 1980. *IAGA/AIGA, Your Earth from the deep interior to outer space, Brochure IAGA*. Pp. 1-10.

Anonymous, 2014r. Rosetta fuels debate on origin of Earth's oceans, *ESA Science release*, issued 10 December.

Anonymous, 2015bd. Simulation of plasma interactions between comet 67P/C-G and the solar wind around perihelion, *ESA, Science and Technology, Rosetta*, issued 29 July.

Arley, N., and K. R. Buch, 1950. *Introduction to the theory of probability and statistics*. Science Editions, John Wiley and Sons, Inc., New York: 1-240.

[Baker](#), H., 2024. Explosive 'devil comet' grows seemingly impossible 2nd tail after close flyby of Earth - but it's not what it seems, *Live Science*, issued 7 June.

Baumgardner, J., J. Wilson, and M. Mendillo, 2008. Imaging the sources and full extent of the sodium tail of the planet Mercury, *Geophysical Research Letters*, 35: L03201; DOI:10.1029/2007GL032337.

Beard, D.B., 1966. A theory of Type-I comet tails. In *The solar wind*, R. J. Jr. Mackin, and M. Neugebauer, Eds., Jet Propulsion Laboratory, Pasadena, Ca.: 373-380.

Becker, R., 1933. *Theorie der Elektrizität, Band I, Einführung in die Maxwellsche Theorie der Elektrizität*, (IX ed., 1941), and *Band II, Elektronen Theorie* (VI ed.), Teubner. Leipzig. (Italian translation published by Sansoni, Firenze, 1949: 313 pp., and 1950: 481 pp.).

Biermann, L., 1941. Der gegenwärtige Stand der Theorie convectiver Sonnenmodelle. *Vierteljahrsschrift der Astronomischen Gesellschaft, Leipzig*, 76: 194-200. [After 1950 the journal continued as *Mitteilungen der Astronomischen Gesellschaft*, Hamburg].

Bingham, R., J. M. Dawson, V. D. Shapiro, D. A. Mendis, and B. J. Kellett, 1997. Generation of X-rays from Comet C/Hyakutake 1996 B2, *Science*, 275, (5296): 49-51; DOI:10.1126/science.275.5296.49.

Brandt, J. C., 1962. A note on the gas tails of comets, *Astron. J.*, 67: 180-180.

Brandt, J. C., L. D. Friedman, and D. K. Yeomans, 1980. *The International Halley Watch. Report of the Science Working Group*. Goddard Space Flight Center, July 1980: 1-72.

Brandt, J. C., R. G. Roosen, S. B. Modali, and P. H. Verdone, 1971. A direct method for the determination of comet tail types. *Bulletin of the Astronomical Society*, 3: 281.

Brandt, J. C., 1968. The physics of comet tails, *Annual Review of Astronomy and Astrophysics*, 6: 267-286.

References

Akasofu, S.-I., 1977. *Physics of magnetospheric substorms*, D. Reidel, Dordrecht, Netherlands: 1-599.

Akasofu, S.-I., 1968. *Polar and magnetospheric substorms*, D. Reidel Publ. Co., Dordrecht: 1-280.

Akasofu, S.-I., 1964. The development of the auroral substorm, *Planetary and Space Science*, 12, (4): 273-282; DOI:10.1016/0032-0633(64)90151-5.

Alfvén, H. O. G., 1957. On the theory of comet tails. *Tellus*, 9, (1): 92-96; DOI:10.1111/j.2153-3490.1957.tb01855.x.

Altwegg, K., H. Balsiger, A. Bar-Nun, J. J. Berthelier, A. Bieler, P. Bochsler, C. Briouis, U. Calmonte, M. Combi, J. De Keyser, P. Eberhardt, B. Fiethe, S. Fuselier, S.

- Brown, J. C., H. E. Potts, L. J. Porter, and G. Le Chat, 2011. Mass loss, destruction and detection of Sun-grazing and -impacting cometary nuclei, *Astronomy and Astrophysics*, 535, A71, [12 p.]; DOI:10.1051/0004-6361/201015660.
- Brownlee, D., 2008. Comets and the early solar system, *Physics Today*, 61, (6): 30-35.
- Bruhat, G., 1963. *Cours de physique générale. Electricité*. Masson, Paris: 1-911.
- Bryans, P., and W. D. Pesnell, 2012. The extreme-ultraviolet emission from Sun-grazing comets, *Astrophysical Journal*, 760, (1): 18; DOI:10.1088/0004-637X/760/1/18.
- Byrd, D., 2018c. Why do comets emit X-rays? Mystery solved, *EarthSky*, issued March 20.
- Campbell, W. H., 1996. Geomagnetic storms, the *Dst* ring-current myth and lognormal distributions. *Journal of Atmospheric and Terrestrial Physics*, 58, (10): 1171-1187; DOI:10.1016/0021-9169(95)00103-4.
- Canup, R. M., 2004. Origin of the terrestrial planets and the Earth-Moon system. *Physics Today*, 57, (4): 56-62.
- Carlson, R. W., P. Drossart, Th. Encrenaz, P. R. Weissman, J. Hui, and M. Segura, 1997. Temperature, size, and energy of the Shoemaker–Levy 9 G-Impact Fireball, *Icarus*, 128, (2): 251-274
- Churyumov, K. I., and S. I. Gerasimenko, 1972. Physical observations of the short-period comet 1969 IV. In G.A. Chebotarev, E.I. Kazimirchack-Polonskaya, and B.G., Marsden, Eds., *The motion, evolution and origin of comets*, IAU Symposium, Leningrad, August, 4-11, 1970, Reidel, Dordrecht etc., (45): 27-34.
- Cofield, C., 2015. Comets are like deep fried ice cream, scientists say, *Space.com*, issued February 23.
- Cosmovici, C. B., P. Mack, P. Maffei, and G. Schwarz, 1993. *An atlas of comet Halley as seen from South Africa*, CNR-IFSI, Frascati (Roma): 1-168.
- Dobrovoiskij, O. V., 1961. Les processus non stationnaires dans les comètes et l'activité solaire, traduit du russe par G. Guigay, *Académie des sciences de la République socialiste soviétique du Tadjikistan, Travaux*, VIII.
- Dungey, J. W., 1961. Interplanetary magnetic field and the auroral zones, *Phys. Rev. Lett.*, 6: 47-48.
- Dungey, J. W., 1963. The structure of the exosphere or adventures in velocity space. In C. deWitt, J. Hieblot, and A. Lebeau, Eds., *Géophysique exterieur-Geophysics, The Earth's environment*, Gordon and Breach, Science Publ., New York and London: 503-550.
- Durand, E., 1968. *Magnétostatique*, Masson, Paris: 1-673.
- [Forsyth, C.](#), [C. S. Arridge](#), [S. E. Milan](#), and [A. P. Walsh](#), 2010. Magnetotails throughout the solar system, *Astronomy and Geophysics*, 51, (6): 6.28–6.30; DOI:10.1111/j.1468-4004.2010.51628.x.
- Galli, D., A. Gasperini, and S. Bianchi, 2016. Il primo spettro di una cometa, *Giornale di Astronomia*, 42, (1): 43-45.
- Goldman, N., 2020. Comets in ancient cultures, *Deep Impact, Univ. Maryland, Ball Aerospace & Technol. Corp., JPL (CalTech)*, retrieved on January 12.
- Goldman, N., 2017. Comets in ancient cultures. *Deep Impact, Univ. of Maryland/ Ball Aerospace & Techn. Corp./ JPL/ Caltech*, last updated November 14.
- Gregori, G. P., 1991. Artificial generation of a magnetospheric substorm. In E. Sindoni, and A.Y. Wong, Eds., *Controlled active global experiments (C.A.G.E.)*, Proceedings of the International School of Plasma Physics "Piero Caldirola", Varenna (Como-Italy), September 5-12, 1989, Editrice Compositori, Società Italiana di Fisica, Bologna: 361-366.
- Gregori, G. P., 2002. Galaxy – Sun – Earth relations. The Origin of the Magnetic Field and of the Endogenous Energy of the Earth, with Implications for Volcanism, Geodynamics and Climate Control, and Related Items of Concern for Stars, Planets, Satellites, and Other Planetary Objects. A Discussion in a Prologue and Two Parts. *Beiträge zur Geschichte der Geophysik und Kosmischen Physik*, Band 3, Heft 3: 1-471 [Available at <http://ncgtjournal.com/additional-resources.html>]
- Gregori, G. P., 2000. Geomagnetism and fundamental science. In W. Schröder, Ed., *Geomagnetism (research, past and present)*, *Newsletter of the IDCH of IAGA*: 12-50.
- Gregori, G. P., M. T. Hovland, B. A. Leybourne, S. Pellis, V. Straser, B. G. Gregori, G. M. Gregori, and A. R. Simonelli, 2025w. Air-earth currents and a universal “law”: filamentary and spiral structures - Repetitiveness, fractality, golden ratio, fine-structure constant, antifragility and “statistics” - The origin of life, *News Concepts in Global Tectonics*, 3, (1): 106-225.
- Gregori, G. P., 2001a. Interaction of a stellar wind with a magnetised planetary object. In F. Giovannelli, Ed., *The Bridge between the big bang and biology-Stars, planetary systems, atmospheres, volcanoes: their link to life*, Proceedings of a meeting held at Stromboli (Messina, Italy), September 13-17, 1999, C.N.R., Roma: 116-135.
- Gregori, G. P., and B. A. Leybourne, 2021. An unprecedented challenge for humankind survival. Energy exploitation from the atmospheric electrical circuit, *American Journal of Engineering and Applied Science*, DOI:10.3844/ajeassp.2021.258.291.
- Gregori, G. P., B. A. Leybourne, and F. Bonavia, 2025u. Hexagonal vs. octagonal vs. other patterns: the logical key, pending publication in *American Journal of Engineering and Applied Science*.
- Gregori, G. P., B. A. Leybourne, and F. Bonavia, 2025v. The origin of lavakas, pending publication in *American Journal of Engineering and Applied Science*.
- Gregori, G. P., B. A. Leybourne, Dong Wenjie, and Gao Xiaoqing, 2025o. Energy release from *ALB*, *CMB* and *ICB* and secular variation. V – Results, pending publication in *American Journal of Engineering and Applied Science*.
- Gregori, G. P., B. A. Leybourne, Dong Wenjie, and Gao

- Xaoqing, 2025l. Energy release from ALB, CMB and ICB and secular variation. II – Methods: the “principle of magnetic energy variation” & Joule heat on a spherical shell of currents, pending publication in *American Journal of Engineering and Applied Science*.
- Gregori, G. P., B. A. Leybourne, and G. Paparo†, 2025b. Introduction – Anomalous lesser air-earth phenomena, pending publication in *American Journal of Engineering and Applied Science*.
- Gregori, G. P., B. A. Leybourne, G. Paparo†, and M. Poscolieri, 2025a. The global Sun-Earth circuit, pending publication in *American Journal of Engineering and Applied Science*.
- Gregori, G. P., W. Soon, V. Straser, and B. A. Leybourne, 2022d. The foundations of physics and axiomatics. III - Superluminal phenomena, mechanisms, matter-antimatter, cosmological implications. *New Concepts in Global Tectonics*, 10, (3): 263-283.
- Gregori, G. P., Leybourne, B. A., 2025b. The electrostatic Sun, pending publication in *American Journal of Engineering and Applied Science*.
- Gregori, G. P., and B. A. Leybourne, 2025e. The physics of electrical discharges – 1. Small-scale phenomena - Fog - atmospheric precipitation – BLs, pending publication in *American Journal of Engineering and Applied Science*.
- Gregori, G. P., Leybourne, B. A., 2025f. The physics of electrical discharges – 2. RB & TGFs - Runaway breakdown – terrestrial gamma flashes – GK effect, pending publication in *American Journal of Engineering and Applied Science*.
- Gregori, G. P., and B. A. Leybourne, 2025g. The physics of electrical discharges – 3. Sparks and lightning - electrostatics of the ionosphere – TLEs - plasma jets collimation – Birkeland currents & sea-urchin spikes - stellar and galactic alignments, pending publication in *American Journal of Engineering and Applied Science*.
- Gregori, G. P., and B. A. Leybourne, 2025c, The solar cycle and MiniMax - Effects on other planets, pending publication in *American Journal of Engineering and Applied Science*.
- Gregori, G. P., B. A. Leybourne, W. Soon, and V. Straser, 2025e. The heuristic meaning of variational principles, pending publication in *American Journal of Engineering and Applied Science*.
- Gregori, G. P., B. A. Leybourne, and J. R. Wright, 2025d. Generalized Cowling theorem and the Cowling dynamo, pending publication in *American Journal of Engineering and Applied Science*.
- Gregori, G. P., B. A. Leybourne, and J. R., Wright, 2025c. The solar cycle and MiniMax, pending publication in *American Journal of Engineering and Applied Science*.
- Gregori, G. P., 1992. Magnetospheric diagnostics by means of observations of polar auroras in Antarctica (electric field and plasma drift in the magnetosphere and in the polar ionosphere). In M. Colacino, G. Giovannelli, and L. Stefanutti, Eds., 3rd Workshop Italian Research on Antarctic Atmosphere, *Conference Proceedings*, SIF, Bologna, Volume 34: 361-374.
- Gregori, G. P., 1998. Natural catastrophes and point-like processes. Data handling and prevision. *Annales de Geofisique*, 41, (5/6): 767-786.
- Gregori, G. P., 1968. On the origin of day-side auroras, *Ann. Géophys.*, 24, (1): 153-158.
- Gregori, G. P., 2001. Self-consciousness in Earth’s sciences - Some personal reflections. In Schröder, W., Ed., *Wege zur Wissenschaft, Gelehrte erzählen aus ihrem Leben – Pathways to science, Scientists tell of their life and work, Beiträge zur Geschichte der Geophysik und Kosmischen Physik des Arbeitskreises Geschichte der Geophysik und Kosmischen Physik*, W. Schröder, AKGGKP, Bremen-Roennebeck. (4): 123-133.
- Gregori, G. P., 2016a. The endogenous energy and the magnetic field of planetary objects: the Pluto/Charon binary system and its seasonal rejuvenation, *New Concepts in Global Tectonics, Journal*, 4, (3): 406-431.
- Gregori, G. P., 1999a. The external magnetic sources over the polar caps. Feasible modelling vs. unrealistic expectations. *Annals of Geofysics.*, 42, (2): 171-189.
- Gregori, G. P., 1998a. The magnetosphere of the Earth. A theory of magnetospheric substorms and of geomagnetic storms. In W. Schröder, Ed., *From Newton to Einstein-A Festschrift in honour of the 70th birthday of Hans-Jürgen Treder, Mitteilungen des Arbeitskreises Geschichte der Geophysik der DDG*, Science Edition / IDCH-IAGA / AKGGKP (Arbeitskreis Geschichte der Geophysik und Kosmischen Physik der DDG), Bremen-Roennebeck and Potsdam. Volume 17, (3/4): 68-106.
- Gregori, G. P., 1999. Variational principles and geomagnetism. In W. Schröder, Ed., *Physics and geophysics (A compilation with special historical case studies)*, History Commission of the German Geophysical Society, *Mitteilungen des Arbeitskreises Geschichte der Geophysik der DGG*, Science Edition/DGG, Bremen 18, Heft 1-3: 268-303.
- Gunell, H., C. Goetz, C. S. Wedlund, J. Lindkvist, M. Hamrin, H. Nilsson, K. Llera, A. Eriksson, and M. Holmström, 2018. The infant bow shock: a new frontier at a weak activity comet, *Astronomy and Astrophysics*: 619, L2; DOI:10.1051/0004-6361/201834225.
- Güttler, C., J. Blum, A. Zsom, C. W. Ormel, and C. P. Dullemond, 2010. The outcome of protoplanetary dust growth: pebbles, boulders, or planetesimals? I. Mapping the zoo of laboratory collision experiments, *Astronomy and Astrophysics*, 513, A56 [16 p.]; DOI:10.1051/0004-6361/200912852.
- Harada, Y., D. L. Mitchell, J. S. Halekas, J. P. McFadden, C. Mazelle, J. E. P. Connerney, J. Espley, D. A. Brain, D. E. Larson, R. J. Lillis, T. Hara, R. Livi, G. A. Di Braccio, S. Ruhunusiri, and B. M. Jakosky, 2016. MAVEN observations of energy-time dispersed electron signatures in Martian crustal magnetic fields. *Geophysical Research Letters*, 43, (3): 939-944; DOI:10.1002/2015GL067040.

- Heikkila, W. J., 1972. Penetration of particles into the polar cap Regions of the magnetosphere. In E.R. Dyer, Ed., *Critical problems in magnetospheric physics*, Proceedings of the Symposium, held 11-13 May, 1972 in Madrid, Spain, IUCSTP Secretariat, National Academy of Sciences, Washington D.C.: 67-82.
- Heins, W., 2014. UT research uncovers forces that hold gravity-defying near-Earth asteroid together, *Tennessee Today*, issued August 13.
- Högner, W., and N. Richter, 1979. *Isophotometric atlas of comets*, Part I, 90 plates; Part II, 55 plates, Springer-Verlag, Berlin etc.
- Howell, E., 2015b. Amazing photo of green comet Lovejoy captured by Dark Energy Camera, *Space.com*, issued March 02.
- Howell, E., 2015c. Speedy particles caught erupting from comet's tail, *Space.com*, issued March 18.
- Hultqvist, B., 1969a. Auroral and polar substorms: observations and theory. *Reviews of Geophysics*, 7, (1/2): 129-177.
- Imster, E., 2016. Close comet flyby plunged Mars' magnetic field into chaos, *Science Wire*, issued March 14.
- Ivanov, K. G., and A. D., Shevnin, 1966. Geomagnetic phenomena observed during the transit of the Earth through the tail of Halley's 1910 II comet, *Geomagnetism and Aeronomy*, 6: 634-637.
- Jewitt, D., J. Agarwal, H. Weaver, M. Mutchler, and S. Larson, 2013. The extraordinary multi-tailed main-belt Comet P/2013 P5. *Astrophysical Journal Letters*, 778, (1): L21.
- Jones, G. H., A. Balogh, and T. S. Horbury, 2000. Identification of comet Hyakutake's extremely long ion tail from magnetic field signatures, *Nature*, 404: 574-576; DOI:10.1038/35007011.
- Killen, R. M., W. E. McClintock, A. E. Potter, E. T. Bradley, N. R. Izenberg, M. C. Kochte, M. R. Lankton, N. Mouawad, A. L. Sprague, and R. J. Jr. Vervack, 2008. Comparison of ground-based sodium observations to measurements of Mercury's exosphere with the MESSENGER ultraviolet and visible spectrometer during the first Mercury flyby, *Lunar Planetary Science*, 39: 1452.
- [Koenders, C.](#), [K.-H. Glassmeier, I. Richter, H. Ranocha, and U. Motschmann](#), 2015. Dynamical features and spatial structures of the plasma interaction region of 67P/Churyumov-Gerasimenko and the solar wind, [Planetary and Space Science](#), 105: 101-116; DOI:10.1016/j.pss.2014.11.014.
- Kramer, M., 2014d. Rosetta spacecraft's comet water discovery: what it means for Earth, *Space.com*, issued December 12.
- Krimigis, S. M., 1973. Light ion releases in the solar wind and the distant magnetotail. In *Workshop on controlled magnetospheric experiments*, held during the *Second Scientific General Assembly of IAGA*, Kyoto, September, 1973.
- Kronk, G. W., 2011. [C/2011 W3 \(Lovejoy\)](#). *Cometography.com*. Retrieved 28 December.
- [Kuthunur, S.](#), 2024. Iconic Crab Nebula shines in gorgeous James Webb Space Telescope views (video, image), *Space.com*, issued June 18.
- Lanzerotti, L. J., and G. P. Gregori, 1986. Telluric currents: the natural environment and interactions with man-made systems. In Krider, E.P., and R.G. Roble, Eds., *The Earth's electrical environment*, National Academy Press, Washington, D. C.; DOI:10.17226/898: 232-257.
- Larmor, Sir J., 1920. How could a rotating body such as the Sun become a magnet?, *Report of the British Association for the Advancement of Science, Bournemouth Meeting, 1919*: 159-160, also in *Mathematical and physical papers*, Vol. II: 611-612, Cambridge University Press, 1929.
- Larmor, Sir J., 1919a. Possible rotational origin of magnetic fields of Sun and Earth. *Electrical Review*, 85: 412 (or 512?).
- Lassen, K., 1967. Polar cap aurora. In B. M. McCormac, Ed., *Aurora and airglow*. Reinhold Publ. Corp., New York etc.: 453-464.
- Lassen, K., 1969. Polar cap emissions. In B. M. McCormac, and A. Omholt, Eds., *Atmospheric emissions*, Van Nostrand Reinhold Company, New York etc.: 63-71.
- Levenspiel, O., T. J. Fitzgerald, and D. Pettit, 2000. Earth's atmosphere before the age of dinosaurs, *Chemical Innovation*, 30, (12): 50-55.
- Levenspiel, O., 2000. DEPARTMENTS-Learning from the past-Earth's early atmosphere. *Chemical Innovation*, 30, (5): 47-51.
- Lyttleton, R. A., 1972. Does a continuous solid nucleus exist in comets? *Astrophysics and Space Science*, 15: 175-184.
- Malaise, D., 1966. Discussion, in *Nature et origine des comètes*, 13 colloque, *Mémoires de la Société Royale des Sciences de Liège*, 5° serie, XII : 385.
- Malik, T., 2013. Russian meteor explosion not caused by asteroid flyby, NASA scientist says. *Space.com*, issued 15 February.
- Malik, T., 2011. [Sun rips tail from comet during solar close encounter](#). *Space.com*. Issued 16 December.
- [Mathewson, S.](#), 2023.10 times the night sky amazed us in 2023, *Space.com News*, issued December 23.
- Mazzucato, M. T., 2007. Sungrazing comets: le comete che sfiorano il Sole, *Giornale di Astronomia*, 33, (2): 17-22.
- McClintock, W. E., E. T. Bradley, N. R. Izenberg, R. M. Killen, M. C. Kochte, M. R. Lankton, N. Mouawad, A. L. Sprague, and R. J. Jr. Vervack, 2008. Observations of Mercury's exosphere by the Mercury atmospheric and surface composition spectrometer during the first MESSENGER flyby. In *39th Lunar and Planetary Science Conference, (Lunar and Planetary Science XXXIX)*, held March 10-14, 2008 in League City, Texas, LPI Contribution No. 1391: p. 1353.
- Möstl, C., T. Amerstorfer, E. Palmerio, A. Isavnin, C. J. Farrugia, C. Lowder, R. M. Winslow, J. M. Donnerer,

- E. K. J. Kilpua, and P. D. Boakes, 2018. Forward modeling of Coronal Mass Ejection flux ropes in the inner heliosphere with 3DCORE, *Space Weather*, 16, (3): 216-229; DOI:10.1002/2017SW001735.
- Ness, N. F., and B. D. Donn, 1966. Concerning a new theory of Type I comet tails, in "Nature et origine des comètes", 13 colloque, *Mémoires de la Société Royale des Sciences de Liège*, 5° serie, XII: 343-362.
- Ness, N. F., and B. D. Donn, 1965. The magnetic tail of the Earth and its implications for Type-I tails-Abstract of a paper given at the 118th meeting of the *American Astronomical Society*, 14-17 March, 1965, Lexington, Univ. of Kentucky, *Astronomical Journal*, 70, (65): 327-328.
- Niedner, M. B., and J. C., Brandt, 1978. Interplanetary gas. XXIII - Plasma tail disconnection events in comets - Evidence for magnetic field line reconnection at interplanetary sector boundaries, *Astrophysical Journal, Part 1*, 223: 655-670, DOI:10.1086/156299.
- Olson, V. P., 1974. Potential experiments with superconducting magnets flown from rockets and satellites. In *Workshop on controlled magnetospheric experiments*, held during the *Second Scientific General Assembly of IAGA*, Kyoto, September 1973, *Space Science Reviews*, 15: 899-904.
- Öpik, E. J., 1964a. The motion of the condensation in the tail of Halley's comet, June 5-8, 1910., *Zeitschrift für Astrophysik*, 58: 192-201.
- Paparo, G., and G. P. Gregori, 2003 Multifrequency acoustic emissions (AE) for monitoring the time evolution of microprocesses within solids. In D. O. Thompson and D. E. Chimenti, Eds., *Reviews of Quantitative Nondestructive Evaluation*, 22, (AIP Conference Proceedings): 1423-1430.
- Paschmann, G., N. Sckopke, H. Grünwaldt, 1976. Plasma in the polar cusp and plasma mantle. In *Magnetospheric particles and fields*, D. Reidel Publishing Co., Dordrecht, etc.: 37-46.
- Philipp, W., and G. Morfill, 1976. The plasma mantle as the origin of the plasmashet. In B. M. McCormac, Ed., *Magnetospheric particles and fields*, D. Reidel Publishing Co., Dordrecht, etc: 55-66.
- Phillips, T., 2012f. Comet corpses in the solar wind, *Science@NASA*, issued January 20.
- Phillips, T., 2011a. Comet Lovejoy plunges into the Sun and survives, *Science News* (NASA.gov), issued December 16.
- Phillips, T., 2013d. Hubble sees an asteroid with six comet-like tails, *Science@NASA*, issued November 7.
- Phillips, T., 2012a. [Some comets like it hot](#). *Science News* (NASA.gov). Issued 12 January.
- Phillips, T., 2013e. What happened to comet ISON? [Science@NASA](#), issued December 4.
- Porter, J. G., 1960. Two bright comets of 1957: II – Cometary physics and the comets Arend-Roland and Mrkos, *Vistas in Astron.*, 3, Part I: 132-137.
- Potter, A. E., R. M. Killen, and T. H. Morgan, 2002. The sodium tail of Mercury, *Bull. Am. Astr. Soc.*, 34, (3).
- Potter, A. E., R. M. Killen, and T. H. Morgan, 2007. Solar radiation acceleration effects on Mercury sodium emission, *Icarus*, 186, (2): 571-580; DOI:10.1016/j.icarus.2006.09.025.
- Potter, A. E., and R. M. Killen, 2008. Observations of the sodium tail of Mercury, *Icarus*, 194, (1): 1-12.
- [Ramanjooloo](#), Y., 2014. How comets reveal structure of the inner heliosphere, *Astronomy and Geophysics*, 55, (1): 1.32-1.35; DOI:10.1093/astgeo/atu038.
- [Reale](#), F., S. [Orlando](#), P. [Testa](#), G. [Peres](#), E. [Landi](#), and C. J. [Schrijver](#), 2013. Bright hot impacts by erupted fragments falling back on the Sun: a template for stellar accretion, *Science*, 341, (6143): 251-253; DOI:10.1126/science.1235692.
- Reid, G. C., 1963. Polar cap absorption. In *Advances in upper atmosphere research*. Landmark, B., Ed., Pergamon Press, Oxford etc., pp. 309-316.
- Richter, N. B., 1963. *The nature of comets*, Methuen & Co. Ltd, London: 1-221.
- Rigby, A., F. Cruz, B. Albertazzi, R. Bamford, A. R. Bell, J. E. Cross, F. Frascchetti, P. Graham, Y. Hara, P. M. Kozłowski, Y. Kuramitsu, D. Q. Lamb, S. Lebedev, J. R. Marques, F. Miniati, T. Morita, M. Oliver, B. Reville, Y. Sakawa, S. Sarkar, C. Spindloe, R. Trines, P. Tzeferacos, L. O. Silva, R. Bingham, M. Koenig, and G. Gregori, 2018. Electron acceleration by wave turbulence in a magnetized plasma, *Nature, Physics*, 145: 475-479; DOI:10.1038/s41567-018-0059-2.
- [Roizitis](#), B., [E. MacLennan](#), and [J. P. Emery](#), 2014. Cohesive forces prevent the rotational breakup of rubble-pile asteroid (29075) 1950 DA, *Nature*, 512: 174-176; DOI:10.1038/nature13632.
- Saito, T., and K. Saito, 1986a. Effect of the heliospheric neutral sheet to the kinked ion tail of Comet Halley on 13 May 1910. In *ESA Proceedings of the 20th ESLAB Symposium, on the Exploration of Halley's Comet*. 1: *Plasma and Gas*: 135-140.
- Saito, T., and K. Saito, 1986. In *Proceedings of the 7th Symp. Solar System Science*, (Institute of Space and Aeronautical Science): 23-24.
- Saito, T., K. Yumoto, K. Hirao, S. Minami, K. Saito, and E. Smith, 1987. Structure and dynamics of the plasma tail of comet P/Halley. I-Knot event on December 31, 1985, *Astronomy and Astrophysics*, 187, (1/2): 209-214.
- Saito, T., K. Yumoto, K. Hirao, T. Nakagawa, and K. Saito, 1986. Interaction between comet Halley and the interplanetary magnetic field observed by Sakigake, *Nature*, 321: 303-307; DOI:10.1038/321303a0.
- Saito, T., K. Yumoto, K. Hirao, K. Saito, T. Nakagawa, and E. J. Smith, 1986a. A disturbance of the ion tail of comet Halley and the heliospheric structure as observed by Sakigake, *Geophysical Research Letters*, 23, (8): 821-824.
- Sapper, K., 1903. *Esplorazione della crosta terrestre. In Universo ed Umanità, Storia dei progressi umani nella conoscenza e nel dominio delle forze naturali*, Kraemer,

- H., *et al.*, Eds.; Italian translation from the German, with notes by L. de Marchi *et al.*, printed by Casa Editrice Dottor Francesco Vallardi, Milano, Volume I: 17-292.
- Schrijver, C. J., C. M. Lisse, and C. Downs, 2013. Comets as solar probes, *Physics Today*, 66, (10): 27-32.
- Schrijver, C. J., J. C. Brown, K. Battams, P. Saint-Hilaire, W. Liu, H. Hudson, and W. D. Pesnell, 2012. Destruction of Sun-grazing comet C/2011 N3 (SOHO) within the low solar corona, *Science*, 335, (6066): 324-328; DOI:10.1126/science.1211688.
- Schröder, W., 2008. Johann Wolfgang von Goethe and the aurora borealis, *Acta Geodetica et Geophysica Hungarica*, 43, (1): 113-113.
- Schulz, M., 1991. The magnetosphere. In Jacobs, J. A., Ed., *Geomagnetism*, Academic Press, Harcourt Brace Jovanovich, Publ., London, etc. Volume 4: 87-293.
- Schwenn, R., 1981. Solar wind and its interaction with the magnetosphere: measured parameters, *Advances in Space Research*, 1: 3-17.
- Schwenn, R., 1988. Transport of energy and mass to the outer boundary of the Earth system. In J. G. Roederer, Ed., STEP, *Solar Terrestrial energy program: Major scientific problems*. Proceedings of a Scostep Symposium, held during the XXVII COSPAR Plenary Meeting, Helsinki, July 23, 1988, SCOSTEP Secretariat, University of Illinois, Urbana, Illinois, USA: 13-30.
- Scopke, N., and G. Paschmann, 1978. The plasma mantle: a survey of magnetotail boundary observations, *Journal of Atmospheric and Terrestrial Physics*, 40: 261-278.
- Sekanina, Z., 2019. Oumuamua as debris of dwarf interstellar comet that disintegrated before perihelion, *arXiv:1901.08704v3 [astro-ph.EP]* 30 January.
- Sekanina, Z., 1966. A note on variations in cometary diameters, in *Nature et origine des comètes*, 13° colloque, *Mémoires de la Société Royale des Sciences de Liège*, 5° serie, XII: 145-153.
- Sekanina, Z., 1968. Non-gravitational forces and comet nuclei, *Sky and Telescopes*, 35: 282-286.
- Shanklin, J., 2003. Meteorites, meteors and comets, *Astronomy and Geophysics*, 44, (5): 5.31-5.32.
- Slavin, J. A., G. Jungman, and E. J. Smith, 1986. The interplanetary magnetic field during solar cycle 21: ISEE-3/ICE observations, *Geophysical Research Letters*, 13, (6): 513-516; DOI:10.1029/GL013i006p00513.
- Stefanik, B. P., 1966. On thirteen split comets, in *Nature et origine des comètes*, 13° colloque, *Mémoires de la Société Royale des Sciences de Liège*, 5° serie, XII: 29-32.
- Vaquero, J. M., 2014. Early sightings of comets near the Sun, *Physics Today*, 67, (5): 9-9.
- Vaquero, J. M., and M. Vázquez, 2009. *The Sun recorded through history: scientific data extracted from historical documents*, Springer, New York: 1-382.
- Vourlidas, A., C. J. Davis, C. J. Eyles, S. R. Crothers, R. A. Harrison, R. A. Howard, J. D. Moses, and D. G. Socker, 2007. First direct observation of the interaction between a comet and a coronal mass ejection leading to a complete plasma tail disconnection, *Astrophysical Journal Letters*, 668, (1): L79-L82; DOI:10.1086/522587.
- Vsekhsvyatskii, S. K., 1964. *Physical characteristics of comets*, Israel Program for Scientific Translations: 1-596.
- Wada, K., H. Tanaka, T. Suyama, H. Kimura, and T. Yamamoto, 2009. Collisional growth conditions for dust aggregates, *Astrophysical Journal*, 702, (2): 1490; DOI:10.1088/0004-637X/702/2/1490.
- Wall, M., 2011b. [Comet Lovejoy survives fiery plunge through Sun, NASA says](#). *Space.com*. Issued 15 December.
- Wall, M., 2013. NASA spacecraft snaps last close-up photos of icy Saturn moon, *Space.com*, issued 15 March.
- Wall, M., 2011a. [Satellites to watch comet's death plunge through Sun today](#)". *Space.com*. Issued 15 December.
- Weaver, H. A., 1997. The impact of comet D/Shoemaker-Levy 9 with Jupiter. In E. F. van Dishoeck, Ed., *Molecules in astrophysics: probes and processes*, IAU Symposium, Leiden, Netherlands, July 1-5, 1996, Kluwer Academic Publishers, (178): 205-218.
- Whipple, F. L. and D. H. Douglas-Hamilton, 1966. Brightness changes in periodic comets, in *Nature et origine des comètes*, 13° colloque, *Mémoires de la Société Royale des Sciences de Liège*, 5° serie, XII: 469-480.
- Whipple, F. L., 1974. The nature of comets, *Scientific American*, 230, (2) (February): 48-57
- Williams, I., 2011. The origin and evolution of meteor showers and meteoroid streams, *Astronomy and Geophysics*, 52, (2): 2.20-2.26.
- Wurm, K., 1959. Die Kometen, *Handbuch der Physik*, 52: 465-518.
- Yagi, M., J. Koda, R. Furusho, T. Terai, H. Fujiwara, J.-I. Watanabe, 2015. Initial speed of knots in the plasma tail of C/2013 R1(Lovejoy), *Astrophysical Journal*, 149, (3): 149-197; DOI:10.1088/0004-6256/149/3/97; [arXiv:1403.1346](#) [astro-ph.EP].
- Yeomans, D. K., 1991. *Comets. A chronological history of observation, science, myth and folklore*. Wiley Science Editors, New York etc.: 1-485.
- Yeomans, D. K., 1981. In *The Comet Halley handbook: an observer's guide*, D.K. Yeomans, Ed., NASA Doc. JPL 400-91. Jet Propulsion Lab. Pasadena, California: pp. 1-44.

- Geophysical model of the tectonosphere of Europe. 1987. Ed. V. V. Gordienko. Kyiv: *Naukova Dumka*. 184 p. (in Russian)
- Gershanok L. A. Popova N. S. Lectures on magnetic exploration, Perm: *Perm State National Research University*, 2007, 68 p. (in Russian)
- Gordienko V. V. 2000. Magnetic models of the earth's crust of the territory of Ukraine. Kyiv: *Znanie*. 92 p. (in Russian)
- Gordienko V. V., Gordienko I. V., Zavgorodnyaya O. V. et al., 2005. Ukrainian shield (geophysics, deep processes). Kyiv: *Korvin press*, 112 p. (in Russian)
- Gordienko V. V. 2019. Earth's crust of the oceans and stripe anomalies of the magnetic field. *Geologiya i poleznye iskopaemye Mirovogo okeana*. 4. P.3-35.(in Russian).
- Gordienko V. 2022. Density models of the tectonosphere of continents and oceans. *Izvestiya, Atmospheric and Oceanic Physics*, № 7, pp. 805-822
- Gordienko V.V., Gordienko I.V. 2023. Temperature distribution the crust and upper mantle of Ukraine. *Geodynamics*. 1. p. 47-56.
- Heines G. 1985. Magsat vertical field anomalies above 400 N from spherical Cap Yarmonic analisis *J.G.R.* 90. B3. P. 2593-2598.
- Hemant K., Maus S. 2005a. Geological modeling of the new CHAMP magnetic anomaly maps using a geographical information system technique. *Journal of Geophysical Research* V. 110. P. 1–23. <https://doi.org/10.1029/2005JB003837>
- Hemant K., Maus S., Haak V. 2005b. Interpretation of CHAMP crustal field anomaly maps using a geographical information system (GIS) technique. in: *Earth Observation with CHAMP: Results from Three Years in Orbit*. P. 249–254. https://doi.org/10.1007/3-540-26800-6_39
- Efremova M. A., Rogozhin E. A. 2010. Geophysical fields and earthquakes in the Voronezh crystalline shield territory. *Geofizicheskie Issledovaniya*. Vol.11. 3. pp. 57-71. (in Russian)
- Kovacicova S., Logvinov I. M., Pek J., Tarasov V. N., 2016. Modeling of the Earth's Crust of Ukraine by the results of the magnetotelluric studies using new methods of inversions. *Geofizicheskiy Zhurnal*. 6. pp. 83-100. (in Russian)
- Maus S., Barckhausen U., Berkenbosch H. et al. 2009. EMAG2: A 2–arc min resolution Earth Magnetic Anomaly Grid compiled from satellite, airborne, and marine magnetic measurements. *Geochemistry, Geophysics, Geosystems*. V. 10. Issue 8 <https://doi.org/10.1029/2009GC002471>
- Nikonov A. A. 1999. Catalog of Tectonic Earthquakes in the Central Part of the East European Platform. Arkhangel'sk. *Geodinamika i Geoekologiya*. pp. 271–273. (in Russian)
- Pashkevich I. K., Markovsky V. S., Orlyuk M. I. 1990. Magnetic Model of the Lithosphere of Europe. Kyiv: *Naukova Dumka*, 168 p. (in Russian)
- Pavlenkova N. I. 1980. Features of Different Approaches to Interpretation of Continuous Profiling Data. Seismic Models of the Lithosphere of the Main Geostuctures of the USSR. Moscow: *Nauka*. pp. 28-40. (in Russian)
- Primdahl F., Luhr H., Lauridsen E.K. 1992. The Effect of Large Uncompensated Transverse Fields on the Fluxgate Magnetic Sensor Output. *Danish Space Research Institute Report*. P. 1–92.
- Rotanova N.M., Kharitonov A.L., Frunze A.Kh., Filippov S.V., Abramova D.Yu. 2005. Anomalous magnetic fields from measurements on the CHAMP satellite for the territory of the Kursk magnetic anomaly. *Geomagnetizm i aeronomiya*. Vol. 45, No. 5. Pp.712-719. (in Russian)
- Varentsov I.M., Gordienko V.V., Gordienko I.V. et al., 2013. Slope of the Voronezh crystalline massif (geophysics, deep processes). Kyiv: *Logos*, 112 p. (in Russian).

5. Cultural rituals and Mythological stories revolving around peat

1. Lori Dorn October 26, 2022, Randall Carlson, <https://laughingsquid.com/randall-carson-halloween/>
2. The Fire Of St. Elmo 1998, Keith C. Heidorn, PhD, www.heidorn.info
3. Babrauskas, V. (2022). Minimum Values of Voltage, Current, or Power for the Ignition of Fire. *Fire*, 5(6), 201. <https://doi.org/10.3390/fire5060201>
4. Plate tectonic issues, the influence of electricity in rock forming processes and a coherent connection between science, mythology and history of Finland, Stefan Ahmala, NCGT Journal, Vol. 0. Nr. 4. 2021, ISSN 2202-0039 (Page 45-70)
5. Robinet, Jean-Christophe & Casalis, Grégoire. (2001). Critical interaction of a shock wave with an acoustic wave. *Physics of Fluids - PHYS FLUIDS*. 13. 10.1063/1.1351548.
6. Study of the Electrical Characteristics, Shock-Wave Pressure Characteristics, and Attenuation Law Based on Pulse Discharge in Water, Dong Yan, Decun Bian, Jinchang Zhao, Shaoqing Niu, First published: 2016 <https://doi.org/10.1155/2016/6412309>
7. Great Lynx, the Thunder, and the Mortals - Mii Dash Geget, February 24, 2019, wordpress.com
8. CHIPPEWA BURIAL AND MOURNING CUSTOMS, Sister M. Inez Hilger, First published: October-December 1944, <https://doi.org/10.1525/aa.1944.46.4.02a00240>
9. Christopher J.M. Lawley, Victoria Tschirhart, Jennifer W. Smith, Sally J. Pehrsson, Ernst M. Schetselaar, Andrew J. Schaeffer, Michel G. Houlié, Bruce M. Eglinton, Prospectivity modelling of Canadian magmatic Ni (\pm Cu \pm Co \pm PGE) sulphide mineral systems, *Ore Geology Reviews*, Volume 132, 2021, 103985, ISSN 0169-1368, <https://doi.org/10.1016/j.oregeorev.2021.103985>
10. Haerendel, G., & Partamies, N. (2024). On the formation of auroral spirals. *Journal of Geophysical Research: Space Physics*, 129, e2024JA032413. <https://doi.org/10.1029/2024JA032413>
11. Nishimura, K., Ikehata, H., Douki, T., Cadet, J., Sugiura, S., & Mori, T. (2021). Seasonal Differences in the UVA/UVB Ratio of Natural Sunlight Influence the Efficiency of the Photoisomerization of (6-4) Photoproducts into their Dewar Valence Isomers. *Photochemistry and photobiology*, 97(3), 582–588. <https://doi.org/10.1111/php.13361>
12. The Electric Universe, Wallace Thornhill & David Talbott, May 24, 2007, Mikamar Publisher
13. The Thunderbolts Project™ Trademark of T-Bolts Group Inc. a 501(c)(3) non-profit organization, www.thunderbolts.info
14. Emily Goodheart | Feb 3, 2018, <https://www.nathab.com/blog/folklore-arctic-animals/>
15. Tables to Correct Eyes and Quickly Answer Differences in Cosmologies, Sf. R. Careaga, BSEE, MSTOM June 2023 www.academia.edu/103064184/PEMC
16. A3Anomalies/ Stefan Ahmala Finnish Copper Playlist https://youtube.com/playlist?list=PLLWZrQb_ZJzX9gB7e7dc9ZxRMW-tGXIEL&si=NAVBqGuc1hQR_9D1
17. Talbott, David N., *The Saturn Myth* ISBN: 0-385-113376-5 Library of Congress Catalog Card Number 76-51986 1980
18. Lahelma, Antti, University of Helsinki Open Repository, Suomen Muinaismuistoyhdistys r.y, A Touch of Red : Archaeological and Ethnographic Approaches to Interpreting Finnish Rock Paintings, <http://urn.fi/URN:ISBN:978-952-10-4845-6>, URN:ISSN:0355-3108
19. Peratt, Anthony. (2004). Characteristics for the Occurrence of a High-Current, Z-Pinch Aurora as Recorded in Antiquity. *Plasma Science, IEEE Transactions on*. 31. 1192 - 1214. 10.1109/TPS.2003.820956.
20. Lobachevsky, P., Forrester, H. B., Ivashkevich, A., Mason, J., Stevenson, A. W., Hall, C. J., Sprung, C. N., Djonov, V. G., & Martin, O. A. (2021). Synchrotron X-Ray Radiation-Induced Bystander Effect: An Impact of the Scattered Radiation, Distance From the Irradiated Site and p53 Cell Status. *Frontiers in oncology*, 11, 685598. <https://doi.org/10.3389/fonc.2021.685598>

ABOUT THE NCGT JOURNAL

The NCGT Newsletter , the predecessor of the NCGT Journal , was begun as a result of discussions at the symposium “Alternative Theories to Plate Tectonics ” held at the 30th International Geological Congress in Beijing in August 1996 . The name is taken from an earlier symposium held in association with the 28th International Geological Congress in Washington , D. C. in 1989 . The first issue of the NCGT Newsletter was December 1996 . The NCGT Newsletter changed its name in 2013 to the NCGT Journal . Aims of the NCGT Journal include:

1. Providing an international forum for the open exchange of new ideas and approaches in the fields of geology, geophysics, solar and planetary physics, cosmology, climatology, oceanography, electric universe, and other fields that affect or are closely related to physical processes occurring on Earth from its core to the top of its atmosphere.
2. Forming an organizational focus for creative ideas not fitting readily within the scope of dominant tectonic models.
3. Forming the basis for the reproduction and publication of such work, especially where there has been censorship or discrimination.